GLIAL CELLS, MALADAPTIVE PLASTICITY AND NEURODEGENERATION: MECHANISMS, TARGETED THERAPIES AND FUTURE DIRECTIONS,
2nd Edition

EDITED BY: Giovanni Cirillo, Andrea Beatriz Cragnolini and Livio Luongo
PUBLISHED IN: Frontiers in Cellular Neuroscience

frontiers Research Topics

ISSN 1664-8714
ISBN 978-2-8325-3663-6
DOI 10.3389/978-2-8325-3663-6

About Frontiers

Frontiers is more than just an open-access publisher of scholarly articles: it is a pioneering approach to the world of academia, radically improving the way scholarly research is managed. The grand vision of Frontiers is a world where all people have an equal opportunity to seek, share and generate knowledge. Frontiers provides immediate and permanent online open access to all its publications, but this alone is not enough to realize our grand goals.

Frontiers Journal Series

The Frontiers Journal Series is a multi-tier and interdisciplinary set of open-access, online journals, promising a paradigm shift from the current review, selection and dissemination processes in academic publishing. All Frontiers journals are driven by researchers for researchers; therefore, they constitute a service to the scholarly community. At the same time, the Frontiers Journal Series operates on a revolutionary invention, the tiered publishing system, initially addressing specific communities of scholars, and gradually climbing up to broader public understanding, thus serving the interests of the lay society, too.

Dedication to Quality

Each Frontiers article is a landmark of the highest quality, thanks to genuinely collaborative interactions between authors and review editors, who include some of the world's best academicians. Research must be certified by peers before entering a stream of knowledge that may eventually reach the public - and shape society; therefore, Frontiers only applies the most rigorous and unbiased reviews.
Frontiers revolutionizes research publishing by freely delivering the most outstanding research, evaluated with no bias from both the academic and social point of view. By applying the most advanced information technologies, Frontiers is catapulting scholarly publishing into a new generation.

What are Frontiers Research Topics?

Frontiers Research Topics are very popular trademarks of the Frontiers Journals Series: they are collections of at least ten articles, all centered on a particular subject. With their unique mix of varied contributions from Original Research to Review Articles, Frontiers Research Topics unify the most influential researchers, the latest key findings and historical advances in a hot research area! Find out more on how to host your own Frontiers Research Topic or contribute to one as an author by contacting the Frontiers Editorial Office: frontiersin.org/about/contact

GLIAL CELLS, MALADAPTIVE PLASTICITY AND NEURODEGENERATION: MECHANISMS, TARGETED THERAPIES AND FUTURE DIRECTIONS,
2nd Edition

Topic Editors:
Giovanni Cirillo, Università degli Studi della Campania Luigi Vanvitelli, Italy
Andrea Beatriz Cragnolini, Universidad Nacional de Cordoba, Argentina
Livio Luongo, University of Campania Luigi Vanvitelli, Italy

Publisher's note: This is a 2nd edition due to an article retraction.

Citation: Cirillo, G., Cragnolini, A. B., Luongo, L., eds. (2023). Glial Cells, Maladaptive Plasticity and Neurodegeneration: Mechanisms, Targeted Therapies and Future Directions, 2nd Edition. Lausanne: Frontiers Media SA.
doi: 10.3389/978-2-8325-3663-6

Table of Contents

frontiers in Cellular Neuroscience

EDITORIAL
published: 30 April 2021
doi: 10.3389/fncel.2021.682524

Editorial: Glial Cells, Maladaptive Plasticity, and Neurodegeneration: Mechanisms, Targeted Therapies, and Future Directions

Sohaib Ali Korai [1†], Giovanna Sepe [1†], Livio Luongo [2,3], Andrea Beatriz Cragnolini [4,5*] and Giovanni Cirillo [1*]*

[1] Division of Human Anatomy – Laboratory of Neuronal Networks, University of Campania "Luigi Vanvitelli", Naples, Italy, [2] Division of Pharmacology, University of Campania "Luigi Vanvitelli", Naples, Italy, [3] IRCSS Neuromed, Pozzilli, Italy, [4] Facultad de Ciencias Exactas, Físicas y Naturales, Universidad Nacional de Córdoba, Córdoba, Argentina, [5] Instituto de Investigaciones Biológicas y Tecnológicas (IIByT), CONICET-Universidad Nacional de Córdoba, Córdoba, Argentina

Keywords: glial cells, neuroinflammation, neurodegeneration, synaptic homeostasis, synaptic plasticity

OPEN ACCESS

Edited and reviewed by:
Enrico Cherubini, European Brain Research Institute, Italy

***Correspondence:**
Livio Luongo
livio.luongo@unicampania.it
Andrea Beatriz Cragnolini
andrea.cragnolini@unc.edu.ar
Giovanni Cirillo
giovanni.cirillo@unicampania.it

[†]These authors have contributed equally to this work

Specialty section:
This article was submitted to Cellular Neurophysiology, a section of the journal Frontiers in Cellular Neuroscience

Received: *18 March 2021*
Accepted: *29 March 2021*
Published: *30 April 2021*

Citation:
Korai SA, Sepe G, Luongo L, Cragnolini AB and Cirillo G (2021) Editorial: Glial Cells, Maladaptive Plasticity, and Neurodegeneration: Mechanisms, Targeted Therapies, and Future Directions. Front. Cell. Neurosci. 15:682524. doi: 10.3389/fncel.2021.682524

Editorial on the Research Topic

Glial Cells, Maladaptive Plasticity, and Neurodegeneration: Mechanisms, Targeted Therapies, and Future Directions

Understanding the biological complexity of the central nervous system (CNS) is a frontier in neuroscience. Morphological organization of the CNS represents the basis for its functional properties underlying higher brain functions; therefore, efforts are needed to boost the comprehension of the organization of the CNS, from the ultrastructural to the functional-networks level.

To date, two highly integrated and interconnected cellular networks substantiate the anatomo-functional organization of CNS: neurons and non-neuronal cells, namely glial cells.

Glial cells, including astrocytes, oligodendrocytes, and microglia, actively participate in many complex functions within the CNS (immunity surveillance and inflammatory response, metabolic and synaptic homeostasis, modulation of blood-brain barrier—BBB) (Volterra and Meldolesi, 2005). Moreover, interaction with the elements of the extracellular matrix (ECM), an active player for long-term plasticity and circuit maintenance, adds another level of complexity to the modern model of the synapse structure (tetrapartite synapse) (Song and Dityatev, 2018). Therefore, if on one hand glial cells allow adaptive synaptic plasticity of CNS in several physiological conditions modulating synaptic transmission, homeostasis, and neural pathways signaling, then on the other, when activated, they boost inflammatory response and perturb neuroglial interactions, synaptic circuitry, and plasticity. This new condition, called maladaptive synaptic plasticity, may represent an early stage of neuroinflammatory processes in neurodegenerative disorders (Papa et al., 2014).

Recently, it has been hypothesized that the morpho-functional heterogeneity of astrocytes in different brain regions might explain the regional diversity of astrocytic response to an external injury and the selectivity of neuronal degeneration (Cragnolini et al., 2018, 2020). Therefore, the comprehension of these mechanisms is relevant for the development of targeted therapies for clinical management of neurodegenerative disorders. Only through unraveling the complex interactions between the different cell types at the synapse, we will truly understand synaptic plasticity, higher brain functions, and how perturbations of these interactions contribute to brain diseases with dramatic clinical impact.

This Research Topic aims to address the role of neuroglia in health and disease through a collection of 12 articles that include two mini-reviews, two reviews, one hypothesis and theory, and seven original research articles, providing an overview on a broad spectrum of molecular and cellular bases of glial function in normal and pathological CNS.

New mechanisms were explored in glial transmission, signaling, and neural circuitry. It has been established that astrocytes which release neurotransmitters such as glutamate and GABA, express a variety of neurotransmitter receptors and participate in synaptic transmission (Araque et al., 2014). Furthermore, GABA released from interneurons participates in astrocyte-mediated control of excitatory synaptic transmission (Perea et al., 2016) through activation of astrocytic GABA-B receptors leading to gliotransmission (Liu et al., 2018b). The coupling between GABA interneuron, astrocytic terminals and pre/post synaptic compartments may underpin both seizure-like activity and neuronal synchrony across different brain regions (Liu et al.). Evidence has also demonstrated that early neuroinflammation, macrophage infiltration, and astrocytic activation have a main role in epileptogenesis (Rossi et al., 2013, 2017). In particular, experimental epileptic seizures after stroke, brain injury, or pilocarpine administration induce the release of small intracellular molecules (called DAMP—damage associated molecular patterns) including the ubiquitous High Mobility Group Box 1 (HMGB1) nuclear protein (Braun et al., 2017). It has been proposed that microglial-astroglial cooperation is required for astrocytes to respond to HMGB-1 and to induce neurodegeneration. Disruption of this HMGB-1 mediated signaling pathway shows beneficial effects by reducing neuroinflammation and neurodegeneration after status epilepticus (Rosciszewski et al.).

Furthermore, thrombin increase in the brain after stroke as a result of brain-blood barrier breakdown or brain tissue intrinsic production enhances PAR1-mediated NMDA receptor activity and increases intracellular calcium levels (Maggio et al., 2013). Altman et al. reviews the events that lead to a hyperexcitable state and to maladaptive plasticity that in turn, through an astrocytic mediated response, synchronize neuronal activity producing epileptic activity.

Astrocytic functions and activity are also affected by general anesthetics (Thrane et al., 2012; Liu et al., 2016), particularly the NMDA antagonist ketamine have an inhibitory role in astrocytic glutamatergic transmission blocking GluN1/GluN2B receptors. The decrease of astrocyte-mediated slow inward current (SICs) synchronization due to ketamine administration at clinical concentration may have serious implications for the development of dissociative cognitive impairment during ketamine anesthesia (Zhang et al.). In addition, anesthesia and surgical stress may cause postoperative cognitive dysfunction (POCD), a highly prevalent condition in elderly patients undergoing major surgery or non-invasive procedures under sedation (Leslie, 2017; Skvarc et al., 2018). Wei et al. hypothesized that mtROS/NLRP3 inflammasome may be part of the upstream pathway mediating the cleavage and release of the microglial interleukin 1 beta into brain areas including hippocampus that might play a pivotal role in POCD.

Besides their role in neural circuitry and signaling, glial cells are also involved in axonal regeneration and nerve repair. Ganglionic satellite glial cells (SGCs) create a structural unit inside the dorsal root ganglion, providing protection against inflammation, structural, and metabolic support to neurons (Hanani, 2005). Slit1 is one of the signaling factors that guides both axon projection and neuronal migration (Blockus and Chédotal, 2016), by mediating the branching of the sensory axon growth cone. Evidence has demonstrated that peripheral nerve injury activates the purinergic system via P2X7 receptors (mainly expressed on SGCs) and upregulates the expression of slit1, promoting axonal repair, and regeneration (Zhang et al.).

The relevance of astrocytes to the neurodegenerative process was highlighted in an experimental model of Parkinson's disease (PD). Astrocytes express the α7 nicotinic acetylcholine receptor (α7nAChR) (Xu et al., 2019) for anti-inflammatory (Egea et al., 2015), antiapoptotic (Kim et al., 2012), and neuroprotective functions in health and disease (Liu et al., 2015; Quik et al., 2015). The α7nAChR agonist PNU-282987 showed neuroprotective effects in astrocytes treated with 1-methyl-4-phenylpyridinium (MPP+), reducing the number of degenerating cells, and alleviating MPP -induced apoptosis. Moreover, PNU-282987 upregulated the expression of the antiapoptotic protein Bcl-2 and downregulated the expression of the apoptotic protein Bax and cleaved caspase-3, mainly via the JNK-p53-caspase-3 signaling (Hua et al.).

The immunological aspects of glial cells were explored by Zhou et al. in a murine model of experimental autoimmune encephalomyelitis (EAE). CD73, an astrocytic membrane ectonucleotidase, quickly converts adenosine monophosphate (AMP) to adenosine (an anti-inflammatory mediator) that interacts with ARA1 receptors controlling excitability, synaptic transmission in brain circuits and neuroinflammation (Liu et al., 2018a). Upon EAE induction, astrocytes lose most of their membrane-localized CD73, thus inhibiting the generation of adenosine in the local microenvironment, boosting the inflammatory process, and facilitating the pathogenesis of EAE (Zhou et al.).

Among the inflammatory disorders of the CNS, neuromyelitis optica spectrum disorder (NMOSD) represents a prototype of antigen-antibody-induced damage (the disease target is the aquaporin-4 (AQP4), a water channel protein expressed on astrocytic end-feet) (Wingerchuk et al., 2015). As in many other CNS disorders, glutamatergic excitotoxicity may play an important role in NMOSD (Zekeridou and Lennon, 2015). Da Silva et al. reviews the pathway that causes AQP4-IgG/AQP4 complex to downregulate the astrocytic glutamate transporter EAAT2 (Yang et al., 2016), leading to the excitotoxic damage.

Activation of glial cells, dysfunction of the endocannabinoid signaling and increased expression of pro-inflammatory factors might also contribute to pathogenesis of autism spectrum disorder (ASD) (Bronzuoli et al., 2018). Using the ASD animal model consisting in prenatal exposure to valproic acid (VPA) (Melancia et al., 2018), it has been demonstrated that an inflammatory reaction and astrocytic/microglia activation restricted to the hippocampus and related to impaired social interactions, stereotypic repetitive behaviors, and

learning and memory defects. Interestingly, treatment with the phytocannabinoid cannabidivarin (CBDV) restores hippocampal endocannabinoid signaling and neuroinflammation induced by prenatal VPA exposure and recovered social impairments, social novelty preference, short-term memory deficits, and repetitive behaviors (Zamberletti et al.).

Connexins and pannexins are widely expressed in glial cells, where they play several roles including channel and non-channel functions. These functions include modulation of synaptic gain, the control of excitability through regulation of the ion and neurotransmitter composition of the extracellular milieu and the promotion of neuronal survival (Abudara et al., 2018). Brocardo et al. review how glial connexins and pannexins are remodeled in different pathological conditions with variable outcomes in the context of a neurodegenerative disease.

The established role of glial cells in many neurological and neuropsychiatric disorders has boosted new glial-targeted therapies, however the unavailability of validated biomarkers to assess and monitor gliosis *in vivo* has limited their clinical application (Garden and Campbell, 2016). Cavaliere et al. present a comprehensive overview on molecular neuroimaging, using positron emission tomography (PET) and magnetic resonance imaging (MRI) and offer a wide panel of non- or minimally invasive techniques to image glial targets.

Altogether, this Research Topic has provided an update on recent developments in glial biology, with many translational insights for a wider understanding of the neural mechanisms in health and disease.

AUTHOR CONTRIBUTIONS

All authors contributed in writing the editorial and organizing the research topic.

FUNDING

This work was supported by grants from the Italian Minister of Research and University (PRIN2017-2017XJ38A4_003 to GC).

REFERENCES

Abudara, V., Retamal, M. A., Del Rio, R., and Orellana, J. A. (2018). Synaptic functions of hemichannels and pannexons: a double-edged sword. *Front. Mol. Neurosci.* 11:435. doi: 10.3389/fnmol.2018.00435

Araque, A., Carmignoto, G., Haydon, P. G., Oliet, S. H. R., Robitaille, R., and Volterra, A. (2014). Gliotransmitters travel in time and space. *Neuron* 81, 728–739. doi: 10.1016/j.neuron.2014.02.007

Blockus, H., and Chédotal, A. (2016). Slit-Robo signaling. *Development* 143, 3037–3044. doi: 10.1242/dev.132829

Braun, M., Vaibhav, K., Saad, N. M., Fatima, S., Vender, J. R., Baban, B., et al. (2017). White matter damage after traumatic brain injury: a role for damage associated molecular patterns. *Biochim. Biophys. Acta - Mol. Basis Dis.* 1863, 2614–2626. doi: 10.1016/j.bbadis.2017.05.020

Bronzuoli, M. R., Facchinetti, R., Ingrassia, D., Sarvadio, M., Schiavi, S., Steardo, L., et al. (2018). Neuroglia in the autistic brain: evidence from a preclinical model. *Mol. Autism* 9:66. doi: 10.1186/s13229-018-0254-0

Cragnolini, A., Lampitella, G., Virtuoso, A., Viscovo, I., Panetsos, F., Papa, M., et al. (2020). Regional brain susceptibility to neurodegeneration: what is the role of glial cells? *Neural Regen. Res.* 15, 838–842. doi: 10.4103/1673-5374.268897

Cragnolini, A. B., Montenegro, G., Friedman, W. J., and Mascó, D. H. (2018). Brain-region specific responses of astrocytes to an *in vitro* injury and neurotrophins. *Mol. Cell. Neurosci.* 88, 240–248. doi: 10.1016/j.mcn.2018.02.007

Egea, J., Buendia, I., Parada, E., Navarro, E., León, R., and Lopez, M. G. (2015). Anti-inflammatory role of microglial alpha7 nAChRs and its role in neuroprotection. *Biochem. Pharmacol.* 97, 463–472. doi: 10.1016/j.bcp.2015.07.032

Garden, G. A., and Campbell, B. M. (2016). Glial biomarkers in human central nervous system disease. *Glia* 64, 1755–1771. doi: 10.1002/glia.22998

Hanani, M. (2005). Satellite glial cells in sensory ganglia: from form to function. *Brain Res. Rev.* 48, 457–476. doi: 10.1016/j.brainresrev.2004.09.001

Kim, S. Y., Kang, K. L., Lee, J.-C., and Heo, J. S. (2012). Nicotinic acetylcholine receptor α7 and β4 subunits contribute nicotine-induced apoptosis in periodontal ligament stem cells. *Mol. Cells* 33, 343–350. doi: 10.1007/s10059-012-2172-x

Leslie, M. (2017). The post-op brain. *Science* 356, 898–900. doi: 10.1126/science.356.6341.898

Liu, G., Zhang, W., Guo, J., Kong, F., Zhou, S., Chen, S., et al. (2018a). Adenosine binds predominantly to adenosine receptor A1 subtype in astrocytes and mediates an immunosuppressive effect. *Brain Res.* 1700, 47–55. doi: 10.1016/j.brainres.2018.06.021

Liu, J., Harkin, J., Maguire, L. P., McDaid, L. J., and Wade, J. J. (2018b). SPANNER: a self-repairing spiking neural network hardware architecture. *IEEE Trans. Neural Networks Learn. Syst.* 29, 1287–1300. doi: 10.1109/TNNLS.2017.2673021

Liu, X., Gangoso, E., Yi, C., Jeanson, T., Kandelman, S., Mantz, J., et al. (2016). General anesthetics have differential inhibitory effects on gap junction channels and hemichannels in astrocytes and neurons. *Glia* 64, 524–536. doi: 10.1002/glia.22946

Liu, Y., Zeng, X., Hui, Y., Zhu, C., Wu, J., Taylor, D. H., et al. (2015). Activation of α7 nicotinic acetylcholine receptors protects astrocytes against oxidative stress-induced apoptosis: implications for Parkinson's disease. *Neuropharmacology* 91, 87–96. doi: 10.1016/j.neuropharm.2014.11.028

Maggio, N., Cavaliere, C., Papa, M., Blatt, I., Chapman, J., and Segal, M. (2013). Thrombin regulation of synaptic transmission: Implications for seizure onset. *Neurobiol. Dis.* 50, 171–178. doi: 10.1016/j.nbd.2012.10.017

Melancia, F., Schiavi, S., Servadio, M., Cartocci, V., Campolongo, P., Palmery, M., et al. (2018). Sex-specific autistic endophenotypes induced by prenatal exposure to valproic acid involve anandamide signalling. *Br. J. Pharmacol.* 175, 3699–3712. doi: 10.1111/bph.14435

Papa, M., De Luca, C., Petta, F., Alberghina, L., and Cirillo, G. (2014). Astrocyte-neuron interplay in maladaptive plasticity. *Neurosci. Biobehav. Rev.* 42, 35–54. doi: 10.1016/j.neubiorev.2014.01.010

Perea, G., Gómez, R., Mederos, S., Covelo, A., Ballesteros, J. J., Schlosser, L., et al. (2016). Activity-dependent switch of gabaergic inhibition into glutamatergic excitation in astrocyte-neuron networks. *Elife* 5:e20362. doi: 10.7554/eLife.20362.016

Quik, M., Zhang, D., McGregor, M., and Bordia, T. (2015). Alpha7 nicotinic receptors as therapeutic targets for Parkinson's disease. *Biochem. Pharmacol.* 97, 399–407. doi: 10.1016/j.bcp.2015.06.014

Rossi, A., Murta, V., Auzmendi, J., and Ramos, A. (2017). Early gabapentin treatment during the latency period increases convulsive threshold, reduces microglial activation and macrophage infiltration in the lithium-pilocarpine model of epilepsy. *Pharmaceuticals* 10:93. doi: 10.3390/ph10040093

Rossi, A. R., Angelo, M. F., Villarreal, A., Lukin, J., and Ramos, A. J. (2013). Gabapentin administration reduces reactive gliosis and neurodegeneration after pilocarpine-induced status epilepticus. *PLoS ONE* 8:e78516. doi: 10.1371/journal.pone.0078516

Skvarc, D. R., Berk, M., Byrne, L. K., Dean, O. M., Dodd, S., Lewis, M., et al. (2018). Post-operative cognitive dysfunction: an exploration of the inflammatory hypothesis and novel therapies. *Neurosci. Biobehav. Rev.* 84, 116–133. doi: 10.1016/j.neubiorev.2017.11.011

Song, I., and Dityatev, A. (2018). Crosstalk between glia, extracellular matrix and neurons. *Brain Res. Bull.* 136, 101–108. doi: 10.1016/j.brainresbull.2017.03.003

Thrane, A. S., Rangroo Thrane, V., Zeppenfeld, D., Lou, N., Xu, Q., Nagelhus, E. A., et al. (2012). General anesthesia selectively disrupts astrocyte calcium signaling in the awake mouse cortex. *Proc. Natl. Acad. Sci. U.S.A.* 109, 18974–18979. doi: 10.1073/pnas.1209448109

Volterra, A., and Meldolesi, J. (2005). Astrocytes, from brain glue to communication elements: the revolution continues. *Nat. Rev. Neurosci.* 6, 626–640. doi: 10.1038/nrn1722

Wingerchuk, D. M., Banwell, B., Bennett, J. L., Cabre, P., Carroll, W., Chitnis, T., et al. (2015). International consensus diagnostic criteria for neuromyelitis optica spectrum disorders. *Neurology* 85, 177–189. doi: 10.1212/WNL.0000000000001729

Xu, S., Yang, B., Tao, T., Zhang, J., Liu, Y., Hu, J., et al. (2019). Activation of α7-nAChRs protects SH-SY5Y cells from 1-methyl-4-phenylpyridinium-induced apoptotic cell death via ERK/p53 signaling pathway. *J. Cell. Physiol.* 234, 18480–18491. doi: 10.1002/jcp.28484

Yang, X., Ransom, B. R., and Ma, J.-F. (2016). The role of AQP4 in neuromyelitis optica: More answers, more questions. *J. Neuroimmunol.* 298, 63–70. doi: 10.1016/j.jneuroim.2016.06.002

Zekeridou, A., and Lennon, V. A. (2015). Aquaporin-4 autoimmunity. *Neurol. - Neuroimmunol. Neuroinflammation* 2:e110. doi: 10.1212/NXI.0000000000000110

Conflict of Interest: The authors declare that the research was conducted in the absence of any commercial or financial relationships that could be construed as a potential conflict of interest.

frontiers in Cellular Neuroscience

HYPOTHESIS AND THEORY
published: 21 February 2019
doi: 10.3389/fncel.2019.00073

The Potential Role of the NLRP3 Inflammasome Activation as a Link Between Mitochondria ROS Generation and Neuroinflammation in Postoperative Cognitive Dysfunction

Penghui Wei[1], *Fan Yang*[1,2], *Qiang Zheng*[1], *Wenxi Tang*[1] *and Jianjun Li*[1]*

[1]*Department of Anesthesiology, Qilu Hospital of Shandong University, Qingdao, China,* [2]*Department of Anesthesiology, Cheeloo College of Medicine, Shandong University, Jinan, China*

Postoperative cognitive dysfunction (POCD) is commonly observed in perioperative care following major surgery and general anesthesia in elderly individuals. No preventive or interventional agents have been established so far. Although the role of interleukin-1β (IL-1β)-mediated neuroinflammation following surgery and anesthesia is strongly implicated in POCD, the exact mechanism of action remains to be explored. Growing evidence has shown that mitochondria-derived reactive oxygen species (mtROS) are closely linked to IL-1β expression through a redox sensor known as the nod-like receptor pyrin domain-containing 3 (NLRP3) inflammasome. Therefore, we hypothesize that the mechanisms underlying POCD involve the mtROS/NLRP3 inflammasome/IL-1β signaling pathway. Furthermore, we speculate that cholinergic anti-inflammatory pathway induced by α7 nicotinic acetylcholine receptor (a7nAChR) may be the potential upstream of mtROS/NLRP3 inflammasome/IL-1β signaling pathway in POCD. For validating the hypotheses, we provide experimental plan involving different paradigms namely; microglial cells and behavioral studies. The link between mtROS, the NLRP3 inflammasome, and IL-1β within and between these different stages in combination with mtROS and NLRP3 inflammasome agonists and inhibitors could be explored using techniques, such as knockout mice, small interference ribonucleic acid, flow cytometry, co-immunoprecipitation, and the Morris Water Maze test. We conclude that the NLRP3 inflammasome is a new preventive and therapeutic target for POCD.

Keywords: postoperative cognitive dysfunction, NLRP3 inflammasome, mitochondria-derived reactive oxygen species, Interleukin-1β, neuroinflammation, microglia, hippocampus

OPEN ACCESS

Edited by:
Giovanni Cirillo,
Second University of Naples, Italy

Reviewed by:
Hermona Soreq,
Hebrew University of Jerusalem, Israel
Dennis Qing Wang,
Zhujiang Hospital, Southern Medical University, China
Carlo Cavaliere,
IRCCS SDN, Italy

***Correspondence:**
Jianjun Li
ljj9573@163.com

Received: *07 December 2018*
Accepted: *13 February 2019*
Published: *21 February 2019*

Citation:
Wei P, Yang F, Zheng Q, Tang W and Li J (2019) The Potential Role of the NLRP3 Inflammasome Activation as a Link Between Mitochondria ROS Generation and Neuroinflammation in Postoperative Cognitive Dysfunction. Front. Cell. Neurosci. 13:73. doi: 10.3389/fncel.2019.00073

INTRODUCTION

Postoperative cognitive dysfunction (POCD) is a highly prevalent condition with significant effects on the prognosis of elderly patients undergoing surgery, experiencing problems with memory, concentration, information processing, language comprehension, and social integration that can last for months or may even be permanent (Leslie, 2017). POCD reportedly

occurs in 25% to 40% of elderly patients undergoing cardiac surgery, non-cardiac surgery, and even minor non-invasive procedures under sedation, such as coronary angiography, across different studies (Evered et al., 2011). The potential risk factors of POCD include advanced age, lower education levels, carrying the APOE4 genotype, alcohol abuse and premedication (Skvarc et al., 2018; Xie et al., 2018). Of note, preoperative treatment with anticholinergic medications (e.g., atropine and scopolamine) or medications with anticholinergic properties (e.g., tricyclic antidepressants and benzodiazepines) have been demonstrated to be associated with increasing risk of POCD in recent years (Wang et al., 2014). Shoair et al. (2015) conducted a subgroup analysis of 69 patients aged 65 years or older, and they found that the incidence of POCD in the patients receiving anticholinergic or sedative-hypnotic drug at home prior to surgery was three times greater than patients without these drug (users 28% vs. nonusers 9.1%). A large longitudinal follow up of patients who had POCD 1 week or 3 months following surgery showed significantly higher mortality [hazard ratio, 1.63 (95% confidence interval, 1.11–2.38); P = 0.01, adjusted for sex, age, and cancer] and risk of leaving the labor market prematurely [hazard ratio, 2.26 (1.24–4.12); P = 0.01], and greater dependency on social security [prevalence ratio, 1.45 (1.03–2.04); P = 0.03] (Steinmetz et al., 2009). As the aging population requiring more surgeries is increasing, POCD is expected to become epidemic.

Inflammation and immune activation are the key mechanism of POCD. Surgery and anesthesia unleash a body-wide inflammation in the elderly, and then peripheral inflammatory cytokines can compromise the integrity of the blood brain barrier (BBB), allowing for increased infiltration of inflammatory factors and macrophages into brain (Terrando et al., 2011; Leslie, 2017). Although current theories regarding the mechanisms underlying POCD highlight the role of neuroinflammation in the hippocampus (Skvarc et al., 2018), the exact cascade remains elusive. interleukin (IL)-1β-mediated neuroinflammation in the hippocampus plays a pivotal role in surgery-induced cognitive dysfunction; both in mice pretreated with IL-1 receptor antagonist and knocked out IL-1 receptor (IL-1R$^{-/-}$), the cognitive impairment induced by surgical trauma was effectively attenuated (Cibelli et al., 2010). Our previous study has also confirmed the critical role of hippocampal IL-1β in the development of POCD (Li et al., 2014; Wei et al., 2018). However, the mechanism by which surgical stress and anesthesia induce production of IL-1β in association with POCD remains unknown.

The nod-like receptor pyrin domain-containing 3 (NLRP3) inflammasome, composed of NLRP3 protein, adapter protein apoptosis-associated speck-like protein (ASC), and pro-caspase-1, is a pivotal upstream target that controls IL-1β cleavage and secretion by the active caspase-1 (Schroder and Tschopp, 2010). Recent studies have revealed that isoflurane-induced cognitive impairment was associated with high levels of NLRP3 in the hippocampus of aged mice and the impairment was reversed by the inhibition of NLRP3-caspase-1 pathway (Wang et al., 2018). Studies have also reported that inhibitors of the NLRP3 inflammasome [e.g., MCC950 and ketone metabolite β-hydroxybutyrate (BHB)] inhibited NLRP3-induced ASC oligomerization and IL-1β expression in systemic macrophages and brain mononuclear cells (Coll et al., 2015; Youm et al., 2015). A recent study demonstrated that MCC950 improved cognitive function in Alzheimer's disease (AD) by clearance of amyloid β $(Aβ)_{1–40}$ and $Aβ_{1–42}$ in apolipoprotein (APP)/presenilin 1 (PS1) mice. The study further showed that the impact of MCC950 on Aβ pathology resulted from its ability to block NLRP3 inflammasome activation in microglia (Dempsey et al., 2017). Therefore, the NLRP3 inflammasome may be a viable target to interrupt the pathogenesis of POCD. Furthermore, exposure to anesthetics may impair mitochondria and potentiate oxidative damage to neurons (Skvarc et al., 2018). The mitochondria are potent activators of the immune system through their ability to generate reactive oxygen species (ROS), which damage the mitochondrial DNA (mtDNA) and interact with the NLRP3 inflammasome during the inflammatory response (Kim et al., 2015; Liu K. et al., 2017). Evidence supported the critical role of mitochondrial ROS (mtROS) in NLRP3 inflammasome activation (Zhou et al., 2011). Zhou et al. (2011) showed that ROS generated by mitochondria having reduced membrane potential could lead to NLRP3 inflammasome activation and addition of the complex I inhibitor (rotenone) resulted in the loss of ROS generation and inflammasome activation. Moreover, a specific mitochondria ROS scavenger, the mito-TEMPO (500 μM), abrogated mtROS release, inhibited NLRP3 inflammasome activation and reduced the up-regulation of IL-1β and IL-18 induced by ethanol or lipopolysaccharide (LPS)/ATP (Alfonso-Loeches et al., 2014). Therefore, we speculate that mtROS/NLRP3 inflammasome-induced IL-1β activation in the hippocampus may play a critical role in the development of POCD, and this signaling pathway may consequently become an attractive drug target.

THE HYPOTHESIS

The hypothesis we present here is that mtROS-induced NLRP3 activation may be a pivotal upstream mechanism that controls microglial IL-1β cleavage and secretion, and subsequent IL-1β-mediated inflammatory cascades in the hippocampus. Therefore, the mtROS/NLRP3 inflammasome/IL-1β signaling pathway may be a new drug target for attenuating POCD (**Figure 1**).

EVALUATION OF THE HYPOTHESIS

IL-1β-Mediated Neuroinflammation Following Surgery and POCD

The activation of microglia induced by surgery and the resulting exacerbated inflammatory response in the hippocampus have been associated with impaired cognitive function (Hovens et al., 2014). Tissue damage following surgery engages the immune system and produces a wide range of inflammatory cytokines and macrophages in the serum

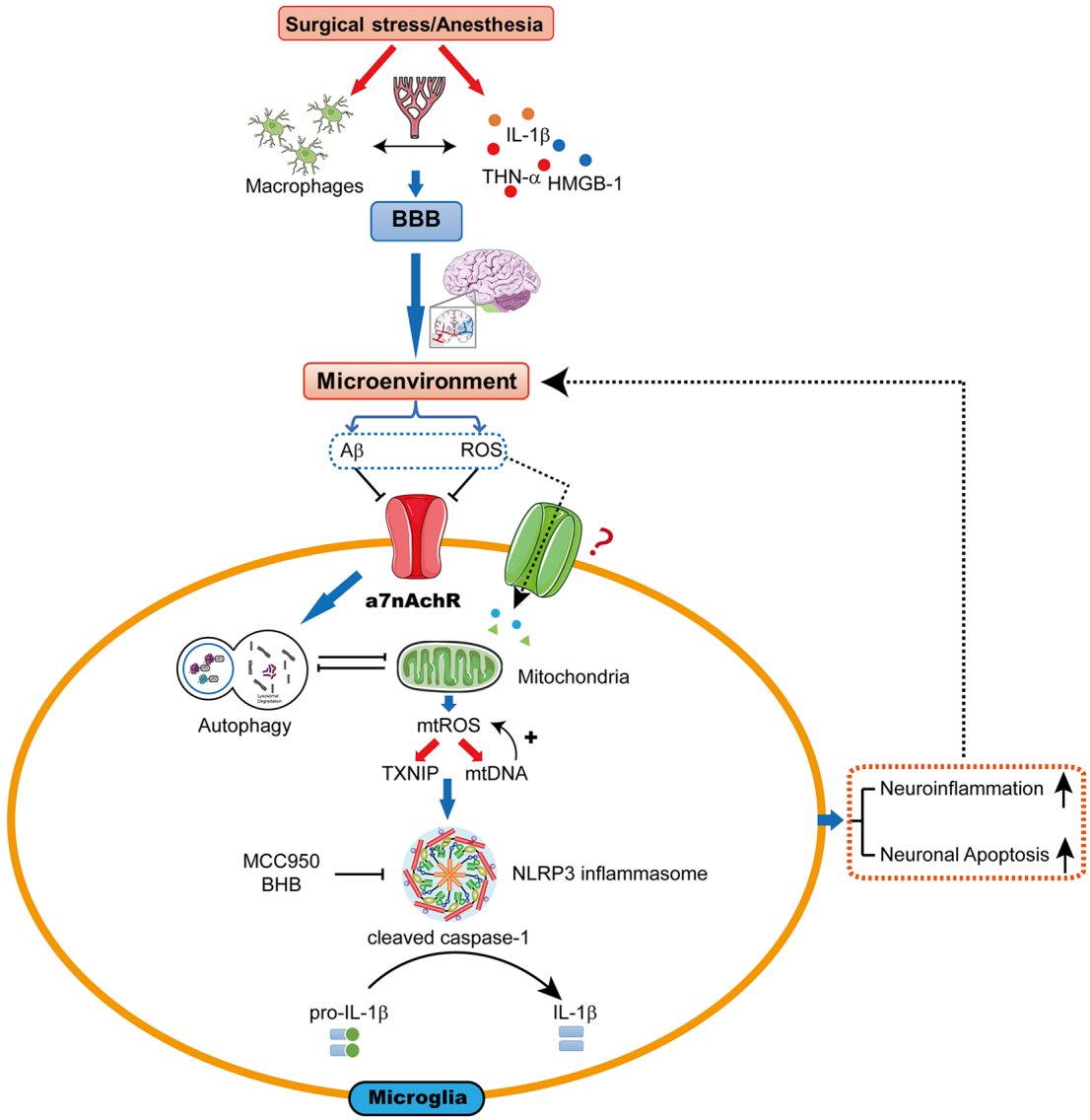

FIGURE 1 | The proposed biological mechanisms for microglia mitochondrial reactive oxygen species (mtROS)/nod-like receptor pyrin domain-containing 3 (NLRP3) inflammasome-induced interleukin-1β (IL-1β) activation in the hippocampus leading to cognitive dysfunction following surgery and anesthesia. Surgical stress and anesthesia, through mechanisms that include inhibition of α7 nicotinic acetylcholine receptor (α7nAChR)-induced cholinergic anti-inflammatory pathway and autophagy, result in mitochondrial damage. The damaged mitochondria overproduce the superoxide anion, which escape the mitochondria to undergo a series of reactions to form mtROS. mtROS overproduction is sensed by TRX-interaction protein (TXNIP) or mitochondrial DNA (mtDNA), which bind to the leucine-rich repeat region of NLRP3 and lead to NLRP3 inflammasome activation. Consequently, the microglia is activated, which further promotes neuroinflammation and induces neuronal apoptosis, contributing to cognitive dysfunction.

(Terrando et al., 2010, 2011). These cytokines, including IL-1β, IL-6, and high mobility group box-1 (HMGB-1), inhibit Wnt/β-catenin/Annexin A1 signaling pathway and disrupt the BBB integrity, which facilitates the migration of macrophages into areas of the brain, in particular, but not restricted to the hippocampus (Hu et al., 2016; Fan et al., 2018). Additionally, surgical stress and anesthetics promote deposition of oligomeric tau and Aβ paralleled by increased levels of ROS in cerebral microvasculature, which disrupts BBB integrity and shifts the balance of neuroimmune microenvironment toward proinflammatory milieu (Arora et al., 2015; Castillo-Carranza et al., 2017; Zou et al., 2018). Subsequently, the inhibition of anti-inflammatory receptors (e.g., nicotinic acetylcholine receptors; Liu P.-R. et al., 2017) and activation of pro-inflammatory receptors [e.g., toll-like receptor 4 (TLR 4)] trigger a cascade of downstream signaling events (Terrando et al., 2010). Consequently, microglia in the hippocampus is activated, which further promotes neuroinflammation and induces neuronal apoptosis, contributing to cognitive dysfunction (Terrando et al., 2011).

POCD involves a wide range of cognitive impairment and multiple brain regions are involved in cognitive processes of POCD, such as hippocampus, prefrontal cortex, striatum and amygdala (Hovens et al., 2015). However, the role of the hippocampus in many of the processes is particularly well established (Skvarc et al., 2018). Since inflammatory cytokine receptors are highly concentrated in areas associated with learning and memory (Parnet et al., 2002), particularly in the regions of the hippocampus, surgery-induced neuroinflammation in the brain may primarily disrupt hippocampus-dependent learning and memory (Zhang et al., 2016). The hippocampus arguably contains the largest number of receptors for IL-1β and is implicated in optimal memory and learning processes (Gemma et al., 2005). This region of the brain is also sensitive to the insults of aging (Huang et al., 2008) and excessive levels of IL-1β are associated with cognitive disorders in aging animal models (Barrientos et al., 2006; Chen et al., 2008). Therefore, we focused on the hippocampus in our hypothesis.

The hippocampal-dependent memory impairment was associated with IL-1β increase in the hippocampal structure of aged rats, while young rats did not present any exacerbated response to surgery and anesthesia (Barrientos et al., 2012). Hippocampal IL-1β-mediated neuroinflammation plays a pivotal role in surgery-induced cognitive impairment in aged rats (Goshen et al., 2007). A recent animal study reported that surgery induced significant morphological changes of microglial reactivity paralleled by elevations of IL-1β at 24 h and day 3 compared to naive and animals treated only with anesthesia, which showed that microglial reactivity after surgery may be the cause of increase in the levels of IL-1β in the hippocampus (Cibelli et al., 2010). Upon peripheral macrophage and resident microglia activation in the hippocampus, IL-1β is activated to enhance expression and release, triggering a cascade of downstream signaling events (Hovens et al., 2014; Skvarc et al., 2018). Elevated levels of IL-1β induce the subsequent production of IL-6 and HMGB-1, which further drive IL-1β expression, in a feed-forward mechanism promoting further activation of inflammatory signaling pathways (Lee et al., 2014). These cytokines have been described to result in impairment of hippocampal long-term potentiation, neuronal activity, and synaptic plasticity through modulation of glutamate receptors and inhibition of glutamate release in rats (Yirmiya and Goshen, 2011; Riazi et al., 2015).

The specificity of IL-1β involvement has been revealed by previous studies. A study conducted showed that a single intracisternal administration of IL-1 receptor antagonist (hIL-1RA; 112 μg) at the time of surgery was sufficient to block both the behavioral deficit and the neuroinflammatory response in the hippocampus of aged rats 4 day after surgery (Barrientos et al., 2012). Cibelli et al. (2010) further highlighted the importance of IL-1β expression in the neuroinflammatory effect of surgery and cognitive impairment. The results showed that reactive microgliosis in the hippocampus was no longer triggered following surgery in mice lacking the IL-1 receptor. These data reinforce the hypothesis that increased IL-1β levels in the hippocampus are likely to play a prominent role in the pathogenesis of POCD.

NLRP3 Inflammasome Activation by mtROS in the Hippocampus and POCD

Evidence supports that IL-1β cleavage and secretion are primarily dependent on activation of the inflammasome, a multiprotein complex localized in the cytoplasm (Dempsey et al., 2017). Numerous inflammasomes, including NLRP1, NLRP3, and NLRC4, have been reported to exhibit inflammasome activity in several diseases (Schroder and Tschopp, 2010). Each NLR forms its own inflammasome and the NLRP3 inflammasome is only described as a central component in the production of IL-1β among them (Lamkanfi and Dixit, 2014). The NLRP3 inflammasome is a pattern recognition receptor and its activation depends on exposure to immune activators such as pathogen-associated molecular patterns, danger-associated molecular patterns, and environmental irritants (Shao et al., 2015). Immune activators cause a conformational change in NLRP3, which allows an interaction between the pyrin domains in NLRP3 and ASC (Cordero et al., 2018; Place and Kanneganti, 2018). Subsequently, ASC recruits pro-caspase-1 through its caspase recruitment domain, causing the activation of the NLRP3 inflammasome. The activated NLRP3 inflammasome triggers pro-caspase-1 self-cleavage and this complex releases cleaved caspase-1 into the cytosol, which induces the conversion of IL-1β from its immature "pro" forms to an active form, which is secreted (Willingham et al., 2009; Shao et al., 2015).

A non-canonical pathway downstream of caspase-1 is also involved in NLRP3-dependent IL-1β processing (Lamkanfi and Dixit, 2014). However, compared to the non-canonical pathway, canonical NLRP3 inflammasome controls systemic low grade age-related sterile inflammation in both periphery and the brain (Youm et al., 2013). Emerging evidence suggests that canonical NLRP3 inflammasome activation is linked to inflammation-mediated cognitive decline and neuropathological changes with aging. Reduction of canonical NLRP3 inflammasome-induced inflammation prevents aged-related cognitive dysfunction (Goldberg and Dixit, 2015; Wang et al., 2018). Studies on microglia and animal models have revealed an important role for the canonical NLRP3 inflammasome in AD pathogenesis (Heneka et al., 2013; Dempsey et al., 2017). Activation of the NLRP3 inflammasome contributes to Aβ accumulation, synaptic dysfunction, and cognitive impairment in APP/PS1 mice, suggesting that blocking the assembly of the inflammasome may constitute a novel therapeutic intervention for attenuating changes that negatively affect neuronal function in AD (Dempsey et al., 2017). Furthermore, preliminary experimental findings have suggested that NLRP3 inflammasome activation was linked to cognitive impairment after isoflurane anesthesia and isoflurane exposure induced the upregulation of NLRP3 and subsequently increased the level of IL-1β in the hippocampus of aged mice (Li et al., 2014; Wang et al., 2018). Despite a shortage of literature on sources of IL-1β in the pathophysiological mechanism of POCD, existing evidence shows that isoflurane-induced IL-1β overproduction in the hippocampus can be partially attenuated but not be repressed completely by an inhibitor of NLRP3-caspase-1 (Wang et al., 2018). Therefore, we hypothesize that canonical NLRP3 inflammasome/IL-1β

axis is likely is implicated in postoperative inflammatory mediators-induced cognitive impairment.

Several theories have been proposed to explain the cellular signal responsible for activation of the NLRP3 inflammasome including cytosolic K^+ efflux, the production of ROS, and the release of mtDNA and ROS (Lamkanfi and Dixit, 2014). The importance of K^+ efflux in NLRP3 activation is supported by the fact that NLRP3 activators, such as ATP, nigericin and pore-forming toxins, result in lower intracellular concentration of K^+, and a higher extracellular concentration of K^+ inhibits activation of the NLRP3 inflammasome (He et al., 2016). The involvement of K^+ efflux in NLRP3 inflammasome activation has been further suggested by a typical study showing that the drop in intracellular K^+ concentration is the common step that is necessary and sufficient to engage the NLRP3 inflammasome activation (Munoz-Planillo et al., 2013). However, the mechanistic link between K^+ efflux-induced NLRP3 activation and inflammation-mediated cognitive dysfunction remains poorly understood.

Alternative models for NLRP3 activation involve ROS production. Recent evidence suggests that ROS are positively correlated with cognitive impairment after surgery (Qiu et al., 2016b). ROS overproduction is an important upstream event that can activate NLRP3 inflammation and amplify the production of IL-1β (Qiu et al., 2016a). The source of ROS is currently unclear. The most studied ROS include nicotinamide adenine dinucleotide phosphate oxidase and mtROS (Circu and Aw, 2010), but mitochondria are considered to be the major source of intracellular ROS (Qiu et al., 2016b). Mitochondrial damage is a key mechanism of neurodegenerative disorders (Gao et al., 2017; Liu K. et al., 2017). Evidence from cellular and animal models indicates that exposure to anesthetics or surgical stress induces deficiencies in mitochondrial respiratory chain components and mtDNA mutations which could result in membrane potential loss and the opening of the mitochondrial permeability transition pore, causing increased leakage of electrons (Zhang et al., 2012; Li et al., 2017). Leaked electrons react with molecular oxygen to produce the superoxide anion, which escape the mitochondria to undergo a series of reactions to form mtROS (Kim et al., 2015). Iron-dependent mtROS is also tightly associated with neurodegenerative diseases (Gao et al., 2017). Increased iron accumulation and oxidative stress in the brain, especially in the hippocampus, may be involved in the pathogenesis of POCD (An et al., 2013). mtROS leads to accumulation of mtDNA mutations, increased superoxide production, and a vicious cycle of oxidative stress, which further accelerates mtDNA mutagenesis and damages mitochondrial function (Xu et al., 2017). Although the role of mtROS in NLRP3 activation is a topic of longstanding controversy, mounting studies have suggested that mtROS production may be linked to NLRP3 inflammasome activation (Schroder and Tschopp, 2010; Choi and Ryter, 2014; Shao et al., 2015; He et al., 2016). A study conducted by Wu et al. (2015) also showed that mtROS blockade by mitochondrion-targeted antioxidant SS-31 suppressed NLRP3 inflammasome activation and alleviated isoflurane-induced cognitive deficits 24 h after anesthesia. Since ROS are short-lived and act as a messenger only for a short distance, NLRP3 is thought to be localized in close proximity to mitochondria, which allows efficient sensing of the presence of ROS produced in the same cell by malfunctioning mitochondria (Zhou et al., 2011). Mechanisms directing mtROS-dependent NLRP3 inflammasome activation have been characterized in detail (Zhou et al., 2011; Alfonso-Loeches et al., 2014; Minutoli et al., 2016). mtROS overproduction is sensed by a complex of thioredoxin (TRX) and TRX-interaction protein (TXNIP) that induce the dissociation of the complex. Subsequently, TXNIP binds to the leucine-rich repeat region of NLRP3, leading to NLRP3 inflammasome activation (Minutoli et al., 2016). Another potential mechanism of mtROS and NLRP3 inflammasome activation is the release of mt DNA. mtDNA preceding mtROS production, escape from the mitochondria to the cytoplasm *via* mitochondrial membrane permeability transition pores and mtDNA directly binds and activates the NLRP3 inflammasome (Kim et al., 2015). While the exact pathway by which mtROS mediates NLRP3 inflammasome activation and assembly remains elusive, these existing findings suggest that mitochondrial dysfunction and mtROS overexpression may at least be partly responsible for expression of cytokines *via* NLRP3 inflammasome activation in POCD.

The Cholinergic Modulation of mtROS/NLRP3 Inflammasome/IL-1β Signaling Pathway

Cholinergic transmission plays a key role in cognitive function. A cerebral cholinergic deficit has been demonstrated to be implicated in age-related cognitive impairment (Rossi et al., 2014). Activation of the cholinergic anti-inflammatory pathway suppresses excessive neuroinflammation in neurodegenerative diseases, such as POCD, AD, multiple sclerosis and Parkinson's disease (Taly et al., 2009; Leslie, 2017). The α7 nicotinic acetylcholine receptor (α7nAChR) is identified as an essential mediator of cholinergic anti-inflammatory pathway (Pavlov and Tracey, 2017). The dysfunctional activity of α7nAchR in the hippocampus in response to surgical stress and anesthesia is now considered to be the critical event in the development of neuroinflammation in aged POCD rats (Liu P.-R. et al., 2017). Recently, we and other research groups have reported that α7nAChR agonists resolved IL-1β-mediated neuroinflammation and reversed cognitive decline after surgery in animal studies (Chen et al., 2018; Wei et al., 2018). Therefore, we speculate that cholinergic deficit induces neuroinflammation in POCD and α7nAChR may be the potential upstream of mtROS/NLRP3 inflammasome/IL-1β signaling pathway in microglia.

Activation of α7nAChR suppresses the NLRP3 inflammasome, but the nature of this suppression is unclear (Hecker et al., 2015; Ke et al., 2017). One potential mechanism involves the autophagic removal of mtROS production. Autophagy is a cellular quality-control system which removes unnecessary or damaged proteins and organelles *via* the lysosomal apparatus (Zhang et al., 2018). Autophagy has been demonstrated to regulate inflammation and immune responses in the Central Nervous System, especially in inflammatory cells such as microglia and astrocyte (De Luca et al., 2018). Deficient autophagy impairs mitochondrial integrity and

promotes generation of mtROS, consequently contributing to activation of inflammasome (Razani et al., 2012). Defects in autophagy, along with neuroinflammation, have been implicated in the pathogenesis of postoperative cognitive decline (von Haefen et al., 2018). Additionally, evidence has shown that activating α7nAChR enhances microglial autophagy, which suppresses neuroinflammation and thus plays an alleviative role in neurodegenerative disorders (Jeong and Park, 2015; Shao et al., 2017). Collectively, these findings support the hypothesis that autophagy deficiency induced by dysfunctional α7nAChR promotes POCD *via* the activation of mtROS/NLRP3 inflammasome/IL-1β signaling pathway in microglia.

Other Potential Signaling Pathways Involved in Modulating of Neuroinflammation in POCD

The mechanism initiating, controlling and modulating neuroinflammation in POCD are complex. The non-canonical inflammasomes/caspase-11 is also required for macrophages to secrete IL-1β (Lamkanfi and Dixit, 2014). The finding highlights the potential benefits of blocking the caspase-11 directly over inhibiting IL-1β expression and its downstream cytokines. Recent studies have identified additional signaling pathways that can regulate cytokine synthesis and release in the pathogenesis of POCD, such as TNF-α/TLR4 (Terrando et al., 2010), ATP/P2X7 (Zheng et al., 2017) and cannabinoid receptor type 2 (CB2R)-related signaling pathways (Sun et al., 2017). Additionally, certain key signaling pathways/molecules associated with the regulation of inflammation, such as AMPK, mTOR, Nur77, and miRNAs, have been demonstrated to play critical roles in chronic age-related diseases (Wei et al., 2016; Xu et al., 2017; Li et al., 2018; Zhang et al., 2018). However, the involvement of these signaling pathways/molecules in POCD remains to be explored.

IMPORTANT IMPLICATIONS OF THE HYPOTHESIS AND PROPOSED EXPERIMENTAL PLAN

Although numerous drugs with neuroprotective action during surgery and anesthesia have been studied, there is no agreement on the efficiency of prophylactic neuroprotectants in POCD. If our hypothesis is verified by future studies, the NLRP3 inflammasome will become a new drug target for attenuating POCD.

Several small molecules including MCC950 (Coll et al., 2015; Dempsey et al., 2017) and BHB (Youm et al., 2015) have been shown to specifically inhibit the NLRP3 inflammasome activation. Other types of NLRP3 inflammasome inhibitors, such as autophagy inducer (Resveratrol, arglabin and CB2R agonist), type I interferon (IFN) and IFN-β (Malhotra et al., 2015) and microRNA223, have also been reported (Shao et al., 2015), although these agents have limited potency and are non-specific. The most promising inhibitor of NLRP3 inflammasome activation was described in a groundbreaking report in *Nature Medicine* in 2015 (Coll et al., 2015). Coll et al. (2015) showed that MCC950 inhibited canonical and non-canonical NLRP3 activation at nanomolar concentrations in mouse bone marrow-derived macrophages (BMDMs) and the half-maximal inhibitory concentration of MCC950 was approximately 7.5 nM in BMDMs. The study further showed that MCC950 specifically inhibited NLRP3 inflammasome but not NLRP1 or NLRC4 activation. MCC950 has been demonstrated to present certain advantages over other inhibitors of the NLRP3 inflammasome. Compared to other inhibitors, MCC950 may have less immunosuppressive effects because it specifically targets NLRP3 and does not result in the complete blockade of IL-1β which is essential during infection and antimicrobial responses, especially for elderly and immunosuppressed populations (Lopez-Castejon and Pelegrin, 2012; Coll et al., 2015). As a small molecule, numerous studies have shown that MCC950 effectively traversed an impaired BBB and attenuated neuroinflammation-related diseases. Dempsey et al. (2017) showed that MCC950-treated APP/PS1 mice performed significantly better than control-treated APP/PS1 mice, and MCC950 promoted non-phlogistic clearance of $A\beta_{1-40}$ and $A\beta_{1-42}$ in APP/PS1 mice. They further showed that the impact of MCC950 on Aβ pathology resulted from its ability to block production of IL-1β while it promoted Aβ phagocytosis by microglia. MCC950 has also been demonstrated to reduce the neurological deficit score of 24 h after cerebral ischemia reperfusion and improved the 28-day survival rate of cerebral ischemia-reperfusion injury in diabetic mice (Hong et al., 2018). Another study has further revealed that MCC950 reduced neuroinflammation and improved the long-term neurological outcomes on the 3, 7, and 14 days after traumatic brain injury in a murine model and the therapeutic window for MCC950 against traumatic brain injury was as long as 6 h (Xu et al., 2018). BHB, produced in the liver, is another promising small molecule inhibitor of NLRP3 inflammasome. BHB serves as an alternative energy source for the brain, heart, and skeletal muscle in mammals during states of energy deficit (Newman and Verdin, 2014). Like MCC950, BHB specifically suppresses activation of the NLRP3 inflammasome, without affecting NLRC4, AIM2 or non-canonical caspase-11 inflammasome activation (Youm et al., 2015). However, their mechanisms differ in key aspects. Youm et al. (2015) discovered that BHB inhibited the NLRP3 inflammasome by preventing K^+ efflux and reducing ASC oligomerization and speck formation. Furthermore, a recent study has shown that BHB attenuated stress-induced behavioral as well as the elevation of IL-1β and TNF-α in the rodent hippocampus by inhibiting NLRP3 inflammasome activation (Yamanashi et al., 2017).

Literature pertaining to clinical trials associated with NLRP3 inflammasome and POCD is scarce. Thus, a basic hypothesis involving microglial cells, mice hippocampi and behavioral studies is provided here. Experimentally, it proposes the use of animal and cellular models of POCD to investigate the following: (i) NLRP3 inflammasome mediated IL-1β activation and hippocampus-dependent cognitive performance; (ii) mitochondrial oxidative stress and NLRP3 inflammasome

activation in the hippocampus and microglia; and (iii) mtROS and its regulatory effect on the NLRP3 inflammasome. To evaluate whether NLRP3 inflammasome mediated IL-1β activation is involved in POCD, NLRP3$^{-/-}$ or caspase-1$^{-/-}$ aged mice carrying mutations (e.g., C57/Bl6 background) and primary microglia prepared from neonatal mice are recommended in future studies (Heneka et al., 2013). Surgery is performed under general anesthesia and the primary microglia are preincubated with LPS and isoflurane (Wang et al., 2018). The Morris Water Maze test should be performed to evaluate the hippocampus-dependent spatial learning and memory, and the assembly and interaction of the complex consisting of NLRP3, ASC, and caspase-1 in microglia should be tested using a series of immunological and biochemical assays, such as small interference ribonucleic acid, immunohistochemistry, and co-immunoprecipitation (Dempsey et al., 2017; Wang et al., 2018). To understand whether mtROS and its regulatory effect on the NLRP3 inflammasome are involved in POCD, flow cytometry and confocal microscopy should be carried out in primary microglia or hippocampus after exposure to the inhibitors or enhancers of NLRP3 inflammasome (e.g., MCC950 and BHB) and mtROS (e.g., Rotenone and SS-31; Zhou et al., 2011).

Future clinical trials with MCC950 and BHB may contribute to the development of new anti-inflammatory therapies for neuroinflammation-associated diseases. Therefore, we hypothesize that the two small molecule inhibitors, especially MCC950, may be viable for the attenuation of patients with POCD in the future.

Additionally, α7nAChR and autophagy may be potential drug targets for attenuating POCD by directly regulating mtROS/NLRP3 inflammasome/IL-1β signaling pathway. Terrando et al. (2011) have highlighted the importance of α7nAChR in resolving the inflammatory pathogenesis of POCD. α7nAChR agonists prevent macrophage migration into the hippocampus and cognitive decline following surgery. A recent research has also shown that activated α7nAChR markedly improved cognitive impairment after cardiopulmonary bypass in rats (Chen et al., 2018). Pre-clinical evidence suggested that inducing autophagy was effective in protecting against several neurodegenerative diseases, though this is not a universal finding (Zou et al., 2017; Weng et al., 2018). Recently, it has been reported that enhancement of autophagy could ameliorate the pathogenesis of cognitive impairment in aged hippocampus after propofol anesthesia (Yang et al., 2017). Activating α7nAChR and inducing autophagy might also provide a potential therapeutic target for POCD.

CONCLUSIONS

In conclusion, mitochondrial dysfunction in POCD triggers mtROS generation and an mtROS-dependent pathway may be responsible for NLRP3 inflammasome complex formation in the hippocampus, which may be regulated by α7nAChR and autophagy. Subsequently, pro-caspase-1 clustering induces autoactivation and caspase-1-dependent maturation and secretion of IL-1β. IL-1β further drives neuroinflammation in a feed-forward mechanism, which promotes subsequent activation of inflammatory cytokines and eventually causes neuronal apoptosis (**Figure 1**). The mtROS/NLRP3 inflammasome/IL-1β signaling pathway may be a potential drug target for therapeutic intervention in POCD.

AUTHOR CONTRIBUTIONS

PW, FY, and JL wrote the draft. PW, QZ, and WT created the figure. JL secured the funds to support this project. All the authors read and approved the manuscript.

FUNDING

This work was supported by grants from the People's Benefit Project of Science and Technology in Qingdao (18-6-1-74-nsh) and the Scientific Research Foundation of Qilu Hospital of Shandong University (Qingdao; Grant Nos. QDKY2016QN01 and QDKY2016ZD05). The open access publication fees was supported by all these funds.

REFERENCES

Alfonso-Loeches, S., Urena-Peralta, J. R., Morillo-Bargues, M. J., Oliver-De La Cruz, J., and Guerri, C. (2014). Role of mitochondria ROS generation in ethanol-induced NLRP3 inflammasome activation and cell death in astroglial cells. *Front. Cell. Neurosci.* 8:216. doi: 10.3389/fncel.2014.00216

An, L. N., Yue, Y., Guo, W. Z., Miao, Y. L., Mi, W. D., Zhang, H., et al. (2013). Surgical trauma induces iron accumulation and oxidative stress in a rodent model of postoperative cognitive dysfunction. *Biol. Trace Elem. Res.* 151, 277–283. doi: 10.1007/s12011-012-9564-9

Arora, K., Cheng, J., and Nichols, R. A. (2015). Nicotinic acetylcholine receptors sensitize a MAPK-linked toxicity pathway on prolonged exposure to β-amyloid. *J. Biol. Chem.* 290, 21409–21420. doi: 10.1074/jbc.m114.634162

Barrientos, R. M., Hein, A. M., Frank, M. G., Watkins, L. R., and Maier, S. F. (2012). Intracisternal interleukin-1 receptor antagonist prevents postoperative cognitive decline and neuroinflammatory response in aged rats. *J. Neurosci.* 32, 14641–14648. doi: 10.1523/JNEUROSCI.2173-12.2012

Barrientos, R. M., Higgins, E. A., Biedenkapp, J. C., Sprunger, D. B., Wright-Hardesty, K. J., Watkins, L. R., et al. (2006). Peripheral infection and aging interact to impair hippocampal memory consolidation. *Neurobiol. Aging* 27, 723–732. doi: 10.1016/j.neurobiolaging.2005.03.010

Castillo-Carranza, D. L., Nilson, A. N., Van Skike, C. E., Jahrling, J. B., Patel, K., Garach, P., et al. (2017). Cerebral microvascular accumulation of tau oligomers in Alzheimer's disease and related tauopathies. *Aging Dis.* 8, 257–266. doi: 10.14336/AD.2017.0112

Chen, J., Buchanan, J. B., Sparkman, N. L., Godbout, J. P., Freund, G. G., and Johnson, R. W. (2008). Neuroinflammation and disruption in working memory in aged mice after acute stimulation of the peripheral innate immune system. *Brain Behav. Immun.* 22, 301–311. doi: 10.1016/j.bbi.2007.08.014

Chen, K., Sun, Y., Dong, W., Zhang, T., Zhou, N., Yu, W., et al. (2018). Activated alpha7nachr improves postoperative cognitive dysfunction and intestinal injury induced by cardiopulmonary bypass in rats: inhibition of the proinflammatory response through the th17 immune response. *Cell. Physiol. Biochem.* 46, 1175–1188. doi: 10.1159/000489068

Choi, A. J., and Ryter, S. W. (2014). Inflammasomes: molecular regulation and implications for metabolic and cognitive diseases. *Mol. Cells* 37, 441–448. doi: 10.14348/molcells.2014.0104

Cibelli, M., Fidalgo, A. R., Terrando, N., Ma, D., Monaco, C., Feldmann, M., et al. (2010). Role of interleukin-1beta in postoperative cognitive dysfunction. *Ann. Neurol.* 68, 360–368. doi: 10.1002/ana.22082

Circu, M. L., and Aw, T. Y. (2010). Reactive oxygen species, cellular redox systems and apoptosis. *Free Radic. Biol. Med.* 48, 749–762. doi: 10.1016/j.freeradbiomed.2009.12.022

Coll, R. C., Robertson, A. A., Chae, J. J., Higgins, S. C., Munoz-Planillo, R., Inserra, M. C., et al. (2015). A small-molecule inhibitor of the NLRP3 inflammasome for the treatment of inflammatory diseases. *Nat. Med.* 21, 248–255. doi: 10.1038/nm.3806

Cordero, M. D., Williams, M. R., and Ryffel, B. (2018). AMP-activated protein kinase regulation of the NLRP3 inflammasome during aging. *Trends Endocrinol. Metab.* 29, 8–17. doi: 10.1016/j.tem.2017.10.009

De Luca, C., Colangelo, A. M., Alberghina, L., and Papa, M. (2018). Neuro-immune hemostasis: homeostasis and diseases in the central nervous system. *Front. Cell. Neurosci.* 12:459. doi: 10.3389/fncel.2018.00459

Dempsey, C., Rubio Araiz, A., Bryson, K. J., Finucane, O., Larkin, C., Mills, E. L., et al. (2017). Inhibiting the NLRP3 inflammasome with MCC950 promotes non-phlogistic clearance of amyloid-beta and cognitive function in APP/PS1 mice. *Brain Behav. Immun.* 61, 306–316. doi: 10.1016/j.bbi.2016.12.014

Evered, L., Scott, D. A., Silbert, B., and Maruff, P. (2011). Postoperative cognitive dysfunction is independent of type of surgery and anesthetic. *Anesth. Analg.* 112, 1179–1185. doi: 10.1213/ANE.0b013e318215217e

Fan, J., An, X., Yang, Y., Xu, H., Fan, L., Deng, L., et al. (2018). MiR-1292 targets FZD4 to regulate senescence and osteogenic differentiation of stem cells in TE/SJ/Mesenchymal tissue system via the wnt/beta-catenin pathway. *Aging Dis.* 9, 1103–1121. doi: 10.14336/AD.2018.1110

Gao, G., Zhang, N., Wang, Y. Q., Wu, Q., Yu, P., Shi, Z. H., et al. (2017). Mitochondrial ferritin protects hydrogen peroxide-induced neuronal cell damage. *Aging Dis.* 8, 458–470. doi: 10.14336/ad.2016.1108

Gemma, C., Fister, M., Hudson, C., and Bickford, P. C. (2005). Improvement of memory for context by inhibition of caspase-1 in aged rats. *Eur. J. Neurosci.* 22, 1751–1756. doi: 10.1111/j.1460-9568.2005.04334.x

Goldberg, E. L., and Dixit, V. D. (2015). Drivers of age-related inflammation and strategies for healthspan extension. *Immunol. Rev.* 265, 63–74. doi: 10.1111/imr.12295

Goshen, I., Kreisel, T., Ounallah-Saad, H., Renbaum, P., Zalzstein, Y., Ben-Hur, T., et al. (2007). A dual role for interleukin-1 in hippocampal-dependent memory processes. *Psychoneuroendocrinology* 32, 1106–1115. doi: 10.1016/j.psyneuen.2007.09.004

He, Y., Hara, H., and Nunez, G. (2016). Mechanism and regulation of NLRP3 inflammasome activation. *Trends Biochem. Sci.* 41, 1012–1021. doi: 10.1016/j.tibs.2016.09.002

Hecker, A., Kullmar, M., Wilker, S., Richter, K., Zakrzewicz, A., Atanasova, S., et al. (2015). Phosphocholine-modified macromolecules and canonical nicotinic agonists inhibit ATP-induced IL-1beta release. *J. Immunol.* 195, 2325–2334. doi: 10.4049/jimmunol.1400974

Heneka, M. T., Kummer, M. P., Stutz, A., Delekate, A., Schwartz, S., Vieira-Saecker, A., et al. (2013). NLRP3 is activated in Alzheimer's disease and contributes to pathology in APP/PS1 mice. *Nature* 493, 674–678. doi: 10.1038/nature11729

Hong, P., Li, F. X., Gu, R. N., Fang, Y. Y., Lai, L. Y., Wang, Y. W., et al. (2018). Inhibition of NLRP3 inflammasome ameliorates cerebral ischemia-reperfusion injury in diabetic mice. *Neural Plast.* 2018:9163521. doi: 10.1155/2018/9163521

Hovens, I. B., Schoemaker, R. G., van der Zee, E. A., Absalom, A. R., Heineman, E., and van Leeuwen, B. L. (2014). Postoperative cognitive dysfunction: involvement of neuroinflammation and neuronal functioning. *Brain Behav. Immun.* 38, 202–210. doi: 10.1016/j.bbi.2014.02.002

Hovens, I. B., van Leeuwen, B. L., Nyakas, C., Heineman, E., van der Zee, E. A., and Schoemaker, R. G. (2015). Postoperative cognitive dysfunction and microglial activation in associated brain regions in old rats. *Neurobiol. Learn. Mem.* 118, 74–79. doi: 10.1016/j.nlm.2014.11.009

Hu, N., Wang, C., Zheng, Y., Ao, J., Zhang, C., Xie, K., et al. (2016). The role of the Wnt/beta-catenin-Annexin A1 pathway in the process of sevoflurane-induced cognitive dysfunction. *J. Neurochem.* 137, 240–252. doi: 10.1111/jnc.13569

Huang, Y., Henry, C. J., Dantzer, R., Johnson, R. W., and Godbout, J. P. (2008). Exaggerated sickness behavior and brain proinflammatory cytokine expression in aged mice in response to intracerebroventricular lipopolysaccharide. *Neurobiol. Aging* 29, 1744–1753. doi: 10.1016/j.neurobiolaging.2007.04.012

Jeong, J. K., and Park, S. Y. (2015). Melatonin regulates the autophagic flux via activation of alpha-7 nicotinic acetylcholine receptors. *J. Pineal. Res.* 59, 24–37. doi: 10.1111/jpi.12235

Ke, P., Shao, B. Z., Xu, Z. Q., Chen, X. W., Wei, W., and Liu, C. (2017). Activating alpha7 nicotinic acetylcholine receptor inhibits NLRP3 inflammasome through regulation of beta-arrestin-1. *CNS Neurosci. Ther.* 23, 875–884. doi: 10.1111/cns.12758

Kim, H. K., Chen, W., and Andreazza, A. C. (2015). The potential role of the NLRP3 inflammasome as a link between mitochondrial complex I dysfunction and inflammation in bipolar disorder. *Neural Plast.* 2015:408136. doi: 10.1155/2015/408136

Lamkanfi, M., and Dixit, V. M. (2014). Mechanisms and functions of inflammasomes. *Cell* 157, 1013–1022. doi: 10.1016/j.cell.2014.04.007

Lee, Y. H., Su, S. B., Huang, C. C., Sheu, H. M., Tsai, J. C., Lin, C. H., et al. (2014). N-acetylcysteine attenuates hexavalent chromium-induced hypersensitivity through inhibition of cell death, ROS-related signaling and cytokine expression. *PLoS One* 9:e108317. doi: 10.1371/journal.pone.0108317

Leslie, M. (2017). The post-op brain. *Science* 356, 898–900. doi: 10.1126/science.356.6341.898

Li, H., Fan, J., Fan, L., Li, T., Yang, Y., Xu, H., et al. (2018). MiRNA-10b reciprocally stimulates osteogenesis and inhibits adipogenesis partly through the TGF-beta/SMAD2 signaling pathway. *Aging Dis.* 9, 1058–1073. doi: 10.14336/ad.2018.0214

Li, X. M., Zhou, M. T., Wang, X. M., Ji, M. H., Zhou, Z. Q., and Yang, J. J. (2014). Resveratrol pretreatment attenuates the isoflurane-induced cognitive impairment through its anti-inflammation and -apoptosis actions in aged mice. *J. Mol. Neurosci.* 52, 286–293. doi: 10.1007/s12031-013-0141-2

Li, Z., Ni, C., Xia, C., Jaw, J., Wang, Y., Cao, Y., et al. (2017). Calcineurin/nuclear factor-kappaB signaling mediates isoflurane-induced hippocampal neuroinflammation and subsequent cognitive impairment in aged rats. *Mol. Med. Rep.* 15, 201–209. doi: 10.3892/mmr.2016.5967

Liu, K., Zang, Y., Guo, X., Wei, F., Yin, J., Pang, L., et al. (2017). The Δ133p53 isoform reduces Wtp53-induced stimulation of DNA Pol γ activity in the presence and absence of D4T. *Aging Dis* 8, 228–239. doi: 10.14336/AD.2016.0910

Liu, P.-R., Zhou, Y., Zhang, Y., and Diao, S. (2017). Electroacupuncture alleviates surgery-induced cognitive dysfunction by increasing α7-nAChR expression and inhibiting inflammatory pathway in aged rats. *Neurosci. Lett.* 659, 1–6. doi: 10.1016/j.neulet.2017.08.043

Lopez-Castejon, G., and Pelegrin, P. (2012). Current status of inflammasome blockers as anti-inflammatory drugs. *Expert Opin. Investig. Drugs* 21, 995–1007. doi: 10.1517/13543784.2012.690032

Malhotra, S., Rio, J., Urcelay, E., Nurtdinov, R., Bustamante, M. F., Fernandez, O., et al. (2015). NLRP3 inflammasome is associated with the response to IFN-beta in patients with multiple sclerosis. *Brain* 138, 644–652. doi: 10.1093/brain/awu388

Minutoli, L., Puzzolo, D., Rinaldi, M., Irrera, N., Marini, H., Arcoraci, V., et al. (2016). ROS-mediated NLRP3 inflammasome activation in brain, heart, kidney and testis ischemia/reperfusion injury. *Oxid. Med. Cell. Longev.* 2016:2183026. doi: 10.1155/2016/2183026

Munoz-Planillo, R., Kuffa, P., Martinez-Colon, G., Smith, B. L., Rajendiran, T. M., and Nunez, G. (2013). K^+ efflux is the common trigger of NLRP3 inflammasome activation by bacterial toxins and particulate matter. *Immunity* 38, 1142–1153. doi: 10.1016/j.immuni.2013.05.016

Newman, J. C., and Verdin, E. (2014). Ketone bodies as signaling metabolites. *Trends Endocrinol. Metab.* 25, 42–52. doi: 10.1016/j.tem.2013.09.002

Parnet, P., Kelley, K. W., Bluthe, R. M., and Dantzer, R. (2002). Expression and regulation of interleukin-1 receptors in the brain. Role in cytokines-induced sickness behavior. *J. Neuroimmunol.* 125, 5–14. doi: 10.1016/s0165-5728(02)00022-x

Pavlov, V. A., and Tracey, K. J. (2017). Neural regulation of immunity: molecular mechanisms and clinical translation. *Nat. Neurosci.* 20, 156–166. doi: 10.1038/nn.4477

Place, D. E., and Kanneganti, T. D. (2018). Recent advances in inflammasome biology. *Curr. Opin. Immunol.* 50, 32–38. doi: 10.1016/j.coi.2017.10.011

Qiu, L. L., Ji, M. H., Zhang, H., Yang, J. J., Sun, X. R., Tang, H., et al. (2016a). NADPH oxidase 2-derived reactive oxygen species in the hippocampus might contribute to microglial activation in postoperative cognitive dysfunction in aged mice. *Brain Behav. Immun.* 51, 109–118. doi: 10.1016/j.bbi.2015.08.002

Qiu, L. L., Luo, D., Zhang, H., Shi, Y. S., Li, Y. J., Wu, D., et al. (2016b). Nox-2-mediated phenotype loss of hippocampal parvalbumin interneurons might contribute to postoperative cognitive decline in aging mice. *Front. Aging Neurosci.* 8:234. doi: 10.3389/fnagi.2016.00234

Razani, B., Feng, C., Coleman, T., Emanuel, R., Wen, H., Hwang, S., et al. (2012). Autophagy links inflammasomes to atherosclerotic progression. *Cell Metab.* 15, 534–544. doi: 10.1016/j.cmet.2012.02.011

Riazi, K., Galic, M. A., Kentner, A. C., Reid, A. Y., Sharkey, K. A., and Pittman, Q. J. (2015). Microglia-dependent alteration of glutamatergic synaptic transmission and plasticity in the hippocampus during peripheral inflammation. *J. Neurosci.* 35, 4942–4952. doi: 10.1523/JNEUROSCI.4485-14.2015

Rossi, A., Burkhart, C., Dell-Kuster, S., Pollock, B. G., Strebel, S. P., Monsch, A. U., et al. (2014). Serum anticholinergic activity and postoperative cognitive dysfunction in elderly patients. *Anesth. Analg.* 119, 947–955. doi: 10.1213/ANE.0000000000000390

Schroder, K., and Tschopp, J. (2010). The inflammasomes. *Cell* 140, 821–832. doi: 10.1016/j.cell.2010.01.040

Shao, B.-Z., Ke, P., Xu, Z.-Q., Wei, W., Cheng, M.-H., Han, B.-Z., et al. (2017). Autophagy plays an important role in anti-inflammatory mechanisms stimulated by alpha7 nicotinic acetylcholine receptor. *Front. Immunol.* 8:553. doi: 10.3389/fimmu.2017.00553

Shao, B. Z., Xu, Z. Q., Han, B. Z., Su, D. F., and Liu, C. (2015). NLRP3 inflammasome and its inhibitors: a review. *Front. Pharmacol.* 6:262. doi: 10.3389/fphar.2015.00262

Shoair, O. A., Grasso Ii, M. P., Lahaye, L. A., Daniel, R., Biddle, C. J., and Slattum, P. W. (2015). Incidence and risk factors for postoperative cognitive dysfunction in older adults undergoing major noncardiac surgery: A prospective study. *J. Anaesthesiol. Clin. Pharmacol.* 31, 30–36. doi: 10.4103/0970-9185.150530

Skvarc, D. R., Berk, M., Byrne, L. K., Dean, O. M., Dodd, S., Lewis, M., et al. (2018). Post-operative cognitive dysfunction: an exploration of the inflammatory hypothesis and novel therapies. *Neurosci. Biobehav. Rev.* 84, 116–133. doi: 10.1016/j.neubiorev.2017.11.011

Steinmetz, J., Christensen, K. B., Lund, T., Lohse, N., and Rasmussen, L. S. (2009). Long-term consequences of postoperative cognitive dysfunction. *Anesthesiology* 110, 548–555. doi: 10.1097/ALN.0b013e318195b569

Sun, L., Dong, R., Xu, X., Yang, X., and Peng, M. (2017). Activation of cannabinoid receptor type 2 attenuates surgery-induced cognitive impairment in mice through anti-inflammatory activity. *J. Neuroinflamm.* 14:138. doi: 10.1186/s12974-017-0913-7

Taly, A., Corringer, P. J., Guedin, D., Lestage, P., and Changeux, J. P. (2009). Nicotinic receptors: allosteric transitions and therapeutic targets in the nervous system. *Nat. Rev. Drug Discov.* 8, 733–750. doi: 10.1038/nrd2927

Terrando, N., Eriksson, L. I., Ryu, J. K., Yang, T., Monaco, C., Feldmann, M., et al. (2011). Resolving postoperative neuroinflammation and cognitive decline. *Ann. Neurol.* 70, 986–995. doi: 10.1002/ana.22664

Terrando, N., Monaco, C., Ma, D., Foxwell, B. M., Feldmann, M., and Maze, M. (2010). Tumor necrosis factor-alpha triggers a cytokine cascade yielding postoperative cognitive decline. *Proc. Natl. Acad. Sci. U S A* 107, 20518–20522. doi: 10.1073/pnas.1014557107

von Haefen, C., Sifringer, M., Endesfelder, S., Kalb, A., Gonzalez-Lopez, A., Tegethoff, A., et al. (2018). Physostigmine restores impaired autophagy in the rat hippocampus after surgery stress and LPS treatment. *J. Neuroimmune. Pharmacol.* 13, 383–395. doi: 10.1007/s11481-018-9790-9

Wang, W., Wang, Y., Wu, H., Lei, L., Xu, S., Shen, X., et al. (2014). Postoperative cognitive dysfunction: current developments in mechanism and prevention. *Med. Sci. Monit.* 20, 1908–1912. doi: 10.12659/MSM.892485

Wang, Z., Meng, S., Cao, L., Chen, Y., Zuo, Z., and Peng, S. (2018). Critical role of NLRP3-caspase-1 pathway in age-dependent isoflurane-induced microglial inflammatory response and cognitive impairment. *J. Neuroinflammation* 15:109. doi: 10.1186/s12974-018-1137-1

Wei, P., Zheng, Q., Liu, H., Wan, T., Zhou, J., Li, D., et al. (2018). Nicotine-induced neuroprotection against cognitive dysfunction after partial hepatectomy involves activation of BDNF/TrkB signaling pathway and inhibition of NF-kappaB signaling pathway in aged rats. *Nicotine. Tob. Res.* 20, 515–522. doi: 10.1093/ntr/ntx157

Wei, X., Gao, H., Zou, J., Liu, X., Chen, D., Liao, J., et al. (2016). Contra-directional coupling of nur77 and nurr1 in neurodegeneration: a novel mechanism for memantine-induced anti-inflammation and anti-mitochondrial impairment. *Mol. Neurobiol.* 53, 5876–5892. doi: 10.1007/s12035-015-9477-7

Weng, R., Wei, X., Yu, B., Zhu, S., Yang, X., Xie, F., et al. (2018). Combined measurement of plasma cystatin C and low-density lipoprotein cholesterol: A valuable tool for evaluating progressive supranuclear palsy. *Parkinsonism Relat. Disord* 52, 37–42. doi: 10.1016/j.parkreldis.2018.03.014

Willingham, S. B., Allen, I. C., Bergstralh, D. T., Brickey, W. J., Huang, M. T., Taxman, D. J., et al. (2009). NLRP3 (NALP3, Cryopyrin) facilitates in vivo caspase-1 activation, necrosis and HMGB1 release via inflammasome-dependent and -independent pathways. *J. Immunol.* 183, 2008–2015. doi: 10.4049/jimmunol.0900138

Wu, J., Li, H., Sun, X., Zhang, H., Hao, S., Ji, M., et al. (2015). A mitochondrion-targeted antioxidant ameliorates isoflurane-induced cognitive deficits in aging mice. *PLoS One* 10:e0138256. doi: 10.1371/journal.pone.0138256

Xie, F., Gao, X., Yang, W., Chang, Z., Yang, X., Wei, X., et al. (2018). Advances in the research of risk factors and prodromal biomarkers of Parkinson's disease. *ACS Chem. Neurosci.* doi: 10.1007/978-0-387-72076-0_6 [Epub ahead of print].

Xu, X., Yin, D., Ren, H., Gao, W., Li, F., Sun, D., et al. (2018). Selective NLRP3 inflammasome inhibitor reduces neuroinflammation and improves long-term neurological outcomes in a murine model of traumatic brain injury. *Neurobiol. Dis.* 117, 15–27. doi: 10.1016/j.nbd.2018.05.016

Xu, Z., Feng, W., Shen, Q., Yu, N., Yu, K., Wang, S., et al. (2017). Rhizoma coptidis and berberine as a natural drug to combat aging and aging-related diseases via anti-oxidation and AMPK activation. *Aging Dis.* 8, 760–777. doi: 10.14336/AD.2016.0620

Yamanashi, T., Iwata, M., Kamiya, N., Tsunetomi, K., Kajitani, N., Wada, N., et al. (2017). Beta-hydroxybutyrate, an endogenic NLRP3 inflammasome inhibitor, attenuates stress-induced behavioral and inflammatory responses. *Sci. Rep.* 7:7677. doi: 10.1038/s41598-017-08055-1

Yang, N., Li, L., Li, Z., Ni, C., Cao, Y., Liu, T., et al. (2017). Protective effect of dapsone on cognitive impairment induced by propofol involves hippocampal autophagy. *Neurosci. Lett.* 649, 85–92. doi: 10.1016/j.neulet.2017.04.019

Yirmiya, R., and Goshen, I. (2011). Immune modulation of learning, memory, neural plasticity and neurogenesis. *Brain Behav. Immun.* 25, 181–213. doi: 10.1016/j.bbi.2010.10.015

Youm, Y. H., Grant, R. W., McCabe, L. R., Albarado, D. C., Nguyen, K. Y., Ravussin, A., et al. (2013). Canonical Nlrp3 inflammasome links systemic low-grade inflammation to functional decline in aging. *Cell Metab.* 18, 519–532. doi: 10.1016/j.cmet.2013.09.010

Youm, Y. H., Nguyen, K. Y., Grant, R. W., Goldberg, E. L., Bodogai, M., Kim, D., et al. (2015). The ketone metabolite beta-hydroxybutyrate blocks NLRP3 inflammasome-mediated inflammatory disease. *Nat. Med.* 21, 263–269. doi: 10.1038/nm.3804

Zhang, M., Deng, Y. N., Zhang, J. Y., Liu, J., Li, Y. B., Su, H., et al. (2018). SIRT3 protects rotenone-induced injury in SH-SY5Y cells by promoting autophagy through the LKB1-AMPK-mTOR pathway. *Aging Dis.* 9, 273–286. doi: 10.14336/ad.2017.0517

Zhang, X., Dong, H., Li, N., Zhang, S., Sun, J., and Qian, Y. (2016). Activated brain mast cells contribute to postoperative cognitive dysfunction by evoking microglia activation and neuronal apoptosis. *J. Neuroinflammation* 13:127. doi: 10.1186/s12974-016-0592-9

Zhang, Y., Xu, Z., Wang, H., Dong, Y., Shi, H. N., Culley, D. J., et al. (2012). Anesthetics isoflurane and desflurane differently affect mitochondrial function, learning and memory. *Ann. Neurol.* 71, 687–698. doi: 10.1002/ana.23683

Zheng, B., Lai, R., Li, J., and Zuo, Z. (2017). Critical role of P2X7 receptors in the neuroinflammation and cognitive dysfunction after surgery. *Brain Behav. Immun.* 61, 365–374. doi: 10.1016/j.bbi.2017.01.005

Zhou, R., Yazdi, A. S., Menu, P., and Tschopp, J. (2011). A role for mitochondria in NLRP3 inflammasome activation. *Nature* 469, 221–225. doi: 10.1038/nature09663

Zou, J., Chen, Z., Liang, C., Fu, Y., Wei, X., Lu, J., et al. (2018). Trefoil factor 3, cholinesterase and homocysteine: potential predictors for Parkinson's disease dementia and vascular parkinsonism dementia in advanced stage. *Aging Dis.* 9, 51–65. doi: 10.14336/AD.2017.0416

Zou, J., Chen, Z., Wei, X., Chen, Z., Fu, Y., Yang, X., et al. (2017). Cystatin C as a potential therapeutic mediator against Parkinson's disease via VEGF-induced angiogenesis and enhanced neuronal autophagy in neurovascular units. *Cell Death Dis.* 8:e2854. doi: 10.1038/cddis.2017.240

Conflict of Interest Statement: The authors declare that the research was conducted in the absence of any commercial or financial relationships that could be construed as a potential conflict of interest.

frontiers in Cellular Neuroscience

REVIEW
published: 12 April 2019
doi: 10.3389/fncel.2019.00142

Role of Glutamatergic Excitotoxicity in Neuromyelitis Optica Spectrum Disorders

Ana Paula Bornes da Silva[1,2], *Débora Guerini Souza*[3], *Diogo Onofre Souza*[3], *Denise Cantarelli Machado*[1,2]* *and Douglas Kazutoshi Sato*[1]*

[1]Molecular and Cellular Biology Laboratory, Brain Institute, Pontifical Catholic University of Rio Grande do Sul (PUCRS), Porto Alegre, Brazil, [2]Medical School, Institute of Geriatrics and Gerontology, Graduate Program in Biomedical Gerontology, Pontifical Catholic University of Rio Grande do Sul (PUCRS), Porto Alegre, Brazil, [3]Graduate Program in Biological Sciences: Biochemistry, Federal University of Rio Grande do Sul (UFRGS), Porto Alegre, Brazil

Neuromyelitis optica spectrum disorder (NMOSD) is an inflammatory disorder mediated by immune-humoral responses directed against central nervous system (CNS) antigens. Most patients are positive for specific immunoglobulin G (IgG) auto-antibodies for aquaporin-4 (AQP4), a water channel present in astrocytes. Antigen-antibody binding promotes complement system cascade activation, immune system cell infiltration, IgG deposition, loss of AQP4 and excitatory amino acid transporter 2 (EAAT2) expression on the astrocytic plasma membrane, triggering necrotic destruction of spinal cord tissue and optic nerves. Astrocytes are very important cells in the CNS and, in addition to supporting other nerve cells, they also regulate cerebral homeostasis and control glutamatergic synapses by modulating neurotransmission in the cleft through the high-affinity glutamate transporters present in their cell membrane. Specific IgG binding to AQP4 in astrocytes blocks protein functions and reduces EAAT2 activity. Once compromised, EAAT2 cannot take up free glutamate from the extracellular space, triggering excitotoxicity in the cells, which is characterized by overactivation of glutamate receptors in postsynaptic neurons. Therefore, the longitudinally extensive myelitis and optic neuritis lesions observed in patients with NMOSD may be the result of primary astrocytic damage triggered by IgG binding to AQP4, which can activate the immune-system cascade and, in addition, downregulate EAAT2. All these processes may explain the destructive lesions in NMOSD secondary to neuroinflammation and glutamatergic excitotoxicity. New or repurposed existing drugs capable of controlling glutamatergic excitotoxicity may provide new therapeutic options to reduce tissue damage and permanent disability after NMOSD attacks.

Keywords: neuromyelitis optica spectrum disorders, aquaporin-4, antibody, astrocytes, glutamate, excitotoxicity

OPEN ACCESS

Edited by:
Andrea Beatriz Cragnolini, Universidad Nacional de Cordoba, Argentina

Reviewed by:
Annalisa Scimemi, University at Albany, United States
Mirko Santello, University of Zurich, Switzerland

***Correspondence:**
Denise Cantarelli Machado
dcm@pucrs.br
Douglas Kazutoshi Sato
douglas.sato@pucrs.br

Received: *17 December 2018*
Accepted: *21 March 2019*
Published: *12 April 2019*

Citation:
Silva APB, Souza DG, Souza DO, Machado DC and Sato DK (2019) Role of Glutamatergic Excitotoxicity in Neuromyelitis Optica Spectrum Disorders. Front. Cell. Neurosci. 13:142. doi: 10.3389/fncel.2019.00142

INTRODUCTION

The central nervous system (CNS) is the target of several pathologies, including CNS autoimmune diseases, a diversified class of disorders that target neuronal and glial antigens. These disorders may be syndromes associated with auto-antibodies that attack intracellular neural antigens or surface antigens. Among the surface antigens, the membrane proteins present on the neuronal or glial surface might be important targets. In the CNS, the antigen-antibody interaction compromises

the homeostasis of the system and may cause damage to neural cells (Zettl et al., 2012; Höftberger, 2015).

Neuromyelitis optica spectrum disorder (NMOSD) is an inflammatory disorder mediated by immune-humoral responses directed against CNS antigens (Sato et al., 2013). Most patients are positive for serum antibodies that target the water channel aquaporin-4 [AQP4–immunoglobulin G (IgG)], a water channel expressed in the end-feet of astrocytes (Wingerchuk et al., 2006, 2015). This inflammatory context is signaled by activated T cells, which cross the cerebral vascular endothelium and impair blood-brain barrier (BBB), promoting the migration of other inflammatory cells, such as macrophages and granulocytes, into the brain and spinal cord tissue (Kurosawa et al., 2015). Moreover, the binding between IgG and AQP4 triggers exacerbation of astrocytic lesions characterized by massive loss of AQP4 and consequent tissue damage that can lead to secondary demyelination due to oligodendrocyte destruction (Kurosawa et al., 2015; Li and Yan, 2015; Zeka et al., 2015; Zekeridou and Lennon, 2015). The lesions are predominantly localized on the optic nerves and spinal cord, compromising the visual and motor capacity of NMOSD patients (Zeka et al., 2015; Zekeridou and Lennon, 2015).

Astrocytes are the main cells regulating glutamatergic homeostasis and, once injured, their ability to perform physiological functions becomes impaired (Zeng et al., 2007; Haruki et al., 2013; Yang et al., 2016). Some studies suggest that the death of oligodendrocytes and secondary demyelination lesions after astrocyte injury may be related to high extracellular concentrations of the neurotransmitter glutamate in the CNS tissue (reviewed by Yang et al., 2016). Neurons are also highly sensitive to high glutamate concentrations, and glutamate excitotoxicity may promote neuronal death, increasing the risk of disability (Marignier et al., 2010; Haruki et al., 2013). The aim of this review is to discuss the relationship between astrocyte damage and glutamatergic excitotoxicity in AQP4-IgG-positive NMOSD.

THE ROLE OF ASTROCYTES IN THE BRAIN

The CNS is composed of neurons and glial cells (**Figure 1**). Glial cells perform critical functions in the CNS, such as modulating and eliminating synapses, supporting neurons with energetic sources and playing an immune role (Allen and Barres, 2009). Glial cells are as numerous as neurons (Allen and Barres, 2009; Gutiérrez Aguilar et al., 2017). This group of cells includes microglia, oligodendrocytes and astrocytes. Their unique biochemical and molecular features allow them to play pivotal roles in CNS physiology (Domingues et al., 2016).

Astrocytes are particularly important among the glial cells since they participate in information processing in the brain from the early stages of development and throughout adult life (Allen and Barres, 2009). They perform various functions in the brain, such as controlling the balance of extracellular ions and water through specialized transmembrane proteins, including AQP4 and ion channels (Papadopoulos and Verkman, 2013; Verkman et al., 2013). Astrocytes can act in CNS repair, maintain BBB homeostasis and regulate the extracellular ionic content to allow an action potential to occur (Maragakis and Rothstein, 2006; Iacovetta et al., 2012; Domingues et al., 2016; Hubbard et al., 2018). Additionally, they secrete growth factors that stimulate surrounding cells, such as molecules that directly influence synapse formation, which is essential in synaptic modulation and synaptic plasticity (Crawford et al., 2012; Fang et al., 2012).

Astrocytes are anatomically associated with neuronal cell bodies and synapses. Therefore, they can regulate the chemical content of the extracellular space and restrict the diffusion of neurotransmitters released into the synaptic cleft (Tritsch and Bergles, 2007; Allen and Barres, 2009; Gutiérrez Aguilar et al., 2017). The classical example is the modulation of the glutamate extracellular concentration through excitatory amino acid transporters (EAATs)/high-affinity glutamate transporters expressed in astrocytic cell membranes (Danbolt, 2001; Danbolt et al., 2016). These cells are responsible for removing glutamate from the extracellular space to promote cerebral homeostasis and prevent excitotoxicity (Benediktsson et al., 2012; Vasile et al., 2017). Therefore, they can regulate extracellular concentrations of substances that can potentially interfere in normal brain functions (Domingues et al., 2016; Hubbard et al., 2018). Recent findings suggest that glial cells are a target of several pathologies. The role of glial cells in health and disease is slowly being elucidated, and the interactions of glia with other CNS cells seem to play fundamental roles in brain performance during normal development and disease states (Domingues et al., 2016).

CEREBRAL GLUTAMATE

Glutamate is the most abundant CNS excitatory molecule and the main neurotransmitter in mammalian brain (Rose et al., 2018). Glutamate excites nerve cells, especially neurons, thus playing a key role in cell signaling (Zhou and Danbolt, 2014). Glutamate is known to be active in several brain processes, such as cognition, memory and learning. In addition, it plays an important role in the induction and elimination of synapses and contributes to cell migration, differentiation and death (Danbolt, 2001). Glutamate also participates in the synthesis of proteins, peptides, and purines (Hackett and Ueda, 2015) and plays a fundamental role in amino acid metabolism (Skytt et al., 2012). Glutamate signaling has been extensively studied, especially due to its vital role in brain normal function and due to its association with pathologies that affect the CNS (Fang et al., 2012; Lewerenz and Maher, 2015).

Glutamate is stored in vesicles at the presynaptic terminal through the action of vesicular glutamate transporters (vGLUTs) and released in the synaptic cleft after presynaptic membrane depolarization. When glutamate is released, it binds to ionotropic glutamate receptors (iGluRs), such as N-methyl-D-aspartate (NMDA) receptors, α-amino-3-hydroxy-5-methyl-4-isoxazole propionic acid (AMPA) receptors, kainate receptors and metabotropic receptors on the postsynaptic membrane, as well as metabotropic receptors on the presynaptic membrane (Reiner and Levitz, 2018). This depolarization excites the postsynaptic neuron, generating an action potential in the

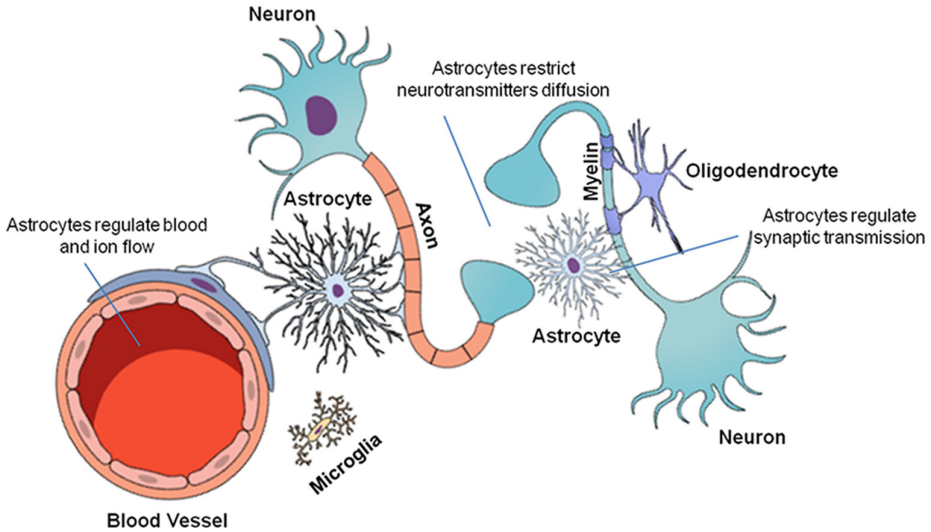

FIGURE 1 | Cellular organization of the central nervous system (CNS). The CNS is composed of neuronal and glial cells (microglia, oligodendrocytes, and astrocytes). Each cell performs a specific function in the CNS. Neurons transmit chemical and electrical signals to other nerve cells. Microglia are immune system cells responsible for the defense of the CNS. Oligodendrocytes form the myelin sheaths of the axons, facilitating saltatory nervous signal conduction. Finally, astrocytes are multifunctional cells that control ion and neurotransmitter diffusion in the nervous parenchyma, in addition to actively participating in the synapses and providing metabolic support to the other cells.

axon to carry the nerve signal (Zhou and Danbolt, 2014; Lewerenz and Maher, 2015; Hayashi, 2018).

The interaction of glutamate with its specific receptors produces postsynaptic excitatory potentials in a precise and controlled manner (Danbolt, 2001; Reiner and Levitz, 2018). The glutamate extracellular concentrations must be well controlled because high glutamate concentrations excessively activate its receptors, generating oxidative stress that may lead to cell death, a process known as excitotoxicity, which impairs both neurons and glial cells (Zhou and Danbolt, 2013, 2014; Stojanovic et al., 2014), causing synaptic transmission dysfunction and interfering in synaptic plasticity (Pál, 2018). For such modulation, glutamate concentrations are controlled by astrocytes through cellular reuptake since these cells present specific proteins in their cell membranes that take up free glutamate as we discuss below (Danbolt, 2001; Larsson et al., 2004; Benarroch, 2010). Glutamate present in the extracellular space cannot be metabolized by any other mechanism (Zhou and Danbolt, 2013). Therefore, astrocytes are essential in the modulation of the glutamatergic system, and any impairment in their highly coordinated action may contribute to the onset of pathologies (Miladinovic et al., 2015).

ASTROCYTES AND GLUTAMATE TRANSPORTERS

Astrocytes express EAATs in their cell membranes, which are also known as glutamate transporters (Lewerenz and Maher, 2015; Al Awabdh et al., 2016). These transporters can retain excess glutamate from the extracellular space inside the cell, thus potentially avoiding excitotoxicity (Gasparini and Griffiths, 2013). Therefore, they transport glutamate in cells against their intra- and extracellular concentration gradients, contributing to the low extracellular glutamate concentration (Lewerenz and Maher, 2015; Underhill et al., 2015; Gutiérrez Aguilar et al., 2017). Glutamate transporters also contribute to physiological synaptic plasticity and function (Rose et al., 2018) and can function as chloride channels (Wadiche et al., 1995a,b; Wadiche and Kavanaugh, 1998) and water transporters (MacAulay et al., 2001, 2004). Five glutamate transporters belonging to the solute-1 carrier family have been identified (Benarroch, 2010; Jiang and Amara, 2011). These transporters are expressed in various tissues, but their main contribution is control of excitatory neurotransmission in brain tissue (Grewer et al., 2014). EAAT1 and EAAT2 are highly expressed in astrocytes, EAAT3 is expressed in neurons (Lewerenz and Maher, 2015; Hayashi, 2018; Schousboe, 2018), EAAT4 is present in the dendritic spines of Purkinje cerebellar cells, and EAAT5 is the retinal glutamate transporter (Gutiérrez Aguilar et al., 2017; Pál, 2018).

Astrocytes are well documented to be the cells responsible for detoxification of metabolic waste and extracellular ions and molecules, such as glutamate (Rose et al., 2018). When glutamate enters in the astrocytic compartment, it can be degraded, recycled or transported out of the brain through the blood or gliolymphatic system (Rose et al., 2018). In the adult brain, approximately 80%–90% of extracellular glutamate is captured by EAAT2 (Danbolt et al., 2016). In addition to glutamate, these transporters cotransport three Na^+ molecules and one proton (H^+) with each glutamate molecule. Additionally, this system is coupled to the reverse transport of one K^+ (Zerangue and Kavanaugh, 1996). Thus, an electrochemical gradient is created on the plasma membrane, allowing transporters to maintain low concentrations of extracellular glutamate (Bergles et al., 2002; Larsson et al., 2004; Lewerenz and Maher, 2015).

Astrocytes also convert glutamate into glutamine through the glutamine synthetase reaction (Norenberg and Martinez-Hernandez, 1979; Jayakumar and Norenberg, 2016), and glutamine is later transported to neurons and converted back to glutamate to be used again in neurotransmission in a process known as the "glutamate-glutamine cycle" (Grewer et al., 2014; Lewerenz and Maher, 2015; Hayashi, 2018; Pál, 2018; Schousboe, 2018; **Figure 2**). Since they regulate glutamatergic signaling, glutamate transporters are essential to brain metabolism (Fang et al., 2012; Grewer et al., 2014; Lewerenz and Maher, 2015). As EAAT2 plays an important role in the physiological functioning of the brain, it is believed to also play a role in the development of chronic and acute CNS disorders (Soni et al., 2014; Grewer et al., 2014). Studies with simultaneous EAAT1- and EAAT2-knockout animals show that they are nonviable because of brain abnormalities and cortical disorganization (Ciappelloni et al., 2017; Rose et al., 2018). Animals deficient only in EAAT2 die after birth due to seizures (Tanaka et al., 1997; Al Awabdh et al., 2016; Danbolt et al., 2016). In adults, impairment in EAAT2 function has been observed to compromise cerebral glutamatergic homeostasis (Hayashi, 2018; Rose et al., 2018). Taken together, the loss of glutamate transporters in astrocytes may contribute to CNS dysfunction and increase neuronal damage in focal inflammatory lesions.

Considering the aforementioned roles of astrocytes and glutamate transporters, understanding astrocyte injury in NMOSD and these entities' contributions to the glutamatergic excitotoxicity observed in this condition is vital since astrocytic impairment can cause serious consequences in brain homeostasis and reduce synaptic function, contributing to the NMOSD physiopathology (Hinson et al., 2008). For these reasons, astrocytic damage in NMOSD is believed to trigger an imbalance in glutamatergic homeostasis, which may contribute to the formation of longitudinally extensive myelitis and optic neuritis lesions (Haruki et al., 2013; Yang et al., 2016).

GLUTAMATE IN NMOSD

Most patients with NMOSD produce IgG auto-antibodies that are highly specific for AQP4, but the cellular and molecular

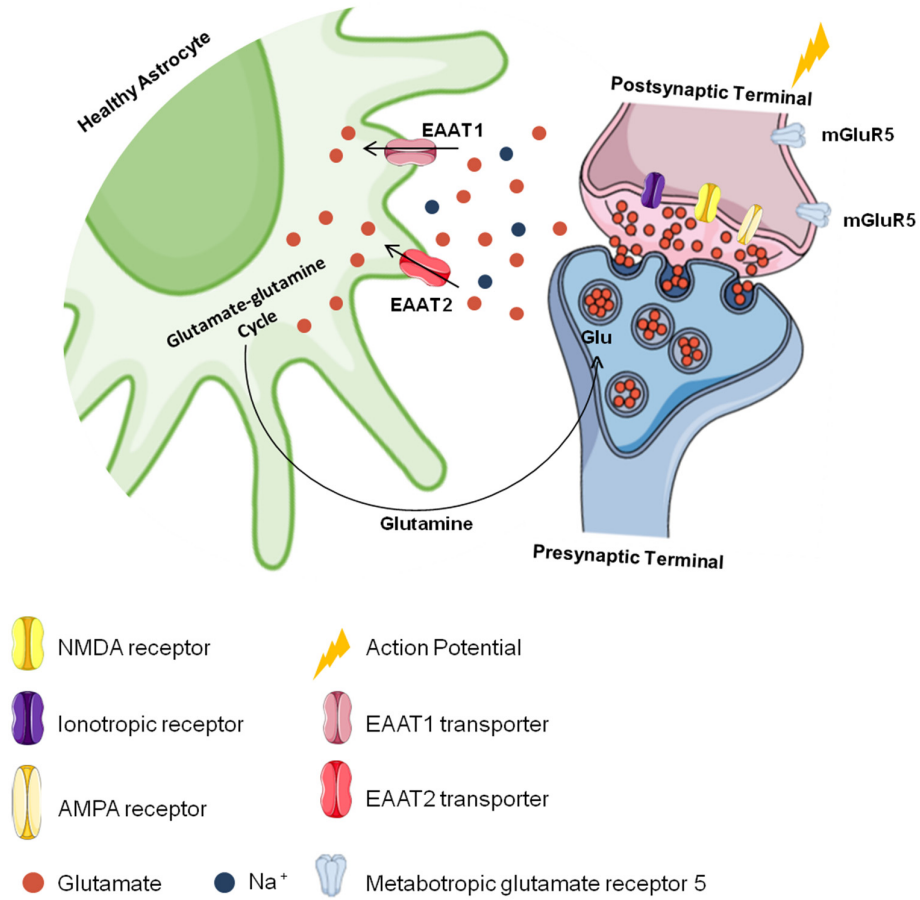

FIGURE 2 | Cerebral glutamate flow. Glutamate is stored presynaptically in vesicles by vesicular glutamate transporters (vGLUTs). It is released after presynaptic membrane depolarization, binds to ionotropic glutamate receptors (iGluRs). like N-methyl-D-aspartate (NMDA) and α-amino-3-hydroxy-5-methyl-4-isoxazole propionic acid (AMPA) receptors in the postsynaptic membrane and generates an action potential. The excess glutamate released into the synaptic cleft is regulated by astrocytes through the excitatory amino acid transporter 1 (EAAT1) and EAAT2 transporters against a concentration gradient. In astrocytes, glutamate is recycled and converted to glutamine, which is transported to neurons and converted into glutamate again to be used in a new synapse.

mechanisms of this interaction are still not clear. Damage occurring in other cells of the CNS, such as neurons and oligodendrocytes, is assumed to be due to a primary astrocytic lesion (Hinson et al., 2008). Astrocytes have been studied for a few decades in both *in vivo* and *in vitro* models of various diseases. Cultivation of astrocytes as primary cultures and lineages represents a powerful tool to explore specific information provided by these cells and to reveal mechanisms related to their function (Hertz et al., 1998). The brain is a complex system in which several cell types interact. While some regions are enriched in a specific cell subtype, an isolated cell type does not occur naturally. Regardless, the use of *in vitro* models of specific cell types has been very helpful in the progress of the neuroscience field (Lange et al., 2012). *In vitro* models of NMOSD have shown that auto-antibodies against AQP4 protein trigger a phenomenon known as antigenic modulation because when such auto-antibodies bind to their targets, a specific IgG alters the functions of AQP4 through its degradation or internalization by astrocytes and interferes in sodium-potassium-dependent glutamate uptake (Hinson et al., 2010). For this reason, *in vitro* NMOSD models are important for identifying cellular interactions that cause nerve tissue damage in this disease.

Such models basically consist of rodent/human astrocyte cultures or immortalized lineages that are exposed to AQP4+ serum samples or only purified IgG, with or without the addition of a human complement, which is used to evaluate the possible deleterious effects of related conditions (Haruki et al., 2013). *In vitro* assays have shown that auto-antibodies present in serum derived from NMOSD patients are cytotoxic and harmful to astrocytes, modifying their morphology and function (Li and Yan, 2015). These conditions induce the internalization of AQP4 protein and consequently other membrane proteins, such as EAAT2, since AQP4 protein forms complexes with other membrane proteins, including glutamate transporters (Zeng et al., 2007; Haruki et al., 2013; Yang et al., 2016).

Haruki et al. (2013) showed that when astrocyte cultures are exposed to AQP4-IgG+ human serum or purified IgG, these cells undergo morphological alterations, with compression of their cell bodies and reduction of cell processes, both in the presence and absence of a human complement. This finding has been confirmed by cell viability assays showing that cells treated with NMOSD patient samples have reduced survival rates compared to cells treated with serum from healthy controls. Astrocyte cultures exposed to AQP4-IgG+ NMOSD patient samples showed reduced EAAT2 transporter expression on cell membranes, suggesting that under these conditions, the AQP4-IgG complex exerts an indirect negative effect on this transporter, impairing its physiological role (Haruki et al., 2013).

NMOSD is characterized by astrocyte death due to binding of the AQP4-IgG complex to AQP4 in astrocyte membranes (Wingerchuk et al., 2015). For this reason, astrocytes cannot capture free glutamate from the extracellular space, causing excitotoxicity and damaging other nerve cells and their cellular structures, such as the myelin sheath, as observed in longitudinally extensive myelitis lesions and optic neuritis (Hinson et al., 2008). Therefore, impairment in glutamatergic homeostasis induces excitotoxicity in neurons and oligodendrocytes, promoting the destruction of myelin (Stojanovic et al., 2014; **Figure 3**).

Excitotoxicity is evident in important CNS disorders and may also be present in NMOSD (Lewerenz and Maher, 2015). *In vitro* studies show that after IgG binding to AQP4, a decrease in the EAAT2 content occurs in the cell membrane, with a consequent decrease in the ability of cells to take up glutamate (Hinson et al., 2017). Since astrocytes are damaged in NMOSD lesions and EAAT2 is not functional, these cells are unable to take up glutamate. Thus, the lesions of longitudinally extensive myelitis and optic neuritis observed in patients with NMOSD may contribute to excess extracellular glutamate since astrocytes are damaged and lose their functionality (Hinson et al., 2008, 2017). Oligodendrocytes and neurons are highly sensitive to extracellular glutamate accumulation, and lesions in NMOSD are characterized by loss of the myelin sheaths that line the neurons, which are produced by oligodendrocytes. Excess glutamate in the extracellular space may contribute to neurotoxic events that lead to oligodendrocyte dysfunction and consequent demyelination (McDonald et al., 1998; Hinson et al., 2008, 2010).

AQP4-IgG DOWNREGULATES EAAT2

Aquaporins are membrane proteins responsible for cellular water balance (Papadopoulos and Verkman, 2013; Verkman et al., 2013; Nakada, 2015). Thirteen proteins have been identified in various mammalian species and are distributed throughout the organism, including the brain (Iacovetta et al., 2012). In the brain, the most expressed aquaporin is AQP4, which can be found in the cerebral cortex, corpus callosum, retina, optic nerves, cerebellum, hypothalamus magnocellular nucleus and brainstem (Papadopoulos and Verkman, 2013; Ikeshima-kataoka, 2016). AQP4 is vital for the brain since it also regulates potassium uptake and release by astrocytes and facilitates cell migration, glial scar formation and cellular communication (Papadopoulos and Verkman, 2013; Verkman et al., 2013; Hubbard et al., 2018). Studies using AQP4-knockout animals have shown that this protein facilitates the movement of water into and out of the CNS. In the absence of AQP4, animals show cytotoxic brain edema due to an osmotic imbalance (Verkman et al., 2013, 2017).

AQP4 forms complexes with other membrane proteins, such as glutamate transporters, especially EAAT2, and can regulate this transporter positively when it is functional or negatively when it is damaged (Chaudhry et al., 1995; MacAulay et al., 2002; Queen et al., 2007; Zeng et al., 2007; Hinson et al., 2008; Xing et al., 2017). Thus, the interaction between IgG and AQP4, which is known as the "antigen-antibody complex" (AQP4-IgG), compromises EAAT2 function, resulting in excitotoxicity and impaired CNS cell function (Zeng et al., 2007; Fang et al., 2012; Haruki et al., 2013; Lewerenz and Maher, 2015; Yang et al., 2016). The AQP4-IgG complex induces downregulation of EAAT2, resulting in high concentrations of glutamate in the brain (Mattson, 2003; Park et al., 2004; Hinson et al., 2010). This process increases extracellular glutamate concentrations, aggravating typical NMOSD lesions associated with the complement system, and provides a cytotoxic

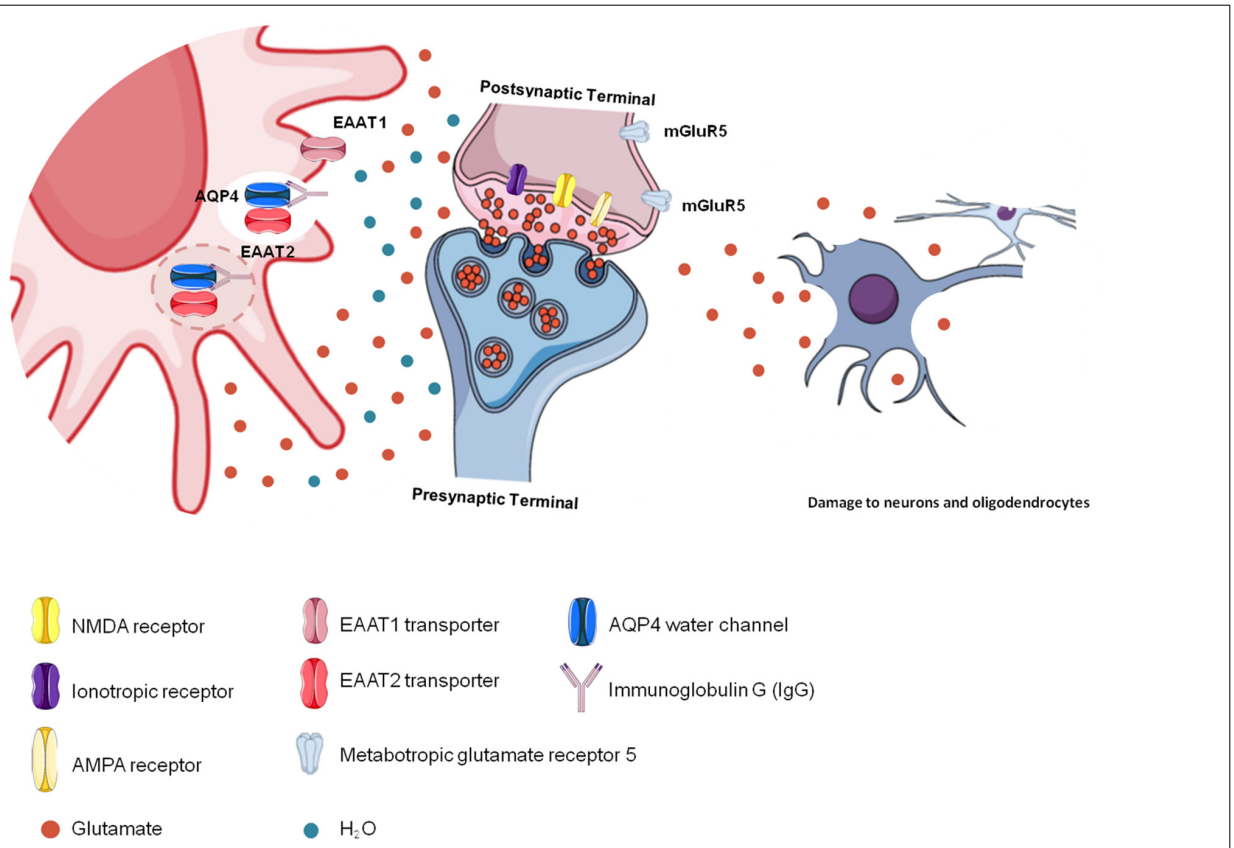

FIGURE 3 | Glutamatergic toxicity in neuromyelitis optica spectrum disorder (NMOSD). Aquaporin-4 (AQP4)-immunoglobulin G (IgG) auto-antibodies binding to AQP4 may promote the internalization of the water channel, thus affecting cellular hydric homeostasis. Antigen-antibody binding promotes immune activation but also affects glutamatergic homeostasis because of reduced glutamate transporter (EAAT2) activity due to its internalization together with AQP4. In the absence of EAAT2, glutamate remains free in the extracellular space, promoting glutamatergic toxicity, which affects other cells, such as neurons and oligodendrocytes.

environment for neurons and oligodendrocytes (Hinson et al., 2010).

Accordingly, Haruki et al. (2013) showed that EAAT2 has diminished expression in human adult astrocyte lineages exposed to specific IgG, suggesting that the AQP4-IgG complex downregulates this transporter in NMOSD. Astrocyte cultures derived from AQP4-knockout animals show low EAAT2 expression as well as a low astrocytic ability to take up glutamate (Zeng et al., 2007). Marignier et al. (2010) observed that purified IgG from patients with NMOSD reduces the number of AQP4+ cells, and the remaining cells exhibit low glutamate uptake. Therefore, in this model, we can conclude that the AQP4-IgG complex results in the loss of EAAT2 and consequently impacts glutamatergic homeostasis. Subsequently, damage to neurons and oligodendrocytes is observed, causing the classic lesions that characterize NMOSD (Marignier et al., 2010; Haruki et al., 2013).

In a glutamate uptake assay, Hinson et al. (2008) observed that cells take up little glutamate (less than 50%) after AQP4+ serum exposure, and EAAT2 expression is as low as AQP4 expression, undetectable by immunofluorescence, after serum exposure. In addition, immunohistochemical assays of human CNS tissue (the cortex and spinal cord) showed that EAAT2 is normally colocalized with AQP4 protein in astrocytes of the gray matter (Chaudhry et al., 1995). The same type of colocalization has also been observed in rodents (Queen et al., 2007), corroborating the hypothesis that AQP4 can form protein complexes and exerts regulatory action on GLT-1 (EAAT2 analogous in rodents) due to the action of the specific IgG (Hinson et al., 2008, 2017).

Under normal physiological conditions, EAAT2 is known to be enriched in the spinal cord (Nakamura et al., 2008). In NMOSD, this tissue is extensively damaged, and the resultant lesions can be explained when considering the theory that AQP4-IgG downregulates EAAT2 (Hinson et al., 2008); therefore, the loss of this transporter may contribute to the destructive lesions of the spinal cord observed in patients with NMOSD. Since the lesions are necrotic, NMOSD lesions may emerge not only from complement activation but also due to the negative control exerted by AQP4-IgG on EAAT2, preventing glutamatergic homeostasis (Wingerchuk et al., 2007; Hinson et al., 2008, 2010; Newcombe et al., 2008). Therefore, impairment of AQP4 functions through AQP4-IgG binding decreases EAAT2's regulation of extracellular glutamate, resulting in glutamatergic excitotoxicity that promotes the death of other nerve cells and contributes to the formation of lesions characteristic of NMOSD (Yang et al., 2016).

THERAPEUTIC INTERVENTIONS

The drug therapies developed to date to treat autoimmune diseases such as NMOSD aim to reduce the inflammatory process through immunosuppression. However, new oral therapies using small molecules that are directly permeable to the BBB may be promising for neuroprotection (Luchtman et al., 2016), so both immunosuppressive and neuroprotective drugs may be combined to treat patients. Therefore, investigating drugs that modulate astrocyte function and glutamate uptake and have a protective effect on other cells may contribute to the treatment of several CNS neuroinflammatory pathologies, such as NMOSD.

Antigen-antibody binding in NMOSD promotes the loss of important astrocyte functions associated with AQP4 and EAAT2, which leaves glutamate at high concentrations in the extracellular space. Considering that excess glutamate contributes to the formation of spinal cord and optic nerve lesions, a therapy that regulates glutamatergic excitotoxicity could be useful to prevent such lesions in NMOSD. Studies with rodents show that ceftriaxone, a beta-lactam antibiotic that increases EAAT2 expression, thus facilitating the removal of free glutamate and preventing glutamatergic excitotoxicity (Hsu et al., 2015), positively regulates EAAT2 acutely and chronically (Rothstein et al., 2005; Szu and Binder, 2016; Zimmer et al., 2017), thus providing neuroprotection under excitotoxic stress conditions. In *in vitro* models derived from spinal cord cultures, ceftriaxone reduces neuronal loss by increasing EAAT2 expression (Bajrektarevic and Nistri, 2017).

Bajrektarevic and Nistri (2017) observed that excitotoxic stress induction with 100 μM kainate promotes EAAT2 immunoreactivity in astrocyte cultures pretreated with ceftriaxone for 3 days, suggesting that ceftriaxone confers neuroprotection against an excitotoxic stimulus/challenge when administered prior to treatment with a glutamate uptake inhibitor. In an experimental model of Parkinson's disease, ceftriaxone has been shown to increase EAAT2 expression in the hippocampus, regardless of whether the treatment started before or after the injury. This drug crosses the BBB and can penetrate into the CNS at therapeutic levels. In the context of NMOSD, ceftriaxone may be studied to determine whether it can reduce acute longitudinally extensive myelitis and optic neuritis lesions based on reduced cell damage secondary to excess glutamate (Hsu et al., 2015).

The deleterious effect of glutamate has already been elucidated in several neurodegenerative diseases such as Alzheimer's. Memantine is a neuroprotective drug recommended for the treatment of Alzheimer's disease, and as a noncompetitive NMDA receptor antagonist, this drug reduces receptor affinity for glutamate (Matsunaga et al., 2018). Memantine may confer neuroprotection through more potent inhibition of extrasynaptic NMDA receptors (Zhao et al., 2006; Léveillé et al., 2008; Okamoto et al., 2009; Milnerwood et al., 2010; Xia et al., 2010) without significantly affecting physiologic glutamatergic transmission. In addition, this drug has few undesirable drug interactions or adverse effects and is a well-tolerated medication for neurological disorders (Seyedsaadat and Kallmes, 2019). Several studies have investigated the effects of memantine on neurons, and the drug is known to increase the release of glial cell neurotrophic factors, contributing to neuronal survival (Wu et al., 2009). Further, the anti-inflammatory action of memantine reduces pro-inflammatory factors (reactive oxygen species and tumor necrosis factor-α), inhibiting the activation of microglia, and may provide neuroprotection (Maciulaitiene et al., 2017).

In addition to Alzheimer's disease, in retinal crush models (a classic glaucoma model), astrocytes treated with intravitreal memantine have been found to exhibit improved survival (Maciulaitiene et al., 2017). Memantine preserves retinal astrocytes by exerting a glioprotective effect. In glaucoma models, an altered ion concentration in cells causes cellular damage due to high sodium influx and elevated intracellular calcium, causing glutamate release and cell death. Under memantine treatment, this process is attenuated, preventing excitotoxicity-induced damage to nerve cells. Memantine, as a noncompetitive NMDA receptor blocker, can reduce the optic neuritis observed in patients with NMOSD as well as retinal damage in some cases (Maciulaitiene et al., 2017; Bradl et al., 2018). In addition to its protective effect, memantine can induce cellular proliferation and increase the production of neural progenitors by up to 2–3 times, which may contribute to the regeneration of injured tissues in NMOSD (Cahill et al., 2018).

Another drug that may be helpful in the treatment of NMOSD is dimethyl fumarate (DMF or BG-12). DMF is used to treat relapsing-remitting multiple sclerosis (MS; Höftberger and Lassmann, 2017; Mills et al., 2018). DMF mainly modulates the immunological profiles of patients in terms of cellular composition and inflammation, reducing the number of peripheral T and B lymphocytes and modulating their inflammatory state to engender an anti-inflammatory profile. Further, DMF has a protective effect on cells that suffer from oxidative stress through activation of nuclear factor-erythroid 2-related factor 2 (Nrf2) and can increase the proliferation of neural progenitors *in vitro* since DMF increases self-renewal and protects neural progenitors, oligodendrocytes and therefore myelin against oxidative stress, reducing death by apoptosis (Hammer et al., 2018; Mills et al., 2018). Although some studies show that DMF plays a neuroprotective role, its mechanism of action is still obscure and requires further clarification because many immunomodulatory drugs used in MS treatment may actually worsen NMOSD. Therefore, any trial with DMF should be performed only after strong experimental evidence is found showing that the beneficial effects observed in MS are also observed in NMOSD (Yamout et al., 2017; Popiel et al., 2018).

CONCLUSIONS

The concept that AQP4-IgG auto-antibodies are deleterious to astrocytes is well established. Protein-antibody binding not only activates the immune system but also modulates AQP4 function and induces its internalization by astrocytes. Some pathological features observed in longitudinally extensive myelitis and optic neuritis lesions may be associated with glutamatergic excitotoxicity since the AQP4-IgG/AQP4 complex downregulates the main astrocytic glutamate transporter

EAAT2. Consequently, neurons and glial cells may be exposed to excitotoxicity, oxidative stress and neuroinflammation. These three aspects may influence the formation and extension of NMOSD lesions. Drugs to control the deleterious effects of excess glutamate in the CNS may provide innovative neuroprotective therapy to reduce NMOSD attacks and their severity. Therefore, promoting future studies with such drugs in monotherapy or in association with currently used immunotherapies is critical to evaluate the safety and efficacy of these strategies in NMOSD.

AUTHOR CONTRIBUTIONS

All authors contributed to the manuscript preparation and wrote, read and approved the submitted version.

FUNDING

This review is based on research supported by the Conselho Nacional de Desenvolvimento Científico e Tecnológico (CNPq Universal/Brazil grant 425331/2016-4), the Instituto Nacional de Ciências e Tecnologia em Exitotoxicidade e Neuroproteção (INCT-EN), Coordenação de Aperfeiçoamento de Pessoal de Nível Superior (CAPES) Finance Code 001—Brazilian Federal Agency for Support and Evaluation of Graduate Education (PROEX Program) and the Fundação de Amparo à Pesquisa do Estado do Rio Grande do Sul (FAPERGS/CAPES/DOCFIX 18/2251-0000504-5).

ACKNOWLEDGMENTS

The authors would like to acknowledge the Conselho Nacional de Desenvolvimento Científico e Tecnlógico (CNPq), the Coordenação de Aperfeiçoamento de Pessoal de Nível Superior (CAPES) Finance Code 001—Brazilian Federal Agency for Support and Evaluation of Graduate Education (PROEX Program) and the Fundação de Amparo à Pesquisa do Estado do Rio Grande do Sul (FAPERGS).

REFERENCES

Al Awabdh, S., Gupta-Agarwal, S., Sheehan, D. F., Muir, J., Norkett, R., Twelvetrees, A. E., et al. (2016). Neuronal activity mediated regulation of glutamate transporter GLT-1 surface diffusion in rat astrocytes in dissociated and slice cultures. *Glia* 64, 1252–1264. doi: 10.1002/glia.22997

Allen, N. J., and Barres, B. A. (2009). Neuroscience: Glia - more than just brain glue. *Nature* 457, 675–677. doi: 10.1038/457675a

Bajrektarevic, D., and Nistri, A. (2017). NeuroToxicology Ceftriaxone-mediated upregulation of the glutamate transporter GLT-1 contrasts neurotoxicity evoked by kainate in rat organotypic spinal cord cultures. *Neurotoxicology* 60, 34–41. doi: 10.1016/j.neuro.2017.02.013

Benarroch, E. E. (2010). Glutamate transporters: diversity, function, and involvement in neurologic disease. *Neurology* 74, 259–264. doi: 10.1212/wnl.0b013e3181cc89e3

Benediktsson, A. M., Marrs, G. S., Tu, J. C., Worley, P. F., Rothstein, J. D., Bergles, D. E., et al. (2012). Neuronal activity regulates glutamate transporter dynamics in developing astrocytes. *Glia* 60, 175–188. doi: 10.1002/glia.21249

Bergles, D. E., Tzingounis, A. V., and Jahr, C. E. (2002). Comparison of coupled and uncoupled currents during glutamate uptake by GLT-1 transporters. *J. Neurosci.* 22, 10153–10162. doi: 10.1523/jneurosci.22-23-10153.2002

Bradl, M., Reindl, M., and Lassmann, H. (2018). Mechanisms for lesion localization in neuromyelitis optica spectrum disorders. *Curr. Opin. Neurol.* 31, 325–333. doi: 10.1097/wco.0000000000000551

Cahill, S. P., Cole, J. D., Yu, R. Q., Clemans-Gibbon, J., and Snyder, J. S. (2018). Differential effects of extended exercise and memantine treatment on adult neurogenesis in male and female rats. *Neuroscience* 390, 241–255. doi: 10.1016/j.neuroscience.2018.08.028

Chaudhry, F. A., Lehre, K. P., Lookeren Campagne, M., Ottersen, O. P., Danbolt, N. C., and Storm-Mathisen, J. (1995). Glutamate transporters in glial plasma membranes: highly differentiated localizations revealed by quantitative ultrastructural immunocytochemistry. *Neuron* 15, 711–720. doi: 10.1016/0896-6273(95)90158-2

Ciappelloni, S., Murphy-royal, C., Dupuis, J. P., and Oliet, S. H. R. (2017). Dynamics of surface neurotransmitter receptors and transporters in glial cells: single molecule insights. *Cell Calcium* 67, 46–52. doi: 10.1016/j.ceca.2017.08.009

Crawford, D. C., Jiang, X., Taylor, A., and Mennerick, S. (2012). Astrocyte-derived thrombospondins mediate the development of hippocampal presynaptic plasticity *in vitro*. *J. Neurosci.* 32, 13100–13110. doi: 10.1523/jneurosci.2604-12.2012

Danbolt, N. C. (2001). Glutamate uptake. *Prog. Neurobiol.* 65, 1–105. doi: 10.1016/s0301-0082(00)00067-8

Danbolt, N. C., Furness, D. N., and Zhou, Y. (2016). Neurochemistry International Neuronal vs. glial glutamate uptake: resolving the conundrum. *Neurochem. Int.* 98, 29–45. doi: 10.1016/j.neuint.2016.05.009

Domingues, H. S., Portugal, C. C., Socodato, R., and Relvas, J. B. (2016). Oligodendrocyte, astrocyte, and microglia crosstalk in myelin development, damage, and repair. *Front. Cell Dev. Biol.* 4:71. doi: 10.3389/fcell.2016.00071

Fang, J., Han, D., Hong, J., Tan, Q., and Tian, Y. (2012). The chemokine, macrophage inflammatory protein-2γ, reduces the expression of glutamate transporter-1 on astrocytes and increases neuronal sensitivity to glutamate excitotoxicity. *J. Neuroinflammation* 9, 01–12. doi: 10.1186/1742-2094-9-267

Gasparini, C. F., and Griffiths, L. R. (2013). The biology of the glutamatergic system and potential role in migraine. *Int. J. Biomed. Sci.* 9, 1–8.

Grewer, C., Gameiro, A., and Rauen, T. (2014). SLC1 glutamate transporters. *Pflugers Arch.* 466, 3–24. doi: 10.1007/s00424-013-1397-7

Gutiérrez Aguilar, G. F., Alquisiras-Burgos, I., Espinoza-Rojo, M., and Aguilera, P. (2017). Glial excitatory amino acid transporters and glucose incorporation. *Adv. Neurobiol.* 16, 269–282. doi: 10.1007/978-3-319-55769-4_13

Hackett, J. T., and Ueda, T. (2015). Glutamate Release. *Neurochem. Res.* 40, 2443–2460. doi: 10.1007/s11064-015-1622-1

Hammer, A., Waschbisch, A., Kuhbandner, K., Bayas, A., Lee, D., Duscha, A., et al. (2018). The NRF2 pathway as potential biomarker for dimethyl fumarate treatment in multiple sclerosis. *Ann. Clin. Transl. Neurol.* 5, 668–676. doi: 10.1002/acn3.553

Haruki, H., Sano, Y., Shimizu, F., Omoto, M., Tasaki, A., Oishi, M., et al. (2013). NMO sera down-regulate AQP4 in human astrocyte and induce cytotoxicity independent of complement. *J. Neurol. Sci.* 331, 136–144. doi: 10.1016/j.jns.2013.05.035

Hayashi, M. K. (2018). Structure-function relationship of transporters in the glutamate-glutamine cycle of the central nervous system. *Int. J. Mol. Sci.* 19:E1177. doi: 10.3390/ijms19041177

Hertz, L., Peng, L., and Lai, J. C. K. (1998). Functional studies in cultured astrocytes. *Methods* 16, 293–310. doi: 10.1006/meth.1998.0686

Hinson, S. R., Clift, I. C., Luo, N., Kryzer, T. J., and Lennon, V. A. (2017). Autoantibody-induced internalization of CNS AQP4 water channel and EAAT2 glutamate transporter requires astrocytic Fc receptor. *Proc. Natl. Acad. Sci. U S A* 114, 5491–5496. doi: 10.1073/pnas.1701960114

Hinson, S. R., McKeon, A., and Lennon, V. A. (2010). Neurological autoimmunity targeting aquaporin-4. *Neuroscience* 168, 1009–1018. doi: 10.1016/j.neuroscience.2009.08.032

Hinson, S. R., Roemer, S. F., Lucchinetti, C. F., Fryer, J. P., Kryzer, T. J., Chamberlain, J. L., et al. (2008). Aquaporin-4-binding autoantibodies in patients with neuromyelitis optica impair glutamate transport by

down-regulating EAAT2. *J. Exp. Med.* 205, 2473–2481. doi: 10.1084/jem.20081241

Höftberger, R. (2015). Neuroimmunology: an expanding frontier in autoimmunity. *Front. Immunol.* 6:206. doi: 10.3389/fimmu.2015.00206

Höftberger, R. H., and Lassmann, H. (2017). Inflammatory demyelinating diseases of the central nervous system. *Handb. Clin. Neurol.* 145, 263–283. doi: 10.1016/B978-0-12-802395-2.00019-5

Hsu, C., Hung, C., Chang, H., Liao, W., Ho, S. C., and Ho, Y. J. (2015). Ceftriaxone prevents and reverses behavioral and neuronal deficits in an MPTP-induced animal model of Parkinson's disease dementia. *Neuropharmacology* 91, 43–56. doi: 10.1016/j.neuropharm.2014.11.023

Hubbard, J. A., Szu, J. I., and Binder, D. K. (2018). The role of aquaporin-4 in synaptic plasticity, memory and disease. *Brain Res. Bull.* 136, 118–129. doi: 10.1016/j.brainresbull.2017.02.011

Iacovetta, C., Rudloff, E., and Kirby, R. (2012). The role of aquaporin 4 in the brain. *Vet. Clin. Pathol.* 41, 32–44. doi: 10.1111/j.1939-165x.2011.00390.x

Ikeshima-kataoka, H. (2016). Neuroimmunological implications of AQP4 in astrocytes. *Int. J. Mol. Sci.* 17:E1306. doi: 10.3390/ijms17081306

Jayakumar, A. R., and Norenberg, M. D. (2016). Glutamine Synthetase: Role in Neurological Disorders. *Adv. Neurobiol.* 13, 327–350. doi: 10.1007/978-3-319-45096-4_13

Jiang, J., and Amara, S. G. (2011). New views of glutamate transporter structure and function: advances and challenges. *Neuropharmacology* 60, 172–181. doi: 10.1016/j.neuropharm.2010.07.019

Kurosawa, K., Misu, T., Takai, Y., Sato, D. K., Takahashi, T., Abe, Y., et al. (2015). Severely exacerbated neuromyelitis optica rat model with extensive astrocytopathy by high affinity anti-aquaporin-4 monoclonal antibody. *Acta Neuropathol. Commun.* 3:82. doi: 10.1186/s40478-015-0259-2

Lange, S. C., Bak, L. K., Waagepetersen, H. S., Schousboe, A., and Norenberg, M. D. (2012). Primary cultures of astrocytes: their value in understanding astrocytes in health and disease. *Neurochem. Res.* 37, 2569–2588. doi: 10.1007/s11064-012-0868-0

Larsson, H. P., Tzingounis, A. V., Koch, H. P., and Kavanaugh, M. P. (2004). Fluorometric measurements of conformational changes in glutamate transporters. *Proc. Natl. Acad. Sci. U S A* 101, 3951–3956. doi: 10.1073/pnas.0306737101

Léveillé, F., El Gaamouch, F., Gouix, E., Lecocq, M., Lobner, D., Nicole, O., et al. (2008). Neuronal viability is controlled by a functional relation between synaptic and extrasynaptic NMDA receptors. *FASEB J.* 22, 4258–4271. doi: 10.1096/fj.08-107268

Lewerenz, J., and Maher, P. (2015). Chronic glutamate toxicity in neurodegenerative diseases-what is the evidence?. *Front. Neurosci.* 9:469. doi: 10.3389/fnins.2015.00469

Li, M., and Yan, Y. (2015). Experimental models of neuromyelitis optica: current status, challenges and future directions. *Neurosci. Bull.* 31, 735–744. doi: 10.1007/s12264-015-1552-6

Luchtman, D., Gollan, R., Ellwardt, E., Birkenstock, J., Robohm, K., Siffrin, V., et al. (2016). *In vivo* and *in vitro* effects of multiple sclerosis immunomodulatory therapeutics on glutamatergic excitotoxicity. *J. Neurochem.* 136, 971–980. doi: 10.1111/jnc.13456

MacAulay, N., Gether, U., Klaerke, D. A., and Zeuthen, T. (2001). Water transport by the human Na^+-coupled glutamate cotransporter expressed in Xenopus oocytes. *J. Physiol.* 530, 367–378. doi: 10.1111/j.1469-7793.2001.0367k.x

MacAulay, N., Gether, U., Klaerke, D. A., and Zeuthen, T. (2002). Passive water and urea permeability of a human Na^+-glutamate cotransporter expressed in *Xenopus* oocytes. *J. Physiol.* 542, 817–828. doi: 10.1113/jphysiol.2002.020586

MacAulay, N., Hamann, S., and Zeuthen, T. (2004). Water transport in the brain: role of cotransporters. *Neuroscience* 129, 1031–1044. doi: 10.1016/j.neuroscience.2004.06.045

Maciulaitiene, R., Pakuliene, G., Kaja, S., Pauza, D. H., Kalesnykas, G., and Januleviciene, I. (2017). Glioprotection of retinal astrocytes after intravitreal administration of memantine in the mouse optic nerve crush model. *Med. Sci. Monit.* 23, 1173–1179. doi: 10.12659/msm.899699

Maragakis, N. J., and Rothstein, J. D. (2006). Mechanisms of disease: astrocytes in neurodegenerative disease. *Nat. Clin. Pract. Neurol.* 2, 679–689. doi: 10.1038/ncpneuro0355

Marignier, R., Nicolle, A., Watrin, C., Touret, M., Cavagna, S., Varrin-Doyer, M., et al. (2010). Oligodendrocytes are damaged by neuromyelitis optica immunoglobulin G via astrocyte injury. *Brain* 133, 2578–2591. doi: 10.1093/brain/awq177

Matsunaga, S., Kishi, T., Nomura, I., Sakuma, K., Okuya, M., Ikuta, T., et al. (2018). The efficacy and safety of memantine for the treatment of Alzheimer's disease. *Expert Opin. Drug Saf.* 17, 1053–1061. doi: 10.1080/14740338.2018.1524870

Mattson, M. P. (2003). Excitotoxic and excitoprotective mechanisms: abundant targets for the prevention and treatment of neurodegenerative disorders. *Neuromolecular Med.* 3, 65–94. doi: 10.1385/NMM:3:2:65

McDonald, J. W., Althomsons, S. P., Hyrc, K. L., Choi, D. W., and Goldberg, M. P. (1998). Oligodendrocytes from forebrain are highly vulnerable to AMPA/kainate receptor-mediated excitotoxicity. *Nat. Med.* 4, 291–297. doi: 10.1038/nm0398-291

Miladinovic, T., Nashed, M. G., and Singh, G. (2015). Overview of glutamatergic dysregulation in central pathologies. *Biomolecules* 5, 3112–3141. doi: 10.3390/biom5043112

Mills, E. A., Ogrodnik, M. A., Plave, A., and Mao-Draayer, Y. (2018). Emerging understanding of the mechanism of action for dimethyl fumarate in the treatment of multiple sclerosis. *Front. Neurol.* 9:5. doi: 10.3389/fneur.2018.00005

Milnerwood, A. J., Gladding, C. M., Pouladi, M. A., Kaufman, A. M., Hines, R. M., Boyd, J. D., et al. (2010). Early increase in extrasynaptic NMDA receptor signaling and expression contributes to phenotype onset in Huntington's disease mice. *Neuron* 65, 178–190. doi: 10.1016/j.neuron.2010.01.008

Nakada, T. (2015). The molecular mechanisms of neural flow coupling: a new concept. *J. Neuroimaging* 25, 861–865. doi: 10.1111/jon.12219

Nakamura, M., Miyazawa, I., Fujihara, K., Nakashima, I., Misu, T., Watanabe, S., et al. (2008). Preferential spinal central gray matter involvement in neuromyelitis optica. an MRI study. *J. Neurol.* 255, 163–170. doi: 10.1007/s00415-008-0545-z

Newcombe, J., Uddin, A., Dove, R., Patel, B., Turski, L., Nishizawa, Y., et al. (2008). Glutamate receptor expression in multiple sclerosis lesions. *Brain Pathol.* 18, 52–61. doi: 10.1111/j.1750-3639.2007.00101.x

Norenberg, M. D., and Martinez-Hernandez, A. (1979). Fine structural localization of glutamine synthetase in astrocytes of rat brain. *Brain Res.* 161, 303–310. doi: 10.1016/0006-8993(79)90071-4

Okamoto, S., Pouladi, M. A., Talantova, M., Yao, D., Xia, P., Ehrnhoefer, D. E., et al. (2009). Balance between synaptic versus extrasynaptic NMDA receptor activity influences inclusions and neurotoxicity of mutant huntingtin. *Nat. Med.* 15, 1407–1413. doi: 10.1038/nm.2056

Pál, B. (2018). Involvement of extrasynaptic glutamate in physiological and pathophysiological changes of neuronal excitability. *Cell. Mol. Life Sci.* 75, 2917–2949. doi: 10.1007/s00018-018-2837-5

Papadopoulos, M. C., and Verkman, A. S. (2013). Aquaporin water channels in the nervous system. *Nat. Rev. Neurosci.* 14, 265–277. doi: 10.1038/nrn3468

Park, E., Velumian, A. A., and Fehlings, M. G. (2004). The role of excitotoxicity in secondary mechanisms of spinal cord injury: a review with an emphasis on the implications for white matter degeneration. *J. Neurotrauma.* 21, 754–774. doi: 10.1089/0897715041269641

Popiel, M., Psujek, M., and Bartosik-Psujek, H. (2018). Severe disease exacerbation in a patient with neuromyelitis optica spectrum disorder during treatment with dimethyl fumarate. *Mult. Scler. Relat. Disord.* 26, 204–206. doi: 10.1016/j.msard.2018.09.011

Queen, S. A., Kesslak, J. P., and Bridges, R. J. (2007). Regional distribution of sodium-dependent excitatory amino acid transporters in rat spinal cord. *J. Spinal Cord Med.* 30, 263–271. doi: 10.1080/10790268.2007.11753935

Reiner, A., and Levitz, J. (2018). Glutamatergic signaling in the central nervous system: ionotropic and metabotropic receptors in concert. *Neuron* 98, 1080–1098. doi: 10.1016/j.neuron.2018.05.018

Rose, C. R., Felix, L., Zeug, A., Dietrich, D., Reiner, A., and Henneberger, C. (2018). Astroglial glutamate signaling and uptake in the hippocampus. *Front. Mol. Neurosci.* 10:451. doi: 10.3389/fnmol.2017.00451

Rothstein, J. D., Patel, S., Regan, M. R., Haenggeli, C., Huang, Y. H., Bergles, D. E., et al. (2005). β-Lactam antibiotics offer neuroprotection by increasing glutamate transporter expression. *Nature* 433, 73–77. doi: 10.1038/nature03180

Sato, D. K., Lana-Peixoto, M. A., Fujihara, K., and de Seze, J. (2013). Clinical spectrum and treatment of neuromyelitis optica spectrum disorders: evolution and current status. *Brain Pathol.* 23, 647–660. doi: 10.1111/bpa.12087

Schousboe, A. (2018). Neuroscience Letters Metabolic signaling in the brain and the role of astrocytes in control of glutamate and GABA neurotransmission. *Neurosci. Lett.* 689, 11–13. doi: 10.1016/j.neulet.2018.01.038

Seyedsaadat, S. M., and Kallmes, D. F. (2019). Memantine for the treatment of ischemic stroke: experimental benefits and clinical lack of studies. *Rev. Neurosci.* 30, 203–220. doi: 10.1515/revneuro-2018-0025

Skytt, D. M., Klawonn, A. M., Stridh, M. H., Pajecka, K., Patruss, Y., Quintana-Cabrera, R., et al. (2012). siRNA knock down of glutamate dehydrogenase in astrocytes affects glutamate metabolism leading to extensive accumulation of the neuroactive amino acids glutamate and aspartate. *Neurochem. Int.* 61, 490–497. doi: 10.1016/j.neuint.2012.04.014

Soni, N., Reddy, B. V. K., and Kumar, P. (2014). GLT-1 transporter: an effective pharmacological target for various neurological disorders. *Pharmacol. Biochem. Behav.* 127, 70–81. doi: 10.1016/j.pbb.2014.10.001

Stojanovic, I. R., Kostic, M., and Ljubisavljevic, S. (2014). The role of glutamate and its receptors in multiple sclerosis. *J. Neural Transm.* 121, 945–955. doi: 10.1007/s00702-014-1188-0

Szu, J. I., and Binder, D. K. (2016). The role of astrocytic aquaporin-4 in synaptic plasticity and learning and memory. *Front. Integr. Neurosci.* 10:8. doi: 10.3389/fnint.2016.00008

Tanaka, K., Watase, K., Manabe, T., Yamada, K., Watanabe, M., Takahashi, K., et al. (1997). Epilepsy and exacerbation of brain injury in mice lacking the glutamate transporter GLT-1. *Science* 276, 1699–1702. doi: 10.1126/science.276.5319.1699

Tritsch, N. X., and Bergles, D. E. (2007). Defining the role of astrocytes in neuromodulation. *Neuron* 54, 497–500. doi: 10.1016/j.neuron.2007.05.008

Underhill, S. M., Wheeler, D. S., and Amara, S. G. (2015). Differential regulation of two isoforms of the glial glutamate transporter EAAT2 by DLG1 and CaMKII. *J. Neurosci.* 35, 5260–5270. doi: 10.1523/jneurosci.4365-14.2015

Vasile, F., Dossi, E., and Rouach, N. (2017). Human astrocytes: structure and functions in the healthy brain. *Brain Struct. Funct.* 222, 2017–2029. doi: 10.1007/s00429-017-1383-5

Verkman, A. S., Phuan, P.-W., Asavapanumas, N., and Tradtrantip, L. (2013). Biology of AQP4 and anti-AQP4 antibody: therapeutic implications for NMO. *Brain Pathol.* 23, 684–695. doi: 10.1111/bpa.12085

Verkman, A. S., Smith, A. J., Phuan, P., Tradtrantip, L., and Anderson, M. O. (2017). The aquaporin-4 water channel as a potential drug target in neurological disorders. *Expert Opin. Ther. Targets* 21, 1161–1170. doi: 10.1080/14728222.2017.1398236

Wadiche, J. I., Arriza, J. L., Amara, S. G., and Kavanaugh, M. P. (1995a). Kinetics of a human glutamate transporter. *Neuron* 14, 1019–1027. doi: 10.1016/0896-6273(95)90340-2

Wadiche, J. I., Amara, S. G., and Kavanaugh, M. P. (1995b). Ion fluxes associated with excitatory amino acid transport. *Neuron* 15, 721–728. doi: 10.1016/0896-6273(95)90159-0

Wadiche, J. I., and Kavanaugh, M. P. (1998). Macroscopic and microscopic properties of a cloned glutamate transporter/chloride channel. *J. Neurosci.* 18, 7650–7661. doi: 10.1523/jneurosci.18-19-07650.1998

Wingerchuk, D. M., Banwell, B., Bennett, J. L., Cabre, P., Carroll, W., Chitnis, T., et al. (2015). International consensus diagnostic criteria for neuromyelitis optica spectrum disorders. *Neurology* 85, 177–189. doi: 10.1212/WNL.0000000000001729

Wingerchuk, D. M., Lennon, V. A., Lucchinetti, C. F., Pittock, S. J., and Weinshenker, B. G. (2007). The spectrum of neuromyelitis optica. *Lancet Neurol.* 6, 805–815. doi: 10.1016/S1474-4422(07)70216-8

Wingerchuk, D. M., Lennon, V. A., Pittock, S. J., Lucchinetti, C. F., and Weinshenker, B. G. (2006). Revised diagnostic criteria for neuromyelitis optica. *Neurology* 66, 1485–1489. doi: 10.1212/01.wnl.0000216139.44259.74

Wu, H. M., Tzeng, N. S., Qian, L., Wei, S. J., Hu, X., Chen, S. H., et al. (2009). Novel neuroprotective mechanisms of memantine: increase in neurotrophic factor release from astroglia and anti-inflammation by preventing microglial activation. *Neuropsychopharmacology* 34, 2344–2357. doi: 10.1038/npp.2009.64

Xia, P., Chen, H. S., Zhang, D., and Lipton, S. A. (2010). Memantine preferentially blocks extrasynaptic over synaptic NMDA receptor currents in hippocampal autapses. *J. Neurosci.* 30, 11246–11250. doi: 10.1523/jneurosci.2488-10.2010

Xing, H. Q., Zhang, Y., Izumo, K., Arishima, S., Kubota, R., Ye, X., et al. (2017). Decrease of aquaporin-4 and excitatory amino acid transporter-2 indicate astrocyte dysfunction for pathogenesis of cortical degeneration in HIV-associated neurocognitive disorders. *Neuropathology* 37, 25–34. doi: 10.1111/neup.12321

Yamout, B. I., Beaini, S., Zeineddine, M. M., and Akkawi, N. (2017). Catastrophic relapses following initiation of dimethyl fumarate in two patients with neuromyelitis optica spectrum disorder. *Mult. Scler.* 23, 1297–1300. doi: 10.1177/1352458517694086

Yang, X., Ransom, B. R., and Ma, J. (2016). The role of AQP4 in neuromyelitis optica: more answers, more questions. *J. Neuroimmunol.* 298, 63–70. doi: 10.1016/j.jneuroim.2016.06.002

Zeka, B., Hastermann, M., Hochmeister, S., Kögl, N., Kaufmann, N., Schanda, K., et al. (2015). Highly encephalitogenic aquaporin 4-specific T cells and NMO-IgG jointly orchestrate lesion location and tissue damage in the CNS. *Acta Neuropathol.* 130, 783–798. doi: 10.1007/s00401-015-1501-5

Zekeridou, A., and Lennon, V. A. (2015). Aquaporin-4 autoimmunity. *Neurol. Neuroimmunol. Neuroinflamm.* 2:e110. doi: 10.1212/NXI.0000000000000110

Zeng, X., Sun, X., Gao, L., Fan, Y., Ding, J., and Hu, G. (2007). Aquaporin-4 deficiency down-regulates glutamate uptake and GLT-1 expression in astrocytes. *Mol. Cell. Neurosci.* 34, 34–39. doi: 10.1016/j.mcn.2006.09.008

Zerangue, N., and Kavanaugh, M. P. (1996). Flux coupling in a neuronal glutamate transporter. *Nature* 383, 634–637. doi: 10.1038/383634a0

Zettl, U. K., Stüve, O., and Patejdl, R. (2012). Autoimmunity Reviews Immune-mediated CNS diseases: a review on nosological classification and clinical features. *Autoimmun. Rev.* 11, 167–173. doi: 10.1016/j.autrev.2011.05.008

Zhao, X., Marszalec, W., Toth, P. T., Huang, J., Yeh, J. Z., and Narahashi, T. (2006). *In vitro* galantamine-memantine co-application: mechanism of beneficial action. *Neuropharmacology* 51, 1181–1191. doi: 10.1016/j.neuropharm.2006.08.007

Zhou, Y., and Danbolt, N. C. (2013). GABA and glutamate transporters in brain. *Front. Endocrinol.* 4:165. doi: 10.3389/fendo.2013.00165

Zhou, Y., and Danbolt, N. C. (2014). Glutamate as a neurotransmitter in the healthy brain. *J. Neural Transm.* 121, 799–817. doi: 10.1007/s00702-014-1180-8

Zimmer, E. R., Parent, M. J., Souza, D. G., Leuzy, A., Lecrux, C., Kim, H. I., et al. (2017). [^{18}F]FDG PET signal is driven by astroglial glutamate transport. *Nat. Neurosci.* 20, 393–395. doi: 10.1038/nn.4492

Conflict of Interest Statement: AS has received a scholarship from Conselho Nacional de Desenvolvimento Científico e Tecnológico (CNPq/Brazil). DKS has received a scholarship from the Ministry of Education, Culture, Sports, Science and Technology (MEXT) of Japan; a Grants-in-Aid for Scientific Research from the Japan Society for the Promotion of Science (KAKENHI 15K19472); research support from CNPq/Brasil (425331/2016-4), FAPERGS/MS/CNPq/SESRS (03/2017) PPSUS/Brazil, TEVA (research grant for EMOCEMP Investigator Initiated Study), and Euroimmun AG (Neuroimmunological Complications associated with Arboviruses); and speaker honoraria from Biogen, Novartis, Genzyme, TEVA, Merck-Serono, Roche, and Bayer and has participated in advisory boards for Shire, Roche, TEVA, Merck-Serono and Quest/Athena Diagnostics.

The remaining authors declare that the research was conducted in the absence of any commercial or financial relationships that could be construed as a potential conflict of interest.

frontiers in Cellular Neuroscience

ORIGINAL RESEARCH
published: 11 June 2019
doi: 10.3389/fncel.2019.00240

Ketamine Within Clinically Effective Range Inhibits Glutamate Transmission From Astrocytes to Neurons and Disrupts Synchronization of Astrocytic SICs

Yu Zhang[1,2†], Sisi Wu[2†], Liwei Xie[2†], Shouyang Yu[3], Lin Zhang[2], Chengxi Liu[3], Wenjing Zhou[2] and Tian Yu[2]*

[1] Department of Anesthesiology, Affiliated Hospital of Zunyi Medical University, Guizhou, China, [2] The Key Laboratory of Anesthesia and Organ Protection, Zunyi Medical University, Guizhou, China, [3] The Key Laboratory of Brain Science, Zunyi Medical University, Guizhou, China

OPEN ACCESS

Edited by:
Giovanni Cirillo,
Second University of Naples, Italy

Reviewed by:
Rheinallt Parri,
Aston University, United Kingdom
Livio Luongo,
Second University of Naples, Italy
Changyu Jiang,
Duke University, United States

***Correspondence:**
Tian Yu
dllyutian@163.com

[†] These authors have contributed equally to this work

Specialty section:
This article was submitted to Cellular Neurophysiology, a section of the journal Frontiers in Cellular Neuroscience

Received: 14 December 2018
Accepted: 14 May 2019
Published: 11 June 2019

Citation:
Zhang Y, Wu S, Xie L, Yu S, Zhang L, Liu C, Zhou W and Yu T (2019) Ketamine Within Clinically Effective Range Inhibits Glutamate Transmission From Astrocytes to Neurons and Disrupts Synchronization of Astrocytic SICs. Front. Cell. Neurosci. 13:240. doi: 10.3389/fncel.2019.00240

Background: Astrocytes are now considered as crucial modulators of neuronal synaptic transmission. General anesthetics have been found to inhibit astrocytic activities, but it is not clear whether general anesthetics within the clinical concentration range affects the astrocyte-mediated synaptic regulation.

Methods: The effects of propofol, dexmedetomidine, and ketamine within clinically effective ranges on the slow inward currents (SICs) were tested by using the whole-cell recording in acute prefrontal cortex (PFC) slice preparations of rats. Astrocytes culture and HPLC were used to measure the effects of different anesthetics on the glutamate release of astrocytes.

Results: Propofol and dexmedetomidine showed no significant effect on the amplitude or frequency of SICs. Ketamine was found to inhibit the frequency of SICs in a concentration-dependent manner. The SICs synchronization rate of paired neurons was inhibited by 30 μM ketamine (from 42.5 ± 1.4% to 9.6 ± 0.8%) and was abolished by 300 μM ketamine. The astrocytic glutamate release induced by DHPG, an agonist of astrocytic type I metabotropic glutamate receptors, was not affected by ketamine, and ifenprodil, a selective antagonist of GluN1/GluN2B receptor, blocked all SICs and enhanced the inhibitory effect of 30 μM ketamine on the frequency of SICs. Ketamine at low concentration (3 μM) could inhibit the frequency of SICs, not the miniature excitatory postsynaptic currents (mEPSCs), and the inhibition rate of SICs was significantly higher than mEPSCs with 30 μM ketamine (44.5 ± 3% inhibition vs. 28.3 ± 6% inhibition).

Conclusion: Our data indicated that ketamine, not propofol and dexmedetomidine, within clinical concentration range inhibits glutamatergic transmission from astrocytes to neurons, which is likely mediated by the extrasynaptic GluN1/GluN2B receptor activation.

Keywords: ketamine, slow inward current, astrocyte, GluN2B receptor, neuromodulation

HIGHLIGHTS

- Astrocytic glutamatergic activity is inhibited by ketamine at clinically relevant concentration.
- Synchronizations of astrocytic SICs are disrupted by ketamine.
- The same dose of ketamine inhibits SICs more obviously than mEPSCs.

INTRODUCTION

Astrocytes, like neurons, are important participants in the brain's integration and processing of information. Neuron-astrocyte network modulates advanced neural activities such as cognition (Yeh et al., 2015), emotion (Oliveira et al., 2015), motor (Acton et al., 2018), and sensory processing (Lopez-Hidalgo et al., 2017). Astrocytes release important neurotransmitters such as glutamate and GABA and participate in synaptic transmission (Araque et al., 2014). Besides, astrocytes express a variety of neurotransmitter receptors and perceive the activity of peripheral neurons (Pannasch and Rouach, 2013). So astrocytes interact with neurons dynamically and regulate pre-synaptic and post-synaptic activities. Recent studies have found that the activities of astrocytes are affected by general anesthetics (Thrane et al., 2012; Liu et al., 2016), but the effects of general anesthetics on the astrocyte-neuron transmission have not been systematically explored.

The glutamate that spontaneously released from astrocytes produces slow inward currents (SICs) via the extrasynaptic, GluN2B-containing NMDA receptors on neighboring neurons (Shigetomi et al., 2008). When compared with the miniature excitatory postsynaptic currents (mEPSCs), SICs exhibit significantly slower rise and decay times (Kovacs and Pal, 2017). SICs persists when neuronal and synaptic activity is suppressed, and both pharmacological and mechanical stimulation of astrocytes can induce SICs in neighboring neurons (Angulo et al., 2004). The physiological significance of SICs is to promote synchrony of neuronal activity, thus coordinating the activity of a brain area in a wider range. For example, in the thalamus, hippocampus and nucleus accumbens, researchers have found this extrasynaptic NMDAR response can occur synchronously in multiple neurons (Fellin et al., 2004; Pirttimaki et al., 2011).

Many studies of the mechanism of anesthesia believe that the loss of consciousness induced by general anesthetics is associated with a temporary breakdown of cortical functional connections, specifically the collapse of the synchronous activity pattern of cortical neurons, which makes the cortex unable to integrate information (Alkire et al., 2008; Lee et al., 2009; Rathmell and Wanderer, 2016). A single astrocyte makes about 100,000 synaptic connections with the surrounding neurons (Perea et al., 2014a), which synchronize the activity of neurons of the local brain area. So it is important to figure out the effects of anesthetics on the astrocyte-neuron activities.

In this work, we selected three anesthetics in clinical concentration: propofol (agonist of $GABA_A$ receptor), ketamine (antagonist of NMDA receptor) and dexmedetomidine (agonist of α2-adrenergic receptors), which are agonist or antagonist of distinct receptors and all three drugs can induce hypnosis or loss of consciousness. The effects of the three distinct anesthetics on the astrocyte-derived SICs in acute cortical slices of rats were investigated. Our research may contribute to improving the understanding of the role of astrocytes in the mechanisms of loss of consciousness induced by general anesthetics.

MATERIALS AND METHODS

Animals

All the experimental protocols were reviewed and approved by the Zunyi Medical University Animal Care and Use Committees (no. 2017-69 for pre-registration). According to the Guide for the Care and Use of Laboratory Animals published by the National Institutes of Health (Eighth Edition, 2011), the infant rats were reared with their mother in a specific pathogen-free animal room with controlled temperature (22–25°C) and a 12-hour light/dark cycle. All the rats had free access to a standard chow diet and purified drinking water.

Slice Preparation

Coronal prefrontal cortex (PFC) slices (300 μm) were prepared from Sprague Dawley rats at postnatal day 21 (P21) to P40. Rats were anesthetized with chloral hydrate (10% wt/vol) and then perfused transcardially with ice-cold oxygenated (95% O_2/ 5% CO_2) high-sucrose solution containing (in mM) 2.5 KCl, 1.25 NaH_2PO_4, 2 Na_2HPO_4, 2 $MgSO_4$, and 26 $NaHCO_3$. The Rats were then decapitated to remove the brains. In a sectioning plate filled with ice-cold oxygenated high-sucrose solution, the isolated brain was sectioned at 300 μm using a vibratome (HM650V, Thermo, United States). After sectioning, the slices were incubated for 1 h at 34°C in an oxygenated artificial cerebrospinal fluid (ACSF) containing (in mM): 124 NaCl, 4.5 KCl, 2.0 $CaCl_2$, 1.0 $MgCl_2$, 1.2 NaH_2PO_4, 26 $NaHCO_3$, 10 glycine, 10 glucose, pH 7.32.

Electrophysiology

Glial cells and neurons were visually identified on an infrared-differential interference contrast optics (Olympus, Japan). Whole-cell patch-clamp recordings were performed from pyramidal neurons in the lateral prefrontal regions. For SICs recording, the internal solution contained (in mM): 135 CsCl, 8 NaCl, 4 Mg-ATP, 10 HEPES, 0.6 EGTA and 0.3 Na_2-GTP, 310 mOsmol/L, pH 7.2. Slices were perfused in a chamber at 2–3 ml/min with an ACSF contained 100 micro molar picrotoxin (antagonist of gamma-aminobutyric acid A subtype receptor, $GABA_A$) and 1 μM tetrodotoxin (TTX) (Angulo et al., 2004), which prevented the interference of action potential and inhibitory synaptic neurotransmission on the SICs recording. Whole-cell patch-clamp experiments were conducted with EPC10 amplifier (HEKA Elektronik, Germany).

According to the nature of whole-cell recording, there is no randomization was performed.

Pharmacology

In this experiment, the concentrations of the three general anesthetics were chosen based on their clinically effective ranges. For propofol, an agonist of $GABA_A$ receptors, the plasma concentration to induce loss of consciousness in rat is around 10 μM (Yang et al., 1995); For ketamine, an antagonist of NMDA receptors, the plasma concentration of rats after intraperitoneal injection is around 30 μM (Ganguly et al., 2018); For dexmedetomidine, an agonist of alpha2-adrenergic receptors, the plasma concentration causing unconsciousness is around 40 nM (Plourde and Arseneau, 2017). The experimental concentrations of three drugs were 0.1, 1, 10, 20, and 40-fold of their clinically relevant concentrations. Propofol injectable emulsion (Diprivan, AstraZeneca, United States) was diluted to a final concentration in perfusion solution, while the perfusion solution containing the same concentration of emulsion (100 mg/mL soybean oil, 22.5 mg/mL glycerol, 12 mg/mL egg lecithin and 0.005% disodium edetate) was used as the control solution for experiments with propofol. Ketamine (Fujian Gutian Pharmaceutical Co., Ltd., China) and dexmedetomidine (Jiangsu Nhwa Pharmaceutical Co., Ltd., China) were diluted to experimental concentrations in perfusion solution.

In certain experiments, slices were treated with DHPG, an agonist of type I metabotropic glutamate receptors, to induce glutamate release from astrocytes (Porter and McCarthy, 1996). Some slices were treated with 1 mM fluorocitrate (a glia-specific metabolic inhibitor) for 1 h to inhibit astrocytic activity (Martín et al., 2007). Other antagonists included ifenprodil (5 μM), a GluN2B-specific NMDA receptor blocker; D(-)-2-Amino-5-phosphonopentanoic acid (D-AP5, 50 μM), a general NMDA receptor antagonist; tetanus neurotoxin (TeNT, 2 μM), which blocks the synaptic release of neurotransmitters; MK-801, 20 μM, a non-competitive antagonist of NMDA receptors; 2,3-Dihydroxy-6-nitro-7- sulfamoyl-benzo[f]quinoxaline (NBQX, 30 μM), a specific antagonist of non-NMDA (AMPA) glutamate receptors; TCN-201, 10 μM, a selective antagonist of GluN2A receptor.

Astrocytes Culture

The dissociated subculture of cortical astrocytes was prepared and maintained as described previously (Zeng et al., 2008). Briefly, neonatal rat (1–2 days) was anesthetized and the prefrontal cortex was dissected surgically under sterile condition. The cortical tissue was cut and then incubated in 0.125% trypsin (Sigma, United States) at 37°C for 30 min, during which the trypsin was shaken once every 10 min. Then DMEM/F12 medium (Gibco, United States) containing 15% (v/v) fetal bovine serum was added to stop the action of trypsin. The cell suspension was centrifuged at 1000 rpm for 5 min to collect cells. The supernatant was discarded and the cells were suspended in complete medium containing DMEM/F12 and 15% (v/v) fetal bovine serum. Cells were planted in a flask and cultured in the incubator at 37°C in a humidified 5% CO_2-95% air atmosphere. After 15 days, flasks were shaken (180 rpm) for 18 h and the medium was replaced by new ones. The subculture of cortical astrocytes was made by two times of digestion and centrifugation in the same procedure as mentioned above.

Immunofluorescence

The subculture of astrocytes was planted in Petri dish containing DMEM/F12 complete medium and cultured for 24 h. Astrocytes were fixed in 4% paraformaldehyde for 30 min, washed with 0.01 mol/L phosphate-buffered saline (PBS) three times, permeated by 0.02 % TritonX-100 for 3 min, washed with 0.01 mol/L PBS three times. Astrocytes were incubated with rabbit anti-GFAP (1:1000, Abcam, United States) at 4°C overnight, followed by incubations with FITC-conjugated goat anti-rabbit IgG (1: 1000 in PBS, Sigma, United States) for 90 min. At last, DAPI (1:2000, Abcam) was applied for 5 min to label the nuclei of all astrocytes. After staining, Petri dishes were examined using a Leica SP2 confocal microscope (Leica, Germany).

Analysis of Extracellular Glutamate Concentration

The concentration of extracellular glutamate was identified using HPLC with a fluorescence detector. HPLC was performed based on the methods previously published with some adjustment (Zeng et al., 2008) and the tester was blinded to the procedure of supernatant harvest. The HPLC system (1260 Infinity, Agilent, United States) comprised of a quaternary pump system (G1311B), fluorescence detector (G1321B, λex = 337 nm, λem = 457 nm), HPLC chemo-station, a 5 μm biophase octadecylsilyl and analytical column (150 mm × 4.6 mm). All astrocytes were seeded in 6-well plates and employed for individual tests when astrocytes produced a confluent layer 5 days after seeding. At this stage, the culturing medium was discarded and washed two times with 0.01 PBS, after that incubated with the free-serum medium. 10 μM DHPG (made with 0.01 M PBS) was added to the various wells and supernatant was harvested at 2, 4, 6, 8, and 10 min, respectively. Supernatants were derivatized with O-phthalaldehyde/beta-mercaptoethanol (OPA) for 2 min prior to injection. The mobile phase was composed of 0. 01 M Na2HPO4, 0.1 mM EDTA and 30% methanol. The system was operated at 38°C with a flow rate of 1 mL/min. The calibration curves and quantifications were deduced on the maximum areas calculated with Agilent Lab Advisor software. Control experiments were performed with adding 0.01 M PBS to wells after which supernatants were harvested to determine the basal amount of glutamate. Effects of the three anesthetics (diluted to 0.1, 1, 10, and 100-fold of their clinically relevant concentrations in 0.01 M PBS) were always compared with the controls performed on the same culture preparation. The same experiments were repeated in five different astrocyte cultures.

Data Collection and Analysis

Patchmaster 2.0 software (HEKA Elektronik, Germany) was used for data acquisition, while data analysis was performed by Spike 2 software (CED, ENGLAND). For recording SICs and mEPSC, voltage-clamp traces were recorded at a holding potential of −60 mV. The noise level of mEPSC was set as 5 pA while SICs as 30 pA. Only stable current traces that exhibit a single peak distribution in the on-line histogram analysis were used for subsequent analysis. Average amplitude and frequency of SICs and mEPSC were calculated from 30 min long current traces before and after drug application. The series resistance was continuously monitored during the recording and was accepted when the series resistance of the current was less than 30 Ω and with less than 10% change. The amplitude of the SICs is the difference between the SICs peak and the average of the current baseline within the 20 ms before the appearance of the SICs. The zero to one hundred percent rise time and 10 to 90% decay time for SIC events were calculated with single exponential fits. Power And Sample Size software was used to predetermine the sample size of recorded neurons. All data were presented as mean ± SD. Statistical analysis of two groups was performed with Student's *t*-test by utilizing GraphPad PRISM 6 Software (GraphPad Software Inc., United States). When multiple groups were compared, statistical analysis was performed with one-way analysis of variance (ANOVA) followed by Brown-Forsythe test. Cumulative probability curves for SICs rise times and decay times were tested by Kolmogorov-Smirnov test. Statistical significance at the $p < 0.05$ level were considered statistically significant.

RESULTS

SICs Is Generated by Glutamate Release From Astrocytes

First, we investigated the presence of SICs on PFC neurons. When we held PFC neurons near their resting membrane potential (−60 mV) in magnesium-free ACSF (as $MgCl_2$ was not administered to the solution), which prevent the voltage-dependent block of glutamate receptors of the NMDA subtype, and 1 μM TTX was applied into the ACSF to block action potential propagation in the neuronal network, we observed spontaneous SICs in 89% of the recorded neurons (63 neurons from 20 rats) with comparable parameters to literature data (Pirttimaki and Parri, 2012). The average frequency of SICs was 0.78 ± 0.16/min, with the amplitude of 96.9 ± 37.9 pA, a rise time of 96.8 ± 30.5 ms and a decay time constant of 269.5 ± 32.8 ms (38 events from 22 neurons, **Figures 1A,C**). The parameters of SICs can be unambiguously separated from miniature excitatory postsynaptic currents (mEPSCs) (**Figures 1A,B**). The decay time constant of mEPSCs were 25.68 ± 2.6 ms (45 events from 9 neurons, **Figures 1B,C**), which were two magnitudes faster than SICs, thus SICs are clearly distinguishable. We then sought evidence to prove whether the neuronal SICs generation could be affected by pharmacological manipulations known to inhibit or activate astrocytes in PFC slices. First, the slices were treated with 1 mM fluorocitrate for 1 h prior to recording. This drug, a specific blocker of astrocytes, inhibits the Krebs cycle of astrocytic metabolism (Largo et al., 1996). Under the same experimental arrangement described above, no SICs was detected from fluorocitrate incubated slices (12 neurons from 3 rats, **Figures 1D,E**). Second, when 10 μM DHPG (agonist of astrocytic type I metabotropic glutamate receptors) were bath applied for pharmacological activation of astrocytes (Porter and McCarthy, 1996), we observed a significant increase in the frequency of the SICs (**Figures 1D,E**). The 10–90% rise and decay time of the slow currents recorded before and during DHPG showed no different (**Figure 1F**). Furthermore, SICs were still present after slice incubation (2 h) with 2 μM tetanus neurotoxin (TeNT) (**Figures 1D,E**), which blocks the synaptic release of neurotransmitters (Link et al., 1992). Altogether, the above observations strongly suggest that SICs are of the astrocytic origin.

The Astrocytic Glutamatergic Transmission Was Inhibited by Ketamine at a Clinically Relevant Concentration

To study the effects of different general anesthetics on the astrocytic glutamatergic transmission, the selected anesthetics were added to oxygenated ACSF for a slice pre-incubation (15 min), the solution containing anesthetic were continuously perfused during whole-cell patch-clamp recordings. Due to the different preparation protocols of the 3 drugs (see section "Materials and Methods"), SICs recording in slices under ASCF containing emulsion was taken as the control for propofol, while SICs recording under normal ASCF was taken as the control for both ketamine and dexmedetomidine. The concentrations tested for each general anesthetic were chosen as 0.1, 1, 10, 20, and 40-fold of their clinically relevant concentrations (see section Materials and Methods). For propofol, the test concentrations were set as 1, 10, 100, 200, and 400 μM. Propofol with all selected concentrations showed no significant effect on the amplitude or frequency of SICs (**Figures 2B,E**). Dexmedetomidine with selected concentrations (4, 40, 400, 800, and 1600 nM) were also found ineffective in changing the amplitude or frequency of SICs (**Figures 2C,E**), indicating propofol and dexmedetomidine exert no effect on the astrocytic glutamatergic transmission within the clinically relevant concentration range. For ketamine, the test concentrations were 3, 30, 300, 600, and 1200 μM. We found that the frequency of SICs dropped to 0.53 ± 0.18 SICs/min at a concentration of 30 μM from 0.77 ± 0.16 SICs/min in control group (10 neurons from 5 slices, **Figure 2D**). The inhibition of the frequency of SICs reached 0.35 ± 0.15 SICs/min at 300 μM (8 neurons from 3 slices, **Figure 2D**). Ketamine with 600 (5 neurons from 3 slices) and 1200 μM (5 neurons from 3 slices) inhibited the frequency of SICs to 0.087 ± 0.06 and 0.083 ± 0.05%, respectively (**Figure 2D**). Ketamine with all selected concentrations did not change the amplitude of SICs (**Figure 2E**). When washed out for 15 min, the frequency of SICs recovered to about 80% (**Figure 2A**, the bottom trace) of the control level,

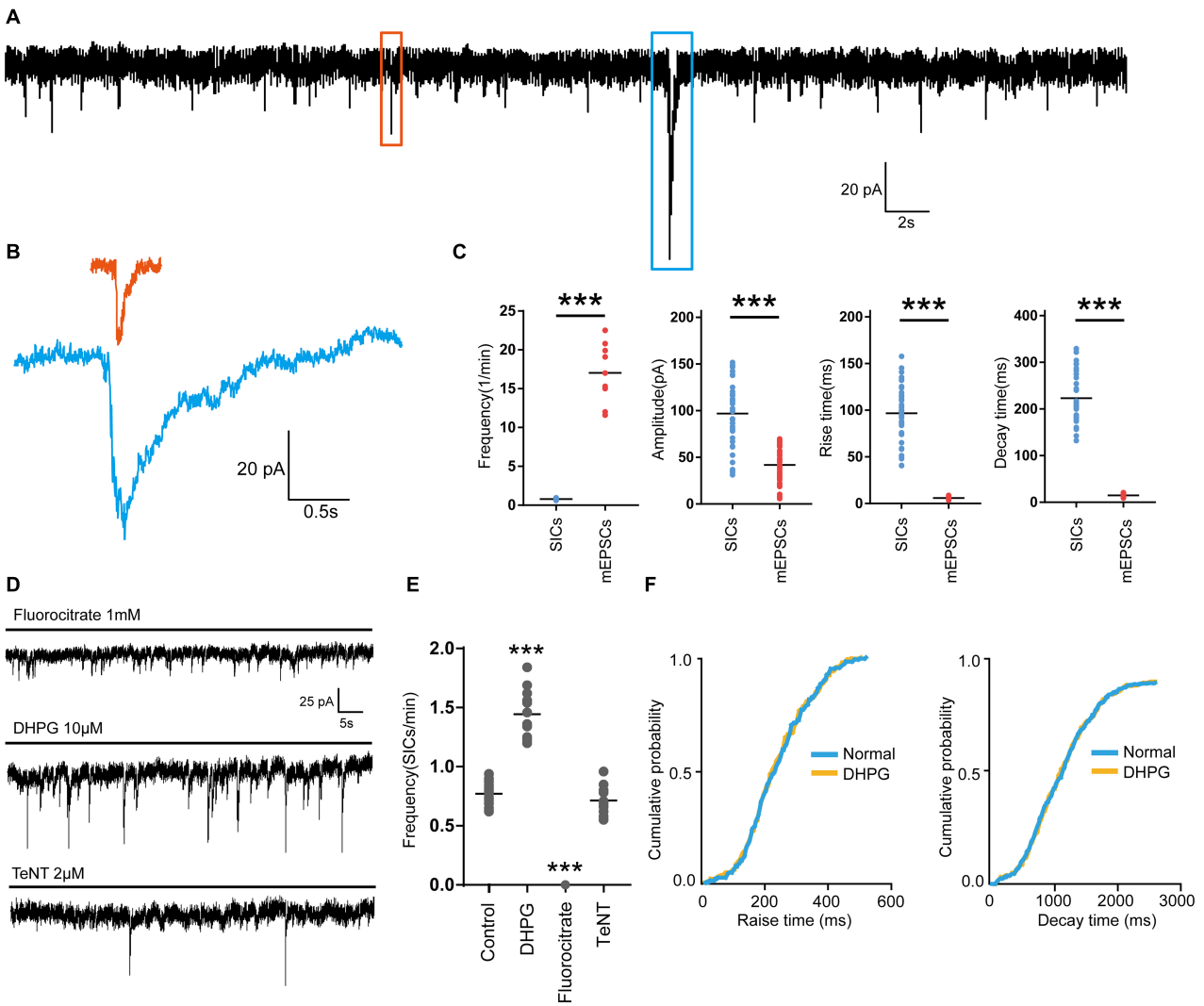

FIGURE 1 | Parameters of SICs and mEPSC from the prefrontal cortex neuron. **(A)**, Representative trace of SICs and mEPSCs recorded from a PFC neuron at a holding potential of –60 mV. The red square marks a mEPSC and a SIC is labeled by the blue square. **(B)** mEPSC (red) and SIC (blue) were showed in a larger scale. **(C)** Statistical summary of frequency, amplitude, rise and decay time of SICs and mEPSCs. Differences with statistically significant (***$p < 0.001$, compared with control) were verified by unpaired *t*-test. **(D)** Representative traces of SICs exposed to fluorocitrate, DHPG and TeNT administration. **(E)** Statistical summary of frequency of SICs recorded in 10 min before and after fluorocitrate, DHPG and TeNT administration. **(F)** Cumulative probability curves for SIC rise times and decay times for normal (blue line) and DHPG treatment (yellow line), no statistical difference, Kolmogorov-Smirnov test. Data were presented as mean ± SD. Dots represent individual data.

demonstrating that the inhibition induced by ketamine is largely reversible.

Synchronization of Astrocytic SICs Was Inhibited by Ketamine

SICs can occur simultaneously in adjacent pyramidal neurons, which promote synchrony of neuronal activity (Perea et al., 2014a). In the next series of experiments, we sought evidence whether ketamine can affect the synchronization of astrocytic SICs. Since propofol and dexmedetomidine at clinically relevant concentration showed no inhibitory action on the frequency of SICs, we did not examine their effects on SICs synchronization. Pairs of PFC neurons were patched where somata were within 20 μm (**Figure 3A**), and spontaneous activity was recorded in parallel in voltage clamp mode in a recording period of 10 min. When the delay between the onset of one SIC recorded in one neuron and the other SIC appearing in the paired neuron was <0.05 s, count as a valid synchronization of SICs (**Figure 3B**). We first record six pairs of PFC neurons distant by <20 μm under normal ACSF, during 10 min period, the occurrence rate of synchronized SICs was 42.5 ± 1.4% (68 SICs were recorded from 12 neurons) (**Figure 3C**, up panel and **Figure 3D**). Then we recorded 6 pairs of PFC neurons distant by <20 μm under ACSF containing 30 μM ketamine, the occurrence rate of synchronized SICs dropped to 9.6 ± 0.8% (36 SICs were recorded from

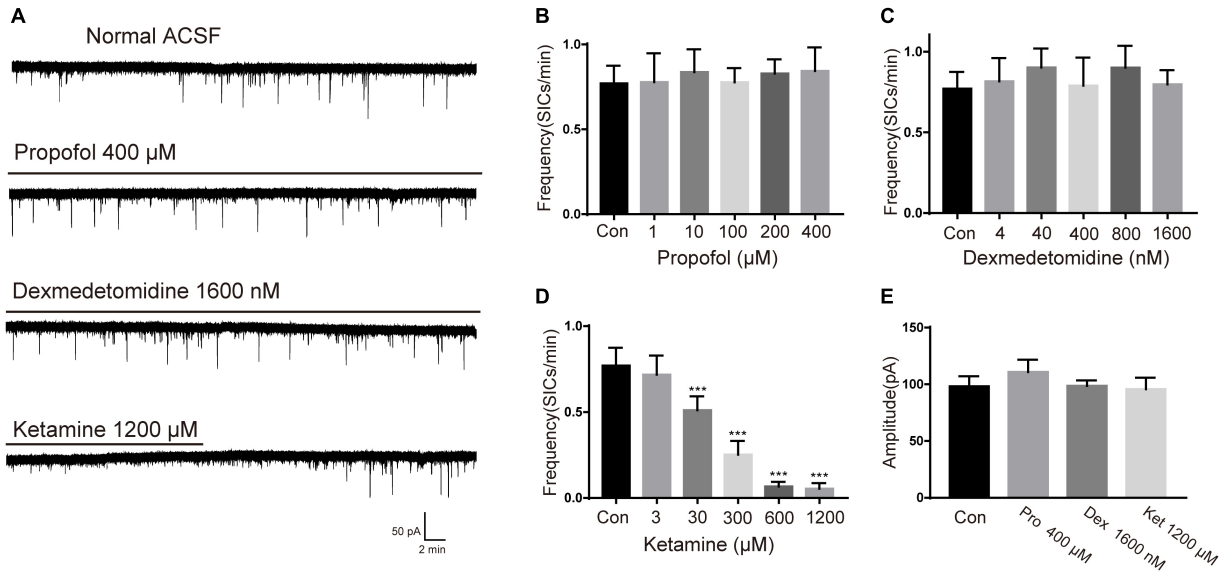

FIGURE 2 | Effects of propofol, dexmedetomidine and ketamine on SICs. **(A)** Example large scale traces of SICs exposed to the highest concentration of propofol, dexmedetomidine and ketamine. **(B–D)** bar graphs illustrate SICs frequency affected by three anesthetics with different concentrations. **(E)** Statistical summary of amplitude of SICs affected by three anesthetics with the highest concentration in this study. Differences with statistically significant (***$p < 0.001$, compared with control) were verified by one-way ANOVA followed by Brown-Forsythe test. Data were presented as mean ± SD. Con = control, Pro = propofol, Dex = dexmedetomidine, Ket = ketamine.

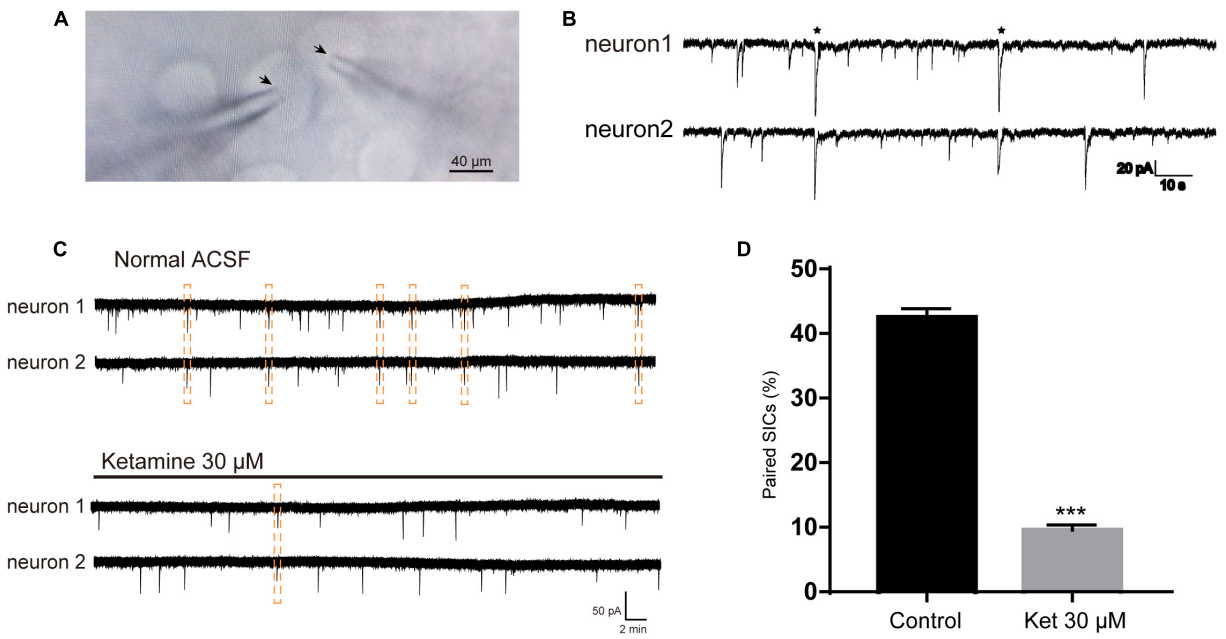

FIGURE 3 | Ketamine inhibit synchronized SICs from pair-recorded PFC neurons. **(A)** Infrared chromatic aberration photo of pair-recorded PFC neurons. Tips of glass microelectrodes were marked with arrow. **(B)** Example traces showed synchronized SICs in two different PFC neurons recorded simultaneously. Two pairs of synchronized SICs were marked by asterisks. **(C)** Example large scale traces of synchronized SICs exposed to normal ACSF and 30 μM ketamine, synchronized SICs were marked by dashed box. **(D)** Statistical summary of the occurrence rate of paired SICs. Differences with statistically significant (***$p < 0.001$, compared with control) were verified by unpaired *t*-test. Data were presented as mean ± SD.

12 neurons) (**Figure 3C**, bottom panel and **Figure 3D**). The occurrence rate of synchronized SICs was 0 when 300 μM ketamine were tested (5 SICs were recorded form 2 pairs of PFC neurons). These data thus indicate that ketamine at clinically relevant concentrations exerts a significant inhibitory effect on the astrocyte-mediated SICs synchronization.

Ketamine Exerts No Effects on the Astrocytic Glutamate Release

SICs are due to the spontaneous release of glutamate from astrocytes, thus the inhibitory actions of ketamine on SICs might be consequences of the decrease of glutamate release from astrocytes caused by ketamine. In order to investigate this possibility, we next explore whether ketamine inhibits DHPG-evoked glutamate release from cultured PFC astrocytes. PFC astrocytes were identified with immunofluorescence stained by mouse GFAP antibody (**Figure 4A**). The immunohistochemical staining after two generations showed that the purity of the astrocytes was more than 95% (data not shown). Glutamate efflux from astrocyte cultures was assayed with HPLC. The base level of glutamate release from cultured prefrontal cortex (PFC) astrocytes was 2.18 ± 0.84 μM (**Figures 4B,C**; five wells). Application of 10 μM DHPG for 10 min increased the concentration of glutamate to 6.18 ± 0.15 μM (**Figures 4B,C**; of five wells). Pre-incubation of ketamine (300 and 1200 μM) for 10 min could not influence the DHPG-induced glutamate efflux (5.96 ± 0.23 μM for ketamine 1200 μM + DHPG 10 μM; **Figures 4B,C**; of five wells), which suggest that DHPG-induced astrocytic glutamate release is not affected by ketamine.

Ketamine-Induced Inhibition of SICs Is Mediated by GluN1/GluN2B Receptors

Negative results with glutamate assay of astrocyte cultures raised the possibility that ketamine-induced inhibition of SICs was due to blockade of NMDA receptors. As ketamine is a non-selective antagonist for the NMDA receptor (Lord et al., 2013), we need to seek the NMDA receptor subtype responsible for SICs. The effects of different antagonists on SICs were present in **Figure 5A**. In the presence of 20 μM MK-801, a non-competitive antagonist of NMDA receptors, the frequency of SICs were dropped to 0.02 ± 0.01/min (**Figure 5B**, 10 neurons). However, spontaneous SICs were observed with normal frequency (0.98 ± 0.10/min) in 30 μM NBQX (**Figure 5B**, 5 neurons), a specific antagonist of non-NMDA (AMPA) glutamate receptors. Then we perfused selective antagonist of GluN1/GluN2B receptor, ifenprodil (5 μM) (Bettini et al., 2010), which inhibited the frequency of SICs significantly (**Figure 5B**, 10 neurons). We also found that 0.5 μM ifenprodil, not 10 μM TCN-201 [selective antagonist of GluN1/GluN2A receptor (Edman et al., 2012)] could significantly enhance the inhibitory effect of 30 μM ketamine on the frequency of SICs (from 0.65 ± 0.10/min to 0.29 ± 0.04/min, **Figure 5B**, 10 neurons). Such results suggest that the ketamine-induced inhibition of the frequency of SICs is due to the blockade of GluN1/GluN2B receptors by ketamine.

Astrocytic SICs Are More Sensitive to Ketamine Than Synaptic mEPSCs

Depending on the subunit composition, GluN1/GluN2A and GluN1/GluN2B receptors have distinct pharmacological and kinetic properties. GluN1/GluN2A receptor is a target of glutamate released from a synaptic source, which is characterized by rapid kinetics (mEPSCs) (Nakanishi et al., 1998). While extrasynaptic GluN1/GluN2B are activated by glutamate released from a non-synaptic (astrocytic) source, which is characterized by slow kinetics (SICs) (Angulo et al., 2004). Different in the source of glutamate and kinetic properties raised the possibility that ketamine may exert a different effect on the fast (synaptic) and slow (non-synaptic) glutamatergic transmission. In order to investigate this possibility, we compared the effect of 3, 30, and 300 μM ketamine on the GluN1/GluN2A and GluN1/GluN2B mediated currents. mEPSCs and SICs were recorded and distinguished by their frequency and decay time as stated above. The frequency of mEPSCs was 22.7 ± 3.4/min in control, and 22.1 ± 3.2/min with 3 μM ketamine, 16.9 ± 1.5/min with 30 μM ketamine, 2.3 ± 0.2/min with 300 μM ketamine. The frequency of SICs was 0.85 ± 0.12/min in control, and 0.72 ± 0.12/min with 3 μM ketamine, 0.48 ± 0.10/min with 30 μM ketamine, 0.06 ± 0.001/min with 300 μM ketamine (**Figure 6A**). In **Figure 6B**, inhibition rate of 3, 30, and 300 μM ketamine on mEPSCs and SICs were presented, which indicated that ketamine at low concentration (3 μM) could inhibit the frequency of SICs, but not mEPSCs. And, the inhibition rate of SICs was significantly higher than mEPSCs with 30 μM ketamine (44.5 ± 3% inhibition vs. 28.3 ± 6% inhibition). Taken together, one might conclude that GluN1/GluN2B mediated astrocytic excitatory current is more sensitive to ketamine.

DISCUSSION

In the present study, we demonstrated that ketamine significantly suppressed GluN1/GluN2B receptor-induced SICs in acute rats brain slice, in a concentration-dependent manner. On the contrary, propofol and dexmedetomidine did not affect SICs, which represent glutamatergic transmission from astrocytes to neurons. Three anesthetics were tested in the ranges that correspond to their respective plasma concentrations during anesthesia. Ketamine inhibited the frequency of SICs by more than 30% when used at 30 μM, which is around the plasma concentration of rats after intraperitoneal injection (Ganguly et al., 2018). Propofol and dexmedetomidine had no effect on the frequency of SICs, even at 40-fold of their clinically relevant concentrations (Franks, 2008; Plourde and Arseneau, 2017).

Connexins form functional gap junction channels that enable electrochemistry communication between adjacent astrocytes and neurons (Nagy and Rash, 2000). Early experiment (Liu et al., 2016) exploring anesthetic mechanism in astrocytes compared the effects of propofol, ketamine, and dexmedetomidine on the connexin channel functions of astrocytes. They reported that propofol was found to inhibit gap junction within clinically relevant ranges (100–150 μM), either ketamine nor dexmedetomidine had an effect on gap junction channels within clinically relevant ranges. Combined with our results, one can infer that both propofol and ketamine, at clinically relevant concentrations, are an effective compound in affecting the activities of astrocytes, however, they aimed at different targets. Propofol may inhibit the functional astrocytic network by inhibiting the activity of connexin channel and decreasing calcium signaling between astrocytes (Parys et al., 2010). While ketamine inhibits the glutamate transmission from astrocytes

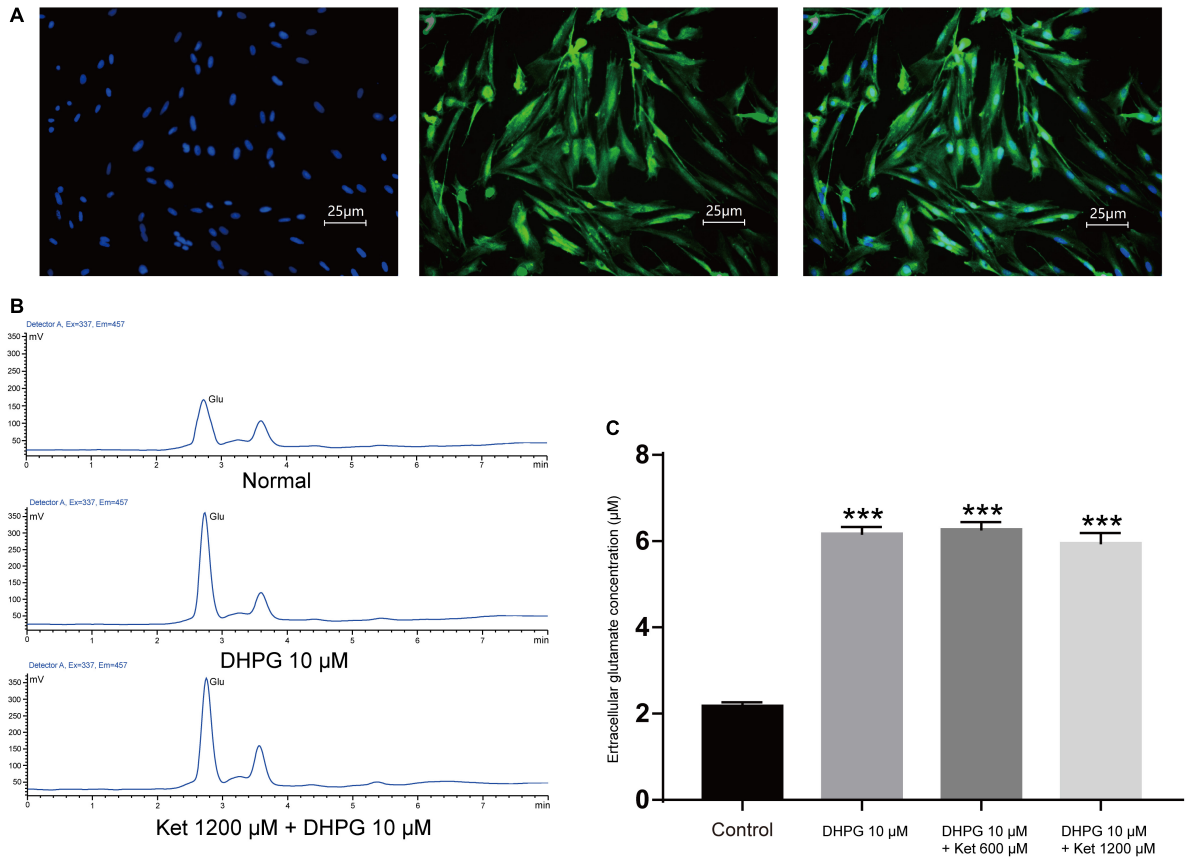

FIGURE 4 | Effect of ketamine on glutamate release from cultured prefrontal cortex astrocytes. **(A)** Micrographs of cultured prefrontal cortex astrocytes labeled for DAPI (left), GFAP (middle) their overlay (right). **(B)** HPLC chromatogram of glutamate in astrocyte culture medium after DHPG (middle) or ketamine (down) administration. **(C)** Statistical summary of the glutamate concentration. Differences with statistically significant (***$p < 0.001$, compared with control) were verified by one-way ANOVA followed by Brown-Forsythe test. Data were presented as mean ± SD. Glu = glutamate, Con = control, Ket = ketamine.

to neurons, thereby inhibiting the astrocytic regulation of neurons, especially the synchronous activity of nearby neurons (Fellin et al., 2004).

In this study, we found direct evidence for the inhibition of astrocyte-mediated SICs synchronization by ketamine at clinical concentrations. A significant 78% inhibition of the occurrence rate of synchronized SICs on paired PFC neurons was produced by 30 μM ketamine. Astrocytes play a key role for the synchrony of regional neurons, stimulation of one astrocyte can activate other astrocytes in the region and trigger continuous depolarization and high-frequency discharge of adjacent neurons (change and maintain new patterns of neuronal activity) (Perea et al., 2014a). Under the control of astrocytes, the cortex forms a wide range of neuronal clusters that receive and output special signals, and eventually from the neuronal basis to encode and integrate advanced neural information.

Astrocytes can release glutamate through calcium-dependent and calcium-independent mechanisms, such as vesicular release (Yaguchi and Nishizaki, 2010), the reverse operation of glutamate transporters (Yoshizumi et al., 2012) and the opening of hemichannels (Ye et al., 2003). Our present research did not focus on the specific mechanism by which astrocytes release glutamate. However, bath applications of DHPG were shown previously to trigger intracellular calcium transients in astrocytes (Muyderman et al., 2001). So DHPG increases the release of glutamate from astrocyte cultures support the involvement of a calcium-dependent release mechanism. Our results of glutamate assay showed that ketamine with 10-fold of the clinical concentration exerts no effects on the astrocytic glutamate release, which indicate that calcium-independent vesicular pattern of astrocytic glutamate release is not a potentially important mechanism in ketamine-induced inhibition of glutamatergic transmission between neurons and astrocytes. However, identifying the actual effects of ketamine or other anesthetics on the glia release glutamate *in vivo* animal model still need additional experiments.

Our work demonstrated that SICs are consequences of astrocytic activity. Stimulation of astrocytes by group I metabotropic glutamate receptor agonist led to the appearance of SICs, and inhibition of astrocytes by fluorocitrate prevented the development of these events. The astrocytic source of SICs was verified by optogenetic activation of astrocytes (Perea et al., 2014b), a more advanced technology allowing specific activation of astrocytes in slice preparations. Our results showed that SICs were prevented by ketamine or GluN1/GluN2B receptors

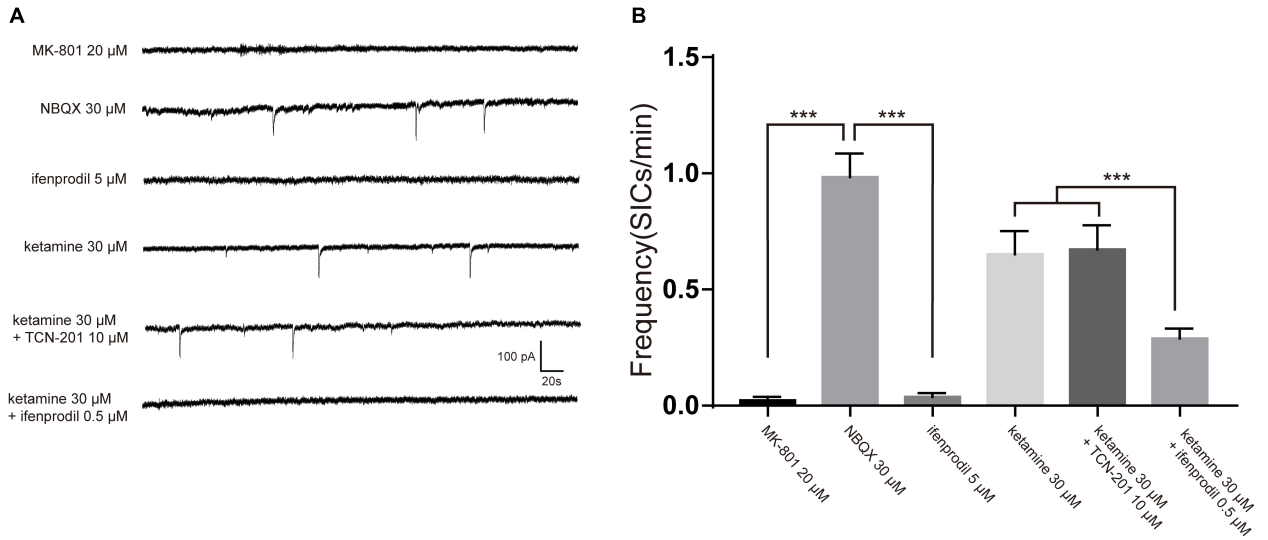

FIGURE 5 | The inhibition of SICs by ketamine was enhanced by selective antagonist of GluN1/GluN2B receptor. **(A)** Example traces of SICs with different antagonists administration. **(B)** Statistical summary of SICs frequency affected by different antagonists. Differences with statistically significant (***$p < 0.001$, compared with control) were verified by one-way ANOVA followed by Brown-Forsythe test. Data were presented as mean ± SD.

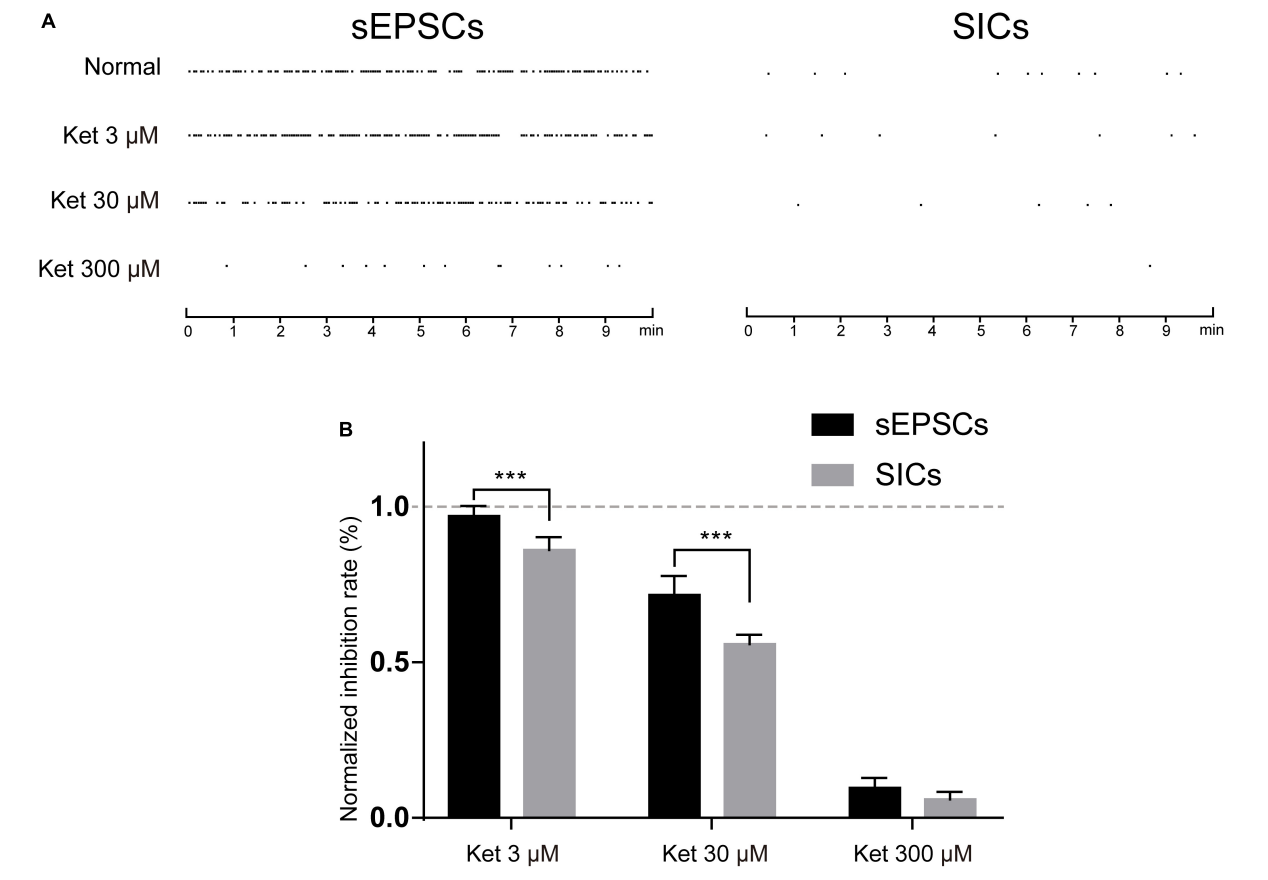

FIGURE 6 | The inhibitory effects of ketamine on mEPSCs and SICs. **(A)** events marker of mEPSCs (left) and SICs (right) in a representative 10 min period. Ketamine inhibited both mEPSCs and SICs in a concentration dependent manner. **(B)** Normalized inhibition rate of ketamine on mEPSCs and SICs. Differences with statistically significant (***$p < 0.001$, compared with control) were verified by two-way ANOVA with post tests. Data were presented as mean ± SD.

antagonists, which indicates that ketamine-induced inhibition of SICs is mediated by the extrasynaptic NMDA receptors containing NR2B subunits. However, it can be a matter debate whether GluN1/GluN2B receptors involved in the astrocyte-neuron modulation of ketamine are neuronal extrasynaptic or astrocytic receptors because functional NMDA receptors were found presenting on cortical astrocytes (Dzamba et al., 2013). As the SICs-blocking effects of ketamine were very similar to the inhibition caused by ifenprodil, we cannot clearly exclude the possibility that astrocytic NMDA receptors contribute to the ketamine-inhibition of SICs. Furthermore, based on the facts that astrocytes express functional AMPA receptors (Matthias et al., 2003) and ketamine is an indirect AMPA receptor agonists (Krystal et al., 2013), one may hypothesize that ketamine potentiates the glutamatergic AMPA transmission while inhibits SICs. We did not add selective AMPA antagonist when evaluating the effects of ketamine on SICs, thus the low concentration of ketamine was insufficient to inhibit mEPSCs may due to the ketamine-induced potentiation of glutamatergic AMPA transmission.

To the best of our knowledge, our present work first found direct evidence prove that astrocyte-neuron glutamatergic transmission, which represented by SICs, were inhibited by ketamine in clinical concentration. The effects of general anesthetics on non-neuronal cells and the potential mechanism by which these drugs induce unconsciousness are not widely appreciated. Most previous studies focused on the effects of general anesthetics on the neuronal injury related to intracellular calcium homeostasis (Mantz et al., 1994; Yang et al., 2008) or glutamate uptake in astrocytes (Miyazaki et al., 1997; Sitar et al., 1999). One study explored the conscious targets of anesthetics (including ketamine) in astrocytes (Thrane et al., 2012). Combined with our findings, it is important that direct suppression of astrocytic activities (such as synchronized calcium signals and SICs) by anesthetics were found as a potential mechanism under their unconsciousness effects. In addition, the previous study reported that anesthetic doses of isoflurane are insufficient to affect neuronal responses but sufficient to obviously inhibit sensory-evoked astrocyte calcium transients (Schummers et al., 2008). Their results are in line with our present finding showed that low concentration of ketamine was insufficient to inhibit mEPSCs but sufficient to inhibit astrocytic SICs. All these studies indicate that, compared with neurons, astrocytes activities are more vulnerable to anesthetics. So the inhibition of astrocytic function may play a key role in the early stage of unconsciousness induced by general anesthetics.

Ketamine at sub-anesthetic doses acts as a fast-acting antidepressant (Krystal et al., 2013). The underlying mechanisms involve activating the mammalian target of rapamycin (mTOR) pathway leading to improvement of synaptic signaling (Li et al., 2010), actions on the glutamatergic system, 5-HT system and dopaminergic system (De Gregorio et al., 2018), improving synaptogenesis (Liu et al., 2012) and neurotrophic function (Abdallah et al., 2015). Thus the ability of ketamine to modulate the SICs at sub-anesthetic doses in its antidepressant effects needs to be discussed. Many factors of stress response such as immunologic attack, increased levels of reactive oxygen species and reduced levels of free radical scavengers lead to astrocytes loss (Banasr and Duman, 2008). Because astrocytes are centrally involved in glutamate inactivation, astrocytes loss may elevate glutamate levels in both synaptic and extrasynaptic spaces. The astrocytic origin of SICs was confirmed by our results, thus the inhibition of astrocytic SICs by ketamine may depress glutamate neurotransmission when extracellular glutamate level was elevated by astrocytes loss, which in turn compromising functional astrocyte–neuron connectivity during the depression. Moreover, the blockade of extrasynaptic NMDA receptors also appears to be critical to the antidepressant effects of ketamine (Krystal et al., 2013), and we proved that ketamine inhibited SICs by blocking the extrasynaptic NMDA receptors containing NR2B subunits supporting such theory.

CONCLUSION

In summary, the present findings suggest that by blocking GluN1/GluN2B receptors, ketamine have an inhibitory role in astrocytic glutamatergic transmission. The decrease of astrocyte-mediated SICs synchronization due to ketamine administration at clinical concentration may have serious implications for the development of dissociative cognitive impairment during ketamine anesthesia.

AUTHOR CONTRIBUTIONS

YZ, SW, and LX analyzed the data and drafted the manuscript. CL, SY, LZ, and WZ collected the data. TY approved the final version of the manuscript.

FUNDING

The study is supported in part by the National Natural Science Foundation of China (Beijing, China) Grant Nos. 81460219 and 81760259 to YZ and 81571026 to TY and Guizhou Science and Technology Project (2017-1430) to YZ.

REFERENCES

Abdallah, C. G., Sanacora, G., Duman, R. S., and Krystal, J. H. (2015). Ketamine and rapid-acting antidepressants: a window into a new neurobiology for mood disorder therapeutics. *Annu. Rev. Med.* 66, 509–523. doi: 10.1146/annurev-med-053013-062946

Acton, D., Broadhead, M. J., and Miles, G. B. (2018). Modulation of spinal motor networks by astrocyte-derived adenosine is dependent on D1-like dopamine receptor signaling. *J. Neurophysiol.* 120, 998–1009. doi: 10.1152/jn.00783.2017

Alkire, M. T., Hudetz, A. G., and Tononi, G. (2008). Consciousness and anesthesia. *Science* 322, 876–880. doi: 10.1126/science.1149213

Angulo, M. C., Kozlov, A. S., Charpak, S., and Audinat, E. (2004). Glutamate released from glial cells synchronizes neuronal activity in the hippocampus. *J. Neurosci.* 24, 6920–6927. doi: 10.1523/JNEUROSCI.0473-04.2004

Araque, A., Carmignoto, G., Haydon, P. G., Oliet, S. H., Robitaille, R., and Volterra, A. (2014). Gliotransmitters travel in time and space. *Neuron* 81, 728–739. doi: 10.1016/j.neuron.2014.02.007

Banasr, M., and Duman, R. S. (2008). Glial loss in the prefrontal cortex is sufficient to induce depressive-like behaviors. *Biol. Psychiatry* 64, 863–870. doi: 10.1016/j.biopsych.2008.06.008

Bettini, E., Sava, A., Griffante, C., Carignani, C., Buson, A., Capelli, A. M., et al. (2010). Identification and characterization of novel NMDA receptor antagonists selective for NR2A- over NR2B-containing receptors. *J. Pharmacol. Exp. Ther.* 335, 636–644. doi: 10.1124/jpet.110.172544

De Gregorio, D., Enns, J. P., Nunez, N. A., Posa, L., and Gobbi, G. (2018). d-Lysergic acid diethylamide, psilocybin, and other classic hallucinogens: mechanism of action and potential therapeutic applications in mood disorders. *Prog. Brain Res.* 242, 69–96. doi: 10.1016/bs.pbr.2018.07.008

Dzamba, D., Honsa, P., and Anderova, M. (2013). NMDA receptors in glial cells: pending questions. *Curr. Neuropharmacol.* 11, 250–262. doi: 10.2174/1570159X11311030002

Edman, S., McKay, S., Macdonald, L. J., Samadi, M., Livesey, M. R., Hardingham, G. E., et al. (2012). TCN 201 selectively blocks GluN2A-containing NMDARs in a GluN1 co-agonist dependent but non-competitive manner. *Neuropharmacology* 63, 441–449. doi: 10.1016/j.neuropharm.2012.04.027

Fellin, T., Pascual, O., Gobbo, S., Pozzan, T., Haydon, P. G., and Carmignoto, G. (2004). Neuronal synchrony mediated by astrocytic glutamate through activation of extrasynaptic NMDA receptors. *Neuron* 43, 729–743. doi: 10.1016/j.neuron.2004.08.011

Franks, P. N. (2008). General anaesthesia. from molecular targets to neuronal pathways of sleep and arousal. *Nat. Rev. Neurosci.* 9, 370–386. doi: 10.1038/nrn2372

Ganguly, S., Panetta, J. C., Roberts, J. K., and Schuetz, E. G. (2018). Ketamine pharmacokinetics and pharmacodynamics are altered by Pgp and Bcrp efflux transporters in mice. *Drug Metab. Dispos.* 46, 1014–1022. doi: 10.1124/dmd.117.078360

Kovacs, A., and Pal, B. (2017). Astrocyte-dependent slow inward currents (SICs) participate in neuromodulatory mechanisms in the pedunculopontine nucleus (PPN). *Front. Cell Neurosci.* 11:16. doi: 10.3389/fncel.2017.00016

Krystal, J. H., Sanacora, G., and Duman, R. S. (2013). Rapid-acting glutamatergic antidepressants: the path to ketamine and beyond. *Biol. Psychiatry* 73, 1133–1141. doi: 10.1016/j.biopsych.2013.03.026

Largo, C., Cuevas, P., Somjen, G. G., Martin, R., and del Rio Herreras, O. (1996). The effect of depressing glial function in rat brain in situ on ion homeostasis, synaptic transmission, and neuron survival. *J. Neurosci.* 16, 1219–1229. doi: 10.1523/jneurosci.16-03-01219.1996

Lee, U., Mashour, G. A., Kim, S., Noh, G. J., and Choi, B. M. (2009). Propofol induction reduces the capacity for neural information integration: implications for the mechanism of consciousness and general anesthesia. *Conscious. Cogn.* 18, 56–64. doi: 10.1016/j.concog.2008.10.005

Li, N., Lee, B., Liu, R. J., Banasr, M., Dwyer, J. M., Iwata, M., et al. (2010). mTOR-dependent synapse formation underlies the rapid antidepressant effects of NMDA antagonists. *Science* 329, 959–964. doi: 10.1126/science.1190287

Link, E., Edelmann, L., Chou, J. H., Binz, T., Yamasaki, S., Eisel, U., et al. (1992). Tetanus toxin action: inhibition of neurotransmitter release linked to synaptobrevin proteolysis. *Biochem. Biophys. Res. Commun.* 189, 1017–1023. doi: 10.1016/0006-291x(92)92305-h

Liu, R. J., Lee, F. S., Li, X. Y., Bambico, F., Duman, R. S., and Aghajanian, G. K. (2012). Brain-derived neurotrophic factor Val66Met allele impairs basal and ketamine-stimulated synaptogenesis in prefrontal cortex. *Biol. Psychiatry* 71, 996–1005. doi: 10.1016/j.biopsych.2011.09.030

Liu, X., Gangoso, E., Yi, C., Jeanson, T., Kandelman, S., Mantz, J., et al. (2016). General anesthetics have differential inhibitory effects on gap junction channels and hemichannels in astrocytes and neurons. *Glia* 64, 524–536. doi: 10.1002/glia.22946

Lopez-Hidalgo, M., Kellner, V., and Schummers, J. (2017). Astrocyte calcium responses to sensory input: influence of circuit organization and experimental factors. *Front. Neural Circuits* 11:16. doi: 10.3389/fncir.2017.00016

Lord, B., Wintmolders, C., Langlois, X., Nguyen, L., Lovenberg, T., and Bonaventure, P. (2013). Comparison of the ex vivo receptor occupancy profile of ketamine to several NMDA receptor antagonists in mouse hippocampus. *Eur. J. Pharmacol.* 715, 21–25. doi: 10.1016/j.ejphar.2013.06.028

Mantz, J., Delumeau, J. C., Cordier, J., and Petitet, F. (1994). Differential effects of propofol and ketamine on cytosolic calcium concentrations of astrocytes in primary culture. *Br. J. Anaesth.* 72, 351–353. doi: 10.1093/bja/72.3.351

Martín, E. D., Fernández, M., Perea, G., Pascual, O., Haydon, P. G., Araque, A., et al. (2007). Adenosine released by astrocytes contributes to hypoxia-induced modulation of synaptic transmission. *Glia* 55, 36–45. doi: 10.1002/glia.20431

Matthias, K., Kirchhoff, F., Seifert, G., Hüttmann, K., Matyash, M., Kettenmann, H., et al. (2003). Segregated expression of AMPA-type glutamate receptors and glutamate transporters defines distinct astrocyte populations in the mouse hippocampus. *J. Neurosci.* 23, 1750–1758. doi: 10.1523/jneurosci.23-05-01750.2003

Miyazaki, H., Nakamura, Y., Arai, T., and Kataoka, K. (1997). Increase of glutamate uptake in astrocytes: a possible mechanism of action of volatile anesthetics. *Anesthesiology* 86, 1359–1366. doi: 10.1097/00000542-199706000-00018

Muyderman, H., Angehagen, M., Sandberg, M., Björklund, U., Olsson, T., Hansson, E., et al. (2001). Alpha 1-adrenergic modulation of metabotropic glutamate receptor-induced calcium oscillations and glutamate release in astrocytes. *J. Biol. Chem.* 276, 46504–46514. doi: 10.1074/jbc.M103849200

Nagy, I. J., and Rash, J. E. (2000). Connexins and gap junctions of astrocytes and oligodendrocytes in the CNS. *Brain Res. Brain Res. Rev.* 32, 29–44. doi: 10.1016/s0165-0173(99)00066-1

Nakanishi, S., Nakajima, Y., Masu, M., Ueda, Y., Nakahara, K., Watanabe, D., et al. (1998). Glutamate receptors: brain function and signal transduction. *Brain Res. Brain Res. Rev.* 26, 230–235.

Oliveira, J. F., Sardinha, V. M., Guerra, S., Araque-Gomes, A., and Sousa, N. (2015). Do stars govern our actions? Astrocyte involvement in rodent behavior. *Trends Neurosci.* 38, 535–549. doi: 10.1016/j.tins.2015.07.006

Pannasch, U., and Rouach, N. (2013). Emerging role for astroglial networks in information processing: from synapse to behavior. *Trends Neurosci.* 36, 405–417. doi: 10.1016/j.tins.2013.04.004

Parys, B., Cote, A., Gallo, V., De, P., and Sik Koninck, A. (2010). Intercellular calcium signaling between astrocytes and oligodendrocytes via gap junctions in culture. *Neuroscience* 167, 1032–1043. doi: 10.1016/j.neuroscience.2010.03.004

Perea, G., Sur, M., and Araque, A. (2014a). Neuron-glia networks. Integral gear of brain function. *Front. Cell Neurosci.* 8:378. doi: 10.3389/fncel.2014.00378

Perea, G., Yang, A., Boyden, E. S., and Sur, M. (2014b). Optogenetic astrocyte activation modulates response selectivity of visual cortex neurons in vivo. *Nat. Commun.* 5:3262. doi: 10.1038/ncomms4262

Pirttimaki, M. T., and Parri, H. R. (2012). Glutamatergic input-output properties of thalamic astrocytes. *Neuroscience* 205, 18–28. doi: 10.1016/j.neuroscience.2011.12.049

Pirttimaki, T. M., Hall, S. D., and Parri, H. R. (2011). Sustained neuronal activity generated by glial plasticity. *J. Neurosci.* 31, 7637–7647. doi: 10.1523/JNEUROSCI.5783-10.2011

Plourde, G., and Arseneau, F. (2017). Attenuation of high-frequency (30-200 Hz) thalamocortical EEG rhythms as correlate of anaesthetic action: evidence from dexmedetomidine. *Br. J. Anaesth.* 119, 1150–1160. doi: 10.1093/bja/aex329

Porter, T. J., and McCarthy, K. D. (1996). Hippocampal astrocytes in situ respond to glutamate released from synaptic terminals. *J. Neurosci.* 16, 5073–5081. doi: 10.1523/jneurosci.16-16-05073.1996

Rathmell, P. J., and Wanderer, J. P. (2016). unraveling the neurobiology of consciousness: anesthesia, loss of behavioral response to stimuli, and functional connectivity in the brain. *Anesthesiology* 124:A21. doi: 10.1097/01.anes.0000480996.68425.66

Schummers, J., Yu, H., and Sur, M. (2008). Tuned responses of astrocytes and their influence on hemodynamic signals in the visual cortex. *Science* 320, 1638–1643. doi: 10.1126/science.1156120

Shigetomi, E., Bowser, D. N., Sofroniew, M. V., and Khakh, B. S. (2008). Two forms of astrocyte calcium excitability have distinct effects on NMDA receptor-mediated slow inward currents in pyramidal neurons. *J. Neurosci.* 28, 6659–6663. doi: 10.1523/JNEUROSCI.1717-08.2008

Sitar, S. M., Hanifi, P., Gelb-Moghaddam, A., Cechetto, D. F., Siushansian, R., and Wilson, J. X. (1999). Propofol prevents peroxide-induced inhibition of glutamate transport in cultured astrocytes. *Anesthesiology* 90, 1446–1453. doi: 10.1097/00000542-199905000-00030

Thrane, A. S., Rangroo Thrane, V., Zeppenfeld, D., Lou, N., Xu, Q., Nagelhus, E. A., et al. (2012). General anesthesia selectively disrupts astrocyte calcium signaling

in the awake mouse cortex. *Proc. Natl. Acad. Sci. U.S.A.* 109, 18974–18979. doi: 10.1073/pnas.1209448109

Yaguchi, T., and Nishizaki, T. (2010). Extracellular high K+ stimulates vesicular glutamate release from astrocytes by activating voltage-dependent calcium channels. *J. Cell Physiol.* 225, 512–518. doi: 10.1002/jcp.22231

Yang, C. H., Shyr, M. H., Kuo, T. B., Tan, P. P., and Chan, S. H. (1995). Effects of propofol on nociceptive response and power spectra of electroencephalographic and systemic arterial pressure signals in the rat: correlation with plasma concentration. *J. Pharmacol. Exp. Ther.* 275, 1568–1574.

Yang, H., Liang, G., Hawkins, B. J., Madesh, M., Pierwola, A., and Wei, H. (2008). Inhalational anesthetics induce cell damage by disruption of intracellular calcium homeostasis with different potencies. *Anesthesiology* 109, 243–250. doi: 10.1097/ALN.0b013e31817f5c47

Ye, Z. C., Wyeth, M. S., Baltan, S., and Ransom-Tekkok, B. R. (2003). Functional hemichannels in astrocytes: a novel mechanism of glutamate release. *J. Neurosci.* 23, 3588–3596. doi: 10.1523/jneurosci.23-09-03588.2003

Yeh, C. W., Yeh, S. H., Shie, F. S., Lai, W. S., Liu, H. K., Tzeng, T. T., et al. (2015). Impaired cognition and cerebral glucose regulation are associated with astrocyte activation in the parenchyma of metabolically stressed APPswe/PS1dE9 mice. *Neurobiol. Aging* 36, 2984–2994. doi: 10.1016/j.neurobiolaging.2015.07.022

Yoshizumi, M., Eisenach, J. C., and Hayashida, K. (2012). Riluzole and gabapentinoids activate glutamate transporters to facilitate glutamate-induced glutamate release from cultured astrocytes. *Eur. J. Pharmacol.* 677, 87–92. doi: 10.1016/j.ejphar.2011.12.015

Zeng, J. W., Liu, X. H., Zhang, J. H., Wu, X. G., and Ruan, H. Z. (2008). P2Y1 receptor-mediated glutamate release from cultured dorsal spinal cord astrocytes. *J. Neurochem.* 106, 2106–2118. doi: 10.1111/j.1471-4159.2008.05560.x

Conflict of Interest Statement: The authors declare that the research was conducted in the absence of any commercial or financial relationships that could be construed as a potential conflict of interest.

frontiers in Cellular Neuroscience

ORIGINAL RESEARCH
published: 23 July 2019
doi: 10.3389/fncel.2019.00335

GABA Regulation of Burst Firing in Hippocampal Astrocyte Neural Circuit: A Biophysical Model

Junxiu Liu[1], Liam McDaid[1], Alfonso Araque[2], John Wade[1], Jim Harkin[1], Shvan Karim[1], David C. Henshall[3,4], Niamh M. C. Connolly[3], Anju P. Johnson[5], Andy M. Tyrrell[5], Jon Timmis[5], Alan G. Millard[5], James Hilder[5] and David M. Halliday[5]*

[1] School of Computing, Engineering and Intelligent Systems, Ulster University, Derry, United Kingdom, [2] Department of Neuroscience, University of Minnesota, Minneapolis, MN, United States, [3] Department of Physiology and Medical Physics, Royal College of Surgeons in Ireland, Dublin, Ireland, [4] FutureNeuro Research Centre, Royal College of Surgeons in Ireland, Dublin, Ireland, [5] Department of Electronic Engineering, University of York, York, United Kingdom

It is now widely accepted that glia cells and gamma-aminobutyric acidergic (GABA) interneurons dynamically regulate synaptic transmission and neuronal activity in time and space. This paper presents a biophysical model that captures the interaction between an astrocyte cell, a GABA interneuron and pre/postsynaptic neurons. Specifically, GABA released from a GABA interneuron triggers in astrocytes the release of calcium (Ca^{2+}) from the endoplasmic reticulum via the inositol 1, 4, 5-trisphosphate (IP_3) pathway. This results in gliotransmission which elevates the presynaptic transmission probability rate (PR) causing weight potentiation and a gradual increase in postsynaptic neuronal firing, that eventually stabilizes. However, by capturing the complex interactions between IP_3, generated from both GABA and the 2-arachidonyl glycerol (2-AG) pathway, and PR, this paper shows that this interaction not only gives rise to an initial weight potentiation phase but also this phase is followed by postsynaptic bursting behavior. Moreover, the model will show that there is a presynaptic frequency range over which burst firing can occur. The proposed model offers a novel cellular level mechanism that may underpin both seizure-like activity and neuronal synchrony across different brain regions.

Keywords: astrocyte cell, GABA interneuron, burst firing, calcium oscillation, potentiation

OPEN ACCESS

Edited by:
Giovanni Cirillo,
Second University of Naples, Italy

Reviewed by:
Stefano Taverna,
San Raffaele Hospital (IRCCS), Italy
Rheinallt Parri,
Aston University, United Kingdom
Gertrudis Perea,
Cajal Institute (CSIC), Spain

****Correspondence:***
Junxiu Liu
j.liu1@ulster.ac.uk

Specialty section:
This article was submitted to Cellular Neurophysiology, a section of the journal Frontiers in Cellular Neuroscience

Received: *16 March 2019*
Accepted: *08 July 2019*
Published: *23 July 2019*

Citation:
Liu J, McDaid L, Araque A, Wade J, Harkin J, Karim S, Henshall DC, Connolly NMC, Johnson AP, Tyrrell AM, Timmis J, Millard AG, Hilder J and Halliday DM (2019) GABA Regulation of Burst Firing in Hippocampal Astrocyte Neural Circuit: A Biophysical Model. Front. Cell. Neurosci. 13:335. doi: 10.3389/fncel.2019.00335

1. INTRODUCTION

Spiking neural networks (SNNs) are considered to be the most biologically plausible representation of brain function (Ghosh-dastidar and Adeli, 2009). Additionally, SNNs capture a Hebbian type learning paradigm where the timing between pre- and post-synaptic spikes dictates whether synaptic depression or potentiation occurs (Song et al., 2000). SNNs have also been shown to be effective in time series prediction (Reid et al., 2014), spatiotemporal pattern recognition (Hu et al., 2013), and system control (Liu et al., 2015) in various application domains. In SNNs, the neurons and synapses are fundamental components in the network, where the information is encoded in spikes or action potentials for transmission between neurons (Izhikevich, 2003). In the central nervous system neurons receive input stimuli and respond by firing spike patterns such as bursting, which has been observed in the hippocampus of rodents (Miles and Wong, 1986), electric fish (Gabbiani et al., 1996), and in the primary motor cortex, brainstem and thalamus within the somatomotor system of humans (Arichi et al., 2017). The bursts can, in some cases, represent

normal brain function and in other cases abnormal brain function (e.g., epilepsy) (Araque et al., 1999; Halassa et al., 2007).

Research has shown that astrocytes, one type of glial cell, modulate neuronal activity (Halassa et al., 2007; Breslin et al., 2018; Flanagan et al., 2018) where a single astrocyte may enwrap a large number of synapses ($\sim 10^5$ synapses), and connect to several neighboring neurons (four-eight). The interplay between an astrocyte and the neighboring neurons is believed to occur at the tripartite synapse (Araque et al., 1999), which is bi-directional and serves, in some cases, to modulate the synaptic transmission probability rate (PR): via the direct/indirect retrograde signaling messenger endocannabinoids (Wade et al., 2012). This gives rise to re-modeling of the SNN connectivity (Wade et al., 2011; Naeem et al., 2015; Johnson et al., 2018; Liu et al., 2018).

It has also been reported that gamma-aminobutyric acidergic (GABA) interneurons participate in astrocyte-mediated control of excitatory synaptic transmission (Perea et al., 2016) and exercises control over the firing frequency of pyramidal cells. Furthermore GABA release synchronizes principal cell population discharge contributing to the generation of rhythmic activity in neuronal networks, such as theta and gamma frequency oscillations (Kullmann, 2011). A recent paper reported that GABA released in proximity to a tripartite synapse can activate GABA-B receptors on the astrocyte leading to gliotransmission, which is known to regulate synaptic transmission probability (Liu et al., 2018). The research reported in Kurosinski and Götz (2002), Kullmann (2011), Liu et al. (2018) provides the underpinning for the work presented here.

In this paper, we investigate the coupling between a GABA interneuron, an astrocyte terminal and the pre and postsynaptic terminals. The main contributions of this paper include (i) a novel biophysical model that describes the signaling pathways at the tripartite synapse and (ii) a novel mechanism that can potentially explain postsynaptic neuron burst firing. The rest of paper is organized as follows. Section 2 presents the biophysical model while section 3 provides simulation results that demonstrate the bursting. Section 4 concludes the paper and discusses future work.

2. BIOPHYSICAL MODEL OF A NETWORK BURSTING

In this section, a detailed discussion of the signaling pathways at the tripartite synapse is presented with a specific focus on GABA signaling between the presynaptic terminal and the nearby astrocyte. It will be shown that this interplay acts as a frequency dependent switch, which modulates the probability of release (PR) at the presynaptic terminal. Our Ca^{2+} dynamics model shows that calcium (Ca^{2+}) oscillations only occur over a range of inositol 1, 4, 5-trisphosphate (IP_3) concentrations and furthermore this paper will show that Ca^{2+} oscillations are periodic and this behavior is key to the bursting behavior.

2.1. Signaling Pathways and Activity Regulations

The conventional tripartite synapse has three terminals: the presynaptic axon, postsynaptic dendrite and the astrocyte cell (Wade et al., 2012; Liu et al., 2018). In this paper we consider earlier work where, in a hippocampal astrocyte neural network, GABA interneurons interact with excitatory tripartite synapses to dynamically change the synaptic transmission behavior from inhibitory to excitatory through modulation of PR (Perea et al., 2016). The signaling pathways between the GABA interneuron and tripartite synapse are shown in **Figure 1**. When an input stimulus of frequency (f_{pre}) is present at the excitatory presynaptic axon, neurotransmitter (glutamate) is released into the cleft and subsequently binds to receptors at the postsynaptic dendrite causing the depolarization of the postsynaptic neuron. While the authors accept that fast-spiking interneurons can fire at much higher frequencies than glutamatergic neurons, in this work we assume for simplicity that the firing rate of the GABA interneuron (f_{GABA}) follows f_{pre}, as the most likely physiological condition would be the activation of GABA interneuron by activation of glutamatergic axons (Serrano et al., 2006; Covelo and Araque, 2018). While GABA initially binds to GABA-A receptors inhibiting synaptic transmission and post-synaptic neuronal activity, recent work (Perea et al., 2016) has shown that with repeated firing of GABA interneurons, GABA also binds to GABA-B receptors on the astrocyte membrane, resulting in a switch from inhibition to excitation at the presynaptic terminal, and an associated excitatory response at the postsynaptic terminal. In this paper we focus on astrocyte-mediated GABA-induced excitation since the postsynaptic inhibition was found negligible, and the transient acute presynaptic inhibition was overpowered by the astrocyte signaling during sustained activity (Perea et al., 2016). Hence, our model dos not incorporate these negligible or transient inhibitory effects, focusing in the sustained mechanisms and effects of inhibitory signaling through astrocyte activation.

As f_{GABA} increases, the GABA concentration level in the extracellular space increases, and a level is reached whereby binding to GABA-B receptors on the astrocyte membrane commences, leading to the production of IP_3: we subsequently refer to IP_3 due to GABA as IP_3^{GABA}, which contributes to the overall cytosolic IP_3 (Perea et al., 2016). IP_3^{GABA} is a secondary messenger which is degraded when released into the cytoplasm: initially cytosolic Ca^{2+} and IP_3 levels are low and therefore degradation of IP_3 will also be low, as the degradation rate correlates with both Ca^{2+} and IP_3 concentrations. This degradation is gradually overcome with increasing levels of GABA and the $PLC\delta$ signaling pathway, which is modulated by Ca^{2+} and is accounted for in this work. Finally IP_3^{GABA} starts to bind to IP_3 receptors (IP_3R_s) on the Endoplasmic Reticulum (ER). When the total cytosolic IP_3 is sufficiently high, Ca^{2+} is released from the ER (De Pittà et al., 2009). At some point both IP_3 and Ca^{2+} reaches a level at which an oscillating Calcium-Induced Calcium Release (CICR) occurs from the ER (Marchant et al., 1999): hereafter referred to as T_{CICR}. Several mechanisms are believed to contribute to Ca^{2+} oscillation but there is still much debate around this topic. For example, IP_3R_s have binding sites for both IP_3 and Ca^{2+}, and Ca^{2+} release from the ER is believed to rely on coincidence binding of these ions. The time between IP_3 and Ca^{2+} binding depends on the concentration of these ions and therefore this could explain why Ca^{2+} is believed to be a regulator of IP_3R_s activity: at low Ca^{2+} levels IP_3R_s

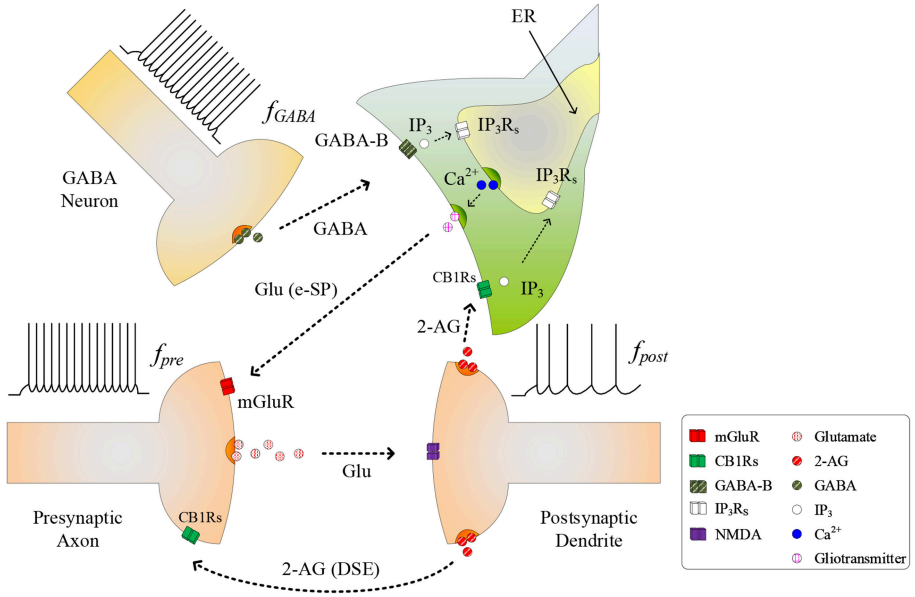

FIGURE 1 | Signaling pathways at the tripartite synapse where GABA released from GABA interneuron binds to GABA-B receptors on the astrocyte membrane and IP_3^{GABA} is released into the astrocyte cytosol. 2-AG released from the postsynaptic neuron binds to the receptors on the astrocyte membrane triggering the generation of IP_3^{AG}. With f_{post} low and IP_3 reached a level, IP_3 induces Ca^{2+} release from the ER and gliotransmitter is released into the synaptic cleft [Glu (e-SP) pathway] where it binds to mGluR receptors on the presynaptic membrane. This causes an increase in PR and the plasticity window opens.

activity is increased, whereas the opposite is true at high Ca^{2+} levels. This is in agreement with other research (Dawson, 1997). However, there is not enough experimental evidence on these receptors to formulate a sufficiently detailed model. Therefore, in this work we revert to a hitherto accepted model (Perea et al., 2016) where Ca^{2+} oscillatory behavior is believed to arise from the feedback interplay between Ca^{2+}, IP_3, and IP_3 degradation. As Ca^{2+} and IP_3 rapidly increase there is a complex dependency between the concentrations of both Ca^{2+} and IP_3 and Ca^{2+}/IP_3-induced degradation of IP_3, which is the dominant process at elevated Ca^{2+}/IP_3 levels. Therefore, a transient elevation of Ca^{2+} and/or IP_3 is followed by a rapid drop in IP_3, which can reduce IP_3 to below T_{CICR}. At this point degradation of IP_3 is weak because both the Ca^{2+} and IP_3 levels have fallen and therefore IP_3 starts to increase again due to IP_3^{GABA}. When the T_{CICR} level is reached again a transient elevation of Ca^{2+} re-occurs. We will demonstrate that our results support this behavior. This oscillatory behavior causes the release of the glutamate from the astrocyte (gliotransmitter) into the synapse [see Glu (e-SP) pathway in **Figure 1**], which binds to pre-synaptic group I metabotropic Glutamate Receptors (mGluRs) at the presynaptic terminal. This signaling pathway results in an increase in PR at the presynaptic terminal (Navarrete and Araque, 2010).

As PR increases more glutamate is released into the cleft and potentiation/depression of the synaptic weight can commence with the availability of glutamate to bind to N-methyl-D-aspartate (NMDA)-type glutamate receptors (Lüscher and Malenka, 2012). While we acknowledge that the biophysical mechanisms regulating the functional dependency between PR and plasticity are complex and not fully understood, we propose that PR acts as a "switch" which can turn on/off potentiation/depression at synaptic sites. To formulate a tractable mathematical model that captures this relationship we modulate the height of the Spike Timing Dependent Plasticity (STDP) associated plasticity window using PR: with $PR \geq PR^*$ (PR^* is defined as the plasticity activation level) the plasticity window fully opens and with $PR < PR^*$ the plasticity window closes. The decision on whether potentiation or depression occurs is governed by the STDP rule (Magee and Johnston, 1997) where potentiation occurs when the presynaptic spike precedes postsynaptic spike, otherwise depression occurs. Additionally, we consider the case where the postsynaptic neuron is sufficiently depolarized such that the retrograde messenger 2-arachidonyl glycerol (2-AG) is released from the postsynaptic neuron. Since the contribution of 2-AG signaling to the observed GABA-mediated regulatory effects of astrocytes on excitatory transmission is negligible (Perea et al., 2016), the authors take the view that 2-AG signaling onto GABAergic terminals would not be a significant factor in network bursting. However, we do consider 2-AG binding to type 1 Cannabinoid Receptors (CB1Rs) on the astrocyte membrane which then initiates the release of the IP_3 into the cytoplasm of the astrocyte: we denote this secondary messenger as IP_3^{AG}.

During the synapse learning phase, the frequency of the postsynaptic neuron, f_{post}, is increasing, as is the 2-AG signal and consequently IP_3^{AG}. As IP_3^{AG} contributes to the total IP_3, IP_3 will eventually reach a level where degradation of IP_3 no longer reduces IP_3 (and therefore Ca^{2+}) to below T_{CICR}. In this instance, both the oscillatory Ca^{2+} transient and Glu (e-SP) pathways cease (Liu et al., 2018) (see **Figure 2**). In addition, the released

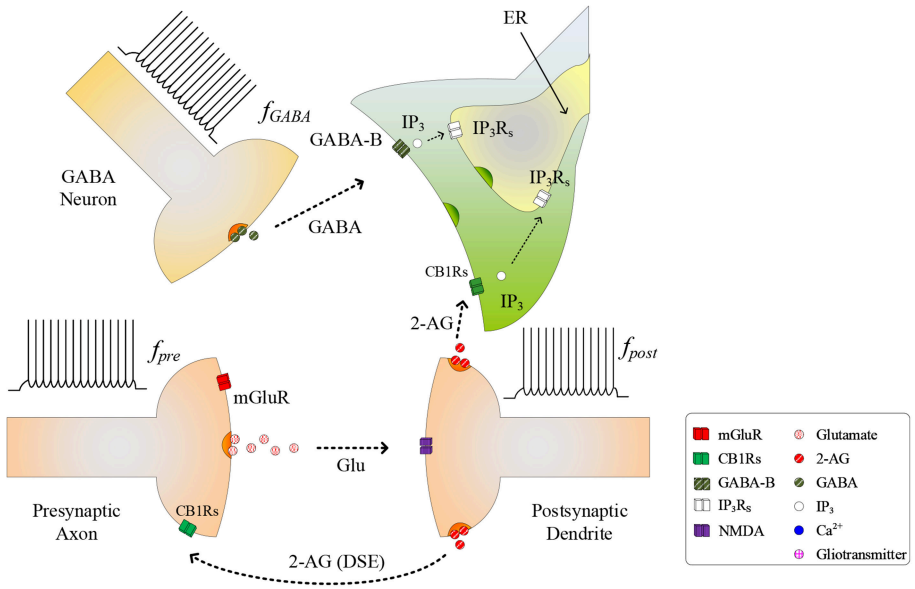

FIGURE 2 | Signaling pathways of the tripartite synapse where for high f_{post} T_{CICR} is reached and hence the Ca^{2+} oscillation and the Glu (e-SP) pathway ceases causing PR to fall and the plasticity window shuts: PR also falls due to the increase in the 2-AG (DSE) pathway. Under this condition the level of neurotransmitter in the cleft falls to baseline and f_{post} diminishes.

2-AG also binds to CB1Rs on the presynaptic terminal triggering the Suppression of Excitation (DSE) pathway, and results in a decrease in PR (Alger, 2002). Due to the reduction in the Glu (e-SP) pathway and the increase in the DSE pathway, PR decreases at the presynaptic terminal, the level of neurotransmitter in the cleft then falls to baseline and the frequency of the postsynaptic f_{post} diminishes which in turn causes IP_3^{AG} to reduce. Furthermore, the total IP_3 degrades due to cytosolic degradation pathways including IP_3 3-kinase IP_3^{3K}, and dephosphorylation by inositol polyphosphate 5-phosphatase (IP_3^{5P}) (see Equation 11). Together, these processes reduce IP_3 levels below T_{CICR}, and the rate of degradation diminishes sufficiently to allow IP_3 to increase again due to IP_3^{GABA}. When the T_{CICR} level is again exceeded, Ca^{2+} oscillations re-commence, the Glu (e-SP) pathway is re-established, PR increases and the level of neurotransmitter in the cleft is raised. In this post-learning phase PR cannot be elevated to a level where the plasticity window opens ($PR < PR^*$), as the postsynaptic neuron is active and therefore the 2-AG pathway leads to a reduction in PR due to the DSE pathway. Consequently, the postsynaptic neuron firing rate reaches a maximum when the T_{CICR} level is reached but it subsequently falls afterwards: a postsynaptic burst has occurred. This is followed by repeated bursts at each Ca^{2+} oscillatory period. We therefore propose that neuronal burst firing directly correlates with astrocytic Ca^{2+} oscillation.

Moreover, it should be noted that the duration of the burst correlated with the frequency of presynaptic terminal f_{pre} at the excitatory presynaptic axon. As f_{pre} increases so does the rate of increase of IP_3 and the burst period is reduced. Therefore, network bursting is f_{pre} dependant and will only occur over a range of f_{pre}.

2.2. Postsynaptic Neuron Model

In this paper, the Leaky Integrate and Fire (LIF) model (Gerstner and Kistler, 2002) is used due to the relatively low computing requirement and minimal parameters tuning. The LIF model is given by

$$\tau_m \frac{dv}{dt} = -v(t) + R_m \sum_{i=1}^{n} I_{syn}^i(t), \tag{1}$$

where τ_m is the neuron membrane time constant, v is the neuron membrane potential, R_m is the membrane resistance, I_{syn}^i is the current injected to the neuron membrane by ith synapse, and n is the total number of synapses associated with the neuron. When the neuron membrane potential v is greater than the firing threshold value, v_{th}, the neuron fires and outputs a spike followed by a reset state or a refractory period ($\sim 2ms$). The release of 2-AG correlates with the postsynaptic neuron activity (Naeem et al., 2015) and this is expressed as

$$\frac{d(AG)}{dt} = \frac{-AG}{\tau_{AG}} + r_{AG}\delta(t - t_{sp}), \tag{2}$$

where AG denotes the released amount of 2-AG, τ_{AG}, and r_{AG} are the 2-AG decay and production rates, and t_{sp} is the postsynaptic spike time. The released 2-AG binds to the CB1Rs at the presynaptic terminal and at the astrocyte terminal, and this will be discussed in section 2.4.

2.3. GABA Interneuron

The spike train at the presynaptic axon also presents at the GABA interneuron causing the release of GABA neurotransmitter

(Perea et al., 2016), which can be described by

$$\frac{d(GABA)}{dt} = \frac{-GABA}{\tau_{GABA}} + r_{GABA}\delta(t - t_{sp}), \tag{3}$$

where GABA denotes the released amount of the neurotransmitter GABA, τ_{GABA}, and r_{GABA} are the GABA decay and production rates, and t_{sp} is the presynaptic spike arrival time. GABA binds to the GABA-B receptors at the astrocyte cell and this is modeled in the next subsection.

2.4. Astrocyte Cell

When GABA binds to GABA-B receptors on the astrocyte membrane, the amount of IP_3 released is given by

$$\frac{d(IP_3^{GABA})}{dt} = \frac{IP_3^{GABA*} - IP_3^{GABA}}{\tau_{ip3}^{GABA}} + r_{ip3}^{GABA}GABA, \tag{4}$$

where IP_3^{GABA} is the quantity of IP_3 generated by GABA within the cytoplasm, IP_3^{GABA*} is the baseline GABA level, τ_{ip3}^{GABA} is the decay rate of IP_3^{GABA} and r_{ip3}^{GABA} is the production rate of IP_3^{GABA}. When the postsynaptic neuron fires, the released 2-AG can also trigger IP_3 generation (Wade et al., 2012) and this is modeled by

$$\frac{d(IP_3^{AG})}{dt} = \frac{IP_3^{AG*} - IP_3^{AG}}{\tau_{ip3}^{AG}} + r_{ip3}^{AG}AG, \tag{5}$$

where IP_3^{AG} is the quantity of IP_3 generated by 2-AG within the cytoplasm, IP_3^{AG*} is the baseline level, τ_{ip3}^{AG} is decay rate of IP_3^{AG}, and r_{ip3}^{AG} is production rate of IP_3^{AG}.

In addition, the IP_3 production is also increased by the hydrolysis of the highly phosphorylated membrane lipid phosphatidylinositol 4, 5–bisphosphate (PIP_2), such as the phosphoinositide-specific phospholipase C (PLC) isoenzyme of $PLC\delta$ (De Pittà et al., 2009). The $PLC\delta$ signaling is agonist independent and modulated by Ca^{2+} (De Pittà et al., 2009), and its activation rate can be modeled by

$$PLC\delta = PLC\delta' Hill(Ca^{2+}, K_{PLC\delta}, 2), \tag{6}$$

where the maximum $PLC\delta$-dependant IP_3 production rate (De Pittà et al., 2009) can be modeled by

$$PLC\delta' = \overline{PLC\delta'}/(1 + IP_3/K_\delta), \tag{7}$$

and K_δ is the inhibition constant of $PLC\delta$ activity. The Hill function (De Pittà et al., 2009) is described by

$$Hill(x, K, n) \equiv \frac{x^n}{x^n + K^n}, \tag{8}$$

where n is the Hill coefficient and K is the midpoint of the Hill function, namely the value of x at which $Hill(x, K, n)|_{x=K} = 1/2$.

The degradation of IP_3 mainly occurs through phosphorylation into inositol 1, 3, 4, 5-tetrakisphosphate (IP_4), catalyzed by IP_3 3-kinase (3K), and dephosphorylation by inositol polyphosphate 5-phosphatase (5P). The rate of IP_3 degradation by IP_3^{5P} (De Pittà et al., 2009) can be modeled by

$$IP_3^{5P} \approx \bar{r}_{5P} IP_3, \tag{9}$$

where $\bar{r}_{5P}$ is the IP_3 degradation rate by IP-5P. The activity of IP_3^{3K} is regulated by Ca^{2+} in a complex fashion (De Pittà et al., 2009). The rate of IP_3 degradation by IP_3^{3K} can be modeled by

$$IP_3^{3K} = \bar{v}_{3K} Hill(Ca^{2+}, K_D, 4) Hill(IP_3, K_3, 1), \tag{10}$$

where $\bar{v}_{3K}$ is the maximum degradation rate by IP_3^{3K}, K_D is the Ca^{2+} affinity of IP_3^{3K}, and K_3 is the IP_3 affinity of IP_3^{3K}. Based on the previous contributions of IP_3, the total IP_3 is given by

$$IP_3 = IP_3^{GABA} + IP_3^{AG} + PLC\delta - IP_3^{5P} - IP_3^{3K}. \tag{11}$$

The Li-Rinzel model (Li and Rinzel, 1994) is used to model the Ca^{2+} dynamics within the astrocyte cell. The model consists of three channels, J_{chan}, J_{leak}, and J_{pump}, where J_{chan} models the Ca^{2+} channel opening based on the mutual gating of the Ca^{2+} and IP_3, J_{leak} models the Ca^{2+} leakage from the ER into the cytoplasm and J_{pump} models how Ca^{2+} is pumped out from the cytoplasm into the ER via Sarco-Endoplasmic-Reticulum Ca^{2+}-ATPase (SERCA) pumps. The Ca^{2+} model in the approach of De Pittà et al. (2009) is used in this work, and it is described by

$$\frac{d(Ca^{2+})}{dt} = J_{chan}(Ca^{2+}, h, IP_3) + J_{leak}(Ca^{2+}) - J_{pump}(Ca^{2+}), \tag{12}$$

$$\frac{dh}{dt} = \frac{h_\infty - h}{\tau_h}, \tag{13}$$

where J_{chan} is Ca^{2+} release depending on the Ca^{2+} and IP_3 concentrations, J_{pump} is the amount of stored Ca^{2+} within the ER via the SERCA pumps, J_{leak} is the Ca^{2+} leaking out of the ER and h is the fraction of activated IP_3R_s. The parameters h_∞ and τ_h are given by

$$h_\infty = \frac{Q_2}{Q_2 + Ca^{2+}}, \tag{14}$$

$$\tau_h = \frac{1}{a_2(Q_2 + Ca^{2+})}, \tag{15}$$

where

$$Q_2 = d_2 \frac{IP_3 + d_1}{IP_3 + d_3}. \tag{16}$$

J_{chan} is given by

$$J_{chan} = r_C m_\infty^3 n_\infty^3 h_\infty^3 (C_0 - (1 + C_1)Ca^{2+}), \tag{17}$$

where r_C is the maximal Calcium-Induced Calcium Release (CICR) rate, C_0 is the total free Ca^{2+} cytosolic concentration, C_1 is the ER/cytoplasm volume ratio, and m_∞ and n_∞ are the IP_3 Induced Calcium Release (IICR) and CICR channels respectively, which are given by

$$m_\infty = \frac{IP_3}{IP_3 + d_1}, \tag{18}$$

and

$$n_\infty = \frac{Ca^{2+}}{Ca^{2+} + d_5}. \tag{19}$$

J_{leak} and J_{pump} are described by

$$J_{leak} = r_L(C_0 - (1 + C_1)Ca^{2+}), \tag{20}$$

and

$$J_{pump} = v_{ER}\frac{(Ca^{2+})^2}{k_{ER}^2 + (Ca^{2+})^2}, \tag{21}$$

where r_L is the Ca^{2+} leakage rate, v_{ER} is the maximum SERCA pump uptake rate and k_{ER} is the SERCA pump activation constant.

The intracellular astrocytic calcium dynamics are used to regulate the release of glutamate from the astrocyte: the Glu pathway. To model this release, it is assumed that when Ca^{2+} crosses the CICR threshold, a quantity of glutamate is released (Wade et al., 2012). It is described by

$$\frac{d(Glu)}{dt} = \frac{-Glu}{\tau_{Glu}} + r_{Glu}\delta(t - t_{Ca}), \tag{22}$$

where Glu is the quantity of released glutamate, τ_{Glu} is decay rate of glutamate, r_{Glu} is production rate of glutamate, and t_{Ca} is the time at which Ca^{2+} crosses the threshold. The released glutamate drives the generation of e-SP (Wade et al., 2012). The level of e-SP is modeled by

$$\tau_{eSP}\frac{d(eSP)}{dt} = -Glu + m_{eSP}Glu(t), \tag{23}$$

where τ_{eSP} is the decay rate of Glu, and m_{eSP} is a constant weight used to control the height of e-SP. It shows that the e-SP level depends on the glutamate released from the astrocyte cell.

The model of DSE in the approach of Wade et al. (2012) is used to describe the relationship between the DSE and the released 2-AG from postsynaptic neuron. The DSE is assumed to change linearly with the cytosolic concentration of 2-AG, which is described by

$$DSE = AG \times K_{AG}, \tag{24}$$

where AG is the concentration of 2-AG and K_{AG} is the scaling factor for the DSE.

2.5. Synapse Model

For the synapse, a probabilistic model is employed which is based on the failure and success mechanisms of synaptic neurotransmitter release (Navarrete and Araque, 2010; Wade et al., 2012). A uniformly distributed pseudo-random number generator is used. If the generated random number *rand* is less than or equal to the PR, a current I_{inj} is injected into the neuron which is shown by

$$I_{syn}^i(t) = \begin{cases} r_I * w_{syn}^i(t), & rand \le PR \\ 0, & rand > PR \end{cases} \tag{25}$$

where r_I is the current production rate, and w_{syn}^i is the weight of the ith synapse. The associated PR of each synapse is determined by the DSE and e-SP together, which is given by

$$PR(t) = PR(t_0) + DSE(t)/100 + eSP(t)/100, \tag{26}$$

where $PR(t_0)$ is the initial PR for each synapse. As discussed in section 2.1, the PR can switch on/off learning at the synaptic terminal by modulating the height of the plasticity learning window. The authors are not aware of any biophysical model that relates PR to the plasticity window weighting parameter A_0 and therefore in this work it is assumed that A_0 is modulated according to

$$A_0 = \begin{cases} 0, & PR \le PR^* \\ (PR - PR^*) * r, & PR > PR^* \end{cases} \tag{27}$$

where PR^* is the learning activation level and r is a constant value which controls the maximum height of the learning window. The STDP rule used in this approach to update the synaptic weights according to the timing difference between the post and presynaptic spikes is described by

$$\delta w\ (\Delta t) = \begin{cases} -A_0 exp(\frac{\Delta t}{\tau_+}), & \Delta t \le 0 \\ A_0 exp(\frac{-\Delta t}{\tau_-}), & \Delta t > 0 \end{cases} \tag{28}$$

where $\delta w(\Delta t)$ is the weight update, Δt is the time difference between the post and presynaptic spikes, A_0 is the height of the plasticity window which limits the maximum levels of weight potentiation and depression, and τ_+ and τ_- control the width of the plasticity window. A symmetrical plasticity window is assumed in this approach, and $\tau_+ = \tau_- = 40ms$.

From the proposed models, it can be seen that if the f_{pre} is large enough, IP_3 is generated sufficiently to cause Ca^{2+} oscillations. Then the Ca^{2+}-induced glutamate binds to the mGluRs receptors at the presynaptic terminal resulting in an increase of the synaptic transmission probability PR. Note that the authors wish to point out that astrocytes are believed to gate LTP and LTD by regulating glutamate levels in the synaptic cleft (Foncelle et al., 2018). Since there are many complex biophysical mechanisms involved in the regulation of glutamate, which are still under debate, the authors take the view that modulating the STDP plasticity window using PR is an effective way to capture this gating function. Elevating PR opens the synaptic plasticity learning window and over time f_{post} gradually increases which, via the 2-AG pathway, contributes to astrocytic IP_3 level until the Ca^{2+} oscillation stops. This is accompanied by a reduction in the Glu (e-SP) pathway and PR falls causing a reduction in f_{post}. Therefore, the bursting activity of the postsynaptic neuron is regulated by the GABA interneuron and the astrocyte cell. The results in the next section show the signaling pathways leading to a bursting postsynaptic neuron.

3. RESULTS

This section provides simulation results which highlight the dynamic behavior at the synapse terminals and how the

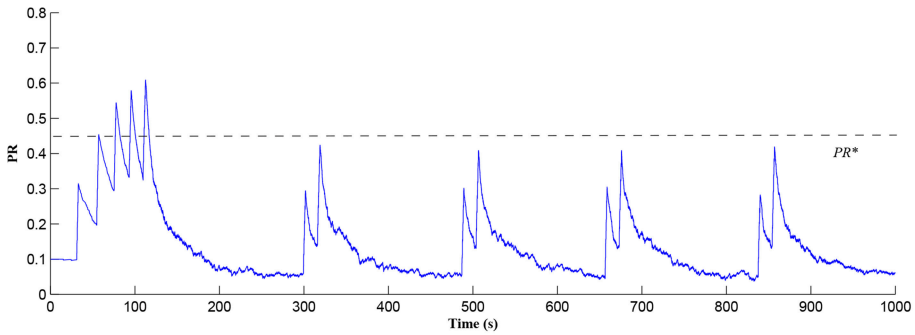

FIGURE 3 | PR as a function of Glu (e-SP) and DSE signals over time. Note that the plasticity window will only be open when $PR > PR^*$ and this can be observed in **Figure 4**.

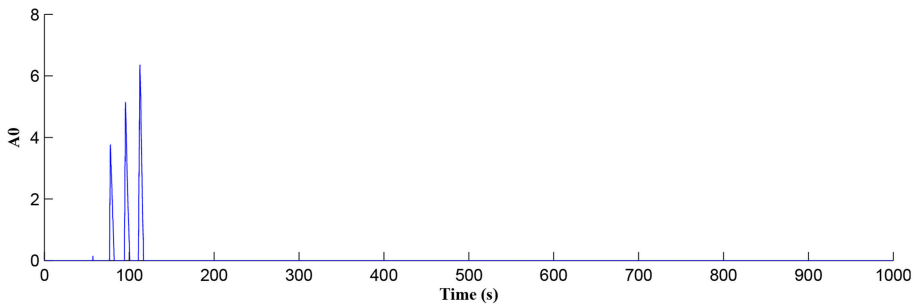

FIGURE 4 | Plasticity window height A_0 as a function of time. Note that PR acts as a switch to open/close the plasticity window controlling the learning period.

interactions between an astrocyte and GABA interneuron can give rise to bursting behavior. The MATLAB simulation platform is used in this work together with the Euler method with the time step of 1 ms. **Tables A1**, **A2** give all the model parameters.

3.1. Bursting Output Spike Pattern

In this simulation both the presynaptic excitatory neuron and the GABA interneuron are stimulated by the same spike train at frequency $f_{pre} = f_{GABA}$ which causes the release of GABA and glutamate (Perea et al., 2016). The presynaptic excitatory neuron/GABA interneuron stimulus is 40 Hz in the following simulations as this is sufficient to produce a cytosolic $[IP_3] > 0.5\mu M$. With $PR > PR^*$ (see **Figure 3**), a significant increase occurs in the level of neurotransmitter in the cleft, the learning window opens (**Figure 4**) and weight potentiation starts (**Figure 5**) resulting in postsynaptic firing. Note that in **Figure 4**, the plasticity window height parameter A_0 increases periodically with a corresponding potentiation of the synaptic weight (**Figure 5**). In our model the resting level for PR is 0.1 and based on the model in Equation (27), if $PR > PR^*$ ($PR^* = 0.45$ in this work), the STDP learning window opens ($A_0 > 0$) at ∼80 s, as shown in **Figure 4**. After the synaptic weight is potentiated, the synapse generates a depolarising current only when the input stimulus is presented at the presynaptic terminal and the PR value is greater than the value of a random number (see probabilistic-based synapse model in Equation 25): this current is injected into the postsynaptic LIF neuron. This injected current increases the postsynaptic potential and the neuron fires a spike if the membrane potential is greater than the firing threshold, v_{th}.

After a period of learning the postsynaptic neuron activity has stabilized and PR drops sufficiently, toward the end of the first set of PR "spikes" (see **Figure 3**), closing the plasticity window ($A_0 = 0$) and the weight stabilizes to ∼610 at 110 s, as shown in **Figure 5**: note that because the postsynaptic neuron is now active, $PR < PR^*$ for all subsequent Ca^{2+} oscillations as the DSE pathway is also active. **Figure 6** shows the amount of GABA released by the GABA interneuron as a function of time where, as expected, GABA increases gradually and then stabilizes at 0.027 μM under the input spike stimulus. IP_3^{GABA} is shown in **Figure 7** (blue) as a function of time and stabilizes at $\sim 0.58\mu M$ which is consistent with the input stimuli profile. **Figure 7** shows the other IP_3 sources that contribute to the total IP_3 in the cytosol.

Initially the total IP_3 increases with IP_3^{GABA} until the T_{CICR} level is reached triggering the release of Ca^{2+}, as shown in **Figure 8**. We have observed from our model that T_{CICR} is consistent with an IP_3 level of approximately 0.5 μM and whenever IP_3 exceeds this threshold a transient elevation in Ca^{2+} occurs, as can be seen in **Figure 8**. Note however that as the IP_3 level increases with IP_3^{AG} the degradation in IP_3 due to elevated Ca^{2+}/IP_3 levels is insufficient to reduce IP_3 to below 0.5 μM and consequently the transient elevations of Ca^{2+} stops just after 100 s followed by a relatively slow degradation of IP_3 and Ca^{2+}: these periodic bursts in Ca^{2+} gives rise to a Ca^{2+} oscillatory wave where the initial Ca^{2+} burst is longer due to synaptic

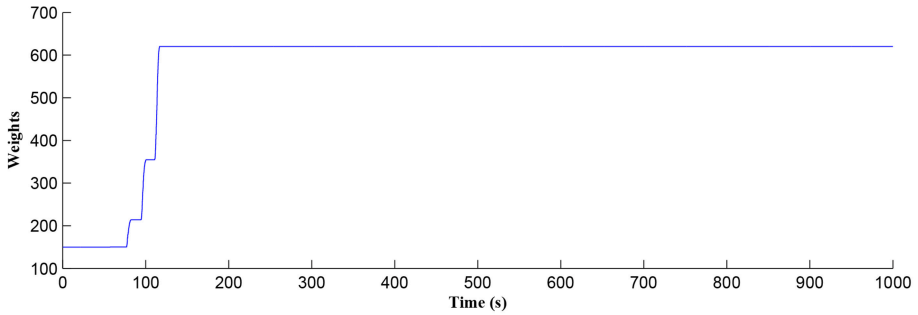

FIGURE 5 | Time dependant synaptic weight update governed by the STDP learning rule. When the plasticity window is open, learning commences, the synaptic weight begins to potentiate and after a period of learning the window shuts off and the synaptic weight stabilizes.

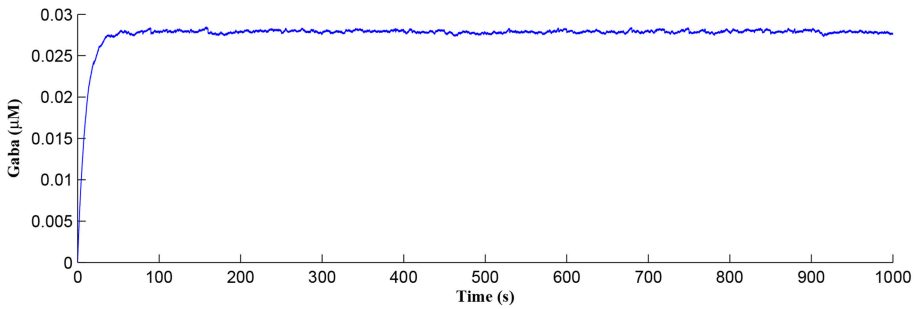

FIGURE 6 | GABA released from the GABA interneuron as a function of time. Under the input spike stimulus of f_{GABA}, GABA increases and then stabilized.

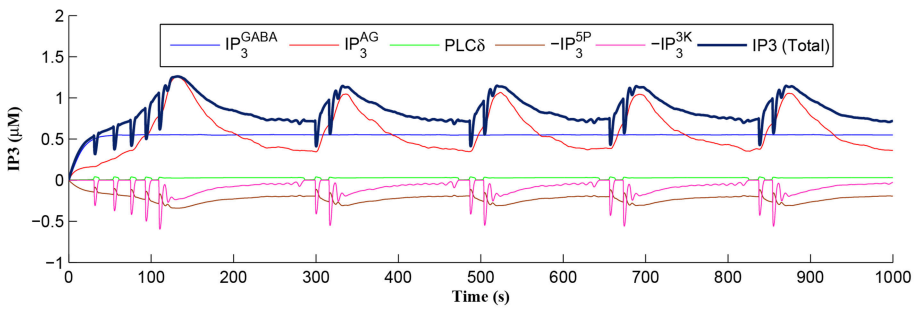

FIGURE 7 | IP_3 dynamics within the astrocyte cell over time. The overall IP_3 includes contributions from IP_3^{GABA}, IP_3^{AG}, $PLC\delta$, IP_3^{5P}, and IP_3^{3K}, where the degradations of IP_3, IP_3^{5P}, and IP_3^{3K}, are shown as negative values.

potentiation. At the onset of each subsequent Ca^{2+} burst the IP_3 level drops sharply and we attribute this to strong dependence of IP_3^{3K} on Ca^{2+} (Equation 10). As the Ca^{2+} level drops J_{chan} (Equation 17) reverses direction perturbing the rate of change in Ca^{2+} (Equation 12) and this causes a rapid increase in IP_3^{3K} and a corresponding decrease in IP_3 (Equation 11).

The Ca^{2+} oscillation is initiated at ∼20 s (T_{CICR} is exceeded; **Figure 8**) and this triggers the release of glutamate targeting group I mGluRs on the presynaptic terminal, i.e., Glu (e-SP) pathway is activated (**Figure 9**). **Figure 9** shows that the Glu (e-SP) signal accumulates at each CICR and rapidly decays after the Ca^{2+} transients have ceased at ∼120 s. Also the DSE pathway increases as the activity of the postsynaptic neuron is increasing, and competes with the Glu (e-SP) pathway to restrict PR to a relatively stable low value for all subsequent Ca^{2+} oscillations that occur post-learning, as shown in **Figure 10**. Again note a longer period of elevation of the DSE signal at the start due to synaptic potentiation but thereafter the DSE profile repeats in time.

Figure 11 shows the firing rate of the postsynaptic neuron, which is calculated based on a sliding time window of 10 s (blue) and 40 s (red), respectively. Note that the first burst reaches a higher level of postsynaptic neuron activity when compared to subsequent bursts. Also, between bursts

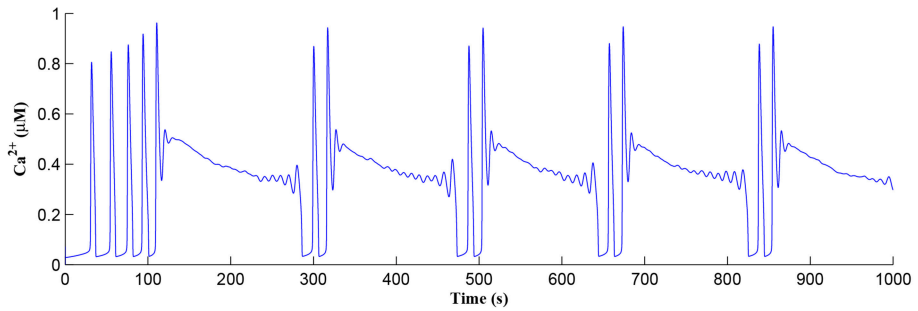

FIGURE 8 | Ca^{2+} oscillations in the astrocyte cell as a function of time. Note a longer oscillatory period at the start due to learning but thereafter the oscillator period stabilizes with constant on/off ratio.

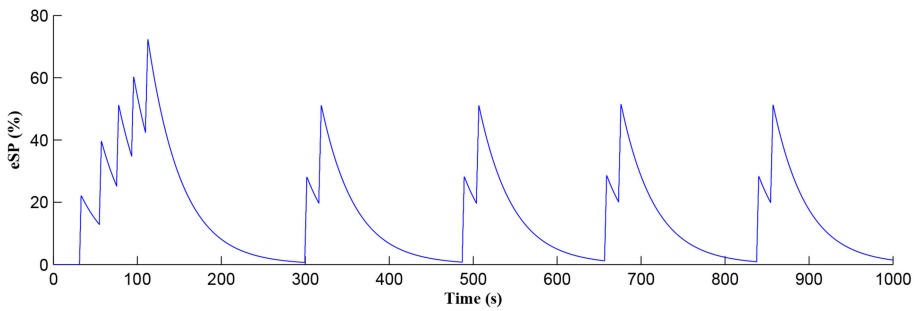

FIGURE 9 | Glu (e-SP) signaling pathway as a function of time. Note a longer period of elevation of Glu (e-SP) at the start due to synaptic potentiation but thereafter the Glu (e-SP) profile repeats in time.

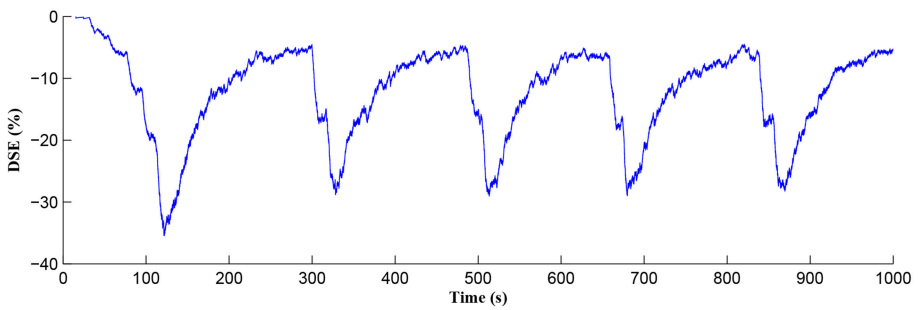

FIGURE 10 | DSE signaling pathway from the postsynaptic neuron, which correlates with the activity of the postsynaptic neuron.

the activity never falls back to zero. This is because the first burst occurs during the weight potentiation phase when the synaptic weight is continually updated and eventually stabilized, whereas in all subsequent neuronal bursts no weight potentiation occurs. Clearly from **Figure 11** a continual postsynaptic bursting behavior is evident.

Referring to **Figure 12**, we show simulations for f_{pre} of 20, 40, and 80 Hz where clearly only $f_{pre} = 40Hz$ results in repeated Ca^{2+} oscillations. This is because at 20Hz the T_{CICR} level cannot be reached whereas at 80Hz the astrocyte cytosol is quickly swamped with both IP_3 and Ca^{2+} and subsequent degradation in IP_3 is insufficient to allow further CICR. Consequently our model shows presynaptic frequency selectivity which is consistent with work reported elsewhere (Bienenstock et al., 1982; Dong et al., 2015).

In addition, as the morphology of GABA interneurons and receptor density at the astrocyte cell differ, the IP_3^{GABA} levels vary under the same input f_{pre}. IP_3^{GABA} is a main contributor to the total IP_3, thus the greater IP_3^{GABA}, the longer the process of IP_3 degradation.

Figure 7 shows that when IP_3 degrades sufficiently to once again enable IP_3 to cross T_{CICR} from below, a transient elevation in Ca^{2+} results and PR increases with a corresponding increase in the postsynaptic neuron burst frequency. Therefore,

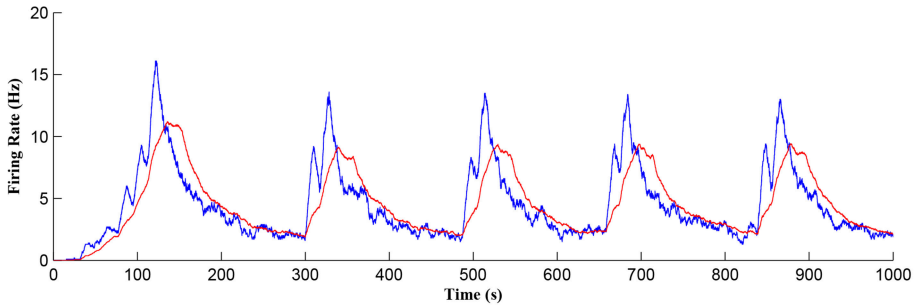

FIGURE 11 | Firing rate of the postsynaptic neuron where a continual bursting behavior is evident. The firing activity was calculated using a sliding time window of 10 s (blue) and again for a sliding window of 40 s (red) where the latter gives a better average.

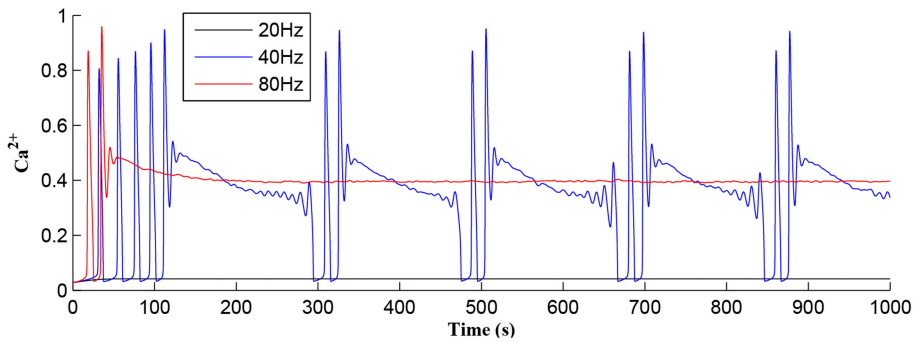

FIGURE 12 | Astrocytic Ca^{2+} as a function of time with f_{pre} of 20, 40, and 80 Hz as a parameter. Note that for the extreme cases of (20 or 80 Hz) no Ca^{2+} oscillations occur: for f_{pre} = 20 Hz T_{CICR} can never be achieved and at 80Hz degradation of IP_3 is insufficient to allow CICR to repeatedly occur. Consequently, there is a frequency window over which oscillations can occur.

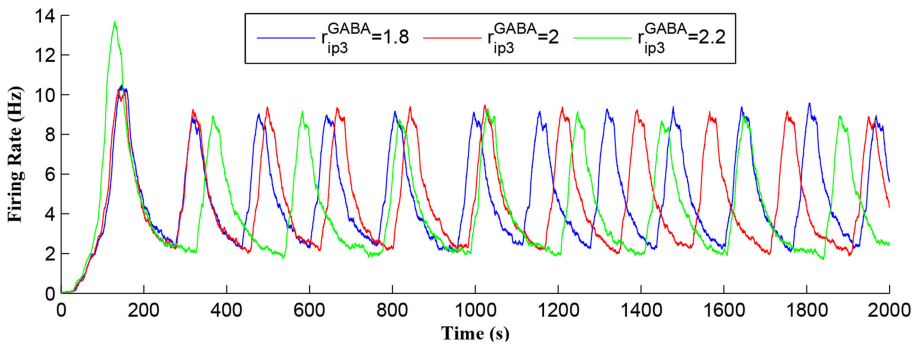

FIGURE 13 | Postsynaptic neuron burst firing as a function of time with IP_3^{GABA} production rates (r_{ip3}^{GABA}) as a parameter. When r_{ip3}^{GABA} increases, IP_3^{GABA} level increases and the frequency of the bursting decreases. Due to a high IP_3^{GABA} level, a long time period is required to degrade the overall IP_3 and to restart the Ca^{2+} oscillation. Thus, the bursting frequency is low.

different IP_3^{GABA} levels lead to different burst frequencies of the postsynaptic neuron. To determine the dependency of neuronal burst frequency on the production rate of IP_3^{GABA}, r_{ip3}^{GABA}, a simulation was carried out (**Figure 13**) which shows the firing rates of the postsynaptic neuron under different production rates with f_{pre} fixed at 40 Hz. It can be seen that when the r_{ip3}^{GABA} increases, the frequency of the bursting decreases. For example, for the first 1,000 s, there are 6, 5, 4 bursts under the IP_3^{GABA} production rates (r_{ip3}^{GABA}) of 1.8, 2, and 2.2, respectively. This is because a high IP_3^{GABA} level requires a significant time period to degrade the total IP_3, and to restart the Ca^{2+} oscillation and bursting behavior, thus the bursting frequency is low. Note that a fixed frequency of the input stimulus (i.e., f_{pre} = 40 Hz) is used in this experiment, however the same results are observed

for other f_{pre} values such as 50 Hz, and the burst frequency variation is not constrained for specific f_{pre} values. The results in **Figures 12**, **13** demonstrate the functionalities of the GABA interneuron including the presynaptic frequency selectivity and postsynaptic bursting frequency regulation.

4. CONCLUSIONS

In this paper, a biophysical model is proposed where it is shown that GABA interneuron regulates the astrocytic IP_3 secondary messenger and thus the probability of release (PR) at the presynaptic terminal. In our model we propose that PR modulates the height of the plasticity window and therefore controls when synaptic potentiation/depression occurs. Specifically, the simulations show that during the weight potentiation phase, increasing IP_3 leads to a cycle of CICR events where each is followed by rapid degradation in IP_3. Over time the firing frequency of the postsynaptic neuron continually increases and eventually the synaptic weights stabilize. Postsynaptic firing results in the release of 2-AG into the extracellular space and this messenger binds to CB1R receptors on the astrocyte membrane. The associated IP_3^{AG} contributes to the total cytosolic IP_3 and eventually Ca^{2+} oscillations, and therefore the Glu (e-SP) pathway ceases: 2-AG also binds to CB1Rs on the presynaptic terminal causing a decrease of the synaptic transmission PR via the DSE pathway. PR therefore decreases at the presynaptic terminal which reduces the level of neurotransmitter in the cleft, and consequently the firing frequency of the postsynaptic neuron diminishes, as does IP_3^{AG}. Thereafter, the total IP_3/Ca^{2+} degrades significantly over time but is replenished by IP_3^{GABA} and a subsequent cycle of CICR events commences—the Glu (e-SP) pathway is re-established with an associated increase in PR and the level of neurotransmitter in the cleft is raised. However, in this instance weight potentiation does not occur as $PR < PR^*$. The postsynaptic neuron firing rate increases again until the Ca^{2+} transients stop and thereafter the activity of the postsynaptic neuron falls off again. A network burst has occurred and this is followed by repeated bursts where each coincides with Ca^{2+} transients: the network burst frequency correlates with the Ca^{2+} oscillatory wave. In addition, the GABA released by the GABA interneuron controls the frequency range within which the network bursts can occur. Future work will further explore other neurotransmitters released by astrocytes such as D-serine and ATP, and also slow inward currents at the postsynaptic terminal as a result of glutamate release by astrocytes.

The authors recognize that this study is based on biological findings of the simplest signaling mechanisms involving astrocytic GABA responses and astrocytic glutamate signaling in presynaptic terminals that regulate network function. Other factors, such as astrocytic ATP/adenosine release from astrocytes (Covelo and Araque, 2018), are not considered in the present model, but may also contribute to further shape of network activity, adding further complexity of the network effects of astrocyte signaling. Further studies incorporating these additional elements are therefore required to get a complete view of the astrocyte roles in network function. Despite this the present findings have potential implications for the generation of normal and pathologic circuit behavior in the brain, relevant to brain diseases that feature altered synaptic properties or where there is a propensity for the episodic synchronized bursting behavior of neurons. The electroencephalogram (EEG) is a composite product of population-level neuronal firing patterns of differing frequencies. Our findings suggest that GABA-B signaling via astrocytes may be relevant to the generation of certain frequencies and behaviors in the EEG. Seizures are the hallmark of the common brain disease epilepsy and are generated by hyper-synchronous discharges of populations of neurons. Notably, gene expression levels of key components modeled here, including the IP_3 receptor and GABA-B receptor, are dysregulated in human epileptic brain tissue or animal models (Matsumoto et al., 1996; Nishimura et al., 2005; Sheilabi et al., 2018) of epilepsy. Mutations in these genes have also been identified in individuals with epilepsy (Møller et al., 2017; Yoo et al., 2017). Indeed, the GABA-B receptor is a long-standing therapeutic target for the treatment of epilepsy (Bowery, 2006), and more recently the IP_3 receptor was reported to be a target of levetiracetam, one of the most effective anti-epileptic drugs (Nagarkatti et al., 2008). The present model offers a novel mechanism to explain how astrocyte-neuron interactions regulate seizure-like activity (Gómez-Gonzalo et al., 2010), and how alterations in the described pathways may contribute to hyper-synchronous firing. It may also offer therapeutic insights through targeted manipulation of the astrocytic GABA-B or IP_3 systems followed by evaluation of the resting electroencephalogram (EEG) and investigating whether this alters the frequency or occurrence of pathophysiological neuronal firing and seizures.

DATA AVAILABILITY

The raw data supporting the conclusions of this manuscript will be made available by the authors, without undue reservation, to any qualified researcher.

AUTHOR CONTRIBUTIONS

JL, LM, AA, JW, JHa, SK, DCH, NC, AT, JT, and DMH investigated and proposed the biophysical model. JL, LM, AA, JW, JHa, DCH, NC, and DMH wrote and revised the manuscript. JL, LM, AA, JW, JHa, DCH, NC, AJ, AT, JT, AM, JHi, and DMH analyzed the results and reviewed the manuscript.

FUNDING

This work acknowledges funding supports from EPSRC (EP/N007141X/1) (EP/N007050/1) and HFSP (RGP0036/2014).

REFERENCES

Alger, B. E. (2002). Retrograde signaling in the regulation of synaptic transmission: focus on endocannabinoids. *Progr. Neurobiol.* 68, 247–286. doi: 10.1016/S0301-0082(02)00080-1

Araque, A., Parpura, V., Sanzgiri, R. P., and Haydon, P. G. (1999). Tripartite synapses: glia, the unacknowledged partner. *Trends Neurosci.* 22, 208–215. doi: 10.1016/S0166-2236(98)01349-6

Arichi, T., Whitehead, K., Barone, G., Pressler, R., Padormo, F., Edwards, A. D., et al. (2017). Localization of spontaneous bursting neuronal activity in the preterm human brain with simultaneous EEG-fMRI. *eLife* 6:27814. doi: 10.7554/eLife.27814

Bienenstock, E. L., Cooper, L. N., and Munro, P. W. (1982). Theory for the development of neuron selectivity: orientation specificity and binocular interaction in visual cortex. *J. Neurosci.* 2, 32–48. doi: 10.1523/JNEUROSCI.02-01-00032.1982

Bowery, N. G. (2006). GABAB receptor: a site of therapeutic benefit. *Curr. Opin. Pharmacol.* 6, 7–43. doi: 10.1016/j.coph.2005.10.002

Breslin, K., Wade, J. J., Wong-Lin, K., Harkin, J., Flanagan, B., Van Zalinge, H., et al. (2018). Potassium and sodium microdomains in thin astroglial processes: a computational model study. *PLoS Comput. Biol.* 14:e1006151. doi: 10.1371/journal.pcbi.1006151

Covelo, A., and Araque, A. (2018). Neuronal activity determines distinct gliotransmitter release from a single astrocyte. *eLife* 7:32237. doi: 10.7554/eLife.32237

Dawson, A. P. (1997). Calcium signalling: how do IP3 receptors work? *Curr. Biol.* 7, 544–547. doi: 10.1016/S0960-9822(06)00277-6

De Pittà, M., Goldberg, M., Volman, V., Berry, H., and Ben-Jacob, E. (2009). Glutamate regulation of calcium and IP3 oscillating and pulsating dynamics in astrocytes. *J. Biol. Phys.* 35, 383–411. doi: 10.1007/s10867-009-9155-y

Dong, W. S., Zeng, F., Lu, S. H., Liu, A., Li, X. J., and Pan, F. (2015). Frequency-dependent learning achieved using semiconducting polymer/electrolyte composite cells. *Nanoscale* 7, 16880–16889. doi: 10.1039/C5NR02891D

Flanagan, B., McDaid, L., Wade, J., Wong-Lin, K., and Harkin, J. (2018). A computational study of astrocytic glutamate influence on post-synaptic neuronal excitability. *PLoS Comput. Biol.* 14, 1–25. doi: 10.1371/journal.pcbi.1006040

Foncelle, A., Mendes, A., Jedrzejewska-Szmek, J., Valtcheva, S., Berry, H., Blackwell, K. T., et al. (2018). Modulation of spike-timing dependent plasticity : towards the inclusion of a third factor in computational models. *Front. Comput. Neurosci.* 12, 1–21. doi: 10.3389/fncom.2018.00049

Gabbiani, F., Metzner, W., Wessel, R., and Koch, C. (1996). From stimulus encoding to feature extraction in weakly electric fish. *Nature* 38, 564–567. doi: 10.1038/384564a0

Gerstner, W., and Kistler, W. M. (2002). *Spiking Neuron Models: Single Neurons, Populations, Plasticity*. Cambridge University Press.

Ghosh-dastidar, S., and Adeli, H. (2009). Spiking neural networks. *Int. J. Neural Syst.* 19, 295–308. doi: 10.1142/S0129065709002002

Gómez-Gonzalo, M., Losi, G., Chiavegato, A., Zonta, M., Cammarota, M., Brondi, M., et al. (2010). An excitatory loop with astrocytes contributes to drive neurons to seizure threshold. *PLoS Biol.* 8:e1000352. doi: 10.1371/journal.pbio.1000352

Halassa, M. M., Fellin, T., Takano, H., Dong, J., and Haydon, P. G. (2007). Synaptic islands defined by the territory of a single astrocyte. *J. Neurosci.* 27, 6473–6477. doi: 10.1523/JNEUROSCI.1419-07.2007

Hu, J., Tang, H., Tan, K. C., Li, H., and Shi, L. (2013). A spike-timing-based integrated model for pattern recognition. *Neural Comput.* 25, 450–472. doi: 10.1162/NECO_a_00395

Izhikevich, E. M. (2003). Simple model of spiking neurons. *IEEE Trans. Neural Netw.* 14, 1569–1572. doi: 10.1109/TNN.2003.820440

Johnson, A. P., Liu, J., Millard, A. G., Karim, S., Tyrrell, A. M., Harkin, J., et al. (2018). Homeostatic fault tolerance in spiking neural networks: a dynamic hardware perspective. *IEEE Trans. Circ. Syst.* 65, 687–699. doi: 10.1109/TCSI.2017.2726763

Kullmann, D. M. (2011). Interneuron networks in the hippocampus. *Curr. Opin. Neurobiol.* 21, 709–716. doi: 10.1016/j.conb.2011.05.006

Kurosinski, P., and Götz, J. (2002). Glial cells under physiologic and pathologic conditions. *Arch. Neurol.* 59, 1524–1528. doi: 10.1001/archneur.59.10.1524

Li, Y.-X., and Rinzel, J. (1994). Equations for InsP3 receptor-mediated calcium oscillations derived from a detailed kinetic model: a Hodgkin-Huxley like formalism. *J. Theor. Biol.* 166, 461–473. doi: 10.1006/jtbi.1994.1041

Liu, J., Harkin, J., Maguire, L. P., Mcdaid, L. J., and Wade, J. J. (2018). SPANNER: a self-repairing spiking neural network hardware architecture. *IEEE Trans. Neural Netw. Learn. Syst.* 29, 1287–1300. doi: 10.1109/TNNLS.2017.2673021

Liu, J., Harkin, J., McElholm, M., McDaid, L., Jimenez-Fernandez, A., and Linares-Barranco, A. (2015). "Case study: bio-inspired self-adaptive strategy for spike-based PID controller," in *IEEE International Symposium on Circuits and Systems (ISCAS)* (Lisbon), 2700–2703.

Liu, J., McDaid, L. J., Harkin, J., Karim, S., Johnson, A. P., Millard, A. G., et al. (2019). Exploring self-repair in a coupled spiking astrocyte neural network. *IEEE Trans. Neural Netw. Learn. Syst.* 30, 865–875. doi: 10.1109/TNNLS.2018.2854291

Lüscher, C., and Malenka, R. C. (2012). NMDA receptor-dependent long-term potentiation and long-term depression (LTP/LTD). *Cold Spring Harb. Perspect. Biol.* 4, 1–15. doi: 10.1101/cshperspect.a005710

Magee, J. C., and Johnston, D. (1997). A synaptically controlled, associative signal for synaptic plasticity in hippocampal neurons. *Science* 275, 209–213. doi: 10.1126/science.275.5297.209

Marchant, J., Callamaras, N., and Parker, I. (1999). Initiation of IP3-mediated Ca2+ waves in Xenopus oocytes. *EMBO J.* 18, 5285–5299. doi: 10.1093/emboj/18.19.5285

Matsumoto, M., Nakagawa, T., Inoue, T., Nagata, E., Tanaka, K., Takano, H., et al. (1996). Ataxia and epileptic seizures in mice lacking type 1 inositol 1,4,5-trisphosphate receptor. *Nature* 379, 168–171. doi: 10.1038/379168a0

Miles, R., and Wong, R. K. (1986). Excitatory synaptic interactions between CA3 neurones in the guinea pig hippocampus. *J. Physiol.* 373, 397–418. doi: 10.1113/jphysiol.1986.sp016055

Møller, R. S., Wuttke, T. V., Helbig, I., Marini, C., Johannesen, K. M., Brilstra, E. H., et al. (2017). Mutations in GABRB3 From febrile seizures to epileptic encephalopathies. *Neurology* 88, 483–492. doi: 10.1212/WNL.0000000000003565

Naeem, M., McDaid, L. J., Harkin, J., Wade, J. J., and Marsland, J. (2015). On the role of astroglial syncytia in self-repairing spiking neural networks. *IEEE Trans. Neural Netw. Learn. Syst.* 26, 2370–2380. doi: 10.1109/TNNLS.2014.2382334

Nagarkatti, N., Deshpande, L. S., and DeLorenzo, R. J. (2008). Levetiracetam inhibits both ryanodine and IP3 receptor activated calcium induced calcium release in hippocampal neurons in culture. *Neurosci. Lett.* 436, 289–293. doi: 10.1016/j.neulet.2008.02.076

Navarrete, M., and Araque, A. (2010). Endocannabinoids potentiate synaptic transmission through stimulation of astrocytes. *Neuron* 68, 113–126. doi: 10.1016/j.neuron.2010.08.043

Nishimura, T., Schwarzer, C., Gasser, E., Kato, N., Vezzani, A., and Sperk, G. (2005). Altered expression of GABA-A and GABA-B receptor subunit mRNAs in the hippocampus after kindling and electrically induced status epilepticus. *Neuroscience* 134, 691–704. doi: 10.1016/j.neuroscience.2005.04.013

Perea, G., Gómez, R., Mederos, S., Covelo, A., Ballesteros, J. J., Schlosser, L., et al. (2016). Activity-dependent switch of GABAergic inhibition into glutamatergic excitation in astrocyte-neuron networks. *eLife* 5, 1–26. doi: 10.7554/eLife.20362

Reid, D., Hussain, A. J., and Tawfik, H. (2014). Financial time series prediction using spiking neural networks. *PLoS ONE* 9:e103656. doi: 10.1371/journal.pone.0103656

Serrano, A., Haddjeri, N., Lacaille, J.-c., and Robitaille, R. (2006). GABAergic network activation of glial cells underlies hippocampal heterosynaptic depression. *J. Neurosci.* 26, 5370–5382. doi: 10.1523/JNEUROSCI.5255-05.2006

Sheilabi, M. A., Battacharyya, D., Caetano, L., Thom, M., Reuber, M., Duncan, J. S., et al. (2018). Quantitative expression and localization of GABA-B receptor protein subunits in hippocampi from patients with refractory temporal lobe epilepsy. *Neuropharmacology* 136, 117–128. doi: 10.1016/j.neuropharm.2017.08.001

Song, S., Miller, K. D., and Abbott, L. F. (2000). Competitive Hebbian learning through spike-timing-dependent synaptic plasticity. *Nat. Neurosci.* 3, 919–926. doi: 10.1038/78829

Wade, J., McDaid, L., Harkin, J., Crunelli, V., and Kelso, S. (2012). Self-repair in a bidirectionally coupled astrocyte-neuron (AN) system based on retrograde signaling. *Front. Comput. Neurosci.* 6:76. doi: 10.3389/fncom.2012.00076

Wade, J. J., McDaid, L. J., Harkin, J., Crunelli, V., Kelso, J. A. S., and Beiu, V. (2011). "Exploring retrograde signaling via astrocytes as a mechanism for self repair," in *International Joint Conference on Neural Networks (IJCNN)* (San Jose, CA: IEEE), 3149–3155.

Yoo, Y., Jung, J., Lee, Y. N., Lee, Y., Cho, H., Na, E., et al. (2017). GABBR2 mutations determine phenotype in rett syndrome and epileptic encephalopathy. *Ann. Neurol.* 82, 466–478. doi: 10.1002/ana.25032

Conflict of Interest Statement: The authors declare that the research was conducted in the absence of any commercial or financial relationships that could be construed as a potential conflict of interest.

APPENDIX

TABLE A1 | GABA interneuron, neuron, and synapse parameters.

Parameter	Parameter description	Value	Source
τ_{GABA}	GABA decay rate	10 s	-
r_{GABA}	GABA production rate	0.07 μMs^{-1}	-
τ_m	Neuron membrane time constant	24 ms	-
R_m	Neuron membrane resistance	1.2GΩ	Wade et al., 2012
τ_{AG}	2-AG decay rate	10 s	Wade et al., 2012
r_{AG}	2-AG production rate	0.27 μMs^{-1}	Wade et al., 2012
r_I	Synaptic current production rate	16	-
PR^*	Learning activation level	0.45	-
r	Maximum height weighting factor of learning window	40	-
τ_+	Potentiation width of the plasticity window	40 ms	Liu et al., 2019
τ_-	Depression width of the plasticity window	40 ms	Liu et al., 2019

TABLE A2 | Astrocyte cell parameters.

Parameter	Parameter description	Value	Source
IP_3^{GABA*}	Baseline value of IP_3^{GABA}	0.16 μM	-
τ_{ip3}^{GABA}	Decay rate of IP_3^{GABA}	7 s	-
r_{ip3}^{GABA}	Production rate of IP_3^{GABA}	2 μM	-
IP_3^{AG*}	Baseline value of IP_3^{AG}	0.16 μM	Wade et al., 2012
τ_{ip3}^{AG}	Decay rate of IP_3^{AG}	7 s	Wade et al., 2012
r_{ip3}^{AG}	Production rate of IP_3^{AG}	5 μM	Wade et al., 2012
$K_{PLC\delta}$	Ca^{2+} affinity of PLCδ	0.1 μM	De Pittà et al., 2009
K_δ	Inhibition constant of PLCδ activity	1.5 μM	De Pittà et al., 2009
$\bar{r}_{5P}$	IP_3 degradation rate by IP-5P	0.27	-
$\bar{v}_{3K}$	Maximum degradation rate by IP_3-3K	2	De Pittà et al., 2009
K_D	Ca^{2+} affinity of IP_3-3K	0.7	De Pittà et al., 2009
K_3	IP_3 affinity of IP_3-3K	1	De Pittà et al., 2009
r_C	Maximal CICR rate	6 s^{-1}	De Pittà et al., 2009
r_L	Ca^{2+} leakage rate from ER	0.11 s^{-1}	De Pittà et al., 2009
v_{ER}	Maximum SERCA pump uptake rate	0.9 μMs^{-1}	De Pittà et al., 2009
k_{ER}	SERCA pump activation constant	0.1 μM	De Pittà et al., 2009
r_{Glu}	Production rate of glutamate	65 μMs^{-1}	-
τ_{Glu}	Decay rate of glutamate	0.1s	Wade et al., 2012
m_{eSP}	e-SP weighting factor	35000	-
τ_{eSP}	Decay rate of e-SP	40 s	Wade et al., 2012
a_2	IP3R Ca^{2+} inactivation binding rate	0.2 μMs^{-1}	Wade et al., 2012
c_0	Total free Ca^{2+} cytosol concentration	2 μM	Wade et al., 2012
c_1	Ratio of ER volume to cytosol volume	0.185	Wade et al., 2012
d_1	IP_3 dissociation constant	0.13 μM	Wade et al., 2012
d_2	Ca^{2+} inactivation dissociation constant	1.049 μM	Wade et al., 2012
d_3	IP_3 dissociation constant	0.9434 μM	Wade et al., 2012
d_5	Ca^{2+} activation dissociation constant	0.08234 μM	Wade et al., 2012
Ca^{2+} threshold	Astrocyte glutamate release Ca^{2+} threshold	0.7 μM	-
K_{AG}	DSE weighting factor	1,000	-

frontiers in Cellular Neuroscience

ORIGINAL RESEARCH
published: 09 August 2019
doi: 10.3389/fncel.2019.00367

Cannabidivarin Treatment Ameliorates Autism-Like Behaviors and Restores Hippocampal Endocannabinoid System and Glia Alterations Induced by Prenatal Valproic Acid Exposure in Rats

Erica Zamberletti[1], Marina Gabaglio[1], Marie Woolley-Roberts[2], Sharon Bingham[2], Tiziana Rubino[1] and Daniela Parolaro[1,3]*

[1] Department of Biotechnology and Life Sciences, University of Insubria, Varese, Italy, [2] GW Research Ltd., Cambridge, United Kingdom, [3] Zardi-Gori Foundation, Milan, Italy

OPEN ACCESS

Edited by:
Giovanni Cirillo, Second University of Naples, Italy

Reviewed by:
Javier Fernández-Ruiz, Complutense University of Madrid, Spain
Viviana Trezza, Roma Tre University, Italy

***Correspondence:**
Erica Zamberletti
erica.zamberletti@uninsubria.it

Specialty section:
This article was submitted to Cellular Neurophysiology, a section of the journal Frontiers in Cellular Neuroscience

Received: *13 June 2019*
Accepted: *29 July 2019*
Published: *09 August 2019*

Citation:
Zamberletti E, Gabaglio M, Woolley-Roberts M, Bingham S, Rubino T and Parolaro D (2019) Cannabidivarin Treatment Ameliorates Autism-Like Behaviors and Restores Hippocampal Endocannabinoid System and Glia Alterations Induced by Prenatal Valproic Acid Exposure in Rats. Front. Cell. Neurosci. 13:367. doi: 10.3389/fncel.2019.00367

Autism spectrum disorder (ASD) is a developmental condition whose primary features include social communication and interaction impairments with restricted or repetitive motor movements. No approved treatment for the core symptoms is available and considerable research efforts aim at identifying effective therapeutic strategies. Emerging evidence suggests that altered endocannabinoid signaling and immune dysfunction might contribute to ASD pathogenesis. In this scenario, phytocannabinoids could hold great pharmacological potential due to their combined capacities to act either directly or indirectly on components of the endocannabinoid system and to modulate immune functions. Among all plant-cannabinoids, the phytocannabinoid cannabidivarin (CBDV) was recently shown to reduce motor impairments and cognitive deficits in animal models of Rett syndrome, a condition showing some degree of overlap with autism, raising the possibility that CBDV might have therapeutic potential in ASD. Here, we investigated the ability of CBDV treatment to reverse or prevent ASD-like behaviors in male rats prenatally exposed to valproic acid (VPA; 500 mg/kg i.p.; gestation day 12.5). The offspring received CBDV according to two different protocols: symptomatic (0.2/2/20/100 mg/kg i.p.; postnatal days 34–58) and preventative (2/20 mg/kg i.p.; postnatal days 19–32). The major efficacy of CBDV was observed at the dose of 20 mg/kg for both treatment schedules. CBDV in symptomatic rats recovered social impairments, social novelty preference, short-term memory deficits, repetitive behaviors and hyperlocomotion whereas preventative treatment reduced sociability and social novelty deficits, short-term memory impairments and hyperlocomotion, without affecting stereotypies. As dysregulations in the endocannabinoid system and neuroinflammatory markers contribute to the development of some ASD phenotypes in the VPA model, neurochemical studies were performed after symptomatic treatment to investigate possible CBDV's effects on the endocannabinoid system, inflammatory markers and microglia activation in the hippocampus and prefrontal cortex. Prenatal VPA exposure increased CB1 receptor, FAAH and MAGL levels, enhanced GFAP, CD11b, and TNFα

levels and triggered microglia activation restricted to the hippocampus. All these alterations were restored after CBDV treatment. These data provide preclinical evidence in support of the ability of CBDV to ameliorate behavioral abnormalities resembling core and associated symptoms of ASD. At the neurochemical level, symptomatic CBDV restores hippocampal endocannabinoid signaling and neuroinflammation induced by prenatal VPA exposure.

Keywords: cannabidivarin, valproate, autism, endocannabinoid system, neuroinflammation

INTRODUCTION

Autism spectrum disorder (ASD) represents a group of developmental disabilities whose primary symptoms include social communication and interaction impairments with restricted or repetitive motor movements, frequently associated with general cognitive deficits (American Psychiatric Association [APA], 2013). About 1% of the global population receives an ASD diagnosis (Baio et al., 2018), with a male to female ratio of 3:1 (Loomes et al., 2017). Diagnosis can be made as early as 2 years of age and patients are expected to have a normal lifespan. Despite the critical medical need, no approved treatments for the core symptoms of ASD are available; hence, reliable animal models are of fundamental importance for identifying and testing new therapeutic strategies. Although ASD is a typical human pathology, endophenotypes including impairments of social interaction, cognitive deficits, repetitive behaviors and motor dysfunctions can be reproduced in rodents by means of genetic and/or environmental manipulations (Ergaz et al., 2016; Kim et al., 2016). Environmentally based models are relevant when the same risk factor contributing to human autism produces similar brain and behavioral alterations in the animal. The use of valproic acid (VPA) in pregnancy has been consistently associated with an increased risk to develop congenital malformations and features of ASD in children (Duncan, 2007; Dufour-Rainfray et al., 2011; Christensen et al., 2013; Roullet et al., 2013; Ornoy et al., 2019). Similar to humans, rodents prenatally exposed to VPA show increased impaired social interactions and preference for social novelty, stereotypic repetitive behaviors, learning and memory defects and hypersensitivity (Schneider and Przewłocki, 2005; Dufour-Rainfray et al., 2010; Gandal et al., 2010; Kim et al., 2011; Mehta et al., 2011; Melancia et al., 2018). Therefore, because of its strong construct and face validity, the VPA animal model has been one of the most widely used to understand the neural underpinnings and to test novel therapeutic possibilities in the context of ASD (Mabunga et al., 2015; Ornoy et al., 2015; Tartaglione et al., 2019).

Recent studies in the prenatal VPA exposure model have implicated the endocannabinoid system in the development of ASD-like features. Changes in components of this neuromodulatory system were reported in different brain regions as a consequence of *in utero* VPA exposure, including alterations in 2-arachidonyilglycerol (2-AG) and anandamide (AEA) signaling and abnormalities in CB1 receptor (Kerr et al., 2013, 2016; Servadio et al., 2016; Melancia et al., 2018). Changes in other targets including PPARα, PPARγ, and GPR55 receptors were also observed (Kerr et al., 2013; Servadio et al., 2016; Melancia et al., 2018). Remarkably, recent studies have confirmed the presence of dysregulations of the endocannabinoid system in ASD patients (Brigida et al., 2017; Yeh and Levine, 2017; Karhson et al., 2018; Aran et al., 2019). A correlation between altered endocannabinoid signaling and ASD traits is supported by the observation that enhancing AEA signaling through inhibition of its degradation partially attenuated the behavioral phenotype induced by prenatal VPA exposure (Kerr et al., 2016; Servadio et al., 2016; Melancia et al., 2018), suggesting that modulation of the endocannabinoid signaling could represent a novel strategy for mitigating ASD symptoms. Besides the endocannabinoid system, recent evidence suggests that modulation of immune dysfunction might be beneficial toward ASD symptomatology. Indeed, signs of neuroinflammation have been reported in the brain of ASD patients, including microglia and astrocyte activation and increased expression of pro-inflammatory factors (Vargas et al., 2005; Morgan et al., 2010; Suzuki et al., 2013; Kern et al., 2016), reinforcing the idea that immunological dysfunction might play a role in ASD. In line with human evidence, signs of neuroinflammation, including increased reactive oxygen species, pro-inflammatory cytokines, astrocyte and microglia activation, have been observed in the VPA-induced ASD animal model (Lucchina and Depino, 2014; Codagnone et al., 2015; Deckmann et al., 2018; Kuo and Liu, 2018; Bronzuoli et al., 2019). The administration of compounds able to reduce this inflammatory response resulted in neuroprotection and amelioration of ASD-like phenotypes (Banji et al., 2011; Bambini-Junior et al., 2014; Pragnya et al., 2014; Al-Amin et al., 2015; Gao et al., 2016; Kumar and Sharma, 2016; Morakotsriwan et al., 2016; Bertolino et al., 2017; Deckmann et al., 2018; Fontes-Dutra et al., 2018), suggesting that inflammatory dysfunction might play a role in the development of ASD symptoms.

In this scenario, phytocannabinoids possess great and interesting pharmacological potentials. In addition to their indirect actions on components of the endocannabinoid system, plant-derived cannabinoids possess a broad range of pharmacological properties including proved anti-inflammatory and anti-oxidant properties (Nagarkatti et al., 2009; Ligresti et al., 2016; Morales et al., 2017; Maroon and Bost, 2018) that may contribute to achieve an overall beneficial effect in the context of ASD.

Recent studies have shown that the plant-derived cannabinoid Cannabidivarin (CBDV) exerts beneficial effects toward neurological and motor impairments as well as cognitive deficits in two animal models of Rett syndrome (Vigli et al., 2018; Zamberletti et al., 2019). CBDV's simultaneous capacity to ameliorate neurological and motor defects as well as cognitive

impairment in these animal models raises the possibility that this phytocannabinoid might have interesting yet unexplored therapeutic potential in ASD, prompting its evaluation in animal models of this disorder.

Therefore, in this study we examined the ability of CBDV treatment to reverse or prevent sociability and preference for social novelty deficits, repetitive behaviors, hyperactivity and recognition memory impairments in rats prenatally exposed to VPA (500 mg/kg i.p.; gestation day 12.5). To this aim, CBDV was administered using two treatment protocols in the male offspring of VPA-treated dams; a symptomatic treatment was performed between postnatal day (PND) 34–58 to assess the ability of CBDV to counteract VPA-induced autism-like behaviors whereas a preventative treatment was carried out from PND 19–32 to test CBDV's ability to prevent the appearance of autism-like traits in the model. In addition to behavioral analysis, neurochemical studies were carried out after symptomatic CBDV treatment to investigate its effect on the endocannabinoid system as well as on inflammatory markers and microglia activation in the hippocampus and prefrontal cortex (PFC).

MATERIALS AND METHODS

Prenatal VPA Administration

Pregnant Sprague-Dawley rats (Charles River, Calco, Italy) received a single intraperitoneal injection of sodium valproate 500 mg/kg (or saline) on gestation day (GD) 12.5. Sodium valproate (Sigma Aldrich, Milan) was dissolved in saline at a concentration of 250 mg/ml. Females were housed individually and were allowed to raise their own litters. Gross toxic effects were not observed in VPA-exposed rats in both dams and pups. No postnatal mortality was observed. Body weight was slightly but significantly reduced in VPA-exposed pups with respect to controls from PND 12–17. Eye opening was delayed in VPA-exposed pups with respect to vehicles between PND 14 and 16. At PND 9, male pups from VPA-treated dams showed significantly increased latencies in nest-seeking behavior compared to controls as well as impaired righting reflex (**Supplementary Methods, Supplementary Results** and **Supplementary Figure S1**). Nine vehicle- and 15 VPA-treated dams were used in this study. Litters were not culled and the offspring was weaned on PND 21, separated by sex and the animals were kept four to a cage, with controlled temperature and light conditions. Rats had free access to food (standard laboratory pellets) and water. All the experiments were performed in the light phase between 09:00 and 15:00. Experimental procedures were performed in accordance with the guidelines released by the Italian Ministry of Health (D.L. 2014/26) and the European Community directives regulating animal research (2010/63/EU). Protocols were approved by the Italian Minister for Scientific Research and all efforts were made to minimize the number of animals used and their suffering.

CBDV Treatment

A total of 54 rats from 9 vehicle-treated dams and 75 rats from 15 VPA-treated dams were used in this study. Pharmacological treatments and behavioral testing were carried out in 5–6 rats per litter during four separate experiments. Pure CBDV was provided by GW Research Ltd. (Cambridge, United Kingdom) and dissolved in ethanol, Kolliphor EL and saline (2:1:18) and was administered according to the treatment schedules reported in **Figures 1A**, **2A**. Symptomatic treatment with CBDV 0.2, 2, 20 or 100 mg/kg/day i.p. was performed starting from PND 34 (early adolescence) to 58 (early adulthood) in the male offspring of dams injected with VPA 500 mg/kg (or saline) on GD 12.5 (**Figure 1A**). Starting from PND 56, a series of behavioral tests was performed. The three chamber test was carried out at PND 56 in order to assess the effect of chronic CBDV on sociability and social novelty preference, the novel object recognition (NOR) test was performed at PND 57 to assess short-term memory, and locomotion and stereotyped/repetitive behaviors were measured in the activity cage at PND 58. Preventative treatment with CBDV 2 or 20 mg/kg/day i.p. was performed starting from PND 19 (pre-weaning) to 32 (post-weaning) in the male offspring of VPA- and vehicle-treated dams (**Figure 2A**). Behavioral analysis was carried out at PND 30 (three chamber test), 31 (NOR test), and 32 (repetitive behavior and locomotion).

Behavioral Studies

Three-Chamber Test

The three-chamber test was performed to measure social approach and social preference. In brief, animals were placed into a novel arena (80 cm × 31.5 cm × 40 cm) composed of three communicating chambers separated by Perspex walls with central openings allowing access to all chambers for 5 min. Distance moved (meters) and time spent (seconds) in the various compartments were recorded during this time to evaluate general locomotor activity and ensure that animals did not have a preference for a particular side of the arena. Following this acclimatization period, animals were briefly confined to the central chamber while an unfamiliar rat confined in a small wire cage was placed in one of the outer chambers. An identical empty wire cage was placed in the other chamber. The unfamiliar rat was randomly either assigned to the right or left chamber of the arena. The test animal was then allowed to explore the arena for a further 5 min. The arena was cleaned between animals with 0.1% acetic acid. Time spent engaging in investigatory behavior with the rat was evaluated with the aid of ANY-maze program (Ugo Basile, Italy) in order to examine social approach. To investigate the preference for social novelty, a novel unfamiliar rat was then placed in the empty cage and the test animal was allowed to explore the arena for a further 5 min. Time spent engaging in investigatory behavior with the novel unfamiliar rat was evaluated with the aid of Anymaze program (Ugo Basile, Italy) in order to examine the preference for social novelty. Sociability index and preference for social novelty index were calculated as the ratio of time spent exploring the stranger rat (sociability) or the unknown rat (preference for novelty) vs. the total time of exploration × 100.

Novel Object Recognition (NOR) Test

The experimental apparatus used for the object recognition test was an open-field box (43 cm × 43 cm × 32 cm)

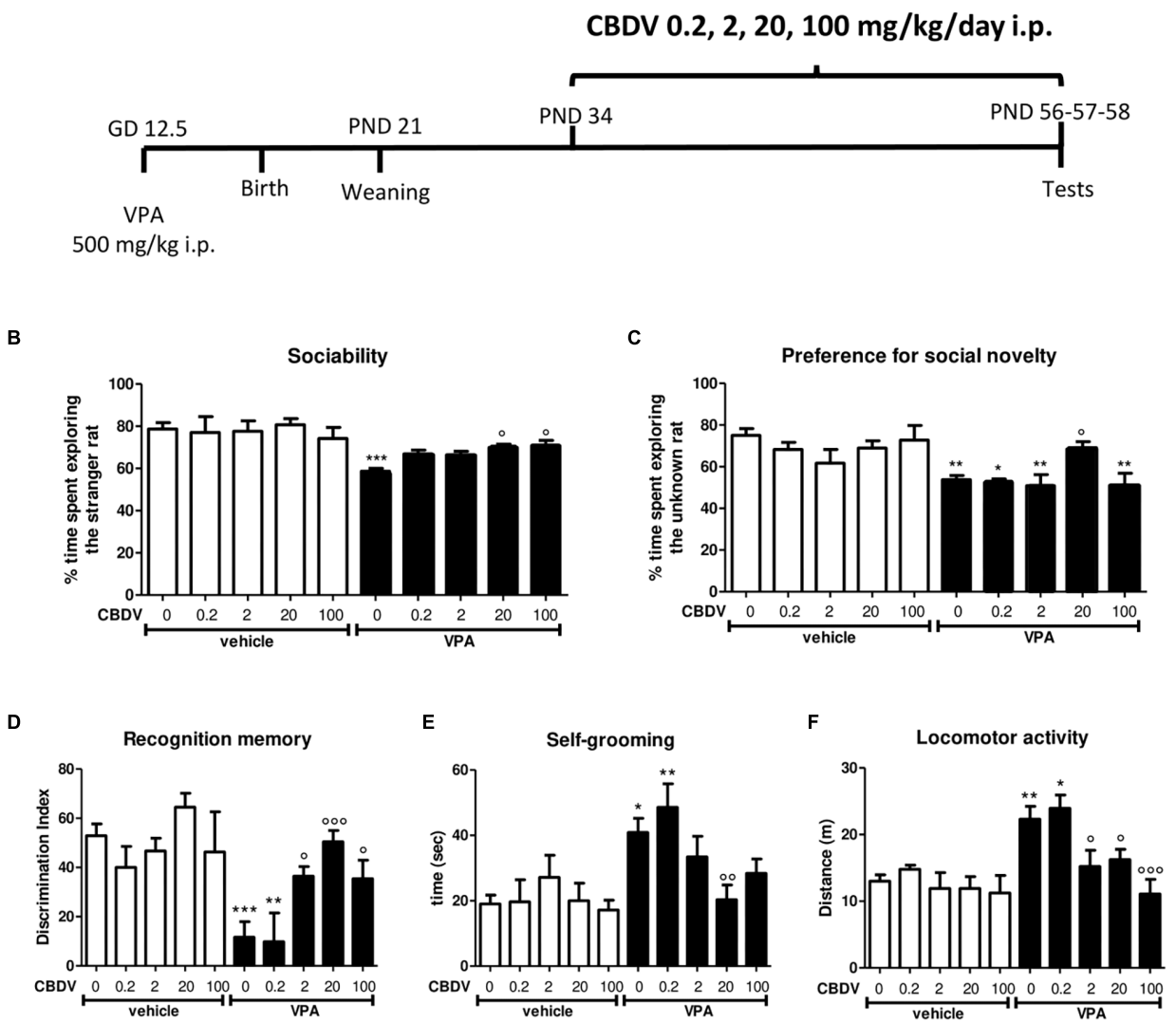

FIGURE 1 | Symptomatic CBDV treatment protocol. Pregnant Sprague-Dawley rats received a single injection of VPA 500 mg/kg i.p. (or vehicle) at GD 12.5. **(A)** Symptomatic treatment with CBDV 0.2, 2, 20, 100 mg/kg/day i.p. was performed from PND 34 and male offspring was tested at PND 56 (three chamber test), 57 (NOR test), and 58 (repetitive behavior and locomotion). Effect of symptomatic CBDV 0.2, 2, 20, 100 mg/kg/day treatment in male offspring of VPA- and vehicle-exposed rats on **(B)** sociability and **(C)** social novelty preference as measured through the three chamber test; **(D)** short-term memory as measured through the novel object recognition; **(E)** compulsive self-grooming and **(F)** locomotor activity as measured in the activity cage. Data represent mean ± SEM of $n = 9$ vehicle-vehicle, $n = 6$ vehicle-CBDV 0.2 mg/kg, $n = 6$ vehicle-CBDV 2 mg/kg, $n = 8$ vehicle-CBDV 20 mg/kg, $n = 6$ vehicle-CBDV 100 mg/kg, $n = 15$ VPA-vehicle, $n = 5$ VPA-CBDV 0.2 mg/kg, $n = 10$ VPA-CBDV 2 mg/kg, $n = 13$ VPA-CBDV 20 mg/kg, $n = 10$ VPA-CBDV 100 mg/kg. Results were analyzed by two-way ANOVA followed by Tukey's *post hoc* test (***$p < 0.001$, **$p < 0.01$, *$p < 0.05$ vs. vehicle-vehicle;°°°$p < 0.001$,°°$p < 0.01$,°$p < 0.05$ vs. VPA-vehicle).

made of Plexiglas, placed in a dimly illuminated room. The experiment was performed and analyzed as previously described (Zamberletti et al., 2014). Animals performed each test individually. Briefly, each animal was placed in the arena and allowed to explore two identical previously unseen objects for 5 min (familiarization phase). After an inter-trial interval of 3 min one of the two familiar objects was replaced by a novel, previously unseen object and rats were returned to the arena for the 5-min test phase. The arena was cleaned between animals with 0.1% acetic acid. During the test phase the time spent exploring the familiar object (Ef) and the new object (En) was videotaped and recorded separately by two observers blind to the treatment groups and the discrimination index was calculated as follows: $[(\mathrm{En} - \mathrm{Ef})/(\mathrm{En} + \mathrm{Ef})] \times 100$.

Activity Cage

Locomotor activity was recorded in an activity cage (40 cm × 40 cm × 40 cm) for 20 min with the aid of Anymaze program (Ugo Basile, Italy). In this period, repetitive behaviors

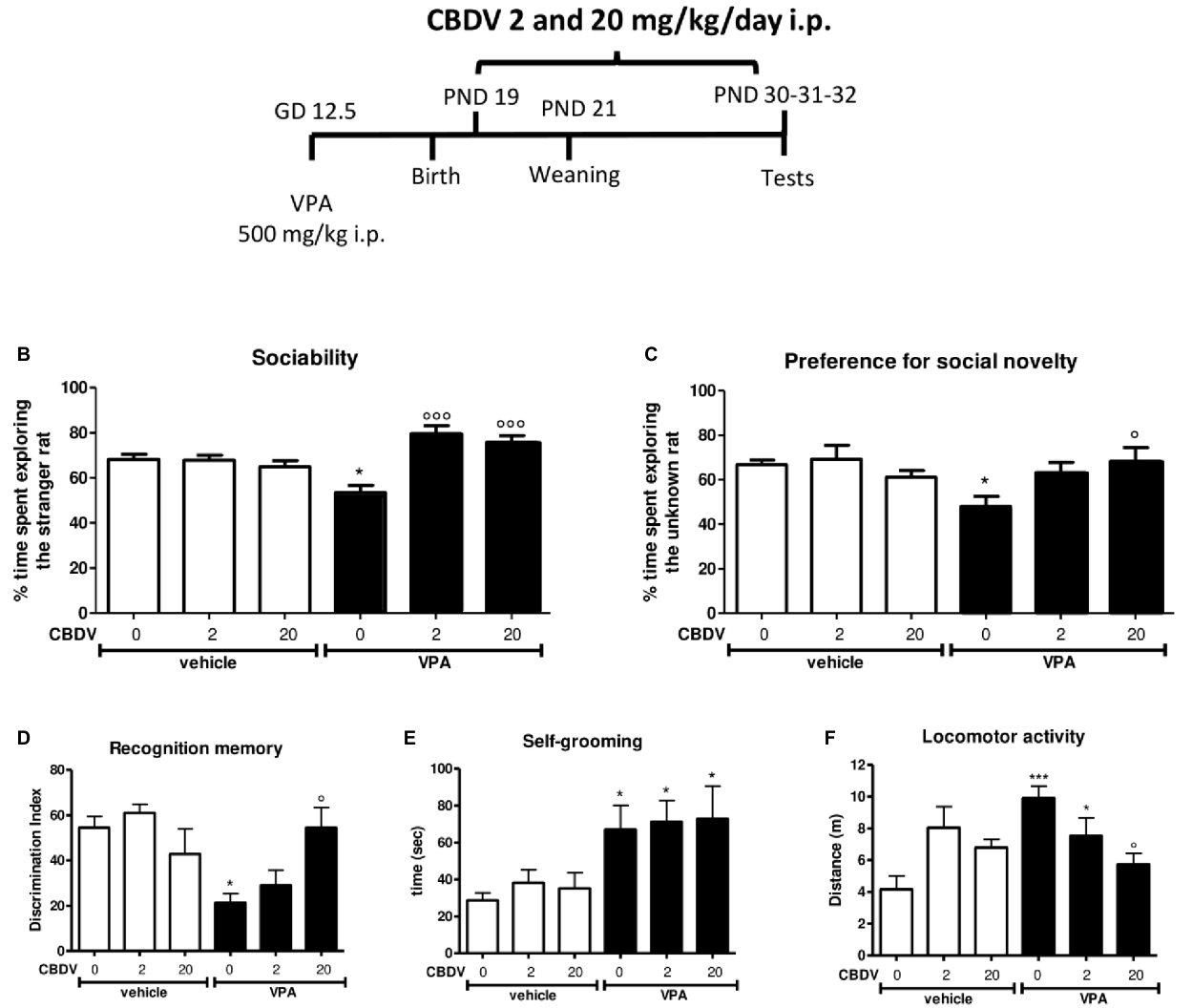

FIGURE 2 | Preventative CBDV treatment protocol. Pregnant Sprague-Dawley rats received a single injection of VPA 500 mg/kg i.p. (or vehicle) at GD 12.5. **(A)** Preventative treatment with CBDV 2 or 20 mg/kg/day i.p. was performed from PND 19 and animals were tested at PND 30 (three chamber test), 31 (NOR test), and 32 (repetitive behavior and locomotion). Effect of preventative CBDV 2, 20 mg/kg/day treatment in male offspring of VPA- and vehicle-exposed rats on **(B)** sociability and **(C)** social novelty preference as measured through the three chamber test; **(D)** short-term memory as measured through the novel object recognition test; **(E)** compulsive self-grooming and **(F)** locomotor activity as measured in the activity cage. Data represent mean ± SEM of $n = 7$ vehicle-vehicle, $n = 6$ vehicle-CBDV 2 mg/kg, $n = 6$ vehicle-CBDV 20 mg/kg, $n = 6$ VPA-vehicle, $n = 8$ VPA-CBDV 2 mg/kg, $n = 8$ VPA-CBDV 20 mg/kg and were analyzed using two-way ANOVA followed by Tukey's *post hoc* test (***$p < 0.001$, *$p < 0.05$ vs. vehicle-vehicle;°°°$p < 0.01$,°$p < 0.05$ vs. VPA-vehicle).

(compulsive self-grooming) were measured by an observer blind to the treatment group. The cage was cleaned between animals with 0.1% acetic acid.

Biochemical Studies

All animals underwent behavioral assessment. 24 h after the last CBDV (or vehicle) injection, all the animals were euthanized, their brain tissues collected and randomly assigned to different procedures for subsequent biochemical analysis. For Western blot analysis, PFC and hippocampi were dissected, frozen in liquid nitrogen and stored at −80°C; for immunohistochemistry, the brains were quickly removed and post-fixed in 4% paraformaldehyde in 100 mM phosphate buffer pH7.4, stored in fixative for 48 h, kept in 30% sucrose for 24 h. Coronal sections were serially collected using a Leica cryostat CM1510 set to 40 μm thickness and a −20°C chamber temperature.

Western Blotting

Cytosolic fractions from rat hippocampus and PFC were obtained using a protocol published by Shen and Chen (2013), with slight modifications. In brief, animals were sacrificed and cerebral areas quickly dissected. Samples were homogenized by 25 strokes in a

glass-glass homogenizer in 0.32 M sucrose solution containing 20 mM HEPES, 1 mM $MgCl_2$, protease inhibition cocktail, and 0.1 mM phenylmethylsulfonyl fluoride (PMSF) (pH 7.4). The homogenized tissue was centrifuged at 500 × *g* for 2 min. Resultant pellets (P1) were resuspended in 500 μL of a solution containing HEPES 20 mM, $MgCl_2$ 1.5 mM, NaCl 420 mM, EDTA 0.2 mM, glycerol 25%, DTT 2 mM, PMSF 2 mM, protease inhibition cocktail and stored as nuclear fraction. The resulting supernatant (S1) was centrifuged at 10,000 × *g* for 10 min to obtain a fraction containing mitochondria and synaptosome-enriched pellets (P2) and the supernatant (S2) containing soluble proteins. S2 fraction was conserved as cytosolic fraction while the P2 fraction was resuspended in 0.32 M sucrose, layered onto 0.8 M sucrose and centrifuged at 4100 rpm for 15 min in a swinging bucket rotor to obtain crude synaptosome fractions. The protein concentrations were determined according to the Micro-BCA assay kit (Pierce, Rockford, IL, United States).

Equal amount of protein lysates from the cytosolic fractions (30 μg) were run on a 10% SDS-polyacrylamide gel. The proteins were then transferred to polyvinylidene difluoride (PVDF) membranes, blocked for 2 h at room temperature in 5% dry skimmed milk in TBS 1×, 0.1% tween-20 before incubation overnight at 4°C with the primary antibody. The following primary antibodies were used: rabbit polyclonal anti-CB1 (1:1000; Cayman Chemical, United States), rabbit polyclonal anti-CB2 (1:1000; Cayman Chemical, United States), rabbit polyclonal anti-FAAH (1:1000; Cayman Chemical, United States), rabbit polyclonal anti-MAGL (1:1000; Cayman Chemical, United States), rabbit polyclonal anti-NAPE-PLD (1:3000; Cayman Chemical, United States), goat polyclonal anti-DAGLα (1:1000; AbCam, United Kingdom), rabbit polyclonal anti-GFAP (1:1000; Sigma Aldrich, United States), rabbit polyclonal anti-CD11b (1:1000; Novus Biologicals, United States), rabbit polyclonal anti-TNF-α (1:2000; Millipore, United States).

Bound antibodies were detected with horseradish peroxidase (HRP) conjugated secondary anti-rabbit, anti-mouse or anti-goat antibodies (1:1000–10000; Santa Cruz Biotechnology, United States) for 1 h at room temperature and visualized using ECL Western Blotting Detection Reagents (Bio-Rad Laboratories, Hercules, CA, United States). For detection of β-actin, the blots were stripped with Restore Western Blot Stripping Buffer (Thermo Scientific, Rockford, IL, United States) and re-blotted with mouse monoclonal anti-β-actin (1:20000; Sigma Aldrich, United States) overnight at 4°C and visualized as described above. Bands were detected with G-Box (Syngene) instrument. For densitometry, images were digitally scanned and optical density of the bands was quantified using ImageJ software (NIH, Bethesda, MD, United States) and normalized to controls. To allow comparison between different blots, the density of the bands was expressed as arbitrary units.

Immunohistochemistry

Free-floating sections containing the dorsal hippocampus were washed three times in 0.05% Tryton X-100 in TBS, incubated with 3% normal goat serum, 0.05% Triton X-100 in TBS for 1 h at room temperature and then overnight at 4°C with rabbit anti-IBA1 antibody (1:1000, Wako, Neuss, Germany) diluted in blocking solution. After blocking peroxidase activity with 0.3% H_2O_2 in TBS for 15 min, sections were washed in TBS and incubated for 4 h at room temperature with HRP-conjugated goat anti-rabbit antibody (1:500; Santa Cruz Biotechnology, United States). The peroxidase activity was revealed with 0.05% diaminobenzidine and 0.03% hydrogen peroxide in PBS for 10 min. After several washes in PBS, sections were mounted on gelatin-coated slides, dehydrated and cover slipped. For each animal, a complete series of one-in-six sections (240 μm apart) through the hippocampus was analyzed. Digital Images were captured using Retiga R1 CCD camera (QImaging, Surrey, BC, Canada) attached to an Olympus BX51 (Tokyo, Japan) polarizing/light microscope. Ocular imaging software (QImaging) was used to import images from the camera. Images of microglia cells in the subgranular zone of the hippocampus were acquired by first delineating the brain sections and the regions of interest at low magnification (×4 objective) and the region of interest outlines were further refined under a ×40 objective. Three mice per each experimental group (four sections/mouse) were analyzed. The morphometric analysis was carried out in DAB-stained microglial cells labeled with IBA-1 antibody. For this purpose, cells were selected and cropped according to the following criteria: (i) random selection in the subgranular zone of the hippocampus; (ii) no overlapping with neighboring cells; and (iii) complete soma and branches (at least apparently). Selection was done blinded to the treatment. Eight cells from each animal were analyzed. Each grayscale single cell cropped image was processed in a systematic way to obtain binary image using the same threshold for all pictures. The binary image was edited to clear the background and transformed into a filled shape and its pairwise outline shape that were used for morphological parameters measurements. Analysis was performed using FIJI free software (NIH, Bethesda, MD, United States). Four parameters, measured on the filled and outlined processed images obtained as described previously (Fernández-Arjona et al., 2017), were analyzed: cell area, cell perimeter, roundness of the soma and soma area.

Statistical Analysis

The Shapiro–Wilk normality test was first used to determine if the data were normally distributed. Results were then expressed as mean ± SEM and quantitative normally distributed data were analyzed by two-way ANOVA (VPA and CBDV as independent variables), followed by Tukey's *post hoc* test. The level of statistical significance was set at $p < 0.05$.

RESULTS

Behavioral Studies

Symptomatic CBDV Treatment

Figure 1 represents the effect of symptomatic CBDV treatment (0.2, 2, 20, and 100 mg/kg/day; PND 34–58; **Figure 1A**)

on autism-like phenotypes in the male offspring of VPA-exposed rats.

Sociability and social novelty preference

In the three-chamber test (**Figures 1B,C**), no differences in the time spent in each compartment of the apparatus were observed during the habituation phase, suggesting that animals belonging to all the experimental groups did not show a preference for a particular side of the arena (data not shown). During the sociability test (**Figure 1B**), two-way ANOVA revealed significant main effects of VPA [$F_{(1,75)} = 34.35$; $p < 0.0001$] and VPA × CBDV interaction [$F_{(4,75)} = 2.636$; $p = 0.0405$] on the percentage of time spent exploring the stranger rat with respect to the empty cage. Indeed, the percentage of time spent by male VPA-exposed rats in the chamber containing the unfamiliar rat was significantly reduced compared to controls (58.673 ± 1.389% in VPA-vehicle vs. 78.668 ± 3.069% in vehicle-vehicle). CBDV at all doses tested did not affect sociability when administered to control animals. CBDV treatment at doses of 20 and 100 mg/kg significantly restored the impairment in sociability observed in VPA rats while doses of 0.2 and 2 mg/kg failed to reverse the sociability deficit in VPA-treated rats.

Concerning the preference for social novelty (**Figure 1C**), significant effects of VPA [$F_{(1,75)} = 21.54$; $p < 0.0001$] and VPA × CBDV interaction [$F_{(4,75)} = 2.556$; $p = 0.0456$] were observed on the percentage of time spent exploring the unknown rat during the test. Control male rats spent a significantly higher percentage of time exploring the novel rat than the known rat (75.021 ± 3.301%). In contrast, VPA animals spent a similar time exploring the two stimuli (53.757 ± 2.072%). Treatment with CBDV 20 mg/kg completely reversed the deficit in social preference in VPA rats, as demonstrated by the fact that VPA-CBDV rats spent significantly more time exploring the novel rats with respect to the familiar one (69.128 ± 2.900%). In contrast, CBDV 0.2, 2, and 100 mg/kg were not able to restore social novelty preference in VPA rats. None of the doses tested had *per se* any effect on social novelty preference when administered to controls.

Short-term recognition memory

Figure 1D represents the effect of chronic CBDV 0.2, 2, 20, and 100 mg/kg/day treatment on short-term memory as evaluated through the NOR test. Total exploration time during the familiarization phase was similar in all the groups under investigation (data not shown). During the test phase, significant effects of VPA [$F_{(1,75)} = 17.47$; $p < 0.0001$] and VPA × CBDV interaction [$F_{(4,75)} = 4.565$; $p = 0.0024$] were observed. Prenatal VPA administration significantly impaired short-term memory, as demonstrated by a significant reduction of the discrimination index by about 81% with respect to controls. Statistical analysis did not reveal any significant effect of CBDV when administered in control rats. Interestingly, CBDV 2, 20, and 100 mg/kg significantly reversed the short-term memory deficit in male VPA rats, without affecting *per se* recognition memory when administered to vehicles. In contrast, CBDV 0.2 mg/kg failed to counteract memory deficits in VPA rats, the discrimination index being still reduced by about 79% with respect to controls.

Compulsive self-grooming and locomotion

The effect of chronic CBDV 0.2, 2, 20, and 100 mg/kg/day treatment on compulsive self-grooming and locomotor activity is reported in **Figures 1E,F** respectively.

Statistical analysis showed significant effects of VPA [$F_{(1,75)} = 17.06$; $p < 0.0001$] and VPA × CBDV interaction [$F_{(4,75)} = 2.518$; $p = 0.0483$] and a trend for CBDV's effect [$F_{(4,75)} = 2.381$; $p = 0.0590$] on self-grooming. VPA exposure significantly increased the time spent by male rats in compulsive self-grooming by about 121% with respect to vehicles. Chronic CBDV administration at the dose of 20 mg/kg significantly normalized the time spent in repetitive behaviors in VPA-treated rats without having any effect when administered to controls. CBDV 2 and 100 mg/kg showed a trend to ameliorate compulsive self-grooming in VPA-vehicle rats. The lowest dose of CBDV was instead ineffective.

Main effects of VPA [$F_{(1,75)} = 17.52$; $p < 0.0001$], CBDV [$F_{(4,75)} = 5.527$; $p = 0.0006$] and VPA × CBDV interaction [$F_{(4,75)} = 2.485$; $p = 0.0500$] were also found on locomotor activity. Indeed, VPA administration significantly increased locomotion by about 69% compared to controls and CBDV administration at the dose of 2, 20, and 100 mg/kg significantly normalized it. In contrast, CBDV 0.2 mg/kg failed to recover hyperlocomotion in VPA-exposed rats. None of the CBDV doses tested affected locomotion in control animals.

Preventative CBDV Treatment

Figure 2 represents the effect of preventative CBDV treatment (2 and 20 mg/kg/day; PND 19–32; **Figure 2A**) on autism-like phenotypes in the male offspring of VPA-exposed rats.

Sociability and social novelty preference

The effect of preventative CBDV 2 and 20 mg/kg/day treatment on sociability in the male offspring of VPA- and vehicle-exposed rats, as measured through the three chamber apparatus is shown in **Figure 2B**. During the habituation phase, VPA and CBDV administration did not affect the time spent in each compartment of the maze and all animals spent similar amounts of time exploring each compartment of the apparatus (data not shown). During the sociability test, significant effects of VPA [$F_{(1,35)} = 9.385$; $p = 0.0005$] and VPA × CBDV interaction [$F_{(2,35)} = 11.78$; $p = 0.0001$] were found. Vehicle-vehicle rats spent significantly more time exploring the unfamiliar rat compared to the empty cage (68.113 ± 2.345%). A similar effect was also observed in vehicle animals treated with CBDV 2 mg/kg (67.773 ± 2.297%) and 20 mg/kg (64.861 ± 2.788%). In contrast, male VPA-exposed rats spent similar amount of time in the chamber containing the unfamiliar rat compared to the time spent in the empty compartment when compared to controls (53.484 ± 3.220%), indicating a deficit in sociability. Chronic CBDV treatment at both doses significantly prevented the deficit in sociability in VPA rats without affecting sociability in control animals.

In the preference for social novelty trial (**Figure 2C**), statistical analysis showed a significant VPA × CBDV interaction [$F_{(2,35)} = 4.426$; $p = 0.0196$] and a trend for VPA [$F_{(1,35)} = 4.088$; $p = 0.0511$] and CBDV [$F_{(2,35)} = 3.174$; $p = 0.0545$] effects.

Control male rats spent a significantly greater percentage of time exploring the novel rat than the known rat (66.819 ± 1,995%). A similar effect was also present in vehicle animals treated with CBDV 2 mg/kg (69.199 ± 6.227%) and 20 mg/kg (61.095 ± 3.0147%). Conversely, VPA animals spent a similar percentage of time exploring the two stimuli (48.003 ± 4.535%). Treatment with CBDV 2 and 20 mg/kg significantly prevented the deficit in social novelty preference in VPA-exposed rats.

Short-term recognition memory

Figure 2D depicts the effect of preventative CBDV 2 and 20 mg/kg/day treatment on short-term memory in vehicle- and VPA-treated rats evaluated through the NOR test. Total exploration time during the familiarization phase was similar in all the groups under investigation (data not shown).

Two-way ANOVA revealed significant effects of VPA [$F_{(1,35)}$ = 8.943; p = 0.0051] and VPA × CBDV interaction [$F_{(2,35)}$ = 6.127; p = 0.0052] on short-term memory. Prenatal VPA administration significantly impaired short-term memory, as demonstrated by a significant reduction of the discrimination index by about 60.9% with respect to controls. Both doses of CBDV did not affect recognition memory when administered to vehicles. CBDV 20 mg/kg significantly prevented the short-term memory deficit in male VPA rats, whereas the lowest dose was ineffective.

Compulsive self-grooming and locomotion

Figures 2E,F represent the effect of preventative CBDV 2 and 20 mg/kg/day treatment on repetitive behaviors (compulsive self-grooming) and locomotion, respectively.

A significant main effect of VPA [$F_{(1,35)}$ = 13.64; p = 0.0008] was found on self-grooming behavior. Indeed, VPA exposure significantly increased the time spent by male rats in compulsive self-grooming by about 133.9% with respect to vehicle-vehicle animals. CBDV treatment did not affect self-grooming in control rats and no dose of CBDV tested was able to prevent compulsive self-grooming in male VPA-exposed rats.

Significant VPA [$F_{(1,35)}$ = 7.301; p = 0.0106] and VPA × CBDV [$F_{(2,35)}$ = 7.554; p = 0.0019] effects were observed on locomotor activity in male rats. VPA administration significantly increased locomotor activity by about 137.9% compared to controls. Chronic CBDV treatment did not affect locomotion when administered to controls while CBDV administration in VPA rats significantly prevented hyperlocomotion only at the dose of 20 mg/kg.

Biochemistry

All biochemical studies were performed 24 h after the last CBDV (or vehicle) injection using the dose of CBDV more efficacious toward ASD-like phenotypes (i.e., 20 mg/kg).

Effect of Symptomatic CBDV Treatment (20 mg/kg) on Components of the Endocannabinoid System in the Hippocampus of Vehicle- and VPA-Exposed Rats

Figure 3 shows the effects of CBDV on the protein levels of components of the endocannabinoid system in the hippocampus of vehicle and VPA rats. Two-way ANOVA revealed significant effects of VPA [$F_{(1,12)}$ = 8.198; p = 0.0143], CBDV [$F_{(1,12)}$ = 13.32; p = 0.0033], and VPA × CBDV interaction [$F_{(1,12)}$ = 15.88; p = 0.0018] on CB1 receptor expression. Prenatal VPA exposure significantly increased CB1 receptor levels in the hippocampus compared to vehicle littermates. CBDV treatment at the behaviorally efficacious dose of 20 mg/kg significantly normalized CB1 receptor expression without affecting its levels when administered to vehicles. A significant effect of VPA [$F_{(1,12)}$ = 10.31; p = 0.0075] was also found on CB2 receptor levels. Indeed, prenatal VPA exposure alone did not affect receptor expression whereas a significant increase in CB2 receptor levels was observed in VPA-exposed rats after chronic administration of CBDV 20 mg/kg. Statistical analysis revealed significant effects of VPA [$F_{(1,12)}$ = 8.722; p = 0.0121] and VPA × CBDV interaction [$F_{(1,12)}$ = 5.830; p = 0.0326] on FAAH protein levels within the hippocampus. FAAH expression was significantly enhanced in VPA exposed rats and it was reduced by chronic CBDV treatment. A similar effect was also found regarding MAGL expression. Indeed, MAGL levels were increased by prenatal VPA exposure and CBDV administration significantly restored MAGL expression in the hippocampus of VPA exposed rats without affecting its levels when administered in controls [VPA: $F_{(1,12)}$ = 7.536; p = 0.0178; VPA × CBDV interaction: $F_{(1,12)}$ = 4.499; p = 0.0564]. Neither VPA exposure nor CBDV treatment alone or in combination affected NAPE-PLD and DAGLα expression in this brain region.

Effect of Symptomatic CBDV Treatment (20 mg/kg) on Neuroinflammatory Markers and Microglia Morphology in the Hippocampus of Vehicle- and VPA-Exposed Rats

Figure 4A shows the effects of prenatal VPA exposure and symptomatic CBDV treatment on the expression of the astrocyte marker GFAP, the microglia marker CD11b and the pro-inflammatory cytokine TNF-α in the hippocampus. Two-way ANOVA showed significant effects of VPA [$F_{(1,12)}$ = 12.12; p = 0.0045], CBDV [$F_{(1,12)}$ = 14.71; p = 0.0024] and VPA × CBDV interaction [$F_{(1,12)}$ = 8.361; p = 0.0135] on GFAP expression. Prenatal VPA exposure significantly increased GFAP protein levels in the hippocampus. Symptomatic CBDV treatment completely restore GFAP expression in VPA rats without affecting the levels of this marker in control animals. Similarly, a significant increase in CD11b expression was found in the hippocampus after VPA exposure *in utero* and CBDV administration showed a trend toward reducing the expression of this marker when given to VPA rats without having any effect *per se* in control animals [VPA: $F_{(1,12)}$ = 5.673; p = 0.0308]. Significant effects of VPA [$F_{(1,12)}$ = 4.902; p = 0.0469] and VPA × CBDV interaction [$F_{(1,12)}$ = 8.531; p = 0.0128] were observed on TNF-α, whose expression was significantly increased in the hippocampus of VPA pre-treated rats. CBDV treatment significantly restored TNF-α levels when chronically administered to VPA rats.

Figures 4B,C shows the effects of prenatal VPA and symptomatic CBDV treatments on some parameters of microglia morphology, namely soma size and roundness as well as surface area and perimeter. Statistical analysis revealed main effects of VPA [$F_{(1-8)}$ = 17.55; p = 0.0030], CBDV [$F_{(1-8)}$ = 18.41;

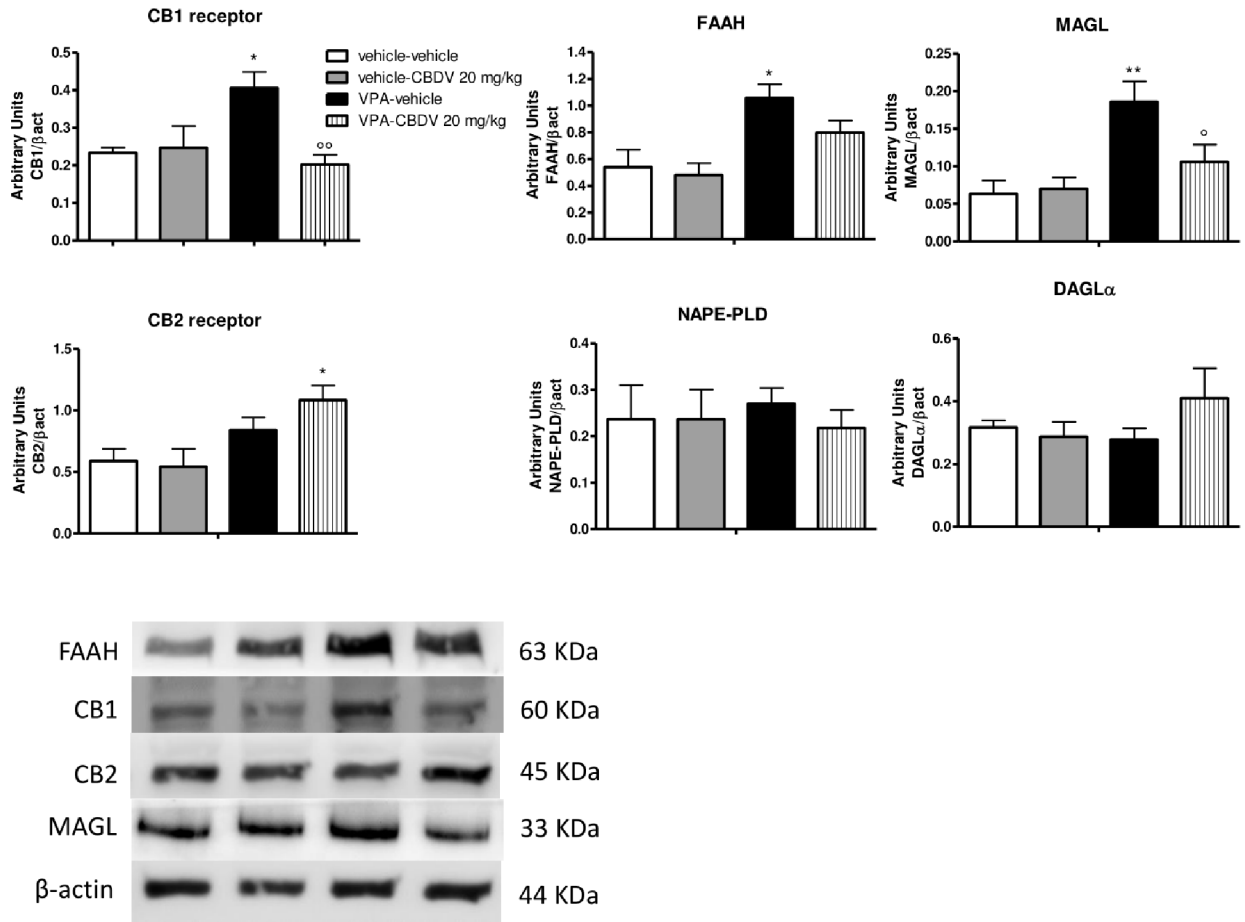

FIGURE 3 | Effect of symptomatic CBDV 20 mg/kg/day treatment on components of the endocannabinoid system in the hippocampus of the male offspring of VPA- and vehicle-exposed rats as measured by means of Western blot analysis in cytosolic fractions. Data represent mean ± SEM of $n = 3$ vehicle-vehicle, $n = 3$ vehicle-CBDV 20 mg/kg, $n = 5$ VPA-vehicle, $n = 5$ VPA-CBDV 20 mg/kg and were analyzed using two-way ANOVA followed by Tukey's *post hoc* test (**$p < 0.01$, *$p < 0.05$ vs. vehicle-vehicle;°°$p < 0.01$,°$p < 0.05$ vs. VPA-vehicle).

$p = 0.0026$], and VPA × CBDV interaction [$F_{(1-8)} = 16.26$; $p = 0.0038$] on soma size. Soma size was significantly increased in rats prenatally exposed to VPA compared to controls. CBDV treatment did not alter soma size in control animals but it significantly restored soma area when administered to VPA-treated rats. Similarly, main effects of VPA [$F_{(1-8)} = 25.21$; $p = 0.0010$], CBDV [$F_{(1-8)} = 7.376$; $p = 0.0264$], and VPA × CBDV interaction [$F_{(1-8)} = 7.221$; $p = 0.0276$] were observed on soma roundness. Prenatal VPA exposure significantly reduced roundness of the soma of Iba-1 positive cells in the hippocampus with respect to controls. CBDV completely rescued this alteration without affecting soma roundness in control rats.

Statistical analysis also revealed main effects of VPA [$F_{(1-8)} = 26.18$; $p = 0.0009$], CBDV [$F_{(1-8)} = 11.98$; $p = 0.0086$], and VPA × CBDV interaction [$F_{(1-8)} = 13.60$; $p = 0.0062$] on surface area and perimeter [VPA: $F_{(1-8)} = 34.68$; $p = 0.0004$, CBDV: $F_{(1-8)} = 17.28$; $p = 0.0032$, and VPA × CBDV interaction: $F_{(1-8)} = 20.71$; $p = 0.0019$]. Morphological analysis showed that prenatal VPA exposure significantly reduced both surface area and perimeter of microglia cells. Again, CBDV did not affect either surface area or perimeter of Iba-1 positive cells in control animals but its administration significantly normalized both parameters in rats prenatally exposed to VPA.

Effect of Symptomatic CBDV Treatment (20 mg/kg) on Components of the Endocannabinoid System and Neuroinflammatory Markers in the PFC of Vehicle- and VPA-Exposed Rats

As shown in **Figure 5A**, no effect of prenatal VPA and symptomatic CBDV treatments were found on CB1 and CB2 receptor, FAAH, MAGL, and NAPE-PLD levels in the PFC. In contrast, statistical analysis revealed significant effects of VPA [$F_{(1,12)} = 11.02$; $p = 0.0041$] and CBDV [$F_{(1,12)} = 13.39$; $p = 0.0033$] on DAGLα expression. Prenatal VPA exposure significantly reduced DAGLα levels in this brain area and a similar effect was observed after CBDV administration both in control and in VPA rats. Concerning the neuroinflammatory markers (**Figure 5B**), neither VPA nor CBDV affected GFAP, CD11b, and TNF-α levels in the PFC.

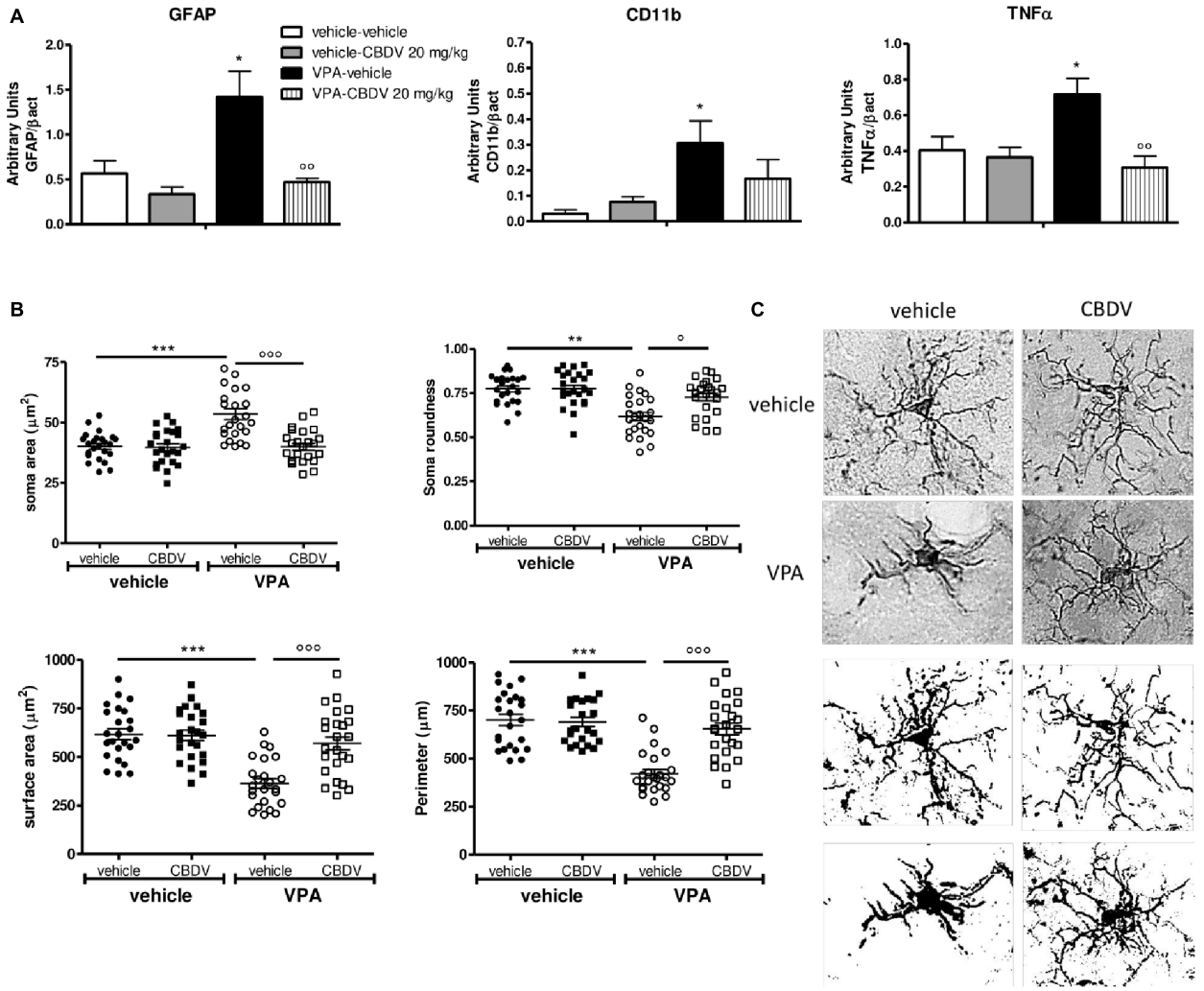

FIGURE 4 | (A) Effects of prenatal VPA exposure and symptomatic CBDV 20 mg/kg/day treatment on the expression of the astrocyte marker GFAP, the microglia marker CD11b and the pro-inflammatory cytokine TNF-α in the hippocampus as measured by means of Western blot analysis in cytosolic fractions. Data represent mean ± SEM of $n = 3$ vehicle-vehicle, $n = 3$ vehicle-CBDV 20 mg/kg, $n = 5$ VPA-vehicle, $n = 5$ VPA-CBDV 20 mg/kg and were analyzed using two-way ANOVA followed by Tukey *post hoc* test. **(B)** Effect of prenatal VPA exposure and CBDV treatment (20 mg/kg/day; PND 34–58) on microglia morphology in the hippocampus as analyzed through Iba1 immunostaining. **(C)** Representative Iba-1 staining and microglia morphology at ×40 magnification (upper panels: grayscale images; lower panels: filled images). Data represent mean ± SEM of three animals per group (4 slices/animal, 240 μm apart; 8 cells/animals) and were analyzed using two-way ANOVA followed by Tukey's *post hoc* test (***$p < 0.001$,**$p < 0.01$, *$p < 0.05$ vs. vehicle-vehicle;°°°$p < 0.001$,°°$p < 0.01$,°$p < 0.05$ vs. VPA-vehicle).

DISCUSSION

This study was performed to determine whether CBDV treatment could be beneficial toward ASD-like features induced by prenatal VPA exposure in rats. In particular, we evaluated CBDV's efficacy toward VPA-induced deficits in sociability and social novelty preference, repetitive self-grooming behavior, recognition memory deficits and hyperactivity in the male offspring of VPA-treated dams using either symptomatic (PND 34–58) and preventative (PND 19–32) treatment protocols.

Results here presented show that chronic CBDV treatment was able to ameliorate ASD-like signs induced by prenatal VPA exposure in the male offspring. Treatment with CBDV at the dose of 20 mg/kg in symptomatic rats rescued deficits in sociability and social novelty preference, repetitive self-grooming, recognition memory impairment and hyperactivity. In contrast, doses of 2 and 100 mg/kg only partially affected the phenotypes under investigation: CBDV 2 mg/kg recovered short-term memory deficits and hyperlocomotion while, at the dose of 100 mg/kg, CBDV's activity against the deficit in social novelty preference and stereotyped behaviors was lost. The lowest dose tested, 0.2 mg/kg, was instead ineffective. Hence, in this experimental model and at the doses tested in this study, CBDV does not show a linear dose-response curve, being more effective at the intermediate dose of 20 mg/kg with respect to doses of 2 and 100 mg/kg. This could suggest that CBDV might display a bell shaped dose-response curve as demonstrated for other phytocannabinoids in some animal

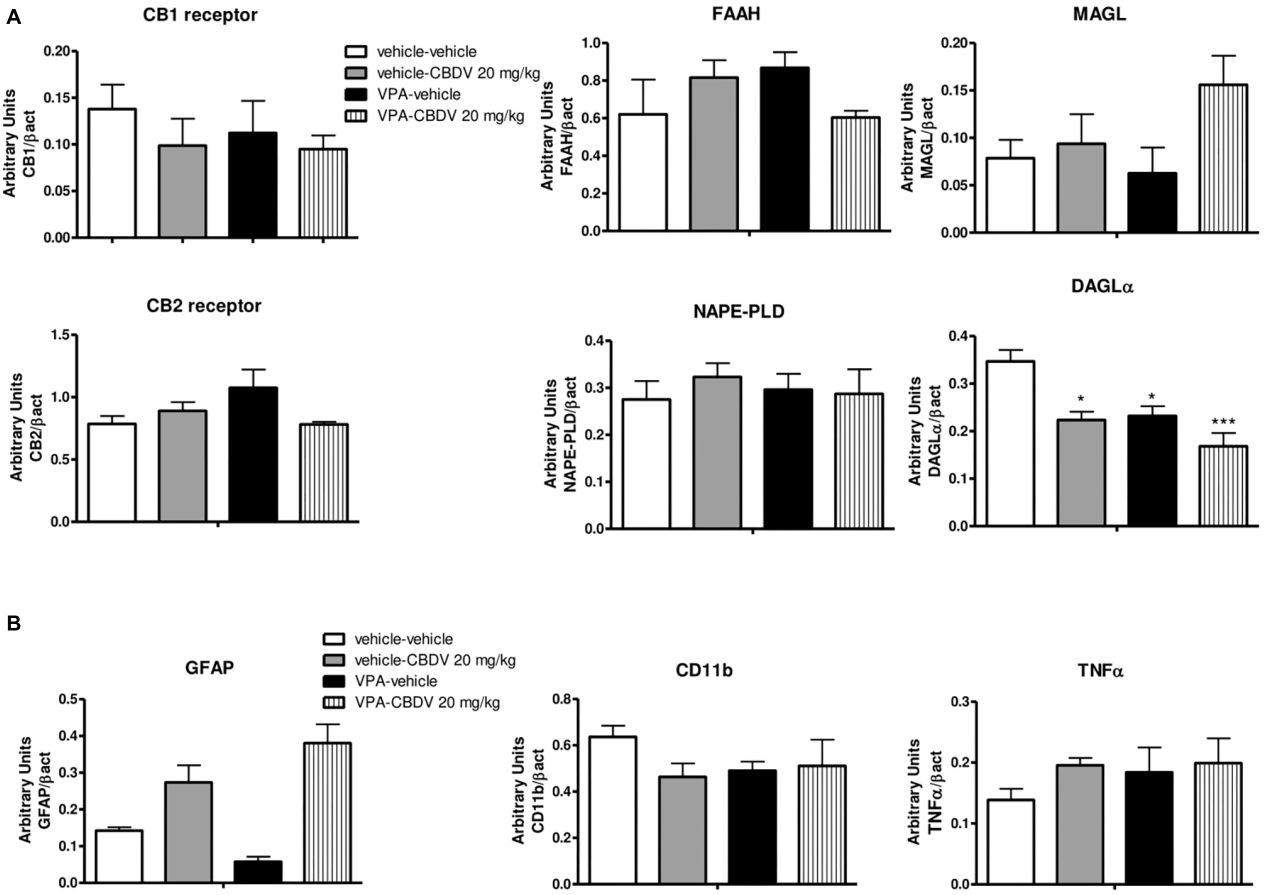

FIGURE 5 | Effect of prenatal VPA exposure and symptomatic CBDV 20 mg/kg/day treatment on protein levels of **(A)** components of the endocannabinoid system and **(B)** the astrocyte marker GFAP, the microglia marker CD11b and the pro-inflammatory cytokine TNF-α in the PFC as measured by means of Western blot analysis in cytosolic fractions. Data represent mean ± SEM of $n = 3$ vehicle-vehicle, $n = 3$ vehicle-CBDV 20 mg/kg, $n = 5$ VPA-vehicle, $n = 5$ VPA-CBDV 20 mg/kg and were analyzed using two-way ANOVA followed by Tukey's *post hoc* test. (**$p < 0.01$, *$p < 0.05$ vs. vehicle-vehicle).

models (Pertwee, 2004; Mishima et al., 2005; Mechoulam et al., 2007; Campos and Guimarães, 2008; Zuardi, 2008; Zanelati et al., 2010; Campos et al., 2012). Alternatively, it could be possible that the experimental paradigm used in our study failed to identify a linear dose response range.

Slightly different results were found in the preventative treatment schedule. Preventative CBDV treatment at the dose of 2 mg/kg significantly prevented sociability and social novelty preference deficits but failed to ameliorate repetitive behaviors, hyperactivity and short-term memory deficits. In contrast, CBDV 20 mg/kg prevented sociability and social novelty preference deficits, normalized locomotor activity and improved short-term memory deficits but was ineffective toward repetitive self-grooming behavior.

An aspect that emerges from these data is the different efficacy of CBDV depending on the time of administration. In fact, while symptomatic treatment at the dose of 20 mg/kg appears to be efficacious in reverting most ASD-like phenotypes, none of CBDV's doses tested in this study completely prevented the behaviors under investigation when administered during early developmental period (i.e., peri-weaning). Nevertheless, independent from the time window of administration, CBDV at all doses was devoid of any side effect when administered to control animals, further supporting the safety profile of this compound (Huizenga et al., 2019).

In the search for possible correlates of the effects observed at the behavioral level, we performed neurochemical analysis in the PFC and hippocampus of VPA-exposed rats treated with CBDV at the dose that showed the maximum behavioral efficacy, i.e., 20 mg/kg. Neurochemical investigations were carried out after symptomatic CBDV treatment only, as the translational value of a preventative treatment in the context of ASD is quite limited at present. In fact, diagnosis of ASD is based on the identification of symptoms and a preventative treatment could only be useful when reliable biomarkers are available. Identifying biomarkers for early disease detection, especially in high-risk populations, is therefore a primary need to allow for earlier pharmacological interventions, with the intent of improving outcomes. Of note, results here presented raise the intriguing possibility that early CBDV treatment might partially prevent/attenuate the development of ASD symptoms.

Recent data from human and animal studies suggest an involvement of the endocannabinoid system in the pathogenesis of ASD. Lower circulating endocannabinoid levels and changes of endocannabinoid receptors and enzymes have been reported in ASD patients (Siniscalco et al., 2013, 2014; Brigida et al., 2017; Karhson et al., 2018; Aran et al., 2019). Animal studies support human data demonstrating the presence of alterations in several components of the endocannabinoid system in the brain of both genetic and environmental ASD models (Maccarrone et al., 2010; Jung et al., 2012; Foldy et al., 2013; Kerr et al., 2013; Speed et al., 2015; Zamberletti et al., 2017). Remarkably, pharmacological modulation of the endocannabinoid signaling can ameliorate some ASD-like phenotypes in animals (Busquets-Garcia et al., 2013; Qin et al., 2015; Gomis-González et al., 2016; Kerr et al., 2016; Servadio et al., 2016; Wei et al., 2016; Melancia et al., 2018), suggesting that interfering with the endocannabinoid system might be beneficial for relieving ASD symptomatology. In line with literature data, we found that prenatal VPA exposure triggers endocannabinoid system alterations in the brain of the male offspring. These changes are more pronounced in the hippocampus with respect to the PFC. Specifically, enhanced FAAH and MAGL expression together with an up-regulation of CB1 receptor were observed in the hippocampus while reduced DAGLα levels were detected in the PFC. Increases in the enzymes responsible for AEA and 2-AG degradation in the hippocampus and the reduction of 2-AG synthesis in the PFC possibly support the presence of a reduced endocannabinoid tone in the brain of VPA-exposed animals, in line with previous findings (Kerr et al., 2013). Interestingly, FAAH, MAGL, and CB1 receptor protein levels returned to control level following CBDV treatment, suggesting that CBDV's ability to restore endocannabinoid system abnormalities might contribute to its beneficial effects on ASD-like behaviors. In addition, we found that CBDV treatment also up-regulated CB2 receptor expression in the hippocampus of VPA-exposed rats. CB2 is emerging as an important regulator of the inflammatory response in the central nervous system (Basu and Dittel, 2011). Although still debated, several authors suggest its immunosuppressive and neuroprotective potential (Ehrhart et al., 2005; Palazuelos et al., 2009; Tumati et al., 2012; Zoppi et al., 2014; Navarro et al., 2016). Its deletion in animals usually exacerbates the inflammatory phenotype in several models and CB2 activation by cannabinoids can slow the progression of some diseases, in addition to reducing inflammation (Turcotte et al., 2016), suggesting that modulation of CB2 receptor could be beneficial for relieving inflammation. Although our data does not allow to establish a causal relationship, we observed that CBDV-induced up-regulation of hippocampal CB2 receptor was associated with the rescue of the neuroinflammatory markers GFAP, CD11b, and TNF-α in the same brain region. Further supporting its either direct or indirect neuroprotective effects, we observed that CBDV treatment can restore microglia activation and consecutive morphological changes in terms of cell size and soma shape in the hippocampus of VPA-treated animals. Hence, CBDV treatment restores the endocannabinoid system and reduces neuroinflammation in the VPA model but, based on the present data, we cannot establish any causality between the two events. Although literature data clearly indicate that alterations of the endocannabinoid system and neuroinflammation co-exist in the brain of VPA-treated rats, there is no evidence about a possible correlation between the two events in the animal model at baseline. Indeed, the consequences of a modulation of either the endocannabinoid system or inflammation have been evaluated in the VPA model but no study has checked whether modulating one of the two events affects the other. Starting from the observation that CBDV does not directly interact with the cannabinoid system at physiologically relevant concentration, we speculate that restoration of the homeostatic endocannabinoid tone by CBDV might be secondary to its effect on neuroinflammation. We hypothesize that CBDV might promote a shift from a pro-inflammatory state, also called the "M1 phenotype," presenting neurotoxic activities and releasing pro-inflammatory signals, to a more neuroprotective profile called the "M2 phenotype" which involves anti-inflammatory responses. Of note, upregulation of CB2 receptors has been associated with a restoration of tissue homeostasis in pathological neuroinflammatory conditions (Miller and Devi, 2011) and our observation that CBDV increases the expression of CB2 receptors in VPA rats further supports its anti-inflammatory action in this model. We speculate that microglia cells shifted to an anti-inflammatory phenotype would then increase endocannabinoid production (Mecha et al., 2015), which by acting autocrinally and/or paracrinally could facilitate/amplify the M2 anti-inflammatory phenotype and might contribute to the restoration of endocannabinoid signaling.

CONCLUSION

This study provides preclinical evidence in support of the ability of CBDV to ameliorate behavioral abnormalities resembling the core and associated symptoms of ASD, a developmental condition for which no cure is available. Restoration of hippocampal endocannabinoid signaling and neuroinflammation are likely to contribute to CBDV's beneficial effects toward ASD-like phenotypes induced by prenatal VPA exposure.

Although further work is required to determine the mechanism(s) of action of CBDV and to evaluate its effect in other animal models, the present results identify for the first time CBDV as a suggested candidate for the treatment of ASD.

DATA AVAILABILITY

The raw data supporting the conclusions of this manuscript will be made available on request, without undue reservation, to any qualified researcher.

AUTHOR CONTRIBUTIONS

EZ performed the histochemical and Western blot experiments and wrote the first draft of the manuscript. MG performed the pharmacological treatments and behavioral experiments. MW-R and SB helped with the manuscript writing and English

editing. TR helped with the data interpretation and manuscript writing. DP conceived the study, supervised the project, helped with the data interpretation and manuscript writing. All authors contributed and have approved the final draft of the manuscript.

FUNDING

This work was supported by the GW Research Ltd. (Cambridge, United Kingdom). EZ has a postdoctoral research fellowship funded by the Zardi-Gori Foundation (Milano, Italy). The funding source had no further role in study design, in the collection, analysis and interpretation of data, decision to publish, and preparation of the manuscript.

SUPPLEMENTARY MATERIAL

The Supplementary Material for this article can be found online at: https://www.frontiersin.org/articles/10.3389/fncel.2019.00367/full#supplementary-material

REFERENCES

Al-Amin, M. M., Rahman, M. M., Khan, F. R., Zaman, F., and Mahmud Reza, H. (2015). Astaxanthin improves behavioral disorder and oxidative stress in prenatal valproic acid-induced mice model of autism. *Behav. Brain Res.* 286, 112–121. doi: 10.1016/j.bbr.2015.02.041

American Psychiatric Association [APA] (2013). *Diagnostic and Statistical Manual of Mental Disorders*, 5th Edn. Washington, DC: American Psychiatric Publishing, Inc.

Aran, A., Eylon, M., Harel, M., Polianski, L., Nemirovski, A., Tepper, S., et al. (2019). Lower circulating endocannabinoid levels in children with autism spectrum disorder. *Mol. Autism.* 10:2. doi: 10.1186/s13229-019-0256-6

Baio, J., Wiggins, L., Christensen, D. L., Maenner, M. J., Daniels, J., Warren, Z., et al. (2018). Prevalence of autism spectrum disorder among children aged 8 years – autism and developmental disabilities monitoring network, 11 sites, United States, 2014. *MMWR Surveill. Summ.* 67, 1–23. doi: 10.15585/mmwr.ss6706a1

Bambini-Junior, V., Zanatta, G., Della Flora Nunes, G., Mueller, de Melo, G., Michels, M., et al. (2014). Resveratrol prevents social deficits in animal model of autism induced by valproic acid. *Neurosci. Lett.* 583, 176–181. doi: 10.1016/j.neulet.2014.09.039

Banji, D., Banji, O. J., Abbagoni, S., Hayath, M. S., Kambam, S., and Chiluka, V. L. (2011). Amelioration of behavioral aberrations and oxidative markers by green tea extract in valproate induced autism in animals. *Brain Res.* 1410, 141–151. doi: 10.1016/j.brainres.2011.06.063

Basu, S., and Dittel, B. N. (2011). Unraveling the complexities of cannabinoid receptor 2 (CB2) immune regulation in health and disease. *Immunol. Res.* 51, 26–38. doi: 10.1007/s12026-011-8210-5

Bertolino, B., Crupi, R., Impellizzeri, D., Bruschetta, G., Cordaro, M., Siracusa, R., et al. (2017). Beneficial effects of co-ultramicronized palmitoylethanolamide/luteolin in a mouse model of autism and in a case report of autism. *CNS Neurosci. Ther.* 23, 87–98. doi: 10.1111/cns.12648

Brigida, A. L., Schultz, S., Cascone, M., Antonucci, N., and Siniscalco, D. (2017). Endocannabinod signal dysregulation in autism spectrum disorders: a correlation link between inflammatory state and neuro-immune alterations. *Int. J. Mol. Sci.* 18:E1425. doi: 10.3390/ijms18071425

Bronzuoli, M. R., Facchinetti, R., Ingrassia, D., Sarvadio, M., Schiavi, S., Steardo, L., et al. (2019). Neuroglia in the autistic brain: evidence from a preclinical model. *Mol. Autism* 9:66. doi: 10.1186/s13229-018-0254-0

Busquets-Garcia, A., Gomis-Gonzalez, M., Guegan, T., Agustin-Pavon, C., Pastor, A., Mato, S., et al. (2013). Targeting the endocannabinoid system in the treatment of fragile X syndrome. *Nat. Med.* 19, 603–607. doi: 10.1038/nm.3127

Campos, A. C., and Guimarães, F. S. (2008). Involvement of 5HT1A receptors in the anxiolytic-like effects of cannabidiol injected into the dorsolateral periaqueductal gray of rats. *Psychopharmacology* 199, 223–230. doi: 10.1007/s00213-008-1168-x

Campos, A. C., Moreira, F. A., Gomes, F. V., Del Bel, E. A., and Guimarães, F. S. (2012). Multiple mechanisms involved in the large-spectrum therapeutic potential of cannabidiol in psychiatric disorders. *Philos. Trans. R. Soc. Lond. B Biol. Sci.* 367, 3364–3378. doi: 10.1098/rstb.2011.0389

Christensen, J., Grønborg, T. K., Sørensen, M. J., Schendel, D., Parner, E. T., Pedersen, L. H., et al. (2013). Prenatal valproate exposure and risk of autism spectrum disorders and childhood autism. *JAMA* 309, 1696–1703. doi: 10.1001/jama.2013.2270

Codagnone, M. G., Podestá, M. F., Uccelli, N. A., and Reinés, A. (2015). Differential local connectivity and neuroinflammation profiles in the medial prefrontal cortex and hippocampus in the valproic acid rat model of autism. *Dev. Neurosci.* 37, 215–231. doi: 10.1159/000375489

Deckmann, I., Schwingel, G. B., Fontes-Dutra, M., Bambini-Junior, V., and Gottfried, C. (2018). Neuroimmune alterations in autism: a translational analysis focusing on the animal model of autism induced by prenatal exposure to valproic acid. *Neuroimmunomodulation* 25, 285–299. doi: 10.1159/000492113

Dufour-Rainfray, D., Vourc'h, P., Le Guisquet, A. M., Garreau, L., Ternant, D., Bodard, S., et al. (2010). Behavior and serotonergic disorders in rats exposed prenatally to valproate: a model for autism. *Neurosci. Lett.* 470, 55–59. doi: 10.1016/j.neulet.2009.12.054

Dufour-Rainfray, D., Vourc'h, P., Tourlet, S., Guilloteau, D., Chalon, S., res, C. R. (2011). Fetal exposure to teratogens: evidence of genes involved in autism. *Neurosci. Biobehav. Rev.* 35, 1254–1265. doi: 10.1016/j.neubiorev.2010.12.013

Duncan, S. (2007). Teratogenesis of sodium valproate. *Curr. Opin. Neurol.* 20, 175–180. doi: 10.1097/WCO.0b013e32805866fb

Ehrhart, J., Obregon, D., Mori, T., Hou, H., Sun, N., Bai, Y., et al. (2005). Stimulation of cannabinoid receptor 2 (CB2) suppresses microglial activation. *J. Neuroinflammation* 2:29. doi: 10.1186/1742-2094-2-29

Ergaz, Z., Weinstein-Fudim, L., and Ornoy, A. (2016). Genetic and non-genetic animal models for autism spectrum disorders (ASD). *Reprod Toxicol.* 64, 116–140. doi: 10.1016/j.reprotox.2016.04.024

Fernández-Arjona, M. D. M., Grondona, J. M., Granados-Durán, P., Fernández-Llebrez, P., and López-Ávalos, M. D. (2017). Microglia morphological categorization in a rat model of neuroinflammation by hierarchical cluster and principal components analysis. *Front. Cell Neurosci.* 11:235. doi: 10.3389/fncel.2017.00235

Foldy, C., Malenka, R. C., and Sudhof, T. C. (2013). Autism-associated neuroligin-3 mutations commonly disrupt tonic endocannabinoid signaling. *Neuron* 78, 498–509. doi: 10.1016/j.neuron.2013.02.036

Fontes-Dutra, M., Santos-Terra, J., Deckmann, I., Brum Schwingel, G., Della-Flora Nunes, G., Hirsch, M. M., et al. (2018). resveratrol prevents cellular and behavioral sensory alterations in the animal model of autism induced by valproic acid. *Front. Synaptic. Neurosci.* 10:9. doi: 10.3389/fnsyn.2018.00009

Gandal, M. J., Edgar, J. C., Ehrlichman, R. S., Mehta, M., Roberts, T. P., and Siegel, S. J. (2010). Validating γ oscillations and delayed auditory responses as translational biomarkers of autism. *Biol. Psychiatry* 68, 1100–1106. doi: 10.1016/j.biopsych.2010.09.031

Gao, J., Wang, X., Sun, H., Cao, Y., Liang, S., Wang, H., et al. (2016). Neuroprotective effects of docosahexaenoic acid on hippocampal cell death and learning and memory impairments in a valproic acid-induced rat autism model. *Int. J. Dev. Neurosci.* 49, 67–78. doi: 10.1016/j.ijdevneu.2015.11.006

Gomis-González, M., Busquets-Garcia, A., Matute, C., Maldonado, R., Mato, S., and Ozaita, A. (2016). Possible therapeutic doses of cannabinoid type 1 receptor antagonist reverses key alterations in fragile X syndrome mouse model. *Genes* 7:E56. doi: 10.3390/genes7090056

Huizenga, M. N., Sepulveda-Rodriguez, A., and Forcelli, P. A. (2019). Preclinical safety and efficacy of cannabidivarin for early life seizures. *Neuropharmacology* 148, 189–198. doi: 10.1016/j.neuropharm.2019.01.002

Jung, K. M., Sepers, M., Henstridge, C. M., Lassalle, O., Neuhofer, D., Martin, H., et al. (2012). Uncoupling of the endocannabinoid signalling complex in a mouse model of fragile X syndrome. *Nat. Commun.* 3:1080. doi: 10.1038/ncomms2045

Karhson, D. S., Krasinska, K. M., Dallaire, J. A., Libove, R. A., Phillips, J. M., Chien, A. S., et al. (2018). Plasma anandamide concentrations are lower in children with autism spectrum disorder. *Mol Autism.* 9:18. doi: 10.1186/s13229-018-0203-y

Kern, J. K., Geier, D. A., Sykes, L. K., and Geier, M. R. (2016). Relevance of neuroinflammation and encephalitis in autism. *Front. Cell. Neurosci.* 9:519. doi: 10.3389/fncel.2015.00519

Kerr, D. M., Downey, L., Conboy, M., Finn, D. P., and Roche, M. (2013). Alterations in the endocannabinoid system in the rat valproic acid model of autism. *Behav. Brain Res.* 249, 124–132. doi: 10.1016/j.bbr.2013.04.043

Kerr, D. M., Gilmartin, A., and Roche, M. (2016). Pharmacological inhibition of fatty acid amide hydrolase attenuates social behavioural deficits in male rats prenatally exposed to valproic acid. *Pharmacol. Res.* 113, 228–235. doi: 10.1016/j.phrs.2016.08.033

Kim, K. C., Gonzales, E. L., Lázaro, M. T., Choi, C. S., Bahn, G. H., Yoo, H. J., et al. (2016). Clinical and neurobiological relevance of current animal models of autism spectrum disorders. *Biomol Ther.* 24, 207–243. doi: 10.4062/biomolther.2016.061

Kim, K. C., Kim, P., Go, H. S., Choi, C. S., Yang, S. I., Cheong, J. H., et al. (2011). The critical period of valproate exposure to induce autistic symptoms in sprague-dawley rats. *Toxicol Lett.* 201, 137–142. doi: 10.1016/j.toxlet.2010.12.018

Kumar, H., and Sharma, B. (2016). Minocycline ameliorates prenatal valproic acid induced autistic behaviour, biochemistry and blood brain barrier impairments in rats. *Brain Res.* 1630, 83–97. doi: 10.1016/j.brainres.2015.10.052

Kuo, H. Y., and Liu, F. C. (2018). molecular pathology and pharmacological treatment of autism spectrum disorder-like phenotypes using rodent models. *Front. Cell Neurosci.* 12:422. doi: 10.3389/fncel.2018.00422

Ligresti, A., De Petrocellis, L., and Di Marzo, V. (2016). From phytocannabinoids to cannabinoid receptors and endocannabinoids: pleiotropic physiological and pathological roles through complex pharmacology. *Physiol. Rev.* 96, 1593–1659. doi: 10.1152/physrev.00002.2016

Loomes, R., Hull, L., and Mandy, W. P. L. (2017). What Is the Male-to-female ratio in autism spectrum disorder? A systematic review and meta-analysis. *J. Am. Acad. Child Adolesc. Psychiatry* 56, 466–474. doi: 10.1016/j.jaac.2017.03.013

Lucchina, L., and Depino, A. M. (2014). Altered peripheral and central inflammatory responses in a mouse model of autism. *Autism Res.* 7, 273–289. doi: 10.1002/aur.1338

Mabunga, D. F., Gonzales, E. L., Kim, J. W., Kim, K. C., and Shin, C. Y. (2015). Exploring the validity of valproic acid animal model of autism. *Exp. Neurobiol.* 24, 285–300. doi: 10.5607/en.2015.24.4.285

Maccarrone, M., Rossi, S., Bari, M., de Chiara, V., Rapino, C., Musella, A., et al. (2010). Abnormal mGlu 5 receptor/endocannabinoid coupling in mice lacking FMRP and BC1 RNA. *Neuropsychopharmacology* 35, 1500–1509. doi: 10.1038/npp.2010.19

Maroon, J., and Bost, J. (2018). Review of the neurological benefits of phytocannabinoids. *Surg. Neurol. Int.* 9:91. doi: 10.4103/sni.sni_45_18

Mecha, M., Feliú, A., Carrillo-Salinas, F. J., Rueda-Zubiaurre, A., Ortega-Gutiérrez, S., de Sola, R. G., et al. (2015). Endocannabinoids drive the acquisition of an alternative phenotype in microglia. *Brain Behav. Immun.* 49, 233–245. doi: 10.1016/j.bbi.2015.06.002

Mechoulam, R., Peters, M., Murillo-Rodriguez, E., and Hanus, L. O. (2007). Cannabidiol–recent advances. *Chem. Biodivers.* 4, 1678–1692. doi: 10.1002/cbdv.200790147

Mehta, M. V., Gandal, M. J., and Siegel, S. J. (2011). mGluR5-antagonist mediated reversal of elevated stereotyped, repetitive behaviors in the VPA model of autism. *PLoS One* 6:e26077. doi: 10.1371/journal.pone.0026077

Melancia, F., Schiavi, S., Servadio, M., Cartocci, V., Campolongo, P., Palmery, M., et al. (2018). Sex-specific autistic endophenotypes induced by prenatal exposure to valproic acid involve anandamide signalling. *Br. J. Pharmacol.* 175, 3699–3712. doi: 10.1111/bph.14435

Miller, L. K., and Devi, L. A. (2011). the highs and lows of cannabinoid receptor expression in disease: mechanisms and their therapeutic implications. *Pharmacol. Rev.* 63, 461–470. doi: 10.1124/pr.110.003491

Mishima, K., Hayakawa, K., Abe, K., Ikeda, T., Egashira, N., Iwasaki, K., et al. (2005). Cannabidiol prevents cerebral infarction via a serotonergic 5-hydroxytryptamine1A receptor-dependent mechanism. *Stroke* 36, 1077–1082. doi: 10.1161/01.STR.0000163083.59201.34

Morakotsriwan, N., Wattanathorn, J., Kirisattayakul, W., and Chaisiwamongkol, K. (2016). Autistic-like behaviors, oxidative stress status, and histopathological changes in cerebellum of valproic acid rat model of autism are improved by the combined extract of purple rice and silkworm pupae. *Oxid. Med. Cell. Longev.* 2016:3206561. doi: 10.1155/2016/3206561

Morales, P., Hurst, D. P., and Reggio, P. H. (2017). Molecular targets of the phytocannabinoids: a complex picture. *Prog. Chem. Org. Nat. Prod.* 103, 103–131. doi: 10.1007/978-3-319-45541-9_4

Morgan, J. T., Chana, G., Pardo, C. A., Achim, C., Semendeferi, K., Buckwalter, J., et al. (2010). Microglial activation and increased microglial density observed in the dorsolateral prefrontal cortex in autism. *Biol. Psychiatry* 68, 368–376. doi: 10.1016/j.biopsych.2010.05.024

Nagarkatti, P., Pandey, R., Rieder, S. A., Hegde, V. L., and Nagarkatti, M. (2009). Cannabinoids as novel anti-inflammatory drugs. *Future Med. Chem.* 1, 1333–1349. doi: 10.4155/fmc.09.93

Navarro, G., Morales, P., Rodríguez-Cueto, C., Fernández-Ruiz, J., Jagerovic, N., and Franco, R. (2016). Targeting cannabinoid cb2 receptors in the central nervous system. medicinal chemistry approaches with focus on neurodegenerative disorders. *Front. Neurosci.* 10:406. doi: 10.3389/fnins.2016.00406

Ornoy, A., Weinstein-Fudim, L., and Ergaz, Z. (2015). Prenatal factors associated with autism spectrum disorder (ASD). *Reprod Toxicol.* 56, 155–169. doi: 10.1016/j.reprotox.2015.05.007

Ornoy, A., Weinstein-Fudim, L., and Ergaz, Z. (2019). Prevention or amelioration of autism-like symptoms in animal models: will it bring us closer to treating human ASD? *Int. J. Mol. Sci.* 20, E1074. doi: 10.3390/ijms20051074

Palazuelos, J., Aguado, T., Pazos, M. R., Julien, B., Carrasco, C., Resel, E., et al. (2009). Microglial CB2 cannabinoid receptors are neuroprotective in Huntington's disease excitotoxicity. *Brain* 132(Pt 11), 3152–3164. doi: 10.1093/brain/awp23

Pertwee, R. G. (2004). "The pharmacology and therapeutic potential of cannabidiol," in *Cannabinoids*, ed. V. Di Marzo (Kluwer: Academic/Plenum Publishers), 32–83.

Pragnya, B., Kameshwari, J., and Veeresh, B. (2014). Ameliorating effect of piperine on behavioral abnormalities and oxidative markers in sodium valproate induced autism in BALB/C mice. *Behav. Brain Res.* 270, 86–94. doi: 10.1016/j.bbr.2014.04.045

Qin, M., Zeidler, Z., Moulton, K., Krych, L., Xia, Z., and Smith, C. B. (2015). Endocannabinoid-mediated improvement on a test of aversive memory in a mouse model of fragile X syndrome. *Behav. Brain Res.* 291, 164–171. doi: 10.1016/j.bbr.2015.05.003

Roullet, F. I., Lai, J. K., and Foster, J. A. (2013). In utero exposure to valproic acid and autism-a current review of clinical and animal studies. *Neurotoxicol Teratol.* 36, 47–56. doi: 10.1016/j.ntt.2013.01.004

Schneider, T., and Przewłocki, R. (2005). Behavioral alterations in rats prenatally exposed to valproic acid: animal model of autism. *Neuropsychopharmacology* 30, 80–89. doi: 10.1038/sj.npp.1300518

Servadio, M., Melancia, F., Manduca, A., di Masi, A., Schiavi, S., Cartocci, V., et al. (2016). Targeting anandamide metabolism rescues core and associated autistic-like symptoms in rats prenatally exposed to valproic acid. *Transl. Psychiatry* 6:e902. doi: 10.1038/tp.2016.182

Shen, C., and Chen, Y. (2013). Preparation of pre- and post-synaptic density fraction from mouse cortex. *Bio Protoc.* 3:e880. doi: 10.21769/BioProtoc.880

Siniscalco, D., Bradstreet, J. J., Cirillo, A., and Antonucci, N. (2014). The in vitro GcMAF effects on endocannabinoid system transcriptionomics, receptor formation, and cell activity of autism-derived macrophages. *J Neuroinflammation* 11:78. doi: 10.1186/1742-2094-11-78

Siniscalco, D., Sapone, A., Giordano, C., Cirillo, A., de Magistris, L., Rossi, F., et al. (2013). Cannabinoid receptor type 2, but not type 1, is up-regulated in peripheral blood mononuclear cells of children affected by autistic disorders. *J. Autism. Dev. Disord.* 43, 2686–2695. doi: 10.1007/s10803-013-1824-9

Speed, H. E., Masiulis, I., Gibson, J. R., and Powell, C. M. (2015). Increased cortical inhibition in autism-linked neuroligin-3R451C mice is due in part to loss of

endocannabinoid signaling. *PLoS One* 10:e0140638. doi: 10.1371/journal.,pone.0140638

Suzuki, K., Sugihara, G., Ouchi, Y., Nakamura, K., Futatsubashi, M., Takebayashi, K., et al. (2013). Microglial activation in young adults with autism spectrum disorder. *JAMA Psychiatry* 70, 49–58. doi: 10.1001/jamapsychiatry.2013.272

Tartaglione, A. M., Schiavi, S., Calamandrei, G., and Trezza, V. (2019). Prenatal valproate in rodents as a tool to understand the neural underpinnings of social dysfunctions in autism spectrum disorder. *Neuropharmacology* doi: 10.1016/j.expneurol.2017.04.017 [Epub ahead of print].

Tumati, S., Largent-Milnes, T. M., Keresztes, A., Ren, J., Roeske, W. R., Vanderah, T. W., et al. (2012). Repeated morphine treatment-mediated hyperalgesia, allodynia and spinal glial activation are blocked by co-administration of a selective cannabinoid receptor type-2 agonist. *J. Neuroimmunol.* 244, 23–31. doi: 10.1016/j.jneuroim.2011.12.021

Turcotte, C., Blanchet, M. R., Laviolette, M., and Flamand, N. (2016). The CB2 receptor and its role as a regulator of inflammation. *Cell. Mol. Life Sci.* 73, 4449–4470. doi: 10.1007/s00018-016-2300-4

Vargas, D. L., Nascimbene, C., Krishnan, C., Zimmerman, A. W., and Pardo, C. A. (2005). Neuroglial activation and neuroinflammation in the brain of patients with autism. *Ann. Neurol.* 57, 67–81. doi: 10.1002/ana.20315

Vigli, D., Cosentino, L., Raggi, C., Laviola, G., Woolley-Roberts, M., and De Filippis, B. (2018). Chronic treatment with the phytocannabinoid cannabidivarin (CBDV) rescues behavioural alterations and brain atrophy in a mouse model of Rett syndrome. *Neuropharmacology* 140, 121–129. doi: 10.1016/j.neuropharm.2018.07.029

Wei, D., Dinh, D., Lee, D., Li, D., Anguren, A., MorenoSanz, G., et al. (2016). Enhancement of anandamide-mediated endocannabinoid signaling corrects autism-related social impairment. *Cannabis Cannabinoid Res.* 1, 81–89. doi: 10.1089/can.2015.0008

Yeh, M. L., and Levine, E. S. (2017). Perspectives on the role of endocannabinoids in autism spectrum disorders. *OBM Neurobiol.* 1:005.

Zamberletti, E., Beggiato, S., Steardo, L. Jr., Prini, P., Antonelli, T., Ferraro, L., et al. (2014). Alterations of prefrontal cortex GABAergic transmission in the complex psychotic-like phenotype induced by adolescent delta-9-tetrahydrocannabinol exposure in rats. *Neurobiol. Dis.* 63, 35–47. doi: 10.1016/j.nbd.2013.10.028

Zamberletti, E., Gabaglio, M., and Parolaro, D. (2017). The endocannabinoid system and autism spectrum disorders: insights from animal models. *Int. J. Mol. Sci.* 18:E1916. doi: 10.3390/ijms18091916

Zamberletti, E., Gabaglio, M., Piscitelli, F., Brodie, J. S., Woolley-Roberts, M., Barbiero, I., et al. (2019). Cannabidivarin completely rescues cognitive deficits and delays neurological and motor defects in male Mecp2 mutant mice. *J. Psychopharmacol.* 33, 894-907. doi: 10.1177/0269881119844184

Zanelati, T. V., Biojone, C., Moreira, F. A., Guimarães, F. S., and Joca, S. R. (2010). Antidepressant-like effects of cannabidiol in mice: possible involvement of 5-HT1A receptors. *Br. J. Pharmacol.* 159, 122–128. doi: 10.1111/j.1476-5381.2009.00521.x

Zoppi, S., Madrigal, J. L., Caso, J. R., García-Gutiérrez, M. S., Manzanares, J., Leza, J. C., et al. (2014). Regulatory role of the cannabinoid CB2 receptor in stress-induced neuroinflammation in mice. *Br. J. Pharmacol.* 171, 2814–2826. doi: 10.1111/bph.12607

Zuardi, A. W. (2008). Cannabidiol: from an inactive cannabinoid to a drug with wide spectrum of action. *Rev. Bras. Psiquiatr.* 30, 271–280. doi: 10.1590/S1516-44462008000300015

Conflict of Interest Statement: DP and TR received research grants from GW Research Ltd. MW-R and SB are employees of GW Research Ltd.

The remaining authors declare that the research was conducted in the absence of any commercial or financial relationships that could be construed as a potential conflict of interest.

frontiers in Cellular Neuroscience

ORIGINAL RESEARCH
published: 27 August 2019
doi: 10.3389/fncel.2019.00380

Detrimental Effects of HMGB-1 Require Microglial-Astroglial Interaction: Implications for the Status Epilepticus -Induced Neuroinflammation

*Gerardo Rosciszewski[1†], Vanesa Cadena[1†], Jerónimo Auzmendi[1], María Belén Cieri[1], Jerónimo Lukin[1], Alicia R. Rossi[1], Veronica Murta[1], Alejandro Villarreal[1], Analia Reinés[2], Flávia C. A. Gomes[3] and Alberto Javier Ramos[1]**

[1] Laboratorio de Neuropatología Molecular, Instituto de Biología Celular y Neurociencia "Prof. E. De Robertis" UBA-CONICET, Facultad de Medicina, Universidad de Buenos Aires, Buenos Aires, Argentina, [2] Laboratorio de Neurofarmacología, Instituto de Biología Celular y Neurociencia "Prof. E. De Robertis" UBA-CONICET, Facultad de Medicina, Universidad de Buenos Aires, Buenos Aires, Argentina, [3] Instituto de Ciências Biomédicas, Universidade Federal do Rio de Janeiro, Rio de Janeiro, Brazil

OPEN ACCESS

Edited by:
Andrea Beatriz Cragnolini, Universidad Nacional de Cordoba, Argentina

Reviewed by:
Rommy Von Bernhardi, Pontifical Catholic University of Chile, Chile
Ingo Gerhauser, University of Veterinary Medicine Hannover, Germany

***Correspondence:**
Alberto Javier Ramos
jramos@fmed.uba.ar

† These authors have contributed equally to this work

Specialty section:
This article was submitted to Non-Neuronal Cells, a section of the journal Frontiers in Cellular Neuroscience

Received: *28 February 2019*
Accepted: *02 August 2019*
Published: *27 August 2019*

Citation:
Rosciszewski G, Cadena V, Auzmendi J, Cieri MB, Lukin J, Rossi AR, Murta V, Villarreal A, Reinés A, Gomes FCA and Ramos AJ (2019) Detrimental Effects of HMGB-1 Require Microglial-Astroglial Interaction: Implications for the Status Epilepticus -Induced Neuroinflammation. Front. Cell. Neurosci. 13:380. doi: 10.3389/fncel.2019.00380

Temporal Lobe Epilepsy (TLE) is the most common form of human epilepsy and available treatments with antiepileptic drugs are not disease-modifying therapies. The neuroinflammation, neuronal death and exacerbated plasticity that occur during the silent period, following the initial precipitating event (IPE), seem to be crucial for epileptogenesis. Damage Associated Molecular Patterns (DAMP) such as HMGB-1, are released early during this period concomitantly with a phenomenon of reactive gliosis and neurodegeneration. Here, using a combination of primary neuronal and glial cell cultures, we show that exposure to HMGB-1 induces dendrite loss and neurodegeneration in a glial-dependent manner. In glial cells, loss of function studies showed that HMGB-1 exposure induces NF-κB activation by engaging a signaling pathway that involves TLR2, TLR4, and RAGE. In the absence of glial cells, HMGB-1 failed to induce neurodegeneration of primary cultured cortical neurons. Moreover, purified astrocytes were unable to fully respond to HMGB-1 with NF-κB activation and required microglial cooperation. In agreement, *in vivo* HMGB-1 blockage with glycyrrhizin, immediately after pilocarpine-induced status epilepticus (SE), reduced neuronal degeneration, reactive astrogliosis and microgliosis in the long term. We conclude that microglial-astroglial cooperation is required for astrocytes to respond to HMGB-1 and to induce neurodegeneration. Disruption of this HMGB-1 mediated signaling pathway shows beneficial effects by reducing neuroinflammation and neurodegeneration after SE. Thus, early treatment strategies during the latency period aimed at blocking downstream signaling pathways activated by HMGB-1 are likely to have a significant effect in the neuroinflammation and neurodegeneration that are proposed as key factors in epileptogenesis.

Keywords: epilepsy, glia, inflammation, seizures, neuronal death

INTRODUCTION

Epilepsy is a devastating neurological disease characterized by recurrent seizures. A significant number of patients develop refractory epilepsy that is unresponsive to currently available treatments, which leaves them with very limited clinical options, being surgical resection of the epileptic focus the most common choice. Retrospective studies have shown that most patients suffering of Temporal Lobe Epilepsy (TLE), the most common human epilepsy, refer an initial precipitating event (IPE) in early childhood, followed by a silent period when the epileptic seizures begin (Cendes et al., 1993; French et al., 1993; Hamati-Haddad and Abou-Khalil, 1998; Theodore et al., 1999; Blume, 2006; Majores et al., 2007). Different types of IPE have been described, but complex febrile seizures with status epilepticus (SE) are frequently associated with adult TLE (Cendes et al., 1993; French et al., 1993; Koyama et al., 2012). The pilocarpine experimental model of TLE reproduces in rodents most features of human TLE, including the IPE induced by acute SE and a latency period before the onset of spontaneous seizures (reviewed in Curia et al., 2008). Previous studies performed in our laboratory, during the latency period that follows pilocarpine-induced seizures, have shown early neuroinflammation, macrophage infiltration and exacerbated neuronal plasticity, which seem to have a main role in the epileptogenesis (Rossi et al., 2013, 2017).

In general terms, acute brain injury causes the release of Damage Associated Molecular Patterns (DAMP). DAMP are intracellular molecules capable of activating the Pattern Recognition Receptors (PRR) such as Toll-Like Receptors (TLR) and the Receptor for Advanced Glycation End products (RAGE). The result of this interaction is the activation of downstream signaling cascades in immune-competent cells eventually leading to the expression of multiple pro-inflammatory mediators, mainly in an NF-κB -dependent manner. High Mobility Group Box 1 (HMGB1) is an ubiquitous nuclear protein that is implicated in the maintenance of chromatin structure (Ellwood et al., 2000; Verrijdt et al., 2002) and that, following Central Nervous System (CNS) injury, is released as a DAMP (Qiu et al., 2008; Maroso et al., 2010). The release of HMGB-1 has been demonstrated in human patients (reviewed in Parker et al., 2017) and in different models of experimental brain injury, including epileptic seizures produced by different experimental paradigms (Maroso et al., 2010); ischemia by middle cerebral artery occlusion (Qiu et al., 2008); traumatic brain injury (TBI) (Laird et al., 2014; Braun et al., 2017); cortical spreading depression (Takizawa et al., 2017); intracerebral hemorrhage (Wang et al., 2017) and it was shown to be increased in aging (Fonken et al., 2016). Moreover, several recent reports have proposed that HMGB-1 release is involved in the epileptogenic process that ultimately develops into overt disease (Fu et al., 2017; Walker et al., 2017a,b; Yang et al., 2017).

The abundant evidence in this regard has raised the hypothesis that blockage of HMGB-1 may blunt the pro-inflammatory activation of PRR that follows brain injury (Yang et al., 2010). In line with this idea, a number of reports have shown that HMGB-1 blockage reduces inflammation and improves behavioral recovery in experimental stroke (Wang C. et al., 2016).

In this work, we investigated the HMGB-1 effects on neuronal survival, and specifically, how glial cells interact to induce neuronal alterations and analyzed the signaling pathways driving those effects. Having in mind that HMGB-1 is released after SE, we aimed to block HMGB-1 signaling pathway with glycyrrhizin after pilocarpine-induced SE. Our results showed that HMGB-1 exposure induces reactive gliosis in astrocytes and microglia, and exerts glia-mediated detrimental effects on neurons. The NF-κB signaling pathway was activated by HMGB-1 by engaging TLR2, TLR4 and RAGE innate immunity receptors. In order to fully activate glial NF-κB signaling, HMGB-1 requires the cooperation between microglia and astrocytes. Finally, we observed that HMGB-1 blockage with glycyrrhizin *in vivo* immediately after pilocarpine-induced seizures reduces neuronal degeneration and reactive gliosis in the long term. Taken together, our results show that HMGB-1 has distinct effects on the different CNS cell types, in the context of the early stages following a typical acute precipitating injury in epilepsy. Thus, early blockage of HMGB-1 is likely to have a beneficial effect, as it would blunt pro-inflammatory cooperation between astrocytes and microglia during a critical period following seizures-induced IPE, a key event related to epileptogenesis.

MATERIALS AND METHODS

Cell culture reagents were obtained from Invitrogen Life Technologies (Carlsbad, United States). Fetal calf serum (FCS) was purchased from Natocor (Córdoba, Argentina). Antibodies were purchased from Chemicon-Millipore (mouse monoclonal anti-Actin, cat# MAB1501; mouse monoclonal anti-NeuN, cat# MAB 377; rabbit polyclonal anti-MAP-2, cat# AB5622), Sigma (mouse monoclonal anti-S100B cat# S2532; mouse monoclonal anti-Glial Fibrillary Acidic Protein, GFAP cat# G3893), Santa Cruz (rabbit polyclonal anti-TREM-2 cat# SC-48765; rabbit polyclonal anti-p65 cat# SC-372), Abcam (goat polyclonal anti-Iba-1, cat# ab5076); Dako (rabbit polyclonal anti-GFAP, cat# Z0334), and Promega (mouse monoclonal anti-β-3-tubulin, cat# G712A). Poly-L-lysine, DAPI (4′,6-diamidino-2-phenylindole); glycyrrhizin, human recombinant HMGB1 and other chemicals were from Sigma (United States). Fluorescent secondary antibodies and peroxidase conjugated secondary antibodies were purchased from Jackson Immunoresearch (United States).

Animals and Lithium-Pilocarpine Model of TLE

Adult male Wistar rats (250–300 g) were obtained from the Animal Facility of the School of Exact and Natural Sciences, University of Buenos Aires. TLR4 (TLR4 B6.B10ScN-*Tlr4*$^{lps-del}$/JthJ) and TLR2 (B6.129-*Tlr2*^{tm1Kir}/J) knockout mice (The Jackson Laboratory, United States) were kindly provided by Dr. P. Iribarren and Dr. M. Maccioni (CIBICI, UNC, Córdoba, Argentina). Animals were housed in a controlled environment (12/12-h light/dark cycle, controlled humidity and temperature, free access to standard laboratory food and water) under the permanent supervision of professional technicians.

All procedures involving animals and their care were conducted in accordance with our institutional guidelines, which comply with the NIH guidelines for the Care and Use of Laboratory Animals, the principles presented in the Guidelines for the Use of Animals in Neuroscience Research by the Society for Neuroscience and the ARRIVE guidelines, and were approved by the CICUAL committee of the School of Medicine, University of Buenos Aires (Res. Nr. 1278/2012). All efforts were made to minimize animal suffering and to reduce the number of animals used.

Rats were randomly assigned to the different treatments groups and subjected to the lithium-pilocarpine model of TLE as described in Rossi et al. (2013). Briefly, animals were intraperitoneally (i.p.) injected with 3 mEq/kg lithium chloride (LiCl) or saline and 20 h later received either i.p. saline or 30 mg/kg pilocarpine (Li-pilo group). Animals that received saline-saline (control group) or Li-saline did not show significant differences either in behavioral or morphometric parameters. The development of behavioral seizures was evaluated according to the Racine scale (Racine et al., 1972) and SE was defined as continuous seizures with a Racine score of 3 to 5, without returning to lower stages for at least 5 min. Approximately 70% of the pilocarpine treated rats showed acute behavioral features of SE between 40 and 60 min after pilocarpine injection (SE group). Thirty percent of the animals that were injected with pilocarpine did not develop SE, showing only behavioral signs corresponding to stages 1–2 of the Racine score and were not used for this study. All animals received 20 mg/kg diazepam 20 min after the onset of SE and doses were repeated as needed to terminate SE. Half of the animals that develop SE received glycyrrhizin i.p. at a dose of 333 mg/kg every 12 h during 4 days. Fifteen days post-SE (DPSE), animals were deeply anesthetized with ketamine/xylazine (90/10 mg/kg, i.p.) and fixed by intracardiac perfusion through the left ventricle. Dissected brains were cryoprotected, snap frozen and coronal 30 μm thick brain sections were cut using a cryostat as previously described (Aviles-Reyes et al., 2010). Free floating sections were kept in a cryoprotective solution (30% glycerol, 20% ethylene glycol in 0.05 M phosphate buffer) at −20°C until use.

Cell Culture

Rat or mice glial cell cultures were performed using the same protocol. Brains from neonatal rats, wild type mice or transgenic mice pups (3 days old) were removed and brain cortices were isolated following the procedure previously described (Villarreal et al., 2014). When mixed glial cultures reached confluence (typically 8–10 days), they were collected following trypsin treatment and seeded for the experimental procedures. Hippocampal neuro-glial cultures (containing glia and neurons), primary cortical neurons, cortical mixed glial cultures (containing approximately 60% astrocytes, 40% microglia), cortical astroglial enriched cultures (99% astrocytes) or microglial cultures (>99% microgliocytes) were obtained as described in Rosciszewski et al. (2018). For immunocytochemistry, primary cell cultures were washed with cold PBS and fixed with 4% paraformaldehyde plus 4% sucrose in PBS pH 7.2 for 15 min at room temperature. The procedure was then followed as stated below. For cell viability analysis, cell survival was measured by the MTT [(3-(4,5-dimethylthiazol-2-yl)-2,5-diphenyltetrazolium bromide)] assay (Mosmann, 1983) with some modifications (Alaimo et al., 2011). Briefly, MTT was added to each well (0.125 mg/ml) and incubated for 2 h at 37°C. Then, formazan reaction product was solubilized in DMSO and absorbance was measured at 570 nm with background subtraction at 655 nm in a microplate reader (BIO-RAD Laboratories, Hercules, CA, United States). The MTT reduction activity was expressed as the absorbance at 570 nm.

Astrocyte conditioned medium (ACM) was prepared as described previously (Diniz et al., 2012). Briefly, confluent astroglial-enriched cultures were washed to eliminate residual FCS and then exposed to 500 ng/ml HMGB-1 for 24 h in serum free medium. Then, cells were washed and cultures were maintained 24 h in serum-free medium. Finally, ACM was centrifuged to remove cellular debris and kept at −80°C until use.

For neuron-glial reconstituted cultures, primary cortical neurons and glial cells were grown separately as stated above and we designed a two-chamber system to allow co-culture without cell contact. Neurons were grown at a density of 7×10^3 cells/cm^2 on poly-L-lysine-coated glass coverslips, and maintained for 10 days in NeuroBasal medium (Invitrogen) supplemented with 2% B27 (Invitrogen) and 0.5 mM glutamine. Glial cells were grown in 12-well plastic plates for 7 days and exposed to HMGB-1 500 ng/ml or LPS 25 ng/ml for 3 h. Glial cells were washed and medium was replaced by a 1:1 mixture of supplemented Neurobasal and DMEM culture medium. Thereafter, a coverslip containing 10 DIV (DIV, days *in vitro*) primary cortical neurons was placed on top of the glial culture supported by U-shape custom-made sterile surgical steel spacers. The coverslips were placed with neurons facing the glial cell layer and the tissue culture medium covered all the system. Plates containing the co-culture were incubated for additional 24 h and then cells were fixed separately to analyze neuronal survival.

RT-PCR Assays

RT-PCR assays were performed as previously described (Rosciszewski et al., 2018). Briefly, RNA was isolated using the RNAeasy Mini kit (Qiagen, Germany). The cDNA was generated using the Omniscript RT kit (Qiagen) with random hexamers (Roche Products, United States). PCR were performed using specific primers: Actin (Fwd: CAC CAC TTT CTA CAA TGA GC; Rev: CGG TCA GGA TCT TCA TGA GG; amplification product: 323 bp); TLR4 (Fwd: GCC GGA AAG TTA TTG TGG TGG T; Rev: ATG GGT TTT AGG CGC AGA GTT T; amplification product: 356 bp). Both TLR4 and actin were amplified by 35 cycles and annealing temperature was 58°C for both genes. PCR products were run in a 1.5% agarose gel and imaged using a VersaDoc 4000 imaging system (Bio-Rad, United States). Each experiment included negative controls in which Omniscript reactions were performed in the absence of reverse transcriptase. All samples were run in triplicate. Detailed PCR protocols are available from authors under request.

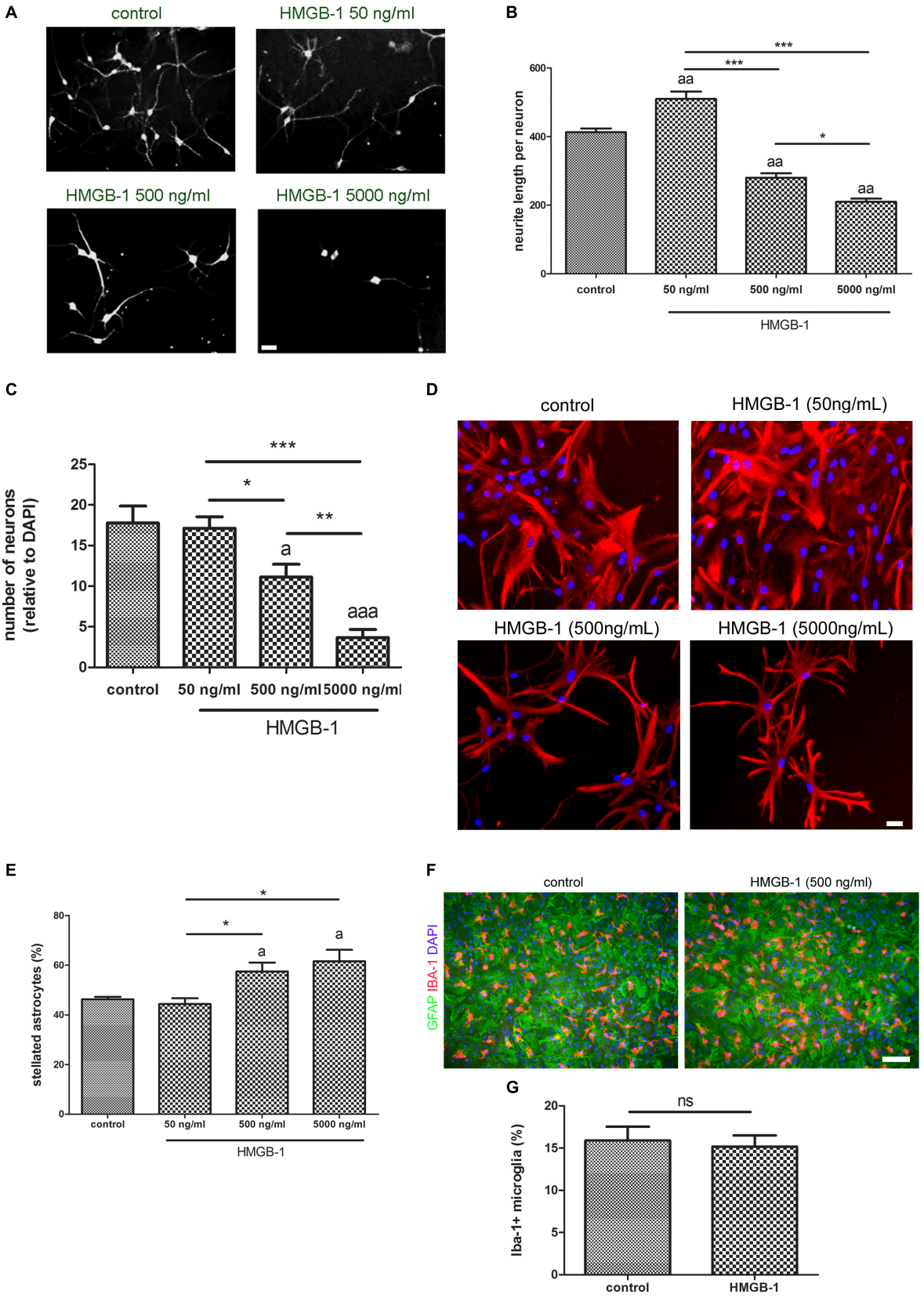

FIGURE 1 | Continued

FIGURE 1 | HMGB-1 effects on hippocampal neuro-glial mixed cultures. Rat hippocampal mixed cultures (10–12 DIV) containing neurons and glial cell types were exposed to HMGB-1 for 24 h. **(A)** Representative images of hippocampal neuron morphology in the mixed culture identified by beta-3-tubulin immunostaining; bar = 20 μm. **(B)** Quantitative analysis of neurites evaluated as the total length of neurites per neuron. **(C)** Quantitative analysis of the surviving neurons after 24 h of exposure to HMGB-1. The number of neurons per field was represented as the ratio of neurons vs. the total number of DAPI + nucleus per field. **(D)** Representative images of GFAP-immunostained astrocytes in hippocampal mixed cultures exposed to HMGB-1; bar = 15 μm. **(E)** Quantitative analysis of the stellated reactive GFAP + astrocytes abundance in hippocampal mixed cultures. Stellated fibrilar GFAP + astrocytes were counted with the ImageJ plugin Cell Counter and expressed as the percent of GFAP + cells in each field. **(F)** Representative images of Iba-1 + microgliocytes in hippocampal mixed cultures co-stained with GFAP astrocytic cell marker; bar = 100 μm. **(G)** Quantitative analysis of the microgliocytes cell abundance in the hippocampal mixed cultures showing that microglial abundance is not significantly affected by HMGB-1 exposure. Statistical analyses were performed by one way ANOVA and Student Newman–Keuls post-test, with statistical significance represented as $*p < 0.05$, $**p < 0.01$, and $***p < 0.001$. In multiple comparisons, statistical significance against control group is shown as "a"; "aa" and "aaa" that represents $p < 0.05$, $p < 0.01$, or $p < 0.001$, respectively. Data presented in the graphs are mean ± SEM from three experiments.

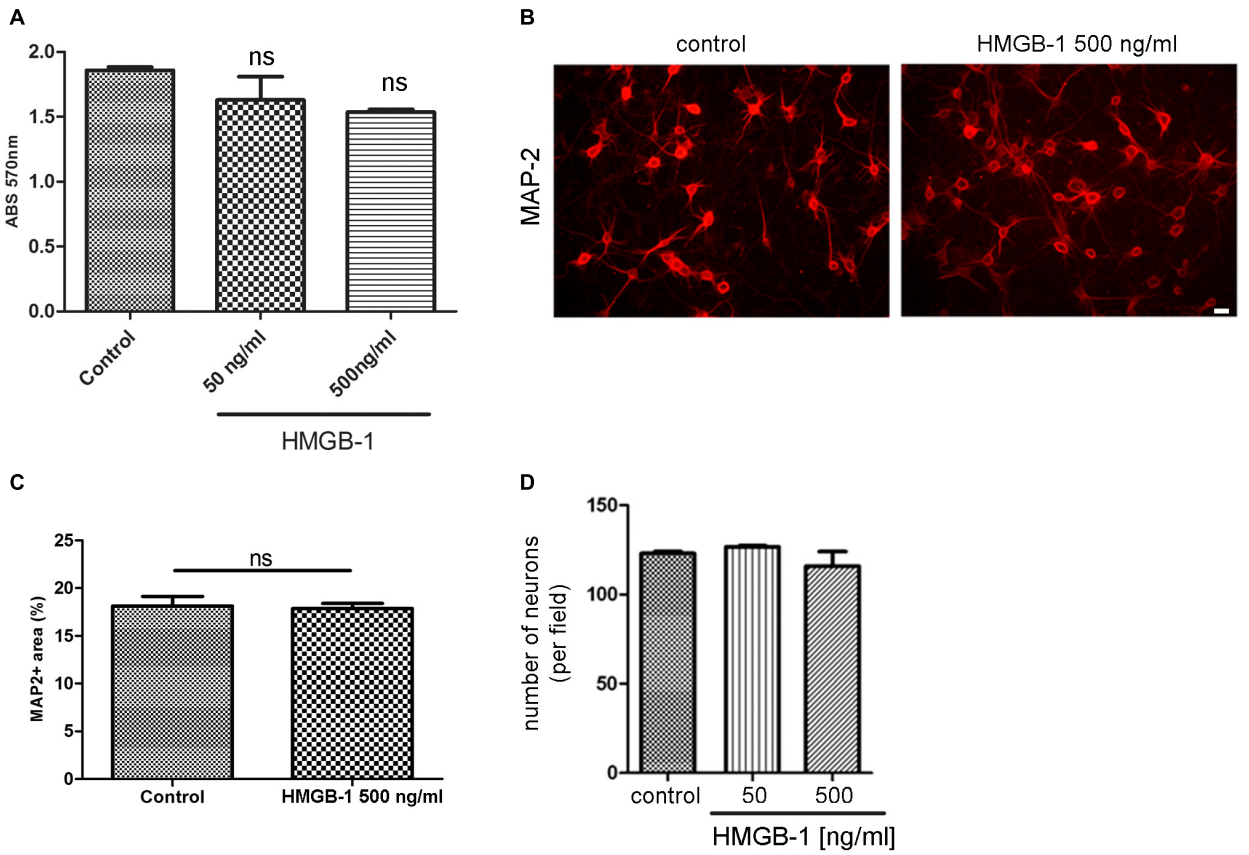

FIGURE 2 | HMGB-1 effects in primary neuronal cultures. **(A)** Quantitative analysis of rat primary cortical neuron survival exposed to HMGB-1 during 24 h and analyzed by the MTT survival assay with results shown as absorbance at 570 nm. **(B)** Representative images of rat primary cortical neurons exposed to HMGB-1 (500 ng/ml) for 24 h and immunostained for MAP-2; bar = 10 μm. **(C)** Quantitative analysis of the area occupied by MAP-2 + neurons after exposure to 500 ng/ml HMGB-1. **(D)** Number of neurons showing normal nuclei per microscopic field analyzed by MAP-2 and DAPI co-staining after 24 h of exposure to HMGB-1 as indicated. Statistical analyses were performed by one way ANOVA. Data presented in the graphs are mean ± SEM from three experiments.

Immunohistochemistry and Immunofluorescence

Brain sections from control and treated animals were simultaneously processed in free-floating state and immunolabelling was detected with diaminobenzidine (DAB) as described previously (Aviles-Reyes et al., 2010; Angelo et al., 2014). For immunofluorescence studies on tissue sections, primary and secondary antibodies were diluted in a solution containing 3% normal horse serum and 1% Triton X-100 in PBS. Isotypic specific secondary antibodies were labeled with Alexa 488 or Alexa 594. Counterstaining was performed with 0.1 μg/ml DAPI. For cell cultures, fixed cells were washed three times with cold PBS and permeabilized with 0.1% Triton X-100. The staining procedure was identical as above except that Triton X-100 was not included in blocking and antibody solutions. Epifluorescence images were obtained using an Olympus IX-81 microscope equipped with a DP71 camera (Olympus, Japan); or a Zeiss Axiophot (Carl Zeiss, Germany) microscope equipped with a Q5 digital camera (Olympus, Japan).

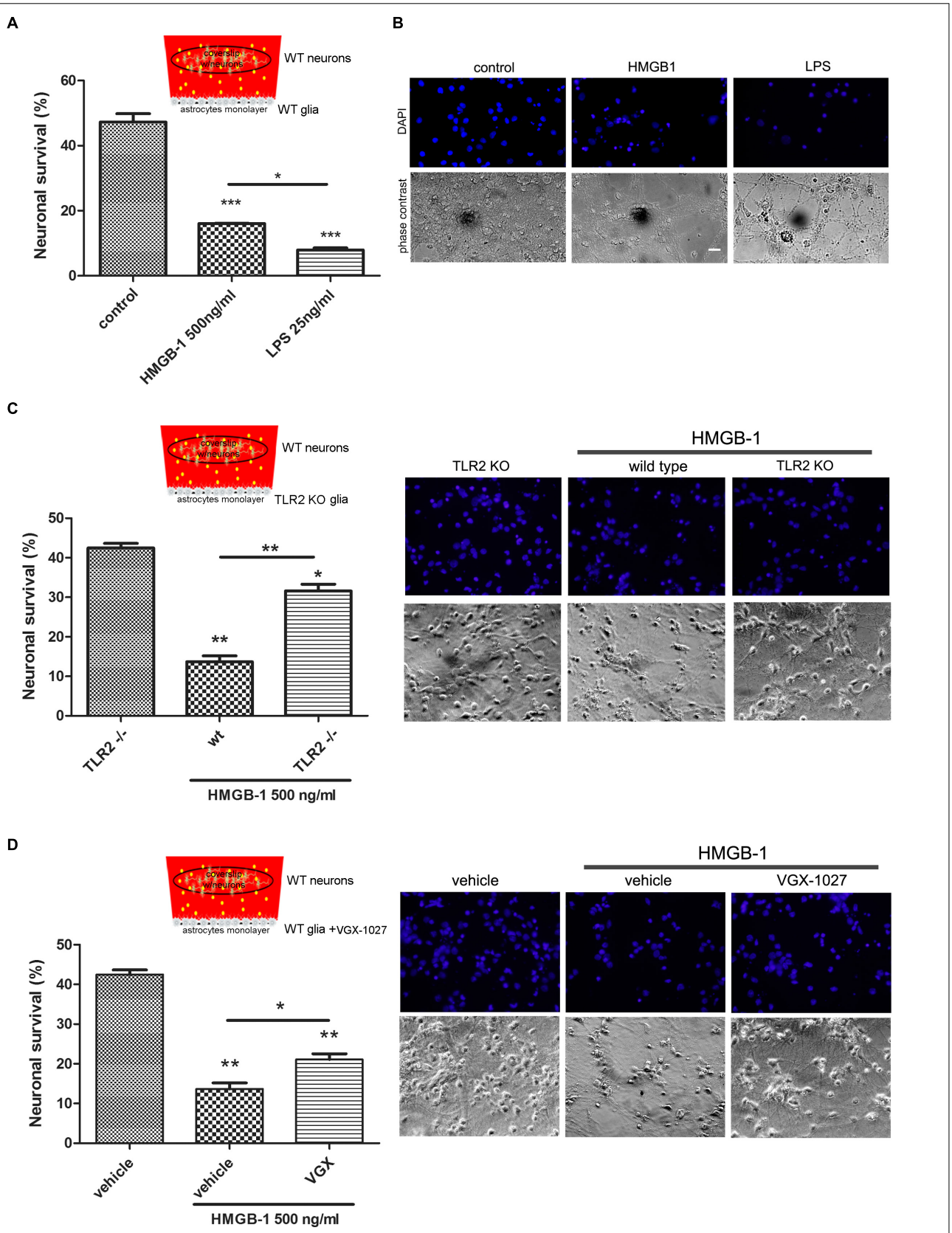

FIGURE 3 | Continued

FIGURE 3 | Pattern Recognition Receptor (PRR) requirement for HMGB-1 effects in neuronal survival. Mice primary cortical neuronal and glial cultures were allowed to grow separately. Glia was exposed to HMGB-1 or LPS during 3 h, medium was replaced and then glia and primary cortical neurons (10DIV) were co-cultured without physical contact but sharing the same culture medium for 24 h to study neuronal survival. **(A)** Quantitative analysis of neuronal survival analyzed by counting homogeneous, non-pycnotic, DAPI-stained neuronal nuclei per field. **(B)** Representative images of primary cortical neurons after co-culture with glial cells exposed to HMGB-1. Bar = 30 μm. **(C,D)** Quantitative analysis of neuronal survival in co-cultures performed as described above but using TLR2 knockout glia or VGX-1027 (TLR4 signaling inhibitor)-treated glia (10 μg/ml; 1 h preincubation). Statistical analyses were performed by one way ANOVA and Student Newman–Keuls post-test, with statistical significance is represented as $*p < 0.05$, $**p < 0.01$, and $***p < 0.001$. Data presented in the graphs are mean ± SEM from three experiments.

Quantitative Studies and Statistical Analysis

Changes in astroglial cell morphology as well as neuronal or glial cell counting were evaluated using the NIH ImageJ software on cells observed with phase contrast or immunostained as mentioned in figure legends. Cell counting was performed with ImageJ Cell Counter plugin. Neurite length and area covered by immunostaining was also done with ImageJ software as previously described (Angelo et al., 2014). Cell viability was analyzed biochemically with MTT assay, as described above, or by observing the nuclear morphology with DAPI as indicated in figure legends. Observers were blinded with respect to the experimental conditions. *In vitro* experiments were run in triplicates, a minimum of ten photographs were taken in each well of the triplicates and experiments were repeated three times. *In vivo* experiments were done with six animals per group and only control animals or those pilocarpine-treated that developed SE were used for glycyrrhizin administration. A minimum of 10 tissue sections per animal were used for each morphometrical analysis. Data were analyzed for normal distribution and homogeneity of variances and subjected to appropriate parametric or non-parametric statistical tests as specified in figure legends. Statistical analyses were performed using GraphPad Prism 5.0 (GraphPad Software, United States) and statistical significance was assumed when $p < 0.05$.

RESULTS

HMGB-1 Exposure Induces Reactive Gliosis and Dendrite Loss in Hippocampal Neuro-Glial Mixed Culture

Primary hippocampal mixed cultures containing neurons and glia were exposed to increasing concentrations of recombinant HMGB-1: 50 ng/ml, 500 ng/ml, and 5000 ng/ml for 24 h. As shown in **Figures 1A,B**, neurons from the neuro-glial culture showed an increase in dendrite length at low 50 ng/ml HMGB-1 and then a dose-dependent reduction in the dendrite length at higher concentrations (500–5000 ng/ml) reaching a significant neurodegenerative toxic effect at 5000 ng/ml. In fact, the relative number of neurons in the mixed culture was dose-dependently reduced after exposure to higher doses of HMGB-1 (**Figure 1C**). An analysis of astroglial cell population in the culture showed that 24 h exposure to HMGB-1 induced astroglial stellation at 500 and 5000 ng/ml HMGB-1 (**Figures 1D,E**). The observation of glial pyknotic cell nuclei at 5000 ng/ml dose precluded further use of this high dose in the next experiments due to toxic effects for astrocytes. Microglial cell population was present in the hippocampal mixed culture as shown in **Figure 1F**, however, HMGB-1 exposure did not significantly altered the microglial cell abundance (**Figure 1G**). Having in mind that astroglial stellation is considered the *in vitro* correlation of reactive gliosis, we conclude that exposure to high HMGB-1 levels induces reactive astrogliosis, dendrite loss and neuronal degeneration in mixed neuro-glial hippocampal cultures.

HMGB-1 Exposure Does Not Affect Neurons in the Absence of Glial Cells

We then tested the effect of HMGB-1 on primary neuronal cultures in the absence of glial cells. For that purpose, primary cortical neurons were exposed to HMGB-1 and neuronal survival was assessed by the MTT survival assay. As shown in **Figure 2A**, neuronal survival was not significantly affected by exposure to neither 50 nor 500 ng/ml HMGB-1. Primary cortical neurons morphology and proximal dendritic trees stained for the dendritic marker MAP-2 were also evaluated in these cultures and they were not significantly affected by HMGB-1 exposure (**Figure 2B**). Quantitative evaluation of MAP-2 + areas in primary cortical neurons is a sensitive parameter that detects not only changes in somatic MAP-2 expression, but also alterations in dendrite morphology and complexity. Following HMGB-1 exposure, this parameter did not show statistical differences between control and HMGB-1-exposed neurons (**Figure 2C**). In addition, there was not a significant neuronal loss in HMGB-1-exposed primary neuronal cultures (**Figure 2D**). We conclude that direct contact with HMGB-1 does not affect neuronal survival in absence of glial cells.

HMGB-1 Neurodegenerative Effects Are Mediated by Glial Cells

Having established that HMGB-1 exposure induces neuronal alterations in neuro-glial mixed cultures, and that direct contact with HMGB-1 does not induce *in vitro* neurodegeneration, we then wondered whether glial-derived factors released by HMGB-1-activated glia could alter neuronal survival in culture. In order to answer this question, we performed glio-neuronal reconstituted co-cultures in a modified two chamber design, which prevents glial-neuronal cell contact, but allows diffusion of soluble molecules among the cells. Mixed glial cultures were seeded separately from neurons and exposed to HMGB-1 or LPS as a positive pro-inflammatory-neurodegenerative stimulus for 3 h. Then, medium was replaced by a 1:1 DMEM/neurobasal mixture and a coverslip with primary cortical neurons was added to the glial culture for 24 h to evaluate neuronal survival. As shown in **Figures 3A,B**, neuronal survival was significantly reduced by HMGB-1-treated glia, but to a lesser extent than in

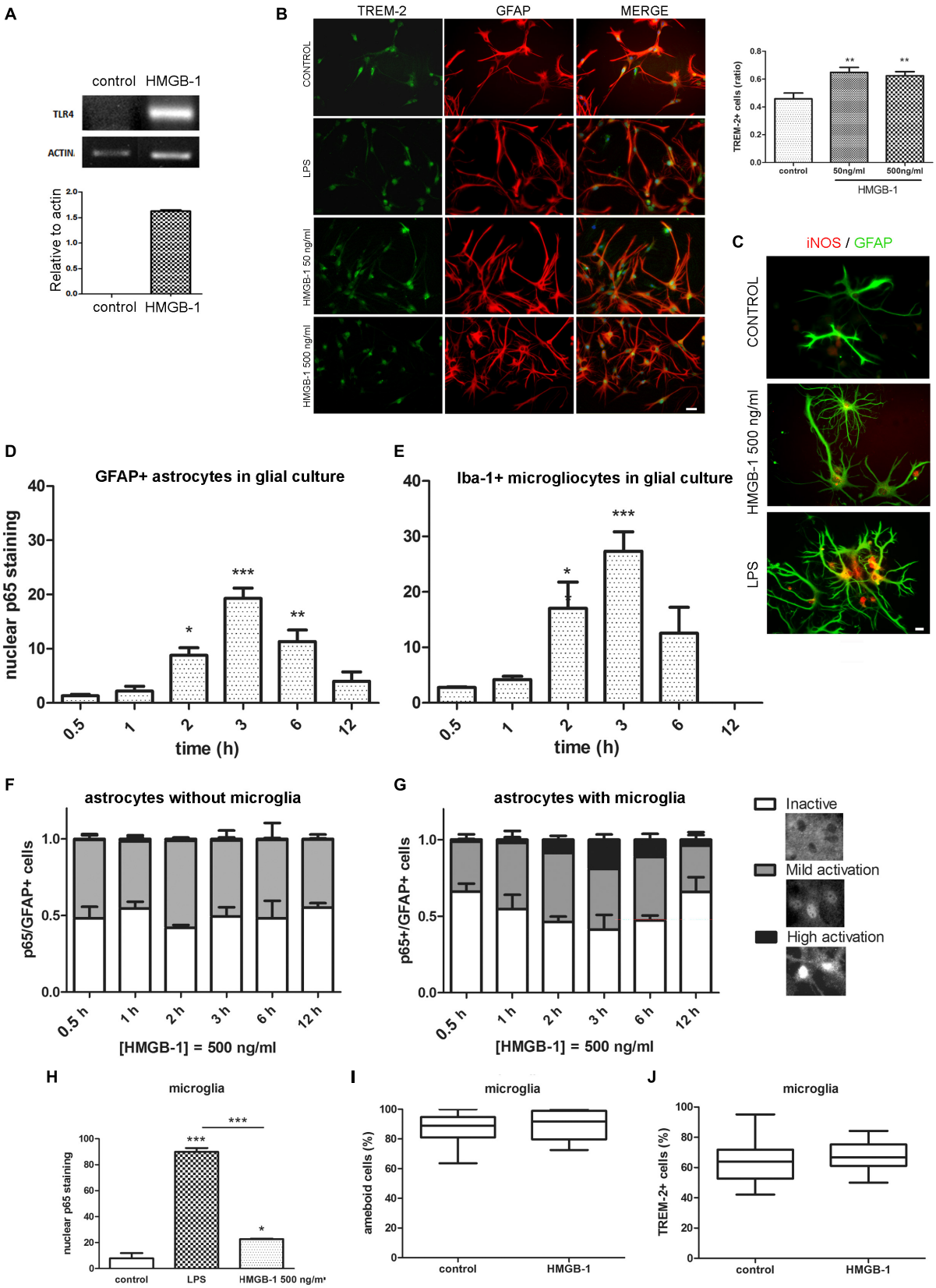

FIGURE 4 | Continued

FIGURE 4 | Differential HMGB-1 effects in astrocytes and microglia. **(A)** End point RT-PCR of rat glial mixed cultures containing astrocytes and microglia were exposed to 500 ng/ml HMGB-1 for 18 h to evaluate TLR4 mRNA expression; Actin was used as loading control. **(B)** Rat mixed glial cultures were exposed to HMGB-1 (50 or 500 ng/ml) or 25 ng/ml LPS and TREM-2 expression was evaluated after 24 h; bar = 20 μm. The graph shows the ratio of TREM-2 + cells in culture relative to the total number of Hoechst + stained cells. **(C)** Representative images of iNOS/GFAP immunostaining showing the differential effects in astroglial morphology and iNOS expression of HMGB-1 and LPS exposure on mixed glial cell cultures after 24 h of exposure; bar = 10 μm. **(D)** Quantitative analysis of p65 nuclear localization over time as the percentage of GFAP + astrocytes from mixed glial cultures showing nuclear p65 staining (NF-κB activation) after 500 ng/ml HMGB-1 exposure. **(E)** A similar experiment in mixed glial culture showing the Iba-1 + microglia with nuclear p65 staining over time after 500 ng/ml HMGB-1 exposure. **(F,G)** Astrocyte enriched cultures (less that 1% microglia) **(F)** or mixed glia **(G)** showing the percentage of GFAP + astrocytes with different patterns of NF-κB p65 subunit localization at different time points after 500 ng/ml HMGB-1 exposure. High activation was defined as predominant nuclear p65; mild activation is nuclear and cytoplasmic p65 of equivalent intensity, and inactive is cytoplasmic-only p65 immunostaining. Insets represent typical patterns of the NF-κB p65 subunit localization in astrocytes. Note the absence of cells showing highly activated NF-κB in astroglial-enriched culture. **(H)** Rat microglial culture (> 99% Iba-1 + microglia) showing the p65 nuclear localization after 3 h exposure to 25 ng/ml LPS (pro-inflammatory control) or 500 ng/ml HMGB-1. **(I,J)** Rat microglial cultures were exposed to 500 ng/ml HMGB-1 for 18 h and the percentage of amoeboid microglia **(I)** or TREM-2 immunostained microgliocytes **(J)** were evaluated. Statistical analyses were performed by one way ANOVA and Student Newman–Keuls post-test, with statistical significance represented as $*p < 0.05$, $**p < 0.01$, and $***p < 0.001$. Data presented in the graphs are mean ± SEM from three experiments. In **(I,J)**, Mann–Whitney non-parametrical test was used and data were represented as the median with box showing the interquartile range and whiskers showing the highest and lowest values.

LPS-exposed glial cells. Considering that HMGB-1 effects are proposed to be mediated by PRR, mainly TLR2 and TLR4, we then performed the same experimental design but using primary glia from TLR2 knockout mice, or exposed to LPS and the antagonist VGX-1027 to block TLR4. As expected, HMBG-1 was less efficient in inducing neuronal death in glial cultures obtained from TLR2 knockout animals or exposed to TLR4 blockade (**Figures 3C,D**). We conclude that detrimental HMGB-1 effects on neurons are mediated by glial cells by engaging TLR2- and TLR4-signaling.

HMGB-1 Induces TLR4 Expression and Activates NF-κB Dependent Signaling in Primary Astroglial Cultures Containing Microglia

In different cell types, including glia, engagement of TLR2 and TLR4 classically activates feed-forward loops that stimulate innate immunity receptor expression and pro-inflammatory polarization by stimulating downstream NF-κB signaling. To evaluate if HMGB-1 was able to induce these effects, mixed glial cultures containing astrocytes and microglia were exposed to HMGB-1, and TLR4, and TREM-2 innate immunity receptor expression was assessed. As shown in **Figure 4A**, HMGB-1 exposure increased TLR4 mRNA expression in glial cells. Immunocytochemistry experiments also showed that HMGB-1 increased TREM-2 (**Figure 4B**) and augmented iNOS expression in glial cells, although to a lesser extent than the classical pro-inflammatory molecule LPS (**Figure 4C**). TREM-2 expression was mainly regarded to myeloid-derived cells and microglia, but some groups, including ours have shown that TREM-2 can be expressed by reactive astrocytes (Rosciszewski et al., 2018). In addition, HMGB-1 induced morphological changes in GFAP + astrocytes toward a stellated and highly ramified reactive phenotype (**Figure 4C**). We then looked into NF-κB activation, which is the canonical TLR2 and TLR4 downstream pathway. Analysis of NF-κB p65 subunit nuclear localization in glial mixed cultures, containing astrocytes and microglia, showed that HMGB-1 exposure induces a time-dependent NF-κB activation in both cell types, identified with GFAP and Iba-1, respectively (**Figures 4D,E**). However, a closer cell-type specific analysis in these glial mixed cultures revealed a higher microglial NF-κB activation following HMGB-1 treatment (**Figures 4D,E**). Then, we compared the results found in mixed glial cultures with experiments in astroglial enriched cultures obtained by reducing the amount of microgliocytes to less than 1% by shacking and subsequent 5-fluorouracyl treatment, as described in Rosciszewski et al. (2018). In these conditions, purified astrocytes did not achieve a high NF-κB activation level (nuclear p65 localization without cytoplasmic p65 staining) following HMGB-1 exposure (**Figure 4F**). They rather became mildly activated, showing similar intensity in nuclear and cytoplasmic p65 staining, while inactive cells showed negative nuclear p65 staining (**Figure 4F**). Conversely, the presence of microglia facilitated astrocytic NF-κB activation, since highly NF-κB -activated astrocytes after HMGB-1 exposure were only observed in the presence of microglia (**Figure 4G**). We conclude that microglia facilitates NF-κB activation in astrocytes following HMGB-1 exposure. Then, we wondered if HMGB-1 had a direct effect on microglia. To test that hypothesis, we exposed pure microglial cultures to HMGB-1 and analyzed NF-κB activation, microglial cell morphology and the expression of TREM-2 as a marker of the M2 anti-inflammatory phenotype. HMGB-1 exposure induced NF-κB activation in microglial cultures, but to a lesser extent than the activation level observed in response to LPS exposure used as a pro-inflammatory control stimulus (**Figure 4H**). On the other hand, neither the morphology nor TREM-2 expression was significantly affected by HMGB-1 exposure (**Figures 4I,J**). We conclude that HMGB-1 activates an NF-κB dependent pathway in glial cells. While HMGB-1 displays a direct effect on microglia, astrocytes require the presence of microglia to achieve the highest level of NF-κB activation.

HMGB-1 –Induced NF-κB Activation in Primary Glial Cultures Is TLR2/TLR4/RAGE-Dependent

Previous reports have shown that HMGB-1 effects are mediated by different PRR including TLR2, TLR4, and RAGE (reviewed in Tian et al., 2017); however, the reported studies comprised different cell types. As stated above, our results have shown that glial-mediated HMGB-1 detrimental effects on neurons

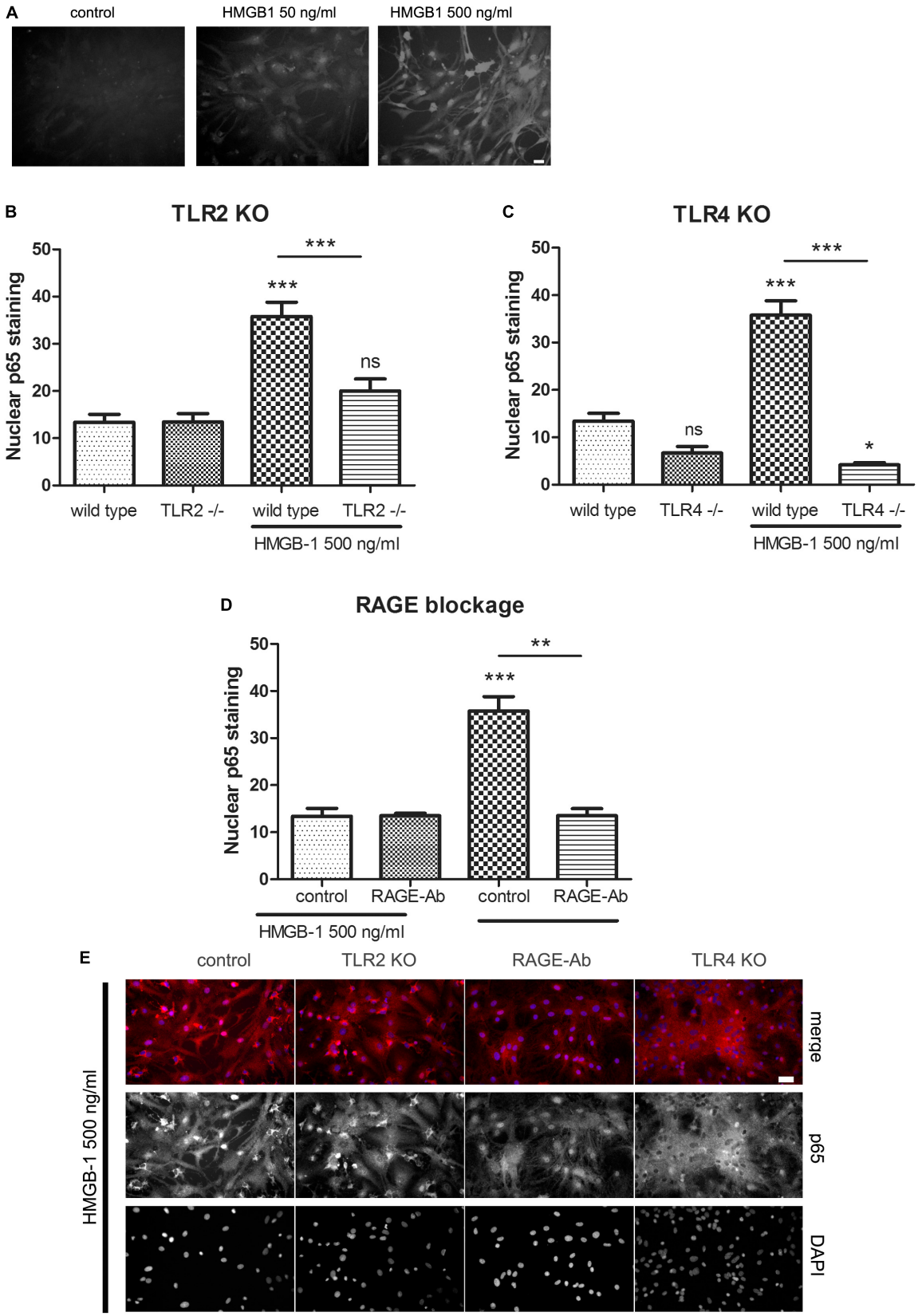

FIGURE 5 | Continued

FIGURE 5 | HMGB-1 –induced NF-κB activation in astrocytes depends on the PRR TLR2, TLR4, and RAGE. **(A)** Representative images of glial cell cultures containing approximately 95% astrocytes (star-like cells) and 5% microglia (small rounded cells) exposed to Histidine-tagged recombinant HMGB-1 for 1 h, medium was replaced and immunocytochemistry for the His-tag was performed; bar = 10 μm. **(B–D)** Quantitative results of the p65 NF-κB subunit nuclear localization in glial cell cultures obtained from wild type, TLR2 **(B)**, TLR4 **(C)** knockout mice or incubated with the RAGE neutralizing antibody (1 ug/ml) **(D)**. **(E)** Representative images of p65 NF-κB subunit nuclear localization in glial cell cultures exposed to HMGB-1 and immunostained for p65 (red) and counterstained with nuclear DAPI. Control cultures were wild type glial cell cultures incubated with an unspecific antibody of the same isotype as anti-RAGE; bar = 40 μm. In all cases, glial cultures were exposed to 500 ng/ml HMGB-1 during 3 h. Data show the percentage of GFAP + astrocytes showing nuclear p65 NF-κB subunit localization. Statistical analyses were performed by one way ANOVA and Student Newman–Keuls post-test, with statistical significance represented as $*p < 0.05$, $**p < 0.01$, and $***p < 0.001$. Data presented in the graphs are mean ± SEM from three experiments.

require TLR2 and TLR4 signaling (**Figure 3**). We then decided to perform a loss-of-function study by analyzing the specific contribution of TLR2, TLR4, and RAGE to the HMGB-1 effects in glial cells. Firstly, we analyzed whether HMGB-1 effectively binds to glial cells *in vitro* by exposing cultures to human recombinant His-tagged HMGB-1, subsequent washing and revealing the bound protein with an anti-His tag specific antibody avoiding the permeabilization step. As shown in **Figure 5A**, immunofluorescence showed a dose-dependent increase in the HMGB-1 binding to microglia and astrocytes, demonstrating that HMGB-1 binds to glial cells. To analyze the signaling pathways activated by HMGB-1 in glial cells and the requirement of TLR2 and TLR4 for downstream HMGB-1-induced NF-κB activation, we exposed mixed glial cultures from TLR4 or TLR2 knockout animals to HMGB-1. As shown in **Figures 5B,C**, the HMGB-1 effect on astrocytes from mixed glial cultures is TLR2- and TLR4-dependent, since a decreased NF-κB activity was observed in the knock out cultures exposed to HMGB-1. RAGE dependence was established by blocking RAGE with neutralizing antibodies, and **Figure 5D** shows that NF-κB activation in glial cells is abolished by pre-incubation with these blocking immunoglobulins. In **Figure 5E**, representative images of the p65 NF-κB subunit nuclear localization patterns in the different loss-of-function paradigms are shown. We conclude that HMGB-1 –induced NF-κB activation in glial cells can be mediated by either TLR2, TLR4, or RAGE-dependent signaling.

In vivo HMGB-1 Blockage With Glycyrrhizin Reduces Reactive Gliosis and Neuronal Degeneration in a Model of TLE

Having established that HMGB-1 activates PRR-dependent signaling pathways in glial cells and that it is detrimental for neuronal survival, we decided to analyze the neuronal and glial effects of HMGB-1 blockage after the SE induced by lithium-pilocarpine administration in rats. The lithium-pilocarpine model of TLE is a well-established epilepsy paradigm that reproduces most of the features of human TLE, by inducing a precipitating event (SE) followed by a silent epileptogenic period, and subsequently developing spontaneous epileptic seizures (reviewed in Curia et al., 2008). SE induced by lithium-pilocarpine treatment produces sustained reactive gliosis and neurodegeneration in piriform cortex and hippocampus, which are hypothesized to be essential for epileptogenesis (Rossi et al., 2013, 2017). Here, animals received the HMGB-1 blocking drug glycyrrhizin twice a day for 4 days, after developing SE (4DPSE) by lithium-pilocarpine administration and were analyzed after 15 days (15DPSE) (**Figure 6**). As shown in **Figure 7**, animals treated with glycyrrhizin showed a significative reduction in reactive microgliosis compared with the SE exposed animals that received vehicle. Early treatment with glycyrrhizin drastically reduced reactive Iba-1 + microglia in hippocampal CA-1 (**Figures 7A–C**) and piriform cortex (**Figures 7D,E**), although glycyrrhicin did not prevent the formation of a necrotic core in the piriform cortex (**Figure 7F**). Reactive astrocytes overexpress GFAP showing evident signs of hypertrophy, enlarged projections and soma size. As shown in **Figure 8**, glycyrrhizin early treatment also attenuated reactive gliosis in the hippocampal CA1 region (**Figures 8A–C**) and piriform cortex (**Figures 8D,E**). In addition, glycyrrhizin treatment prevented neuronal alterations evidenced by atypical NeuN mobilization from the nucleus to the cytoplasm, in the pyramidal cell layer of hippocampal CA-1 area (**Figures 9A–C**). However, glycyrrhizin treatment was not able to prevent NeuN alypical sub-cellular distribution in the piriform cortical neurons, but successfully reduced neuronal loss in that brain area (**Figures 9D–F**). It should be noted that NeuN mobilization to the neuronal cytoplasm is an early marker of reversible neuronal alterations, while its disappearance evidence neuronal loss (Robertson et al., 2006; Angelo et al., 2014). We conclude that HMGB-1 blockage immediately after SE, during the silent period that follows this IPE, is beneficial to reduce reactive gliosis and to improve neuronal survival.

DISCUSSION

HMGB-1 is a prototypical DAMP released after cell injury and capable of activating innate immune responses. In the CNS,

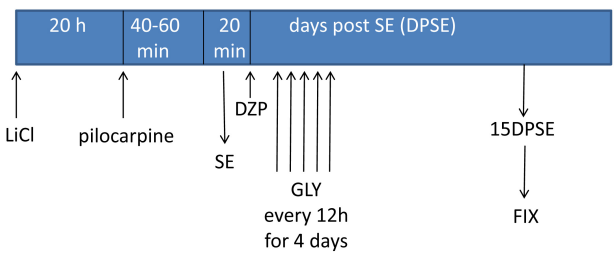

FIGURE 6 | Schematic representation of the *in vivo* treatment with HMGB-1 antagonist glycyrrhizin after pilocarpine-induced status epilepticus (SE).

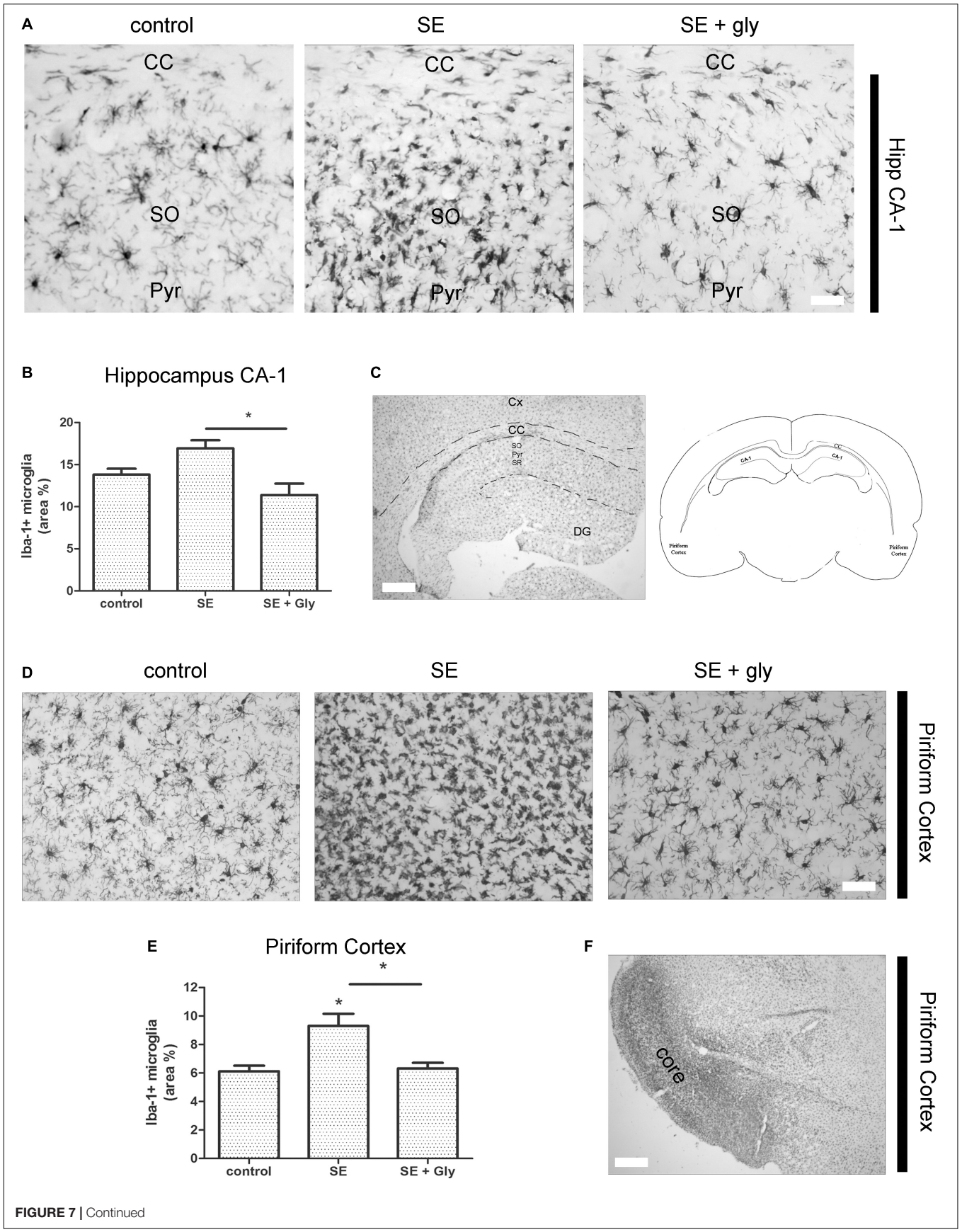

FIGURE 7 | Continued

FIGURE 7 | HMGB-1 antagonist glycyrrhizin reduces reactive microgliosis after pilocarpine-induced SE. Rats were exposed to pilocarpine-induced SE, treated with glycyrrhizin or vehicle for 4 days and analyzed after 15 days. **(A)** Representative images of Iba-1-immunostained microgliocytes in the CA-1 hippocampal area showing hippocampal Stratum Oriens (SO), hippocampal pyramidal layer (Pyr), and also the Corpus Callosum (CC). Note the increased microglial cell abundance in SE exposed animals and the decrease in microglial cell abundance in SE glycyrrhizin-treated animals. Scale bar: 15 μm. **(B)** Quantitative analysis of the Iba-1 + microglial cell abundance hippocampus of control, SE and SE animals treated with glycyrrhizin. **(C)** Low magnification of the Iba-1-immunostained hippocampus to visualize the different regions (scale bar: 350 μm) and the schematic representation of the analyzed areas in a coronal rat brain section. Cx, Brain cortex; CC, Corpus Callosum; DG, Dentate Gyrus; CA-1, Hippocampal CA-1 area; SR, Stratum Radiatum; SO, Stratum Oriens; Pyr, Pyramidal neurons. **(D)** Representative images of Iba-1-immunostained microgliocytes in the piriform cortex. Scale bar = 30 μm. Note that necrotic core has been colonized by microgliocytes and thus it is not distinguished in these images but noticeable in the low magnification image **(F)**. **(E)** Quantitative analysis of Iba-1-immunostained cell area in the piriform cortex and hippocampus of control, SE and SE animals treated with glycyrrhizin. Statistical analyses were performed by one way ANOVA and Student Newman–Keuls post-test, with statistical significance represented as $^{*}p < 0.05$, $^{**}p < 0.01$, and $^{***}p < 0.001$. Control animals were exposed to lithium chloride and saline was used as vehicle. The number of animals were $n = 6$ per experimental group.

HMGB-1 was shown to be released after different types of acute injury (Muhammad et al., 2008; Qiu et al., 2008, 2010; Gao et al., 2012, 2018; Laird et al., 2014; Sun et al., 2014; Haruma et al., 2016; Parker et al., 2017) and after SE (Fu et al., 2017). Extracellular HMGB-1 interacts with TLR2, TLR4, and RAGE to induce innate immunity activation and neuroinflammation within the CNS (Qiu et al., 2010; Yang et al., 2010; Weber et al., 2015; reviewed in Tian et al., 2017). Once released into the brain parenchyma, HMGB-1 can reach the blood, where brain-derived HMGB1 can be redox modified in the circulation; the oxidized form acts as a cytokine targeting peripheral organs, specifically bone marrow and spleen, to recruit myeloid cells and activate peripheral immune cells (Liesz et al., 2015; Singh et al., 2016). Activated immune competent cells also actively release an acetylated form of HMGB-1, probably as a result of maturation in the periphery (Venereau et al., 2016; Singh et al., 2016).

In epilepsy studies, HMGB-1 has gathered increasing attention because it has been hypothesized that it may play a role in epileptogenesis, being both a pharmacological target and a biomarker for the silent phase of the disease (reviewed in Paudel et al., 2018). Animal models of acute and chronic seizures have shown that HMGB-1 receptors are expressed after experimental seizures (Maroso et al., 2010; Rossi et al., 2017) and that HMGB-1/TLR4 signaling plays a role in generating and perpetuating seizures by modifying ionotropic glutamatergic subunit NR2B phosphorylation (Maroso et al., 2010). Human tissue from epileptic lesions has shown overexpression of HMGB-1 and the proposed binding receptors TLR2, TLR4, and RAGE (Zurolo et al., 2011).

Our present results support the assumption that HMGB-1 dependent signaling pathways appear to be centrally involved in the well-characterized initial neuroinflammation and neurodegeneration that follow the IPE (Rossi et al., 2013, 2017). HMGB-1 is released after SE (Fu et al., 2017) and we here propose that, acting on astrocytes and microglia, HMGB-1 activates TLR2/TLR4/RAGE signaling pathways that facilitate neurodegeneration. Undoubtedly, our results also support that HMGB-1-dependent signaling pathways are also likely to be involved in other acute injuries in the CNS such as TBI and ischemia where HMGB-1 was shown to be released from the necrotic core (Muhammad et al., 2008; Kim et al., 2018).

In vitro experiments using hippocampal mixed cultures containing glial cells and neurons showed the ability of HMGB-1 to induce neurite retraction and reactive gliosis. The dose-response studies show that neurodegenerative HMGB-1 effects correlate with reactive gliosis. This neurotoxic effect is abolished when neurons are seeded in absence of microglia and astrocytes. These observations remarkably show that glial cells are required for the detrimental HMGB-1 effects on neuronal survival to become evident. Previous reports have proposed that neurodegenerative HMGB-1 effects after SE and TBI are due to HMGB-1-induced alterations in blood-brain barrier permeability (Laird et al., 2014; Fu et al., 2017). We here report that exogenously applied HMGB-1 is able to induce neuronal degeneration when glial cells are present in the culture, showing that HMGB-1 requires glial cells to promote neurodegeneration.

As a DAMP, HMGB-1 has the ability of activating PRR, which are innate immunity receptors that are also activated by PAMP. By comparing HMGB-1 with the prototypical pro-inflammatory PAMP LPS, we here show that both HMGB-1 or LPS-treated glia induces neuronal death. Signaling pathways activated by HMGB-1 in different cell types, including the professional immune cells, are triggered by engaging the classical innate immunity receptors RAGE, TLR2, and TLR4 (Pedrazzi et al., 2007; Choi et al., 2017; Paudel et al., 2018). By combining glial cell cultures obtained from TLR2 knockout mice brains and TLR4 pharmacological blockade with the chemical inhibitor VGX-1027, we demonstrate here that detrimental HMGB-1 effects on neurons are mediated by glial TLR2 and TLR4. Upon ligand binding, TLR2 or TLR4 initiate a well-characterized signal transduction pathway, that leads to the activation of NF-κB and expression of pro-inflammatory target genes (reviewed in Crack and Bray, 2007; Tajalli-Nezhad et al., 2018). By using glial cell cultures containing astrocytes and microglia, we here show that both cell types exhibit a significant NF-κB activation following HMGB-1 exposure, and that this activation is TLR2/TLR4/RAGE-dependent. However, astroglial enriched cultures containing less than 1% microglia showed a reduced NF-κB activation, thus suggesting that microglial cells are necessary to achieve a significant level of NF-κB activation in astrocytes after HMGB-1 exposure. Microglial cultures lacking astrocytes, on the other hand, still responded to HMGB-1 but to a lesser extent than to the prototypical PAMP LPS, and failed to show the phenotypical switch to the amoeboid activated state, or to change the expression of the classical M2 phenotype marker TREM-2. HMGB-1-induced AQP4 expression was previously shown to depend on microglia-astroglial interaction through soluble mediators (Ohnishi et al., 2014). Moreover, Gao et al.

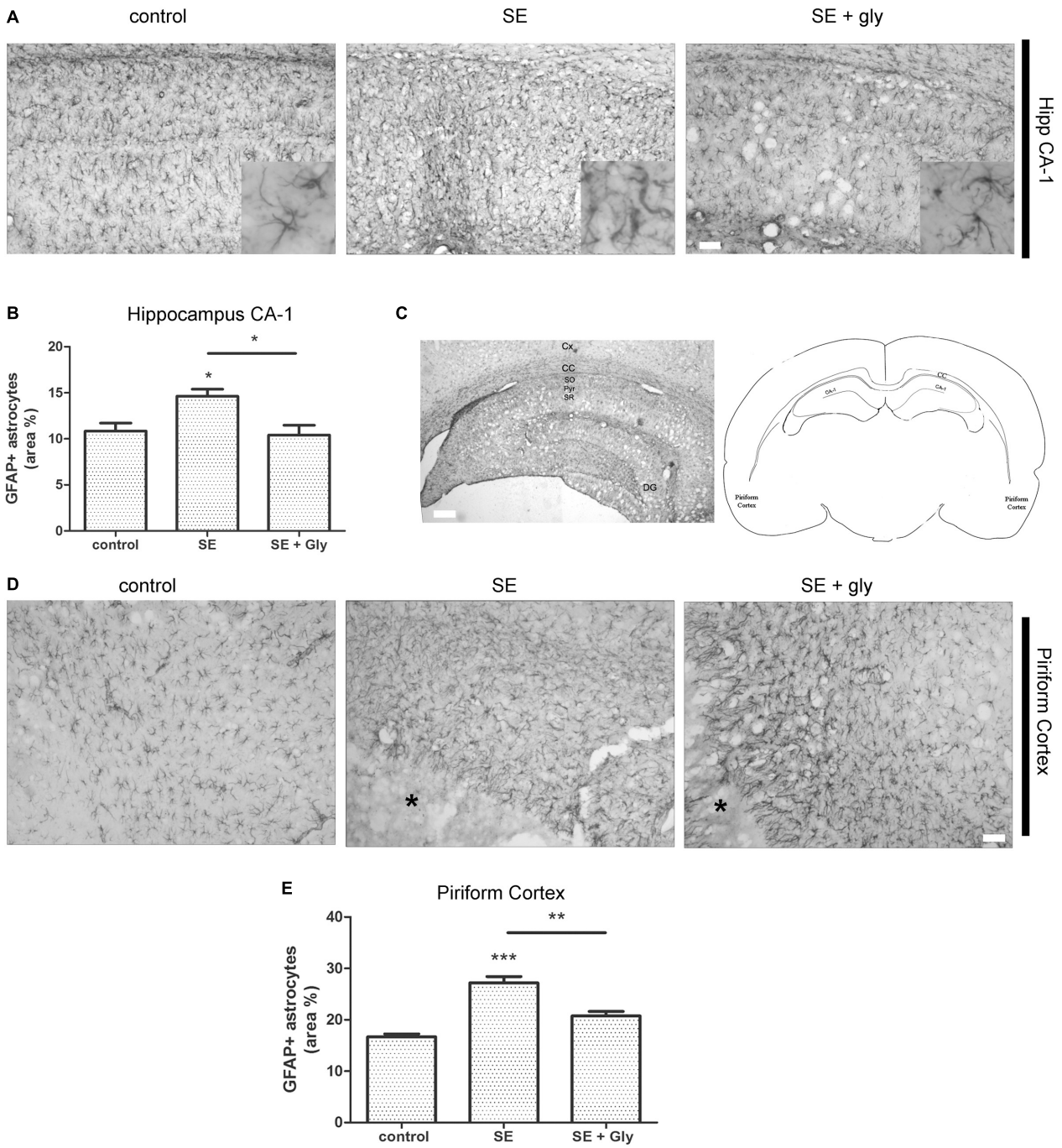

FIGURE 8 | HMGB-1 antagonist glycyrrhizin reduces reactive astrogliosis after pilocarpine-induced SE. Rats were exposed to pilocarpine-induced SE, treated with glycyrrhizin or vehicle for 4 days and analyzed after 15 days. **(A)** Representative images of GFAP-immunostained astrocytes showing the CA-1 hippocampal area. The insets depict astroglial cell morphology in detail. Note the increased astroglial hypertrophy with enlarged projection and increased soma size in SE-exposed animals and the decreased hypertrophy in SE glycyrrhizin-treated animals. Scale bar: 30 μm. **(B)** Quantitative analysis of the GFAP + astroglial cell morphology in the hippocampus of control, SE and SE animals treated with glycyrrhizin. **(C)** Low magnification of the GFAP-immunostained hippocampus to visualize the different regions (scale bar: 300 μm) and a schematic representation of the analyzed areas in a coronal rat brain section. Cx, Brain cortex; CC, Corpus Callosum; DG, Dentate Gyrus; CA-1, Hippocampal CA-1 area; SR, Stratum Radiatum; SO, Stratum Oriens; Pyr, Pyramidal neurons. **(D)** Representative images of GFAP-immunostained astrocytes in the piriform cortex. Note the necrotic core (*) that is characteristic of SE-exposed animals surrounded by highly hypertrophied astrocytes. Scale bar = 35 μm. **(E)** Quantitative analysis of GFAP-immunostained cell area in the piriform cortex and hippocampus of control, SE and SE animals treated with glycyrrhizin. Statistical analyses were performed by one way ANOVA and Student Newman–Keuls post-test, with statistical significance represented as $^{*}p < 0.05$, $^{**}p < 0.01$, and $^{***}p < 0.001$. Control animals were exposed to lithium chloride and saline was used as vehicle. The number of animals were $n = 6$ per experimental group.

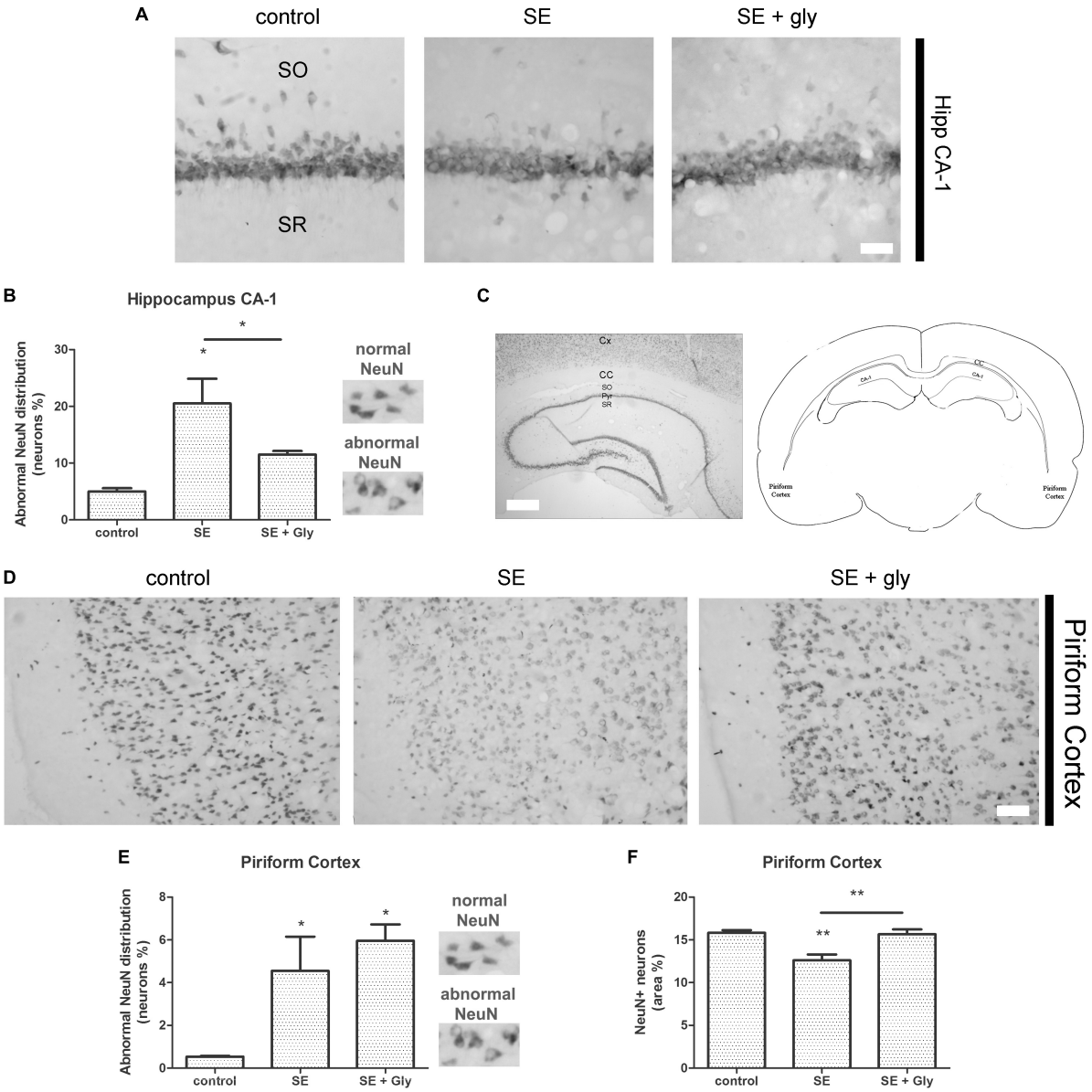

FIGURE 9 | HMGB-1 antagonist glycyrrhizin improves neuronal survival after pilocarpine-induced SE. Rats were exposed to pilocarpine-induced SE, treated with glycyrrhizin or vehicle for 4 days and analyzed after 15 days. **(A)** Representative images of NeuN immunostaining that labels the CA-1 hippocampal pyramidal neurons. Stratum Oriens (SO) and Stratum Radiatum (SR) are also shown. Note the decreased NeuN immunostaining and NeuN relocalization to the cytoplasm, both features of neurodegeneration, in SE-exposed animals and the partial recovery induced by glycyrrhizin treatment. Scale bar: 28 μm. **(B)** Quantitative analysis of NeuN-immunostained neurons showing atypical NeuN localization in the cytoplasm in the CA-1 pyramidal cell layer of control, SE and SE animals treated with glycyrrhizin. **(C)** Low magnification of the NeuN-immunostained hippocampus to visualize the different regions and the typical NeuN labeling of hippocampal neurons. Scale bar: 350 μm. Cx, Brain cortex; CC, Corpus Callosum; SO, Stratum Oriens; Pyr, Pyramidal cell layer; SR, Stratum Radiatum; CA-1, Hippocampal CA-1 area. The scheme shows the localization of the analyzed areas in a coronal rat brain section **(D)** Representative images of NeuN-immunostained neurons in the piriform cortex, images were taken in caudal position to the necrotic core. The absence of NeuN immunostaining in the brain cortical layer I (*moleculare*), scale bar: 40 μm. **(E)** Quantitative analysis of the atypical NeuN-immunostained neurons showing the NeuN redistribution to the cytoplasm in the piriform cortex of control, SE and SE animals treated with glycyrrhizin. **(F)** Quantitative analysis of the total area of NeuN-immunostained neurons in the piriform cortex of control, SE and SE animals treated with glycyrrhizin. Note that glycyrrhizin treatment did not prevent the atypical NeuN localization but significantly reduced neuronal loss induced by SE. Statistical analyses were performed by one way ANOVA and Student Newman–Keuls post-test, with statistical significance represented as $^{*}p < 0.05$, $^{**}p < 0.01$, and $^{***}p < 0.001$. The number of animals were $n = 6$ per experimental group.

(2011) have shown that dopaminergic neurodegeneration in experimental Parkinson Disease requires HMGB-1-activated microglia and downstream NF-κB signaling (Gao et al., 2011). HMGB-1 exposure also seems to induce pro-inflammatory priming in microglial cells of aged brains (Fonken et al., 2016) and the microglial inhibitor named minocicline reduces reactive

microgliosis and HMGB-1 release by activated glia (Hayakawa et al., 2008) Stroke. In this scenario, our results support the notion that microglial-astroglial interaction is required for glial cells to fully respond to HMGB-1, and that this interaction is also required for the HMGB-1 neurodegenerative effects to become evident, since HMGB-1 was unable to reduce neuronal survival in primary cultures lacking glial cells. In addition, our findings in reconstituted cultures that prevent cell contact support the notion that soluble glial cell-derived neurotoxic mediators released upon HMGB-1 stimulation are those able to induce neuronal degeneration without requiring cell contact to exert their effect. The obvious candidate molecules to mediate this effect are classical proinflammatory cytokines such as IL-1β and TNF-α as well as the complement molecule C1q. All these molecules have shown to facilitate astroglial polarization to the proinflammatory-neurodegenerative phenotype (Liddelow et al., 2017). However, more complex cell-to-cell communication pathways like extracellular vesicles can not be ruled out. This area requires further studies in the near future.

Upon binding to target receptors, extracellular HMGB-1 behaves as a typical DAMP, activating PRR-dependent signaling pathways (reviewed in Paudel et al., 2018). We here demonstrated that HMGB-1 induces the translocation of NF-κB to the glial cell nucleus in a TLR2-, TLR4-, and RAGE-dependent manner. The NF-κB-dependent pro-inflammatory responses are probably centrally involved in the neurodegeneration induced by HMGB-1-activated glial cells. Taken together, our results show a novel microglial-astroglial cooperation required for the DAMP HMGB-1 to induce neurodegeneration. This cellular interaction reflects the astroglial engagement in innate immunity and is likely to be a common pathway in brain injury.

A growing body of evidence shows the beneficial role of interfering with HMGB-1 effects after brain injury. HMGB-1 blockade using neutralizing antibodies has been repeatedly shown to be beneficial for brain ischemia and TBI (Okuma et al., 2012; Wang C. et al., 2016), to prevent BBB disruption in a model of Alzheimer's disease (Festoff et al., 2016), reduce 6 hydroxydopamine induced neuronal death (Sasaki et al., 2016) and to reduce neuroinflammation and neurocognitive dysfunction in the aged brain (Fonken et al., 2016; Terrando et al., 2016).

The natural molecule glycyrrhizin, a component from the liquorice root, has also been tested to block HMGB-1 effects since it directly binds to HMGB-1 preventing its interaction with ligand receptors (Okuma et al., 2014). Glycyrrhizin administration was shown to reduce dopamine neuronal death in experimental models of Parkinson's disease (Qi et al., 2015; Santoro et al., 2016). Glycyrrhizin treatment after experimental stroke was effective in reducing infarction (Kim et al., 2012) and neuroinflammation (Xiong et al., 2016), ameliorated intracerebral hemorrhage-induced edema and neuronal loss (Ohnishi et al., 2011), reduced isofluorane-induced neuronal death in neonatal brains (Wang W. et al., 2016) and diminished motor deficits as well as neuroinflammation after experimental TBI (Okuma et al., 2014).

It has been reported that a transient induction of HMGB-1 release occurs after pilocarpine-induced seizures (Fu et al., 2017) in a striking similarity to the HMGB-1 release previously reported in other acute brain injuries (Muhammad et al., 2008; Kim et al., 2018). Accordingly, anti-HMGB-1 antibody administration after seizures reduces neuronal death, acute cytokine release, and astroglial and microglial reactivity in the acute time frame (Fu et al., 2017). In addition, glycyrrhizin administration 30 min before initiating kainic acid-induced seizures in mice suppresses HMGB-1 release (Luo et al., 2014), and consequently reduces reactive gliosis and neuronal death (Luo et al., 2013, 2014). Very recently, Li et al. (2018) have shown that glycyrrhizin treatment ameliorates acute hippocampal neuronal damage and reduces BBB disruption after lithium-pilocarpine treatment (Li et al., 2018). Together, this evidence points toward a main role of HMGB-1 released in the early stages that follow an IPE. In agreement with this, and extending these previous findings, we here show that glycyrrhizin administrated 30 min after pilocarpine-induced seizures partially protects neurons and reduces reactive gliosis in the long term. Thus, having in mind our *in vitro* and *in vivo* mechanistic findings, we propose that early interference with HMGB-1 released by seizure-damaged neurons during the initial latency period that follows the IPE is able to reduce glial conversion to the pro-inflammatory-neurodegenerative phenotype, and that this interference produces beneficial long-lasting effects in neuronal survival and neuroinflammation. Thus, either HMGB-1 blockage or TLR4/TLR2/RAGE antagonist molecules would be able to reduce neuroinflammation and neurodegeneration, phenomena which are proposed as key early steps in epileptogenesis. Taking together our present results with the available previous published data, HMGB-1 and its receptors emerge as a tempting pathway to target in order to change the development of epileptogenesis and probably the natural history of epilepsy as a disease. Lastly, the novel astroglial-microglial cooperation required for HMGB-1 to produce its effects on neuronal survival described here, emerges as a potentially shared common pathway in the acute injury in the CNS. Thus our findings could be extended to several other types of acute brain injury, most notably to TBI and brain ischemia where HMGB-1 has been shown to play a major role.

DATA AVAILABILITY

All datasets generated for this study are included in the manuscript and/or the supplementary files.

ETHICS STATEMENT

All procedures involving animals and their care were conducted in accordance with our institutional guidelines, which comply with the NIH guidelines for the Care and Use of Laboratory Animals, the principles presented in the Guidelines for the Use of Animals in Neuroscience Research by the Society for Neuroscience, the ARRIVE guidelines and were approved by the CICUAL committee of the School of Medicine, University of Buenos Aires (Res. Nr. 1278/2012). All efforts were made to minimize animal suffering and to reduce the number of animal used.

AUTHOR CONTRIBUTIONS

AJR conceived the project, designed the experiments, analyzed the data, and wrote the manuscript. FG, ARR, AR, VM, and AV designed the experiments, discussed results and revised the manuscript. GR, VC, JL, JA, MC, and ARR did the experiments and analyzed the data.

FUNDING

This study was supported by grants from the ANPCYT-FONCYT PICT 2015-1451 and 2017-2203 (AJR), UBACYT (AJR), PICT 2014-2178 (JA), CNPq (FG), and DECIT/MS (FG). GR, VC, and JL are doctoral fellows from CONICET. MC is a doctoral fellow of UBACYT. GR received a research visit grant from IBRO-LARC. AJR, VM, JA, and AV are researchers from CONICET (Argentina).

ACKNOWLEDGMENTS

We thank Biot. Andrea Pecile and Manuel Ponce for the animal care, and Dr. Carla Bonavita for proofreading the manuscript.

REFERENCES

Alaimo, A., Gorojod, R. M., and Kotler, M. L. (2011). The extrinsic and intrinsic apoptotic pathways are involved in manganese toxicity in rat astrocytoma C6 cells. *Neurochem. Int.* 59, 297–308. doi: 10.1016/j.neuint.2011.06.001

Angelo, M. F., Aguirre, A., Avilés Reyes, R. X., Villarreal, A., Lukin, J., Melendez, M., et al. (2014). The pro-inflammatory RAGE/NF-κB pathway is involved in neuronal damage and reactive gliosis in a model of sleep apnea by intermittent hypoxia. *PLoS One* 9:e107901. doi: 10.1371/journal.pone.0107901

Aviles-Reyes, R. X., Angelo, M. F., Villarreal, A., Rios, H., Lazarowski, A., and Ramos, A. J. (2010). Intermittent hypoxia during sleep induces reactive gliosis and limited neuronal death in rats: implications for sleep apnea. *J. Neurochem.* 112, 854–869. doi: 10.1111/j.1471-4159.2009.06535.x

Blume, W. T. (2006). The progression of epilepsy. *Epilepsia* 47, 71–78. doi: 10.1111/j.1528-1167.2006.00665.x

Braun, M., Vaibhav, K., Saad, N. M., Fatima, S., Vender, J. R., Baban, B., et al. (2017). White matter damage after traumatic brain injury: a role for damage associated molecular patterns. *Biochim. Biophys. Acta Mol. Basis Dis.* 1863(10 Pt B), 2614–2626. doi: 10.1016/j.bbadis.2017.05.020

Cendes, F., Andermann, F., Dubeau, F., Gloor, P., Evans, A., Jones-Gotman, M., et al. (1993). Early childhood prolonged febrile convulsions, atrophy and sclerosis of mesial structures, and temporal lobe epilepsy: an MRI volumetric study. *Neurology* 43, 1083–1087.

Choi, J. Y., Cui, Y., Chowdhury, S. T., and Kim, B. G. (2017). High-mobility group box-1 as an autocrine trophic factor in white matter stroke. *Proc. Natl. Acad. Sci. U.S.A.* 114, E4987–E4995. doi: 10.1073/pnas.1702035114

Crack, P. J., and Bray, P. J. (2007). Toll-like receptors in the brain and their potential roles in neuropathology. *Immunol. Cell Biol.* 85, 476–480. doi: 10.1038/sj.icb.7100103

Curia, G., Longo, D., Biagini, G., Jones, R. S., and Avoli, M. (2008). The pilocarpine model of temporal lobe epilepsy. *J. Neurosci. Methods* 172, 143–157. doi: 10.1016/j.jneumeth.2008.04.019

Diniz, L. P., Almeida, J. C., Tortelli, V., Vargas Lopes, C., Setti-Perdigão, P., Stipursky, J., et al. (2012). Astrocyte-induced synaptogenesis is mediated by transforming growth factor β signaling through modulation of D-serine levels in cerebral cortex neurons. *J. Biol. Chem.* 287, 41432–41445. doi: 10.1074/jbc.m112.380824

Ellwood, K. B., Yen, Y. M., Johnson, R. C., and Carey, M. (2000). Mechanism for specificity by HMG-1 in enhanceosome assembly. *Mol. Cell Biol.* 20, 4359–4370. doi: 10.1128/mcb.20.12.4359-4370.2000

Festoff, B. W., Sajja, R. K., van Dreden, P., and Cucullo, L. (2016). HMGB1 and thrombin mediate the blood-brain barrier dysfunction acting as biomarkers of neuroinflammation and progression to neurodegeneration in Alzheimer's disease. *J. Neuroinflammation* 13:194. doi: 10.1186/s12974-016-0670-z

Fonken, L. K., Frank, M. G., Kitt, M. M., D'Angelo, H. M., Norden, D. M., Weber, M. D., et al. (2016). The alarmin HMGB1 mediates age-induced neuroinflammatory priming. *J. Neurosci.* 36, 7946–7956. doi: 10.1523/JNEUROSCI.1161-16.2016

French, J. A., Williamson, P. D., Thadani, V. M., Darcey, T. M., Mattson, R. H., Spencer, S. S., et al. (1993). Characteristics of medial temporal lobe epilepsy: I. Results of history and physical examination. *Ann. Neurol.* 34, 774–780. doi: 10.1002/ana.410340604

Fu, L., Liu, K., Wake, H., Teshigawara, K., Yoshino, T., Takahashi, H., et al. (2017). Therapeutic effects of anti-HMGB1 monoclonal antibody on pilocarpine-induced status epilepticus in mice. *Sci. Rep.* 7:1179. doi: 10.1038/s41598-017-01325-y

Gao, H. M., Zhou, H., Zhang, F., Wilson, B. C., Kam, W., and Hong, J. S. (2011). HMGB1 acts on microglia Mac1 to mediate chronic neuroinflammation that drives progressive neurodegeneration. *J. Neurosci.* 31, 1081–1092. doi: 10.1523/JNEUROSCI.3732-10.2011

Gao, T., Chen, Z., Chen, H., Yuan, H., Wang, Y., Peng, X., et al. (2018). Inhibition of HMGB1 mediates neuroprotection of traumatic brain injury by modulating the microglia/macrophage polarization. *Biochem. Biophys. Res. Commun.* 497, 430–436. doi: 10.1016/j.bbrc.2018.02.102

Gao, T. L., Yuan, X. T., Yang, D., Dai, H. L., Wang, W. J., Peng, X., et al. (2012). Expression of HMGB1 and RAGE in rat and human brains after traumatic brain injury. *J. Trauma Acute Care Surg.* 72, 643–649. doi: 10.1097/TA.0b013e31823c54a6

Hamati-Haddad, A., and Abou-Khalil, B. (1998). Epilepsy diagnosis and localization in patients with antecedent childhood febrile convulsions. *Neurology* 50, 917–922. doi: 10.1212/wnl.50.4.917

Haruma, J., Teshigawara, K., Hishikawa, T., Wang, D., Liu, K., Wake, H., et al. (2016). Anti-high mobility group box-1 (HMGB1) antibody attenuates delayed cerebral vasospasm and brain injury after subarachnoid hemorrhage in rats. *Sci. Rep.* 6:37755. doi: 10.1038/srep37755

Hayakawa, K., Mishima, K., Nozako, M., Hazekawa, M., Mishima, S., Fujioka, M., et al. (2008). Delayed treatment with minocycline ameliorates neurologic impairment through activated microglia expressing a high-mobility group box1-inhibiting mechanism. *Stroke* 39, 951–958. doi: 10.1161/STROKEAHA.107.495820

Kim, I. D., Lee, H., Kim, S. W., Lee, H. K., Choi, J., Han, P. L., et al. (2018). Alarmin HMGB1 induces systemic and brain inflammatory exacerbation in post-stroke infection rat model. *Cell Death Dis.* 9:426. doi: 10.1038/s41419-018-0438-8

Kim, S. W., Jin, Y., Shin, J. H., Kim, I. D., Lee, H. K., Park, S., et al. (2012). Glycyrrhizic acid affords robust neuroprotection in the postischemic brain via anti-inflammatory effect by inhibiting HMGB1 phosphorylation and secretion. *Neurobiol. Dis.* 46, 147–156. doi: 10.1016/j.nbd.2011.12.056

Koyama, R., Tao, K., Sasaki, T., Ichikawa, J., Miyamoto, D., Muramatsu, R., et al. (2012). GABAergic excitation after febrile seizures induces ectopic granule cells and adult epilepsy. *Nat. Med.* 18, 1271–1278. doi: 10.1038/nm.2850

Laird, M. D., Shields, J. S., Sukumari-Ramesh, S., Kimbler, D. E., Fessler, R. D., Shakir, B., et al. (2014). High mobility group box protein-1 promotes cerebral edema after traumatic brain injury via activation of toll-like receptor 4. *Glia* 62, 26–38. doi: 10.1002/glia.22581

Li, Y. J., Wang, L., Zhang, B., Gao, F., and Yang, C. M. (2018). Glycyrrhizin, an HMGB1 inhibitor, exhibits neuroprotective effects in rats after lithium-pilocarpine-induced status epilepticus. *J. Pharm. Pharmacol.* 71, 390–399. doi: 10.1111/jphp.13040

Liddelow, S. A., Guttenplan, K. A., Clarke, L. E., Bennett, F. C., Bohlen, C. J., Schirmer, L., et al. (2017). Neurotoxic reactive astrocytes are induced by activated microglia. *Nature* 541, 481–487. doi: 10.1038/nature21029

Liesz, A., Dalpke, A., Mracsko, E., Antoine, D. J., Roth, S., Zhou, W., et al. (2015). DAMP signaling is a key pathway inducing immune modulation after brain injury. *J. Neurosci.* 35, 583–598. doi: 10.1523/JNEUROSCI.2439-14.2015

Luo, L., Jin, Y., Kim, I. D., and Lee, J. K. (2013). Glycyrrhizin attenuates kainic Acid-induced neuronal cell death in the mouse hippocampus. *Exp. Neurobiol.* 22, 107–115. doi: 10.5607/en.2013.22.2.107

Luo, L., Jin, Y., Kim, I. D., and Lee, J. K. (2014). Glycyrrhizin suppresses HMGB1 inductions in the hippocampus and subsequent accumulation in serum of a kainic acid-induced seizure mouse model. *Cell Mol. Neurobiol.* 34, 987–997. doi: 10.1007/s10571-014-0075-4

Majores, M., Schoch, S., Lie, A., and Becker, A. J. (2007). Molecular neuropathology of temporal lobe epilepsy: complementary approaches in animal models and human disease tissue. *Epilepsia* 48, 4–12. doi: 10.1111/j.1528-1167.2007.01062.x

Maroso, M., Balosso, S., Ravizza, T., Liu, J., Aronica, E., Iyer, A. M., et al. (2010). Toll-like receptor 4 and high-mobility group box-1 are involved in ictogenesis and can be targeted to reduce seizures. *Nat. Med.* 16, 413–419. doi: 10.1038/nm.2127

Mosmann, T. (1983). Rapid colorimetric assay for cellular growth and survival: application to proliferation and cytotoxicity assays. *J. Immunol. Methods* 65, 55–63. doi: 10.1016/0022-1759(83)90303-4

Muhammad, S., Barakat, W., Stoyanov, S., Murikinati, S., Yang, H., Tracey, K. J., et al. (2008). The HMGB1 receptor RAGE mediates ischemic brain damage. *J. Neurosci.* 28, 12023–12031. doi: 10.1523/JNEUROSCI.2435-08.2008

Ohnishi, M., Katsuki, H., Fukutomi, C., Takahashi, M., Motomura, M., Fukunaga, M., et al. (2011). HMGB1 inhibitor glycyrrhizin attenuates intracerebral hemorrhage-induced injury in rats. *Neuropharmacology* 61, 975–980. doi: 10.1016/j.neuropharm.2011.06.026

Ohnishi, M., Monda, A., Takemoto, R., Fujimoto, Y., Sugitani, M., Iwamura, T., et al. (2014). High-mobility group box 1 up-regulates aquaporin 4 expression via microglia-astrocyte interaction. *Neurochem. Int.* 75, 32–38. doi: 10.1016/j.neuint.2014.05.007

Okuma, Y., Liu, K., Wake, H., Liu, R., Nishimura, Y., Hui, Z., et al. (2014). Glycyrrhizin inhibits traumatic brain injury by reducing HMGB1-RAGE interaction. *Neuropharmacology* 85, 18–26. doi: 10.1016/j.neuropharm.2014.05.007

Okuma, Y., Liu, K., Wake, H., Zhang, J., Maruo, T., Date, I., et al. (2012). Anti-high mobility group box-1 antibody therapy for traumatic brain injury. *Ann. Neurol.* 72, 373–384. doi: 10.1002/ana.23602

Parker, T. M., Nguyen, A. H., Rabang, J. R., Patil, A. A., and Agrawal, D. K. (2017). The danger zone: systematic review of the role of HMGB1 danger signalling in traumatic brain injury. *Brain Inj.* 31, 2–8. doi: 10.1080/02699052.2016.1217045

Paudel, Y. N., Shaikh, M. F., Chakraborti, A., Kumari, Y., Aledo-Serrano, Á., Aleksovska, K., et al. (2018). HMGB1: a common biomarker and potential target for TBI, Neuroinflammation, epilepsy, and cognitive dysfunction. *Front. Neurosci.* 12:628. doi: 10.3389/fnins.2018.00628

Pedrazzi, M., Patrone, M., Passalacqua, M., Ranzato, E., Colamassaro, D., Sparatore, B., et al. (2007). Selective proinflammatory activation of astrocytes by high-mobility group box 1 protein signaling. *J. Immunol.* 179, 8525–8532. doi: 10.4049/jimmunol.179.12.8525

Qi, L., Sun, X., Li, F. E., Zhu, B. S., Braun, F. K., Liu, Z. Q., et al. (2015). HMGB1 promotes mitochondrial dysfunction-triggered striatal neurodegeneration via autophagy and apoptosis activation. *PLoS One* 10:e0142901. doi: 10.1371/journal.pone.0142901

Qiu, J., Nishimura, M., Wang, Y., Sims, J. R., Qiu, S., Savitz, S. I., et al. (2008). Early release of HMGB-1 from neurons after the onset of brain ischemia. *J. Cereb. Blood Flow Metab.* 28, 927–938. doi: 10.1038/sj.jcbfm.9600582

Qiu, J., Xu, J., Zheng, Y., Wei, Y., Zhu, X., Lo, E. H., et al. (2010). High-mobility group box 1 promotes metalloproteinase-9 upregulation through Toll-like receptor 4 after cerebral ischemia. *Stroke* 41, 2077–2082. doi: 10.1161/STROKEAHA.110.590463

Racine, R. J., Gartner, J. G., and Burnham, W. M. (1972). Epileptiform activity and neural plasticity in limbic structures. *Brain Res.* 47, 262–268. doi: 10.1016/0006-8993(72)90268-5

Robertson, C. L., Puskar, A., Hoffman, G. E., Murphy, A. Z., Saraswati, M., and Fiskum, G. (2006). Physiologic progesterone reduces mitochondrial dysfunction and hippocampal cell loss after traumatic brain injury in female rats. *Exp. Neurol.* 197, 235–243. doi: 10.1016/j.expneurol.2005.09.014

Rosciszewski, G., Cadena, V., Murta, V., Lukin, J., Villarreal, A., Roger, T., et al. (2018). Toll-like receptor 4 (TLR4) and triggering receptor expressed on myeloid cells-2 (TREM-2) activation balance astrocyte polarization into a proinflammatory phenotype. *Mol. Neurobiol.* 55, 3875–3888. doi: 10.1007/s12035-017-0618-z

Rossi, A., Murta, V., Auzmendi, J., and Ramos, A. J. (2017). Early gabapentin treatment during the latency period increases convulsive threshold, reduces microglial activation and macrophage infiltration in the lithium-pilocarpine model of epilepsy. *Pharmaceuticals* 10:E93. doi: 10.3390/ph10040093

Rossi, A. R., Angelo, M. F., Villarreal, A., Lukin, J., and Ramos, A. J. (2013). Gabapentin administration reduces reactive gliosis and neurodegeneration after pilocarpine-induced status epilepticus. *PLoS One* 8:e78516. doi: 10.1371/journal.pone.0078516

Santoro, M., Maetzler, W., Stathakos, P., Martin, H. L., Hobert, M. A., Rattay, T. W., et al. (2016). In-vivo evidence that high mobility group box 1 exerts deleterious effects in the 1-methyl-4-phenyl-1,2,3,6-tetrahydropyridine model and Parkinson's disease which can be attenuated by glycyrrhizin. *Neurobiol. Dis.* 91, 59–68. doi: 10.1016/j.nbd.2016.02.018

Sasaki, T., Liu, K., Agari, T., Yasuhara, T., Morimoto, J., Okazaki, M., et al. (2016). Anti-high mobility group box 1 antibody exerts neuroprotection in a rat model of Parkinson's disease. *Exp. Neurol.* 275(Pt 1), 220–231. doi: 10.1016/j.expneurol.2015.11.003

Singh, V., Roth, S., Veltkamp, R., and Liesz, A. (2016). HMGB1 as a key mediator of immune mechanisms in ischemic stroke. *Antioxid. Redox Signal.* 24, 635–651. doi: 10.1089/ars.2015.6397

Sun, Q., Wu, W., Hu, Y. C., Li, H., Zhang, D., Li, S., et al. (2014). Early release of high-mobility group box 1 (HMGB1) from neurons in experimental subarachnoid hemorrhage in vivo and in vitro. *J. Neuroinflammation* 11:106. doi: 10.1186/1742-2094-11-106

Tajalli-Nezhad, S., Karimian, M., Beyer, C., Atlasi, M. A., and Azami Tameh, A. (2018). The regulatory role of Toll-like receptors after ischemic stroke: neurosteroids as TLR modulators with the focus on TLR2/4. *Cell Mol. Life Sci.* 76, 523–537. doi: 10.1007/s00018-018-2953-2

Takizawa, T., Shibata, M., Kayama, Y., Shimizu, T., Toriumi, H., Ebine, T., et al. (2017). High-mobility group box 1 is an important mediator of microglial activation induced by cortical spreading depression. *J. Cereb. Blood Flow Metab.* 37, 890–901. doi: 10.1177/0271678X16647398

Terrando, N., Yang, T., Wang, X., Fang, J., Cao, M., Andersson, U., et al. (2016). Systemic HMGB1 neutralization prevents postoperative neurocognitive dysfunction in aged rats. *Front. Immunol.* 7:441. doi: 10.3389/fimmu.2016.00441

Theodore, W. H., Bhatia, S., Hatta, J., Fazilat, S., DeCarli, C., Bookheimer, S. Y., et al. (1999). Hippocampal atrophy, epilepsy duration, and febrile seizures in patients with partial seizures. *Neurology* 52, 132–136.

Tian, X., Liu, C., Shu, Z., and Chen, G. (2017). Review: therapeutic targeting of HMGB1 in stroke. *Curr. Drug Deliv.* 14, 785–790. doi: 10.2174/1567201813666160808111933

Venereau, E., De Leo, F., Mezzapelle, R., Careccia, G., Musco, G., and Bianchi, M. E. (2016). HMGB1 as biomarker and drug target. *Pharmacol. Res.* 111, 534–544. doi: 10.1016/j.phrs.2016.06.031

Verrijdt, G., Haelens, A., Schoenmakers, E., Rombauts, W., and Claessens, F. (2002). Comparative analysis of the influence of the high-mobility group box 1 protein on DNA binding and transcriptional activation by the androgen, glucocorticoid, progesterone and mineralocorticoid receptors. *Biochem. J.* 361(Pt 1), 97–103. doi: 10.1042/bj3610097

Villarreal, A., Seoane, R., González Torres, A., Rosciszewski, G., Angelo, M. F., Rossi, A., et al. (2014). S100B protein activates a RAGE-dependent autocrine loop in astrocytes: implications for its role in the propagation of reactive gliosis. *J. Neurochem.* 131, 190–205. doi: 10.1111/jnc.12790

Walker, L. E., Frigerio, F., Ravizza, T., Ricci, E., Tse, K., Jenkins, R. E., et al. (2017a). Molecular isoforms of high-mobility group box 1 are mechanistic biomarkers for epilepsy. *J. Clin. Invest.* 127, 2118–2132. doi: 10.1172/JCI92001

Walker, L. E., Griffiths, M. J., McGill, F., Lewthwaite, P., Sills, G. J., Jorgensen, A., et al. (2017b). A comparison of HMGB1 concentrations between cerebrospinal

fluid and blood in patients with neurological disease. *Biomarkers* 22, 635–642. doi: 10.1080/1354750X.2016.1265003

Wang, C., Jiang, J., Zhang, X., Song, L., Sun, K., and Xu, R. (2016). Inhibiting HMGB1 reduces cerebral ischemia reperfusion injury in diabetic mice. *Inflammation* 39, 1862–1870. doi: 10.1007/s10753-016-0418-z

Wang, D., Liu, K., Wake, H., Teshigawara, K., Mori, S., and Nishibori, M. (2017). Anti-high mobility group box-1 (HMGB1) antibody inhibits hemorrhage-induced brain injury and improved neurological deficits in rats. *Sci. Rep.* 7:46243. doi: 10.1038/srep46243

Wang, W., Chen, X., Zhang, J., Zhao, Y., Li, S., Tan, L., et al. (2016). Glycyrrhizin attenuates isoflurane-induced cognitive deficits in neonatal rats via its anti-inflammatory activity. *Neuroscience* 316, 328–336. doi: 10.1016/j.neuroscience.2015.11.001

Weber, M. D., Frank, M. G., Tracey, K. J., Watkins, L. R., and Maier, S. F. (2015). Stress induces the danger-associated molecular pattern HMGB-1 in the hippocampus of male Sprague Dawley rats: a priming stimulus of microglia and the NLRP3 inflammasome. *J. Neurosci.* 35, 316–324. doi: 10.1523/JNEUROSCI.3561-14.2015

Xiong, X., Gu, L., Wang, Y., Luo, Y., Zhang, H., Lee, J., et al. (2016). Glycyrrhizin protects against focal cerebral ischemia via inhibition of T cell activity and HMGB1-mediated mechanisms. *J. Neuroinflammation* 13:241. doi: 10.1186/s12974-016-0705-5

Yang, Q. W., Xiang, J., Zhou, Y., Zhong, Q., and Li, J. C. (2010). Targeting HMGB1/TLR4 signaling as a novel approach to treatment of cerebral ischemia. *Front. Biosci.* 2, 1081–1091. doi: 10.2741/s119

Yang, W., Li, J., Shang, Y., Zhao, L., Wang, M., Shi, J., et al. (2017). HMGB1-TLR4 axis plays a regulatory role in the pathogenesis of mesial temporal lobe epilepsy in immature rat model and children via the p38MAPK signaling pathway. *Neurochem. Res.* 42, 1179–1190. doi: 10.1007/s11064-016-2153-0

Zurolo, E., Iyer, A., Maroso, M., Carbonell, C., Anink, J. J., Ravizza, T., et al. (2011). Activation of Toll-like receptor, RAGE and HMGB1 signalling in malformations of cortical development. *Brain* 134(Pt 4), 1015–1032. doi: 10.1093/brain/awr032

Conflict of Interest Statement: The authors declare that the research was conducted in the absence of any commercial or financial relationships that could be construed as a potential conflict of interest.

frontiers in Cellular Neuroscience

MINI REVIEW
published: 13 September 2019
doi: 10.3389/fncel.2019.00397

Post Stroke Seizures and Epilepsy: From Proteases to Maladaptive Plasticity

*Keren Altman[1], Efrat Shavit-Stein[1] and Nicola Maggio[1,2,3]**

[1] Department of Neurology, The Chaim Sheba Medical Center, Ramat Gan, Israel, [2] Sackler Faculty of Medicine and Sagol School of Neuroscience, Tel Aviv University, Tel Aviv-Yafo, Israel, [3] Talpiot Medical Leadership Program, The Chaim Sheba Medical Center, Ramat Gan, Israel

Post stroke epilepsy (PSE) is the most common cause of seizures in the elderly, yet its underlying mechanism is poorly understood. The classification of PSE is confusing, and there is neither a clear agreement on its incidence and prognosis nor a consensus about specific treatments. The diagnosis of PSE requires the occurrence of late seizures: epileptic events occurring 1 week or more after an ischemic stroke. Late seizures differ from early seizures by the presence of permanent structural changes in the brain. Those structural changes cause a shift in the regulation of neuronal firing and lead to circuit dysfunctions, and thus to a long-term epileptic condition. The coagulation cascade and some of its major components, serine proteases such as thrombin, are known to participate in the acute phase of a stroke. Recent discoveries found that thrombin and its protease-activated receptor 1 (PAR1), are involved in the development of maladaptive plasticity. Therefore, we suggest that thrombin and PAR1 may have a role in the development of PSE by inducing permanent structural changes after the ischemic events toward the development of epileptic focuses. We are confident that future studies will lead to a better understanding of the pathophysiology of PSE, as well as development of more directed therapies for its treatment.

Keywords: thrombin, seizure, post stroke epilepsy, proteases-activated receptor 1, ischemic stroke

OPEN ACCESS

Edited by:
Giovanni Cirillo,
Università degli Studi della Campania Luigi Vanvitelli, Italy

Reviewed by:
Hongyu Sun,
Carleton University, Canada
Moran Rubinstein,
Tel Aviv University, Israel

***Correspondence:**
Nicola Maggio
nicola.maggio@sheba.health.gov.il

Specialty section:
This article was submitted to Cellular Neurophysiology, a section of the journal Frontiers in Cellular Neuroscience

Received: *15 June 2019*
Accepted: *16 August 2019*
Published: *13 September 2019*

Citation:
Altman K, Shavit-Stein E and Maggio N (2019) Post Stroke Seizures and Epilepsy: From Proteases to Maladaptive Plasticity. Front. Cell. Neurosci. 13:397. doi: 10.3389/fncel.2019.00397

INTRODUCTION

Cerebrovascular diseases are a major cause of disability worldwide and are the most common cause of seizure in the elderly population (Tomari et al., 2017) As stroke contributes to a significant portion of newly diagnosed epilepsy cases (Beghi and Giussani, 2018; Feyissa et al., 2019), there is an urgent need to further investigate this co-morbidity, which is yet poorly understood. A major cause for this lack of information lies in the high variance of the incidence of stroke-related seizures which range from 2 to 20% among different studies (Wang et al., 2017). The lack of clear epidemiological data both alters the ability to assess the impact and significance of post stroke epilepsy (PSE) as well as humpers clinical care by leaving many cases misdiagnosed and untreated. The major causes for this variability derive from multiple stroke etiologies (Stefanidou et al., 2017), inconsistent

definitions of stroke related seizure and PSE (Stefanidou et al., 2017; Zhao et al., 2018), variations in time of follow up (Stefanidou et al., 2017; Zhao et al., 2018) and lack of organized protocols (Pitkänen et al., 2016).

As a consequence of these discrepancies, little is known about the relatively common condition of stroke related seizure. A limited comprehension of the mechanisms underlying the connection between stroke and epilepsy are significant as it contributes to the faults described in clinical evaluation and treatment. Fortunately, recent discoveries involving activation of the coagulation cascade in the context of blood brain barrier (BBB) breakdown after stroke are providing novel data on the possible pathophysiological mechanisms of PSE which may lead to novel diagnostic and therapeutic tools. In this review, we will shortly describe the state-of-the-art knowledge on early seizure (ES) and PSE, discuss the role of the proteases involved in this process and try to elucidate how proteases are related to development of circuit dysfunction and maladaptive plasticity leading to epilepsy in the context of ischemic stroke.

POST STROKE SEIZURES AND EPILEPSY

In an attempt to settle the discrepancies mentioned above, *The International League Against Epilepsy* defined criteria that try to differentiate between two types of stroke related seizure by their time of onset. ES occurs within a week after stroke and a late seizure (LS) takes place at least a week or more after an ischemic event (Arboix et al., 2003; Lamy et al., 2003; Xu, 2019). This separation has a critical and functional importance: the pathological mechanisms underlying both conditions seem to have distinct differences. ES is related to acute ischemic changes such as hypoperfusion, variations in calcium and sodium concentrations and glutamate release (Myint, 2006). This temporary ischemia may lead to uncontrolled epileptic activity that halts when the patient passes the acute phase. Differently, LS is a long-term continuing disorder resulting from the permanent structural and functional remodeling of damaged brain areas after an ischemic stroke. Importantly, unlike ES, this long term condition has high probability to lead to permanent changes in neuronal excitability (Silverman et al., 2002), an hyperexcitability state leading to increased risk of epileptic activity. PSE diagnosis is based on the presence of two recurrent seizures, which were not provoked by any factor (metabolic, toxic or other) and did not occur in the acute phase of stroke (Sarecka-Hujar and Kopyta, 2019). Therefore, PSE diagnosis does not follow ES, only the occurrence of a LS is required (Zhao et al., 2018).

It is hard to predict which patient will develop ES, LS, and PSE, but certain risk factors are involved. For example, specific stroke types, such as hemorrhagic stroke and total anterior circulation stroke are strongly correlated with increased chance of PSE (Leone et al., 2009; Graham et al., 2013). ES, with an overall prevalence of 3.8% (Feher et al., 2019), is also correlated with similar stroke groups, being more common after hemorrhagic (8.4%) compared to ischemic stroke (2.4%) (Szaflarski et al., 2008). The extent of cortical injury is also considered to be an important issue for both ES and LS, as studies have shown that the involvement of the parietotemporal cortex, supramarginal gyrus and superior temporal gyrus seems to be connected to post stroke epileptogenesis (Zhao et al., 2018). Lacunar strokes are also associated with PSE, accounting for 11% of PSE cases (Pitkänen et al., 2016; Zhao et al., 2018). However, they are less representative than ischemic events with significant cortical involvement (Pitkänen et al., 2016).

Management of ES and PSE is of major importance, yet the present guidelines do not give a definitive curriculum for the management of those patients. While the current criteria for antiepileptic drug selection are based on the specific individual background of the patient, no consideration on either seizures pathogenesis or risk factors to develop ES and PSE in the future (De Reuck, 2009; Gilad, 2012) are part of the clinical decision process. The identification of the risk for developing ES and PSE through better classification may allow precise treatment that will benefit patients that are currently managed as generic focal epilepsy with no regard to prior cerebrovascular event (Wang et al., 2017). According to recent studies, nearly 35% of the patients with ES, LS, and PSE are resistant to antiepileptic treatment. Critically, both the drug resistant and seizure free patients suffer more of drugs adverse effects than general epilepsy patients (Xu, 2019). Additional limitations can be found regarding the prediction of PSE patient outcome. Different studies have shown either an increased (Arntz et al., 2015) or no association (Arntz et al., 2013) of PSE to risk of mortality or disability based on Modified Rankin Scale. If in the future better diagnostic and prognostic tools will be found, medical decisions regarding PSE management may be dealt in a more precise manner then it is today.

PROTEINS AND PROTEASES INVOLVED IN ES AND PSE

In recent years, several studies have suggested a novel approach which may be key for understanding the basic pathological mechanisms associated with the development of ES and PSE. This novel approach is targeting a number of key proteins and proteases involved in the acute phase of stroke that can increase the risk to develop epileptic conditions (Lee et al., 1997; Isaeva et al., 2012; Terunuma et al., 2019). Thrombin, a serine protease derived from the prothrombin cleavage by activated factor X, has a major role in the coagulation cascade (Coughlin, 2000; Göbel et al., 2018) since it mediates the conversion of fibrinogen to fibrin and activates other coagulation factors V, VIII, XI, XIII, and protein C. Thrombin signaling depends on binding to its receptor, the protease-activated receptor (PAR1), a member of the G coupled receptor family, and has a major influence on endothelial disruption, cytotoxicity and inflammation (Coughlin, 2000; Chen et al., 2010; Pleşeru and Mihailă, 2018). Thrombin also serves as an important therapeutic target. Dabigatran, a non-vitamin K antagonist oral anticoagulant approved for stroke prevention in atrial fibrillation patients, is a direct thrombin inhibitor (Alberts et al., 2012).

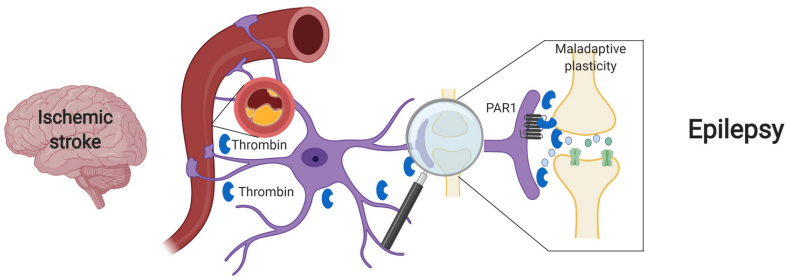

FIGURE 1 | Suggested model – Ischemic stroke leading to maladaptive plasticity and PSE: Following a cerebral vascular occlusion, thrombin increases in the brain. This increase may be as a result of BBB breakdown and entrance of vary blood components into the brain parenchyma or by brain tissue intrinsic production. Thrombin and its main receptor PAR1 enhance NMDA receptor activity and calcium entry, thus leading to a hyperexcitable state and to maladaptive plasticity. Eventually, synchronized epileptic activity occurs as a part of a PSE condition. Created with BioRender.

Beyond its major role in cerebrovascular disease, thrombin has also been pointed as main character in the development of ES after stroke. In acute stroke, cytokine activity promotes an intense neuroinflammation, which underlies BBB disruption. Loss of BBB integrity induces an increase in permeability, facilitating influx of blood components into the brain parenchyma (Abdullahi et al., 2018; Yang et al., 2019). Among various blood components, there is also penetration of serine proteases, such as plasmin and thrombin (Gingrich and Traynelis, 2000), that in turn activates PAR receptors (Ben Shimon et al., 2015). This activation enhances NMDA receptor and calcium overload, thus inducing glutamate mediated neurotoxicity (Gingrich et al., 2000; Stein et al., 2015). Excitatory and inhibitory synapses may be both involved in this process, either through Bestrophin-1 anion channel opening and consequent PAR1 activation in astrocytes (Park et al., 2015) and/or a direct activation of PAR1 in inhibitory interneurons (Maggio et al., 2013). In the former case, through an astrocytic mediated response, an increase in synchronous neuronal firing is achieved (De Pittà and Brunel, 2016; Murphy et al., 2017). In the latter scenario, the activation of PAR1 in interneurons might directly affect IPSCs and thus enhance the excitability of the neuronal network (Maggio et al., 2013). In both cases, a significant hyperexcitable state is established and contributes to seizure onset in the acute phase of stroke (**Figure 1**).

Thrombin and PAR1 signaling contribution to ES is relatively clear. However, knowledge about their action in late cortical remodeling remains limited. A possible late outcome of their signaling could modify physiological plasticity and eventually lead to the development of maladaptive plasticity that can trigger PSE. Future research should seek to unravel how and when this critical shift occurs.

STROKE AS A LEADING CAUSE FOR MALADAPTIVE PLASTICITY AND CIRCUIT DYSFUNCTION

One of the main phenomena involved in synaptic plasticity is long term potentiation (LTP), a process which induces active strengthening of synapses, thus posing an important part of memory and learning processes (Rumpel, 2005; Nabavi et al., 2014). LTP requires the activation of NMDA receptors (NMDAR), which in turn leads to increased calcium influx, a hallmark of synaptic plasticity. The calcium influx induces the expression of more NMDAR as well as increasing axonal sprouting and the formation of new synapses, further strengthening the synapse in the process of positive feedback (Zhou et al., 2015; He and Jin, 2016). LTP is input specific, since it is originated and spread only through relevant synapses that will participate in plasticity process (Luscher and Malenka, 2012).

Proteins and proteases involved in ES and PSE pathophysiology also contribute to homeostatic plasticity. Under normal conditions, PAR1 has several functions in the CNS, such as mediating nerve growth factor release and astrocyte proliferation (Noorbakhsh et al., 2003). In the hippocampus, the major expression of PAR1 is in astrocytes, which are responsible for glutamate release and NMDAR enhancement, crucial for LTP process (Almonte et al., 2013). Additionally, it has been shown that thrombin effects, via PAR1 activation, are dose dependent. Low doses of thrombin enhances plasticity, contributing to learning and memory formation, while high concentration, which typically occurs after stroke, inhibit this physiological pathway and activate a pathological form of plasticity (Ben Shimon et al., 2015).

Under stress, such as the one caused by oxygen and glucose deprivation, the role of ischemic LTP (iLTP), a pathological form of LTP, alters physiological plasticity.

Ischemic LTP and LTP have shared mechanisms, since both work through activation of NMDAR, but also bear major differences. iLTP is not input specific like physiological LTP, since it is more specific to NMDA and not necessarily linked to memory (Lenz et al., 2015). Additionally, it has been shown that iLTP can inhibit physiological LTP (Lyubkin et al., 1997), resulting in deficits of hippocampal LTP thus leading to cognitive deficits (Orfila et al., 2018). Therefore, iLTP can enhance a process called maladaptive plasticity, which leads to a restructure of neuronal network and consequently disruption of function (Ben Shimon et al., 2015).

Under acute ischemic conditions, an excessive glutamate influx drives toxic processes such as extreme excitotoxicity and hyperexcitability (Lai et al., 2014). To protect the brain and compensate for neuronal loss, plasticity processes occur through mechanisms such as iLTP (Stein et al., 2015). However, as mentioned above, iLTP can also lead to pathological forms of plasticity, or maladaptive plasticity and consequently a loss of function. This process can lead eventually to the formation of synchronized neuronal circuits, that in turn can end up as epileptic focuses (Cerasa et al., 2014). Interestingly, it has been shown that, under normal conditions, PAR1 inhibition has no influence on dendritic morphology, which is affected during iLTP process. This implicates that PAR1 targeted therapy could be effective under iLTP conditions, without altering normal brain tissue (Schuldt et al., 2016). While iLTP processes occur in the early phase of ischemic stroke and lead to ES, the mechanism leading to PSE remains unclear. Accumulating evidence suggests that BBB damage and exposure to blood protein and proteases may be involved also in LS and epilepsy (**Figure 1**). For example, recent studies point that albumin plays a role in epileptogenesis after BBB breakdown. In this context, albumin, through TGF-β signaling activation in astrocytes, leads to abnormal reorganization of neuronal circuits and excitatory synaptogenesis, facilitating seizure. Similar mechanisms could also play a role in PSE, as a synergic interaction of proteins and proteases such as thrombin can result in long-term maladaptive plasticity (Friedman et al., 2009; Kim et al., 2017).

Another consequence of maladaptive plasticity is linked to the cognitive outcome. Stroke is known as a major cause of long term cognitive decline (Cao et al., 2015). Additionally, recent studies have shown that thrombin induced neurotoxicity also plays a role in neurodegenerative processes and leads to cognitive deficits (Mhatre, 2004; Stein et al., 2015) which involve damage to reference memory and latency (Mhatre, 2004). Specific analysis of thrombin toxicity in ischemic stroke animal models has also identified damage to similar cognitive functions that could be rescued using direct thrombin inhibitors (Chen et al., 2012).

The role of the serine proteases in the late phase of ischemia and their contribution to maladaptive plasticity and PSE development remains still unclear. A better comprehension of the influence of brain thrombin in the development of seizures is required to gain deeper understanding of these pathological processes for the development of targeted therapy.

SUMMARY AND CONCLUSION

Post stroke epilepsy is a significant cause of epilepsy, yet the underlying mechanisms leading to this condition are mostly unknown. Better understanding of PSE pathology and its connection to ES is a crucial step forward, since it is possible that proper management and treatment of ES might modify the processes of maladaptive plasticity and delay or prevent PSE development. The lack of precise therapies will continue to be a major obstacle going forward, as yet no clinical trials have been set to compare the effectiveness of existing antiepileptic drugs in PSE management.

Additionally, emerging mechanisms found in recent years might provide a possibility to repurpose drugs indicated to other pathologies such as ischemic stroke to ES and PSE patients. In acute stroke, as a result of thrombin enhancement and iLTP induction, the strengthening of excitatory synapses leads to an hyperexcitable state and facilitates ES. Therefore, it can be beneficial to asses in future studies whether treatment of stroke patients with anticoagulants, specifically thrombin inhibitors, might prevent the onset of maladaptive plasticity and possibly reduce the incidence of PSE. If a significant difference is found, it may be beneficial to also study the impact of anticoagulation therapy on seizure frequency among other populations of epileptic patients. Surely, careful selection of patients is needed to test this latter hypothesis: patients with generalized tonic clonic seizures may be at high risk for hemorrhages in case of falls.

All in all, as the incidence of PSE is expected to increase in the incoming decade, more research toward the understanding of PSE mechanisms is urgently needed. A possible search for better PSE animal models as well as the seek of possible biomarkers (i.e., levels of in thrombin CSF) will improve patient management in the future.

AUTHOR CONTRIBUTIONS

All authors conceived and wrote the manuscript.

REFERENCES

Abdullahi, W., Tripathi, D., and Ronaldson, P. T. (2018). Blood-brain barrier dysfunction in ischemic stroke: targeting tight junctions and transporters for vascular protection. *Am. J. Physiol. Physiol.* 315, C343–C356. doi: 10.1152/ajpcell.00095.2018

Alberts, M. J., Bernstein, R. A., Naccarelli, G. V., and Garcia, D. A. (2012). Using dabigatran in patients with stroke. *Stroke* 43, 271–279. doi: 10.1161/STROKEAHA.111.622498

Almonte, A. G., Qadri, L. H., Sultan, F. A., Watson, J. A., Mount, D. J., Rumbaugh, G., et al. (2013). Protease-activated receptor-1 modulates hippocampal memory formation and synaptic plasticity. *J. Neurochem.* 124, 109–122. doi: 10.1111/jnc.12075

Arboix, A., Comes, E., García-Eroles, L., Massons, J. B., Oliveres, M., and Balcells, M. (2003). Prognostic value of very early seizures for In-Hospital mortality in atherothrombotic infarction. *Eur. Neurol.* 50, 78–84. doi: 10.1159/000072503

Arntz, R. M., Maaijwee, N. A. M., Rutten-Jacobs, L. C. A., Schoonderwaldt, H. C., Dorresteijn, L. D., van Dijk, E. J., et al. (2013). Epilepsy after TIA or stroke in young patients impairs long-term functional outcome: the FUTURE Study. *Neurology* 81, 1907–1913. doi: 10.1212/01.wnl.0000436619.25532.f3

Arntz, R. M., Rutten-Jacobs, L. C. A., Maaijwee, N. A. M., Schoonderwaldt, H. C., Dorresteijn, L. D., van Dijk, E. J., et al. (2015). Poststroke epilepsy is associated with a high mortality after a stroke at young age. *Stroke* 46, 2309–2311. doi: 10.1161/STROKEAHA.115.010115

Beghi, E., and Giussani, G. (2018). Aging and the epidemiology of epilepsy. *Neuroepidemiology* 51, 216–223. doi: 10.1159/000493484

Ben Shimon, M., Lenz, M., Ikenberg, B., Becker, D., Shavit Stein, E., Chapman, J., et al. (2015). Thrombin regulation of synaptic transmission and plasticity:

implications for health and disease. *Front. Cell Neurosci.* 9:151. doi: 10.3389/fncel.2015.00151

Cao, L., Pokorney, S. D., Hayden, K., Welsh-Bohmer, K., and Newby, L. K. (2015). Cognitive function: is there more to anticoagulation in atrial fibrillation than stroke? *J. Am. Heart Assoc.* 4:e001573. doi: 10.1161/JAHA.114.001573

Cerasa, A., Fasano, A., Morgante, F., Koch, G., and Quattrone, A. (2014). Maladaptive plasticity in levodopa-induced dyskinesias and tardive dyskinesias: old and new insights on the effects of dopamine receptor pharmacology. *Front. Neurol.* 5:49. doi: 10.3389/fneur.2014.00049

Chen, B., Cheng, Q., Yang, K., and Lyden, P. D. (2010). Thrombin mediates severe neurovascular injury during ischemia. *Stroke* 41, 2348–2352. doi: 10.1161/STROKEAHA.110.584920

Chen, B., Friedman, B., Whitney, M. A., Winkle, J. A., Lei, I. F., Olson, E. S., et al. (2012). Thrombin activity associated with neuronal damage during acute focal ischemia. *J. Neurosci.* 32, 7622–7631. doi: 10.1523/JNEUROSCI.0369-12.2012

Coughlin, S. R. (2000). Thrombin signalling and protease-activated receptors. *Nature* 407, 258–264. doi: 10.1038/35025229

De Pittà, M., and Brunel, N. (2016). Modulation of synaptic plasticity by glutamatergic gliotransmission: a modeling study. *Neural Plast.* 2016, 1–30. doi: 10.1155/2016/7607924

De Reuck, J. (2009). Management of stroke-related seizures. *Acta Neurol. Belg.* 109, 271–276.

Feher, G., Gurdan, Z., Gombos, K., Koltai, K., Pusch, G., Tibold, A., et al. (2019). Early seizures after ischemic stroke: focus on thrombolysis. *CNS Spectr.* doi: 10.1017/S1092852919000804 [Epub ahead of print].

Feyissa, A. M., Hasan, T. F., and Meschia, J. F. (2019). Stroke-related epilepsy. *Eur. J. Neurol.* 26, 18–e3. doi: 10.1111/ene.13813

Friedman, A., Kaufer, D., and Heinemann, U. (2009). Blood-brain barrier breakdown-inducing astrocytic transformation: novel targets for the prevention of epilepsy. *Epilepsy Res.* 85, 142–149. doi: 10.1016/j.eplepsyres.2009.03.005

Gilad, R. (2012). Management of seizures following a stroke. *Drugs Aging* 29, 533–538. doi: 10.2165/11631540-000000000-00000

Gingrich, M. B., Junge, C. E., Lyuboslavsky, P., and Traynelis, S. F. (2000). Potentiation of NMDA receptor function by the serine protease thrombin. *J. Neurosci.* 20, 4582–4595. doi: 10.1523/jneurosci.20-12-04582.2000

Gingrich, M. B., and Traynelis, S. F. (2000). Serine proteases and brain damage – is there a link? *Trends Neurosci.* 23, 399–407. doi: 10.1016/S0166-2236(00)01617-9

Göbel, K., Eichler, S., Wiendl, H., Chavakis, T., Kleinschnitz, C., and Meuth, S. G. (2018). The coagulation factors fibrinogen, thrombin, and factor XII in inflammatory disorders—a systematic review. *Front. Immunol.* 9:1731. doi: 10.3389/fimmu.2018.01731

Graham, N. S. N., Crichton, S., Koutroumanidis, M., Wolfe, C. D. A., and Rudd, A. G. (2013). Incidence and associations of poststroke epilepsy. *Stroke* 44, 605–611. doi: 10.1161/STROKEAHA.111.000220

He, Z., and Jin, Y. (2016). Intrinsic control of axon regeneration. *Neuron* 90, 437–451. doi: 10.1016/j.neuron.2016.04.022

Isaeva, E., Hernan, A., Isaev, D., and Holmes, G. L. (2012). Thrombin facilitates seizures through activation of persistent sodium current. *Ann. Neurol.* 72, 192–198. doi: 10.1002/ana.23587

Kim, S. Y., Senatorov, V. V., Morrissey, C. S., Lippmann, K., Vazquez, O., Milikovsky, D. Z., et al. (2017). TGFβ signaling is associated with changes in inflammatory gene expression and perineuronal net degradation around inhibitory neurons following various neurological insults. *Sci. Rep.* 7:7711. doi: 10.1038/s41598-017-07394-3

Lai, T. W., Zhang, S., and Wang, Y. T. (2014). Excitotoxicity and stroke: identifying novel targets for neuroprotection. *Prog. Neurobiol.* 115, 157–188. doi: 10.1016/j.pneurobio.2013.11.006

Lamy, C., Domigo, V., Semah, F., Arquizan, C., Trystram, D., Coste, J., et al. (2003). Early and late seizures after cryptogenic ischemic stroke in young adults. *Neurology* 60, 400–404. doi: 10.1212/WNL.60.3.400

Lee, K. R., Drury, I., Vitarbo, E., and Hoff, J. T. (1997). Seizures induced by intracerebral injection of thrombin: a model of intracerebral hemorrhage. *J. Neurosurg.* 87, 73–78. doi: 10.3171/jns.1997.87.1.0073

Lenz, M., Vlachos, A., and Maggio, N. (2015). Ischemic long-term-potentiation (iLTP), perspectives to set the threshold of neural plasticity toward therapy. *Neural Regen. Res.* 10, 1537–1539. doi: 10.4103/1673-5374.165215

Leone, M. A., Tonini, M. C., Bogliun, G., Gionco, M., Tassinari, T., Bottacchi, E., et al. (2009). Risk factors for a first epileptic seizure after stroke: a case control study. *J. Neurol. Sci.* 277, 138–142. doi: 10.1016/j.jns.2008.11.004

Luscher, C., and Malenka, R. C. (2012). NMDA Receptor-Dependent Long-term potentiation and long-term depression (LTP/LTD). *Cold Spring Harb. Perspect. Biol.* 4:a005710. doi: 10.1101/cshperspect.a005710

Lyubkin, M., Durand, D. M., and Haxhiu, M. A. (1997). Interaction between tetanus long-term potentiation and hypoxia-induced potentiation in the rat hippocampus. *J. Neurophysiol.* 78, 2475–2482. doi: 10.1152/jn.1997.78.5.2475

Maggio, N., Cavaliere, C., Papa, M., Blatt, I., Chapman, J., and Segal, M. (2013). Thrombin regulation of synaptic transmission: implications for seizure onset. *Neurobiol. Dis.* 50, 171–178. doi: 10.1016/j.nbd.2012.10.017

Mhatre, M. (2004). Thrombin, a mediator of neurotoxicity and memory impairment. *Neurobiol. Aging* 25, 783–793. doi: 10.1016/S0197-4580(03)00192-1

Murphy, T. R., Binder, D. K., and Fiacco, T. A. (2017). Turning down the volume: astrocyte volume change in the generation and termination of epileptic seizures. *Neurobiol. Dis.* 104, 24–32. doi: 10.1016/j.nbd.2017.04.016

Myint, P. K. (2006). Post-stroke seizure and post-stroke epilepsy. *Postgrad. Med. J.* 82, 568–572. doi: 10.1136/pgmj.2005.041426

Nabavi, S., Fox, R., Proulx, C. D., Lin, J. Y., Tsien, R. Y., and Malinow, R. (2014). Engineering a memory with LTD and LTP. *Nature* 511, 348–352. doi: 10.1038/nature13294

Noorbakhsh, F., Vergnolle, N., Hollenberg, M. D., and Power, C. (2003). Proteinase-activated receptors in the nervous system. *Nat. Rev. Neurosci.* 4, 981–990. doi: 10.1038/nrn1255

Orfila, J. E., McKinnon, N., Moreno, M., Deng, G., Chalmers, N., Dietz, R. M., et al. (2018). Cardiac arrest induces ischemic long-term potentiation of hippocampal CA1 neurons that occludes physiological long-term potentiation. *Neural Plast.* 2018:9275239. doi: 10.1155/2018/9275239

Park, H., Han, K.-S., Seo, J., Lee, J., Dravid, S. M., Woo, J., et al. (2015). Channel-mediated astrocytic glutamate modulates hippocampal synaptic plasticity by activating postsynaptic NMDA receptors. *Mol. Brain* 8:7. doi: 10.1186/s13041-015-0097-y

Pitkänen, A., Roivainen, R., and Lukasiuk, K. (2016). Development of epilepsy after ischaemic stroke. *Lancet Neurol.* 15, 185–197. doi: 10.1016/S1474-4422(15)00248-3

Pleşeru, A.-M., and Mihailă, R. G. (2018). The role of thrombin in central nervous system activity and stroke. *Clujul Med.* 91, 368–371. doi: 10.15386/cjmed-973

Rumpel, S. (2005). Postsynaptic receptor trafficking underlying a form of associative learning. *Science* 308, 83–88. doi: 10.1126/science.1103944

Sarecka-Hujar, B., and Kopyta, I. (2019). Poststroke epilepsy: current perspectives on diagnosis and treatment. *Neuropsychiatr. Dis. Treat.* 15, 95–103. doi: 10.2147/NDT.S169579

Schuldt, G., Galanis, C., Strehl, A., Hick, M., Schiener, S., Lenz, M., et al. (2016). Inhibition of protease-activated receptor 1 does not affect dendritic homeostasis of cultured mouse dentate granule cells. *Front. Neuroanat.* 10:64. doi: 10.3389/fnana.2016.00064

Silverman, I. E., Restrepo, L., and Mathews, G. C. (2002). Poststroke Seizures. *Arch. Neurol.* 59:195. doi: 10.1001/archneur.59.2.195

Stefanidou, M., Das, R. R., Beiser, A. S., Sundar, B., Kelly-Hayes, M., Kase, C. S., et al. (2017). Incidence of seizures following initial ischemic stroke in a community-based cohort: the framingham heart study. *Seizure* 47, 105–110. doi: 10.1016/j.seizure.2017.03.009

Stein, E. S., Itsekson-Hayosh, Z., Aronovich, A., Reisner, Y., Bushi, D., Pick, C. G., et al. (2015). Thrombin induces ischemic LTP (iLTP), implications for synaptic plasticity in the acute phase of ischemic stroke. *Sci. Rep.* 5:7912. doi: 10.1038/srep07912

Szaflarski, J. P., Rackley, A. Y., Kleindorfer, D. O., Khoury, J., Woo, D., Miller, R., et al. (2008). Incidence of seizures in the acute phase of stroke: a population-based study HHS Public Access. *Epilepsia* 49, 974–981. doi: 10.1111/j.1528-1167.2007.01513.x

Terunuma, M., Xu, J., Vithlani, M., Pangalos, M., Pg, H., and Da, C. (2019). *Current Literature in Basic Science Impact of Protein Kinase C*

Activation on Status Epilepticus And Epileptogenesis: Oh, What A Tangled Web Deficits in Phosphorylation of GABA A Receptors by Intimately Associated Protein Kinase C Activity Underlie Com-Promised Synaptic Inhibition during Status Epilepticus. Available at: https://www.ncbi.nlm.nih.gov/pmc/articles/PMC2442157/pdf/epc0008-0110.pdf (accessed May 13, 2019).

Tomari, S., Tanaka, T., Ihara, M., Matsuki, T., Fukuma, K., Matsubara, S., et al. (2017). Risk factors for post-stroke seizure recurrence after the first episode. *Seizure* 52, 22–26. doi: 10.1016/j.seizure.2017.09.007

Wang, J. Z., Vyas, M. V., Saposnik, G., and Burneo, J. G. (2017). Incidence and management of seizures after ischemic stroke. *Neurology* 89, 1220–1228. doi: 10.1212/WNL.0000000000004407

Xu, M. Y. (2019). Poststroke seizure: optimising its management. *Stroke Vasc. Neurol.* 4, 48–56. doi: 10.1136/svn-2018-000175

Yang, C., Hawkins, K. E., Doré, S., and Candelario-Jalil, E. (2019). Neuroinflammatory mechanisms of blood-brain barrier damage in ischemic stroke. *Am. J. Physiol. Physiol.* 316, C135–C153. doi: 10.1152/ajpcell.00136.2018

Zhao, Y., Li, X., Zhang, K., Tong, T., and Cui, R. (2018). The progress of epilepsy after stroke. *Curr. Neuropharmacol.* 16, 71–78. doi: 10.2174/1570159X15666170613083253

Zhou, H.-H., Tang, Y., Zhang, X.-Y., Luo, C. X., Gao, L. Y., Wu, H. Y., et al. (2015). Delayed administration of Tat-HA-NR2B9c promotes recovery after stroke in rats. *Stroke* 46, 1352–1358. doi: 10.1161/STROKEAHA.115.008886 doi: 10.1161/strokeaha.115.008886

Conflict of Interest Statement: The authors declare that the research was conducted in the absence of any commercial or financial relationships that could be construed as a potential conflict of interest.

frontiers in Cellular Neuroscience

ORIGINAL RESEARCH
published: 19 September 2019
doi: 10.3389/fncel.2019.00420

The ATP-P2X7 Signaling Pathway Participates in the Regulation of Slit1 Expression in Satellite Glial Cells

*Quanpeng Zhang[1,2], Jiuhong Zhao[1,2], Jing Shen[3], Xianfang Zhang[1,2], Rui Ren[1,2], Zhijian Ma[1,2], Yuebin He[2], Qian Kang[4], Yanshan Wang[5], Xu Dong[6], Jin Sun[7], Zhuozhou Liu[7] and Xinan Yi[1,2]**

[1] Department of Anatomy, Hainan Medical University, Haikou, China, [2] Joint Laboratory for Neuroscience, Hainan Medical University, Fourth Military Medical University, Haikou, China, [3] Department of Ophthalmology, First Affiliated Hospital of Hainan Medical University, Haikou, China, [4] Infection Control Department, People's Hospital of Xing'an County, Guilin, China, [5] Quality Inspection Department, Minghui Industry (Shenzhen) Co., Ltd., Shenzhen, China, [6] Hainan Provincial Key Laboratory of Carcinogenesis and Intervention, Hainan Medical University, Haikou, China, [7] Department of Clinical Medicine, Hainan Medical University, Haikou, China

OPEN ACCESS

Edited by:
Giovanni Cirillo,
Università degli Studi della Campania Luigi Vanvitelli, Italy

Reviewed by:
Parisa Gazerani,
Aalborg University, Denmark
Luigi Catacuzzeno,
University of Perugia, Italy
Bin Yu,
Nantong University, China

***Correspondence:**
Xinan Yi
XinanYi2019@163.com

Specialty section:
This article was submitted to Non-Neuronal Cells, a section of the journal Frontiers in Cellular Neuroscience

Received: 15 July 2019
Accepted: 02 September 2019
Published: 19 September 2019

Citation:
Zhang QP, Zhao JH, Shen J, Zhang XF, Ren R, Ma ZJ, He YB, Kang Q, Wang YS, Dong X, Sun J, Liu ZZ and Yi XN (2019) The ATP-P2X7 Signaling Pathway Participates in the Regulation of Slit1 Expression in Satellite Glial Cells. Front. Cell. Neurosci. 13:420. doi: 10.3389/fncel.2019.00420

Slit1 is one of the known signaling factors of the slit family and can promote neurite growth by binding to its receptor, Robo2. Upregulation of Slit1 expression in dorsal root ganglia (DRG) after peripheral nerve injury plays an important role in nerve regeneration. Each sensory neuronal soma in the DRG is encapsulated by several surrounding satellite glial cells (SGCs) to form a neural structural unit. However, the temporal and spatial patterns of Slit1 upregulation in SGCs in DRG and its molecular mechanisms are not well understood. This study examined the spatial and temporal patterns of Slit1 expression in DRG after sciatic nerve crush by immunohistochemistry and western blotting. The effect of neuronal damage signaling on the expression of Slit1 in SGCs was studied *in vivo* by fluorescent gold retrograde tracing and double immunofluorescence staining. The relationship between the expression of Slit1 in SGCs and neuronal somas was also observed by culturing DRG cells and double immunofluorescence labeling. The molecular mechanism of Slit1 was further explored by immunohistochemistry and western blotting after intraperitoneal injection of Bright Blue G (BBG, P2X7R inhibitor). The results showed that after peripheral nerve injury, the expression of Slit1 in the neurons and SGCs of DRG increased. The expression of Slit1 was presented with a time lag in SGCs than in neurons. The expression of Slit1 in SGCs was induced by contact with surrounding neuronal somas. Through injured cell localization, it was found that the expression of Slit1 was stronger in SGCs surrounding injured neurons than in SGCs surrounding non-injured neurons. The expression of vesicular nucleotide transporter (VNUT) in DRG neurons was increased by injury signaling. After the inhibition of P2X7R, the expression of Slit1 in SGCs was downregulated, and the expression of VNUT in DRG neurons was upregulated. These results indicate that the ATP-P2X7R pathway is involved in signal transduction from peripheral nerve injury to SGCs, leading to the upregulation of Slit1 expression.

Keywords: Slit1, dorsal root ganglia, P2X7R, satellite glial cells, sciatic nerve crush

INTRODUCTION

It is well established that peripheral nerves can be regenerated (Stoll, 1999; Vogelaar et al., 2004; Scheib and Hoke, 2013; Cattin and Lloyd, 2016; Sanna et al., 2017; Mahar and Cavalli, 2018; Tajdaran et al., 2018; Duraikannu et al., 2019). However, the factors affecting neuron generation are very complicated. In addition to endogenous gene regulation, external factors such as nerve regeneration chambers (Cattin and Lloyd, 2016), neurotrophic factors (Duraikannu et al., 2019), cytokines (Fitzgerald and McKelvey, 2016) and inflammation responses (Cattin and Lloyd, 2016) should also be taken into account. Intensive previous studies have focused on Schwann cells (SCs) (Court et al., 2008; Nave and Trapp, 2008; Parrinello et al., 2010; Arthur-Farraj et al., 2012; Fontana et al., 2012; Beirowski et al., 2014; Kang et al., 2014; Painter et al., 2014; Rosenberg et al., 2014; Gomez-Sanchez et al., 2015; Isaacman-Beck et al., 2015; Jessen et al., 2015), while little research has been conducted on satellite glial cells (SGCs), a type of glial cells in the ganglion, to study their involvement in nerve regeneration (Hanani, 2005). SGCs are flattened glial cells in the peripheral nervous system that encircle the neuronal bodies in sensory ganglia, thus supporting and protecting sensory neurons (Hanani, 2005). SGCs are laminar and have no true processes (Hanani, 2005). Each sensory neuronal soma is encapsulated by several SGCs to form a unique SGCs health; thus, the neuron and its surrounding SGCs form a structural unit (Hanani et al., 2002; Hanani, 2005, 2015; Wang et al., 2016). Inside the dorsal root ganglion (DRG), SGCs provide support for neurons by mediating the response against inflammation (Hanani, 2005) and synthesizing multiple neurotrophic factors to support the survival of the neurons (Hanani, 2010, 2012; Hanani et al., 2014). Slit1 is one of the known signaling factors of the slit family and can guide both axon projection and neuronal migration (Blockus and Chedotal, 2016). Slit can guide axon projection by mediating the branching of the sensory axon growth cone (Ma and Tessier-Lavigne, 2007). In a previous study (Yi et al., 2006), we observed that Slit1 expression was increased in the SGCs of damaged DRG. However, SGCs express specific patterns of Slit1, and the signal transduction mechanism between neurons and SGCs was not identified. Signal communication between neurons and SGCs is bidirectional (Christie et al., 2015). The interacting molecules include adenosine triphosphate (ATP) (Zhang et al., 2007), nitric oxide (NO) (Bradman et al., 2010), endothelin 1 (Giaid et al., 1989; Milner and Burnstock, 2000; Hanani, 2012), glutamic acid (Kung et al., 2013) and calcium ions (Suadicani et al., 2010; Castillo et al., 2011). ATP is a neurotransmitter secreted by many cell types including sensory neurons (Chaudhari, 2014), and it participates in signal transduction between neurons and SGCs (Zhang et al., 2007). ATP is stored in many types of neurons and is released not only at synapses but also in axons and cell bodies (Zhang et al., 2007). ATP is an important extracellular signaling molecule that communicates through complex purine energy signaling pathways (Burnstock, 2006). This signaling pathway consists of many membrane receptors and extracellular enzymes including the P2X7 receptor (P2X7R), which belongs to the P2X family (Yegutkin, 2008). P2X7R, an important member of the purine receptor family, is a trimer ATP-gated cation channel encoded by the P2X7R gene (Coddou et al., 2011). P2X7R can be activated by extracellular ATP, and it participates in the regulation of cell biological functions such as cell signaling pathways, cytokine secretion, and the growth and apoptosis of cells (Sluyter, 2017). P2X7R expressed in the SGCs is involved in DRG neuron – SGC communication in adult rats (Chen et al., 2012a). P2X7R is the main receptor in SGCs (Zhang et al., 2007; Kushnir et al., 2011; Song et al., 2018). Similar to the closely related dorsal root ganglion neurons, the membrane capacitance of cultured trigeminal ganglion neurons increased significantly after electrical stimulation, which resulted in the release of vesicles content in the extracellular space of the ganglion (Sforna et al., 2019). The increase of membrane capacitance is an indicator of somatic exocytosis. Sforna et al. (2019) identified Ca^{2+} -dependent and Ca^{2+} -independent somatic vesicular release from trigeminal neurons and the Ca^{2+} channel types involved in the process. The vesicular nucleotide transporter (VNUT) is a key molecule for the vesicular storage and nucleotide release of ATP from neutrophils (Sawada et al., 2008). Injured DRG neurons increase the secretion of ATP and VNUT (Goto et al., 2017). After the cell is stimulated, ATP is secreted from the cell body to become an extracellular signaling molecule that binds to purinoreceptors at the surface of SGCs. It triggers intracellular signal transduction (Zhang et al., 2007). ATP is used as the signaling molecule for signal transmission between neurons and SGCs, and SGCs receive signaling stimuli, leading to the production of a series of reactions (Zhang et al., 2007).The molecular mechanisms of the protective effect of SGCs on DRG neurons and the promotion of the regeneration of DRG neurons have not been clarified. In this study, we further clarified the effect of damage signals on the expression of Slit1 in DRG neurons and their SGCs and clarified the role of ATP and its receptors.

RESULTS

Expression of Slit1 in Intact DRG Neurons and SGCs *in vivo* and *in vitro*

Preliminary analyses were performed to verify the specificity of the Slit1, microtubule-associated protein 2 (MAP2), glutamine synthetase (GS), activating transcription factor 3 (ATF3) and VNUT and P2X7R antibodies used in this study (**Supplementary Figure S1**). The expression of MAP2 and Slit1 co-localized in DRG cells subjected to double labeling of Slit1 and MAP2 [neuron biomarker (Pellegrino et al., 2011)], (**Supplementary Figures S2A–C**). Expression of Slit1 was not observed in the SGCs of intact DRG double labeled for Slit1 and GS [biomarker for SGCs (Donegan et al., 2013)], (**Supplementary Figures S2D–F**). To observe the expression of Slit1 in cultured neurons and SGCs, double immunofluorescence labeling of Slit1 and MAP2 or GS in cultured DRG cells was performed. The results showed that Slit1 was expressed in the cultured sensory neuronal soma of DRG but not in neurites and weakly in SGCs (**Supplementary Figures S2G–L**).

Neural Trunk Injury Can Up-Regulate the Expression of Slit1 in DRG Neurons and SGCs

To observe the effect of nerve injury on the expression of Slit1 in DRG neurons and SGCs, we used a unilateral rat sciatic nerve crush model (SNC). The immunohistochemistry results revealed that Slit1 was expressed in the sensory neurons on the DRG of both sides. However, the expression of Slit1 in the SNC DRG was higher than that in the contralateral DRG (**Figures 1A–J**). At days 1, 3, and 7 after SNC, the numbers of strongly Slit1-positive neurons were 24.4 ± 2, 32.5 ± 5, and 21.2 ± 3.8, respectively, and a significant difference was observed compared with the contralateral side ($P < 0.05$, **Figure 1K**). The number of Slit1-positive neurons was increased at day 1 and peaked at day 3, followed by a gradual decrease and a return to normal levels at day 14 after SNC (**Figure 1K**). The results of Slit1 western blotting after SNC (**Figures 1K,L**) were basically consistent with the immunohistochemistry results (**Figure 1L**). Slit1 expression was not observed in SGCs in intact DRG (**Figure 2A**) and was observed occasionally in SGCs at day 1, then increased between day 3 and day 14 after SNC according to double immunofluorescence labeling of Slit1 and GS (**Figures 2C–F** and **Supplementary Figure S4**). Although the level of Slit1 expression was decreased at day 28 after SNC, it was still higher than in the contralateral DRG (**Figures 2C–F**). At each time point after injury, the Slit1 relative fluorescence intensity (RFI) in SGCs on the ipsilateral side was higher than that on the opposite side, and the difference was statistically significant according to one-way ANOVA ($P < 0.001$) (**Figure 2I**). Interestingly, following SNC, the peak expression of Slit1 in SGCs appeared later than in the neuronal somas (**Figure 2J**).

A Neuronal Damage Signal Can Induce Up-Regulation of Slit1 Expression in SGCs in the Structural Unit

Because the nerve crush model only causes partial damage to DRG neurons, it is convenient to observe the effect of neuron damage signals on SGCs in the anatomical unit of neurons. Fluor-Gold (FG) is a slow retrograde axonal tracer, a volume of 0.1 μl of 4% FG solution was inserted into the epineurium 2 mm from the distal to the injured site of the sciatic nerve and the neurons that are reached by retrograde FG transport can be considered uninjured neurons. Additionally, ATF3 was used as an immunofluorescence marker for injured neuronal somas (Donegan et al., 2013). The combination of Slit1 immunofluorescence and the FG retrograde labeling method with Slit1 and ATF3 double immunofluorescence labeling was used to show the expression of Slit1 in SGCs around normal or injured neurons. 7 days after SNC, L5-6 DRG from the injured side were subjected to Slit1 immunofluorescence staining. The results showed that the expression of Slit1 in SGCs around ATF3-positive neurons was significantly higher than that around ATF3-negative neurons (**Figures 3A–C**). Conversely, the expression of Slit1 in SGCs around FG-positive neurons was significantly lower than that around FG-negative neurons (**Figures 3D–F**). According to analysis of the RFI with the paired *t*-test at a significance level of $P < 0.01$ (**Figures 3G,H**).

Contact of Neuronal Soma With SGCs Induces the Expression of Slit1

In the process of DRG cell culture, an interesting phenomenon was found. When cultured for 2–7 h, some glial cells detached from the neuronal soma, while others remained in contact with the neuronal soma (**Figures 4A,D**). Significantly, glial cells that maintained contact with neuronal somas exhibited a strong expression of Slit1, while those located far from neurons presented very weak expression of Slit1 (**Figures 4A,D**). Immunofluorescence showed that both populations of glial cells expressed GS. RFI analysis showed that the expression of Slit1 in SGCs in contact with neurons was stronger than that in SGCs located far from neurons (**Figure 4E**) (2.51 ± 0.19 folds, $P < 0.01$).

Damage Signaling Induces an Increase in VNUT in DRG Neurons

It has been reported that the changes in the contents of VNUT and ATP are positively associated (Yuri et al., 2013; Menéndez-Méndez et al., 2015; Pérez de Lara et al., 2015; Harada et al., 2018). To observe the effect of an injury signal on ATP production in DRG neurons, we chose to evaluate the changes in VNUT. Double-labeling of ATF3 and VNUT showed that both were co-expressed after SNC (**Figures 5A–G**). Compared to the RFI of VNUT in ATF3-negative neurons, VNUT expression in ATF3-positive neurons was stronger than that in ATF3-negative neurons (**Figure 5H**) ($P < 0.01$).

After Inhibiting the P2X7 Receptor, the Expression of VNUT Increased, While the Expression of Slit1 in SGCs Decreased

It has been reported that ATP can interact with the P2X7 receptor on SGC membranes, thus activating a series of molecular events in SGCs (Zhang et al., 2005, 2007; Ryu and McLarnon, 2008; Chen et al., 2012a; Song et al., 2018). BBG is a P2X7 receptor inhibitor (Jiang et al., 2000; Remy et al., 2008; Ryu and McLarnon, 2008). BBG was injected intraperitoneally after unilateral SNC in rats. VNUT immunofluorescence and western blotting showed that the expression of VNUT in DRG neurons on the ipsilateral side increased significantly (**Figure 6**). After BBG injection, the expression of VNUT in the neurons of both sides was significantly up-regulated ($P < 0.01$) (**Figure 6F**). Double immunofluorescence labeling was performed by using Slit1 and GS antibodies. The results showed that the expression of Slit1 in DRG neurons and SGCs was increased at 7 days after SNC (**Figures 7B,F**). After BBG treatment, the expression of Slit1 in neurons and SGCs was downregulated (**Figures 7D,H**). The results of western blotting detection were similar to those of immunofluorescence (**Figure 7I**). After BBG injection, the expression of Slit1 on the operated side was significantly lower than that on the contralateral side (**Figure 7J**) according to a paired *t*-test ($p < 0.01$). Double immunofluorescence labeling was

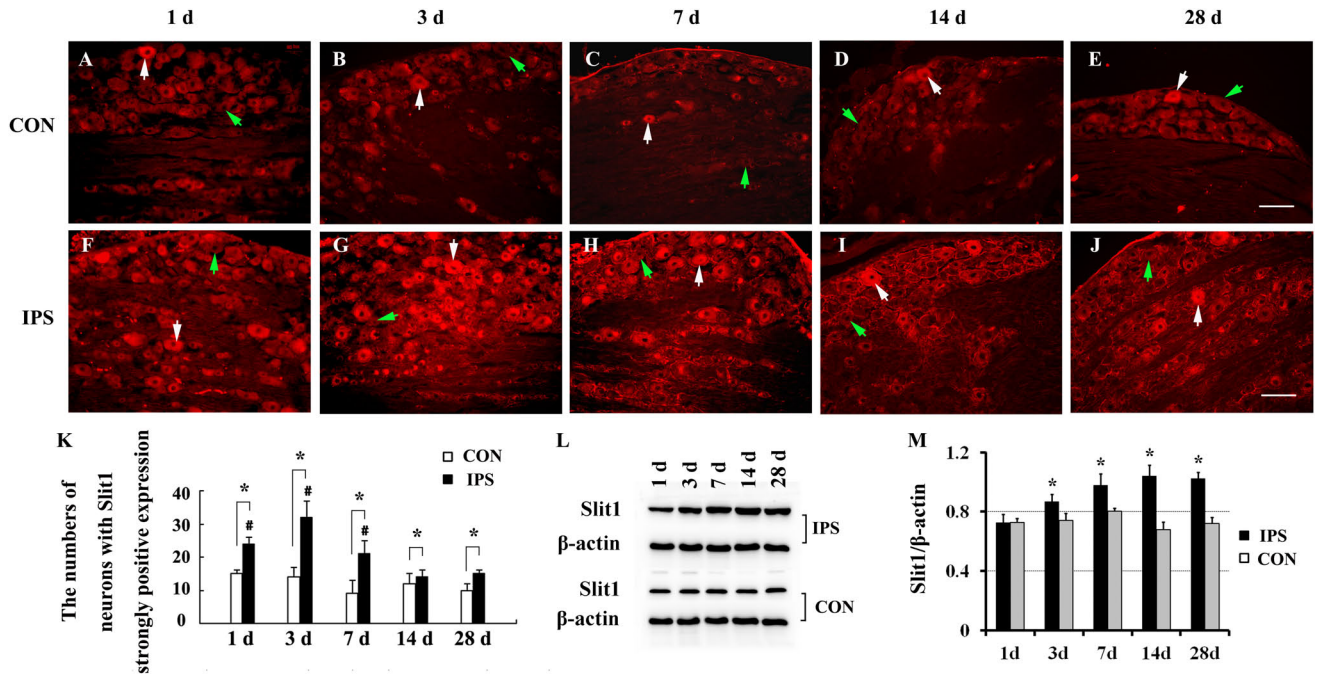

FIGURE 1 | Dynamic changes in Slit1 expression in DRG after sciatic nerve injury. The expression of Slit1 in DRG was detected by immunofluorescence histochemistry and western blotting at different time points after SNC. **(A–E)** Contralateral DRG sections. **(F–J)** Ipsilateral DRG sections. The white arrows indicate strongly Slit1-positive neurons, and the green arrow indicates weakly Slit1-positive neurons. Scale bar = 100 μm. **(K)** At different time points, the numbers of strongly Slit1-positive DRG neurons on both sides were compared, and one-way repeated measures ANOVA and paired *t*-tests were used for statistical analysis. "*" in comparison with the control side, the difference is statistically significant at $P < 0.05$; "#" in comparisons of the groups at 1, 3 or 7 days after injury with the group at 14 days after injury, the difference is statistically at $P < 0.01$. **(L)** Detection of DRG Slit1 protein expression at different time points by western blotting ($N = 3$). The level of β-actin was detected as loading control. **(M)** At different time points, the relative gray values of DRG Slit1 expression on the two sides were compared. $N = 3$, and one-way repeated measures ANOVA and paired *t*-tests were used for statistical analysis, "*" compared to the contralateral side, $P < 0.01$. CON: contralateral DRG, IPS: ipsilateral (crush side) DRG.

performed with the P2X7R and GS antibodies, and the results showed that the P2X7R and GS antibodies were co-expressed in the SGCs of the DRG of both sides. After BBG injection, no expression of P2X7R was found in DRG on the operated side (**Supplementary Figure S3**).

DISCUSSION

This study shows that after peripheral nerve injury, the expression of Slit1 in the neurons and SGCs of DRG increased. The expression of Slit1 was presented with a time lag in SGCs than in neurons. The expression in SGCs of Slit1 was induced by contacting neuronal somas. Through injured cell localization, it was found that the expression of Slit1 was stronger in SGCs surrounding injured neurons than in SGCs surrounding healthy neurons. This result indicates that the damage signal could induce upregulation of Slit1 expression in the SGCs of the DRG neural unit. The expression of VNUT in DRG neurons was increased by the injury signal. After the inhibition of P2X7R, the expression of Slit1 in SGCs was downregulated, and the expression of VNU in DRG neurons was upregulated. These results indicate that the ATP-P2X7R pathway is involved in signal transduction from peripheral nerve injury to SGCs, leading to the upregulation of Slit1 expression. These findings suggest that maintaining the integrity of DRG neurons is beneficial to nerve regeneration and that the ATP-P2X7 pathway between neurons and SGCs plays an important role in the regeneration of peripheral nerves following injury.

Slit, which is generated in glial cells during the development phase, is the guidance molecule for the growth of neurites. There are 4 subtypes of the Slit family: Slit1, Slit2, Slit3 and Slit 4. Slit1, Slit2 and Slit3 all bind to the Robo receptor, which is present in the neuronal cell membrane, to participate in the guidance of axons (Ma and Tessier-Lavigne, 2007; Blockus and Chedotal, 2016; Carr et al., 2017). Previous studies on Slit focusing on SCs suggested that peripheral nerve injury could lead to the expression of various neurotrophic factors in SCs, including NGF, BDNF, neurotrophin 4/5, insulin growth factor 1 and 2 (Scheib and Hoke, 2013), and Slit2 and Slit3 (Carr et al., 2017). Temporarily increased expression of these neurotrophic factors can promote the regeneration of sensory neurons (Scheib and Hoke, 2013). However, we used a mouse polyclonal primary antibody against Slit1 (ab115892, immunogen: Synthetic peptide corresponding to mouse Slit1 aa 497–504 conjugated to keyhole limpet hemocyanin), which was predicted to be able to react with rat Slit1. The results from three repeated experiments were

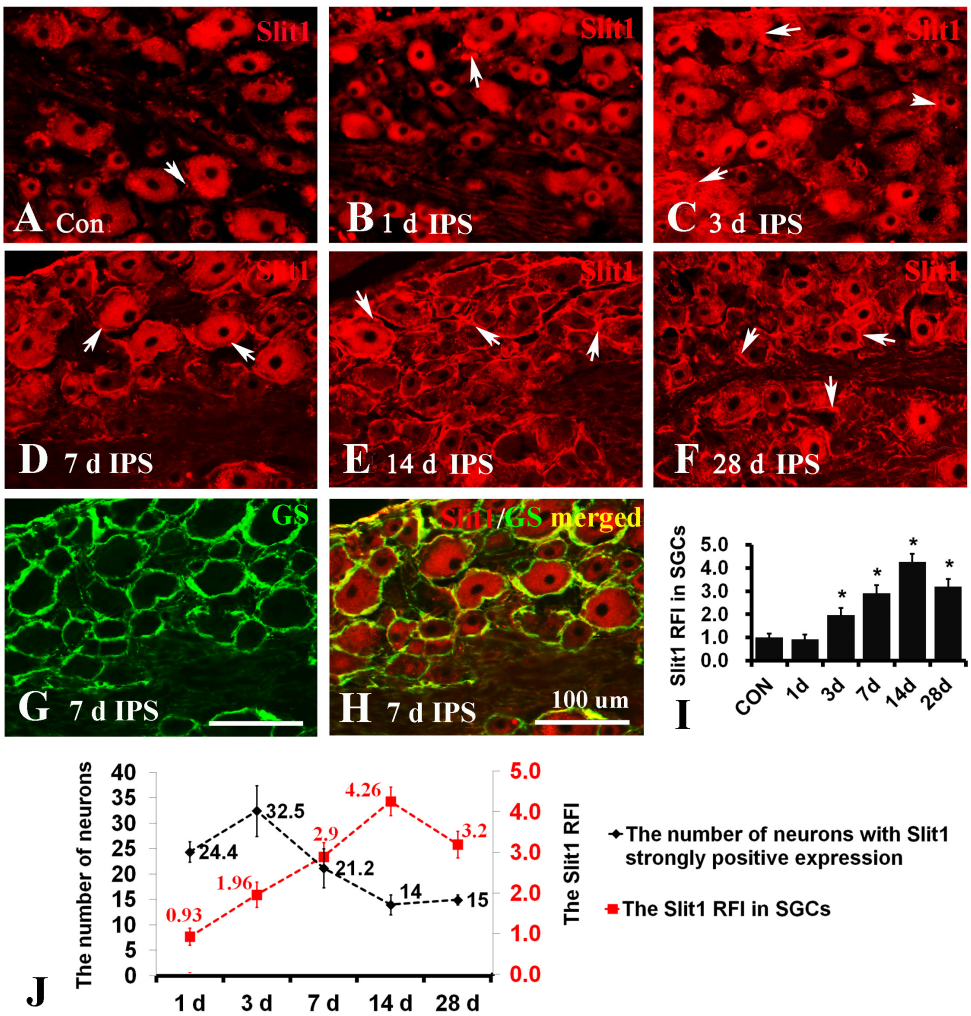

FIGURE 2 | Slit1 expression in SGCs of injured DRG. Slit1 expression in the SGCs of injured DRG was detected by immunofluorescence histochemistry. **(A)** Slit1 (red) immunofluorescence staining of contralateral DRG sections randomly selected from the different groups. **(B–F)** Slit1 immunofluorescence staining of ipsilateral DRG at different time points after operation. The arrow indicates Slit1-positive SGCs. **(G)** GS (green) immunofluorescence staining of DRG sections on the 7th day after sciatic nerve crush. **(H)** Merged images from panels **(D,E)**. **(I)** Summary histograms depicting the changes in the Slit1 RFI in SGCs (one-way repeated measures ANOVA, * $P < 0.01$); RFI, relative fluorescence intensity. **(J)** Changes in the number of strongly Slit1-positive DRG neurons and the RFI of Slit1 expression in SGCs at different time points after injury are shown. Scale bar = 100 μm.

consistent (**Supplementary Figures S1**, **S2**), indicating the reliability of the Slit1 primary antibody (ab115892). Through double labeling of Slit1 and MAP2 (neuron biomarker) and Slit1 and GS (biomarker for SGCs), it was found that Slit1 was strongly expressed in the DRG neuronal soma *in vivo* and *in vitro*, but not expressed in SGCs *in vivo* and weakly *in vitro* (**Supplementary Figure S2**). These results are consistent with the literature (Carr et al., 2017).

In this study, an improved SNC model (Gordon and Borschel, 2017) was used to achieve partial DRG neuron injury, allowing effective evaluation of the regeneration and repair of DRG after neuron injury (Wood et al., 2011; Faroni et al., 2015; Cattin and Lloyd, 2016; Gordon and Borschel, 2017; Mahar and Cavalli, 2018). This model resulted in successful injury of some neurons in the DRG and retention of the integrity of others, which is helpful for observing and comparing Slit1 expression in SGCs located in damaged and undamaged neuron units. In the rat SNC model, DRG neurons are partially injured, that is to say, there are two types of neuron subpopulations in DRG: injured neurons (ATF3 positive, which is a marker of injured neurons) and uninjured neurons (ATF3 negative) (**Figure 3** and **Supplementary Figure S5**). Combining the fluorescence double-label staining data of Slit1 and ATF3, VNUT and ATF3 in this study, we found that there were two mainly types of neuron subpopulations in 7 days post-SNC DRG with using the analytical method of Luigi Catacuzzeno (Catacuzzeno et al., 2014) (**Supplementary Table S1**). There must be existence of the subpopulations $Slit1^{-}VNUT^{+}ATF3^{+}$ on injured neurons, it is suggested that VNUT is mainly expressed in injured neurons. Other subpopulations such as $Slit1^{+}VNUT^{+}ATF3^{+}$,

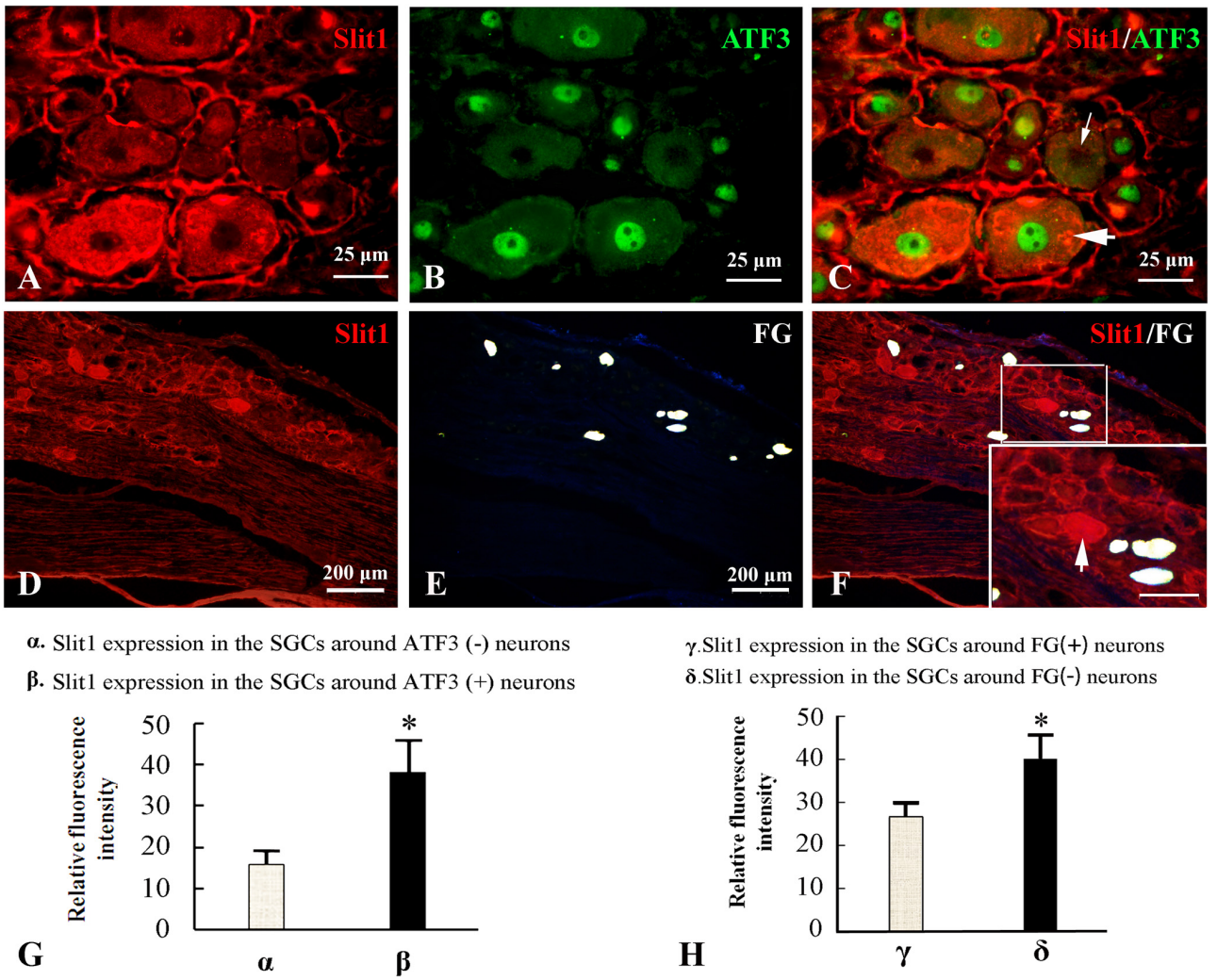

FIGURE 3 | Effects of DRG-injured neuronal soma on Slit1 expression in SGCs. The Slit1 and ATF3 double immunofluorescence labeling method and the Slit1 and FG retrograde labeling method were used to show the expression of Slit1 in SGCs around normal and injured neurons. **(A–C)** Double immunofluorescence labeling of Slit1 and ATF3 was carried out on DRG sections from 7 days after sciatic nerve crush. **(A)** Slit1 (red) immunofluorescence staining. **(B)** ATF3 (green) immunofluorescence staining. **(C)** Merged images of panels **(A,B)**. The thick arrow indicates ATF3-positive neurons, and the thin arrow indicates ATF3-negative neurons, scale bar = 25 μm. **(D–F)** Slit1 immunofluorescence staining and FG retrograde labeling. **(D)** DRG Slit1 immunofluorescence on the 7th day after the operation. **(E)** FG (white)-traced positive neurons. **(F)** Merged images of panels **(D,E)**. Scale bar = 200 μm. The large framed image is an enlargement of the small frame, and thin arrows indicate FG-negative neurons in panels **(F)**. **(G)** Summary histograms depict the changes in the RFI of Slit1 in SGCs surrounding ATF3-positive and negative neurons determined with paired *t*-tests, * $P < 0.001$; bars represent the standard error of the mean; RFI, relative fluorescence intensity. **(H)** Summary histograms depict the changes in the RFI of Slit1 expression in SGCs surrounding FG-negative and FG-positive neurons determined with paired *t*-tests, *$P < 0.001$; bars represent the standard error of the mean; RFI, relative fluorescence intensity.

$Slit1^{+}VNUT^{-}ATF3^{+}$ and $Slit1^{-}VNUT^{-}ATF3^{+}$ on injured neurons may also exist. Among the uninjured neurons (ATF3 negative), there is only one subpopulation $Slit1^{-}VNUT^{-}ATF3^{-}$, and no other subpopulations exists. Slit1 or VNUT expression was observed in the uninjured neurons on the control side, which indicated that their expression was not related to the injury signal. It was reported from another study (Seijffers et al., 2006; Carriel et al., 2017) that only a few hours after peripheral nerve injury, neurons exhibit changes in gene and protein expression. Most of the affected genes are associated with neuronal growth factors such as GAP43 and ATF3. ATF3 is used as a marker of injured neurons, and the uninjured neurons do not express ATF3 (Donegan et al., 2013). FG is a slow retrograde axonal tracer with a retrograde tracing speed of approximately 1–12 mm/day. On average, the distance between the sites of SNC and DRG is 35 ± 3 mm in adult rats. Therefore, it was estimated that it would take at least 3 days to reach the DRG, which was in agreement with our experimental results (**Figure 3**). In this study, FG was injected into the distal point of the injured site to label uninjured neuronal somas through retrograde tracing. ATF3 was used as an immunofluorescence marker for injured neuronal somas.

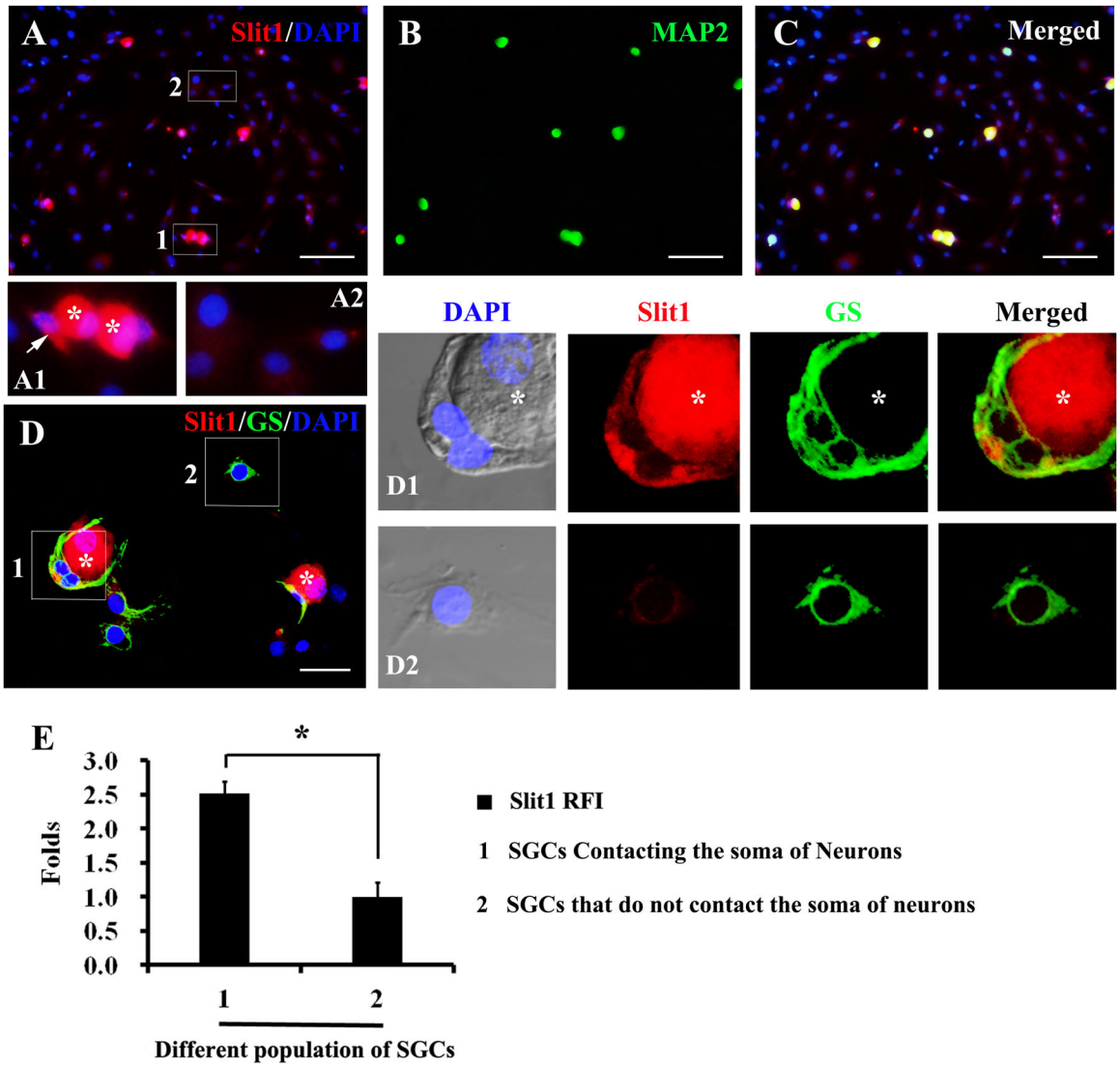

FIGURE 4 | Expression of Slit1 in SGCs directly in contact with the neuronal soma *in vitro* **(A–C)** Primary cultured DRG cells were double labeled with Slit1 and MAP2 immunochemistry, nuclear staining by DAPI. **(A)** Slit1 (red) and DAPI (blue) merged image. The box 1 shows SGCs in contact with neuron bodies, Panel **(A1)** is its enlarged image, with arrows indicating SGCs in contact with neuronal soma (white asterisks); and the box 2 shows SGCs located far from neuron bodies as showed in its enlarged image **(A2)**. **(B)** MAP2 (green) image. **(C)** Slit1 (red), MAP2 (green) and DAPI (blue) merged image. **(D)** Slit1 and GS double immunostaining were performed on cultured DRG cells, nuclear staining by DAPI. The box 1 shows SGCs in contact with Slit1-positive neuronal soma (white asterisks). The box 2 shows SGCs located far from neuron bodies. Panels **(D1,D2)** lines of pictures were local enlarged images of the box 1 and box 2 showed in panel **(D)**, respectively. The white asterisk indicates the neuronal soma. Slit1 (red), MAP2 (green) and DAPI (blue) were showed in panels **(D,D1,D2)**. **(E)** Summary histograms depict the changes in Slit1 expression in two different populations of SGCs, * shows the expression of Slit1 in SGCs of population 1 compared with that in SGCs of population 2 analyzed with paired *t*-tests, * $P < 0.001$; bars represent the standard error of the mean; RFI, relative fluorescence intensity. Scale bar = 50 μm was showed in panels **(A–C)**; Scale bar = 15 μm was showed in panel **(D)**.

Thus, we could compare the difference in Slit1 expression in the SGCs between the injured neuron units and the undamaged neuron units. We found that the expression of Slit1 was higher in the SGCs that were in contact with injured DRG neuronal somas than in those in contact with uninjured DRG neurons. Many studies (Sebert and Shooter, 1993; Kim et al., 2011) simply include contralateral comparisons, which would not meet our experimental requirements. The experimental animal model and the markers of damaged and undamaged neurons that we chose ensure that we could achieve the goal of the experiment.

The expression of Slit1 in SGCs lags behind that in neurons (**Figures 1**, **2**). One possible explanation is that there is no direct link between DRG glial cells and the peripheral nerve trunk (Arkhipova et al., 2010). The peripheral nerve injury signal must reach the neuronal soma first and is subsequently transmitted to SGCs. In respond to nerve injury, SGCs are activated, and upregulate GFAP protein expression, undergo

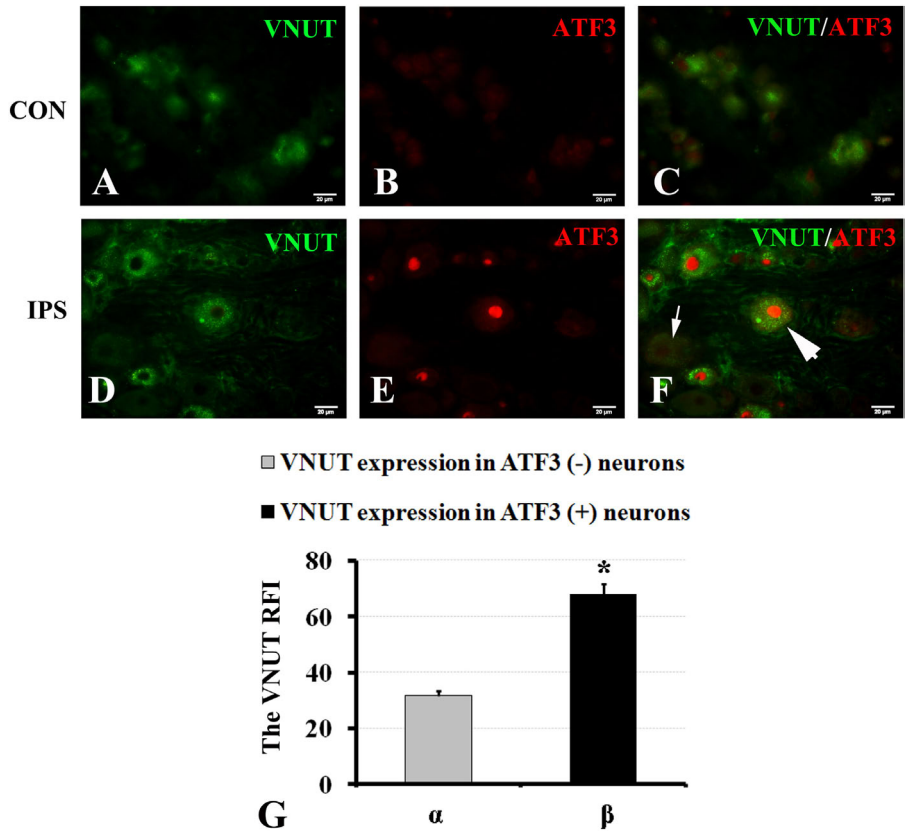

FIGURE 5 | Upregulation of VNUT expression in injured neurons. At 7 days after right sciatic nerve crush, double labeling of VNUT and ATF3 was performed in DRG sections. **(A–C)** Contralateral DRG images, **(D–F)** ipsilateral DRG images following sciatic nerve crush. Panels **(B,E)** immunofluorescence staining for ATF3 (red); Panels **(C,F)** merged images of panels **(A,B)** or **(D,E)**, respectively. A thick arrow indicates ATF3-positive neurons, and a thin arrow indicates ATF3-negative neurons; scale bar = 20 μm. **(G)** Summary histograms depicting the changes in VNUT expression in ATF3-positive neurons and ATF3-negative neurons on the crush side with the paired *t*-test, α and β, * $P < 0.001$; bars represent the standard error of the mean; RFI, relative fluorescence intensity.

cell division, activated SGCs generate and release inflammatory cytokines and neurotransmitters such as bradykinin, interleukin-1β (IL-1β), tumor necrosis factor-α (TNF-α), neurotrophins, and ATP into its surroundings (Elson et al., 2004; Zhang et al., 2009). Wu et al. (2017) reported that SGCs were activated and NGF was up-regulated after sciatic nerve injury, the increase was significant on day 7 and 14. This also suggests that it takes a time for SGCs to receive damage signals to be activated and express GFAP and NGF. Therefore, this signal transmission process delays the effect of the injury signal on SGCs. The continuous increase in Slit1 in SGCs coincides with the regeneration of damaged sensory neurons induced by nerve crush injury (Kovacic et al., 2004). Our previous research (Zhang et al., 2010; Chen et al., 2012b) found that Slit1 promotes neuronal neurite outgrowth by binding with Robo2, Slit1- Robo2-srGAP3 pathway plays an important regulatory role in DRG neuron regeneration. In this study, we observed that the expression of Slit1 in SGCs was up-regulated after neuronal injury, which may promote the outgrowth of neuronal processes.

Neurons within the DRG are pseudounipolar neurons, and each sensory neuronal soma is encapsulated by several SGCs to form a unique anatomic unit (Hanani, 2005). Therefore, Hanani (2005) proposed that the unique structure and relationship of SGCs and neuronal somas might have special physiological and pharmacological effects. Thus, we hypothesized that the continuous increase in Slit1 expression observed in the SGCs of DRG is closely associated with this unique anatomical structure. Our experiments showed that 7 days after SNC, Slit1 expression in SGCs was significantly lower in the FG-positive neuron unit than in the FG-negative neuron unit (in which the axon was injured, and axoplasmic transport was blocked); in comparison, Slit1 expression in SGCs was significantly stronger in the ATF3-positive neuron unit than in the ATF3-negative neuron unit (ATF3-negative neuronal somas may indicate uninjured neurons) (**Figure 3**). This result indicated that upon neuronal injury, Slit1 expression is increased not only in the injured neurons but also in the SGCs of the unit.

Using cultured primary DRG neurons and glial cells and applying double immunofluorescence labeling of Slit1 and GS, we found that the expression of Slit1 in SGCs that accumulated around the neuronal soma was much stronger than that in SGCs located at distal sites in the neuronal somas (**Figure 4**). This

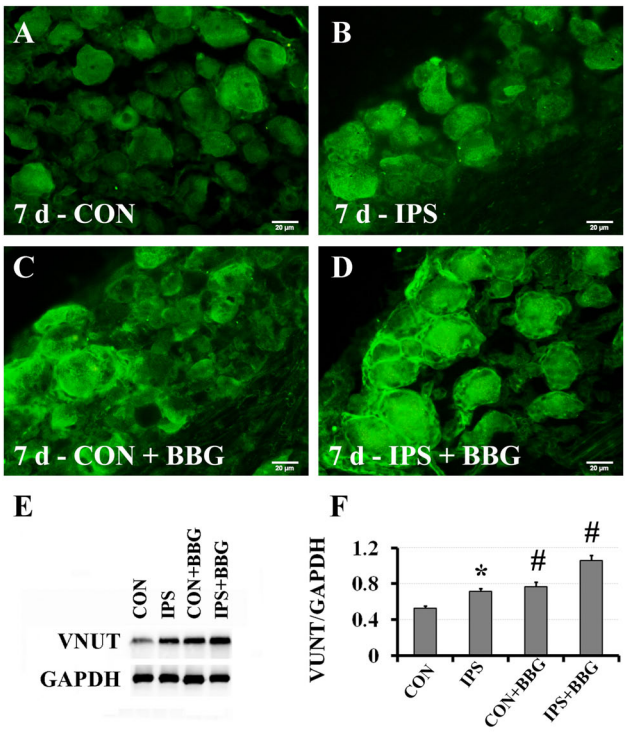

FIGURE 6 | Upregulation of VNUT expression after inhibition of the P2X7 receptor with BBG. After right sciatic nerve crush, BBG (P2X7 receptor inhibitor) was injected intraperitoneally. VNUT immunofluorescence in DRG was detected on the 7th day. **(A–D)** VNUT immunofluorescence staining (green), scale bar = 20 μm. **(E)** The level of VNUT protein was detected by western blotting ($N = 3$). The level of GAPDH was detected as loading control. **(F)** The expression of VNUT before and after BBG treatment on the 7th day after SNC was analyzed with the paired *t*-test, "*" compared with the control side, $P < 0.001$; "#" compared with the contralateral side and the ipsilateral side before BBG treatment, $P < 0.001$. CON: contralateral DRG, IPS: ipsilateral DRG.

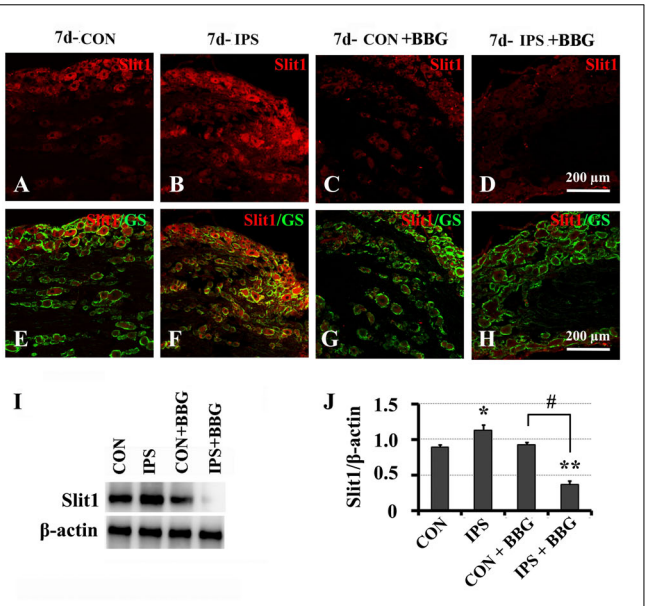

FIGURE 7 | Slit1 expression in SGCs decreased after inhibition of the P2X7 receptor with BBG. After right sciatic nerve crush, BBG (P2X7 receptor inhibitor) was injected intraperitoneally. The expression of Slit1 on the 7th day DRG was detected by double immunofluorescence staining and western blotting. **(A–D)** Slit1 immunofluorescence staining (red). **(E–H)** Merged images of Slit1 (red) and GS (green) immunofluorescence staining. Scale bar = 200 μm. **(I)** the level of Slit1 protein was detected by western blotting ($N = 3$), the level of β-actin was detected as loading control. **(J)** The level of Slit1 before and after BBG treatment on the 7th day post-SNC DRG was analyzed with the paired *t*-test. "*" compared with the control side, the level of Slit1 in IPS side was upregulated, $P < 0.001$; "#" compared with the control side and the ipsilateral side before BBG treatment respectively, the level of Slit1 in "IPS + BBG" was downregulated, $P < 0.001$; The change was not significant in "CON + BBG", $P > 0.05$. "**" compared with "CON + BBG" group, the level of Slit1 in "IPS + BBG" was much lower than that in "CON + BBG" group, $P < 0.001$. CON: contralateral DRG, IPS: ipsilateral DRG.

result suggests that direct contact between neuronal somas and SGCs could induce the upregulation of SGC Slit1 expression (**Figure 4**). SGCs express a series of receptors which can respond to the neurotransmitters released by neurons (Elson et al., 2004; Zhang et al., 2009). Therefore, in the process of cell culture, SGCs contact with neuronal soma, making SGCs more easily activated by signal molecules released by neuron, while SGCs that are not in contact with neuron bodies are less likely to be activated, possibly because the signal molecules are diluted by the culture medium. It was shown that signal transmission between the neuronal soma and SGCs depends on the physical distance, which indirectly indicates that it is very important to maintain the functional relationship between neurons and SGC anatomical units *in vivo*. These results suggest that the transmission of injury signals from the neuronal soma to SGCs is closely associated with the anatomic unit. The molecular mechanisms underlying the transmission of neuronal injury signals to SGCs, which subsequently show increased Slit1 expression, remain unknown.

Signal transmission between neurons and SGCs is bidirectional (Zhang et al., 2007; Kung et al., 2013; Christie et al., 2015). The interacting molecules between neurons and SGCs identified to date include ATP (Zhang et al., 2007), NO (Bradman et al., 2010), glutamic acid (Kung et al., 2013) and calcium ions (Suadicani et al., 2010; Castillo et al., 2011). Additionally, Christie et al. (2015) found that SGCs can sense the injury signal from the distal axons of adjacent neurons via cell enlargement and cell proliferation, and neurons can also transmit some small molecules to the surrounding SGCs. Under pathological and physiological conditions, activation of the receptors of glial cells can promote the interaction between neurons and glial cells (Karadottir et al., 2005; Salter and Fern, 2005; Micu et al., 2006; Castillo et al., 2011). Zhang et al. (2007) reported that ATP released from the neuronal soma activates P2X7 receptors in perineuronal SGCs and triggers communication between neuronal somas and glial cells. They further showed that activation of P2X7 receptors can lead to the release of tumor necrosis factor-α (TNF-α) from SGCs. TNF-α in turn potentiates P2X3 receptor-mediated responses

and increases the excitability of DRG neurons. Therefore, we hypothesized that the transmission of damage signals to SGCs may have been achieved through the ATP-P2X7R pathway. The VNUT, which is stored in neurons and releases ATP, was selected as the experimental indicator of changes in the P2X7R pathway. We found that a damage signal could increase the expression of VNUT in DRG neurons. The double immunofluorescence staining of VNUT and ATF3 showed that the expression of VNUT in injured neurons was stronger than that in uninjured neurons (**Figure 5**, $P < 0.01$). These results indirectly suggest that injured neurons release more ATP than uninjured neurons.

Brilliant blue G (BBG) has been reported to be a P2X7-selective antagonist (Jiang et al., 2000); BBG also shows a neuroprotective effect and no toxicity (Gourine et al., 2005). Furthermore, BBG can be used for intraperitoneal injection *in vivo*, which is simple and convenient (Ryu and McLarnon, 2008; Coddou et al., 2011). Based on these advantages, intraperitoneal injection of BBG, a specific inhibitor of P2X7R, was used as an intervention method. GS and P2X7R double immunofluorescence labeling showed that P2X7R was expressed in SGCs, but P2X7R was not expressed in SGCs after BBG injection (**Supplementary Figure S3**). Brilliant blue G produced a non-competitive inhibition of rat P2X7 receptors with IC50 values of 10 nM and it exerts a specific inhibitory effect on P2X7 receptor by allosteric modulation (Jiang et al., 2000). The specific antibody of P2X7 receptor could not recognize and bind to the allosteric P2X7 receptor, so the expression of P2X7 receptor could not be detected by immunofluorescence staining after BBG injection. This result illustrates that the peritoneal injection of BBG was effective, and after inhibition of P2X7R, the expression of Slit1 in SGCs was downregulated (**Figure 7**), and the expression of VNUT in DRG neurons was upregulated (**Figure 6**). This result may be explained by the increased feedback secretion of the ATP ligand after the receptor is inhibited. It is necessary to further validate this feedback regulation phenomenon using the P2X7 gene knockout method.

CONCLUSION

Our experiments have demonstrated that an injury signal from DRG neurons can activate P2X7R on the SGC membrane and upregulate the expression of Slit1 in SGCs. These results show that the ATP-P2X7 pathway is involved in signal transduction from peripheral nerve injury to SGCs, leading to upregulation of Slit1 expression. Combined with our previous research (Zhang et al., 2010; Chen et al., 2012b), these findings indicate that Slit1 expressed in perineuronal SGCs can bind to Robo2 receptors on neuronal membranes and mediate neuronal process outgrowth through the Robo2-srGAP3 pathway. Our study complements the molecular mechanism of bidirectional signal transmission between neurons and SGCs in the anatomical unit of DRG neurons and clarifies the role of SGCs in nerve injury and regeneration, as shown in the schematic diagram (**Figure 8**).

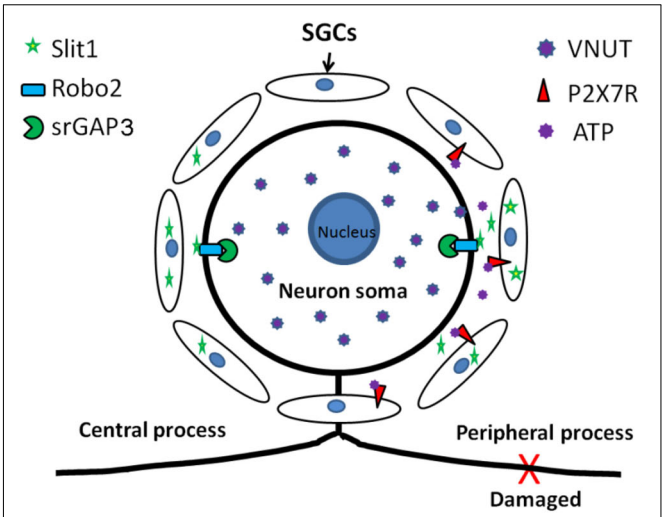

FIGURE 8 | Schematic diagram of the role of Slit1 in the communication between neurons and SGCs. After peripheral nerve injury, neurons activate perineuronal SGCs, leading to upregulation of Slit1 expression through the VNUT-ATP-P2X7R pathway, and SGCs then promote the regeneration of injured neurons through the Slit1-Robo2-srGAP3 pathway (Zhang et al., 2010; Chen et al., 2012b).

MATERIALS AND METHODS

Animals

Adult Sprague-Dawley (SD) rats of 250–300 g were purchased from the Experimental Animal Department of Hunan Agricultural University (Changsha, Hunan, China) and housed in a standard rat cage with unlimited access to water and food under 12 h of continuous light every 24 h. Animal scarification and tissue collection were approved by the animal ethics committee of Hainan Medical University (Haikou, China) and were performed according to the guidelines of the Chinese Care and Use legislation. All efforts were made to minimize animal suffering and the number of animals used.

Surgeries, FG Injection, Brilliant Blue G (BBG) Intraperitoneal Injection, Tissue Preparation and Sectioning

SD rats were used to generate the SNC model as previously described (Zou et al., 2016). The rats were anesthetized using 2% sodium pentobarbital (40 mg/kg, intraperitoneal). The crush lesion was induced by non-serrated forceps with a smoothed surface. The forceps were instrumented with strain gauges and calibrated by a force-sensing resistor (FSR400, Interlink Electronics, CA, United States) linked to an Avometer. The applied force was 1000 g; the duration of the crush was 1 min; and the left sciatic nerve was subjected to a sham control surgery without crush injury. The wounds were sutured after surgery with nylon 5-0 sutures.

Three SD rats were used for retrograde tracing of Fluor-Gold (FG; Fluorochrome; 80014; Sigma-Aldrich, St. Louis,

MO) as previously described (Li et al., 2016). The modified procedure was as follows: A glass micropipette (tip diameter 40–60 μm) connected to a microsyringe (1 μl, Hamilton, Reno, NV, United States) was inserted into the epineurium 2 mm from the distal point of the injured site of the sciatic nerve. A volume of 0.1 μl of 4% FG solution dissolved in normal saline was gradually pressure injected (continuously for over 1 min) into the target site. The needle tip was kept at the target site for another 10 min to avoid FG leakage. Three rats were kept alive for 7 days after FG injection.

The preparation and administration of BBG (P2X7R antagonist) followed the procedures used in a previous study (Ryu and McLarnon, 2008). To prepare a 10 mg/ml BBG solution, 0.3 g of BBG powder (Sigma-Aldrich, 27815-25-f) was dissolved in 30 ml of 0.9% saline. After SNC, the BBG solution (30 mg/kg) was used for intraperitoneal injection at a dose of 50 mg/kg, and the animals that survived for 7 days were subjected to daily injection of this dose for 7 days. Control animals were injected with an equivalent amount of saline.

Following the operation, 30 rats were divided into five groups (n = 6) and kept alive for 1, 3, 7, 14 or 28 days. These rats were used for Slit1 western blotting (n = 3) and immunohistochemistry (n = 3) experiments. Six rats were used for VNUT and Slit1 western blotting at 7 days post-SNC with BBG injection. The remaining rats that were not used for western blotting were anesthetized with an overdose of sodium pentobarbital solution (100 mg/kg, i.p.) and perfused through the ascending aorta with 100 ml of 0.9% (w/v) saline, followed by 500 ml of 4% (w/v) paraformaldehyde and 30% (v/v) saturated picric acid in 0.1 M phosphate buffer (PB, pH 7.4).

L5-L6 DRG from both sides were removed and incubated in 4% paraformaldehyde for 3 h. The tissues were then dehydrated with sucrose density gradient buffer. DRG were embedded with optimum cutting temperature medium (O.C.T. Compound 4583, Tissue-Tek, SAKURA, CA United States), subjected to cryosectioning and kept at 4°C. Sections of the DRG were cut at a 10 μm thickness on a freezing microtome (Shandon Cryotome E, Thermo Electron Corp., United States). The sections were mounted on gelatine-coated glass slides, air dried, and kept at 4°C in the freezer for later use.

DRG Cell Culture

Dorsal Root Ganglia cell culture was performed as described previously (Castillo et al., 2011). Following the administration of anesthesia through intraperitoneal injection with 2% pentobarbital solution (40 mg/kg), L5-L6 DRG were isolated from 3- to 4-week-old SD rats of both sexes. To minimize the interference caused by SCs, nerve roots at both ends of the ganglion were removed as much as possible. Additionally, to avoid interference from fibroblasts, the outer membrane of the ganglion should be removed completely. DRG neurons and glial cells were cultured in Dulbecco's modified Eagle's medium (Sigma, St. Louis, MO, United States) supplemented with 10% FBS (Sigma, St. Louis, MO, United States). After 4 h of culturing, cultured cells were fixed with 4% paraformaldehyde.

Western Blotting

Rat dorsal root ganglia (DRG) (L5-L6) were homogenized with homogenization buffer (20 mM Tris, pH 8, 137 mM NaCl, 1% NP-40, 1 mM sodium orthovanadate, and protease inhibitor cocktail). The supernatant was removed and subjected to protein quantification with a Pierce BCA reagent kit (Thermo Fisher Scientific, 23227). Then, 50 μg of the protein lysate was loaded onto a 10% SDS-PAGE gel for electrophoresis and subsequently transferred to a polyvinylidene-fluoride (PVDF) membrane. After 4 h of blocking with a 5% milk-PBS solution, the membrane was incubated with the primary antibody at 4°C overnight. Thereafter, the membrane was washed three times and incubated with an HRP-conjugated secondary antibody. Membranes developed by incubation with β-actin, GAPDH and rabbit HRP-conjugated secondary antibodies (**Table 1**) were used as controls. Protein was visualized using the Pierce ECL reagent kit (Thermo Fisher Scientific, 32132). Quantitative analysis of proteins was carried out on the protein bands with ImageJ (National Institutes of Health) and Microsoft Excel (Microsoft Corp.). The amount of the Slit1 protein was normalized to the amount of the β-actin protein. The amount of the VNUT protein was normalized to the amount of the GAPDH protein. All the western blot experiments were repeated three times.

Primary and secondary antibodies used for immunohistochemistry, immunocytochemistry and western blotting in this study (**Table 1**).

Immunohistochemistry

Dorsal Root Ganglia sections were incubated with 5% donkey serum for 1 h at room temperature before being incubated with the primary antibodies in the refrigerator overnight. Subsequently, in a dark chamber, the sections were incubated with the secondary antibodies for 2 h at room temperature. Sections incubated with 2% donkey serum without a primary antibody were used as a negative control.

Slit1, MAP2, GS, ATF3, VNUT and P2X7 was used for single labeling of DRG sections, and Slit1 was used for single labeling of sections of 7-day DRG subjected to retrograde tracing with FG. VNUT was used for single labeling in sections of DRG at 7 days post-SNC, and dual labeling of GS and Slit1 was performed in sections from the intact DRG and injured DRG. MAP2 and Slit1 dual labeling was performed in sections from intact DRG. Dual labeling with ATF3 (Santa Cruz, sc-188) and Slit1 or ATF3 (Abcam, ab58668) and VNUT was performed in sections of DRG at 7 days post-SNC. Dual labeling of GS and P2X7 or GS and Slit1 was performed sections of DRG at 7 days post-SNC with BBG injection.

Immunocytochemistry

Staining for immunocytochemistry was carried out as described previously (Castillo et al., 2011). In brief, slides with fixed cells were blocked with 5% donkey serum and permeabilized in 0.1% Triton-X-100 PBS buffer. Then, the slides were incubated with primary antibodies at 4°C overnight and subsequently incubated with secondary antibodies for 2 h at room temperature. DAPI (4', 6-diamidino-2-phenylindole, Boster, AR1176, China) was used to

TABLE 1 | Primary and secondary antibodies used in this study.

Category	Antibody	Manufacturer	Catalog number	Dilution
Primary antibody	Polyclonal mouse anti-Slit1	Abcam	Ab115892	1:200 IF 1:1000 WB
	Polyclonal rabbit anti-GS	Abcam	ab16802	1:400 IF
	Chicken polyclonal anti-MAP2	Abcam	ab5392	1:2000 IF
	Rabbit anti-ATF3	Santa Cruz	sc-188	1:800 IF
	Mouse monoclonal anti-ATF3	Abcam	Ab58668	1:100 IF
	Goat polyclonal anti-P2RX7	Abcam	Ab93354	1:100 IF
	Guinea pig polyclonal anti-VNUT	Millipore	ABN83	1:1000 IF 1:500 WB
	Rabbit polyclonal anti-ß-actin-loading control	Abcam	Ab1801	1:2000 WB
	Rabbit polyclonal anti-GAPDH-loading control	Abcam	Ab9485	1:2500 WB
Secondary antibody	Alexa Fluor 594-donkey anti-mouse IgG	Jackson	715-585-1	1:200 IF
	FITC-rabbit anti-chicken	Millipore	AP162F	1:100 IF
	Alexa Fluor 488-donkey anti-rabbit IgG	Jackson	711-546-1	1:200 IF
	Cy3-donkey polyclonal Anti Chicken IgY	Millipore	703-175-155	1:200 IF
	Alexa Fluor 488-donkey anti-goat IgG(H + L)	Jackson	705-545-147	1:200 IF
	Alexa Fluor 594-donkey anti-rabbit IgG(H + L)	Jackson	711-585-152	1:200 IF
	Alexa Fluor 488-donkey anti-guinea pig IgG(H + L)	Jackson	706-545-148	1:200 IF
	Goat anti-mouse IgG(H + L) (HRP)	Abcam	Ab205719	1:10000 WB
	HRP-conjugated AffiniPure goat anti-guinea pig IgG(H + L)	Proteintech	SA00001-12	1:5000 WB
	Goat anti-rabbit IgG(H + L) (HRP)	Abcam	Ab205718	1:10000 WB

stain nuclei. Slides incubated with 2% donkey serum without a primary antibody were used as a negative control.

GS and Slit1, MAP2 and Slit1 were dual labeled in the cultured DRG cells.

Semi-Quantitative Analysis of the Immunofluorescence Images

All the sections were first used for quantitative analysis and determination of the relative changes in the immunofluorescence intensity in each group. The same slide was used to avoid bias regarding slide-to-slide variations in labeling intensity. Similar trends in Slit1 expression were observed between the five experimental groups for all animals in each experimental group. The fluorescence images of DRG sections (Slit1 and GS double-labeled) subjected to BBG treatment were captured by laser scanning confocal microscopy (FV1000, Olympus, Japan), and fluorescence images of the other groups were captured with a fluorescence microscope (Olympus IX51 and Olympus BX51, Japan) by photographing each DRG slide under the same conditions with the same exposure. Semi-quantification of the fluorescence intensity was performed on images captured with 20× or 40× objective lenses using CellSens Dimension software (Olympus, Japan) integrated with the fluorescence microscope.

The method for the quantification of the fluorescence signal referred to a previous publication (Nadeau et al., 2014). For the profiling of Slit1 expression levels in SGCs, the processing and analysis of fluorescence signals from the cytoplasm of the SGCs were performed as follows: fifteen L5 DRG from different time points and three DRG (randomly chosen from the contralateral side of the experimental condition) were analyzed to determine the Slit1 relative fluorescence intensity (RFI) in SGCs. Using ImageJ (National Institutes of Health), fluorescence images with similar numbers of neurons obtained with a 20-fold objective lens were converted into 8-bit gray-scale images, and the background was subtracted (50 pixels selected). Neurons were individually selected with the "Free Selection Tool" in Photoshop software (Adobe Systems Inc.), and the images were deleted and saved, then inverted with ImageJ. The relative fluorescence intensity of the processed images was analyzed with ImageJ software. The obtained data are expressed as the mean and standard error of the mean (SEM). The data of each group were normalized to the data of the corresponding control group, and the obtained data were mapped by Excel software (Microsoft Corp.).

For the profiling of Slit1 protein expression levels in SGCs surrounding FG-positive and FG-negative neurons, a total of 1453 neurons from L5 to L7 days post-SNC DRG (n = 3) were used. The immunofluorescence signals in the cytoplasm of the SGCs surrounding the 688 FG-positive and 765 FG-negative neurons were traced separately, with the obtained values representing the average SGC labeling intensity around each respective neuron. The semi-quantified Slit1 protein levels in SGCs surrounding 723 AFT3-positive and 751 AFT3-negative neurons and the levels of VNUT protein on 955 AFT3-positive neurons and 896 AFT3-negative neurons were analyzed using the same method. The obtained data were expressed as the mean ± SEM.

For confocal fluorescence images of cultured cells, 100 40-fold objective fluorescence images were taken for analysis. SGCs contacted with neuronal soma were grouped into population 1

and non-contacted into population 2. A total of 347 SGCs of population 1 and 702 SGCs of population 2 were used to measure the average RFI of Slit1 in each satellite cell. The Slit1 RFI was expressed as the mean ± SEM. Slit1 RFI of population 1 SGCs was normalized by population 2 SGCs.

The processing of images and data analysis were performed with Photoshop CS5.1 (Adobe Systems Inc.), ImageJ (National Institutes of Health) and Microsoft Excel (Microsoft Corp.).

Neuron Counting

For Slit1, similar qualitative trends were observed between the five experimental groups for all animals in each experimental group ($n = 3$). Three slides from five different groups of animals were selected for the experimental analysis of Slit1 such that similar numbers of neurons were present in the DRG sections representing each of the five experimental groups ($n = 3$). The numbers of neurons were counted in the fluorescence images of DRG slices from different time points, and the image pixels of SGCs around the intact neuronal soma were defined as the background. Neurons with a fluorescence intensity three times stronger than the background were defined as strongly positive neurons, and their numbers were counted with CellSens Dimension software. The number of neurons is expressed as the mean ± SEM.

Statistical Analysis

Statistical analysis was performed with SPSS18.0 software (Statistical Product and Service Solutions 18.0, Al Monk, NY, United States). Paired *t* tests were used for comparisons between paired data. All the other data were analyzed using one-way repeated measures ANOVA. *P*-values of less than 0.05 were considered statistically significant.

DATA AVAILABILITY

The datasets generated for this study are available on request to the corresponding author.

ETHICS STATEMENT

The animal study was reviewed and approved by Animal scarification and tissue collection were approved by the animal ethics committee of Hainan Medical University (Haikou, China) and were performed according to the guidelines of the Chinese Care and Use legislation.

AUTHOR CONTRIBUTIONS

QP Z and XN Y designed the experiment, carried out data analysis, and wrote the manuscript. QP Z, JH Z, J Sh, XF Z, R R, ZJ M, YB H, Q K, YS W, X D, J Su, and ZZ L performed the experiment. XN Y provided the experimental reagents and access to the data analysis software.

FUNDING

This work was supported by the National Natural Science Foundation of China (grant numbers 81660217 to QP Z; 8116015 and 81100246 to XN Y). This work was also supported by the Hainan Key Research and Development Program of China (grant number ZDYF2016110 to ZJ M).

ACKNOWLEDGMENTS

We would like to thank Prof. YunQing Li and Dr. Le Xiao for his meticulous guidance concerning this research and manuscript writing.

SUPPLEMENTARY MATERIAL

The Supplementary Material for this article can be found online at: https://www.frontiersin.org/articles/10.3389/fncel.2019.00420/full#supplementary-material

REFERENCES

Arkhipova, S. S., Raginov, I. S., Mukhitov, A. R., and Chelyshev, Y. A. (2010). Satellite cells of sensory neurons after various types of sciatic nerve trauma in the rat. *Neurosci. Behav. Physiol.* 40, 609–614. doi: 10.1007/s11055-010-9303-7

Arthur-Farraj, J.-P., Latouche, M., Wilton, D. K., Quintes, S., Chabrol, E., Banerjee, A., et al. (2012). c-Jun reprograms Schwann cells of injured nerves to generate a repair cell essential for regeneration. *Neuron* 75, 633–647. doi: 10.1016/j.neuron.2012.06.021

Beirowski, B., Babetto, E., Golden, J. P., Chen, Y. J., Yang, K., Gross, R. W., et al. (2014). Metabolic regulator LKB1 is crucial for Schwann cell-mediated axon maintenance. *Nat. Neurosci.* 17, 1351–1361. doi: 10.1038/nn.3809

Blockus, H., and Chedotal, A. (2016). Slit-Robo signaling. *Development* 143, 3037–3044. doi: 10.1242/dev.132829

Bradman, M. J., Arora, D. K., Morris, R., and Thippeswamy, T. (2010). How do the satellite glia cells of the dorsal root ganglia respond to stressed neurons?–nitric oxide saga from embryonic development to axonal injury in adulthood. *Neuron Glia Biol.* 6, 11–17. doi: 10.1017/S1740925X09990494

Burnstock, G. (2006). Pathophysiology and therapeutic potential of purinergic signaling. *Pharmacol. Rev.* 58, 58–86. doi: 10.1124/pr.58.1.5

Carr, L., Parkinson, D. B., and Dun, X. P. (2017). Expression patterns of Slit and Robo family members in adult mouse spinal cord and peripheral nervous system. *PLoS One* 12:e0172736. doi: 10.1371/journal.pone.0172736

Carriel, V., Garzon, I., Campos, A., Cornelissen, M., and Alaminos, M. (2017). Differential expression of GAP-43 and neurofilament during peripheral nerve regeneration through bio-artificial conduits. *J. Tissue Eng. Regen. Med.* 11, 553–563. doi: 10.1002/term.1949

Castillo, C., Norcini, M., Baquero-Buitrago, J., Levacic, D., Medina, R., Montoya-Gacharna, J. V., et al. (2011). The N-methyl-D-aspartate-evoked cytoplasmic calcium increase in adult rat dorsal root ganglion neuronal somata was potentiated by substance P pretreatment in a protein kinase C-dependent manner. *Neuroscience* 177, 308–320. doi: 10.1016/j.neuroscience.2010.12.040

Catacuzzeno, L., Sforna, L., D'Adamo, M. C., Pessia, M., and Franciolini, F. (2014). A method to identify tissue cell subpopulations with distinct multi-molecular profiles from data on co-localization of two markers at a time: the case of sensory ganglia. *J. Neurosci. Methods* 224, 88–95. doi: 10.1016/j.jneumeth.2013.12.015

Cattin, A. L., and Lloyd, A. C. (2016). The multicellular complexity of peripheral nerve regeneration. *Curr. Opin. Neurobiol.* 39, 38–46. doi: 10.1016/j.conb.2016.04.005

Chaudhari, N. (2014). Synaptic communication and signal processing among sensory cells in taste buds. *J. Physiol.* 592, 3387–3392. doi: 10.1113/jphysiol.2013.269837

Chen, Y., Li, G., and Huang, L. Y. (2012a). P2X7 receptors in satellite glial cells mediate high functional expression of P2X3 receptors in immature dorsal root ganglion neurons. *Mol. Pain* 8:9. doi: 10.1186/1744-8069-8-9

Chen, Z. B., Zhang, H. Y., Zhao, J. H., Zhao, W., Zhao, D., Zheng, L. F., et al. (2012b). Slit-Robo GTPase-activating proteins are differentially expressed in murine dorsal root ganglia: modulation by peripheral nerve injury. *Anat. Rec.* 295, 652–660. doi: 10.1002/ar.22419

Christie, K., Koshy, D., Cheng, C., Guo, G., Martinez, J. A., Duraikannu, A., et al. (2015). Intraganglionic interactions between satellite cells and adult sensory neurons. *Mol. Cell. Neurosci.* 67, 1–12. doi: 10.1016/j.mcn.2015.05.001

Coddou, C., Yan, Z., Obsil, T., Huidobro-Toro, J. P., and Stojilkovic, S. S. (2011). Activation and regulation of purinergic P2X receptor channels. *Pharmacol. Rev.* 63, 641–683. doi: 10.1124/pr.110.003129

Court, F. A., Hendriks, W. T., MacGillavry, H. D., Alvarez, J., and van Minnen, J. (2008). Schwann cell to axon transfer of ribosomes: toward a novel understanding of the role of glia in the nervous system. *J. Neurosci.* 28, 11024–11029. doi: 10.1523/JNEUROSCI.2429-08.2008

Donegan, M., Kernisant, M., Cua, C., Jasmin, L., and Ohara, P. T. (2013). Satellite glial cell proliferation in the trigeminal ganglia after chronic constriction injury of the infraorbital nerve. *Glia* 61, 2000–2008. doi: 10.1002/glia.22571

Duraikannu, A., Krishnan, A., Chandrasekhar, A., and Zochodne, D. W. (2019). Beyond trophic factors: exploiting the intrinsic regenerative properties of adult neurons. *Front. Cell. Neurosci.* 13:128. doi: 10.3389/fncel.2019.00128

Elson, K., Simmons, A., and Speck, P. (2004). Satellite cell proliferation in murine sensory ganglia in response to scarification of the skin. *Glia* 45, 105–109. doi: 10.1002/glia.10294

Faroni, A., Mobasseri, S. A., Kingham, P. J., and Reid, A. J. (2015). Peripheral nerve regeneration: experimental strategies and future perspectives. *Adv. Drug Deliv. Rev.* 82-83, 160–167. doi: 10.1016/j.addr.2014.11.010

Fitzgerald, M., and McKelvey, R. (2016). Nerve injury and neuropathic pain - a question of age. *Exp. Neurol.* 275(Pt 2), 296–302. doi: 10.1016/j.expneurol.2015.07.013

Fontana, X., Hristova, M., Da Costa, C., Patodia, S., Thei, L., Spencer-Dene, B., et al. (2012). c-Jun in Schwann cells promotes axonal regeneration and motoneuron survival via paracrine signaling. *J. Cell Biol.* 198, 127–141. doi: 10.1083/jcb.201205025

Giaid, A., Gibson, S. J., Ibrahim, B. N., Legon, S., Bloom, S. R., Yanagisawa, M., et al. (1989). Endothelin 1, an endothelium-derived peptide, is expressed in neurons of the human spinal cord and dorsal root ganglia. *Proc. Natl. Acad. Sci. U.S.A.* 86, 7634–7638. doi: 10.1073/pnas.86.19.7634

Gomez-Sanchez, A.-J., Carty, L., Iruarrizaga-Lejarreta, M., Palomo-Irigoyen, M., Varela-Rey, M., Griffith, M., et al. (2015). Schwann cell autophagy, myelinophagy, initiates myelin clearance from injured nerves. *J. Cell Biol.* 210, 153–168. doi: 10.1083/jcb.201503019

Gordon, T., and Borschel, G. H. (2017). The use of the rat as a model for studying peripheral nerve regeneration and sprouting after complete and partial nerve injuries. *Exp. Neurol.* 287, 331–347. doi: 10.1016/j.expneurol.2016.01.014

Goto, T., Iwai, H., Kuramoto, E., and Yamanaka, A. (2017). Neuropeptides and ATP signaling in the trigeminal ganglion. *Jpn. Dent. Sci. Rev.* 53, 117–124. doi: 10.1016/j.jdsr.2017.01.003

Gourine, A. V., Poputnikov, D. M., Zhernosek, N., Melenchuk, E. V., Gerstberger, R., Spyer, K. M., et al. (2005). P2 receptor blockade attenuates fever and cytokine responses induced by lipopolysaccharide in rats. *Br. J. Pharmacol.* 146, 139–145. doi: 10.1038/sj.bjp.0706287

Hanani, H. T. M., Cherkas, P. S., Ledda, M., and Pannese, E. (2002). Glial cell plasticity in sensory ganglia induced by nerve damage. *Neuroscience* 114, 279–283. doi: 10.1016/s0306-4522(02)00279-8

Hanani, M. (2005). Satellite glial cells in sensory ganglia: from form to function. *Brain Res. Brain Res. Rev.* 48, 457–476. doi: 10.1016/j.brainresrev.2004.09.001

Hanani, M. (2010). Satellite glial cells: more than just 'rings around the neuron'. *Neuron Glia Biol.* 6, 1–2. doi: 10.1017/s1740925x10000104

Hanani, M. (2012). Intercellular communication in sensory ganglia by purinergic receptors and gap junctions: implications for chronic pain. *Brain Res.* 1487, 183–191. doi: 10.1016/j.brainres.2012.03.070

Hanani, M. (2015). Role of satellite glial cells in gastrointestinal pain. *Front. Cell. Neurosci.* 9:412. doi: 10.3389/fncel.2015.00412

Hanani, M., Blum, E., Liu, S., Peng, L., and Liang, S. (2014). Satellite glial cells in dorsal root ganglia are activated in streptozotocin-treated rodents. *J. Cell Mol. Med.* 18, 2367–2371. doi: 10.1111/jcmm.12406

Harada, Y., Kato, Y., Miyaji, T., Omote, H., Moriyama, Y., and Hiasa, M. (2018). Vesicular nucleotide transporter mediates ATP release and migration in neutrophils. *J. Biol. Chem.* 293, 3770–3779. doi: 10.1074/jbc.M117.810168

Isaacman-Beck, J., Schneider, V., Franzini-Armstrong, C., and Granato, M. (2015). The lh3 glycosyltransferase directs target-selective peripheral nerve regeneration. *Neuron* 88, 691–703. doi: 10.1016/j.neuron.2015.10.004

Jessen, K. R., Mirsky, R., and Lloyd, A. C. (2015). Schwann cells: development and role in nerve repair. *Cold Spring Harb. Perspect. Biol.* 7:a020487. doi: 10.1101/cshperspect.a020487

Jiang, L. H., Mackenzie, A. B., North, R. A., and Surprenant, A. (2000). Brilliant Blue G selectively blocks ATP-Gated rat P2X7 receptors. *Mol. Pharmacol.* 58, 82–88. doi: 10.1124/mol.58.1.82

Kang, H., Tian, L., Mikesh, M., Lichtman, J. W., and Thompson, W. J. (2014). Terminal Schwann cells participate in neuromuscular synapse remodeling during reinnervation following nerve injury. *J. Neurosci.* 34, 6323–6333. doi: 10.1523/JNEUROSCI.4673-13.2014

Karadottir, R., Cavelier, P., Bergersen, L. H., and Attwell, D. (2005). NMDA receptors are expressed in oligodendrocytes and activated in ischaemia. *Nature* 438, 1162–1166. doi: 10.1038/nature04302

Kim, S. H., Nam, J. S., Choi, D. K., Koh, W. W., Suh, J. H., Song, J. G., et al. (2011). Tumor necrosis factor-alpha and apoptosis following spinal nerve ligation injury in rats. *Korean J. Pain* 24, 185–190. doi: 10.3344/kjp.2011.24.4.185

Kovacic, U., Zele, T., Osredkar, J., Sketelj, J., and Bajrovic, F. F. (2004). Sex-related differences in the regeneration of sensory axons and recovery of nociception after peripheral nerve crush in the rat. *Exp. Neurol.* 189, 94–104. doi: 10.1016/j.expneurol.2004.05.015

Kung, L. H., Gong, K., Adedoyin, M., Ng, J., Bhargava, A., Ohara, P. T., et al. (2013). Evidence for glutamate as a neuroglial transmitter within sensory ganglia. *PLoS One* 8:e68312. doi: 10.1371/journal.pone.0068312

Kushnir, R., Cherkas, P. S., and Hanani, M. (2011). Peripheral inflammation upregulates P2X receptor expression in satellite glial cells of mouse trigeminal ganglia: a calcium imaging study. *Neuropharmacology* 61, 739–746. doi: 10.1016/j.neuropharm.2011.05.019

Li, Q., Chen, J., Chen, Y., Cong, X., and Chen, Z. (2016). Chronic sciatic nerve compression induces fibrosis in dorsal root ganglia. *Mol. Med. Rep.* 13, 2393–2400. doi: 10.3892/mmr.2016.4810

Ma, L., and Tessier-Lavigne, M. (2007). Dual branch-promoting and branch-repelling actions of Slit/Robo signaling on peripheral and central branches of developing sensory axons. *J. Neurosci.* 27, 6843–6851. doi: 10.1523/jneurosci.1479-07.2007

Mahar, M., and Cavalli, V. (2018). Intrinsic mechanisms of neuronal axon regeneration. *Nat. Rev. Neurosci.* 19, 323–337. doi: 10.1038/s41583-018-0001-8

Menéndez-Méndez, A., Diaz-Hernandez, J. I, and Miras-Portugal, M. T. (2015). The vesicular nucleotide transporter (VNUT) is involved in the extracellular ATP effect on neuronal differentiation. *Purinergic Signal.* 11, 239–249. doi: 10.1007/s11302-015-9449-4

Micu, I., Jiang, Q., Coderre, E., Ridsdale, A., Zhang, L., Woulfe, J., et al. (2006). NMDA receptors mediate calcium accumulation in myelin during chemical ischaemia. *Nature* 439, 988–992. doi: 10.1038/nature04474

Milner, L. A., and Burnstock, G. P. (2000). Endothelin immunoreactivity and mRNA expression in sensory and sympathetic neurones following selective denervation. *Int. J. Dev. Neurosci.* 18, 727–734. doi: 10.1016/s0736-5748(00)00054-x

Nadeau, J. R., Wilson-Gerwing, T. D., and Verge, V. M. (2014). Induction of a reactive state in perineuronal satellite glial cells akin to that produced by nerve injury is linked to the level of p75NTR expression in adult sensory neurons. *Glia* 62, 763–777. doi: 10.1002/glia.22640

Nave, K. A., and Trapp, B. D. (2008). Axon-glial signaling and the glial support of axon function. *Annu. Rev. Neurosci.* 31, 535–561. doi: 10.1146/annurev.neuro.30.051606.094309

Painter, M. W., Brosius Lutz, A., Cheng, Y. C., Latremoliere, A., Duong, K., Miller, C. M., et al. (2014). Diminished Schwann cell repair responses underlie age-associated impaired axonal regeneration. *Neuron* 83, 331–343. doi: 10.1016/j.neuron.2014.06.016

Parrinello, S., Napoli, I., Ribeiro, S., Wingfield Digby, P., Fedorova, M., Parkinson, D. B., et al. (2010). EphB signaling directs peripheral nerve regeneration through Sox2-dependent Schwann cell sorting. *Cell* 143, 145–155. doi: 10.1016/j.cell.2010.08.039

Pellegrino, C., Gubkina, O., Schaefer, M., Becq, H., Ludwig, A., Mukhtarov, M., et al. (2011). Knocking down of the KCC2 in rat hippocampal neurons increases intracellular chloride concentration and compromises neuronal survival. *J. Physiol.* 589, 2475–2496. doi: 10.1113/jphysiol.2010.203703

Pérez de Lara, M. J., Guzmán-Aránguez, A., de la Villa, P., Díaz-Hernández, J. I., Miras-Portugal, M. T., and Pintor, J. (2015). Increased levels of extracellular ATP in glaucomatous retinas: possible role of the vesicular nucleotide transporter during the development of the pathology. *Mol. Vis.* 21, 1060–1070.

Remy, M., Thaler, S., Schumann, R. G., May, C. A., Fiedorowicz, M., Schuettauf, F., et al. (2008). An in vivo evaluation of Brilliant Blue G in animals and humans. *Br. J. Ophthalmol.* 92, 1142–1147. doi: 10.1136/bjo.2008.138164

Rosenberg, A. F., Isaacman-Beck, J., Franzini-Armstrong, C., and Granato, M. (2014). Schwann cells and deleted in colorectal carcinoma direct regenerating motor axons towards their original path. *J. Neurosci.* 34, 14668–14681. doi: 10.1523/JNEUROSCI.2007-14.2014

Ryu, J. K., and McLarnon, J. G. (2008). Block of purinergic P2X(7) receptor is neuroprotective in an animal model of Alzheimer's disease. *Neuroreport* 19, 1715–1719. doi: 10.1097/WNR.0b013e3283179333

Salter, M. G., and Fern, R. (2005). NMDA receptors are expressed in developing oligodendrocyte processes and mediate injury. *Nature* 438, 1167–1171. doi: 10.1038/nature04301

Sanna, M. D., Ghelardini, C., and Galeotti, N. (2017). HuD-mediated distinct BDNF regulatory pathways promote regeneration after nerve injury. *Brain Res.* 1659, 55–63. doi: 10.1016/j.brainres.2017.01.019

Sawada, K., Echigo, N., Juge, N., Miyaji, T., Otsuka, M., Omote, H., et al. (2008). Identification of a vesicular nucleotide transporter. *Proc. Natl. Acad. Sci. U.S.A.* 105, 5683–5686.

Scheib, J., and Hoke, A. (2013). Advances in peripheral nerve regeneration. *Nat. Rev. Neurol.* 9, 668–676. doi: 10.1038/nrneurol.2013.227

Sebert, M. E., and Shooter, E. M. (1993). Expression of mRNA for neurotrophic factors and their receptors in the rat dorsal root ganglion and sciatic nerve following nerve injury. *J. Neurosci. Res.* 36, 357–367. doi: 10.1002/jnr.490360402

Seijffers, R., Allchorne, A. J., and Woolf, C. J. (2006). The transcription factor ATF-3 promotes neurite outgrowth. *Mol. Cell. Neurosci.* 32, 143–154. doi: 10.1016/j.mcn.2006.03.005

Sforna, L., Franciolini, F., and Catacuzzeno, L. (2019). Ca(2+) -dependent and Ca(2+) -independent somatic release from trigeminal neurons. *J. Cell. Physiol.* 234, 10977–10989. doi: 10.1002/jcp.27901

Sluyter, R. (2017). The P2X7 receptor. *Adv. Exp. Med. Biol.* 1051, 17–53.

Song, J., Ying, Y., Wang, W., Liu, X., Xu, X., Wei, X., et al. (2018). The role of P2X7R/ERK signaling in dorsal root ganglia satellite glial cells in the development of chronic postsurgical pain induced by skin/muscle incision and retraction (SMIR). *Brain Behav. Immun.* 69, 180–189. doi: 10.1016/j.bbi.2017.11.011

Stoll, M. H. G. (1999). Nerve injury, axonal degeneration, and neural regeneration: basic insights. *Brain Pathol.* 9, 313–325. doi: 10.1111/j.1750-3639.1999.tb00229.x

Suadicani, S. O., Cherkas, P. S., Zuckerman, J., Smith, D. N., Spray, D. C., and Hanani, M. (2010). Bidirectional calcium signaling between satellite glial cells and neurons in cultured mouse trigeminal ganglia. *Neuron Glia Biol.* 6, 43–51. doi: 10.1017/S1740925X09990408

Tajdaran, K., Chan, K., Gordon, T., and Borschel, G. H. (2018). Matrices, scaffolds, and carriers for protein and molecule delivery in peripheral nerve regeneration. *Exp. Neurol.* 319:112817. doi: 10.1016/j.expneurol.2018.08.014

Vogelaar, C. F., Vrinten, D. H., Hoekman, M. F., Brakkee, J. H., Burbach, J. P., and Hamers, F. P. (2004). Sciatic nerve regeneration in mice and rats: recovery of sensory innervation is followed by a slowly retreating neuropathic pain-like syndrome. *Brain Res.* 1027, 67–72. doi: 10.1016/j.brainres.2004.08.036

Wang, F., Xiang, H., Fischer, G., Liu, Z., Dupont, M. J., Hogan, Q. H., et al. (2016). HMG-CoA synthase isoenzymes 1 and 2 localize to satellite glial cells in dorsal root ganglia and are differentially regulated by peripheral nerve injury. *Brain Res.* 1652, 62–70. doi: 10.1016/j.brainres.2016.09.032

Wood, M. D., Kemp, S. W., Weber, C., Borschel, G. H., and Gordon, T. (2011). Outcome measures of peripheral nerve regeneration. *Ann. Anat.* 193, 321–333. doi: 10.1016/j.aanat.2011.04.008

Wu, J. R., Chen, H., Yao, Y. Y., Zhang, M. M., Jiang, K., Zhou, B., et al. (2017). Local injection to sciatic nerve of dexmedetomidine reduces pain behaviors, SGCs activation, NGF expression and sympathetic sprouting in CCI rats. *Brain Res. Bull.* 132, 118–128. doi: 10.1016/j.brainresbull.2017.04.016

Yegutkin, G. G. (2008). Nucleotide- and nucleoside-converting ectoenzymes: important modulators of purinergic signalling cascade. *Biochim. Biophys. Acta* 1783, 673–694. doi: 10.1016/j.bbamcr.2008.01.024

Yi, X. N., Zheng, L. F., Zhang, J. W., Zhang, L. Z., Xu, Y. Z., Luo, G., et al. (2006). Dynamic changes in Robo2 and Slit1 expression in adult rat dorsal root ganglion and sciatic nerve after peripheral and central axonal injury. *Neurosci. Res.* 56, 314–321. doi: 10.1016/j.neures.2006.07.014

Yuri, H., Kato, O., and Miyaji, T. (2013). Inhibitors of ATP release inhibit vesicular nucleotide transporter. *Biol. Pharm. Bull.* 36, 1688–1691. doi: 10.1248/bpb.b13-00544

Zhang, H., Mei, X., Zhang, P., Ma, C., White, F. A., Donnelly, D. F., et al. (2009). Altered functional properties of satellite glial cells in compressed spinal ganglia. *Glia* 57, 1588–1599. doi: 10.1002/glia.20872

Zhang, H. Y., Zheng, L. F., Yi, X. N., Chen, Z. B., He, Z. P., Zhao, D., et al. (2010). Slit1 promotes regenerative neurite outgrowth of adult dorsal root ganglion neurons in vitro via binding to the Robo receptor. *J. Chem. Neuroanat.* 39, 256–261. doi: 10.1016/j.jchemneu.2010.02.001

Zhang, X., Chen, Y., Wang, C., and Huang, L. Y. (2007). Neuronal somatic ATP release triggers neuron-satellite glial cell communication in dorsal root ganglia. *Proc. Natl. Acad. Sci. U.S.A.* 104, 9864–9869. doi: 10.1073/pnas.0611048104

Zhang, X. F., Han, P., Faltynek, C. R., Jarvis, M. F., and Shieh, C. C. (2005). Functional expression of P2X7 receptors in non-neuronal cells of rat dorsal root ganglia. *Brain Res.* 1052, 63–70. doi: 10.1016/j.brainres.2005.06.022

Zou, Y., Xu, F., Tang, Z., Zhong, T., Cao, J., Guo, Q., et al. (2016). Distinct calcitonin gene-related peptide expression pattern in primary afferents contribute to different neuropathic symptoms following chronic constriction or crush injuries to the rat sciatic nerve. *Mol. Pain* 12:1744806916681566. doi: 10.1177/1744806916681566

Conflict of Interest Statement: The authors declare that the research was conducted in the absence of any commercial or financial relationships that could be construed as a potential conflict of interest.

frontiers in Cellular Neuroscience

REVIEW
published: 06 November 2019
doi: 10.3389/fncel.2019.00491

Beneficial and Detrimental Remodeling of Glial Connexin and Pannexin Functions in Rodent Models of Nervous System Diseases

*Lucila Brocardo, Luis Ernesto Acosta, Ana Paula Piantanida† and Lorena Rela**

Grupo de Neurociencia de Sistemas, Facultad de Medicina, Instituto de Fisiología y Biofísica Bernardo Houssay (IFIBIO Houssay), Consejo Nacional de Investigaciones Científicas y Técnicas (CONICET), Universidad de Buenos Aires, Buenos Aires, Argentina

OPEN ACCESS

Edited by:
Giovanni Cirillo, Università degli Studi della Campania Luigi Vanvitelli, Italy

Reviewed by:
Parisa Gazerani, Aalborg University, Denmark
Kenji Fabricio Shoji, IRSET, France

***Correspondence:**
Lorena Rela
lorena.rela@fmed.uba.ar

†Present address:
Ana Paula Piantanida
Instituto de Virología, CICVyA, Instituto Nacional de Tecnología Agropecuaria (INTA), Buenos Aires, Argentina

Received: *31 July 2019*
Accepted: *17 October 2019*
Published: *06 November 2019*

Citation:
Brocardo L, Acosta LE, Piantanida AP and Rela L (2019) Beneficial and Detrimental Remodeling of Glial Connexin and Pannexin Functions in Rodent Models of Nervous System Diseases. Front. Cell. Neurosci. 13:491. doi: 10.3389/fncel.2019.00491

A variety of glial cell functions are supported by connexin and pannexin proteins. These functions include the modulation of synaptic gain, the control of excitability through regulation of the ion and neurotransmitter composition of the extracellular milieu and the promotion of neuronal survival. Connexins and pannexins support these functions through diverse molecular mechanisms, including channel and non-channel functions. The former comprise the formation of gap junction-mediated networks supported by connexin intercellular channels and the formation of pore-like membrane structures or hemichannels formed by both connexins and pannexins. Non-channel functions involve adhesion properties and the participation in signaling intracellular cascades. Pathological conditions of the nervous system such as ischemia, neurodegeneration, pathogen infection, trauma and tumors are characterized by distinctive remodeling of connexin expression and function. However, whether these changes can be interpreted as part of the pathogenesis, or as beneficial compensatory effects, remains under debate. Here we review the available evidence addressing this matter with a special emphasis in mouse models with selective manipulation of glial connexin and pannexin proteins *in vivo*. We postulate that the beneficial vs. detrimental effects of glial connexin remodeling in pathological conditions depend on the impact of remodeling on the different connexin and pannexin channel and non-channel functions, on the characteristics of the inflammatory environment and on the type of interaction among glial cells types.

Keywords: connexins, pannexins, gap junctions, hemichannels, astrocytes, microglia, plasticity

INTRODUCTION

Connexins are transmembrane proteins with a variety of physiological roles including channel and non-channel functions. Channel functions involve the formation of gap junctions, which are intercellular connections, permeable to ions and small metabolites, formed by the apposition of connexin hexamers (connexons) provided by each of the participating cells.

Gap junction-mediated glial networks are ubiquitous in the central nervous system and involve astrocytes and oligodendrocytes. The type of connexins involved in the interaction depends on the cell types participating in the connection (Rouach et al., 2002; Giaume and Theis, 2010; Takeuchi and Suzumura, 2014; Abudara et al., 2018). Connexins can also function as membrane hemichannels with the potential to release mediators such as ATP and glutamate from astrocytes and microglia (Orellana et al., 2013; Gajardo-Gómez et al., 2016; Nielsen et al., 2017). Non-channel functions of connexins involve adhesion properties and intracellular cascade signaling (Zhou and Jiang, 2014; Leithe et al., 2018).

The ubiquitous nature and diversity of connexin functional properties make them versatile mediators of glial cell physiology and a putative locus for maladaptive plasticity in pathological conditions. Plastic changes in abundance and/or functions of glial connexins have been reported in a variety of pathology models (Belousov et al., 2017; De Bock et al., 2017; Xing et al., 2019). However, whether connexin plasticity is causal to the pathology, or is an epiphenomenon of pathological conditions, is becoming to be elucidated only recently, owing to the availability of tools for selective manipulation of glial connexins *in vivo* (Giaume and Theis, 2010). Here we review the available work using rodent models with glia-selective connexin manipulations to evaluate causal relations between glial connexin plasticity and neuropathology, focusing on traumatic and neurodegenerative diseases, ischemia and brain tumors. Most of the cases reviewed here will focus on connexin 43 (Cx43), which is by far the most studied glial connexin and dominates the available literature. We will also review the scarce literature available on glia-selective pannexin manipulations in these models, and discuss the glia-selective data in the context of additionally more abundant data using global connexin and pannexin manipulations.

Modulation of connexin expression and function that may emerge in the context of hypoxia, inflammation and injury, both *in vitro* and *in vivo*, have been thoroughly reviewed and putative mechanisms underlying the observed changes have been proposed (Rouach et al., 2002; Contreras et al., 2004; Farahani et al., 2005; Kielian, 2008; Orellana et al., 2009; Eugenin et al., 2012; Koulakoff et al., 2012; Quintanilla et al., 2012; Bosch and Kielian, 2014; Freitas-Andrade and Naus, 2016). A few important points emerging from the body of available literature are worth mentioning before we focus on glia-selective *in vivo* manipulations, which is the focus of this review. The first point is that a change in connexin immunolabeling needs to be interpreted with caution. Connexin channels in the context of gap junction plaques or in a disassembled state can have dramatically different immunoreactive properties, thus connexins may appear absent owing to epitope masking (Theriault et al., 1997). This highlights the importance of using independent approaches to measure connexin abundance and function. A second point is that changes in the expression of glial connexins in pathological conditions are connexin-, time-, region- and model-specific. As an example, Borna virus infection of neonatal rats results in neurodegeneration and widespread reactivity of hippocampal astrocytes when analyzed 2 months after infection (Köster-Patzlaff et al., 2007). This astrocytic activation is accompanied by an increase of Cx43 in all layers of the dentate gyrus of the hippocampus and a decrease of the same connexin in the CA3 pyramidal layer. Another typically astrocytic connexin, connexin 30 (Cx30), increased in all the hippocampal regions mentioned above (Köster-Patzlaff et al., 2007). In contrast, in a mouse model proposed to mimic features of aging and Alzheimer's disease induced by ovariectomy and chronic D-galactose administration, a reduction of Cx43 in the dentate gyrus and CA1 regions of the hippocampus was observed, while no change was observed in the CA3 hippocampal region (Liu et al., 2010). This was suggested to reflect differential resistance to neuronal damage of CA3 compared to CA1, as was observed in a model of ischemia in rats (Rami et al., 2001). Thus, generalizations about connexin plasticity across brain regions and pathologies should be cautious. A third issue is that changes in the abundance of glial connexin proteins in pathological conditions is challenging to interpret without parallel assessments of functional studies of connexin functions, such as the extent of gap junction coupling, the permeability of connexin hemichannels available at the membrane surface (Sáez et al., 2013) and the phosphorylation state of specific connexin sites that can mediate intracellular signaling. These functions may be oppositely modulated and/or have opposing effects on the severity of the pathology (Retamal et al., 2007; Karpuk et al., 2011). Therefore, when manipulations target more than one connexin function—e.g., both gap junctions and hemichannels—this has to be clearly stated and the effects of the manipulation should be interpreted with care. Finally, an important idea, emerging mostly from *in vitro* studies is that different connexins are expressed in different cell types of the nervous system—i.e., neurons, astrocytes, oligodendrocytes and microglia—and may interact in complex ways when modulated in pathologic conditions. Even more, glial pannexin proteins, which form membrane channels showing structure and function similarity to connexin hemichannels, can also be modulated in inflammatory conditions and have been proposed to play a role in pathologic conditions (Freitas-Andrade and Naus, 2016; Lapato and Tiwari-Woodruff, 2018). The contribution of Cx43 and pannexin-1 (Px1) to hemichannel activity in astrocytes has been a matter of debate as different studies assigned a preponderant role to one or the other, depending on the conditions analyzed (Iglesias et al., 2009; Orellana et al., 2011). Hence, cell type-selective manipulations of connexins and pannexins are essential to achieve a comprehensive idea of their roles in pathology. With these general ideas in mind, we will review the available literature that aims at using *in vivo* selective manipulations of glial connexin and pannexin functions to address their roles in a subset of pathologic conditions.

For this purpose, we used keyword search in PubMed and Scopus citation databases using combinations of keywords (**Table 1**). We then reviewed the methods section of all articles yielded by each search and selected those articles that used *in vivo* rodent models. A final selection of work using global and cell-specific connexin and pannexin manipulations were selected for detailed analysis.

TABLE 1 | Number of original research articles found for the keyword combinations used for the literature search in PubMed and Scopus citation databases.

	Connexin	Pannexin
Astrocyte	875	83
Microglia	150	39
Oligodendrocyte	212	5
Ependymal	28	1
Endothelial + Brain	93	6
Tumor + Brain	212	19

NEURODEGENERATIVE DISEASES

We mentioned that connexins are expressed in different glial types and may interact in complex ways. To illustrate these complex interactions, we can mention a study by Orellana et al. (2011) that addressed the involvement of glial connexins and pannexins in neuronal death associated with exposure to a toxic fragment of the amyloid precursor protein, whose accumulation is associated with Alzheimer's disease. Orellana et al. (2011) observed that in cultured cortical astrocytes and microglia, toxic amyloid fragments increased hemichannel activity. While astrocyte hemichannel activity was explained mainly by Cx43 availability, microglial hemichannel activity involved both Cx43 and Px1 (Orellana et al., 2011). This amyloid-induced glial hemichannel activity was associated with the release of metabolites that are toxic for neurons, likely ATP and glutamate. While microglia-mediated neurotoxicity could be prevented by combined application of Px1 and Cx43 blockers, astrocyte-mediated neurotoxicity was abolished by Cx43 block alone (Orellana et al., 2011). In this same study, hippocampal slices in organotypic culture exposed to the toxic amyloid fragment showed increased hemichannel activity. This effect was revealed by dye uptake first in microglia, then in astrocytes and finally in neurons. While Cx43 blockers and microglia inactivation with minocycline completely prevented amyloid-induced neuronal death, in hippocampal slices obtained from mice with astrocyte-selective deficiency of Cx43 there was only a partial protection (Orellana et al., 2011). These data suggest that astrocytic recruitment is downstream microglial activation, however, pure astrocyte cultures can produce neurotoxic conditioned medium in the presence of toxic amyloid fragments. The relative contributions of microglia and astrocyte connexins to amyloid-induced neurotoxicity will need microglia-selective manipulations (Parkhurst et al., 2013; Yona et al., 2013; Zhao et al., 2019) of connexin and/or pannexin proteins for further clarification.

It is important to note that amyloid neurotoxicity modeled in cell and organotypic slice culture systems involve a rather homogeneous exposure to the toxic fragment. This homogeneous exposure does not reproduce the neurotoxicity gradients generated in the pathology characterized by amyloid deposition in the form of amyloid plaques. The relevance of these gradients for glial plasticity in Alzheimer's disease was nicely illustrated in a mouse model of familial Alzheimer's disease ($APP_{swe}/PS1_{dE9}$ mice, or APP/PS1 mice) characterized by aging-dependent plaque formation. Hemichannel activity assessed using dye uptake in acute brain slices was enhanced in hippocampal astrocytes of APP/PS1 mice when compared to control mice. Interestingly, hemichannel hyperactivity in APP/PS1 astrocytes involved Cx43 and Px1 when astrocytes were located near amyloid plaques, while the increased hemichannel activity observed in astrocytes far from plaques involved only Cx43 (Yi et al., 2016). Microglial inhibition by minocycline partially reduced hemichannel hyperactivity in astrocytes near plaques, while astrocytes far from plaques remained unaffected. When the effects of the APP/PS1 mutations on hemichannel activity were analyzed in the context of a selective deficiency of Cx43 in astrocytes, almost no hemichannel activity was observed in astrocytes far from plaques, but a Px1 component of hemichannel activity remained in astrocytes near plaques. Thus, Px1 appears to contribute to astrocyte hemichannel activity in some *in vivo* conditions (Yi et al., 2016). Together with the prevention of hemichannel activity in astrocytes, the astrocyte-selective Cx43 deficiency in APP/PS1 mice was associated with less mitochondrial oxidative stress assessed by MitoSOX superoxide indicator and less dystrophic dendrites, assessed by reticulon 3 (RTN3) immunoreactivity (Yi et al., 2016), indicating that astrocyte Cx43 worsened the neurotoxicity of the environment. Of interest, no differences were observed in indicators of astrocytic gap junction coupling between APP/PS1 and control mice, assessed by fluorescence recovery after photobleaching (FRAP; Yi et al., 2016), strengthening the idea that the neurotoxic effect of astrocytes was exerted *via* Cx43 hemichannels. Further, APP/PS1 mice with astrocyte Cx43 deficiency had dramatically reduced astrogliosis and improved cognitive performance compared with APP/PS1 mice. Even more, re-expression of Cx43 in Cx43-deficient APP/PS1 mice using an astrocyte-directed adeno-associated viral vector reinstated the cognitive impairment (Ren et al., 2018). These results indicate that in the sequence of events of microglial and astrocytic activation that were proposed to lead to neuronal damage in Alzheimer's disease based on *in vitro* studies, the increase of Cx43 hemichannel activity in astrocytes is a deleterious process and this is confirmed in an *in vivo* model that selectively manipulates connexins in astrocytes.

Evidence for the idea that connexins participate in the complex interaction between astrocytes and microglia during neuroinflammation was provided as well by studies done in experimental autoimmune encephalomyelitis, a mouse model of multiple sclerosis. In this model, the pathologic condition is produced by subcutaneous immunization with myelin oligodendrocyte glycoprotein MOG_{35-55} peptide and intraperitoneal administration of Pertussis toxin on the day of immunization and 2 days after (Chen and Brosnan, 2006). This model is characterized by progressive paralysis followed by partial remission after an acute peak of clinical signs, associated with inflammatory infiltrate, demyelination and axonal damage (Chen and Brosnan, 2006). Mice with a selective astrocytic Cx43 deficiency or with this deficiency in a global Cx30 knockout background to prevent compensatory effects were not statistically different from wild type mice in terms of a clinical score that

evaluates the severity and time course of the motor signs of experimental autoimmune encephalomyelitis up to 3–4 weeks after immunization (Lutz et al., 2012). These mice were not different either in terms of the degree of immune cell reactivity in the spinal cord, evaluated using ionized calcium binding adaptor molecule 1 (Iba1) immunostaining at the endpoint of clinical evaluation. Interestingly, the global Cx30 deficiency reduced the severity of the chronic phase (8 weeks after the insult) in this model and this effect was correlated with the emergence of an anti-inflammatory phenotype in both spinal cord astrocytes and microglia (Fang et al., 2018). Given that a reduction in the abundance of Cx43 during the chronic phase of experimental autoimmune encephalomyelitis was observed in global Cx30 deficient mice, the neuroprotective effect could be mediated indirectly *via* astrocytic Cx43. This possibility will need to be specifically tested ideally using conditional astrocytic-selective and inducible Cx43 deficiency alone or in combination with Cx30 deficiency. Furthermore, global Px1 deficiency delayed the onset of symptoms in this model of experimental autoimmune encephalomyelitis, improving the clinical state of mice in the acute phase. However, Px1-deficient mice reached a clinical score that was comparable to the one observed in wild type mice during the chronic phase (Lutz et al., 2013). When ATP release was evaluated in the bathing medium of spinal cord slices, the authors observed that the enhancement of ATP release that the insult produced was significantly smaller in slices obtained from Px1-deficient mice when compared to wild type slices (Lutz et al., 2013). The former results are compatible with a sequential involvement of Px1 and Cx30 -and possibly Cx43- in the progression of experimental autoimmune encephalomyelitis. Further experiments using glial cell type-selective pannexin and connexin manipulations will help to determine whether an early microglia dependent process involving Px1 elicits a late astrocyte-dependent process involving connexins as part of the pathogenesis of experimental autoimmune encephalomyelitis.

The importance of connexin and pannexin functions to explain pathological conditions characterized by neuronal dysfunction and degeneration is highlighted by data coming from studies of human diseases linked to connexin and pannexin mutations. X-linked Charcot-Marie-Tooth disease type 1 (OMIM #302800) is characterized by progressive muscle weakness and atrophy associated with mutations in the *GJB1* gene, coding for connexin Cx32 (Cx32). These mutations are linked to peripheral demyelination and axonal degeneration that can be accompanied by central manifestations (Wang and Yin, 2016). Deletions of the *GJB1* coding sequence in humans produce a predominantly peripheral phenotype that is compatible with the alterations observed in Cx32 null mice (Hahn et al., 2000; Nakagawa et al., 2001). The central manifestations can be transient, do not appear to correlate with the severity of peripheral neuropathy and may be triggered by a variety of stress stimuli (Wang and Yin, 2016). Besides peripheral signs of neuropathy, Cx32 knockout mice show increased signs of widespread central nervous system inflammation when compared to wild type mice, both in basal conditions and after a systemic challenge with lipopolysaccharide (Olympiou et al., 2016). Interestingly, Cx32 knockout mice bearing a human Cx32 mutation associated with central manifestations of X-linked Charcot-Marie-Tooth disease (Cx32KOT55I) display an enhanced widespread central nervous system inflammatory response not associated with oligodendrocyte loss after lipopolysaccharide challenge, when compared with Cx32 knockout mice that do not carry this mutation (Olympiou et al., 2016). These data suggest that Cx32 mutations contribute to the disease not only through loss-of-function mechanisms that promote central neuroinflammation in addition to peripheral neuropathy, but also through gain-of-function mechanisms that increase the susceptibility to inflammatory challenges. The signals underlying the enhanced neuroinflammation remain to be elucidated.

Another demyelinating disease associated with mutations in the *GJC2* gene coding for connexin 47 (Cx47) is Pelizaeus-Merzbacher-like disease type 1 (OMIM #608804), characterized by progressive spasticity and ataxia. When compared with wild type mice, both knockout mice for Cx47 and mice carrying a mutation associated with the disease in humans (Cx47KOM282T) show delayed myelination and mild motor impairment during the juvenile stage, together with cerebellar astro- and microgliosis, that is no longer observable in the adult stage owing to compensation by Cx32 (Tress et al., 2011). As is the case for Cx32-deficient and mutant mice, Cx47-deficient and mutant mice show evidence of gap junction disassembly, not only in relation to oligodendrocyte-oligodendrocyte connections but also for oligodendrocyte-astrocyte connections (Tress et al., 2011; Olympiou et al., 2016). Whether augmented signs of neuroinflammation in these connexin-deficient mice is associated with oligodendrocytic, astrocytic or neuronal dysfunction, or with a combination of signals from these cell types, remains to be established.

ISCHEMIA

The question whether astrocytic connexins are beneficial or detrimental in pathological conditions fueled a rich debate and is well illustrated for the case of ischemia (Giaume et al., 2007). Correlational evidence and nonselective manipulations aiming at inhibition of Cx43 function in astrocytes led to the idea that Cx43 contributed to the amplification of ischemic damage, as the treatment with octanol, a nonselective connexin and gap junction blocker, reduced the infarct size in rat models of cerebral ischemia by carotid or middle cerebral artery occlusion (Rawanduzy et al., 1997; Rami et al., 2001).

Contrasting with the former data, in a mouse model of ischemia produced by middle cerebral artery occlusion during 45 min with evaluation 24 h later, the infarct size was larger in mice with a selective Cx43 astrocytic deficiency when compared to wild type mice (Lin et al., 2008). In addition, an experience of hypoxic preconditioning of 5 h at 8% oxygen 3 days prior to artery occlusion produced an approximate 50% reduction in infarct size in wild type mice, and was absent in mice with astrocytic Cx43 deficiency (Lin et al., 2008). The protective effect of hypoxic preconditioning needed the

availability of adenosine A1 receptors and it was proposed to be produced by ATP release by Cx43 hemichannels and subsequent metabolization to adenosine extracellularly (Lin et al., 2008). Given that astrocytic Cx43 deficiency is partly compensated by an increase in Cx30 expression, the mice used in these experiments were also global Cx30 knockouts (Wallraff et al., 2006). Cx43 was proposed as pivotal for neuroprotection in this cerebral ischemia model and was reinforced by consistent results obtained in mice with conditional deletion of Cx43 in astrocytes and no deletion of Cx30 (Nakase et al., 2003). In these mice, more cell death and enhanced number of inflammatory cells were observed in the area of penumbra without significant changes in the volume affected by astrogliosis, when compared with control mice (Nakase et al., 2004). The protective effect of Cx43 against ischemic damage was further reinforced by another study using a mouse line bearing a Cx43 mutation that affects Cx43-mediated gap junction and hemichannel activity ($Gja1^{Jrt}$; Kozoriz et al., 2013). Thus, in contrast to what was observed for the inflammatory environment of Alzheimer's disease models, Cx43 was regarded as neuroprotective under hypoxic conditions. One important difference called into attention to explain the difference between these two conditions is the chronicity of the insult in Alzheimer's disease models compared to the acute insult in the models of ischemia.

Genetic models that allow researchers to restrict the connexin deficiency to specific glial types were a big step forward to address glial connexin functions in nervous system pathology; however, there are a series of confounding effects that the strategy does not address. First, most of the data come from constitutive lines that tie the connexin deletion of interest to the timing of expression of a particular promoter, such as the promoter for glial fibrillary acidic protein (GFAP), which is also expressed by neural progenitor cells (Giaume and Theis, 2010). This caveat can be minimized with new tools that spare neural progenitor cells (Tsai et al., 2012; García-Cáceres et al., 2016; Srinivasan et al., 2016; Koh et al., 2017) or inducible tools that allow the researchers to evaluate phenomena in time windows shorter than the time needed for generation of new neurons (Burns et al., 2007; Rivers et al., 2008). Second, the deletion of connexin coding sequences eliminates all connexin functions, thus, it cannot address hemichannel, gap junction and non-channel connexin functions separately. This is particularly relevant in light of data showing that the permeability of gap junction channels and hemichannels can be oppositely modulated in an *in vitro* model of injury in which hemichannels were activated and gap junction coupling was reduced (Retamal et al., 2007). A promising tool to dissociate Cx43 hemichannel and gap junction channel functions is the connexin mimetic peptide Gap19, which blocks Cx43 hemichannels within the hour after exposure without affecting Cx43-mediated gap junction coupling. At larger exposure times, it slightly enhances gap junction coupling, so it nicely dissociates the two functions (Wang et al., 2013). A recent study assessed the effects of this peptide in male mice subjected to a cerebral ischemia-reperfusion protocol (45 min of middle cerebral artery occlusion and assessment 24 h after initiation of reperfusion). Intracerebroventricular administration of Gap19 30 min before ischemia had a protective effect, significantly reducing infarct volume (Chen et al., 2019). This result indicates that Cx43 hemichannel function is deleterious in ischemia and suggests that the increase in infarct volume observed in mice with astrocytic Cx43 deficiency (Nakase et al., 2004) obeys to a neuroprotective role of Cx43-mediated gap junction channels that overrides the neurotoxic action of hemichannels. However, as Gap19 also downregulated Cx43 expression by about 30% and astrocytic gap junction connectivity was not assessed (Chen et al., 2019), a contribution of astrocytic gap junctions to explain the neuroprotective effect of Gap19 cannot be ruled out. Potential effects of Gap19 in microglia or other targets could also explain the results, as the manipulation was not cell-type selective. Further support for the idea that an increment of astrocytic Cx43 hemichannel activity in response to ischemic insults is detrimental comes from a study using mice with global site-directed mutagenesis to eliminate functional phosphorylation sites that are a substrate for mitogen-activated protein kinase in the C-terminus of Cx43 (Freitas-Andrade et al., 2019). These mice (MK4 mice) show reduced infarct size after permanent middle cerebral artery occlusion when compared with wild type mice and two other mouse lines targeting phosphorylation sites for protein kinase C and caseine kinase 1, these two displaying no protection. Cultured astrocytes from MK4 mice showed reduced hemichannel activity assessed using dye uptake and electrophysiological measurements. In addition, MK4 astrocyte gap junction coupling assessed through a scrape-loading assay in cortical brain slices was indistinguishably increased in MK4 and wild type mice after the ischemic insult (Freitas-Andrade et al., 2019). Given that this was a global manipulation, it remains to be confirmed that the protective effect is astrocytic Cx43-dependent.

Non-channel functions of Cx43 involve adhesion properties and the participation in intracellular signaling *via* the C-terminal domain. Cx43 is codified by the *Gja1* gene, which can produce alternative carboxyl-terminal fragments *via* translation at alternative initiation sites (Ul-Hussain et al., 2014). Among these fragments, the GJA1-20k variant is selectively upregulated in a rat model of brain hypoxia-ischemia and may explain at least part of the neuroprotective effects produced by Cx43 in hypoxic conditions. Mice with a C-terminal-truncation in the Cx43 coding region show more vulnerability to brain ischemia, however, as astrocytic gap junction and hemichannel functions are partially disrupted as well in these mice, a neuroprotective role of the carboxyl-terminal fragment of Cx43, independent of its impact in channel functions, cannot be confirmed (Kozoriz et al., 2010).

Multiple connexins and glial types likely contribute to the outcome after ischemic damage. This idea is reinforced by the observation that male null mice for Cx32 are more vulnerable to global cerebral ischemia produced by transient (10 min) bilateral common carotid artery occlusion (Oguro et al., 2001). This enhanced vulnerability was observed 7 days after the insult as increased neuronal loss in the CA1 hippocampal region of null mice when compared with wild type mice (Oguro et al., 2001). Given that Cx32 is expressed by oligodendrocytes and by parvalbumin-positive inhibitory interneurons in the

hippocampus, the locus of origin of the Cx32-dependent neuroprotective effect could not be elucidated in this model, highlighting the need of glia type-selective manipulations of connexin proteins to address their functions (Doerflinger et al., 2003; Piantanida et al., 2019).

The contribution of pannexin proteins to the outcome after ischemic brain damage has been addressed using global knockout mice for Px1 and pannexin-2 (Px2), two pannexin proteins expressed in the nervous system. Contrasting with the deleterious effects of global Cx32 deficiency and astrocytic Cx43 deficiency, global combined deficiency of Px1 and Px2 results in protection against ischemic damage when evaluated 48 h after permanent middle cerebral artery occlusion (Bargiotas et al., 2011, 2012). Interestingly, astrocytes in primary culture with combined Px1 and Px2 deficiency show normal ATP release and membrane conductance, indicating that pannexins do not contribute significantly to astrocytic channel function in these *in vitro* conditions. In contrast, Px1- and Px2-deficient cortical neurons in primary culture show defective dye release (Bargiotas et al., 2011). These results suggest that pannexins contribute to ischemic damage expansion through a neuron-dependent mechanism. This is supported by a study showing comparable degrees of protection against ischemia-reperfusion damage in retinas of global and neuron-selective Px1 deficiency (Dvoriantchikova et al., 2012). Interestingly, microglial cells of Px1 deficient mice retain their ability to display rapid morphologic plasticity in response to extracellular ATP and other stimuli associated with injury (Dissing-Olesen et al., 2014). However, a possible contribution of microglia or endothelial cells (Gaynullina et al., 2014; Sharma et al., 2018) to explain the neuroprotective effect of global Px1 and Px2 deletion cannot be ruled out and needs to be specifically tested.

The availability of new mouse lines to achieve conditional deletion of Px1 using Cre-lox technology (Dvoriantchikova et al., 2012) and conditional expression of tamoxifen-inducible Cre recombinase in microglia and leptomeninges, sparing blood monocytes (Kaiser and Feng, 2019) is much promising. Given that Px2 can compensate for Px1 deficiency, and vice versa (Bargiotas et al., 2011) an *in vivo* approach to address the impact of microglia-selective Px1 deficiency on ischemic damage and other pathologic conditions will likely need to combine the conditional microglia-selective Px1 deletion with a global (or conditional, when available) Px2 deletion. This is an analogous strategy to the one used to address the roles of astrocytic Cx43 without compensation by Cx30 (Wallraff et al., 2006). One additional factor that has to be taken into consideration is the observation of sexual dimorphism in the neuroprotective effect of global Px1 deficiency. When evaluated 48 h after middle cerebral artery occlusion without sex discrimination, global Px1 deficiency did not show protection against ischemic damage (Bargiotas et al., 2011). Of note, another study using a middle cerebral artery occlusion lesion model in an independently generated Px1-knockout line observed that females with Px1 deficiency showed approximately 50% smaller size infarcts 4 days after the lesion when compared with wild type females (Freitas-Andrade et al., 2017). In contrast, males with Px1 deficiency displayed lesion sizes that were indistinguishable from lesions in wild type male mice. The differential susceptibility to ischemic damage between males and females correlated with differential astrocytic reactivity and degree of neuroinflamation, assessed through GFAP and Iba1 immunostaining, respectively, which were less dramatic in Px1-deficient female mice when compared to wild type female mice and males of either genotype (Freitas-Andrade et al., 2017). These data highlight the need to analyze the possibility for sexually dimorphic responses to nervous system insults before concluding a lack of effect of manipulations.

Overall, the current available data strongly suggest that therapeutic interventions to prevent ischemic damage will benefit from strengthening the efforts to develop tools to counteract connexin and pannexin hemichannel activity while preserving connexin gap junction function.

SPINAL CORD INJURY

Female mice with selective astrocytic Cx43 deficiency in a Cx30-knockout background were also assessed to evaluate their response to spinal cord contusion injury, and compared to controls that had only the global Cx30 deficiency (Huang et al., 2012). This study reported that the response to weight-drop spinal cord injury involved less ATP release in the peritraumatic area 1 h after injury in mice with astrocytic Cx43 deficiency. These mice also showed reduced astrocytic and microglial reactivity 1 week after injury and smaller lesion sizes than control mice when evaluated 8 weeks after injury, accompanied by an improved functional recovery that was observed as early as 3 days after damage (Huang et al., 2012). Thus, in this injury model, Cx43 availability was deleterious. In another model of spinal cord contusion injury in rats, peptide5, a Cx43 mimetic peptide that blocks Cx43 hemichannels and gap junctions (O'Carroll et al., 2008), administered at the lesion site 1 h after the lesion, diminished astrocytic activation and inflammatory cell numbers at the lesion site, promoted neuronal survival, and improved locomotor recovery when compared with the administration of a control peptide (O'Carroll et al., 2013). These data are consistent with the more selective astrocyte-directed manipulation of Cx43 mentioned above and support the idea that Cx43 is deleterious for the outcome of traumatic spinal cord injury. Interestingly, comparable results were obtained when peptide5 was administered systemically to rats with spinal cord contusion (Mao et al., 2017b). Consistent results were obtained in yet another study using female mice treated systemically with INI-0602, a derivative of the broadly used non-selective connexin and pannexin blocker carbenoxolone (Bruzzone et al., 2005; Dahl et al., 2013), that prevents the release of glutamate from mouse cultured microglia in response to lipopolysaccharide administration (Takeuchi et al., 2011). Administration of INI-0602, starting at the time of injury and during a month, improved the outcome of transection spinal cord injury, reducing astrogliosis and inflammation, and improving motor recovery (Umebayashi et al., 2014). These results emphasize the idea that even when cell-type

selective manipulations are essential to address the mechanisms behind the resolution of injuries, non-selective manipulations have potential as useful treatments, provided that there are no significant undesired off-targets for the therapeutic agent (Mao et al., 2017a).

In contrast to what was reported in spinal cord injury models, mice with astrocytic Cx43 deletion in a wild type Cx30 background increased the extent of astrogliosis and inflammatory cells around the lesioned area in a brain stab wound injury model (Theodoric et al., 2012). A number of factors may explain these differences, such as the type of injury, the lesion site, the time of observation after injury and the cellular microenvironment around the wound.

NEUROPATHIC PAIN

The development of neuropathic pain after peripheral or central damage involves plastic changes in spinal nociceptive circuits that involve glial plasticity as well. Selective manipulation of astrocytes and microglia have recently revealed that connexin and pannexin proteins in these glial types are critical for the development of neuropathic pain. In a mouse model of mild spinal cord injury, selective astrocytic Cx43 deficiency in a Cx30 knockout background reduced the development of mechanical allodynia and heat hyperalgesia, when compared with Cx30 knockout and wild type mice (Chen et al., 2012). On the other hand, Px1 deficiency in myeloid cells including microglia attenuated the development of mechanical allodynia in a model of induced osteoarthritis by intra-articular administration of monosodium iodoacetate. Interestingly, the hyperactivity of spinal dorsal horn neurons associated with the development of mechanical allodynia was also attenuated by myeloid cell-selective deletion of Px1 (Mousseau et al., 2018). It is important to note that this study used an inducible knock-in/knock-out Cre-lox system that allowed the researchers to evaluate the acute effects of eliminating Px1 expression in the myeloid lineage. Another study used a model in which mechanical allodynia also develops after spared nerve injury of the sciatic nerve. This study did not observe a reduction of pain thresholds in mice with Px1 deficiency in the myeloid lineage using a non-inducible transgenic Cre-lox system under comparable regulatory sequences (the Cx3cr1 promoter; Weaver et al., 2017). In contrast, this same study did observe a prevention of nerve injury-induced mechanical allodynia in global Px1-deficient mice. These results suggest that the non-inducible deletion of Px1 from myeloid cells can be developmentally compensated, while the global Px1 deletion cannot. Strikingly, Weaver et al. could reinstate the capability for nerve injury-induced mechanical allodynia in global Px1-deficient mice after wild type bone marrow transplantation, indicating that bone marrow-derived immune cells confer at least part of the Px1 dependence of nerve injury-induced mechanical allodynia. Combined manipulations of astrocytic connexins and microglial pannexins in specific time windows will help elucidate whether and how these cell types and molecules interact for the development of neuropathic pain. The availability of tools to genetically manipulate astrocytes and microglia with different inductor drugs (Tanaka et al., 2012; Srinivasan et al., 2016) is a promising new avenue with potential to assess interactions between these cell types. The generation of new tools designed to achieve targeted deletions of a broader diversity of connexins and pannexins than what is available (Liao et al., 2001; Cohen-Salmon et al., 2002; Poon et al., 2014; Clasadonte et al., 2017) will overcome one of the current limitations.

TUMORS

Besides their participation in the resolution of nervous system damage, astrocytes are determinants of the microenvironment in which brain tumors develop. In addition, tumor cells express connexins and there is evidence using dye transfer *in vitro* and *in vivo* that they can establish connexin-mediated gap junctions with non-tumor cells (Zhang et al., 1999, 2003). However, a direct electrophysiological measurement of gap junction coupling between astrocytes and tumor cells is still lacking. Data supporting the relevance of connexin proteins as potential targets for antitumor therapy have been reviewed recently (Aasen et al., 2017; Umans and Sontheimer, 2018; Uzu et al., 2018). Whether connexin gap junction, hemichannel and/or non-channel functions are important for tumor progression has not been resolved. However, there is compelling evidence that some tumor cells downregulate connexin proteins and that restoring connexin expression reduces malignancy. As an example, C6 rat glioma cells express low levels of Cx43 and Cx30. When implanted intracranially, they produce well-defined large tumors in the brain parenchyma, resulting in a survival rate of 43% of transplanted individuals after 30 days of implantation. However, rats implanted with Cx30 cDNA-transfected C6 glioma cells exhibited 66% of survival rate, and smaller tumor masses were detected by MRI analysis (Arun et al., 2017). Interestingly, Px1-transfected C6 glioma cells in culture showed reduced proliferation and motility and displayed dye coupling, which was virtually absent in untransfected C6 cells (Lai et al., 2007). When inoculated to nude mice, Px1-transfected C6 glioma cells produced significantly smaller tumors than cells transfected with a control construct. Similar results were observed for Px2-transfected C6 glioma cells (Lai et al., 2009).

Contrasting with the former results, in a brain metastasis model using nude mice inoculated with mammary adenocarcinoma cells of human origin *via* the left cardiac ventricle, shRNA-mediated depletion of Cx43 from cancerous cells reduced metastatic growth in the brain parenchyma when assessed 2 weeks after inoculation (Chen et al., 2016, 2017). Wild-type Cx43 re-expression in Cx43-depleted cancerous cells rescued metastatic activity, whereas re-expression of a mutated variant of Cx43 that does not form functional channels [Cx43(T154A)] did not (Beahm et al., 2006). Interestingly, Cx43 promoted proliferation of metastatic cells in the brain, but not extravasation across the blood-brain barrier, as Cx43 depletion in cancer cells did not significantly diminish the number of cancer cells in the

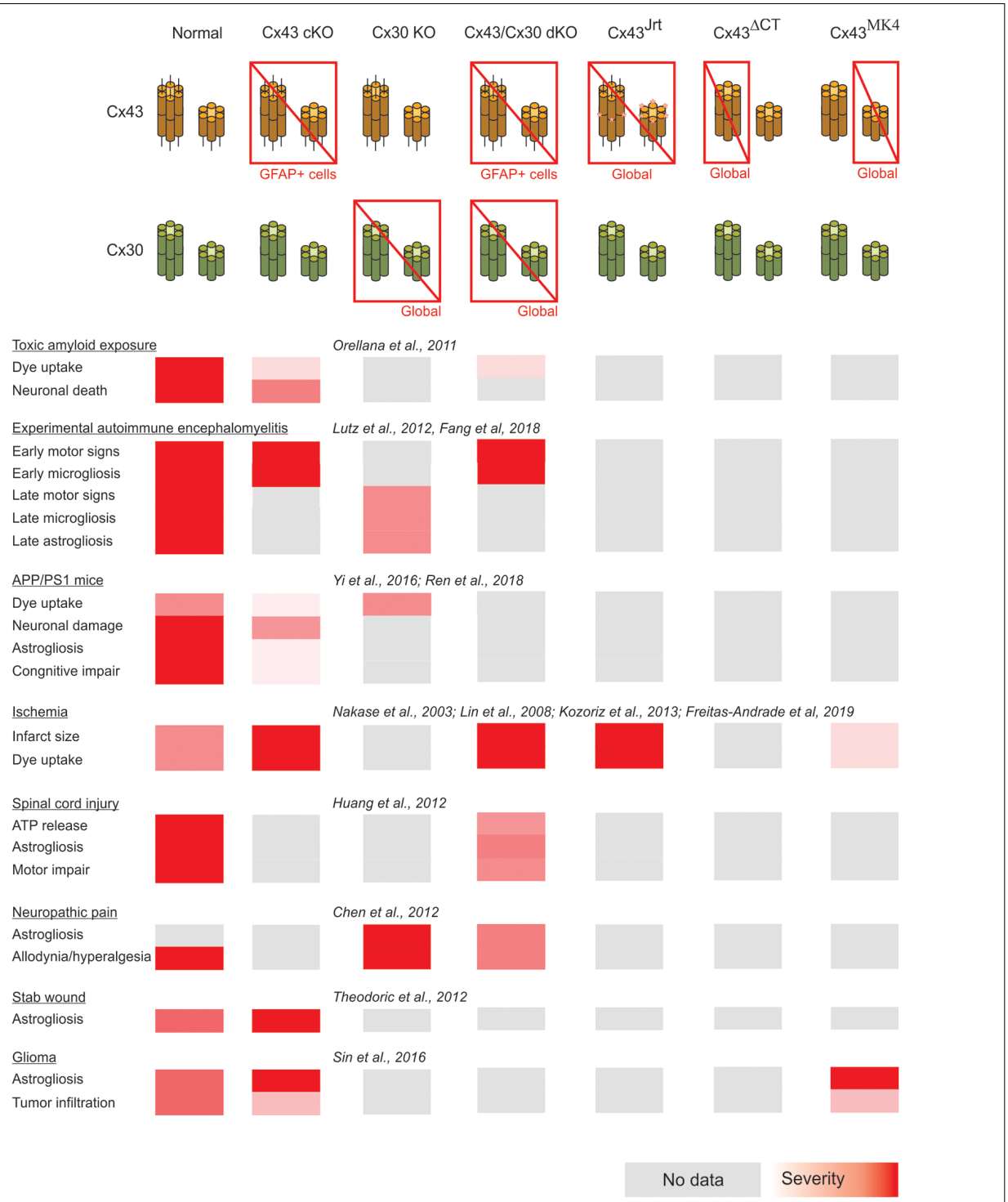

FIGURE 1 | Summary of the impact of global and astrocyte-selective connexin function disruption in the context of *in vivo* models of central nervous system disease.

brain parenchyma, but micrometastases showed decreased proliferative activity when assessed 1 week after cancer cell inoculation. Based on a large body of accompanying *in vitro* data, the authors proposed a model in which gap junctions between tumor cells and astrocytes are required for cancer cell growth and survival (Chen et al., 2016). However, a potential hemichannel function of Cx43 in this process cannot be discarded.

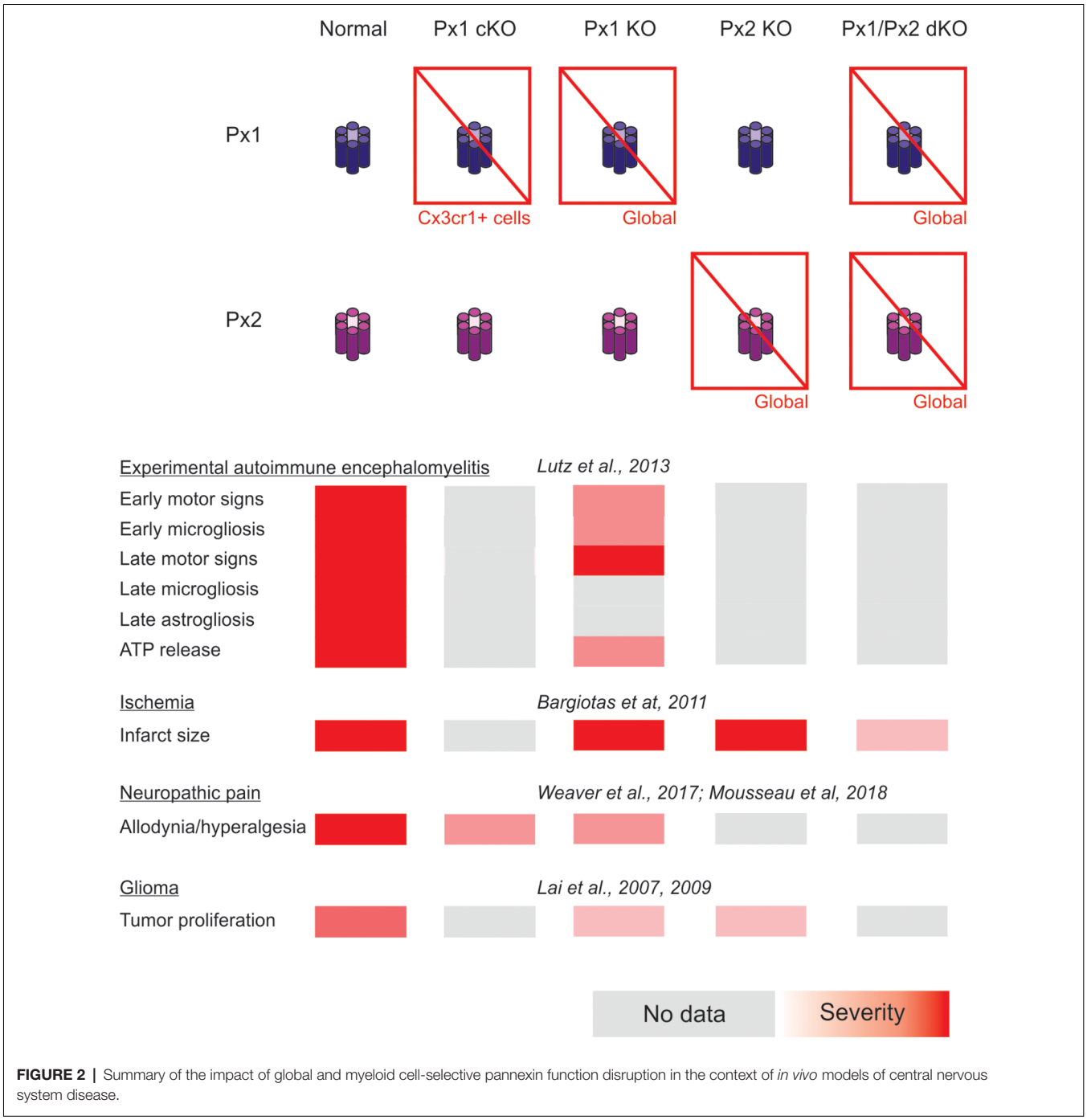

FIGURE 2 | Summary of the impact of global and myeloid cell-selective pannexin function disruption in the context of *in vivo* models of central nervous system disease.

Further research with *in vivo* models and tumor cell manipulations targeting specific connexin functions will shed light on the roles of connexins expressed by cancer cells for their capacity to invade the brain parenchyma, their proliferation and survival, which may differ depending on cancer cell type. To conclude, we will focus on the analysis of plasticity of astrocyte connexin functions in the proximity of tumor cells and their possible detrimental or beneficial effects for tumor progression.

In mice with Cx43-deficient astrocytes, brain implantation of mouse GL261 glioma cells resulted in a larger extent of astrogliosis near the tumor implant, together with reduced invasion of tumor cells into the brain parenchyma. This result was replicated when Cx43-knockdown glioma cells were implanted in wild type mice (Sin et al., 2016). To determine which Cx43 function was taking part in this process, glioma cells were transfected with cDNA coding for the channel-defective Cx43 mutant variant, Cx43(T154A),

TABLE 2 | Genetic tools of potential application to achieve inducible connexin and pannexin manipulations of glial cells *in vivo*.

Cre-expressing lines				
Cell-type selectivity (in nervous system)	**Construct**	**Induction method**	**RRID**	**Reference**
Astrocytes	Aldh1l1-Cre/ERT2 BAC transgene	Tamoxifen	IMSR_JAX:029655	Srinivasan et al. (2016)
Astrocytes, adult neural progenitors cells	Nestin-CreER transgene	Tamoxifen	IMSR_JAX:012906	Burns et al. (2007)
Astrocytes, adult neural progenitors cells	PAC Fgfr3-icreERT2 transgene	Tamoxifen	IMSR_JAX:025809	Rivers et al. (2008)
Oligodendrocytes, Schwann cells, olfactory ensheathing glia, adult neural progenitors	PLP1-Cre/ERT transgene	Tamoxifen	IMSR_JAX:005975	Doerflinger et al. (2003), Guo et al. (2010) and Piantanida et al. (2019)
NG2 cells (oligodendrocyte and astrocyte precursors)	NG2-Cre/ER^{TM} BAC transgene	Tamoxifen	IMSR_JAX:008538	Zhu et al. (2011)
Microglia, mononuclear phagocyte system	Cx3cr1-Cre/ER transgene	Tamoxifen	IMSR_JAX:020940	Yona et al. (2013) and Zhao et al. (2019)
Microglia, mononuclear phagocyte system	Cx3cr1-Cre/ER/YFP transgene	Tamoxifen	IMSR_JAX:021160	Parkhurst et al. (2013)
Microglia, mononuclear phagocyte system	Iba1-tTA transgene	Doxicycline	IMSR_RBRC05769	Tanaka et al. (2012)
Cre-responding lines				
Cell-type selectivity (in nervous system)	**Construct**	**Expressed protein/s**	**RRID**	**Reference**
Astrocytes	Aldh1l1-loxP-EGFP-4XpolyA-loxP-diptheria toxin A (DTA)-polyA BAC transgene	EGFP before recombination, DTA after recombination	IMSR_JAX:026033	Tsai et al. (2012)
Viral vectors				
Cell-type selectivity (in nervous system)	**Construct**	**Expressed protein/s**	**RRID**	**Reference**
Astrocytes (adult non-neurogenic regions)	AAV(5)-GFAP(2.2)-iCre	Cre recombinase		García-Cáceres et al. (2016)
Astrocytes	AAV-DJ-hALDH1L1-Cre	Cre recombinase		Koh et al. (2017)
Connexin and pannexin floxed lines				
Targeted gene	**Targeted sequence**	**Targeted connexins**	**RRID**	**Reference**
Gja1	Exon 2	Cx43	IMSR_JAX:008039	Liao et al. (2001) and Clasadonte et al. (2017)
Gjb2 *Panx1*	Exon 2 Exon 3/4	Cx26 Px1		Cohen-Salmon et al. (2002) Dvoriantchikova et al. (2012) and Poon et al. (2014)

and implanted in astrocyte-selective Cx43-deficient mice, or control mice. Tumor invasion was compromised only in the astrocyte Cx43 null background, suggesting that heterocellular (glioma-astrocyte) gap junction channel activity is not necessary for tumor invasion. However, release of astrocyte gliotransmitters *via* Cx43 hemichannels cannot be discarded. In addition, the outcome of implanted glioma cells was assessed in $Cx43^{\Delta CT/-}$ mice carrying one astrocyte-selective null Cx43 allele and one ΔCT allele that consists in a truncated Cx43 variant (Cx43K258stop). This variant lacks a cytoplasmic tail that carries phosphorylation sites and protein-interacting domains (Freitas-Andrade et al., 2019) and exhibits reduced gap junction activity and increased hemichannel activity when assessed in cultured astrocytes using dye transfer and uptake techniques (Sin et al., 2016). $Cx43^{\Delta CT/-}$ mice displayed compromised invasion of tumor cells in the brain parenchyma and increased astrogliosis when compared with $Cx43^{+/-}$ (mice carrying one astrocyte-selective Cx43 null allele and one wild type allele; Sin et al., 2016). These results indicate that astrocytic Cx43 constitutes a means for tumor invasion in the brain. The channel and non-channel functions directly involved in tumor invasion and survival are still elusive; however, at least in the former case, the results seem to discard adhesive

properties of the extracellular loops, which remained intact in the mutant variants used, provided that Cx43 expression levels and traffic to the membrane remained invariant.

CONCLUDING REMARKS AND FUTURE DIRECTIONS

A summary of the cases of connexin- and pannexin-deficient mouse models reviewed is shown in **Figures 1**, **2**. One interesting feature to highlight is that astrogliosis appears dissociated from the availability of functional astrocytic connexins and is likely more related with the inflammatory environment associated with each particular case. The data reviewed gives support to the idea that the hyperactivation of glial hemichannels leads to circuit dysfunction and worsens neurodegeneration in a variety of contexts. The generally beneficial effect of pannexin deficiency vs. the more variable outcomes observed for connexin deficiency supports the idea that connexin proteins can form both hemichannels and gap junctions, while pannexin proteins are predominantly identified with hemichannel function. Efforts to develop blood-brain barrier-permeant connexin hemichannel blockers for systemic administration appear as promising therapeutic tools. Tools to favor the bias of connexins towards gap junction assembly at the expense of hemichannel availability are expected to be beneficial.

Future studies exploiting the advantages of cell-type specific connexin and/or pannexin disruption, time control provided by inducible genetic drivers or vector administration (**Table 2**) and dissociated manipulation of gap junction channel, hemichannel and non-channel functions will contribute to address the roles of connexins in different nervous system pathologies to better design adequate therapeutic interventions. The focus on cell types whose roles are only beginning to be explored as participants in neuroinflammation (**Table 1**) is a fertile field for new research. One interesting case is NG2 glia, known to be precursors of mature oligondendrocytes present in numbers comparable to astrocytes in many brain areas (Nishiyama et al., 2005) and to be components of the glial scar after traumatic injury (Schäfer and Tegeder, 2018). Of particular importance is the availability of genetic tools to manipulate NG2 glia selectively (Zhu et al., 2011).

In addition, forthcoming studies will need to address complex interactions arising from combined selective connexin deficiency in more than one cell type. We should not be surprised by finding regional, age and pathology-dependent differences instead of a more general rule. **Figures 1**, **2** highlight the complexity of drawing unequivocal conclusions regarding the relevance of hemichannel, gap junction and non-channel functions of connexins and pannexins. Despite the availability of a substantial diversity of genetic tools to distinguish among these functions, it is uncommon to find comparisons of their effects in the same disease model with experiments run in parallel to minimize factors of variability. We envision that collaborative work of different groups with the aim of shedding light on this question will generate invaluable new and confirmative data crucial for the design of new therapies.

AUTHOR CONTRIBUTIONS

LB and LR wrote the manuscript. LA and AP revised the manuscript and made important editions.

FUNDING

This work was supported by Secretaría de Ciencia, Tecnología e Innovación Productiva, Fondo para la Investigación Científica y Tecnológica (PICT 2014-1954, Argentina), that provided funding for research cited in this review, stipend for LA and access to subscription-based journals, Universidad de Buenos Aires (136901), that provided infrastructure and salary for LR and Consejo Nacional de Investigaciones Científicas y Técnicas (142692), that provided salary for LR, AP and LB.

ACKNOWLEDGMENTS

We wish to thank the members of the Glia Club at the School of Medicine, University of Buenos Aires, for providing an encouraging environment for critical discussion about glia functions.

REFERENCES

Aasen, T., Mesnil, M., Naus, C. C., Lampe, P. D., and Laird, D. W. (2017). Gap junctions and cancer: communicating for 50 years. *Nat. Rev. Cancer* 17:74. doi: 10.1038/nrc.2016.142

Abudara, V., Retamal, M. A., Del Rio, R., and Orellana, J. A. (2018). Synaptic functions of hemichannels and pannexons: a double-edged sword. *Front. Mol. Neurosci.* 11:435. doi: 10.3389/fnmol.2018.00435

Arun, S., Ravisankar, S., and Vanisree, A. J. (2017). Implication of connexin30 on the stemness of glioma: connexin30 reverses the malignant phenotype of glioma by modulating IGF-1R, CD133 and cMyc. *J. Neurooncol.* 135, 473–485. doi: 10.1007/s11060-017-2608-4

Bargiotas, P., Krenz, A., Hormuzdi, S. G., Ridder, D. A., Herb, A., Barakat, W., et al. (2011). Pannexins in ischemia-induced neurodegeneration. *Proc. Natl. Acad. Sci. U S A* 108, 20772–20777. doi: 10.1073/pnas.1018262108

Bargiotas, P., Krenz, A., Monyer, H., and Schwaninger, M. (2012). Functional outcome of pannexin-deficient mice after cerebral ischemia. *Channels* 6, 453–456. doi: 10.4161/chan.22315

Beahm, D. L., Oshima, A., Gaietta, G. M., Hand, G. M., Smock, A. E., Zucker, S. N., et al. (2006). Mutation of a conserved threonine in the third transmembrane helix of α- and β-connexins creates a dominant-negative closed gap junction channel. *J. Biol. Chem.* 281, 7994–8009. doi: 10.1074/jbc.m506533200

Belousov, A. B., Fontes, J. D., Freitas-Andrade, M., and Naus, C. C. (2017). Gap junctions and hemichannels: communicating cell death in neurodevelopment and disease. *BMC Cell Biol.* 18:4. doi: 10.1186/s12860-016-0120-x

Bosch, M., and Kielian, T. (2014). Hemichannels in neurodegenerative diseases: is there a link to pathology? *Front. Cell. Neurosci.* 8:242. doi: 10.3389/fncel.2014.00242

Bruzzone, R., Barbe, M. T., Jakob, N. J., and Monyer, H. (2005). Pharmacological properties of homomeric and heteromeric pannexin hemichannels expressed in

Xenopus oocytes. *J. Neurochem.* 92, 1033–1043. doi: 10.1111/j.1471-4159.2004.02947.x

Burns, K. A., Ayoub, A. E., Breunig, J. J., Adhami, F., Weng, W. L., Colbert, M. C., et al. (2007). Nestin-CreER mice reveal DNA synthesis by nonapoptotic neurons following cerebral ischemia hypoxia. *Cereb. Cortex* 17, 2585–2592. doi: 10.1093/cercor/bhl164

Chen, Q., Boire, A., Jin, X., Valiente, M., Er, E. E., Lopez-Soto, A., et al. (2016). Carcinoma-astrocyte gap junctions promote brain metastasis by cGAMP transfer. *Nature* 533, 493–498. doi: 10.1038/nature18268

Chen, Q., Boire, A., Jin, X., Valiente, M., Emrah Er, E., Lopez-Soto, A., et al. (2017). Corrigendum: carcinoma-astrocyte gap junctions promote brain metastasis by cGAMP transfer. *Nature* 544:124. doi: 10.1038/nature21730

Chen, L., and Brosnan, C. F. (2006). Exacerbation of experimental autoimmune encephalomyelitis in $P2X_7R^{-/-}$ mice: evidence for loss of apoptotic activity in lymphocytes. *J. Immunol.* 176, 3115–3126. doi: 10.4049/jimmunol.176.5.3115

Chen, M. J., Kress, B., Han, X., Moll, K., Peng, W., Ji, R. R., et al. (2012). Astrocytic CX43 hemichannels and gap junctions play a crucial role in development of chronic neuropathic pain following spinal cord injury. *Glia* 60, 1660–1670. doi: 10.1002/glia.22384

Chen, B., Yang, L., Chen, J., Chen, Y., Zhang, L., Wang, L., et al. (2019). Inhibition of Connexin43 hemichannels with Gap19 protects cerebral ischemia/reperfusion injury *via* the JAK2/STAT3 pathway in mice. *Brain Res. Bull.* 146, 124–135. doi: 10.1016/j.brainresbull.2018.12.009

Clasadonte, J., Scemes, E., Wang, Z., Boison, D., and Haydon, P. G. (2017). Connexin 43-mediated astroglial metabolic networks contribute to the regulation of the sleep-wake cycle. *Neuron* 95, 1365.e5–1380.e5. doi: 10.1016/j.neuron.2017.08.022

Cohen-Salmon, M., Ott, T., Michel, V., Hardelin, J. P., Perfettini, I., Eybalin, M., et al. (2002). Targeted ablation of connexin26 in the inner ear epithelial gap junction network causes hearing impairment and cell death. *Curr. Biol.* 12, 1106–1111. doi: 10.1016/s0960-9822(02)00904-1

Contreras, J. E., Sánchez, H. A., Véliz, L. P., Bukauskas, F. F., Bennett, M. V., and Sáez, J. C. (2004). Role of connexin-based gap junction channels and hemichannels in ischemia-induced cell death in nervous tissue. *Brain Res. Rev.* 47, 290–303. doi: 10.1016/j.brainresrev.2004.08.002

Dahl, G., Qiu, F., and Wang, J. (2013). The bizarre pharmacology of the ATP release channel pannexin1. *Neuropharmacology* 75, 583–593. doi: 10.1016/j.neuropharm.2013.02.019

De Bock, M., Leybaert, L., and Giaume, C. (2017). Connexin channels at the glio-vascular interface: gatekeepers of the brain. *Neurochem. Res.* 42, 2519–2536. doi: 10.1007/s11064-017-2313-x

Dissing-Olesen, L., LeDue, J. M., Rungta, R. L., Hefendehl, J. K., Choi, H. B., and MacVicar, B. A. (2014). Activation of neuronal NMDA receptors triggers transient ATP-mediated microglial process outgrowth. *J. Neurosci.* 34, 10511–10527. doi: 10.1523/JNEUROSCI.0405-14.2014

Doerflinger, N. H., Macklin, W. B., and Popko, B. (2003). Inducible site-specific recombination in myelinating cells. *Genesis* 35, 63–72. doi: 10.1002/gene.10154

Dvoriantchikova, G., Ivanov, D., Barakat, D., Grinberg, A., Wen, R., Slepak, V. Z., et al. (2012). Genetic ablation of Pannexin1 protects retinal neurons from ischemic injury. *PLoS One* 7:e31991. doi: 10.1371/journal.pone.0031991

Eugenin, E. A., Basilio, D., Sáez, J. C., Orellana, J. A., Raine, C. S., Bukauskas, F., et al. (2012). The role of gap junction channels during physiologic and pathologic conditions of the human central nervous system. *J. Neuroimmune Pharmacol.* 7, 499–518. doi: 10.1007/s11481-012-9352-5

Fang, M., Yamasaki, R., Li, G., Masaki, K., Yamaguchi, H., Fujita, A., et al. (2018). Connexin 30 deficiency attenuates chronic but not acute phases of experimental autoimmune encephalomyelitis through induction of neuroprotective microglia. *Front. Immunol.* 9:2588. doi: 10.3389/fimmu.2018.02588

Farahani, R., Pina-Benabou, M. H., Kyrozis, A., Siddiq, A., Barradas, P. C., Chiu, F. C., et al. (2005). Alterations in metabolism and gap junction expression may determine the role of astrocytes as "good samaritans" or executioners. *Glia* 50, 351–361. doi: 10.1002/glia.20213

Freitas-Andrade, M., Bechberger, J. F., MacVicar, B. A., Viau, V., and Naus, C. C. (2017). Pannexin1 knockout and blockade reduces ischemic stroke injury in female, but not in male mice. *Oncotarget* 8, 36973–36983. doi: 10.18632/oncotarget.16937

Freitas-Andrade, M., and Naus, C. C. (2016). Astrocytes in neuroprotection and neurodegeneration: the role of connexin43 and pannexin1. *Neuroscience* 323, 207–221. doi: 10.1016/j.neuroscience.2015.04.035

Freitas-Andrade, M., Wang, N., Bechberger, J. F., De Bock, M., Lampe, P. D., Leybaert, L., et al. (2019). Targeting MAPK phosphorylation of Connexin43 provides neuroprotection in stroke. *J. Exp. Med.* 216, 916–935. doi: 10.1084/jem.20171452

Gajardo-Gómez, R., Labra, V. C., and Orellana, J. A. (2016). Connexins and pannexins: new insights into microglial functions and dysfunctions. *Front. Mol. Neurosci.* 9:86. doi: 10.3389/fnmol.2016.00086

García-Cáceres, C., Quarta, C., Varela, L., Gao, Y., Gruber, T., Legutko, B., et al. (2016). Astrocytic insulin signaling couples brain glucose uptake with nutrient availability. *Cell* 166, 867–880. doi: 10.1016/j.cell.2016.07.028

Gaynullina, D., Tarasova, O. S., Kiryukhina, O. O., Shestopalov, V. I., and Panchin, Y. (2014). Endothelial function is impaired in conduit arteries of pannexin1 knockout mice. *Biol. Direct.* 9:8. doi: 10.1186/1745-6150-9-8

Giaume, C., and Theis, M. (2010). Pharmacological and genetic approaches to study connexin-mediated channels in glial cells of the central nervous system. *Brain Res. Rev.* 63, 160–176. doi: 10.1016/j.brainresrev.2009.11.005

Giaume, C., Kirchhoff, F., Matute, C., Reichenbach, A., and Verkhratsky, A. (2007). Glia: the fulcrum of brain diseases. *Cell Death Differ.* 14, 1324–1335. doi: 10.1038/sj.cdd.4402144

Guo, F., Maeda, Y., Ma, J., Xu, J., Horiuchi, M., Miers, L., et al. (2010). Pyramidal neurons are generated from oligodendroglial progenitor cells in adult piriform cortex. *J. Neurosci.* 30, 12036–12049. doi: 10.1523/JNEUROSCI.1360-10.2010

Hahn, A. F., Ainsworth, P. J., Naus, C. C., Mao, J., and Bolton, C. F. (2000). Clinical and pathological observations in men lacking the gap junction protein connexin 32. *Muscle Nerve Suppl.* 9, S39–S48. doi: 10.1002/1097-4598(2000)999:9<::aid-mus8>3.3.co;2-3

Huang, C., Han, X., Li, X., Lam, E., Peng, W., Lou, N., et al. (2012). Critical role of connexin 43 in secondary expansion of traumatic spinal cord injury. *J. Neurosci.* 32, 3333–3338. doi: 10.1523/JNEUROSCI.1216-11.2012

Iglesias, R., Dahl, G., Qiu, F., Spray, D. C., and Scemes, E. (2009). Pannexin 1: the molecular substrate of astrocyte "hemichannels". *J. Neurosci.* 29, 7092–7097. doi: 10.1523/JNEUROSCI.6062-08.2009

Kaiser, T., and Feng, G. (2019). Tmem119-EGFP and Tmem119-CreERT2 transgenic mice for labeling and manipulating microglia. *eNeuro* 6:ENEURO.0448-18.2019. doi: 10.1523/ENEURO.0448-18.2019

Karpuk, N., Burkovetskaya, M., Fritz, T., Angle, A., and Kielian, T. (2011). Neuroinflammation leads to region-dependent alterations in astrocyte gap junction communication and hemichannel activity. *J. Neurosci.* 31, 414–425. doi: 10.1523/JNEUROSCI.5247-10.2011

Kielian, T. (2008). Glial connexins and gap junctions in CNS inflammation and disease. *J. Neurochem.* 106, 1000–1016. doi: 10.1111/j.1471-4159.2008.05405.x

Koh, W., Park, Y. M., Lee, S. E., and Lee, C. J. (2017). AAV-mediated astrocyte-specific gene expression under human. *Exp. Neurobiol.* 26, 350–361. doi: 10.5607/en.2017.26.6.350

Köster-Patzlaff, C., Hosseini, S. M., and Reuss, B. (2007). Persistent Borna Disease Virus infection changes expression and function of astroglial gap junctions *in vivo* and *in vitro*. *Brain Res.* 1184, 316–332. doi: 10.1016/j.brainres.2007.09.062

Koulakoff, A., Mei, X., Orellana, J. A., Sáez, J. C., and Giaume, C. (2012). Glial connexin expression and function in the context of Alzheimer's disease. *Biochim. Biophys. Acta* 1818, 2048–2057. doi: 10.1016/j.bbamem.2011.10.001

Kozoriz, M. G., Bechberger, J. F., Bechberger, G. R., Suen, M. W., Moreno, A. P., Maass, K., et al. (2010). The connexin43 C-terminal region mediates neuroprotection during stroke. *J. Neuropathol. Exp. Neurol.* 69, 196–206. doi: 10.1097/nen.0b013e3181cd44df

Kozoriz, M. G., Lai, S., Vega, J. L., Sáez, J. C., Sin, W. C., Bechberger, J. F., et al. (2013). Cerebral ischemic injury is enhanced in a model of oculodentodigital dysplasia. *Neuropharmacology* 75, 549–556. doi: 10.1016/j.neuropharm.2013.05.003

Lai, C. P., Bechberger, J. F., and Naus, C. C. (2009). Pannexin2 as a novel growth regulator in C6 glioma cells. *Oncogene* 28, 4402–4408. doi: 10.1038/onc.2009.283

Lai, C. P., Bechberger, J. F., Thompson, R. J., MacVicar, B. A., Bruzzone, R., and Naus, C. C. (2007). Tumor-suppressive effects of pannexin 1 in C6 glioma cells. *Cancer Res.* 67, 1545–1554. doi: 10.1158/0008-5472.can-06-1396

Lapato, A. S., and Tiwari-Woodruff, S. K. (2018). Connexins and pannexins: at the junction of neuro-glial homeostasis and disease. *J. Neurosci. Res.* 96, 31–44. doi: 10.1002/jnr.24088

Leithe, E., Mesnil, M., and Aasen, T. (2018). The connexin 43 C-terminus: a tail of many tales. *Biochim. Biophys. Acta Biomembr.* 1860, 48–64. doi: 10.1016/j.bbamem.2017.05.008

Liao, Y., Day, K. H., Damon, D. N., and Duling, B. R. (2001). Endothelial cell-specific knockout of connexin 43 causes hypotension and bradycardia in mice. *Proc. Natl. Acad. Sci. U S A* 98, 9989–9994. doi: 10.1073/pnas.171305298

Lin, J. H., Lou, N., Kang, N., Takano, T., Hu, F., Han, X., et al. (2008). A central role of connexin 43 in hypoxic preconditioning. *J. Neurosci.* 28, 681–695. doi: 10.1523/JNEUROSCI.3827-07.2008

Liu, L., Su, Y., Yang, W., Xiao, M., Gao, J., and Hu, G. (2010). Disruption of neuronal-glial-vascular units in the hippocampus of ovariectomized mice injected with D-galactose. *Neuroscience* 169, 596–608. doi: 10.1016/j.neuroscience.2010.05.028

Lutz, S. E., González-Fernández, E., Ventura, J. C., Pérez-Samartín, A., Tarassishin, L., Negoro, H., et al. (2013). Contribution of pannexin1 to experimental autoimmune encephalomyelitis. *PLoS One* 8:e66657. doi: 10.1371/journal.pone.0066657

Lutz, S. E., Raine, C. S., and Brosnan, C. F. (2012). Loss of astrocyte connexins 43 and 30 does not significantly alter susceptibility or severity of acute experimental autoimmune encephalomyelitis in mice. *J. Neuroimmunol.* 245, 8–14. doi: 10.1016/j.jneuroim.2012.01.007

Mao, Y., Nguyen, T., Tonkin, R. S., Lees, J. G., Warren, C., O'Carroll, S. J., et al. (2017a). Characterisation of Peptide5 systemic administration for treating traumatic spinal cord injured rats. *Exp. Brain Res.* 235, 3033–3048. doi: 10.1007/s00221-017-5023-3

Mao, Y., Tonkin, R. S., Nguyen, T., O'Carroll, S. J., Nicholson, L. F., Green, C. R., et al. (2017b). Systemic administration of connexin43 mimetic peptide improves functional recovery after traumatic spinal cord injury in adult rats. *J. Neurotrauma* 34, 707–719. doi: 10.1089/neu.2016.4625

Mousseau, M., Burma, N. E., Lee, K. Y., Leduc-Pessah, H., Kwok, C. H. T., Reid, A. R., et al. (2018). Microglial pannexin-1 channel activation is a spinal determinant of joint pain. *Sci. Adv.* 4:eaas9846. doi: 10.1126/sciadv.aas9846

Nakagawa, M., Takashima, H., Umehara, F., Arimura, K., Miyashita, F., Takenouchi, N., et al. (2001). Clinical phenotype in X-linked Charcot-Marie-Tooth disease with an entire deletion of the connexin 32 coding sequence. *J. Neurol. Sci.* 185, 31–37. doi: 10.1016/s0022-510x(01)00454-3

Nakase, T., Fushiki, S., Söhl, G., Theis, M., Willecke, K., and Naus, C. C. (2003). Neuroprotective role of astrocytic gap junctions in ischemic stroke. *Cell Commun. Adhes.* 10, 413–417. doi: 10.1080/714040461

Nakase, T., Söhl, G., Theis, M., Willecke, K., and Naus, C. C. (2004). Increased apoptosis and inflammation after focal brain ischemia in mice lacking connexin43 in astrocytes. *Am. J. Pathol.* 164, 2067–2075. doi: 10.1016/s0002-9440(10)63765-0

Nielsen, B. S., Hansen, D. B., Ransom, B. R., Nielsen, M. S., and MacAulay, N. (2017). Connexin hemichannels in astrocytes: an assessment of controversies regarding their functional characteristics. *Neurochem. Res.* 42, 2537–2550. doi: 10.1007/s11064-017-2243-7

Nishiyama, A., Yang, Z., and Butt, A. (2005). Astrocytes and NG2-glia: what's in a name? *J. Anat.* 207, 687–693. doi: 10.1111/j.1469-7580.2005.00489.x

O'Carroll, S. J., Alkadhi, M., Nicholson, L. F., and Green, C. R. (2008). Connexin 43 mimetic peptides reduce swelling, astrogliosis and neuronal cell death after spinal cord injury. *Cell Commun. Adhes.* 15, 27–42. doi: 10.1080/15419060802014164

O'Carroll, S. J., Gorrie, C. A., Velamoor, S., Green, C. R., and Nicholson, L. F. (2013). Connexin43 mimetic peptide is neuroprotective and improves function following spinal cord injury. *Neurosci. Res.* 75, 256–267. doi: 10.1016/j.neures.2013.01.004

Oguro, K., Jover, T., Tanaka, H., Lin, Y., Kojima, T., Oguro, N., et al. (2001). Global ischemia-induced increases in the gap junctional proteins connexin 32 (Cx32) and Cx36 in hippocampus and enhanced vulnerability of Cx32 knock-out mice. *J. Neurosci.* 21, 7534–7542. doi: 10.1523/jneurosci.21-19-07534.2001

Olympiou, M., Sargiannidou, I., Markoullis, K., Karaiskos, C., Kagiava, A., Kyriakoudi, S., et al. (2016). Systemic inflammation disrupts oligodendrocyte gap junctions and induces ER stress in a model of CNS manifestations of X-linked Charcot-Marie-Tooth disease. *Acta Neuropathol. Commun.* 4:95. doi: 10.1186/s40478-016-0369-5

Orellana, J. A., Martinez, A. D., and Retamal, M. A. (2013). Gap junction channels and hemichannels in the CNS: regulation by signaling molecules. *Neuropharmacology* 75, 567–582. doi: 10.1016/j.neuropharm.2013.02.020

Orellana, J. A., Shoji, K. F., Abudara, V., Ezan, P., Amigou, E., Sáez, P. J., et al. (2011). Amyloid β-induced death in neurons involves glial and neuronal hemichannels. *J. Neurosci.* 31, 4962–4977. doi: 10.1523/JNEUROSCI.6417-10.2011

Orellana, J. A., Sáez, P. J., Shoji, K. F., Schalper, K. A., Palacios-Prado, N., Velarde, V., et al. (2009). Modulation of brain hemichannels and gap junction channels by pro-inflammatory agents and their possible role in neurodegeneration. *Antioxid. Redox Signal.* 11, 369–399. doi: 10.1089/ars.2008.2130

Parkhurst, C. N., Yang, G., Ninan, I., Savas, J. N., Yates, J. R., Lafaille, J. J., et al. (2013). Microglia promote learning-dependent synapse formation through brain-derived neurotrophic factor. *Cell* 155, 1596–1609. doi: 10.1016/j.cell.2013.11.030

Piantanida, A. P., Acosta, L. E., Brocardo, L., Capurro, C., Greer, C. A., and Rela, L. (2019). Selective Cre-mediated gene deletion identifies connexin 43 as the main connexin channel supporting olfactory ensheathing cell networks. *J. Comp. Neurol.* 527, 1278–1289. doi: 10.1002/cne.24628

Poon, I. K., Chiu, Y. H., Armstrong, A. J., Kinchen, J. M., Juncadella, I. J., Bayliss, D. A., et al. (2014). Unexpected link between an antibiotic, pannexin channels and apoptosis. *Nature* 507, 329–334. doi: 10.1038/nature13147

Quintanilla, R. A., Orellana, J. A., and von Bernhardi, R. (2012). Understanding risk factors for Alzheimer's disease: interplay of neuroinflammation, connexin-based communication and oxidative stress. *Arch. Med. Res.* 43, 632–644. doi: 10.1016/j.arcmed.2012.10.016

Rami, A., Volkmann, T., and Winckler, J. (2001). Effective reduction of neuronal death by inhibiting gap junctional intercellular communication in a rodent model of global transient cerebral ischemia. *Exp. Neurol.* 170, 297–304. doi: 10.1006/exnr.2001.7712

Rawanduzy, A., Hansen, A., Hansen, T. W., and Nedergaard, M. (1997). Effective reduction of infarct volume by gap junction blockade in a rodent model of stroke. *J. Neurosurg.* 87, 916–920. doi: 10.3171/jns.1997.87.6.0916

Ren, R., Zhang, L., and Wang, M. (2018). Specific deletion connexin43 in astrocyte ameliorates cognitive dysfunction in APP/PS1 mice. *Life Sci.* 208, 175–191. doi: 10.1016/j.lfs.2018.07.033

Retamal, M. A., Froger, N., Palacios-Prado, N., Ezan, P., Sáez, P. J., Sáez, J. C., et al. (2007). Cx43 hemichannels and gap junction channels in astrocytes are regulated oppositely by proinflammatory cytokines released from activated microglia. *J. Neurosci.* 27, 13781–13792. doi: 10.1523/jneurosci.2042-07.2007

Rivers, L. E., Young, K. M., Rizzi, M., Jamen, F., Psachoulia, K., Wade, A., et al. (2008). PDGFRA/NG2 glia generate myelinating oligodendrocytes and piriform projection neurons in adult mice. *Nat. Neurosci.* 11, 1392–1401. doi: 10.1038/nn.2220

Rouach, N., Avignone, E., Même, W., Koulakoff, A., Venance, L., Blomstrand, F., et al. (2002). Gap junctions and connexin expression in the normal and pathological central nervous system. *Biol. Cell* 94, 457–475. doi: 10.1016/s0248-4900(02)00016-3

Sáez, P. J., Orellana, J. A., Vega-Riveros, N., Figueroa, V. A., Hernández, D. E., Castro, J. F., et al. (2013). Disruption in connexin-based communication is associated with intracellular Ca^{2+} signal alterations in astrocytes from Niemann-Pick type C mice. *PLoS One* 8:e71361. doi: 10.1371/journal.pone.0071361

Schäfer, M. K. E., and Tegeder, I. (2018). NG2/CSPG4 and progranulin in the posttraumatic glial scar. *Matrix Biol.* 68–69, 571–588. doi: 10.1016/j.matbio.2017.10.002

Sharma, A. K., Charles, E. J., Zhao, Y., Narahari, A. K., Baderdinni, P. K., Good, M. E., et al. (2018). Pannexin-1 channels on endothelial cells mediate vascular inflammation during lung ischemia-reperfusion injury. *Am. J. Physiol. Lung Cell. Mol. Physiol.* 315, L301–L312. doi: 10.1152/ajplung.00004.2018

Sin, W. C., Aftab, Q., Bechberger, J. F., Leung, J. H., Chen, H., and Naus, C. C. (2016). Astrocytes promote glioma invasion *via* the gap junction protein connexin43. *Oncogene* 35, 1504–1516. doi: 10.1038/onc.2015.210

Srinivasan, R., Lu, T. Y., Chai, H., Xu, J., Huang, B. S., Golshani, P., et al. (2016). New Transgenic mouse lines for selectively targeting astrocytes and studying

calcium signals in astrocyte processes *in situ* and *in vivo*. *Neuron* 92, 1181–1195. doi: 10.1016/j.neuron.2016.11.030

Takeuchi, H., and Suzumura, A. (2014). Gap junctions and hemichannels composed of connexins: potential therapeutic targets for neurodegenerative diseases. *Front. Cell. Neurosci.* 8:189. doi: 10.3389/fncel.2014.00189

Takeuchi, H., Mizoguchi, H., Doi, Y., Jin, S., Noda, M., Liang, J., et al. (2011). Blockade of gap junction hemichannel suppresses disease progression in mouse models of amyotrophic lateral sclerosis and Alzheimer's disease. *PLoS One* 6:e21108. doi: 10.1371/journal.pone.0021108

Tanaka, K. F., Matsui, K., Sasaki, T., Sano, H., Sugio, S., Fan, K., et al. (2012). Expanding the repertoire of optogenetically targeted cells with an enhanced gene expression system. *Cell Rep.* 2, 397–406. doi: 10.1016/j.celrep.2012.06.011

Theodoric, N., Bechberger, J. F., Naus, C. C., and Sin, W. C. (2012). Role of gap junction protein connexin43 in astrogliosis induced by brain injury. *PLoS One* 7:e47311. doi: 10.1371/journal.pone.0047311

Theriault, E., Frankenstein, U. N., Hertzberg, E. L., and Nagy, J. I. (1997). Connexin43 and astrocytic gap junctions in the rat spinal cord after acute compression injury. *J. Comp. Neurol.* 382, 199–214. doi: 10.1002/(sici)1096-9861(19970602)382:2<199::aid-cne5>3.3.co;2-5

Tress, O., Maglione, M., Zlomuzica, A., May, D., Dicke, N., Degen, J., et al. (2011). Pathologic and phenotypic alterations in a mouse expressing a connexin47 missense mutation that causes Pelizaeus-Merzbacher-like disease in humans. *PLoS Genet.* 7:e1002146. doi: 10.1371/journal.pgen.1002146

Tsai, H. H., Li, H., Fuentealba, L. C., Molofsky, A. V., Taveira-Marques, R., Zhuang, H., et al. (2012). Regional astrocyte allocation regulates CNS synaptogenesis and repair. *Science* 337, 358–362. doi: 10.1126/science.1222381

Ul-Hussain, M., Olk, S., Schoenebeck, B., Wasielewski, B., Meier, C., Prochnow, N., et al. (2014). Internal ribosomal entry site (IRES) activity generates endogenous carboxyl-terminal domains of Cx43 and is responsive to hypoxic conditions. *J. Biol. Chem.* 289, 20979–20990. doi: 10.1074/jbc.m113.540187

Umans, R. A., and Sontheimer, H. (2018). Combating malignant astrocytes: Strategies mitigating tumor invasion. *Neurosci. Res.* 126, 22–30. doi: 10.1016/j.neures.2017.09.010

Umebayashi, D., Natsume, A., Takeuchi, H., Hara, M., Nishimura, Y., Fukuyama, R., et al. (2014). Blockade of gap junction hemichannel protects secondary spinal cord injury from activated microglia-mediated glutamate exitoneurotoxicity. *J. Neurotrauma* 31, 1967–1974. doi: 10.1089/neu.2013.3223

Uzu, M., Sin, W. C., Shimizu, A., and Sato, H. (2018). Conflicting roles of connexin43 in tumor invasion and growth in the central nervous system. *Int. J. Mol. Sci.* 19:E1159. doi: 10.3390/ijms19041159

Wallraff, A., Kohling, R., Heinemann, U., Theis, M., Willecke, K., and Steinhauser, C. (2006). The impact of astrocytic gap junctional coupling on potassium buffering in the hippocampus. *J. Neurosci.* 26, 5438–5447. doi: 10.1523/jneurosci.0037-06.2006

Wang, N., De Vuyst, E., Ponsaerts, R., Boengler, K., Palacios-Prado, N., Wauman, J., et al. (2013). Selective inhibition of Cx43 hemichannels by Gap19 and its impact on myocardial ischemia/reperfusion injury. *Basic Res. Cardiol.* 108:309. doi: 10.1007/s00395-012-0309-x

Wang, Y., and Yin, F. (2016). A review of X-linked Charcot-Marie-Tooth disease. *J. Child Neurol.* 31, 761–772. doi: 10.1177/0883073815604227

Weaver, J. L., Arandjelovic, S., Brown, G., Mendu, S. K., Schappe, M. S., Buckley, M. W., et al. (2017). Hematopoietic pannexin 1 function is critical for neuropathic pain. *Sci. Rep.* 7:42550. doi: 10.1038/srep42550

Xing, L., Yang, T., Cui, S., and Chen, G. (2019). Connexin hemichannels in astrocytes: role in CNS disorders. *Front. Mol. Neurosci.* 12:23. doi: 10.3389/fnmol.2019.00023

Yi, C., Mei, X., Ezan, P., Mato, S., Matias, I., Giaume, C., et al. (2016). Astroglial connexin43 contributes to neuronal suffering in a mouse model of Alzheimer's disease. *Cell Death Differ.* 23, 1691–1701. doi: 10.1038/cdd.2016.63

Yona, S., Kim, K. W., Wolf, Y., Mildner, A., Varol, D., Breker, M., et al. (2013). Fate mapping reveals origins and dynamics of monocytes and tissue macrophages under homeostasis. *Immunity* 38, 79–91. doi: 10.1016/j.immuni.2012.12.001

Zhang, W., Couldwell, W. T., Simard, M. F., Song, H., Lin, J. H., and Nedergaard, M. (1999). Direct gap junction communication between malignant glioma cells and astrocytes. *Cancer Res.* 59, 1994–2003.

Zhang, W., DeMattia, J. A., Song, H., and Couldwell, W. T. (2003). Communication between malignant glioma cells and vascular endothelial cells through gap junctions. *J. Neurosurg.* 98, 846–853. doi: 10.3171/jns.2003.98.4.0846

Zhao, X. F., Alam, M. M., Liao, Y., Huang, T., Mathur, R., Zhu, X., et al. (2019). Targeting microglia using Cx3cr1-Cre lines: revisiting the specificity. *eNeuro* 6:ENEURO.0114-19.2019. doi: 10.1523/eneuro.0114-19.2019

Zhou, J. Z., and Jiang, J. X. (2014). Gap junction and hemichannel-independent actions of connexins on cell and tissue functions—an update. *FEBS Lett.* 588, 1186–1192. doi: 10.1016/j.febslet.2014.01.001

Zhu, X., Hill, R. A., Dietrich, D., Komitova, M., Suzuki, R., and Nishiyama, A. (2011). Age-dependent fate and lineage restriction of single NG2 cells. *Development* 138, 745–753. doi: 10.1242/dev.047951

Conflict of Interest: The authors declare that the research was conducted in the absence of any commercial or financial relationships that could be construed as a potential conflict of interest.

frontiers in Cellular Neuroscience

ORIGINAL RESEARCH
published: 12 November 2019
doi: 10.3389/fncel.2019.00507

Activation of α7 Nicotinic Acetylcholine Receptor Protects Against 1-Methyl-4-Phenylpyridinium-Induced Astroglial Apoptosis

Ye Hua[1], Beibei Yang[2], Qiang Chen[2], Ji Zhang[3], Jun Hu[4] and Yi Fan[2]†*

[1] Department of Neurology, The Affiliated Wuxi No. 2 People's Hospital of Nanjing Medical University, Wuxi, China, [2] Department of Pharmacology, Neuroprotective Drug Discovery Center, Nanjing Medical University, Nanjing, China, [3] Division of Clinical Pharmacy, Department of Pharmacy, The First Affiliated Hospital of Nanjing Medical University, Nanjing, China, [4] Department of Orthopedics, The First Affiliated Hospital of Nanjing Medical University, Nanjing, China

OPEN ACCESS

Edited by:
Livio Luongo,
Second University of Naples, Italy

Reviewed by:
Yu-Feng Wang,
Harbin Medical University, China
Rheinallt Parri,
Aston University, United Kingdom

***Correspondence:**
Yi Fan
yfan@njmu.edu.cn

†ORCID:
Yi Fan
orcid.org/0000-0003-1783-3220

Specialty section:
This article was submitted to Non-Neuronal Cells, a section of the journal Frontiers in Cellular Neuroscience

Received: 06 September 2019
Accepted: 28 October 2019
Published: 12 November 2019

Citation:
Hua Y, Yang B, Chen Q, Zhang J, Hu J and Fan Y (2019) Activation of α7 Nicotinic Acetylcholine Receptor Protects Against 1-Methyl-4-Phenylpyridinium-Induced Astroglial Apoptosis. Front. Cell. Neurosci. 13:507. doi: 10.3389/fncel.2019.00507

Astrocytes, as the largest population of glial subtype, play crucial roles in normal brain function and pathological conditions, such as Parkinson's disease (PD). Restoring the functions of astrocyte is a promising new therapeutic target for PD. Astrocytes can express multiple types of neurotransmitter receptors, including functional α7 nicotinic acetylcholine receptor (α7nAChR). Previously, we found that a non-selective α7nAChR agonist nicotine exerted a protective effect against H_2O_2-induced astrocyte apoptosis *via* an α7nAChR-dependent pathway. However, the molecular mechanism of the antiapoptotic response of astroglial α7nAChR has not been studied. In the present study, using pharmacological inhibition and genetic knockout of α7nAChR, we assessed the antiapoptotic effects of an α7nAChR agonist PNU-282987 in primary cultured astrocytes treated with 1-methyl-4-phenylpyridinium (MPP^+). PNU-282987 promoted the viability of astrocytes, alleviated MPP^+ induced apoptosis, and decreased the number of $GFAP^+/TUNEL^+$ cells. Meanwhile, PNU-282987 upregulated the expression of the antiapoptotic protein Bcl-2 and downregulated the expression of the apoptotic protein Bax and cleaved-caspase-3. Moreover, the suppression of the JNK-p53-caspase-3 signaling may underlie the neuroprotective property of PNU-282987. Therefore, PNU-282987 ameliorates astroglial apoptosis induced by MPP^+ through α7nAChR-JNK-p53 signaling. Our findings suggest that PNU-282987 may be a potential drug for restoring astroglial functions in the treatment of PD.

Keywords: α7 nicotinic receptor, astrocyte, PNU-282987, apoptosis, 1-methyl-4-phenylpyridinium

INTRODUCTION

As the largest population of glial subtype in the central nervous system, astrocytes play crucial roles in maintaining normal brain function and homeostasis (Santello et al., 2019; Valori et al., 2019). Astrocytes provide multiple physiological support functions for neurons, and loss of these critical functions can contribute to the disruption of neuronal function and neurodegeneration

(Li et al., 2019; Sorrentino et al., 2019). Besides, astrocytes become activated with heterogeneous and progressive changes in response to pathological conditions, such as inflammatory disease (Iglesias et al., 2017), acute traumatic brain injury (Burda et al., 2016), ischemia/hypoxia (Liu and Chopp, 2016), Alzheimer's disease (Acosta et al., 2017), and Parkinson's disease (PD) (Booth et al., 2017). Activated astrocytes leave their quiescent state and are characterized by cellular swelling, proliferation (astrocytosis), and hypertrophy-hyperplasia (astrogliosis) (Pekny and Nilsson, 2005). At the early stage of injury, activated astrocytes are believed to be beneficial to neurons by participating in regulating brain energy metabolism, recycling extracellular ions and neurotransmitter levels, and secreting neuroprotective substances (Efremova et al., 2017; Martin-Jiménez et al., 2017). However, the specific role of prolonged activated astrocytes is still controversial. Activated astrocytes are essential for neuronal survival and functional recovery by the release of neurotrophins (Gozes et al., 1999; Albrecht et al., 2002) and the existence of gap junction (Cotrina et al., 1998; Lin et al., 2010). In contrast, activated astrocytes produce potential toxic mediators and kill neighboring cells in brain injury (Pekny and Nilsson, 2005; Li et al., 2019). Thus, astrocytes act as initiators or contributors in neuropathological conditions *via* both gain-of-function and loss-of-function mechanisms.

As a common neurodegenerative disease, PD is pathologically characterized by the loss of dopaminergic neurons in the substantia nigra pars compacta (SNpc) (Kalia and Lang, 2015). The origin of PD and mechanisms of neuronal degeneration have not yet been fully understood. Compelling evidence certainly indicates that astrocytes have an initiating role in the pathophysiology of PD (Booth et al., 2017). The presence of reactive astrocytes is a crucial aspect of PD pathophysiology in the SNpc (Miklossy et al., 2006). There is also growing evidence that many of the PD-associated genes, such as α-synuclein, DJ-1, ATP13A2, PINK1, and Parkin, are involved in astrocyte-specific functions, including glutamate uptake (Gu et al., 2010; Kim et al., 2016), inflammatory response (Waak et al., 2009; Fellner et al., 2013; Qiao et al., 2016), fatty acid metabolism (Xu et al., 2003; Castagnet et al., 2005), and neurotrophic capacity (Mullett and Hinkle, 2009; Gu et al., 2010; Qiao et al., 2016). Notably, a recent study found that postmortem tissue from PD patients have shown an increase in astrocytic senescence, and removing these senescent cells prevented the symptoms of PD in a mouse model (Chinta et al., 2018). These studies suggest that astrocyte dysfunction plays an essential role in the development and exacerbation of PD, and targeting and restoring the functions of astrocyte are promising new therapeutic targets of neuroprotection.

Alpha7 nicotinic acetylcholine receptor (α7nAChR) is one of the most abundant nAChRs in the mammalian brain (Bertrand et al., 2015). Recent studies suggest that α7nAChR activation may be a crucial mechanism underlying the anti-inflammatory (Egea et al., 2015; Echeverria et al., 2016), antiapoptotic (Kim et al., 2012), and neuroprotective potential of nicotine (Quik et al., 2015; Liu et al., 2017) in several neuropathological conditions. Our previous studies found that α7nAChRs may mediate the protective effects of nicotine *in vivo* in PD model mice (Liu et al., 2015, 2017) and *in vitro* in cultured 1-methyl-4-phenylpyridinium (MPP^+)-induced SH-SY5Y cells (Xu et al., 2019). The expression of functional α7nAChRs has also been reported to be present in astrocytes (Teaktong et al., 2003; Xu et al., 2019). Given that the impairment of astrocyte functions can critically influence neuronal survival, it is critical to evaluate the potential role of astroglial α7nAChR. Recently, we have demonstrated that nicotine exerted a protective effect against H_2O_2-induced astrocyte apoptosis, which was abolished by an α7nAChR-selective antagonist (Liu et al., 2015). Astrocyte apoptosis is believed to contribute to the pathogenesis of chronic neurodegenerative disorders, including PD (Takuma et al., 2004). Therefore, targeting astroglial α7nAChR for their antiapoptotic properties may be necessary for guiding disease-modifying therapies for PD. However, the molecular mechanism of the observed antiapoptotic response of astroglial α7nAChR has not been studied.

In this study, we firstly confirmed *in vitro* the neuroprotective effect of an α7nAChR agonist PNU-282987 in astrocytes treated with 1-methyl-4-phenylpyridinium (MPP^+, a neurotoxin used in cellular models of PD). Then, we showed that PNU-282987 decreased the number of $TUNEL^+/GFAP^+$ cells and alleviated MPP^+-induced apoptosis. Meanwhile, PNU-282987 upregulated the expression of the antiapoptotic protein Bcl-2 and downregulated the expression of the apoptotic protein Bax and cleaved caspase-3. Moreover, the suppression of the JNK-p53-caspase-3 signaling may underlie the antiapoptotic property of PNU-282987.

MATERIALS AND METHODS

Reagents

Dulbecco's modified Eagle's medium (DMEM) and fetal bovine serum (FBS) were purchased from Gibco Lab (Carlsbad, CA, United States). The tetrazolium salt 3-[4,5-dimethylthiazol-2-yl]-2,5-diphenyltetrazolium bromide (MTT), dimethyl sulfoxide (DMSO), 0.25% trypsin solution, PNU-282987, methyllycaconitine (MLA), Triton X-100, penicillin, and streptomycin were purchased from Sigma-Aldrich (St. Louis, MO, United States). Hoechst 33342 staining was purchased from AAT BioQuest (Montreal, CA, United States). Terminal deoxynucleotidyl transferase dUTP nick end labeling (TUNEL)-staining kit was purchased from Roche Applied Science (South San Francisco, CA, United States). ProLong Gold Antifade with 4′,6-diamidino-2-phenylindole (DAPI) was purchased from Invitrogen (Carlsbad, CA, United States). The lactate dehydrogenase (LDH) cytotoxicity detection kit was purchased from Nanjing Jiancheng Bioengineering Institute (Jiangsu, China). The Annexin-V fluorescein isothiocyanate (FITC) apoptosis detection kit was purchased from BD Biosciences (San Jose, CA, United States). Protease inhibitor cocktail and phosphotransferase inhibitor cocktail were purchased from Roche (Indianapolis, IN, United States).

Animal

Alpha7-nAChR knockout (KO) mice (C57BL/6J background) were purchased from the Jackson Laboratory (B6.129S7-charna7tm1bay, number 003232; Bar Harbor, ME, United States) (Liu et al., 2017). Wild-type (WT) C57BL/6J mice were purchased from the Animal Core Facility of Nanjing Medical University (Nanjing, Jiangsu, China). All mice were housed in animal facilities under a standardized light-dark cycle and had free access to food and water.

Cell Culture and Treatment

Primary astrocyte cultures were established from midbrain of 1- to 2-day-old KO and WT mice as previously described (Hua et al., 2019). After washing twice with Dulbecco's phosphate-buffered saline (DPBS), tissues were digested with 0.25% trypsin solution at 37°C for 20 min and stopped by DMEM supplemented with 10% FBS to avoid overtrypsinization, which can severely damage the cells. After centrifugation at 1,500 rpm at room temperature (RT) for 5 min, the cell pellets were resuspended and cultured at 37°C in DMEM with 10% FBS, 100 mg/ml streptomycin, and 100 U/ml penicillin. The culture medium was replaced twice a week. Since neuronal cultures need a higher nutrient-rich media with neuronal supplements (e.g., B-27), neurons cannot survive in astrocyte growth medium without these neuronal supplements. Astrocytic cultures were subjected to one passage for purification purposes. The purity of astrocyte was more than 95% determined by immunostaining with antibodies against glial fibrillary acidic protein (GFAP). Astrocytes were incubated for 24 h with 800 μM MPP^+ after preincubation with 0.001∼100 μM PNU-282987 with or without an antagonist of α7nAChR MLA for 30 min.

MTT Assay

As previously described (Hua et al., 2019), cell viability was determined through the MTT assay. Briefly, cultures of astrocytes were plated on 96-well plates in growth media and were treated following the experimental design. After the supernatants were removed, the cells were incubated with 200 μl of 0.5 mg/ml MTT for 4 h at 37°C in a humidified atmosphere. Then, the MTT medium was removed and replaced with 200 μl DMSO at RT for 30 min. The absorbance of each well was measured at 570 nm with a microplate reader. After background OD subtraction, the results were expressed as a percentage in comparison to the control.

LDH Release

Using the LDH cytotoxicity detection kit, cell viability was measured by LDH release from mouse astrocytes. According to the manufacturer's instructions, the samples were quantified at 490 nm with a microplate reader.

Hoechst 33342 Staining

The apoptosis of astrocytes was detected by the Hoechst 33342 staining. Briefly, cultured astrocytes were fixed with 4% paraformaldehyde in 0.1 M phosphate-buffered saline (PBS) for 15 min and then stained with 5 mg/ml Hoechst 33342 for 15 min. After three rinses with PBS for 5 min, apoptotic cells characterized by nuclear condensation or fragmentation were visualized by fluorescence microscopy (Olympus BX 60, Tokyo, Japan).

Flow Cytometry Analysis of Apoptosis

The apoptosis of astrocytes was estimated using the Annexin V-FITC apoptosis detection kit according to the manufacturer's instructions. The samples from cultured astrocytes were incubated for 15 min in the dark with Annexin V-FITC and PI and then analyzed in a Guava easyCyte^{TM} 8HT system (Millipore, Billerica, MA, United States). The number of cells in each category is expressed as the percentage of the total number of cells counted.

TUNEL Assay

Primary astrocytes were grown on poly-d-lysine precoated glass slides, fixed, and permeabilized in 0.1% Triton X-100 (vol/vol) and 5% (vol/vol) bovine serum albumin (BSA) in PBS for 30 min. Subsequently, the percentage of apoptotic astrocytes was determined by double immunofluorescence staining for TUNEL and GFAP (1:1,000, #ab53554, Abcam, Cambridge, MA, United States) overnight at 4°C. Then, the slides were washed three times with PBS and incubated with the appropriate secondary antibody for 1 h at RT. After incubation with the anti−fade reagent with DAPI, the green fluorescein-labeled DNA was visualized by fluorescence microscopy (Olympus BX 60, Tokyo, Japan).

Western Blotting

As previously described (Hua et al., 2019), cell pellets were homogenized in 150 μl lysis buffer (50 mM Tris–HCl, pH 7.4, 150 mM NaCl, 1% Nonidet P-40, 1 mM sodium orthovanadate, protease inhibitor cocktail, and phosphotransferase inhibitor cocktail). After being electro-transferred to polyvinylidene fluoride membranes, proteins were incubated in tris-buffered saline with tween (TBST, pH 7.4, 10 mM Tris–HCl, 150 mM NaCl, 0.1% Tween-20) with 5% BSA at RT for 1 h. Then, the following primary antibodies were incubated with: anti-Bax (1:1,000, #2772, Cell Signaling Technology, Danvers, MA, United States), anti-Bcl2 (1:1,000, #2876, Cell Signaling Technology, Danvers, MA, United States), anti-cleaved-caspase-3 (1:500, #9664, Cell Signaling Technology, Danvers, MA, United States), anti- caspase-3 (1:1,000, #9662, Cell Signaling Technology, Danvers, MA, United States), anti-p-p53 (1:500, #9284, Cell Signaling Technology, Danvers, MA, United States), anti-p53 (1:1,000, #2524, Cell Signaling Technology, Danvers, MA, United States), anti-p-JNK (1:1,000, #4668, Cell Signaling Technology, Danvers, MA, United States), anti-JNK (1:1,000, #9252, Cell Signaling Technology, Danvers, MA, United States), and β-actin (BL005B, 1:5,000, Biosharp, Beijing, China) in TBST at 4°C overnight. Followed by four washes, the membranes were incubated for 1 h in TBST containing a secondary antibody. The blots were incubated in HRP-conjugated secondary antibodies, and signals were detected by enhanced chemiluminescence (ECL) reagents (Pierce, Rockford, IL, United States). The membranes

were scanned and analyzed using the Tanon 5200 (Tanon, Shanghai, China).

Statistical Analysis

All data were expressed as mean ± SEM. Differences among means were analyzed using SPSS 17.0 statistical software by means of one-way or two-way analysis of variance (ANOVA), followed by Tukey's multiple comparison *post hoc* test. In all values, $p < 0.05$ was considered statistically significant.

RESULTS

PNU-282987 Reverses MPP^+-Induced Cytotoxicity in Primary Cultured Astrocytes

To explore the protective effect of the α7nAChR agonist PNU-282987 on the MPP^+-induced cell injury, we pretreated cultured astrocytes with different concentrations of PNU-282987 (0.001, 0.01, 0.1, 1, 10, and 100 μM) for 30 min and then incubated with 800 μM MPP^+ for 24 h, as shown in **Figure 1**. In cultured astrocytes, 800 μM MPP^+ caused a 23.3% reduction in control cell viability (100.4% ± 0.6 and 76.7% ± 0.7; control and MPP^+ alone, respectively; $p < 0.0001$ by one-way ANOVA). PNU-282987 treatment significantly enhanced cell viability in a concentration-dependent manner (80.5% ± 1.7, 81.7% ± 1.9, 87.2% ± 2.2, 90.6% ± 2.2, 99.0% ± 1.0, and 100.4% ± 1.3; 0.001, 0.01, 0.1, 1, 10, and 100 μM of PNU-282987, respectively; $p = 0.067$ for 0.001 μM, $p = 0.031$ for 0.01 μM, $p = 0.001$ for 0.1 μM, $p < 0.001$ for 1∼100 μM by one-way ANOVA) compared with the MPP^+ only group (**Figure 1A**). Meanwhile, MPP^+ alone for 24 h increased LDH leakage by 56.0% compared to the control cells (100.0% ± 0.4 and 156.0% ± 1.7; control and MPP^+ alone, respectively; $p < 0.001$ by one-way ANOVA), whereas pretreatment with PNU-282987 attenuated this LDH leakage (150.3% ± 1.2, 143.2% ± 2.5, 133.3% ± 2.4, 128.6% ± 1.9, 108.0% ± 3.2, and 103.9% ± 1.7; 0.001, 0.01, 0.1, 1, 10, and 100 μM of PNU-282987, respectively; $p = 0.050$ for 0.001 μM, $p = 0.014$ for 0.01 μM, $p = 0.002$ for 0.1 μM, $p < 0.001$

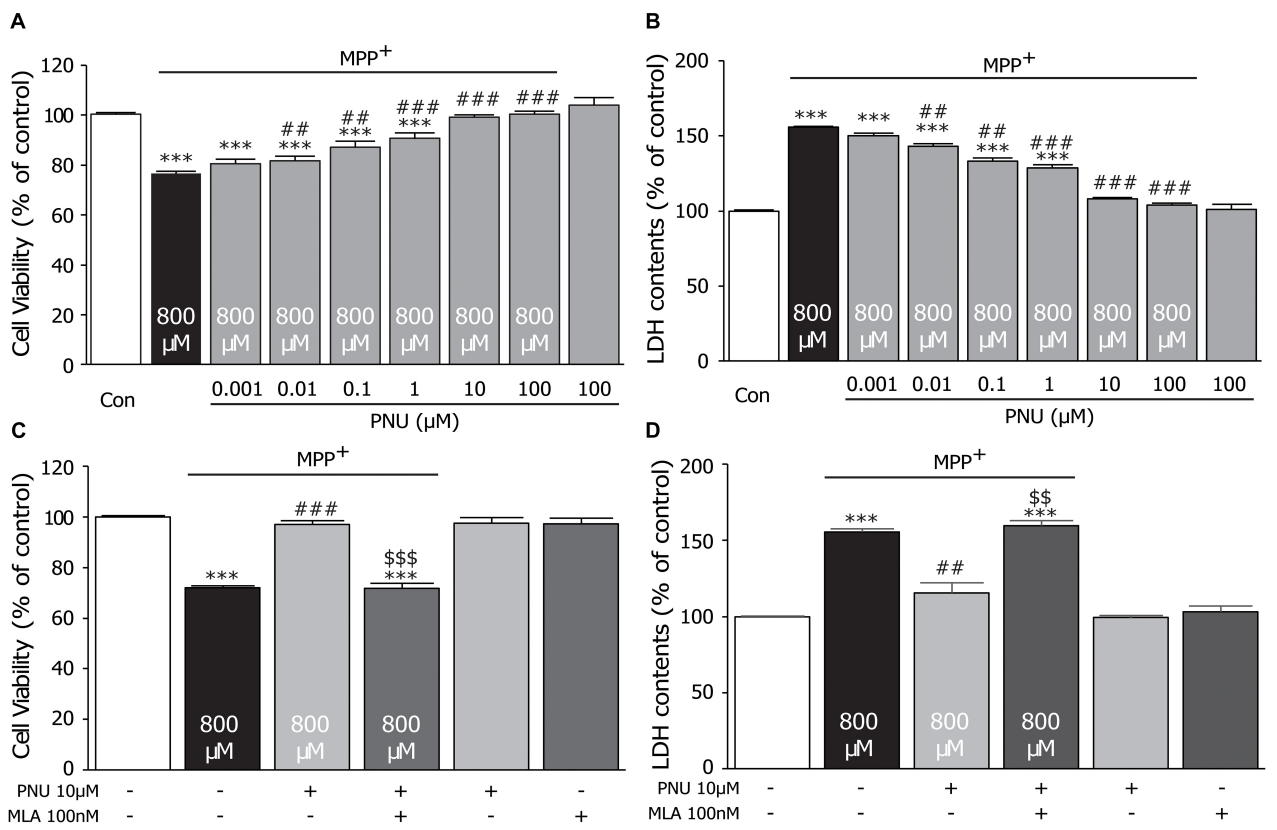

FIGURE 1 | The protective effects of PNU-282987 on cell viability of primary cultured astrocytes after MPP^+ injury. A 30-min pretreatment with PNU-282987 (0.001, 0.01, 0.1, 1, 10, or 100 μM) inhibited 800 μM MPP^+-induced cultured astroglial death after 24 h. **(A)** Pretreatment with PNU-282987 significantly promoted the viability of astrocytes in a concentration-dependent manner after MPP^+ injury. **(B)** Pretreatment with PNU-282987 decreased the release of LDH from astrocytes in a concentration-dependent manner after MPP^+ injury. **(C)** Pretreatment with 10 μM PNU-282987 with 100 nM MLA abolished the increased viability of astrocytes shown in the pretreatment with PNU-282987 only after MPP^+ injury. **(D)** Pretreatment with 10 μM PNU-282987 with 100 nM MLA abolished the reduced release of LDH from astrocytes shown in the pretreatment with PNU-282987 only after MPP^+ injury. Data are presented as mean ± SEM of three independent experiments. $^{***}p < 0.001$ vs. control group; $^{\#\#\#}p < 0.001$, $^{\#\#}p < 0.01$ vs. MPP^+ treatment group; $^{\$\$\$}p < 0.001$, $^{\$\$}p < 0.01$ vs. PNU-282987 treatment group. Con, control; PNU, PNU-282987; MLA, methyllycaconitine; LDH, lactate dehydrogenase.

for 1∼100 μM by one-way ANOVA) in cultured astrocytes (**Figure 1B**). There was no significant difference in the viability of cells (103.9% ± 3.2) or the leakage of LDH (101.2% ± 1.8) with 100 μM PNU-282987 alone. Furthermore, the neuroprotective effects of PNU-282987 on cell viability (100.0% ± 1.3 in control; 72.1% ± 0.7 in MPP^+ alone, $p < 0.001$; 96.9% ± 1.8 in MPP^+ + PNU-282987, $p < 0.001$ vs. MPP^+ alone; 71.9% ± 1.7 in MPP^+ + PNU-282987 + MLA, $p < 0.001$ vs. control, $p < 0.001$ vs. MPP^+ + PNU-282987; one-way ANOVA) and LDH leakage (100.0% ± 0.3 in control; 155.6% ± 2.1 in MPP^+ alone, $p < 0.001$; 115.5% ± 6.8 in MPP^+ + PNU-282987, $p = 0.005$ vs. MPP^+ alone; 159.8% ± 3.3 in MPP^+ + PNU-282987 + MLA, $p < 0.001$ vs. control, $p = 0.004$ vs. MPP^+ + PNU-282987; one-way ANOVA) of cultured astrocytes were blocked by 100 nM MLA (**Figures 2C,D**). MLA alone did not affect cell viability (97.3% ± 2.9) and LDH leakage (103.1% ± 3.7) of cultured astrocytes. These results indicate that PNU-282987 protects against MPP^+-induced astrocyte damage and also supports the hypothesis that the neuroprotective effects of PNU-282987 on astrocytes are mediated through α7nAChRs. Based on the observations, we chose 10 μM PNU-282987 as the optimal concentration for the following experiment.

PNU-282987 Alleviates MPP^+-Induced Apoptosis in Primary Cultured Astrocytes

To further investigate the effects of PNU-282987 on the neurotoxicity of MPP^+ the MPP^+-induced apoptotic changes of cultured astrocytes with or without PNU-282987 were investigated, as shown in **Figure 2**. The Hoechst 33258 staining assay revealed that the rate of apoptotic cells, as indicated by dense granular fluorescence, was increased in MPP^+ only group compared with the control group (**Figures 2A,B**; 100.3% ± 1.1 and 583.1% ± 8.8; control and MPP^+ alone, respectively; $p < 0.001$ by one-way ANOVA). When pretreated with 10 μM PNU-282987 before exposure to 800 μM MPP^+ for 24 h, the rate of apoptotic cells was significantly reduced (**Figures 2A,B**; 119.7% ± 8.1 in MPP^+ + PNU-282987; $p < 0.001$ vs. MPP^+ alone by one-way ANOVA), revealing that PNU-282987 can

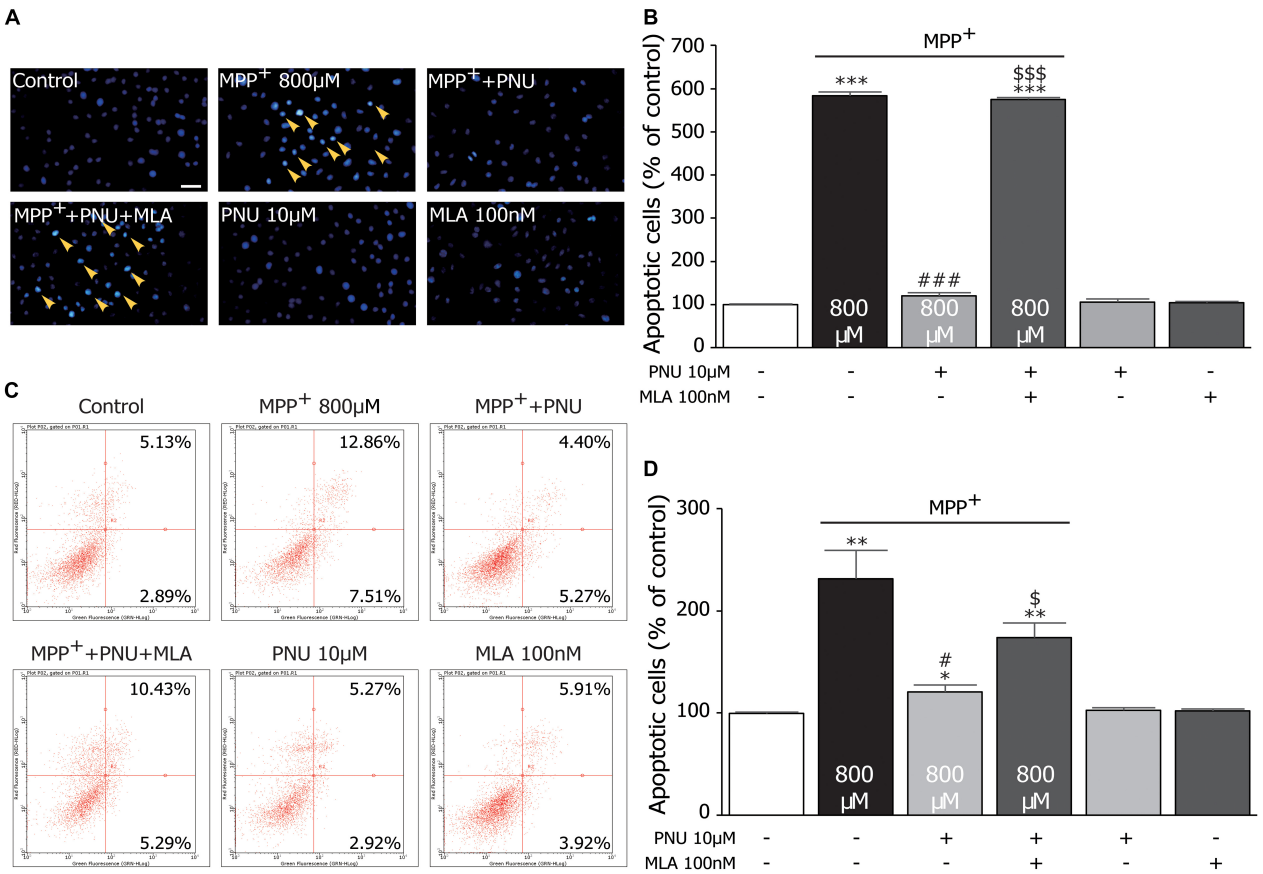

FIGURE 2 | The protective effects of PNU-282987 on MPP^+-induced apoptosis in primary cultured astrocytes. **(A)** Apoptotic cells characterized by cell shrinkage and chromatin condensation were examined by Hoechst 33342 staining and indicated by a yellow arrow. Scale bar: 200 μm. **(B)** Quantification for staining analysis was presented. **(C)** Apoptosis cells were stained with Annexin-V and propidium iodide and analyzed by flow cytometry. Representative picture and quantification for analysis treatment were shown. **(D)** Quantification for flow cytometry analysis was presented. Data are presented as mean ± SEM of three independent experiments. $^{***}p < 0.001$, $^{**}p < 0.01$, and $^{*}p < 0.05$ vs. control group; $^{###}p < 0.001$ and $^{#}p < 0.05$ vs. MPP^+ treatment group; $^{\$\$\$}p < 0.001$ and $^{\$}p < 0.05$ vs. PNU-282987 treatment group. Con, control; PNU, PNU-282987.

protect cultured astrocytes against MPP^+-induced apoptosis. Similarly, a flow cytometric analysis for apoptosis also indicated that 800 μM MPP^+ caused significant apoptosis (99.8% ± 1.3 and 231.5% ± 28.0; control and MPP^+ alone, respectively; $p = 0.009$ by one-way ANOVA), which was inhibited by pretreatment with 10 μM PNU-282987 in cultured astrocytes (**Figures 2C,D**; 173.7% ± 14.2 in MPP^+ + PNU-282987; $p = 0.018$ vs. MPP^+ alone by one-way ANOVA). These antiapoptotic effects of PNU-282987 were expectedly reversed by pretreatment with 100 nM MLA (**Figure 2B**; 575.2% ± 3.9 in MPP^+ + PNU-282987 + MLA; $p < 0.001$ vs. MPP^+ + PNU-282987 by one-way ANOVA; **Figure 2D**; 173.7% ± 14.2 in MPP^+ + PNU-282987 + MLA; $p = 0.028$ vs. MPP^+ + PNU-282987 by one-way ANOVA). These findings confirm that PNU-282987 produces antiapoptotic effects in MPP^+-stimulated neurotoxicity *via* astroglial α7nAChRs.

PNU-282987 Decreases the Number of $TUNEL^+/GFAP^+$ Cells in Primary Cultured Astrocytes

To confirm the effect of PNU-282987 on astroglial apoptosis, we examined MPP^+-stimulated astrocytes using GFAP and TUNEL double labeling. As shown in **Figure 3**, very few $TUNEL^+$ cells were observed in control cultures, whereas substantial $TUNEL^+$ cells were detected after 24 h exposure to MPP^+ (100.2% ± 1.1 and 555.9% ± 40.8; control and MPP^+ alone, respectively; $p < 0.001$ by one-way ANOVA). Pretreatment with 10 μM PNU-282987 decreased the number of $TUNEL^+/GFAP^+$ cells (127.0% ± 3.9; $p < 0.001$ vs. MPP^+ alone by one-way ANOVA), which could be blocked by 100 nM MLA (580.2% ± 42.8; $p < 0.001$ vs. MPP^+ + PNU-282987 by one-way ANOVA). Altogether, these results indicate that α7nAChR activation has been shown to protect astrocytes from MPP^+-induced apoptosis.

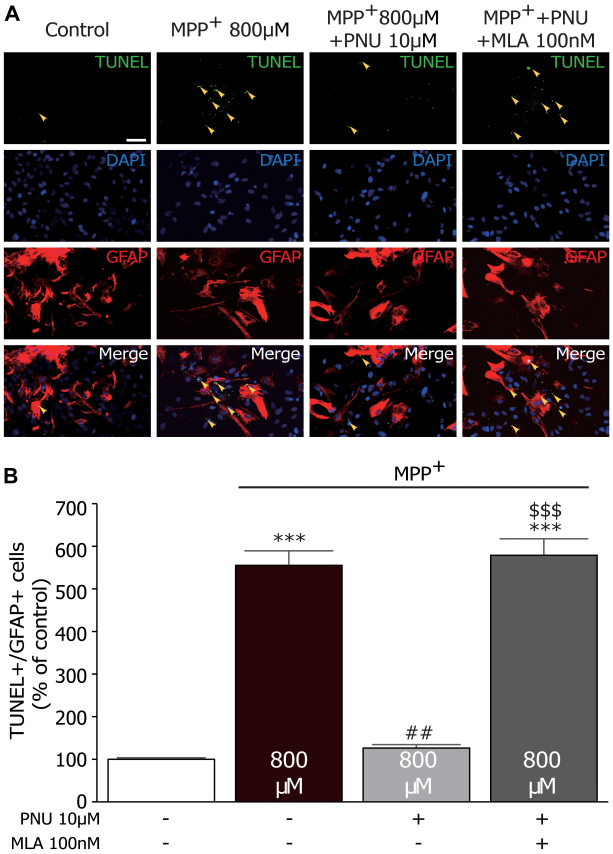

FIGURE 3 | The effects of PNU-282987 on MPP^+-induced increase of $TUNEL^+/GFAP^+$ cells in primary cultured astrocytes. **(A)** Astrocytes were incubated with primary antibody against GFAP and TUNEL. Images were collected on the fluorescence microscopy. The yellow arrows show significantly increased expression of TUNEL staining in the nucleus of astrocytes. **(B)** Quantitative analysis of PNU-282987-induced protection as measured by $TUNEL^+/GFAP^+$ staining produced a significant neuroprotective effect. $^{***}p < 0.001$ vs. control group; $^{\#\#}p < 0.01$ vs. MPP^+ treatment group; $^{\$\$\$}p < 0.001$ vs. PNU-282987 treatment group. Con, control; PNU, PNU-282987; TUNEL, terminal deoxynucleotidyl transferase dUTP nick end labeling; GFAP, glial fibrillary acidic protein.

Pnu-282987 Exerts the Antiapoptotic Effect *via* Suppression of Jnk-p53-Caspase-3 Signaling in Primary Cultured Astrocytes

To examine the expression levels of apoptosis-associated proteins in cultured astrocytes exposed to MPP^+, the levels of cleaved-caspase-3, Bax, and Bcl-2 were analyzed by Western blot assay. As shown in **Figure 4**, MPP^+ stimulated the expression of cleaved-caspase-3 (100.3% ± 1.1 and 210.1% ± 12.3; control and MPP^+ alone, respectively; $p < 0.001$ by one-way ANOVA) and the ratio of Bax/Bcl-2 (99.5% ± 1.3 and 284.9% ± 6.1; control and MPP^+ alone, respectively; $p < 0.001$ by one-way ANOVA) compared to the control group. Pretreatment with 10 μM PNU-282987 reversed the MPP^+-induced alterations of cleaved-caspase-3 (**Figures 4A,D**; 136.6% ± 6.0; $p = 0.006$ vs. MPP^+ alone by one-way ANOVA) and Bax/Bcl-2 (**Figures 4A,E**; 94.0% ± 6.0; $p < 0.001$ vs. MPP^+ alone by one-way ANOVA). These results suggest that PNU-282987 reduces the ratios of cleaved-caspase-3/caspase-3 and Bax/Bcl-2, preventing MPP^+-induced apoptosis.

It is worth noting that JNK pathways have been implicated in many forms of neuronal apoptosis, including dopaminergic neurons in 1-methyl-4-phenyl-1,2,3,6-tetrahydropyridine (MPTP)-induced dopaminergic neurotoxicity (Saporito et al., 2000) and MPP^+-induced cell death (Choi et al., 1999). Furthermore, the phosphorylation of p53 is critically required for the apoptotic pathway by JNK signaling (Fuchs et al., 1998; Miller et al., 2000; Wang and Friedman, 2000). Thus, we hypothesize that these antiapoptotic effects of PNU-282987 in astrocytes are possibly involved in the regulation of JNK/p53 signaling pathways. Compared to the control group, 800 μM MPP^+ upregulated the expressions of p-JNK (**Figures 4A,B**; 100.2% ± 1.2 and 149.0% ± 6.4; control and MPP^+ alone, respectively; $p = 0.002$ by one-way ANOVA) and p-p53 (**Figures 4A,C**; 100.3% ± 1.3 and 218.6% ± 11.4; control and MPP^+ alone, respectively; $p < 0.001$ by one-way ANOVA)

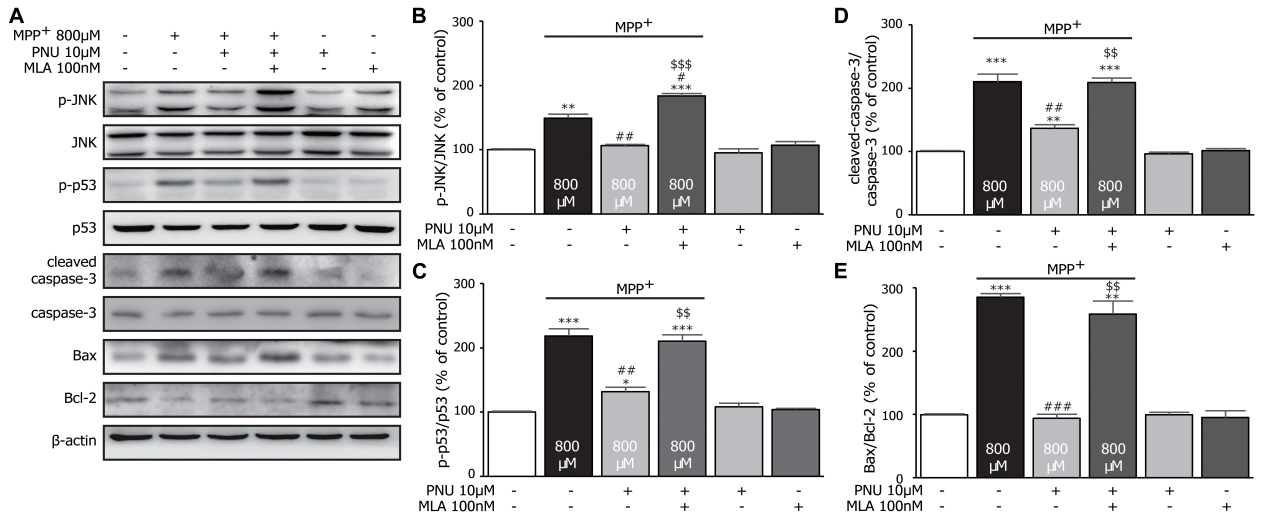

FIGURE 4 | The effects of PNU-282987 on MPP^+-induced expression of JNK-p53-caspase-3 signaling pathway in primary cultured astrocytes. **(A)** Representative immunoblot of p-JNK, JNK, p-p53, p53, cleaved-caspase-3, caspase-3, Bax, and Bcl-2 in cultured astrocytes. **(B)** Quantitation of p-JNK and JNK levels at baseline and in response to MPP^+ and PNU-282987 with or without MLA. **(C)** Quantitation of p-p53 and p53 levels at baseline and in response to MPP^+ and PNU-282987 with or without MLA. **(D)** Quantitation of cleaved-caspase-3 and caspase-3 levels at baseline and in response to MPP^+ and PNU-282987 with or without MLA. **(E)** Quantitation of Bax and Bcl-2 levels at baseline and in response to MPP^+ and PNU-282987 with or without MLA. Data are presented as mean ± SEM of three independent experiments. $^{***}p < 0.001$, $^{**}p < 0.01$, and $^{*}p < 0.05$ vs. control group; $^{###}p < 0.001$, $^{##}p < 0.01$, and $^{#}p < 0.05$ vs. MPP^+ treatment group; $^{\$\$\$}p < 0.001$ and $^{\$\$}p < 0.01$ vs. PNU-282987 treatment group. Con, control; PNU, PNU-282987; MLA, methyllycaconitine.

after 24 h exposure. Meanwhile, the pretreatment of 10 μM PNU-282987 decreased MPP^+-induced phosphorylation of JNK (106.2% ± 2.0; $p = 0.003$ vs. MPP^+ alone by one-way ANOVA) and p53 (132.0% ± 6.8; $p = 0.003$ vs. MPP^+ alone by one-way ANOVA), which was reversed by 100 nM MLA. Thus, we concluded that PNU-282987 was able to inhibit the phosphorylation of JNK-p53 signaling to prevent MPP^+-induced astroglial apoptosis.

Deficiency of α7nAChR Diminishes the Antiapoptotic Effects of PNU-282987

Furthermore, we used primary astrocytes derived from KO mice to investigate the roles of α7nAChR in regulating the antiapoptotic effects of PNU-282987 after MPP^+ exposure. As shown in **Figures 5A,B**, two-way ANOVA revealed a highly significant difference in cell viability and LDH leakage by genotype (cell viability: $F_{1,17} = 19.825$, $p = 0.001$; LDH leakage: $F_{1,17} = 45.246$, $p < 0.001$), treatment (cell viability: $F_{2,17} = 74.184$, $p < 0.001$; LDH leakage: $F_{2,17} = 293.169$, $p < 0.001$), and genotype × treatment (cell viability: $F_{2,17} = 17.137$, $p < 0.001$; LDH leakage: $F_{2,17} = 51.483$, $p < 0.001$). As found in the *in vivo* PD animal model (Liu et al., 2017) and *in vitro* SH-SY5Y cells (Xu et al., 2019), α7nAChR deficiency/knockdown did not affect the neurotoxicity of MPP^+ both in cell viability (**Figure 5A**; WT: 100.6% ± 0.8 in control and 75.0% ± 1.6 in MPP^+ alone, KO: 100.4% ± 2.2 in control and 74.1% ± 2.3 in MPP^+ alone) and LDH leakage (**Figure 5B**; WT: 100.4% ± 1.1 in control and 155.6% ± 2.1 in MPP^+ alone, KO: 99.5% ± 0.8 in control and 154.9% ± 1.7 in MPP^+ alone). However, compared to astrocytes derived from WT mice, the neuroprotective effects of PNU-282987 on cell viability (WT: 96.3% ± 3.6; KO: 74.0% ± 1.2, $p < 0.001$) and LDH leakage (WT: 116.2% ± 2.6; KO: 156.1% ± 4.1, $p < 0.001$) were abolished in astrocytes derived from KO mice. In addition, the antiapoptotic effect of PNU-282987 confirmed by a decrease in the number of apoptotic nuclei was also eliminated in astrocytes derived from KO mice (**Figures 5C,D**). These results indicate that the antiapoptotic effect of PNU-282987 in cultured astrocytes stimulated by MPP^+ is *via* an α7nAChR-dependent mechanism.

Deficiency of α7nAChR Abolishes the Inhibitory Effect of PNU-282987 on JNK-p53-Caspase-3 Signaling

Next, we tested whether α7nAChR deficiency changed the JNK-p53-caspase-3 signaling pathway in MPP^+-induced astroglial apoptosis. As shown in **Figure 6A**, two-way ANOVA revealed a highly significant difference in the expressions of p-JNK (genotype: $F_{1,17} = 69.269$, $p < 0.001$; treatment: $F_{2,17} = 162.551$, $p < 0.001$; genotype × treatment: $F_{2,17} = 77.330$, $p < 0.001$), p-p53 (genotype: $F_{1,17} = 42.936$, $p < 0.001$; treatment: $F_{2,17} = 227.694$, $p < 0.001$; genotype × treatment: $F_{2,17} = 44.312$, $p < 0.001$), leaved-caspase-3 (genotype: $F_{1,17} = 85.225$, $p < 0.001$; treatment: $F_{2,17} = 503.821$, $p < 0.001$; genotype × treatment: $F_{2,17} = 84.738$, $p < 0.001$), and the ratio of Bax/Bcl-2 (genotype: $F_{1,17} = 105.085$, $p < 0.001$; treatment: $F_{2,17} = 282.153$, $p < 0.001$; genotype × treatment: $F_{2,17} = 90.586$, $p < 0.001$). After 24 h exposure to MPP^+, both KO astrocytes and WT astrocytes exhibited the same alterations in the phosphorylation of JNK and p53, the increased expression of cleaved-caspase-3, and the upregulated ratio of Bax/Bcl-2 (**Figure 6**). However, α7nAChR

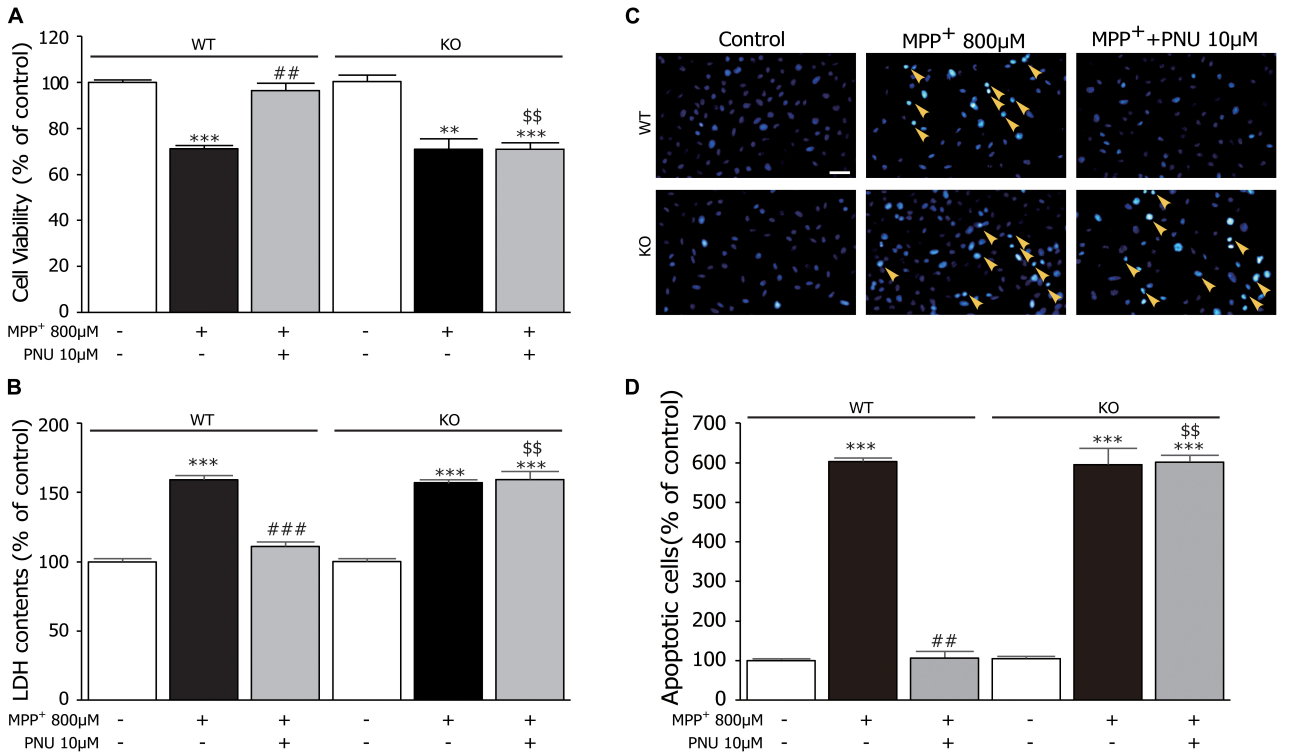

FIGURE 5 | α7nAChR deficiency abrogates the protective effects of PNU-282987 on primary cultured astrocytes after MPP^+ injury. **(A)** The effects of PNU-282987 on the viability of cells were abolished in cultured astrocytes from KO mice. **(B)** The effects of PNU-282987 on the release of LDH were abolished in cultured astrocytes from KO mice. **(C)** Apoptotic cells characterized by cell shrinkage and chromatin condensation were examined by Hoechst 33342 staining and indicated by a yellow arrow. Scale bar: 200 μm. **(D)** Quantification for Hoechst 33342 staining analysis was presented. Data are presented as mean ± SEM of three independent experiments. $^{***}p < 0.001$ and $^{**}p < 0.01$ vs. corresponding control group; $^{\#\#\#}p < 0.001$ and $^{\#\#}p < 0.01$ vs. corresponding MPP^+ treatment group; $^{\$\$}p < 0.01$ vs. PNU-282987-treated WT group. WT, astrocyte from wild-type mice; KO, astrocytes from α7nAChR KO mice; PNU, PNU-282987; LDH, lactate dehydrogenase.

deficiency diminished the inhibitory effect of PNU-282987 on the phosphorylation of JNK and p53. As expected, α7nAChR deficiency also abolished the regulation of PNU-282987 on the expressions of caspase-3/Bax/Bcl-2 signaling pathways. These data indicated that PNU-282987 alleviated apoptotic cell death induced by MPP^+ in cultured astrocytes mainly *via* the α7nAChR-JNK-p53 pathway.

DISCUSSION

The neuroprotective effects of activating α7nAChR on neurodegenerative disorders are receiving increasing attention. Previous studies suggest that α7nAChR activation exerts neuroprotective actions in PD models *in vitro* (Quik et al., 2015) and *in vivo* (Liu et al., 2015, 2017; Quik et al., 2015). We also confirmed that α7-nAChR agonists protected against MPP^+-induced apoptosis in SH-SY5Y cells *via* activating the ERK/p53 signaling pathway (Xu et al., 2019). In the present study, we further found the antiapoptotic effect of PNU-282987 *in vitro* using primary astrocytes exposed to MPP^+. PNU-282987 reversed the reduction of cell viability and the increase of cell apoptosis in primary astrocytes after MPP^+ exposure. Using α7nAChR KO mice, we indicate that the underlying protective mechanism of PNU-282987 was mediated through activating α7nAChR, suppressing the phosphorylation of JNK and p53, and then regulating the caspase-3/Bax/Bcl-2 signaling pathway. Therefore, the antiapoptotic effect of PNU-282987 on astrocytes may offer therapeutic benefits for neurodegenerative disorders such as PD.

MPP^+ is the toxic metabolite of MPTP and is formed by the oxidation of monoamine oxidase B, which is predominantly located in the astrocyte (Ransom et al., 1987). After taking up the dopamine reuptake system, MPP^+ can inhibit the function of mitochondrial complex I and subsequently induce selective dopaminergic neuronal degeneration in the substantia nigra (Langston et al., 1984). MPP^+ also has a direct toxic effect on astrocytes and results in the impairment of astrocyte functions, such as glutamate homeostasis (Di Monte et al., 1999), mitochondrial damage (Di Monte et al., 1992), oxidative stress (Wong et al., 1999), and apoptosis (Zhang et al., 2007). In agreement with these previous studies, we also found in the present study that treating the primary astrocytes with MPP^+ induced a loss of cell viability, cell shrinkage, and caspase-3 activation, which was associated with the increased Bax/Bcl-2 ratio. Furthermore, *via* a pharmacologic approach (using a

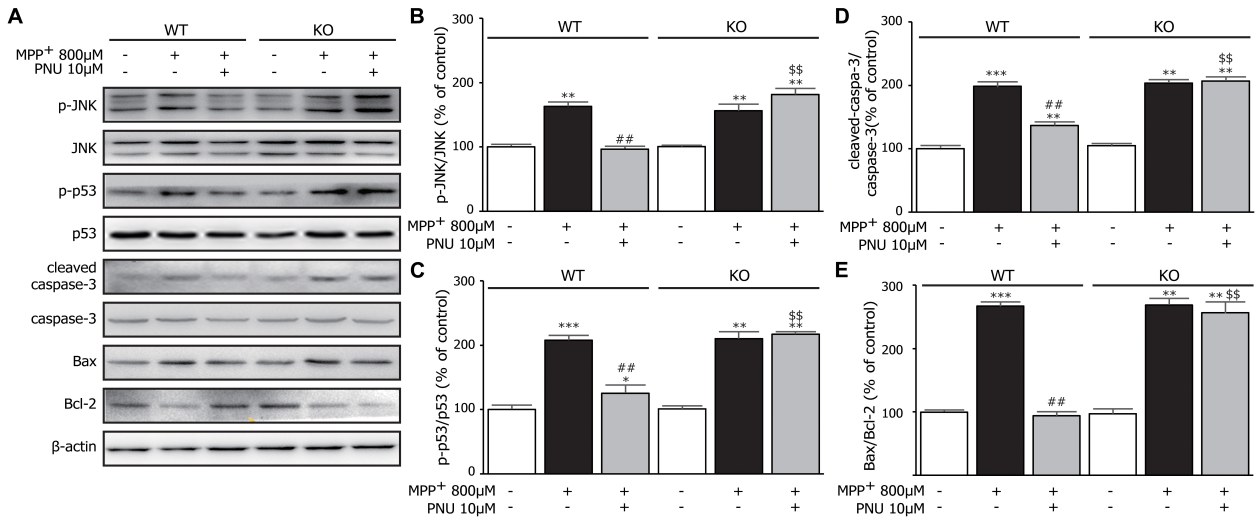

FIGURE 6 | The effects of α7nAChR deficiency on MPP^+-induced expression of the JNK-p53-caspase-3 signaling pathway in primary cultured astrocytes. **(A)** Representative immunoblot of p-JNK, JNK, p-p53, p53, cleaved-caspase-3, caspase-3, Bax, and Bcl-2 in WT and KO cultured astrocytes. **(B)** Quantitation of p-JNK and JNK levels at baseline and in response to MPP^+ and PNU-282987. **(C)** Quantitation of p-p53 and p53 levels at baseline and in response to MPP^+ and PNU-282987. **(D)** Quantitation of cleaved-caspase-3 and caspase-3 levels at baseline and in response to MPP^+ and PNU-282987. **(E)** Quantitation of Bax and Bcl-2 levels at baseline and in response to MPP^+ and PNU-282987. Data are presented as mean ± SEM of three independent experiments. $^{***}p < 0.001$, $^{**}p < 0.01$, and $^{*}p < 0.05$ vs. corresponding control group; $^{\#\#}p < 0.01$ vs. corresponding MPP^+ treatment group; $^{\$\$}p < 0.01$ vs. PNU-282987-treated WT group. WT, astrocyte from wild-type mice; KO, astrocytes from α7nAChR KO mice; PNU, PNU-282987.

selective α7nAChR inhibitor) and a genomic strategy (using α7nAChR KO mice), we characterized the functional role of α7nAChR in astrocytes and found that PNU-282987 attenuated MPP^+-induced astroglial apoptosis mainly *via* the α7nAChR-JNK-p53 pathway. The protective effect of PNU-282987 on astroglial survival may have a beneficial effect on the maintenance of astroglial function and attenuate delayed neuronal death in PD. Notably, previous studies indicate no vulnerability to MPTP/MPP^+ in α7nAChR KO mice (Liu et al., 2017) or knockdown SH-SY5Y cell (Xu et al., 2019). The findings in this study also showed no significant effect of α7nAChR deficiency on MPP^+ toxicity in cultured astrocytes, with no observed difference in alterations in cell apoptosis and JNK-p53-caspase-3 signaling. These data suggest that the expression of α7nAChR may not be necessary for MPTP/MPP^+-induced neurotoxicity both in neurons and astrocytes.

Increasing evidence reveals that apoptotic cell death serves an essential role in the pathogenesis of PD, causing the death of dopamine neurons in the substantia nigra (Burke, 1998). Astrocyte apoptosis is identified after reactive astrocytosis and contributes to the pathogenesis of brain injuries, including cerebral ischemia, Alzheimer's disease, and PD (Takuma et al., 2004). Several signals, such as glutamate toxicity, cytosolic Ca^{2+} elevation, oxidative stress, mitochondrial dysfunction, and inflammatory injury, can induce apoptosis in astrocytes *in vivo* and *in vitro*. As one of the major signaling cassettes of the mitogen-activated protein kinase (MAPK) signaling pathway, JNK signaling is a known important mediator of MPTP/MPP^+-induced apoptosis (Choi et al., 1999; Saporito et al., 2000). Additionally, numerous studies reported the ability of JNK to bind to and phosphorylate p53 (Fuchs et al., 1998; Wang and Friedman, 2000). During stress, the JNK signaling pathway can increase p53 transactivation and phosphorylation and then potentiate p53-dependent apoptosis (Miller et al., 2000). In the present study, we found that MPP^+ induced an increase in the cellular levels of p-JNK, p-p53, and cleaved caspase-3. Moreover, pharmacologic inhibition or genetic KO of α7nAChR diminished the inhibitory effects of PNU-282987 on MPP^+-induced activation of JNK, p53, and caspase-3. Thus, it is reasonable to indicate that α7nAChR activation prevents MPP^+-induced astroglial apoptosis *via* the inhibition of the JNK-p53-pathway.

Our previous study showed the regulative effects of PNU−282987 on the phosphorylation of JNK in SH−SY5Y cells *via* α7nAChRs−independent signaling (Xu et al., 2019). Notably, these inhibitory effects can be reversed by antagonism of α7nAChR but not by knockdown of α7−nAChR. Indeed, gene KO of α7nAChR involves the deletion strategy targeted exons 8–10 (Orr-Urtreger et al., 1997). KO mice show an absence of high-affinity [I-125] alpha-bungarotoxin sites, although no detectable abnormalities of high-affinity nicotine binding sites. However, gene knockdown leads to the degradation of that mRNA and abortive protein translation only. The expression of functional α7−nAChR was still detectable in α7−siRNA−transfected SH−SY5Y cells. In addition, there are lots of differences between adult and newborn rodents, such as GABA-dependent action potentials (Wang et al., 2001). The JNK and p53 pathways may play distinct roles in neonatal and adult astrocytes, and adult astrocyte cultures may be more useful in the studies of PD. Therefore, considering astrocyte cultures

from newborn mice in our present study, further experiments using conditional KO mice of α7−nAChR or adult astrocyte cultures are needed to examine how PNU−282987 modulates the JNK-p53 pathway.

CONCLUSION

In the present study, using either pharmacological inhibition or genetic KO of α7nAChR, we found that PNU−282987 protected against the MPP^+−induced apoptosis of cultured astrocytes *via* α7nAChR-JNK-p53 signaling pathway. These findings indicate the important roles of JNK-p53 signaling in the antiapoptotic response of astroglial α7nAChR and suggest that α7nAChR agonists may be validated as a potential target for modulating astrocyte activity to treat PD.

DATA AVAILABILITY STATEMENT

The data that support the findings of this study are available from the corresponding author upon reasonable request.

ETHICS STATEMENT

The animal study was reviewed and approved by the Institutional Animal Care and Use Committee of Nanjing Medical University. Written informed consent was obtained from the owners for the participation of their animals in this study.

AUTHOR CONTRIBUTIONS

YH, JH, and YF conceived and planned the experiments. YH and BY carried out the cellular experiments and performed the biochemical analysis. QC and JZ designed and performed the animal experiments. YH and JZ contributed to the interpretation of the results. YH and YF wrote the manuscript. All the authors reviewed and approved the final manuscript.

FUNDING

This study was supported by the grants from the National Natural Science Foundation of China (Nos. 81673408, 81703485, and 81603092).

REFERENCES

Acosta, C., Anderson, H. D., and Anderson, C. M. (2017). Astrocyte dysfunction in Alzheimer disease. *J. Neurosci. Res.* 95, 2430–2447. doi: 10.1002/jnr.24075

Albrecht, P. J., Dahl, J. P., Stoltzfus, O. K., Levenson, R., and Levison, S. W. (2002). Ciliary neurotrophic factor activates spinal cord astrocytes, stimulating their production and release of fibroblast growth factor-2, to increase motor neuron survival. *Exp. Neurol.* 173, 46–62. doi: 10.1006/exnr.2001.7834

Bertrand, D., Lee, C. H., Flood, D., Marger, F., and Donnelly-Roberts, D. (2015). Therapeutic potential of α7 nicotinic acetylcholine receptors. *Pharmacol. Rev.* 67, 1025–1073.

Booth, H. D. E., Hirst, W. D., and Wade-Martins, R. (2017). The role of astrocyte dysfunction in Parkinson's disease pathogenesis. *Trends Neurosci.* 40, 358–370. doi: 10.1016/j.tins.2017.04.001

Burda, J. E., Bernstein, A. M., and Sofroniew, M. V. (2016). Astrocyte roles in traumatic brain injury. *Exp. Neurol.* 275(Pt 3), 305–315. doi: 10.1016/j.expneurol.2015.03.020

Burke, R. E. (1998). Programmed cell death and Parkinson's disease. *Mov. Disord.* 13(Suppl. 1), 17–23.

Castagnet, P. I., Golovko, M. Y., Barceló-Coblijn, G. C., Nussbaum, R. L., and Murphy, E. J. (2005). Fatty acid incorporation is decreased in astrocytes cultured from alpha-synuclein gene-ablated mice. *J. Neurochem.* 94, 839–849. doi: 10.1111/j.1471-4159.2005.03247.x

Chinta, S. J., Woods, G., Demaria, M., Rane, A., Zou, Y., Mcquade, A., et al. (2018). Cellular senescence is induced by the environmental neurotoxin paraquat and contributes to neuropathology linked to Parkinson's disease. *Cell Rep.* 22, 930–940. doi: 10.1016/j.celrep.2017.12.092

Choi, W. S., Yoon, S. Y., Oh, T. H., Choi, E. J., O'malley, K. L., and Oh, Y. J. (1999). Two distinct mechanisms are involved in 6-hydroxydopamine- and MPP+-induced dopaminergic neuronal cell death: role of caspases. ROS, and JNK. *J. Neurosci. Res.* 57, 86–94. doi: 10.1002/(sici)1097-4547(19990701)57:1<86::aid-jnr9>3.3.co;2-5

Cotrina, M. L., Kang, J., Lin, J. H., Bueno, E., Hansen, T. W., He, L., et al. (1998). Astrocytic gap junctions remain open during ischemic conditions. *J. Neurosci.* 18, 2520–2537. doi: 10.1523/jneurosci.18-07-02520.1998

Di Monte, D. A., Tokar, I., and Langston, J. W. (1999). Impaired glutamate clearance as a consequence of energy failure caused by MPP(+) in astrocytic cultures. *Toxicol. Appl. Pharmacol.* 158, 296–302. doi: 10.1006/taap.1999.8717

Di Monte, D. A., Wu, E. Y., Delanney, L. E., Irwin, I., and Langston, J. W. (1992). Toxicity of 1-methyl-4-phenyl-1,2,3,6-tetrahydropyridine in primary cultures of mouse astrocytes. *J. Pharmacol. Exp. Ther.* 261, 44–49.

Echeverria, V., Yarkov, A., and Aliev, G. (2016). Positive modulators of the α7 nicotinic receptor against neuroinflammation and cognitive impairment in Alzheimer's disease. *Prog. Neurobiol.* 144, 142–157. doi: 10.1016/j.pneurobio.2016.01.002

Efremova, L., Chovancova, P., Adam, M., Gutbier, S., Schildknecht, S., and Leist, M. (2017). Switching from astrocytic neuroprotection to neurodegeneration by cytokine stimulation. *Arch. Toxicol.* 91, 231–246. doi: 10.1007/s00204-016-1702-2

Egea, J., Buendia, I., Parada, E., Navarro, E., León, R., and Lopez, M. G. (2015). Anti-inflammatory role of microglial alpha7 nAChRs and its role in neuroprotection. *Biochem. Pharmacol.* 97, 463–472. doi: 10.1016/j.bcp.2015.07.032

Fellner, L., Irschick, R., Schanda, K., Reindl, M., Klimaschewski, L., Poewe, W., et al. (2013). Toll-like receptor 4 is required for α-synuclein dependent activation of microglia and astroglia. *Glia* 61, 349–360. doi: 10.1002/glia.22437

Fuchs, S. Y., Adler, V., Pincus, M. R., and Ronai, Z. (1998). MEKK1/JNK signaling stabilizes and activates p53. *Proc. Natl. Acad. Sci. U.S.A.* 95, 10541–10546. doi: 10.1073/pnas.95.18.10541

Gozes, I., Bassan, M., Zamostiano, R., Pinhasov, A., Davidson, A., Giladi, E., et al. (1999). A novel signaling molecule for neuropeptide action: activity-dependent neuroprotective protein. *Ann. N. Y. Acad. Sci.* 897, 125–135. doi: 10.1111/j.1749-6632.1999.tb07884.x

Gu, X. L., Long, C. X., Sun, L., Xie, C., Lin, X., and Cai, H. (2010). Astrocytic expression of Parkinson's disease-related A53T alpha-synuclein causes neurodegeneration in mice. *Mol. Brain* 3:12. doi: 10.1186/1756-6606-3-12

Hua, J., Yin, N., Xu, S., Chen, Q., Tao, T., Zhang, J., et al. (2019). Enhancing the astrocytic clearance of extracellular α-synuclein aggregates by ginkgolides attenuates neural cell injury. *Cell. Mol. Neurobiol.* 39, 1017–1028. doi: 10.1007/s10571-019-00696-2

Iglesias, J., Morales, L., and Barreto, G. E. (2017). Metabolic and inflammatory adaptation of reactive astrocytes: role of PPARs. *Mol. Neurobiol.* 54, 2518–2538. doi: 10.1007/s12035-016-9833-2

Kalia, L. V., and Lang, A. E. (2015). Parkinson's disease. *Lancet* 386, 896–912. doi: 10.1016/S0140-6736(14)61393-3

Kim, J. M., Cha, S. H., Choi, Y. R., Jou, I., Joe, E. H., and Park, S. M. (2016). DJ-1 deficiency impairs glutamate uptake into astrocytes via the regulation of flotillin-1 and caveolin-1 expression. *Sci. Rep.* 6:28823. doi: 10.1038/srep28823

Kim, S. Y., Kang, K. L., Lee, J. C., and Heo, J. S. (2012). Nicotinic acetylcholine receptor α7 and β4 subunits contribute nicotine-induced apoptosis in periodontal ligament stem cells. *Mol. Cells* 33, 343–350. doi: 10.1007/s10059-012-2172-x

Langston, J. W., Irwin, I., Langston, E. B., and Forno, L. S. (1984). 1-Methyl-4-phenylpyridinium ion (MPP+): identification of a metabolite of MPTP, a toxin selective to the substantia nigra. *Neurosci. Lett.* 48, 87–92. doi: 10.1016/0304-3940(84)90293-3

Li, K., Li, J., Zheng, J., and Qin, S. (2019). Reactive astrocytes in neurodegenerative diseases. *Aging Dis.* 10, 664–675. doi: 10.14336/AD.2018.0720

Lin, Q., Balasubramanian, K., Fan, D., Kim, S. J., Guo, L., Wang, H., et al. (2010). Reactive astrocytes protect melanoma cells from chemotherapy by sequestering intracellular calcium through gap junction communication channels. *Neoplasia* 12, 748–754. doi: 10.1593/neo.10602

Liu, Y., Hao, S., Yang, B., Fan, Y., Qin, X., Chen, Y., et al. (2017). Wnt/β-catenin signaling plays an essential role in α7 nicotinic receptor-mediated neuroprotection of dopaminergic neurons in a mouse Parkinson's disease model. *Biochem. Pharmacol.* 140, 115–123. doi: 10.1016/j.bcp.2017.05.017

Liu, Y., Zeng, X., Hui, Y., Zhu, C., Wu, J., Taylor, D. H., et al. (2015). Activation of α7 nicotinic acetylcholine receptors protects astrocytes against oxidative stress-induced apoptosis: implications for Parkinson's disease. *Neuropharmacology* 91, 87–96. doi: 10.1016/j.neuropharm.2014.11.028

Liu, Z., and Chopp, M. (2016). Astrocytes, therapeutic targets for neuroprotection and neurorestoration in ischemic stroke. *Prog. Neurobiol.* 144, 103–120. doi: 10.1016/j.pneurobio.2015.09.008

Martin-Jiménez, C. A., García-Vega, Á, Cabezas, R., Aliev, G., Echeverria, V., González, J., et al. (2017). Astrocytes and endoplasmic reticulum stress: a bridge between obesity and neurodegenerative diseases. *Prog. Neurobiol.* 158, 45–68. doi: 10.1016/j.pneurobio.2017.08.001

Miklossy, J., Doudet, D. D., Schwab, C., Yu, S., Mcgeer, E. G., and Mcgeer, P. L. (2006). Role of ICAM-1 in persisting inflammation in Parkinson disease and MPTP monkeys. *Exp. Neurol.* 197, 275–283. doi: 10.1016/j.expneurol.2005.10.034

Miller, F. D., Pozniak, C. D., and Walsh, G. S. (2000). Neuronal life and death: an essential role for the p53 family. *Cell Death. Differ.* 7, 880–888. doi: 10.1038/sj.cdd.4400736

Mullett, S. J., and Hinkle, D. A. (2009). DJ-1 knock-down in astrocytes impairs astrocyte-mediated neuroprotection against rotenone. *Neurobiol. Dis.* 33, 28–36. doi: 10.1016/j.nbd.2008.09.013

Orr-Urtreger, A., Göldner, F. M., Saeki, M., Lorenzo, I., Goldberg, L., De Biasi, M., et al. (1997). Mice deficient in the alpha7 neuronal nicotinic acetylcholine receptor lack alpha-bungarotoxin binding sites and hippocampal fast nicotinic currents. *J. Neurosci.* 17, 9165–9171. doi: 10.1523/jneurosci.17-23-09165.1997

Pekny, M., and Nilsson, M. (2005). Astrocyte activation and reactive gliosis. *Glia* 50, 427–434. doi: 10.1002/glia.20207

Qiao, C., Yin, N., Gu, H. Y., Zhu, J. L., Ding, J. H., Lu, M., et al. (2016). Atp13a2 deficiency aggravates astrocyte-mediated neuroinflammation via NLRP3 inflammasome activation. *CNS Neurosci Ther.* 22, 451–460. doi: 10.1111/cns.12514

Quik, M., Zhang, D., Mcgregor, M., and Bordia, T. (2015). Alpha7 nicotinic receptors as therapeutic targets for Parkinson's disease. *Biochem. Pharmacol.* 97, 399–407. doi: 10.1016/j.bcp.2015.06.014

Ransom, B. R., Kunis, D. M., Irwin, I., and Langston, J. W. (1987). Astrocytes convert the parkinsonism inducing neurotoxin, MPTP, to its active metabolite, MPP+. *Neurosci. Lett.* 75, 323–328. doi: 10.1016/0304-3940(87)90543-x

Santello, M., Toni, N., and Volterra, A. (2019). Astrocyte function from information processing to cognition and cognitive impairment. *Nat. Neurosci.* 22, 154–166. doi: 10.1038/s41593-018-0325-8

Saporito, M. S., Thomas, B. A., and Scott, R. W. (2000). MPTP activates c-Jun NH(2)-terminal kinase (JNK) and its upstream regulatory kinase MKK4 in nigrostriatal neurons in vivo. *J. Neurochem.* 75, 1200–1208. doi: 10.1046/j.1471-4159.2000.0751200.x

Sorrentino, Z. A., Giasson, B. I., and Chakrabarty, P. (2019). α-Synuclein and astrocytes: tracing the pathways from homeostasis to neurodegeneration in Lewy body disease. *Acta Neuropathol.* 138, 1–21. doi: 10.1007/s00401-019-01977-2

Takuma, K., Baba, A., and Matsuda, T. (2004). Astrocyte apoptosis: implications for neuroprotection. *Prog. Neurobiol.* 72, 111–127. doi: 10.1016/j.pneurobio.2004.02.001

Teaktong, T., Graham, A., Court, J., Perry, R., Jaros, E., Johnson, M., et al. (2003). Alzheimer's disease is associated with a selective increase in alpha7 nicotinic acetylcholine receptor immunoreactivity in astrocytes. *Glia* 41, 207–211. doi: 10.1002/glia.10132

Valori, C. F., Guidotti, G., Brambilla, L., and Rossi, D. (2019). Astrocytes: emerging therapeutic targets in neurological disorders. *Trends Mol. Med.* 25, 750–759. doi: 10.1016/j.molmed.2019.04.010

Waak, J., Weber, S. S., Waldenmaier, A., Görner, K., Alunni-Fabbroni, M., Schell, H., et al. (2009). Regulation of astrocyte inflammatory responses by the Parkinson's disease-associated gene DJ-1. *FASEB J.* 23, 2478–2489. doi: 10.1096/fj.08-125153

Wang, J., and Friedman, E. (2000). Downregulation of p53 by sustained JNK activation during apoptosis. *Mol. Carcinog.* 29, 179–188. doi: 10.1002/1098-2744(200011)29:3<179::aid-mc7>3.0.co;2-k

Wang, Y. F., Gao, X. B., and Van Den Pol, A. N. (2001). Membrane properties underlying patterns of GABA-dependent action potentials in developing mouse hypothalamic neurons. *J. Neurophysiol.* 86, 1252–1265. doi: 10.1152/jn.2001.86.3.1252

Wong, S. S., Li, R. H., and Stadlin, A. (1999). Oxidative stress induced by MPTP and MPP(+): selective vulnerability of cultured mouse astrocytes. *Brain Res.* 836, 237–244. doi: 10.1016/s0006-8993(99)01661-3

Xu, J., Yu, S., Sun, A. Y., and Sun, G. Y. (2003). Oxidant-mediated AA release from astrocytes involves cPLA(2) and iPLA(2). *Free Radic. Biol. Med.* 34, 1531–1543. doi: 10.1016/s0891-5849(03)00152-7

Xu, S., Yang, B., Tao, T., Zhang, J., Liu, Y., Hu, J., et al. (2019). Activation of α7-nAChRs protects SH-SY5Y cells from 1-methyl-4-phenylpyridinium-induced apoptotic cell death via ERK/p53 signaling pathway. *J. Cell. Physiol.* 234, 18480–18491.

Zhang, S., Zhou, F., Ding, J. H., Zhou, X. Q., Sun, X. L., and Hu, G. (2007). ATP-sensitive potassium channel opener iptakalim protects against MPP-induced astrocytic apoptosis via mitochondria and mitogen-activated protein kinase signal pathways. *J. Neurochem.* 103, 569–579. doi: 10.1111/j.1471-4159.2007.04775.x

Conflict of Interest: The authors declare that the research was conducted in the absence of any commercial or financial relationships that could be construed as a potential conflict of interest.

frontiers in Cellular Neuroscience

MINI REVIEW
published: 02 April 2020
doi: 10.3389/fncel.2020.00075

Gliosis and Neurodegenerative Diseases: The Role of PET and MR Imaging

Carlo Cavaliere†, Liberatore Tramontano†, Dario Fiorenza, Vincenzo Alfano, Marco Aiello and Marco Salvatore*

IRCCS SDN, Naples, Italy

Glial activation characterizes most neurodegenerative and psychiatric diseases, often anticipating clinical manifestations and macroscopical brain alterations. Although imaging techniques have improved diagnostic accuracy in many neurological conditions, often supporting diagnosis, prognosis prediction and treatment outcome, very few molecular imaging probes, specifically focused on microglial and astrocytic activation, have been translated to a clinical setting. In this context, hybrid positron emission tomography (PET)/magnetic resonance (MR) scanners represent the most advanced tool for molecular imaging, combining the functional specificity of PET radiotracers (e.g., targeting metabolism, hypoxia, and inflammation) to both high-resolution and multiparametric information derived by MR in a single imaging acquisition session. This simultaneity of findings achievable by PET/MR, if useful for reciprocal technical adjustments regarding temporal and spatial cross-modal alignment/synchronization, opens still debated issues about its clinical value in neurological patients, possibly incompliant and highly variable from a clinical point of view. While several preclinical and clinical studies have investigated the sensitivity of PET tracers to track microglial (mainly TSPO ligands) and astrocytic (mainly MAOB ligands) activation, less studies have focused on MR specificity to this topic (e.g., through the assessment of diffusion properties and T2 relaxometry), and only few exploiting the integration of simultaneous hybrid acquisition. This review aims at summarizing and critically review the current state about PET and MR imaging for glial targets, as well as the potential added value of hybrid scanners for characterizing microglial and astrocytic activation.

Keywords: PET, MRI, gliosis, microglia, astrocytes, hybrid imaging, dual PET/MR agents, molecular imaging

OPEN ACCESS

Edited by:
Giovanni Cirillo, Universitá degli Studi della Campania Luigi Vanvitelli, Italy

Reviewed by:
Jorge Matias-Guiu, Complutense University of Madrid, Spain
Mathias Hoehn, Max-Planck-Gesellschaft (MPG), Germany

****Correspondence:***
Carlo Cavaliere
ccavaliere@sdn-napoli.it;
carlocavaliere1983@yahoo.it

† These authors have contributed equally to this work

Specialty section:
This article was submitted to Non-Neuronal Cells, a section of the journal Frontiers in Cellular Neuroscience

Received: *23 September 2019*
Accepted: *13 March 2020*
Published: *02 April 2020*

Citation:
Cavaliere C, Tramontano L, Fiorenza D, Alfano V, Aiello M and Salvatore M (2020) Gliosis and Neurodegenerative Diseases: The Role of PET and MR Imaging. Front. Cell. Neurosci. 14:75. doi: 10.3389/fncel.2020.00075

INTRODUCTION

Selective cortical or subcortical atrophy, neuronal death and shrinkage characterize pathological feature across different neurodegenerative diseases and brain disorders (Chi et al., 2018).

Nevertheless, exclusively neuron-centric approaches to neuropathological phenomena have not returned new breakthroughs in the prevention and therapy of brain disorders (Verkhratsky et al., 2014). This gap is due to the complexity of neuronal networks that cannot only be explained by neuronal activity, addressing research efforts to different actors in the central nervous system (CNS): the glia (Papa et al., 2014).

Glial cells, mainly represented by microglia and astrocytes, are key components for development and maintenance of brain functions and circuitry. Microglial cells correspond to the brain-resident macrophage playing an essential role for synaptic pruning, CNS repair, and mainly, as cellular mediators of neuroinflammation that characterizes different brain disorders (Colonna and Butovsky, 2017). Astrocytes instead, initially deputed to support neuronal activity, have now gained a central role in brain function, for example being part of the concept of tripartite synapse and gliotransmission for their effects on neuronal communication and plasticity (Pérez-Alvarez and Araque, 2013).

Increasing evidences support the role of an altered glial function as an underlying dynamic feature in psychiatric and neurological disorders (Garden and Campbell, 2016).

As pharmaceutical efforts begin to focus on glial specific targets, a limiting step in knowledge consists of the unavailability of validated biomarkers to assess and monitor gliosis longitudinally, supporting clinical management and potentially identifying best responders to cells-specific drugs (Garden and Campbell, 2016).

Accordingly, the interest in the development of novel methods to investigate glial activation and, more in general, neuroinflammation, has surged over the past 15 years. Neuroimaging offers a wide panel of non- or minimally invasive techniques to characterize neuroinflammatory processes.

Among different imaging techniques, non-invasive brain functional measurements using positron emission tomography (PET) and detailed morpho-functional information provided by magnetic resonance imaging (MRI) appeared the more appealing for translational purposes, being both used in preclinical and clinical settings.

In this context, hybrid PET/MR scanner represent the most advanced tool for molecular imaging, combining the functional specificity of PET radiotracers (e.g., targeting metabolism, hypoxia, inflammation, and specific membrane receptors) to both high-resolution and multiparametric information derived by MR in a single imaging acquisition session.

Aims of this review are: to summarize preclinical and clinical studies employing both PET and MRI techniques to investigate glial contribute in brain disorders; to critically review the main evidences raised up by PET glial tracers in neurodegenerative disorders and their feasibility in a clinical context; to investigate the potential added value of hybrid PET/MRI for characterizing microglial and astrocytic activation in neurological and psychiatric diseases.

HYBRID PET/MR SCANNER

Compared to other more widespread and validated hybrid imaging techniques, like PET/computed tomography (CT), PET/MR scanner constitutes the first real effort to effectively integrate two modalities by simultaneous acquisition, going beyond the serial PET/CT, assuring naturally co-registered multimodal images (Monti et al., 2017). The integration and coregistration of multimodal information achieved by different imaging techniques is essential for a complete understanding of the brain processes, representing a crucial step both for visual qualitative assessment and for multiparametric quantitative analysis. The retrospective coregistration of complex diagnostic datasets serially acquired on different scanners is typically achieved via software, through transformation algorithms based on the anatomical information of the CT component of PET/CT. Despite of the cost effectiveness of this approach compared to hybrid solutions, retrospective coregistration could be particularly challenging and technically demanding in un-collaborative patients (Monti et al., 2017). This problem is intrinsically overcome by hybrid scanners that allow you to simultaneously acquire images that share the same coordinate system (Zaidi and Guerra, 2011).

This innovation has been possible after the development of dedicated hardware components for each modality, and not mutually influenced by the magnetic field or photon pathway (Aiello et al., 2018).

Nowadays, integrated PET/MRI represents the most advanced tool for molecular imaging, opening new insights for the characterization of neurological and psychiatric disorders, and possibly for a multifaceted patient management (Aiello et al., 2015, 2016; Cavaliere et al., 2018a). Indeed, this innovative clinical diagnostic scanner allows to combine the functional specificity of PET radiotracers (e.g., targeting metabolism, hypoxia, inflammation, specific ligands, or receptors) to both high-resolution and multiparametric information derived by MR in a single imaging acquisition session (Herzog et al., 2010; Aiello et al., 2019). This simultaneity of findings achievable by PET/MR, if useful for reciprocal technical adjustments regarding temporal and spatial cross-modal alignment/synchronization, opens still debated insights about its clinical value in neurological patients, possibly incompliant and highly variable from a clinical point of view (Zaidi and Guerra, 2011; Cavaliere et al., 2018b).

Nuclear medicine imaging techniques, like PET, offer the unique opportunity to investigate *in vivo* and in a mini- or not-invasively manner, a plethora of molecular mechanisms, depending on the selectivity of the radio-tracer used. This potentiality has pushed radio-chemists and drug industries to test and investigate new potentially innovative tracers able to specifically target pathophysiological pathways, such as neuroinflammation, glial cells or membrane receptors to disentangle neurodegenerative phenomena (Herzog et al., 2010). However, stand-alone PET imaging is still limited by low spatial resolution, that obliges it to be co-registered to an higher resolution imaging techniques, such as CT and MR. Compared to CT, MRI provides different quantitative information (e.g., water and metabolites diffusion, metabolites concentrations, regional perfusion, and activation), simply modifying sequences' parameters, representing the gold standard for soft tissue and brain study and providing complementary information compared to PET imaging (Cavaliere et al., 2018b; Marchitelli et al., 2018). Moreover, the higher contrast resolution provided by MR can be more suitable for the segmentation of regions of reference useful to normalize PET signal in order to extract quantitative uptake parameters.

While, similarly to PET/CT scanners, findings derived by MRI and PET can be sequentially achieved in two different times, for highly dynamic systems like the brain this temporal gap could bias intermodality comparison. Indeed, sequential approach supposes that no significant modifications have occurred in the underlying state of the subject between two imaging sessions — a statement that could be ineffective both in physiological terms (e.g., changes in cognitive states or alertness) and in pathological conditions (e.g., psychiatric or neurological disorders) or as a result of medical interventions through psychological counseling, drugs or electrical/magnetic brain stimulations (Aiello et al., 2018; Cavaliere et al., 2018b). For these reasons, hybrid PET/MR scanners allow to overcome these limitations by simultaneously acquiring morphological, functional, molecular or metabolic information derived by both MRI and PET in a single shot.

PET AND MR IMAGING OF MICROGLIAL ACTIVATION

Neuroinflammation is a dynamic flogistic response which involve a complex multicellular cascade including the activation of both microglia and astrocytes, and the release of different neuroactive compounds.

Previous experimental studies have provided overwhelming evidence of the pivotal involvement of microglia-related molecular networks in the pathophysiology of many neurodegenerative and psychiatric diseases (Condello et al., 2018). However, the precise mechanisms by which microglia affect the disease's progression and modify neuropathology remain poorly understood.

Different activation phenotypes seem characterize chronic brain pathologies, ranging from a neuroprotective and anti-inflammatory M2 phenotype, mainly represented in an early stage, to the shift into the pro-inflammatory M1 phenotype, typical of later stages and contributing to neuronal dysfunction, injury, and disease progression (**Figure 1**) (Shen et al., 2018).

Therefore, the development of non-invasive molecular imaging methods able to dynamically characterize the spatio-temporal profile of neuroinflammatory biomarkers is widely attracting scientific and clinical interest, also for the application of immunomodulatory therapies both in clinical and preclinical settings (Narayanaswami et al., 2018).

Positron emission tomography imaging of microglia has emerged over recent years, through the development of target-specific radiotracers and, among these, mainly the translocator protein-18 kDa (TSPO) (**Table 1**) (**Figure 2**).

The first-generation radioligand [^{11}C](R)-PK11195 has been the most widely studied in clinical studies and different neurodegenerative diseases, including multiple sclerosis (Airas et al., 2018), Creutzfeldt-Jakob disease (Iaccarino et al., 2018), and also in psychiatric disorders such as schizophrenia (Di Biase et al., 2017). Although the findings of an increased uptake of this tracer in these pathologies, limitations including low signal-to-noise ratio and high non-specific binding has addressed for the synthesis of second- and third-generation TSPO-specific radiopharmaceuticals, linked to [^{11}C] or [^{18}F] and including

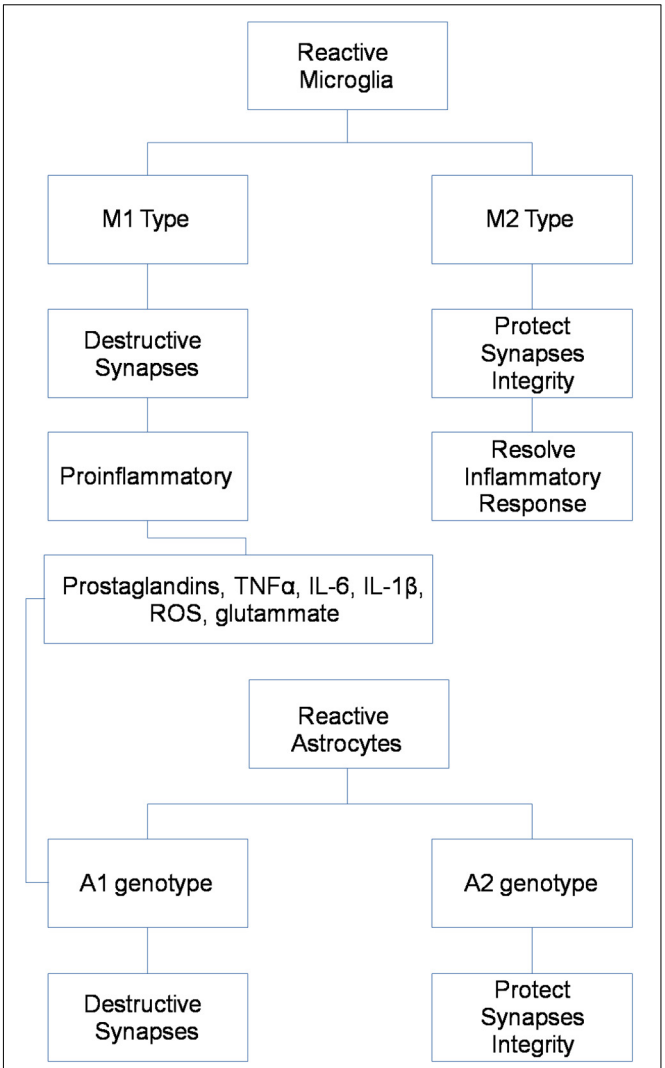

FIGURE 1 | Microglial and astrocytic phenotypes as possible targets for *in vivo* PET/MR imaging.

[^{11}C]-PBR28, [^{18}F]-DPA-714, [^{18}F]-PBR06, [^{18}F]-FEPPA, and [^{18}F]-GE-180 (all used in a clinical context, except for [^{18}F]-DPA-714) (Luo et al., 2018; Singhal et al., 2018; Best et al., 2019). Similarly, different studies have reported selective microglial uptake of these tracers in multiple sclerosis animal models and patients (Hagens et al., 2018; Herranz et al., 2019; Nack et al., 2019), amyotrophic lateral sclerosis (Zürcher et al., 2015; Datta et al., 2017), Alzheimer's disease (Alam et al., 2017; Keller et al., 2018; Focke et al., 2019), and Lyme disease on humans (Coughlin et al., 2018), and stroke experimental models (Miyajima et al., 2018), with more discordant results for psychiatric patients, suffering from schizophrenia (Di Biase et al., 2017; Hafizi et al., 2017; Ottoy et al., 2018; Selvaraj et al., 2018) and major depression (Li et al., 2018), probably due to the different stage of disease. Interestingly, one study on fibromyalgia subjects attempts to demonstrate specificity of TSPO tracers for microglia, considering that an high expression of this molecule was also

TABLE 1 | Main PET radiotracers used to investigate selective microglial and astrocytic activation.

PET radiotracer	Chemical structure	Target	Cellular target	Applications	References
2′-[^{18}F]-Fluoro-2′-deoxy-D-glucopyranose ([^{18}F]-FDG)	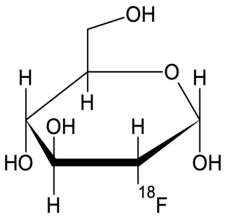	Glucose metabolism	Microglia and astrocytes	Human	Carter et al., 2019
[^{11}C]-PK11195	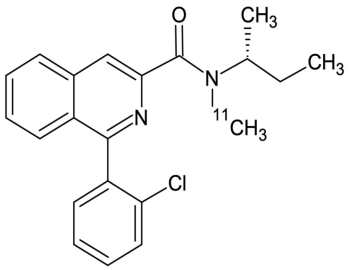	Translocator protein-18 kDa (TSPO)	Microglia and astrocytes	Human	Airas et al., 2018
[^{18}F]-GE-180	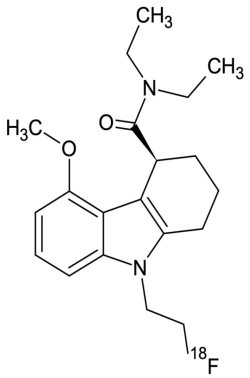	Translocator protein-18 kDa (TSPO)	Microglia and astrocytes	Human	Unterrainer et al., 2018
[^{18}F]-DPA-714	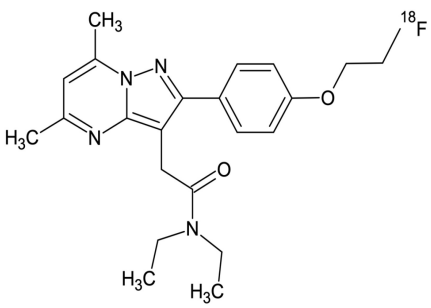	Translocator protein-18 kDa (TSPO)	Microglia and astrocytes	Animal	Luo et al., 2018
[^{18}F]-PBR06	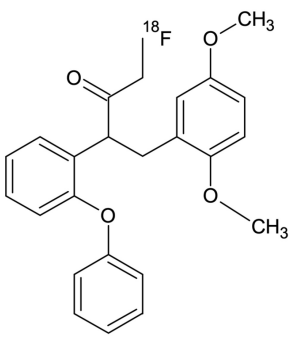	Translocator protein-18 kDa (TSPO)	Microglia and astrocytes	Human	Singhal et al., 2018

(Continued)

TABLE 1 | Continued

PET radiotracer	Chemical structure	Target	Cellular target	Applications	References
[^{11}C]-PBR28	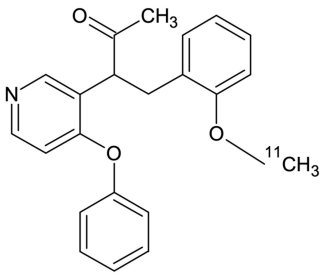	Translocator protein-18 kDa (TSPO)	Microglia and Astrocytes	Human	Albrecht et al., 2019
[^{18}F]-FEPPA	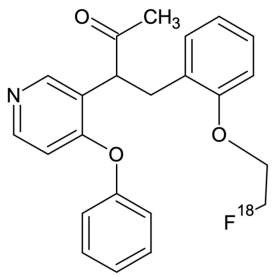	Translocator protein-18 kDa (TSPO)	Microglia and astrocytes	Human	Hafizi et al., 2017
[^{18}F]-Δ^8-THC	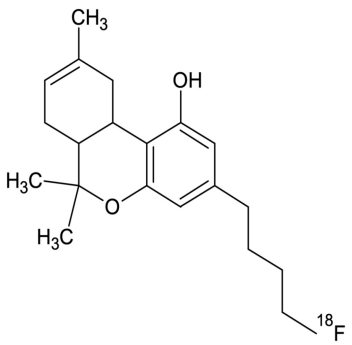	Endogenous cannabinoid system (CB2 receptor)	Microglia and astrocytes	Animal	Gifford et al., 2002
[^{11}C]-NE40	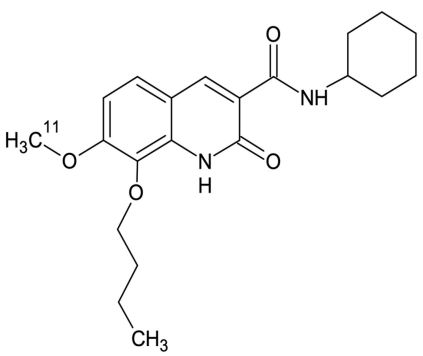	Endogenous cannabinoid system (CB2 receptor)	Microglia and astrocytes	Human	Ahmad et al., 2013
[^{11}C]-GSK1482160	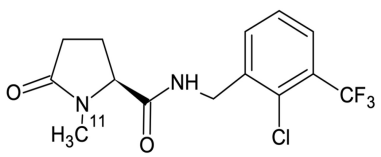	Purinergic receptor ($P2X_7R$)	Microglia	Human	Green et al., 2018

(Continued)

TABLE 1 | Continued

PET radiotracer	Chemical structure	Target	Cellular target	Applications	References
[^{11}C]-SMW139	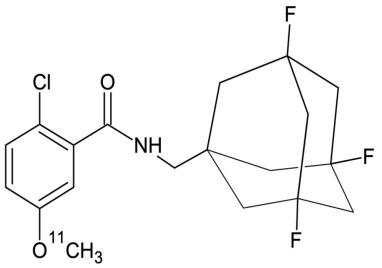	Purinergic receptor ($P2X_7R$)	Microglia	Human	Hagens et al., 2019
[^{18}F]-JNJ-64413739	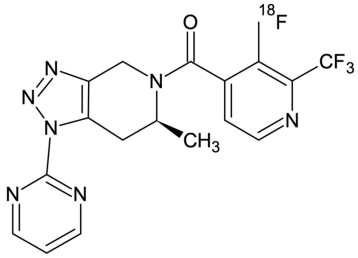	Purinergic receptor ($P2X_7R$)	Microglia	Animal	Kolb et al., 2019
[^{11}C]-Ketoprofen methyl ester	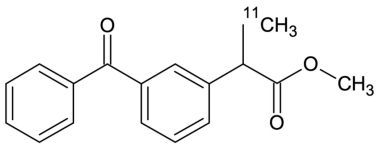	Cyclo-oxygenase 1 (COX-1)	Microglia	Human	Shukuri et al., 2011
[^{11}C]-Celecoxib	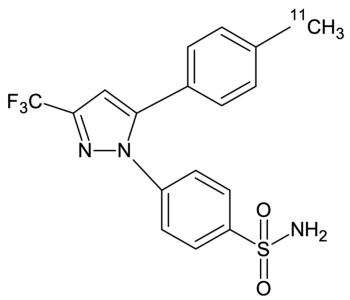	Cyclo-oxygenase 2 (COX-2)	Microglia	Animal	Kumar et al., 2018
[^{11}C]-CPPC	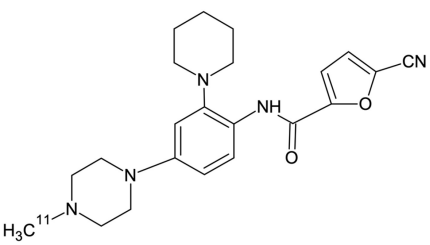	Macrophage colony-stimulating factor 1	Microglia	Animal	Horti et al., 2019
[^{11}C]-L-deprenyl-D_2	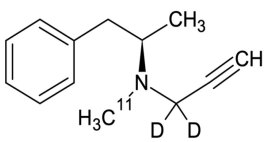	Mono-amine oxidase type B (MAOB)	Astrocytes	Human	Albrecht et al., 2019

(Continued)

TABLE 1 | Continued

PET radiotracer	Chemical structure	Target	Cellular target	Applications	References
[^{18}F]-THK5351	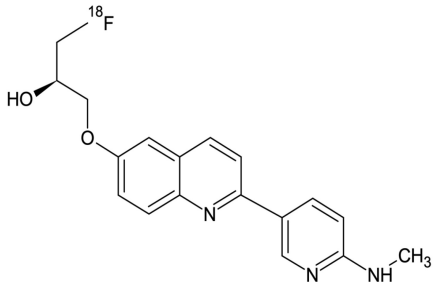	Mono-amine oxidase type B (MAOB)	Astrocytes	Human	Ishiki et al., 2018

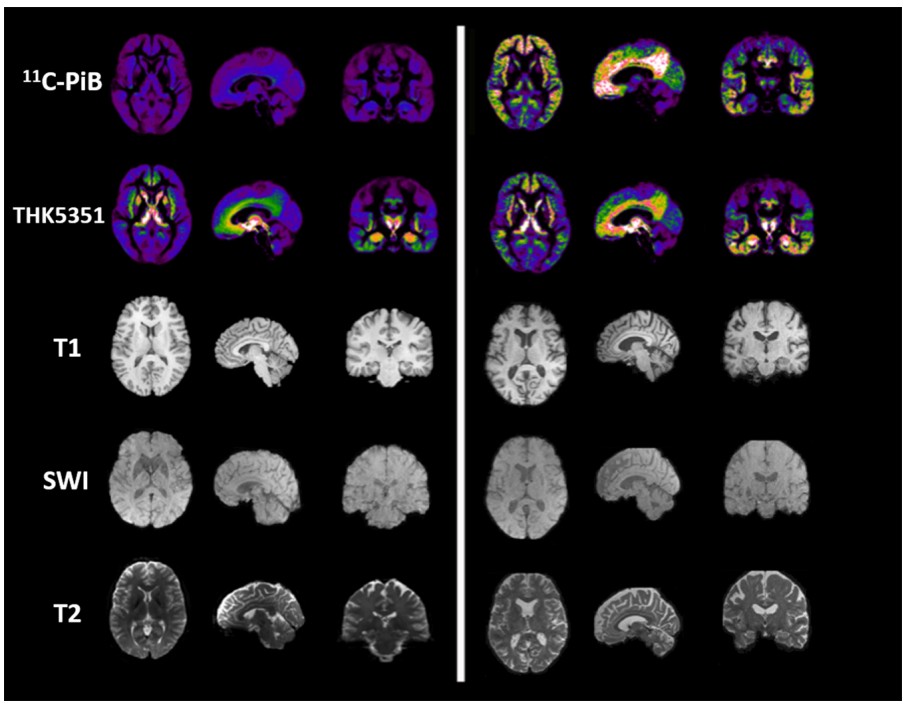

FIGURE 2 | Imaging examples in PET and MR imaging. The figure depicts, from left to right, axial, sagittal and coronal projections of healthy **(Left)** and AD spectrum **(Right)** brain for different PET (Shigemoto et al., 2018) and MR contrasts. From top to bottom row: microglial uptake as revealed by 11C-PiB PET tracer; astrocytic uptake as revealed by 18F-THK5351 PET tracer; structural 3D T1-weighted MR used as anatomical reference for PET and to highlight cortical atrophy and ventricular enlargement; 3D Susceptibility-weighted imaging MR linked to iron deposition and microgliosis; T2-weighted MR scan used for T2 mapping and astrogliosis.

detected in activated astrocytes (Albrecht et al., 2019). The authors, using [^{11}C]PBR28, which binds to the TSPO, and [^{11}C]-DED thought to primarily reflect astrocytic (but not microglial) signal, demonstrated although in a small size sample, a selective cortical uptake of microglial tracer but not of the astrocytic one (Albrecht et al., 2019).

Nevertheless, the application of TSPO tracers is affected by significant inter-subjects variability, essentially due to a rs6971 polymorphism that affects TSPO binding mainly in first- and second-generation radioligands (Hafizi et al., 2017), and more importantly, they are not able to differentiate microglial phenotype, distinguishing between conservative and detrimental activation. Moreover, although TSPO is upregulated in activated glial cells, its function and role in the immunity response is still unclear. Finally, considering that major evidences emerged by TSPO uptake in multiple sclerosis patients, and the very low brain uptake in healthy subjects, several doubts have been raised for the blood–brain barrier permeability of these tracers in physiological conditions (Albert et al., 2019).

For this reason, other microglial targets have been identified for specific radiotracers in animal models, such as the cannabinoid receptor type 2 ([18F]-D8-THC) (Ni et al., 2019; Gifford et al., 2002), the P2X7 receptor ([^{11}C]-GSK1482160) (Han et al., 2017), the cyclo-oxygenase 1

([^{11}C]-Ketoprofen methyl ester) (Shukuri et al., 2011), the cyclo-oxygenase 2 ([^{11}C]-Celecoxib) (Kumar et al., 2018), and the macrophage colony-stimulating factor 1 ([^{11}C]CPPC [5-cyano-N-(4-(4-[^{11}C]methylpiperazin-1-yl)-2-(piperidin-1-yl) phenyl)furan-2-carboxamide]) (Horti et al., 2019).

Regarding the use of MRI for microgliosis identification, less studies have tried to directly characterize microglial activation in specific brain regions. Changes of iron deposition, quantified using quantitative susceptibility mapping in MR, have been correlated with activated microglia/macrophages at edges of some chronic demyelinated lesions in patients suffering from multiple sclerosis (Dal-Bianco et al., 2017; Gillen et al., 2018; Hametner et al., 2018). Advanced diffusion models, based on neurite orientation dispersion and density imaging (NODDI) in MR, have been proved to be sensitive to microglial density and to the cellular changes associated with microglial activation in a preclinical setting (Yi et al., 2019). Finally, in amyotrophic lateral sclerosis patients, a technique based on diffusion spectroscopy has been applied to identify the increase of the predominantly glial metabolites (unspecific for microglia and astrocytes) tCr (creatine + phosphocreatine) and tCho (choline-containing compounds) in the primary motor cortex (Reischauer et al., 2018).

Despite the proved potential of both PET and MRI for the microglial imaging, very few studies have integrated both the modalities in humans and, generally, the majority use MRI to simply colocalize TSPO-uptake with multiple sclerosis plaques identified by MRI (Colasanti et al., 2014; Kang et al., 2018; Unterrainer et al., 2018; Kaunzner et al., 2019). Up to now, only three studies performed a simultaneous PET/MRI to investigate microglial activation in neurodegenerative diseases. The first one, using a selective P2X7R radiotracers in patients affected by Parkinson's disease, was not able to identify significant differences in PET uptake between patients and control subjects (van Weehaeghe et al., 2019). The second one, using a second-generation TSPO radiotracer in patients affected by multiple sclerosis, demonstrated microglial activation in both normal appearing cerebellum and segmented lesions (Barletta et al., 2019). The latter combines magnetic resonance spectroscopy of glial metabolites to TSPO-radiotracer uptake in patients affected by amyotrophic lateral sclerosis demonstrating a positive correlation between MR and PET biomarkers of neuroinflammation (Ratai et al., 2018) (**Figure 2**).

PET AND MR IMAGING OF ASTROCYTIC ACTIVATION

Astrocytes are the most abundant cell type in the brain, and participate to complex neuronal-glial interactions to assure synaptic homeostasis and metabolic sustainment for neurons (Miller, 2018). As for microglial cells, different phenotypes seem characterize astrocytic activation in physiological and pathological conditions, ranging from a pro-inflammatory A1 phenotype to a protective and anti-inflammatory A2 phenotype (**Figure 1**) (Miller, 2018).

Previously considered only as a supporting neuronal cells, astrocytic contributions to different neurodegenerative and psychiatric diseases has been recently revised (Papa et al., 2014).

Compared to microglial visualization, PET radiotracers specific for astrocytic function have been only recently applied for clinical purpose, mainly binding the mono-amine oxidase type B (MAOB) enzyme, highly expressed by activated astrocytes (**Table 1**) (**Figure 2**) (Ishibashi et al., 2019). PET studies using the MAOB radiotracers 11C-DED or [18F]THK5351 in patients affected by Alzheimer's disease have demonstrated an high correlation between brain tau deposition and astrocytic uptake (Harada et al., 2018) and between cortical glucose hypometabolism, detected by 18F-fluorodeoxyglucose [18F]-FDG PET, and longitudinal decline in astrocytic function detected by 11C-DED (Carter et al., 2019). These findings are in agreement with another clinical paper that demonstrate an increase of FDG uptake following selective activation of astrocytic glutamate transport (Zimmer et al., 2017). A specific regional increase of astrocytic function was also detected in two cases of progressive sopranuclear palsy studied with [18F]THK5351 PET (Ishiki et al., 2018).

Regarding the use of MRI to highlight astrocytic involvement in neurological and psychiatric diseases, few research groups have stressed MR potentiality to achieve this aim (**Figure 2**). Several preclinical studies proposed magnetic resonance spectroscopy to highlight lactate (Blanc et al., 2019) or acetate (Dehghani et al., 2017) peaks changes as surrogate markers specific for astrocytic metabolic homeostasis. However, magnetic field strength of clinically available scanner is not able to spectrally resolve these metabolites by surrounding peaks. In another clinical study (Alshelh et al., 2018), regional alterations in T2 relaxation times have been speculated as indicative of astroglial activation in patients suffered of neuropathic pain. More recently, the origin of signal used by functional MRI to investigate large-group of neuronal activations has been debated, considering preclinical evidences that evoked astrocytic Ca^{2+} waves can correlate with increased EEG power signal (Wang et al., 2018), astrocyte-evoked BOLD fluctuations (Takata et al., 2018), and transcranial direct current stimulation response (Monai and Hirase, 2018). These findings render furtherly more appealing the use of hybrid scanner that can acquire simultaneously PET, fMRI, and EEG signal (Mele et al., 2019).

Anyway, evidences derived by MRI on astrocytic activation are still confined to few groups, and often on limited samples. Few studies have serially used both PET and MRI with this purpose, and employing MR findings to colocalize PET uptake. In a longitudinal study on patients affected by corticobasal syndrome, [18F]THK5351 binding have been demonstrated to detect dynamical astrogliosis in specific cortical regions (Ezura et al., 2019). In a case of multiple sclerosis, instead, the authors demonstrated the coregistration of [18F]THK5351 uptake with demyelinating plaques (Ishibashi et al., 2019). Another study compared the spatial uptake patterns of [18F]THK5351 and fMRI network alterations in patients with early AD and healthy controls, showing a similar pattern for the precuneus, a region crucial for Alzheimer progression (Yokoi et al., 2018).

Finally, in patients suffering of semantic variant primary progressive aphasia, several authors demonstrated that the MAOB tracers can be more sensitive to detective neurodegenerative alterations compared to MRI (Kobayashi et al., 2018).

GLIAL PET RADIOTRACERS: A CRITICAL POINT OF VIEW

Despite the remarkable development of radiotracers for numerous molecular targets implicated in the process of neuroinflammation, only a few have been used on patients successfully.

TSPO PET Tracers

The main problems of TSPO tracers are that they cannot distinguish pro- and anti-inflammatory responses, they have a low signal-to-noise ratio and high non-specific binding, low dynamic response variation during neurodegenerative pathologies (**Figure 2**). Furthermore the main problem in the clinical use of these PET tracers is given the presence of polymorphism (SNP) in TSPO gene. These problems have been reduced and/or eliminated with second and third generation TSPO PET tracers, however, there is still no possible differentiation between the M1 (neurotoxic) and M2 (neuroprotective) genotypes. Moreover, even if the 3D pentameric structure of the TSPO has been revealed, the role of this receptor does not yet appear to be clear, since the influence of receptor upregulation as an immune reaction is not clear. Currently [18F] -GE180 is used as a third-generation tracer in clinical trials. Although [18F] -GE180 is able to pass in CNS only in case of blood–brain barrier breakdown, with low BBB permeability in human healthy brain, this radiotracer is a very important neuroinflammation imaging agent in various CNS diseases (Albert et al., 2019).

Cannabinoid Receptor Type 2 PET Tracers

Due to its high brain density, this receptor has been subjected to *in vivo* imaging using PET techniques using radioligands, such as Δ^8-Tetrahydrocannabinol (Δ^8-THC) labeled with fluorine-18. However, the PET images obtained after injection of [18F]-Δ^8-THC in primates do not show a particular specific region of cerebral localization, so much so that the radiotracer appears to be widely diffused in all regions of the brain (Gifford et al., 2002). Some of the synthetic derivatives of classic cannabinoids, which show nano affinity for CB2 receptors, may prove to be successful candidates for *in vivo* imaging of these receptors, including pyrazole derivatives and aminoalkylindole derivatives. Since the level of expression of CB2 receptors in the healthy brain is low and there is an increase of these receptors in pathological conditions, much research has focused on these receptors. To date only the radiotracer [^{11}C] -NE40 has been used in humans for biodistribution studies on healthy patients, to verify the uptake and washout (Ahmad et al., 2013). CB2 ligands are still in the preclinical evaluation phase, however, they can represent a valid alternative in the evaluation of microglial activation (Yamagishi et al., 2019).

Cyclooxygenase-2 PET Tracers

Despite the potential given by the study of the increase in cyclooxygenases (COX1 and COX2) in inflammation, actually only very few radiotracers have been synthesized and studied. For neuroinflammation studies it is mandatory to use selective radioligands for the respective isoforms COX1 and COX2. The advantage in the use of [^{11}C]-celecoxib is certainly represented by the ability to pass the blood–brain barrier, even when it is not damaged (Kumar et al., 2018).

$P2X_7$ Receptor PET Tracers

P2X7 receptor is an adenosine triphosphate ATP-gated purinoreceptor that is widely expressed in microglia and astrocytes. The activation of P2X7 receptor leads to the release of the proinflammatory mediators such as cytokine IL-1β in the brain. In fact the increase in the expression of this receptor leads to the activation of microglia, more than its over-expression is a consequence of the activation of microglia. Over the last years, research has focused on the synthesis and study of ligands of this receptor. The most promising are certainly: [^{11}C]-GSK1482160, [^{11}C]-SMW139, and [^{18}F]-JNJ-64413739. The first [^{11}C]-GSK1482160 has been studied in healthy volunteer patients for the estimation of radiopharmaceutical radiation dosimetry and biodistribution (Green et al., 2018). The first PET/MRI study, even if preliminary, on patients affected by multiple sclerosis was conducted in 2019 with the administration of [^{11}C]-SMW139 (Hagens et al., 2019). The Janssen compound [^{18}F]-JNJ-64413739 is labeled with fluorine-18, which certainly represents an advantage from a clinical point of view considering the longer radioisotope half-life (Kolb et al., 2019). [^{18}F]-JNJ-64413739 is still under evaluation in preclinical study phase and data on patients are not yet available, however, the first studies on animals show its potential as a PET tracer for neuroinflammation.

Macrophage Colony-Stimulating Factor 1 Receptor (CSF1R) PET Tracer

CSF1R is a surface receptor (tyrosine kinase family receptors) mainly expressed by microglia. Recently a specific radioligand of this receptor was synthesized and studied, [^{11}C]-CPPC (Horti et al., 2019). Even if this PET ligand is still in a preclinical phase of animal experiments, this new class of radioligands could be very promising for the study of microglial PET/MRI activation.

Monoamine Oxidase-B PET Tracers

During neuroinflammation, astrocytic increased MAO-B (amine oxidases) activity which leads to an oxidative stress due to the formation of hydrogen peroxides (Gulyás et al., 2011). Among PET ligands MAO-B studied and synthesized over the years, two radiotracers were successfully used in

patients, one of which containing carbon-11([^{11}C]-L-deprenyl-D2) (Arakawa et al., 2017), the other containing fluorine-18 ([^{18}F]-THK5351) (Ishibashi et al., 2019). The last one was used in a patient with relapsing-remitting multiple sclerosis (MS), it was seen that [^{18}F]-THK5351 accumulation corresponded to sites identified in MRI where there were MS plaques, in lesions undergoing astrogliosis.

BIMODAL PROBES AS FUTURE PERSPECTIVES

Although PET/MRI has been often addressed as the new frontier of molecular imaging (Chen and Chen, 2010), very few studies have employed this technique in glial imaging, and often limiting MR to a structural reference for PET signal. One possible innovation in this field could be represented by the development of an efficient and reliable PET/MR dual imaging probe, that if challenging for chemists and neuroscientists (Bouziotis et al., 2013; Vecchione et al., 2017), can help to identify killer applications for PET/MRI.

A general issue for new single- or multi-modal imaging probes that target the brain and that have to be taken into account is the permeability of the blood–brain barrier, a complex multicellular structure that protect CNS by external neurotoxic substances and which functions are assured also by astrocytic endfeet (Poupot et al., 2018). A possible solution is represented by the use of physiological transfer existing across the barrier, like the use of specific carriers or the transcytosis phenomenon (Pulgar, 2019).

Among novel imaging tools, different nanoparticles (usually smaller than 100 nm) have been extensively used in preclinical settings as MRI contrast agent combined with a PET tracer, mainly for oncological and more recently cardiovascular imaging (Aime et al., 2002; Uppal et al., 2011; Lewis et al., 2015; Kirschbaum et al., 2016; Vecchione et al., 2017; Grimaldi et al., 2019). Recently, a potential multimodal PET/MRI probe has been described to target microglia and neuroinflammation in a mouse model (Tang et al., 2018). The proposed nanoparticle selectively binds to the scavenger receptor class A (SR-A) expressed on activated microglia and is iron-oxide coated and so detectable by T2* -weighted MRI.

CONCLUSION

In this review main PET and MR imaging biomarkers for microglial and astrocytic activation have been summarized. Furthermore, these studies also demonstrate potential benefits for the integration of findings achievable by simultaneous PET/MRI scanners, although still few employed in the literature. While the technological challenges seem to be overcome with new powerful scanners able to *in vivo* characterize molecular processes, more efforts to identify selective glial targets and efficient multimodal imaging probes, potentially useful for tailored treatments targeting glial activation, are needed.

AUTHOR CONTRIBUTIONS

CC designed and wrote the manuscript. LT, DF, and VA wrote the manuscript and prepared figures/tables. MA and MS revised and approved the text.

REFERENCES

Ahmad, R., Koole, M., Evens, N., Serdons, K., Verbruggen, A., Bormans, G., et al. (2013). Whole-body biodistribution and radiation dosimetry of the cannabinoid type 2 receptor ligand [11C]-NE40 in healthy subjects. *Mol. Imaging Biol.* 15, 384–390. doi: 10.1007/s11307-013-0626-y

Aiello, M., Cavaliere, C., Fiorenza, D., Duggento, A., Passamonti, L., and Toschi, N. (2019). Neuroinflammation inneurodegenerative diseases: current multi-modal imaging studies and future opportunities for hybridPET/MRI. *Neuroscience* 403, 125–135. doi: 10.1016/j.neuroscience.2018.07.033

Aiello, M., Cavaliere, C., Marchitelli, R., d'Albore, A., De Vita, E., and Salvatore, M. (2018). Hybrid PET/MRIMethodology. *Int. Rev. Neurobiol.* 141, 97–128. doi: 10.1016/bs.irn.2018.07.026

Aiello, M., Cavaliere, C., and Salvatore, M. (2016). Hybrid PET/MR imaging and brain connectivity. *Front. Neurosci.* 10:64. doi: 10.3389/fnins.2016.00064

Aiello, M., Monti, S., Inglese, M., Forte, E., Cavaliere, C., Catalano, O. A., et al. (2015). A multimodalfusion scheme for the enhancement of PET/MR viewing. *Ejnmmi. Phys.* 2(Suppl.1):A32. doi: 10.1186/2197-7364-2-S1-A32

Aime, S., Frullano, L., and Crich, S. G. (2002). Compartmentalization of a gadolinium complex in the apoferritin cavity: a route to obtain high relaxivity contrast agents for magnetic resonance imaging. *Angewandte Chem. Int. Ed.* 41, 1017–1019. doi: 10.1002/1521-3773(20020315)41:6<1017::aid-anie1017>3.0.co;2-p

Airas, L., Nylund, M., and Rissanen, E. (2018). Evaluation of microglial activation in multiple sclerosis patients using positron emission tomography. *Front. Neurol.* 9:181. doi: 10.3389/fneur.2018.00181

Alam, M. M., Lee, J., and Lee, S. Y. (2017). Recent progress in the development of TSPO PET ligands for neuroinflammation imaging in neurological diseases. *Nucl. Med. Mol. Imaging* 51, 283–296. doi: 10.1007/s13139-017-0475-8

Albert, N. L., Unterrainer, M., Brendel, M., Kaiser, L., Zweckstetter, M., Cumming, P., et al. (2019). In response to: the validity of 18F-GE180 as a TSPO imaging agent. *Eur, J. Nucl. Med. Mol. Imaging* 46, 1208–1211. doi: 10.1007/s00259-019-04294-8

Albrecht, D. S., Forsberg, A., Sandström, A., Bergan, C., Kadetoff, D., Protsenko, E., et al. (2019). Brain glial activation in fibromyalgia - A multi-site positron emission tomography investigation. *Brain Behav. Immun.* 75, 72–83. doi: 10.1016/j.bbi.2018.09.018

Alshelh, Z., Di Pietro, F., Mills, E. P., Vickers, E. R., Peck, C. C., Murray, G. M., et al. (2018). Altered regional brain T2 relaxation times in individuals with chronic orofacial neuropathic pain. *Neuroimage Clin.* 19, 167–173. doi: 10.1016/j.nicl.2018.04.015

Arakawa, R., Stenkrona, P., Takano, A., Nag, S., Maior, R. S., and Halldin, C. (2017). Test-retest reproducibility of [11C]-L-deprenyl-D2 binding to MAO-B in the human brain. *Ejnmmi Res. Dec* 7:54. doi: 10.1186/s13550-017-0301-4

Barletta, V. T., Herranz, E., Treaba, C. A., Ouellette, R., Mehndiratta, A., Loggia, M., et al. (2019). Evidence of diffuse cerebellar neuroinflammation in multiple sclerosis by 11C-PBR28 MR-PET. *Mult. Scler.* doi: 10.1177/1352458519843048 [Epub ahead of print].

Best, L., Ghadery, C., Pavese, N., Tai, Y. F., and Strafella, A. P. (2019). New and old TSPO PET radioligands for imaging brain microglial activation in neurodegenerative disease. *Curr. Neurol. Neurosci. Rep* 19:24. doi: 10.1007/s11910-019-0934-y

Blanc, J., Roumes, H., Mazuel, L., Massot, P., Raffard, G., Biran, M., et al. (2019). Functional magnetic resonance spectroscopy at 7 T in the rat barrel cortex during whisker activation. *J. Vis. Exp.* 8:e58912. doi: 10.3791/58912

Bouziotis, P., Psimadas, D., Tsotakos, T., Stamopoulos, D., and Tsoukalas, C. (2013). Radiolabeled iron oxide nanoparticles as dual-modality SPECT/MRI and PET/MRI agents. *Curr. Top. Med. Chem.* 12, 2694–2702. doi: 10.2174/1568026611212230007

Carter, S. F., Chiotis, K., Nordberg, A., and Rodriguez-Vieitez, E. (2019). Longitudinal association between astrocyte function and glucose metabolism in autosomal dominant Alzheimer's disease. *Eur. J. Nucl. Med. Mol. Imaging* 46, 348–356. doi: 10.1007/s00259-018-4217-7

Cavaliere, C., Kandeepan, S., Aiello, M., Ribeiro de Paula, D., Marchitelli, R., Fiorenza, S., et al. (2018a). Multimodal neuroimaging approach to variability of functional connectivity in disorders ofconsciousness: a PET/MRI pilot study. *Front. Neurol.* 9:861. doi: 10.3389/fneur.2018.00861

Cavaliere, C., Longarzo, M., Orsini, M., Aiello, M., and Grossi, D. (2018b). Fronto-temporal circuits in musicalhallucinations: a PET-MR case study. *Front. Hum. Neurosci.* 12:385. doi: 10.3389/fnhum.2018.00385

Chen, K., and Chen, X. (2010). Design and development of molecular imaging probes. *Curr. Top. Med. Chem.* 10, 1227–1236. doi: 10.2174/156802610791384225

Chi, H., Chang, H. Y., and Sang, T. K. (2018). Neuronal cell death mechanisms in major neurodegenerative diseases. *Int. J. Mol. Sci.* 19:3082. doi: 10.3390/ijms19103082

Colasanti, A., Guo, Q., Muhlert, N., Giannetti, P., Onega, M., Newbould, R. D., et al. (2014). In vivo assessment of brain white matter inflammation in multiple sclerosis with (18)F-PBR111 PET. *J. Nucl Med.* 55, 1112–1118. doi: 10.2967/jnumed.113.135129

Colonna, M., and Butovsky, O. (2017). Microglia function in the central nervous system during health and neurodegeneration. *Annu. Rev. Immunol.* 35, 441–468. doi: 10.1146/annurev-immunol-051116-052358

Condello, C., Yuan, P., and Grutzendler, J. (2018). Microglia-mediated neuroprotection, trem2, and alzheimer's disease: evidence from optical imaging. *Biol. Psychiatry* 83, 377–387. doi: 10.1016/j.biopsych.2017.10.007

Coughlin, J. M., Yang, T., Rebman, A. W., Bechtold, K. T., Du, Y., Mathews, W. B., et al. (2018). Imaging glial activation in patients with post-treatment Lyme disease symptoms: a pilot study using [11C]DPA-713 PET. *J. Neuroinflammation* 15:346. doi: 10.1186/s12974-018-1381-1384

Dal-Bianco, A., Grabner, G., Kronnerwetter, C., Weber, M., Höftberger, R., Berger, T., et al. (2017). Slow expansion of multiple sclerosis iron rim lesions: pathology and 7 T magnetic resonance imaging. *Acta Neuropathol.* 133, 25–42. doi: 10.1007/s00401-016-1636-z

Datta, G., Colasanti, A., Kalk, N., Owen, D., Scott, G., Rabiner, E. A., et al. (2017). 11C-PBR28 and 18F-PBR111 detect white matter inflammatory heterogeneity in multiple sclerosis. *J. Nucl. Med.* 58, 1477–1482. doi: 10.2967/jnumed.116.187161

Dehghani, M., Kunz, N., Lanz, B., Yoshihara, H. A. I., and Gruetter, R. (2017). Diffusion-weighted MRS of acetate in the rat brain. *NMR Biomed* 30:e3768. doi: 10.1002/nbm.3768

Di Biase, M. A., Zalesky, A., O'keefe, G., Laskaris, L., Baune, B. T., Weickert, C. S., et al. (2017). PET imaging of putative microglial activation in individuals at ultra-high risk for psychosis, recently diagnosed and chronically ill with schizophrenia. *Transl. Psychiatry* 7:e1225. doi: 10.1038/tp.2017.193

Ezura, M., Kikuchi, A., Ishiki, A., Okamura, N., Hasegawa, T., Harada, R., et al. (2019). Longitudinal changes in 18 F-THK5351 positron emission tomography in corticobasal syndrome. *Eur. J. Neurol.* 26, 1205–1211. doi: 10.1111/ene.13966

Focke, C., Blume, T., Zott, B., Shi, Y., Deussing, M., Peters, F., et al. (2019). Early and Longitudinal microglial activation but not amyloid accumulation predicts cognitive outcome in PS2APP mice. *J. Nucl. Med.* 60, 548–554. doi: 10.2967/jnumed.118.217703

Garden, G. A., and Campbell, B. M. (2016). Glial biomarkers in human central nervous system disease. *Glia* 64, 1755–1771. doi: 10.1002/glia.22998

Gifford, A. N., Makriyannis, A., Volkow, N. D., and Gatley, S. J. (2002). In vivo imaging of the brain cannabinoid receptor. *Chem.Phys. Lipids* 121, 65–72. doi: 10.1016/s0009-3084(02)00148-2

Gillen, K. M., Mubarak, M., Nguyen, T. D., and Pitt, D. (2018). Significance and in vivo detection of iron-laden microglia in white matter multiple sclerosis lesions. *Front. Immunol.* 9:255. doi: 10.3389/fimmu.2018.00255

Green, M., Hutchins, G., Fletcher, J., Territo, W., Polson, H., Trussell, H., et al. (2018). Distribution of the P2X7-receptor-targeted [11C]GSK1482160 radiopharmaceutical in normal human subjects. *J. Nucl. Med.* 59(Suppl. 1):1009.

Grimaldi, A. M., Forte, E., Infante, T., Cavaliere, C., Salvatore, M., Cademartiri, F., et al. (2019). Future perspectives of nanoparticle-based contrast agents for cardiac magnetic resonance in myocardial infarction. *Nanomedicine* 17, 329–341. doi: 10.1016/j.nano.2019.02.003

Gulyás, B., Pavlova, E., Kása, P., Gulya, K., Bakota, L., and Várszegi, S. (2011). Activated MAO-B in the brain of Alzheimer patients, demonstrated by [11C]-L-deprenyl using whole hemisphere autoradiography. *Neurochem. Int.* 58, 60–68. doi: 10.1016/j.neuint.2010.10.013

Hafizi, S., Da Silva, T., Gerritsen, C., Kiang, M., Bagby, R. M., Prce, I., et al. (2017). Imaging Microglial activation in individuals at clinical high risk for psychosis: an In Vivo PET Study with [18F]FEPPA. *Neuropsychopharmacology* 42, 2474–2481. doi: 10.1038/npp.2017.111

Hagens, M. H. J., Golla, S. S. V., Janssen, B., Vugts, D. J., Beaino, W., and Windhorst, A. D. (2019). The P2X7 receptor tracer [11C]SMW139 as an in vivo marker of neuroinflammation in multiple sclerosis: a first-in man study. *Eur. J. Nucl. Med. Mol. Imaging* 47, 379–389. doi: 10.1007/s00259-019-04550-x

Hagens, M. H. J., Golla, S. V., Wijburg, M. T., Yaqub, M., Heijtel, D., Steenwijk, M. D., et al. (2018). In vivo assessment of neuroinflammation in progressive multiple sclerosis: a proof of concept study with [18F]DPA714 PET. *J. Neuroinflammation* 15:314. doi: 10.1186/s12974-018-1352-9

Hametner, S., Dal Bianco, A., Trattnig, S., and Lassmann, H. (2018). Iron related changes in MS lesions and their validity to characterize MS lesion types and dynamics with Ultra-high field magnetic resonance imaging. *Brain Pathol.* 28, 743–749. doi: 10.1111/bpa.12643

Han, J., Liu, H., Liu, C., Jin, H., Perlmutter, J. S., Egan, T. M., et al. (2017). Pharmacologic characterizations of a P2X7 receptor-specific radioligand, [11C]GSK1482160 for neuroinflammatory response. *Nucl. Med. Commun.* 38, 372–382. doi: 10.1097/MNM.0000000000000660

Harada, R., Ishiki, A., Kai, H., Sato, N., Furukawa, K., Furumoto, S., et al. (2018). Correlations of 18F-THK5351 PET with Postmortem Burden of Tau and Astrogliosis in Alzheimer Disease. *J. Nucl. Med.*59, 671–674. doi: 10.2967/jnumed.117.197426

Herranz, E., Louapre, C., Treaba, C. A., Govindarajan, S. T., Ouellette, R., Mangeat, G., et al. (2019). Profiles of cortical inflammation in multiple sclerosis by 11C-PBR28 MR-PET and 7 Tesla imaging. *MultScler* 1:1352458519867320. doi: 10.1177/1352458519867320

Herzog, H., Pietrzyk, U., Shah, N. J., and Ziemons, K. (2010). The current state, challenges and perspectives of MR-PET. *NeuroImage* 49, 2072–2082. doi: 10.1016/j.neuroimage.2009.10.036

Horti, A. G., Naik, R., Foss, C. A., Minn, I., Misheneva, V., Du, Y., et al. (2019). PET imaging of microglia by targeting macrophage colony-stimulating factor 1 receptor (CSF1R). *Proc. Natl. Acad. Sci. U.S.A.* 116, 1686–1691. doi: 10.1073/pnas.1812155116

Iaccarino, L., Moresco, R. M., Presotto, L., Bugiani, O., Iannaccone, S., Giaccone, G., et al. (2018). An In Vivo 11C-(R)-PK11195 PET and in vitro pathology study of microglia activation in creutzfeldt-jakob disease. *Mol. Neurobiol.* 55, 2856–2868. doi: 10.1007/s12035-017-0522-6

Ishibashi, K., Miura, Y., Hirata, K., Toyohara, J., and Ishii, K. (2019). 18F-THK5351 PET can identify astrogliosis in multiple sclerosis plaques. *Clin. Nucl. Med.* 2019:24. doi: 10.1097/RLU.0000000000002751

Ishiki, A., Harada, R., Kai, H., Sato, N., Totsune, T., Tomita, N., et al. (2018). Neuroimaging-pathological correlations of [18F]THK5351 PET in progressive supranuclear palsy. *Acta Neuropathol. Commun.* 6:53. doi: 10.1186/s40478-018-0556-7

Kang, Y., Schlyer, D., Kaunzner, U. W., Kuceyeski, A., Kothari, P. J., and Gauthier, S. A. (2018). Comparison of two different methods of image analysis for the assessment of microglial activation in patients with multiple sclerosis using (R)-[N-methyl-carbon-11]PK11195. *PLoS One* 13:e0201289. doi: 10.1371/journal.pone.0201289

Kaunzner, U. W., Kang, Y., Zhang, S., Morris, E., Yao, Y., Pandya, S., et al. (2019). Quantitative susceptibility mapping identifies inflammation in a subset of chronic multiple sclerosis lesions. *Brain* 142, 133–145. doi: 10.1093/brain/awy296

Keller, T., López-Picón, F. R., Krzyczmonik, A., Forsback, S., Kirjavainen, A. K., Takkinen, J. S., et al. (2018). [18F]F-DPA for the detection of activated microglia

in a mouse model of Alzheimer's disease. *Nucl. Med. Biol.* 67, 1–9. doi: 10.1016/j.nucmedbio.2018.09.001

Kirschbaum, K., Sonner, J. K., Zeller, M. W., Deumelandt, K., Bode, J., Sharma, R., et al. (2016). In vivo nanoparticle imaging of innate immune cells can serve as a marker of disease severity in a model of multiple sclerosis. *Proc. Natl. Acad. Sci. U.S.A.* 113, 13227–13232. doi: 10.1073/pnas.1609397113

Kobayashi, R., Hayashi, H., Kawakatsu, S., Ishiki, A., Okamura, N., Arai, H., et al. (2018). [18F]THK-5351 PET imaging in early-stage semantic variant primary progressive aphasia: a report of two cases and a literature review. *BMC Neurol.* 18:109. doi: 10.1186/s12883-018-1115-3

Kolb, H. C., Barret, O., Bhattacharya, A., Chen, G., Constantinescu, C., and Huang, C. (2019). Preclinical evaluation and nonhuman primate receptor occupancy study of 18F-JNJ-64413739, a PET radioligand for P2X7 receptors. *J. Nucl. Med.* 60, 1154–1159. doi: 10.2967/jnumed.118.212696

Kumar, J. S. D., Bai, B., Zanderigo, F., DeLorenzo, C., Prabhakaran, J., Parsey, R. V., et al. (2018). In vivo brain imaging, biodistribution, and radiation dosimetry estimation of [11C]Celecoxib, a COX-2 PET ligand, in nonhuman primates. *Molecules* 23:E1929. doi: 10.3390/molecules23081929

Lewis, C. M., Graves, S. A., Hernandez, R., Valdovinos, H. F., Barnhart, T. E., Cai, W., et al. (2015). 52Mn production for PET/MRI tracking of human stem cells expressing divalent metal transporter 1 (DMT1). *Theranostics* 5, 227–239. doi: 10.7150/thno.10185

Li, H., Sagar, A. P., and Kéri, S. (2018). Translocator protein (18kDa TSPO) binding, a marker of microglia, is reduced in major depression during cognitive-behavioral therapy. *Prog. Neuropsychopharmacol. Biol. Psychiatry* 83, 1–7. doi: 10.1016/j.pnpbp.2017.12.011

Luo, S., Kong, X., Wu, J. R., Wang, C. Y., Tian, Y., Zheng, G., et al. (2018). Neuroinflammation in acute hepatic encephalopathy rats: imaging and therapeutic effectiveness evaluation using 11C-PK11195 and 18F-DPA-714 micro-positron emission tomography. *Metab. Brain Dis.* 33, 1733–1742. doi: 10.1007/s11011-018-0282-7

Marchitelli, R., Aiello, M., Cachia, A., Quarantelli, M., Cavaliere, C., Postiglione, A., et al. (2018). Simultaneous resting- state FDG-PET/fMRI in Alzheimer disease: relationship between glucose metabolism and intrinsic activity. *NeuroImage* 176, 246–258. doi: 10.1016/j.neuroimage.2018.04.048

Mele, G., Cavaliere, C., Alfano, V., Orsini, M., Salvatore, M., and Aiello, M. (2019). Simultaneous EEG-fMRI for functional neurological assessment. *Front. Neurol.* 10:848. doi: 10.3389/fneur.2019.00848

Miller, S. J. (2018). Astrocyte heterogeneity in the adult central nervous system. *Front. Cell Neurosci.* 2018:15. doi: 10.3389/fncel.2018.00401

Miyajima, N., Ito, M., Rokugawa, T., Iimori, H., Momosaki, S., Omachi, S., et al. (2018). Detection of neuroinflammation before selective neuronal loss appearance after mild focal ischemia using [18F]DPA-714 imaging. *EJNMMI Res.* 8:43. doi: 10.1186/s13550-018-0400-x

Monai, H., and Hirase, H. (2018). Astrocytes as a target of transcranial direct current stimulation (tDCS) to treat depression. *Neurosci. Res.* 126, 15–21. doi: 10.1016/j.neures.2017.08.012

Monti, S., Cavaliere, C., Covello, M., Nicolai, E., Salvatore, M., and Aiello, M. (2017). An evaluation of the benefits of simultaneous acquisition on PET/MR coregistration in head/neck imaging. *J. Healthcare Eng.* 2017:2634389. doi: 10.1155/2017/2634389

Nack, A., Brendel, M., Nedelcu, J., Daerr, M., Nyamoya, S., Beyer, C., et al. (2019). Expression of translocator protein and [18F]-ge180 ligand uptake in multiple sclerosis animal models. *Cells* 8, E94. doi: 10.3390/cells8020094

Narayanaswami, V., Dahl, K., Bernard-Gauthier, V., Josephson, L., Cumming, P., and Vasdev, N. (2018). Emerging PET radiotracers and targets for imaging of neuroinflammation in neurodegenerative diseases: outlook beyond TSPO. *Mol. Imaging* 17:1536012118792317. doi: 10.1177/1536012118792317

Ni, R., Mu, L., and Ametamey, S. (2019). Positron emission tomography of type 2 cannabinoid receptors for detecting inflammation in the central nervous system. *Acta Pharmacol. Sin.* 40, 351–357. doi: 10.1038/s41401-018-0035-5

Ottoy, J., De Picker, L., Verhaeghe, J., Deleye, S., Wyffels, L., Kosten, L., et al. (2018). 18F-PBR111 PET imaging in healthy controls and schizophrenia: test-retest reproducibility and quantification of neuroinflammation. *J. Nucl. Med.* 59, 1267–1274. doi: 10.2967/jnumed.117.203315

Papa, M., De Luca, C., Petta, F., Alberghina, L., and Cirillo, G. (2014). Astrocyte-neuron interplay in maladaptive plasticity. *Neurosci. Biobehav. Rev.* 42, 35–54. doi: 10.1016/j.neubiorev.2014.01.010

Pérez-Alvarez, A., and Araque, A. (2013). Astrocyte-neuron interaction at tripartite synapses. *Curr. Drug Targets* 14, 1220–1224. doi: 10.2174/13894501113149990203

Poupot, R., Bergozza, D., and Fruchon, S. (2018). Nanoparticle-based strategies to treat Neuro-inflammation. *Materials* 11:270. doi: 10.3390/ma11020270

Pulgar, V. M. (2019). Transcytosis to cross the blood brain barrier, new advancements and challenges. *Front. Neurosci.* 12, 1019.

Ratai, E. M., Alshikho, M. J., Zürcher, N. R., Loggia, M. L., Cebulla, C. L., Cernasov, P., et al. (2018). Integrated imaging of [11C]-PBR28 PET, MR diffusion and magnetic resonance spectroscopy 1H-MRS in amyotrophic lateral sclerosis. *Neuroimage Clin.* 20, 357–364. doi: 10.1016/j.nicl.2018.08.007

Reischauer, C., Gutzeit, A., Neuwirth, C., Fuchs, A., Sartoretti-Schefer, S., Weber, M., et al. (2018). In-vivo evaluation of neuronal and glial changes in amyotrophic lateral sclerosis with diffusion tensor spectroscopy. *Neuroimage Clin.* 20, 993–1000. doi: 10.1016/j.nicl.2018.10.001

Selvaraj, S., Bloomfield, P. S., Cao, B., Veronese, M., Turkheimer, F., and Howes, O. D. (2018). Brain TSPO imaging and gray matter volume in schizophrenia patients and in people at ultra high risk of psychosis: an [11C]PBR28 study. *Schizophr Res.* 195, 206–214. doi: 10.1016/j.schres.2017.08.063

Shen, Z., Bao, X., and Wang, R. (2018). Clinical PET imaging of microglial activation: implications for microglial therapeutics in Alzheimer's Disease. *Front. Aging Neurosci.* 10:314. doi: 10.3389/fnagi.2018.00314

Shigemoto, Y., Sone, D., Maikusa, N., Okamura, O., Furumoto, S., Kudo, Y., et al., (2018). Association of deposition of tau and amyloid-β proteins with structural connectivity changes in cognitively normal older adults and alzheimer's disease spectrum patients. *Brain Behav.* 8:e01145. doi: 10.1002/brb3.1145

Shukuri, M., Takashima-Hirano, M., Tokuda, K., Takashima, T., Matsumura, K., Inoue, O., et al. (2011). In vivo expression of cyclooxygenase-1 in activated microglia and macrophages during neuroinflammation visualized by PET with 11C-ketoprofen methyl ester. *J. Nucl. Med.* 52, 1094–1101. doi: 10.2967/jnumed.110.084046

Singhal, T., O'Connor, K., Dubey, S., Belanger, A. P., Hurwitz, S., Chu, R., et al. (2018). 18F-PBR06 Versus 11C-PBR28 PET for assessing white matter translocator protein binding in multiple sclerosis. *Clin. Nucl. Med.* 43, e289–e295. doi: 10.1097/RLU.0000000000002179

Takata, N., Sugiura, Y., Yoshida, K., Koizumi, M., Hiroshi, N., Honda, K., et al. (2018). Optogenetic astrocyte activation evokes BOLD fMRI response with oxygen consumption without neuronal activity modulation. *Glia.* 66, 2013–2023. doi: 10.1002/glia.23454

Tang, T., Valenzuela, A., Petit, F., Chow, S., Leung, K., Gorin, F., et al. (2018). In Vivo MRI of functionalized iron oxide nanoparticles for brain inflammation. *Contrast Media Mol. Imaging* 25:3476476. doi: 10.1155/2018/3476476

Unterrainer, M., Mahler, C., Vomacka, L., Lindner, S., Havla, J., Brendel, M., et al. (2018). TSPO PET with [18F]GE-180 sensitively detects focal neuroinflammation in patients with relapsing-remitting multiple sclerosis. *Eur. J. Nucl. Med. Mol. Imaging* 45, 1423–1431. doi: 10.1007/s00259-018-3974-7

Uppal, R., Catana, C., Ay, I., Benner, T., Sorensen, A. G., and Caravan, P. (2011). Bimodal thrombus imaging: simultaneous PET/MR imaging with a fibrin-targeted dual PET/MR probe—Feasibility study in rat model. *Radiology* 258, 812–820. doi: 10.1148/radiol.10100881

van Weehaeghe, D., Koole, M., Schmidt, M. E., Deman, S., Jacobs, A. H., Souche, E., et al. (2019). [11C]JNJ54173717, a novel P2X7 receptor radioligand as marker for neuroinflammation: human biodistribution, dosimetry, brain kinetic modelling and quantification of brain P2X7 receptors in patients with Parkinson's disease and healthy volunteers. *Eur. J. Nucl. Med. Mol. Imaging* 46, 2051–2064. doi: 10.1007/s00259-019-04369-6

Vecchione, D., Aiello, M., Cavaliere, C., Nicolai, E., Netti, P. A., and Torino, E. (2017). Hybrid core shell nanoparticles entrapping Gd-DTPA and 18F-FDG for simultaneous PET/MRI acquisitions. *Nanomedicine* 12, 2223–2231. doi: 10.2217/nnm-2017-0110

Verkhratsky, A., Parpura, V., Pekna, M., Pekny, M., and Sofroniew, M. (2014). Glia in the pathogenesis of neurodegenerative diseases. *Biochem. Soc. Trans.* 42, 1291–1301. doi: 10.1042/BST20140107

Wang, M., He, Y., Sejnowski, T. J., and Yu, X. (2018). Brain-state dependent astrocytic Ca2+ signals are coupled to both positive and negative BOLD-fMRI signals. *Proc. Natl. Acad. Sci. U.S.A.* 115, E1647–E1656. doi: 10.1073/pnas.1711692115

Yamagishi, S., Iga, Y., Nakamura, M., Takizawa, C., Fukumoto, D., and Kakiuchi, T. (2019). Upregulation of cannabinoid receptor type 2, but not TSPO, in senescence-accelerated neuroinflammation in mice: a positron emission tomography study. *J. Neuroinflammation.*10 16:208. doi: 10.1186/s12974-019-1604-3

Yi, S. Y., Barnett, B. R., Torres-Velázquez, M., Zhang, Y., Hurley, S. A., Rowley, P. A., et al. (2019). Detecting microglial density with quantitative multi-compartment diffusion MRI. *Front. Neurosci.* 13:81. doi: 10.3389/fnins.2019.00081

Yokoi, T., Watanabe, H., Yamaguchi, H., Bagarinao, E., Masuda, M., Imai, K., et al. (2018). Involvement of the precuneus/posterior cingulate cortex is significant for the development of Alzheimer's Disease: a PET (THK5351, PiB) and resting fMRI Study. *Front. Aging Neurosci.* 10:304. doi: 10.3389/fnagi.2018.00304

Zaidi, H., and Guerra, A. D. (2011). An outlook on future design of hybrid PET/MRI systems. *Med. Phys.*38, 5667–5689. doi: 10.1118/1.3633909

Zimmer, E. R., Parent, M. J., Souza, D. G., Leuzy, A., Lecrux, C., Kim, H. I., et al. (2017). [18F]FDG PET signal is driven by astroglial glutamate transport. *Nat. Neurosci.* 20, 393–395. doi: 10.1038/nn.4492

Zürcher, N. R., Loggia, M. L., Lawson, R., Chonde, D. B., Izquierdo-Garcia, D., Yasek, J. E., et al. (2015). Increased in vivo glial activation in patients with amyotrophic lateral sclerosis: assessed with [(11)C]-PBR28. *Neuroimage Clin.* 7, 409–414. doi: 10.1016/j.nicl.2015.01.009

Conflict of Interest: The authors declare that the research was conducted in the absence of any commercial or financial relationships that could be construed as a potential conflict of interest.

Advantages of publishing in Frontiers

OPEN ACCESS
Articles are free to read for greatest visibility and readership

FAST PUBLICATION
Around 90 days from submission to decision

HIGH QUALITY PEER-REVIEW
Rigorous, collaborative, and constructive peer-review

TRANSPARENT PEER-REVIEW
Editors and reviewers acknowledged by name on published articles

Frontiers
Avenue du Tribunal-Fédéral 34
1005 Lausanne | Switzerland

Visit us: www.frontiersin.org
Contact us: frontiersin.org/about/contact

REPRODUCIBILITY OF RESEARCH
Support open data and methods to enhance research reproducibility

DIGITAL PUBLISHING
Articles designed for optimal readership across devices

FOLLOW US
@frontiersin

IMPACT METRICS
Advanced article metrics track visibility across digital media

EXTENSIVE PROMOTION
Marketing and promotion of impactful research

LOOP RESEARCH NETWORK
Our network increases your article's readership